Clays and Clay Minerals

Geological Origin, Mechanical Properties and Industrial Applications

Earth Sciences in the 21st Century

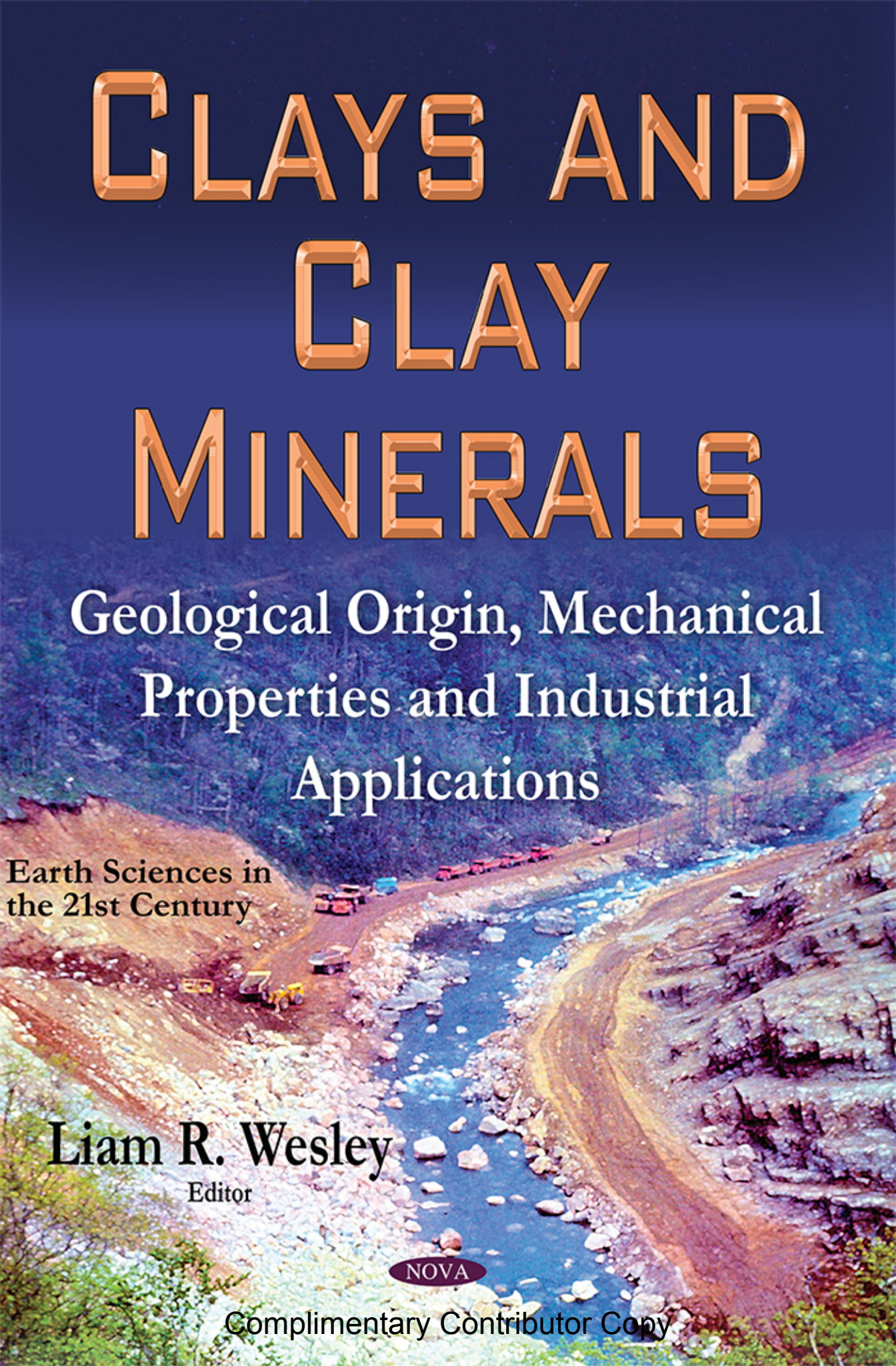

Liam R. Wesley
Editor

NOVA

EARTH SCIENCES IN THE 21ST CENTURY

CLAYS AND CLAY MINERALS

GEOLOGICAL ORIGIN, MECHANICAL PROPERTIES AND INDUSTRIAL APPLICATIONS

EARTH SCIENCES IN THE 21ST CENTURY

Additional books in this series can be found on Nova's website
under the Series tab.

Additional e-books in this series can be found on Nova's website
under the e-book tab.

EARTH SCIENCES IN THE 21ST CENTURY

CLAYS AND CLAY MINERALS

GEOLOGICAL ORIGIN, MECHANICAL PROPERTIES AND INDUSTRIAL APPLICATIONS

LIAM R. WESLEY
EDITOR

nova publishers
New York

Library of Congress Cataloging-in-Publication Data

Clays and clay minerals : geological origin, mechanical properties and industrial applications / [edited by] Liam R. Wesley.
pages cm. -- (Earth sciences in the 21st century)
Includes bibliographical references and index.
ISBN: 978-1-63117-780-4 (eBook)
1. Clay minerals. 2. Clay minerals--Industrial applications. I. Wesley, Liam R., editor of compilation.
QE389.625.C57 2014
552'.5--dc23

2014013219

Published by Nova Science Publishers, Inc. † New York

CONTENTS

PREFACE

The peculiar characteristics of clays provide it with very interesting adsorption qualities, especially for polar or ionizable molecules. Some of these characteristics include the silicates' sheet structure that makes a large surface area accessible for adsorption; the usually significant surface charge that can be responsible for strong electrostatic interactions; and clays' swelling properties and presence of exchangeable surface cations that facilitate ion-exchange mechanisms. Added to their wide availability and associated low cost, these characteristics have motivated in recent years an increasing interest in utilizing natural, processed or chemically-modified clays for the removal of organic contaminants from aqueous solutions. This book discusses the application of clay materials for the removal of organic compounds from contaminated waters. It also discusses several other topics that include time and temperature related behavior of clays; mechanical treatment of clay minerals; the workability of natural clays and clays in the ceramics industry; recent advances in hydraulic performance of clay liners; and the genesis, properties and industrial applications of bauxitic lithomargic clay.

Chapter 1 - The prediction of stresses, deformations and temperature as a function of time in a material subjected to simultaneous thermal and mechanical loading is one of the most challenging and complex problems in engineering mechanics. In the field of Geomechanics a number of important problems exist that necessitate the realistic prediction of time dependent thermal-mechanical behavior. Thermal-mechanical analyses of soils are complicated by the nature of these materials. Soils consist of a porous skeleton whose voids are filled with fluid and gas. Consequently, soils are non-homogeneous materials. Macroscopically such materials exhibit an anisotropic, inelastic, path-dependent, strain hardening (and softening), time-, rate- and temperature-dependent behavior. To further complicate matters, the thermal properties of such materials are not as well known as those for other materials such as metals. The variability in a soil’s composition and subsequent degrees of thermal and mechanical dependency further increase the complexity of the thermomechanical behavior of such material. Finally, natural soils are also subject to sample disturbance that makes the task of representative testing all the more difficult. Local variations in soil composition often preclude the obtaining of reproducible test results, and thus impose limitations on the confidence associated with the analytical description of the soil behavior. This chapter briefly discusses the rudimentary microscopic and physicochemical aspects associated with saturated cohesive soils. This is followed by a discussion of the macroscopically observed time- and temperature-dependent behavior of such soils. Finally, a combined and coupled thermo-

elastoplastic-viscoplastic framework for modeling the anisotropic, time-, rate- and temperature-dependent behavior of cohesive soils in the context of a bounding surface formulation is proposed.

Chapter 2 - Clay-rich soil lenses and layers in the subsurface play an important role in determining the efficiency of remediation of waste sites contaminated with hazardous organic compounds. Often organic solvents, such as trichloroethylene or tetrachloroethylene, are spilled or disposed of in such a manner that they enter the subsurface. There they dissolve in the groundwater and accumulate over time in the clayey lenses and layers located in the saturated zone. During the remediation of these waste sites, the contaminants are then slowly released, contributing to elevated concentrations in groundwater over an extended period of time. Because of the low permeability of the clayey lenses and layers, the main transport process into and out of these locations is considered to be diffusion. Thus, estimating the rates of diffusion in clayey soil materials is key to determining the rates at which these hazardous compounds may be released during clean-up activities.

Correlations have been developed to estimate diffusion coefficients in soil media based on the diffusion coefficient of the compound in water and the porosity of the soil. However, the use of these methods may be limited as they suggest an increase in the diffusion coefficient with an increasing porosity whereas lower diffusion coefficients are usually measured in clay materials despite their higher porosity. Furthermore, the flexibility of the structure of smectitic clay minerals can result in variable porosities. Because remediation time frames depend on the diffusional rate of release of hazardous organic solutes from clayey soils, this study quantitatively assessed the performance of commonly-used methodologies to estimate the diffusion coefficient of organic solutes in saturated clay-silt mixtures. The results suggest that the performance of these methodologies is acceptable (average relative error of 61%) if the soil contains less than 25% clay, whereas high relative errors (> 151%) may occur for soils containing more than 25% clay. To improve predictions for the materials with high clay contents, two methodologies were developed from literature data to estimate the effective diffusion coefficient as a function of dry bulk density, which yielded relative errors of 83% and 48%. Consequently, these methods are recommended as alternatives to those commonly used to estimate effective diffusion coefficients of organic solutes in saturated clayey soils.

Chapter 3 - Physico-chemical changes during the dry grinding of clays produce mechanochemical effects, as in other solids subjected to mechanical stress by impact and friction forces among particles, such as planetary mills. Thus, the reactivity of ground materials is enhanced and, therefore, it leads to mechanochemical reactions. The effects of dry grinding on clays and clay minerals have been extensively studied. It is associated to their relevant importance in some industrial applications as ceramic raw materials and processing of advanced ceramics.

In the present research, kaolinite (1:1 layer silicate), pyrophyllite and talc (2:1) and raw clay materials have been selected. Dry grinding experiments using planetary milling have been performed using selected samples. Several techniques have been used to follow the evolution of the layer silicates, mainly XRD, surface area (nitrogen adsorption), SEM, TEM, MAS-NMR, FTIR, particle size analysis and thermal methods (DTA-TGA).

The mechanical stress during grinding clays are quite diverse, producing important changes such as lattice distortions, amorphization, decrease in particle size, formation of nanostructures and an increase in surface area. Modifications of surface area, particle size and

shape of short and prolonged grinding on the crystal structure of the layer silicates have been evaluated. These observed changes have been related to a progressive delamination and structural breakdown during grinding, with final formation of a turbostratic-type structure. Short grinding times resulted in the breakdown and drastic size reduction of relatively thin particles. It has been found an inverse relationship between coherent X-ray domain and lattice microstrains in the ground powders. It can be also observed an increasing in amorphization as a consequence of the loss of long-range order. On the other hand, the rate of size reduction decreased with time and a limit was reached for each layer silicate producing more rounded particles and aggregates, with a decrease of surface area. Grinding produced a loss of periodicity perpendicular to the layer silicate plane, and the dimensions of the crystallites along the c-direction resulted too small to produce coherent X-ray scattering. Microscopy techniques (TEM and SEM) allowed to observe the formation of nanometer size ground powders and further particle agglomeration. Modifications in the coordination of Si and Al nuclei have been also deduced from MAS-NMR spectroscopy, demonstrating a short-range order.

The present results are interesting in clay research to analyze the formation of nanostructured powders, with enhanced surface properties and reactivity, when grinding clays and to compare the effects of grinding on 1:1 and 2:1 layer silicates, the modifications of tetrahedral and octahedral sheets, the mechanochemical effects induced by grinding and the influence of experimental conditions.

Chapter 4 - The peculiar characteristics of clays (namely, among others, the silicates' sheet structure that makes a large surface area accessible for adsorption; the usually significant surface charge that can be responsible for strong electrostatic interactions; and clays' swelling properties and presence of exchangeable surface cations that facilitate ion-exchange mechanisms) provide these materials with very interesting adsorption qualities, especially for polar or ionizable molecules. Added to their wide availability and associated low cost, these characteristics have motivated in recent years an increasing interest in utilizing natural, processed or chemically-modified clays for the removal of organic contaminants from aqueous solutions. In fact, organic xenobiotic compounds have been emerging in the latest years as a serious environmental concern, as many of these pollutants have a proven ecotoxicity and may even be a threat to human health. Associated to the fact that many such substances are not efficiently removed from wastewaters by conventional wastewater treatment processes (which has resulted in many reports of the detection of organic xenobiotics presence in treated wastewaters, natural waters and even drinking waters) urges for the development and implementation of alternative or complementary water and wastewater treatment technologies, of which adsorption-based processes have been recognized as one of the most economic possibilities (depending on the cost of the adsorbent materials). The aim of this work is to present a review on the extensive amount of studies on the adsorption of organic compounds to several clay-based materials. The discussion is focused on the environmental applications, specifically for the decontamination of water and wastewater polluted with organic xenobiotics, and with the aim of highlighting the possibilities presented by this type of generally cheap materials, and to provide resources for the screening of prospective adsorbents with potential to be used as efficient and economic water and wastewater treatment alternatives.

Chapter 5 - The large quantities of sewage sludge that are currently generated require new alternatives for its recycling and final destination, beyond already known methods in the

agriculture and cement industry. The use of this sludge as raw material for the production of structural ceramics, such as clay bricks, may become an interesting alternative, both from an industrial and environmental point of view.

This chapter is focused on the use of solid wastes, such as for example sewage sludge or forest residues, to serve as additive raw materials for the production of clay bricks. It is based on the author's experience with the Ecobrick® material and their subsequent research on producing some raw materials from WWTP sludge suitable for the ceramic industry. The chapter shows some formulations of raw materials in ceramic mixtures, their physical properties and to analyze their environmental characteristics. The final purpose is to illustrate the possibility of designing tailor-made ceramics that fulfill custom-physical properties, which are appropriate for particular construction use.

Chapter 6 - The property of workability is important in the ceramics industry, particularly in association with extrusion processes, in the construction industry where natural and stabilised clay soils are required to be worked, moulded and compacted and in the agricultural industry where the conditions for good tillage and ploughing are related to a friable or brittle condition close to the plastic limit. The work required to carry out the processes of extrusion and compaction of clays in the plastic state can be related to their toughness which in turn depends on the clay mineralogy, water content, particle size distribution and soil fabric. Toughness has previously only been studied in an indirect and qualitative manner. The results of tests conducted with an apparatus developed by the author to produce rolling of a soil thread comparable to the procedure in the Atterberg plastic limit test are discussed. A well-defined ductile-brittle transition in relation to water content is achieved resulting in a much more accurate determination of the plastic limit compared to the poor reproducibility of the standard test. The toughness of a ductile clay can be determined as a measure of work/unit volume from a stress-strain curve over a range of water contents. Unique toughness-water content relationships are obtained for a wide variety of natural clays, ball clays and brick clays. The range of water contents between the liquid and plastic limit, conventionally referred to as the plasticity index, can be distinguished into three regions, described as adhesive-plastic, soft-plastic and stiff-plastic regions and these are defined by the water content at zero toughness, the toughness limit, the water content at the stiffness transition between the soft-plastic and stiff-plastic regions and the plastic limit. The effects of coarse-grained particles, silts and sands, on toughness is small at low contents but at high contents is affected by the requirements not only to mould the clay component but to displace the coarse particles. Mixing different clays together is found to produce non-linear variations in their properties, depending on the total clay content and the content of a dominant clay mineral.

Chapter 7 - In the last decades, our planet has been systematically harmed by contamination processes, mainly by the industrial activity. Within such context, the textile industry is responsible by the generation of great amount of highly colored effluents, composed of dyes which are harmful both for men and the environment. Amongst the several methods of dyes removal, adsorption has been increasingly applied, due to low cost and simplicity of this this technique. Therefore, the development and study of low cost adsorbent materials with good adsorption capability have been carried out. Nowadays, hybrid materials present great appeal, as they have unique features, which are not seen in the precursors when isolated. Clays are amongst the most used materials, as they are low cost material and have lamellar structure which might serve as a support to other substances interlayer in the preparation of mixed materials. In this study, a composite material obtained from the mixture

of bentonite clay and *pinus* activated charcoal, which presented very interesting properties regarding reactive dye adsorption, was used. In order to evaluate the composite adsorption potential to remove dyes in aqueous solution, a reactive navy blue dye was used and some parameters which influence the process, such as pH, ionic strength and temperature were evaluated by factorial design. Results revealed that all variables under study influenced the reactive navy blue dye adsorption process, as well as the interaction between pH and temperature, ionic strength and temperature and also amongst the three variables. Thus, the results of experimental design showed that the variables pH, ionic strength and temperature cannot be studied separately. Besides this, it enabled reduction in the number of experiments carried out.

Chapter 8 - Since ancient times that the fired clay bricks have been used as building materials. In general, the common clays are the most widely used raw materials for clay bricks. It is known fact that the clay brick bodies are empirically formulated with clays of different technical characteristics. This empirical approach makes the economically unviable industrial experiments, since the costs and execution time are high. On the other hand, the technological properties of clay bricks are influenced primarily by the combination of the raw materials and processing conditions. When the processing conditions are kept constant, the experimental design technique with mixture could be used to optimize the clay body formulation. In this context, the present chapter focuses on the use of experimental design in simplex lattice to optimize a clay brick formulation using two distinct sedimentary clays from south-eastern Brazil. Emphasis special is given on the effect of the clayey formulation on the technical properties of clay bricks.

Chapter 9 - This chapter presents recent advances on the hydraulic performance of clay liners. Due to their low hydraulic conductivity, clay liners are used as hydraulic barriers in many engineering and environmental applications including earth dams, embankments, levees, landfills, and pond liners, to prevent leakage of water or leachate from reservoirs and/or landfills. The hydraulic performance of clay liners is related to the mineralogy, the manner of deposition and the exposure conditions, which could involve chemical exposure, potentially large physical stresses, thermal and freeze-thaw cycles, and elevated operating temperatures due to waste biodegradation in landfills. Changes in the clay hydraulic conductivity by several orders of magnitude have been reported in the literature upon exposure to thermal cycles or permeation with high-concentration leachate solutions. The latest findings on the hydraulic performance of clay liners under various field conditions such as daily thermal and wet-dry cycles, elevated temperatures, leachate exposure, and the combined effect of temperature and chemical exposure conditions are described. The hydraulic performance of composite liners (i.e., clay liner along with a layer of geomembrane) under simulated field conditions is also discussed.

Chapter 10 - The kaolins are a group of dioctahedral 1:1 layer silicates, in which each layer consists of a combination of one sheet of tetrahedral and one sheet of octahedral cations linked by bridging oxygen atoms. The surface of the tetrahedral sheet consists of oxygen atoms, whereas that of the octahedral sheet contains hydroxyl groups, and neighbouring layers are held together by hydrogen bonds. Kaolin deposits are widely distributed throughout the World, but they also exhibit considerable variations in both their chemical and structural compositions; the latter are exhibited both in the nature of the stacking of adjacent layers, but also in the inclusion of water molecules in the interlayer region. The kaolin minerals are used extensively in the ceramics, paint and paper industries, and can also be used as source

materials for the production of higher-value products for a wide range of industrial uses. In addition, kaolins can be modified to produce new materials with a wide range of physical and chemical properties that have the potential for the development of additional uses for the mineral.

This chapter reviews recent publications on the generation, characterization, and properties of modified kaolins, and these results are supplemented by the inclusion of some previously unpublished results obtained using materials from two of the main kaolin deposits in Thailand. A final section discusses potential uses for some of these products and possible further developments in the production of novel kaolin-derived materials.

Chapter 11 - Clay mineral surfaces have been important for the prebiotic organization and protection of nucleic acids. The adsorption of DNA to mineral surfaces is of great interest because of gene transfer, drug release, bio-adhesion (cell capture) and origins of life studies. Here, the authors present the morphology observation to provide insight into the adsorption structure and characteristics of DNA by natural allophane particles. The molecular orbital computer simulation has been used to probe the interaction of DNA and/or adenosine 5'-monophosphate and allophane with active sites. The author's simulations predicted the strand undergoes some extent of the elongation, which induces the alteration of the conformation of the phosphate backbone, base-base distance and excluded volume correlation among bases. The authors discuss the general adsorption mechanism for the DNA/allophane complexation and hydrogel formation.

Chapter 12 - Direct observations of physical structures and chemical composition of the seismogenic zones of active faults are rare, due to the difficulty in reaching the fault zone at depth. Thus, the physico-chemical processes, triggered by energies released from coseismic faulting, remain largely unknown. The Chelungpu thrust fault was northward ruptured as a result of the Mw 7.6 Chi-Chi earthquake which struck central Taiwan on 21st September 1999. To fill the knowledge gaps raised by the 1999 Chi-Chi earthquake, such as what the absolute stress levels was on the fault during the earthquake, how the stresses recover afterward to prepare for the next event, and how the material properties of the Chelungpu fault affect its propensity to catastrophically slide rather than creep, the Taiwan Chelungpu fault Drilling Project (TCDP) was conducted in 2005 and drilled to a depth of 2,003 m. On the basis of continuous coring, a suite of geophysical measurements, and microstructural observation, three fault zones of the Chelungpu fault were identified at the depth of 1,111 m, 1,153 m, and 1,222 m (described as FZ1111, FZ1153, and FZ1222 hereafter). The active fault zone of the Chelungpu fault corresponding to the 1999 Chi-Chi earthquake was recognized at the depth of 1,111 m (FZ1111). By characterizing clay mineral assemblages with continuous sampling from fresh materials of the Chelungpu fault, the authors aim at achieving the objectives of (1) characterization of clay mineralogy of the Chelungpu fault zones, (2) recognition of the PSZ within the active fault zone(s) corresponding to the 1999 Chi-Chi earthquake, (3) determination of the physico-chemical processes occurred during seismic slip and plausible slip weakening mechanism operated at seismic rates, and (4) estimation of earthquake source parameters (e.g., estimate of temperature for calculating associated frictional energy and thickness of the PSZ for calculating associated surface fracture energy). Distinct clay mineral assemblage within the principal slip zone (PSZ) of FZ1111 show that (1) a decrease in clay content; and (2) significant decline of illite, disappearance of chlorite and kaolinite, and a spike in smectite. Meanwhile, the microstructural observation provides the evidence of melting, and the temperature within the fresh black gouge is estimated to be

from 900°C to 1100°C by comparing the SEM images of in-situ natural samples with those of heated materials. The interval of clay anomaly within the PSZ resulted from frictional melting was determined by state-of-art in-situ synchrotron X-ray diffraction analysis and was estimated to be 1 mm. Thus, the characteristics of clay within the PSZ suggest that pseudotachylyte were possibly produced during the 1999 Chi-Chi earthquake and promptly altered to smectite. In addition, based on the estimation of the thickness of the PSZ, the contribution of surface fracture energy to earthquake breakdown work is quantified to be 1.9%. The huge remaining part of the breakdown work would be turned into chemical work (mineral transformation) and mechanic work associated with several processes to lubricate the Chelungpu fault such as thermal pressurization, elastohydrodynamic lubrication, and melting lubrication.

Chapter 13 - Free radicals and other paramagnetic centres are a common occurrence in mineral species. Paramagnetic metal ions may be incorporated into mineral structures during or after formation, whereas free radical centres are mainly generated by natural radiation, although they can also be the consequence of chemical and physical processes during and after mineral formation. This chapter reviews the types of paramagnetic centre that have been observed in clay minerals and their characterization by electron paramagnetic resonance (EPR) spectroscopy, with special attention being given to natural kaolin samples, which illustrate the diversity of these minerals from different parts of the World. In addition, clay minerals contain reactive surfaces, and have important function in controlling the mobility and stability of ions and molecules in environmental situations, as well as having potential uses as catalysts. Examples are also presented of potentially useful free radical reactions that are catalyzed by clay mineral surfaces.

Chapter 14 - Inhalation of dust is an important cause of lung disease, and it has long been associated with premature deaths in the mining industry. However, it is now also becoming recognized as an important problem associated with air pollution. Reactions associated with the surfaces of clay mineral particles can generate highly toxic reactive oxygen species (ROS) such as the hydroxyl radical and the superoxide radical anion, and also lead to lipid peroxidation in the lungs after inhalation. The production of free radicals can be identified by a combination of electron paramagnetic resonance (EPR) spectroscopy and spin trapping technology, which converts highly reactive radicals into long(er) lived species that can be studied and identified. In this chapter the authors review the evidence for the generation of these free radical species by the surfaces of silicate mineral particles, and discuss their implications for health problems associated with mineral dust inhalation.

Chapter 15 - Clays are among the most widespread sedimentary rocks, which are mainly composed of clay minerals like kaolinite, illite, montmorillonite and other aluminum silicates as well as other various ingredients, e.g., quartz grains, apatite, granite, iron hydroxide, etc. According to their mineralogical composition, there are three main groups of clays: kaolinite, montmorillonite and illite as well as around 30 different types of pure clays within these categories. However most of natural clays are mixtures of these different types. Due to their specific properties, e.g., high capillarity, unique rheological properties, hardening, plasticity, thixotropy, high degree of swelling, clays are widely used in various industries. For example, because of their excellent colloidal properties clays are often used as drilling fluids for oil and gas wells as well as other boreholes to lubricate and cool the cutting tools, to remove cuttings, and help prevent blowouts. The possibility of swelling allowes clays to occupy an important role in mining and geology while the high swelling degree of clays is exploited in the

construction industry. In contact with freshly poured concrete, clays swell and create a waterproof barrier that is used during construction of underground facilities, sewerage systems, water tanks, nuclear and other waste storages, etc. Clays have been widely used as a foundary-sand bond in the steelmaking industry as well as a binding agents in the manufacturing of iron ore pellets. One of the important properties of clays is adsorption and ability to interact with the metal ions from the surrounding environment. Therefore clays take a prominent place in the list of natural sorbents and can be used to remove heavy metals ions and organic compounds from industrial water, that represents one of the major challenges of the modern civilization. Besides being used in environmental protection, the use of clays as adsorbents is found in the food industry as well, e.g., for clarification of wine. In addition, clays are also very important in medicine and cosmetics where mixed with water create a colloidal solution, which when consumed acts as a natural laxative absorbing both organic and inorganic contaminants, heavy metals and free radicals. Clays and clay minerals are ingredients in a large number of skin care products as creams but also independently applied to eczema and different types of rashes. Recently a lot of studies have been performed in order to investigate the use of clays as a thermal energy storage medium since they are able to perform reversible direct hydration/dehydration process. The first results clearly showed that a few types of clays can be even considered as an efficient energy storage materials compared to the others used in this purpose.

Chapter 16 - Clay as inorganic material present naturally is considered as additional mater for immobilization and containment of radioactive wastes. The use of natural clays as an additive to facilitate the incorporation of organic radioactive wastes seems to be an acceptable route to counteract the retarding effect of these hazardous wastes and to obtain a well-standing structural stable monolith. The waste form composite has to optimally comply with the advised requirements of chemical, physical and mechanical characterizations for the safe long-term disposal even at very exaggerating conditions. Radioactive waste generated from the nuclear applications should be properly isolated by a suitable containment such as, multi-barrier systems. Multi-barrier technology is a promising method for keeping the radioactive waste safe against the flooding events and keeping the radiation dose in the permissible level during the transportation and long-term disposing processes.

The capacity of a multi-barrier system including economical material and other additives such as clays and clay minerals to isolate radioactive wastes is an important point for study.

Chapter 17 - Primary clays underlying Awaso lateritic bauxite deposits in southwestern Ghana, known as lithomargic clays are thought to have resulted from an indirect or incomplete bauxitization process. The physical, genetic, geochemical and mineralogical relations characterizing these clay types have been examined enabling their potential use for the production of alumino-silicate refractories and aluminium sulphate (alum). Kaolinite and gibbsite are the dominant minerals whilst accessory minerals found included goethite, rutile, biotite and muscovite with quartz conspicuously absent. The gibbsitic fraction has successfully been separated from the kaolinitic fraction using a 90 μm sieve making it possible to produce refractories of varying alumina content. Being residual, lithomargic clays of low iron content (< 1.5%) are not plastic and therefore difficult to produce refractory bodies. An improvement in the plasticity of the clay has been achieved by addition of a clay binder. This report reviews the advances made towards the industrial utilization of lithomargic clays. The effect of processing route on the structure, physical and mechanical properties as well as performance of products from lithomargic clay is discussed.

Chapter 18 - In many studies, vermiculite, hydrobiotite and a mixture of vermiculite, mica and hydrobiotite are grouped together as ‘vermiculite’. This is due to the fact that the name ‘vermiculite’ is used as a mineral at the same time as a traded commodity. Any mineral that shows the property of exfoliation when flash-heated is named as ‘vermiculite’, regardless whether is vermiculite, hydrobiotite or a mixture of vermiculite, hydrobiotite and/or mica. This generalisation is making confusion and difficult to compare available data in literature. True vermiculite does not expand when heated or treated with chemicals and it is rarely used as a commercial commodity in civil engineering works because of high bulk density and poor thermal exfoliation. It differs significantly from other minerals that are regarded as commercial vermiculites in chemical compositions as well as in physic-chemical properties. Thus, it is recommended in this chapter that this generalisation should stop because it is misleading the public.

In: Clays and Clay Minerals
Editor: Liam R. Wesley
ISBN: 978-1-63117-779-8

Chapter 1

THE TIME- AND TEMPERATURE-RELATED BEHAVIOR OF CLAYS: MICROSCOPIC CONSIDERATIONS AND MACROSCOPIC MODELING

***Victor N. Kaliakin*[1*], *Meysam Mashayekhi*[1†] *and Andrés Nieto-Leal*[2, ‡]**
[1]University of Delaware, Newark, DE, US
[2]Universidad Militar Nueva Granada, Colombia
& University of Delaware, Newark, DE, US

Abstract

The prediction of stresses, deformations and temperature as a function of time in a material subjected to simultaneous thermal and mechanical loading is one of the most challenging and complex problems in engineering mechanics. In the field of Geomechanics a number of important problems exist that necessitate the realistic prediction of time-dependent thermal-mechanical behavior. Thermal-mechanical analyses of soils are complicated by the nature of these materials. Soils consist of a porous skeleton whose voids are filled with fluid and gas. Consequently, soils are non-homogeneous materials. Macroscopically such materials exhibit an anisotropic, inelastic, path-dependent, strain hardening (and softening), time-, rate- and temperature-dependent behavior. To further complicate matters, the thermal properties of such materials are not as well known as those for other materials such as metals. The variability in a soil's composition and subsequent degrees of thermal and mechanical dependency further increase the complexity of the thermo-mechanical behavior of such material. Finally, natural soils are also subject to sample disturbance that makes the task of representative testing all the more difficult. Local variations in soil composition often preclude the obtaining of reproducible test results, and thus impose limitations on the confidence associated with the analytical description of the soil behavior. This chapter briefly discusses the rudimentary microscopic and physicochemical aspects associated with saturated cohesive soils. This is followed by a discussion of the macroscopically observed time- and temperature-dependent behavior of such soils. Finally, a combined and coupled thermo-elastoplastic-viscoplastic framework for modeling the

*E-mail address: kaliakin@udel.edu
†E-mail address: meysam@udel.edu
‡E-mail address: andres.nieto@unimilitar.edu.co

anisotropic, time-, rate- and temperature-dependent behavior of cohesive soils in the context of a bounding surface formulation is proposed.

Keywords: Cohesive soils, time-dependent, temperature-dependent, micromechanics, elastoplasticity **A**MS Subject Classification: 53D, 37C, 65P

1. Introduction

The nature of most engineering materials is quite complex. It is therefore difficult to devise a general mathematical (constitutive) model that will cover all possible ranges and types of excitation and behavior of a given material. As a result, the development of mathematical models is based upon simplifying assumptions regarding material behavior. The level of sophistication of the model, therefore, significantly dictates the extent to which the complexities of a given engineering material are taken into consideration.

Soils are prime examples of complex engineering materials. Whereas in elementary physics, solid, liquid and gaseous states are distinguished, soils are not simple bodies that can be placed in either of these three groups. Soils are generally composed of solid, liquid and gas, with the solid part being a porous medium made up of numerous particles whose voids are filled with fluid and gas (typically water and air, respectively, with the former possibly containing contaminants). Consequently, soils are non-homogeneous materials. Macroscopically such materials exhibit an anisotropic, path-dependent, inelastic, strain hardening (and softening), time-, rate- and temperature-dependent behavior. Thermal-mechanical analyses of soils are thus complicated by the nature of these materials. Consequently, the prediction of stresses, deformations and temperature as a function of time in a material subjected to simultaneous thermal and mechanical loading is one of the most challenging and complex problems in engineering mechanics.

To further complicate matters, the thermal properties of such materials are not as well known as those for other materials such as metals. In addition, the variability in a soil's composition and subsequent degrees of thermal and mechanical dependency further increase the complexity of the thermo-mechanical behavior of such material. Finally, natural soils are also subject to sample disturbance that makes the task of representative testing all the more difficult. Local variations in soil composition often preclude the obtaining of reproducible test results, and, thus, impose limitations on the confidence associated with the analytical description of the soil behavior.

The above deficiencies in material testing and description, along with fairly limited computational capabilities, have imposed severe restrictions on past attempts to model the complex nature of soils. Historically, problems involving geomaterials have, by necessity, been solved using extremely simplistic and highly idealized mathematical models. However, over the past few decades, the aforementioned experimental and computational limitations have been greatly reduced. In the area of geotechnical testing, significant advances have been made not only in laboratory apparatus, but, more importantly, in equipment that measures the behavior and properties of soils in situ. Of even greater significance has been the rapid development of high-speed computers and efficient numerical techniques such as the finite element and finite difference methods. These computational advances have facilitated the application of improved models of soil behavior to problems of practical interest. As a result of the above experimental and computational advances, much research has, in

recent years, been directed towards the development of sophisticated mathematical constitutive models that can more accurately predict diverse stress-strain phenomena exhibited by actual soils.

In the field of Geomechanics a number of important problems exist that necessitate the realistic prediction of time-dependent thermal-mechanical behavior. Examples of such problems include: 1) creep, relaxation and strain-rate effects under both isothermal and non-isothermal conditions, 2) the disposal of radioactive waste in deep underground repositories deep ocean sediment, or in hard rock; 3) the interaction between soils and piles in conjunction with energy pile applications; 4) the performance of geothermal structures as affected by long-term deformations such as de-bonding effects in soils; 5) the investigation of land subsidence in connection with shallow geothermal energy production; 6) the realistic simulation of thermal and/or hydraulic fracturing of oil reservoirs, as well as deep geothermal energy production; 7) the injectivity and reactive transport in sequestration of emitted gas in deep geothermal wells; 8) the interaction between soils and buried conduits transporting high-temperature fluids or high-voltage cables; 9) the loss of heat from buried buildings and its subsequent affect on energy consumption; 10) the integrity of pavement-soil systems subjected to diurnal (cyclic) temperature changes; 11) the prediction of sample disturbance due to temperature changes during sampling, handling, storage or testing, and 12) the increased stability of earth masses through heating.

This chapter briefly discusses the rudimentary microscopic and physicochemical aspects associated with cohesive soils. This is followed by a description of macroscopically observed the time- and temperature-dependent behavior of such soils. Finally, a combined and coupled thermo-elastoplastic-viscoplastic framework for modeling the anisotropic, time-, rate- and temperature-dependent behavior of cohesive soils in the context of a bounding surface formulation is proposed. In the remainder of this document cohesive soils are assumed to be fully saturated; i.e., the soil is assumed to be a two-phase continuum, consisting of a solid skeleton with fluid-filled pores. Furthermore, unless stated otherwise, the pore fluid is assumed to be water.

2. Microscopic Aspects Related to Clays

This section presents an overview of the rudimentary microscopic and physicochemical aspects associated with cohesive soils. The intent is not to present an exhaustive discourse on this subject, but to introduce certain terms and concepts that will be used in subsequent sections of this chapter. More thorough discussions of the physicochemical and microscopic aspects of soils are presented in a number of publications, of which the books by Scott (1963) and Mitchell & Soga (2005) are prime examples.

The microscopic and submicroscopic mineral particles formed, for the most part, by chemical rather than by physical weathering processes are crystalline, and are called *clay* or *clay colloids*. The minerals that combine to produce clay are chemically the same as those forming the parent rock, but they have a different crystalline structure arising from the solution and recombination, or crystallization, of the original materials (Scott 1963).

The word "clay" is generally understood to refer to a material composed of a mass of small mineral particles that are plastic within a moderate to wide range of water content. In this context, plasticity refers to a soil's ability to be molded. Minerals in a finely ground

state do not all exhibit plasticity; those that do are referred to as *clay minerals*, among which there are several groups of different chemical compositions. The finest sizes on the grain-size distribution chart, typically smaller than $0.075\,mm$, are referred to as *clay sizes* only for purposes of definition. To say that a given soil falls in the range of clay sizes does not imply that it is composed of clay minerals, although this frequently may be true. In the fine and very fine fractions, any one grain usually consists of only a single mineral. The particles may be angular, plate-shaped or, rarely, tubular. Rounded particles are absent (Terzaghi & Peck 1967). In general, the percentage of platy particles in a given soil increases with decreasing grain size of the soil fraction, and is associated with a sheeted crystal structure in which the particle diameters may be as great as several hundred times the plate thickness (Scott 1963).

Soils possessing clay particles often deform plastically at varying water contents. In addition, the particles in such soils produce a mass that holds together even when unconfined. Clays are thus often referred to as *cohesive soils*, for this cohesive quality results from the presence of some proportion of clay minerals. Those soils that do not exhibit this cohesion are called *cohesionless*. Soils composed of bulky grains are cohesionless regardless of the fineness of their particles (Sowers & Sowers 1970).

2.1. The Solid Phase

In soils, mineral grains comprise the solid phase. By means of mechanical analysis, it has been found that most natural soils contain grains representative of two or more soil fractions. It might be expected that the type of mineral occurring in a soil would influence the engineering properties of the soil. However, in coarser grained soils it is found that properties related to the mass of the material do not depend upon the constituent minerals, although locally the mineral present will control the frictional characteristics of the individual grains (Tschebotarioff 1952). The character of mixed-grained soils is known however to be determined almost entirely by the character of the smallest soil constituents (Terzaghi & Peck 1967). In general, the greater the quantity of clay mineral in a soil, the higher the plasticity, the greater the potential shrinkage and swell, the lower the permeability, the higher the compressibility, the higher the true cohesion, and the lower the true angle of internal friction (Mitchell 1976). The inert portion of a mixed-grained soil comprises about 80 to 90 percent of the total dry weight, with the decisive or active portion making up the remainder.

The changes in behavior with diminished particle size are due to the increasing influence of the forces between the molecules of adjacent particle surfaces. In most mineral particles with high sphericites (e.g. those particles making up silts, sands, and larger sizes), the ratio of the area of the surface to the volume of the sample is relatively small, and as a result their behavior is principally dependent on the bulk or volume of the grains. In a small particle, however, the molecules forming the surface constitute a large proportion of the total number of molecules, and the electrical charges of these molecules dictate the behavior of the particles. The influence of these surface effects relative to the influence of mass forces (i.e., the weight of the particle) is directly related to the surface area per unit mass of particles. A useful index of the relative importance of surface effects is thus the specific surface (i.e., the magnitude of surface area per unit mass of dry soil) of a grain, that becomes larger as the particle decreases in size (Grim 1968, Mitchell 1976).

2.2. Interatomic Bonding

Clay particles at one time were believed to be amorphous. However, investigations carried out with improved equipment and techniques since the 1920's have shown them to be predominantly crystalline (Scott 1963). The type of crystal structure associated with a particular material is determined by the strength and directionality of interatomic bonds together with the relative sizes of the bonded atoms (Mitchell 1976). There are two main groups of interatomic bonds: *primary* or high-energy bonds that hold atoms together and *secondary* or weak bonds that link molecules.

2.2.1. Primary Bonds

In the formation of primary bonds, only the outer shell (or valence) electrons participate. There are two types of primary bonds of importance in the study of soils: covalent and ionic. In an arbitrary system of measure, both bonds are considered to be strong (Mitchell 1976).

If one or more bonding electrons are shared by two atomic nuclei so that they serve to complete the outer shell for each atom, then the bond is termed covalent. In the nonmetallic state, covalent bonds form primarily between nonmetallic atoms such as oxygen, chlorine, and nitrogen. Since only certain electrons participate in the bonding, covalent bonds are directional. Atoms bonded covalently thus pack in such a way that fixed bond angles are developed, resulting in strong bonds (Mitchell 1976).

Ionic bonds result from the electrostatic attraction between positive and negative ions formed from free atoms through loss or gain of electrons. The loss or gain of electrons does not, however, leave the atoms in an electrically neutral state. Strong electrostatic attractions and repulsions may thus develop. Ionic bonds are non-directional; each cation (positively charged atoms) attracts all neighboring anions (negatively charged atoms) and vice-versa. In most minerals, purely ionic and purely covalent bonds are limiting conditions that are the exception rather than the rule. Instead, a combination of the two types is common (Mitchell 1976). For example, in the case of silicate minerals, which are the most abundant constituents of the majority of soils, the interatomic bond in silica (SiO_2) is about half covalent and half ionic.

2.2.2. Secondary Bonds

In addition to the primary bonds described above, other types of weaker, secondary bonds exist between units of matter. Although these bonds are weak relative to ionic and covalent bonds, they are often strong enough to be important sources of attraction between very small particles and between solid particles and liquids. Although there are several different types of secondary bonds, only hydrogen bonds, van der Waals forces and electric forces are pertinent to the present discussion.

If hydrogen represents the positive end of a dipole, its attraction to the negative end of another dipole forms a hydrogen bond. Although hydrogen bonds do not have the strength of a covalent bond, their strength is, however, considerably greater than the other types of secondary bonds (Mitchell 1976).

As a result of the movements of electrons in their orbits spinning around atoms and the associated fluctuating polarizations, any molecule possesses an electric field that is ca-

pable of interacting with the field of nearby molecules to give rise to an attractive force between the molecules called a van der Waals force. Although the resulting molecular bonds are weak, typically an order of magnitude weaker than a hydrogen bond, they are non-directional and additive between atoms (Mitchell 1976). This force is essentially independent of the characteristic of the fluid between the particles (Lambe & Whitman 1979). Instead, it depends primarily on the crystal structure of the minerals and on the distance of separation between two flat particles. The net attraction from Van der Waals forces is believed to be the main cause of cohesion in fine-grained soils (Scott 1963, Mitchell 1976).

Although a clay particle as a whole is electrically neutral, it will, owing to typically large values of specific surface, carry a net surface charge. Theoretically, the surface charge may be of either sign, yet only negative charges have been measured (Lambe & Whitman 1979). The net negative electrical charge primarily arises due to isomorphous substitution, a process in which metallic ions in the clay mineral lattice are replaced by other metallic ions of lower valency without modifying the crystal structure. Since clay particles have a finite, small size, breaks must occur in the crystal structure at the plate edges. There, other, normally internal, ions may now be exposed. Most of these ions are positive, and therefore the edge may attract dipole molecules, negative ions, or be itself attracted to the negatively charged surface of another clay particle. There are localized areas of high and low charge, and the total charge per unit of mass varies with the charge per unit area and with the specific surface.

2.3. Clay Minerals

Although soils may contain virtually any element found in the earth's crust, by far the most abundant elements found in soils are oxygen, silicon, hydrogen, and aluminum (Mitchell 1976). Atoms of these elements are organized into various crystallographic forms along with lesser amounts of other elements to form the common soil-forming minerals with a relatively complicated structure. Clay minerals are formed through the decomposition of feldspars, micas, and ferro-magnetism minerals (Sowers & Sowers 1970).

As previously noted, clay minerals that are found in soils are crystalline substances. Chemically, they are hydrous aluminum silicates that also contain other metallic ions. Clay minerals belong to the larger mineral family called *phyllosilicates* (Mitchell & Soga 2005). The crystals are colloidal sized and have a large specific surface. Mineralogical investigations reveal that clay particles consist of many molecular sheets. The sheets have a repeating atomic structure consisting of essentially two basic structural units help together by ionic bonds. These are the *silica tetrahedron* and the *aluminum* or *magnesium octahedron* (Mitchell & Soga 2005). Multiple sheets stack together to form layers; multiple layers then form crystals.

A silica tetrahedron consists of a central silicon ion (Si^{4+}) surrounded by four oxygen ions (O^{2-}), each of which contributes one valence link to the central silicon (Figure 1). A number of such tetrahedra may combine to form the sheet structure. In this formation, there is a central plane of silicon atoms above which project single oxygen ions that are charged negatively and are free to combine with external cations because their valences are incompletely satisfied.

The aluminum or magnesium octahedron is more complex (Scott 1963). It consists of

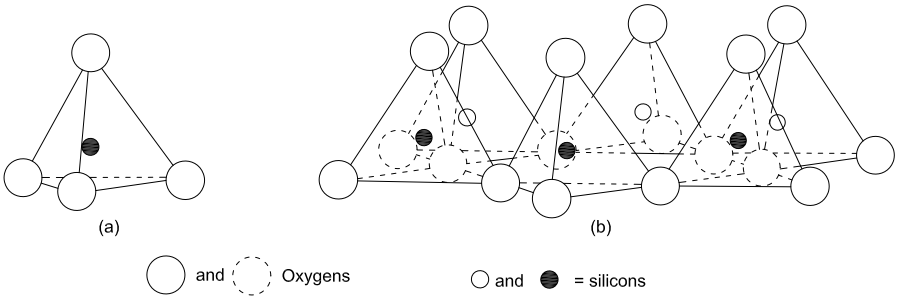

Figure 1. Silica tetrahedron and silica tetrahedra arranged in a hexagonal network (Grim 1959.)

six oxygen or hydroxyl ions enclosing an aluminum, magnesium, iron or other metallic ion that occupies the center of the structure (Mitchell & Soga 2005) (Figure 2). If the central ions are replaced by other of the same valency, the charge balance is maintained. If, however, ions of different valency enter the lattice, a charge imbalance occurs that can materially increase the surface activity of the clay mineral (Scott 1980).

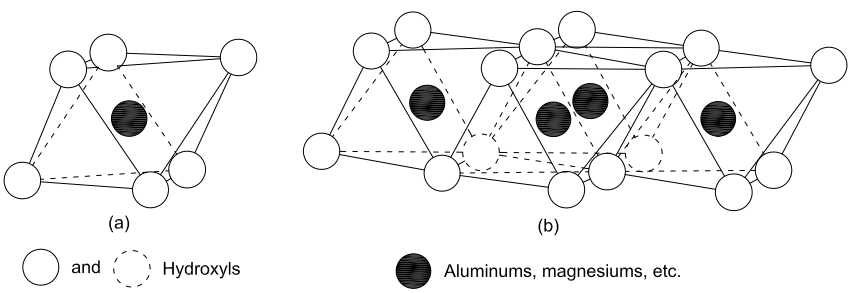

Figure 2. Octahedral units and sheet structure of octahedral units.
(Grim 1959)

Although the tetrahedral and octahedral sheets are capable of indefinite extension in the direction of the planes, the resulting particles generally have a hexagonal shape, with the sheets tightly bonded in the plates (Scott 1963). Since cleavage takes place between the sheets and the plates are interrupted at their edges, it follows that while the electric charges for a sheet are theoretically neutral, broken bonds will be found at the edges, resulting in positively charged particle edges and negatively charged surfaces. The particles are thus electrically non-neutral.

All clay minerals consist of the two aforementioned basic structural units, stacked in certain ways to form plates, with certain cations present. There are many forms of clay minerals, with some similarities and wide differences in composition, structure and behavior (Sowers & Sowers 1970). Differences among clay mineral groups arise mainly from differences in the type and amount of isomorphous substitution within the crystal structure (Mitchell 1976). For example, if all the anions of the octahedral sheet are hydroxyls and

two-thirds of the cation positions are filled with aluminum, the mineral is called *gibbsite*. In this case the valences are not balanced as in the case of silica, so an occasional unit octahedra will contain no aluminum. This makes the sheet non-symmetrical and non-uniform (Scott 1963). If magnesium is substituted for the aluminum and it fills the cation positions, then the mineral is called *brucite* (Holtz, Kovacs & Sheahan 2011).

Although dozens of clay minerals have been identified, only a few groups are typically associated with geotechnical applications. These include the kaolinite-serpentine group (minerals in this group consist of alternating octahedral and silica tetrahedral sheets), the smectite minerals (consisting of an octahedral sheet between two silica tetrahedral sheets), and the micalike minerals (possessing sheet structures similar to the smectites, only with ions bonding the respective sheets together. The most common members of the above three groups are kaolinite, montmorillonite and illite.

Towhata, Kuntiwattanakul & Kobayashi (1993) examined whether heating clay powders affects their fundamental properties. Two clays, one having a mineral content similar to kaolin and the other bentonite, were heated in an oven to temperatures of 200^oC. Following cooling, conventional laboratory tests (Atterberg limits, free swelling and unconfined compression) were performed on the clays. The results of these tests indicated that heating does not influence the fundamental nature of clay powders, and that thermal effects should occur only through the interaction between clay grains and pore fluid. These conclusions are in agreement with the findings of Houston & Lin (1987), who found that heating marine clays to 200^oC resulted in no appreciable mineralogical changes.

2.4. The Liquid Phase

The properties of any cohesive soil are greatly influenced by the presence of water (Rosenqvist 1959, Mitchell 1976). In a general cohesive soil, water is present in the following forms: (a) As ordinary ("free" or "bulk") liquid water, (b) As adsorbed water, and, particularly in low-porosity clays (c) As an "organized" fluid. Each of the above forms is briefly discussed below.

2.4.1. Free Water

Even in low-porosity clays some "free" (liquid) water may be present in inactive zones in pores formed by non-clayey particles. The amount of this water corresponds to the shrinkage limit of the clay (Yong & Warkentin 1975). The viscosity of the free water is known to decrease exponentially with temperature (Houwink 1953). It follows that at points of higher temperature the viscosity thus decreases, allowing for a greater flow. This, in turn, causes the solid particles to re-arrange themselves in such a manner as to be in equilibrium under the applied load.

2.4.2. Adsorbed Water and the Diffuse Double Layer

The properties of any clay, with sufficiently large voids, are greatly influenced by the amount of water present through the process of *adsorption*. When water contacts a clay particle, both the mineral surfaces and exchangeable ions pick up water; i.e., they hydrate.

To better understand this phenomenon, recall that the ions in the surface layers of clay crystals are oxygen ions (O^{2-}) or hydroxyls (OH^{-}). Thus water, being a polar molecule, is held against these surfaces by hydrogen bonds. Unlike exchangeable ions, these water dipoles are tightly held and strongly oriented at the surface due to the high electrical forces attracting them to the clay surface; they form an adsorbed, diffused water film. It is generally considered that within this layer of "adsorbed water," the water molecules closest to the particle surface are tightly held and strongly oriented (Terzaghi 1941, Rosenqvist 1959). As a result, the adsorbed water is anisotropic with respect to directions perpendicular and parallel to the particle surfaces (Michaels 1959), and appears to be denser and more viscous than "free" water (Kèzdi 1974). Indeed, several investigators (Hogentogler 1937, Scott 1963, Grim 1968) have proposed that due to the spacing and/or structure of water molecules closest to the surface of a clay crystal, this water appears to have properties of a solid substance.

The density of the adsorbed water may vary from 1.0 Mg/m^3 for free water to 1.4 Mg/m^3 or more for the first layers of water molecules at the solid surface (DeWit & Arens 1950, Martin 1960, Mitchell 1976, Mooney, Keenan & Wood 1952, Yong & Warkentin 1975). It would appear, however, that the thermal expansion of adsorbed water should be different from that associated with free water at the usual density (Baldi, Hueckel & Pellegrini 1988), though this has not always been assumed. Movement of water is largely restricted to slow migration parallel to the surface; in this way the adsorbed water appears to have a higher viscosity than ordinary water (Iler 1955, Sowers & Sowers 1970).

The amount of water that can be bound to a particle is greatly dependent on the size of the particle. The greater the specific surface, the higher the water content bound to the particle and the less of the water is "free" (i.e., not strongly attracted to the mineral skeleton and thus constituting a separate phase). Farther from a clay particle's surface, the hydrogen bonds become weaker, the degree of orientation is less regular, and the apparent viscosity is lower. This results in more random motion of water molecules; water at sufficiently large distances from the particle surface approaches the behavior of normal water and is more easily expelled from the pores.

Upon hydration, the exchangeable cations grow about sevenfold, and are quite mobile, being in ceaseless motion due to thermal agitation. They are too large to fit into a monoionic layer on the mineral particles and move away from the mineral surfaces to positions of equilibrium (Lambe & Whitman 1979). They distribute themselves statistically in an assemblage having the greatest density of ions near the surface and a decreasing density with increasing distance. They constitute a positively charged zone which, together with the negatively charged surface of the particle itself, is known as the electric or *diffuse double layer*. The effective thickness of the double layer depends on the concentration of the electrolyte in the pore fluid, on the dielectric constant, and on the valence of exchangeable cations. Monovalent cations (e.g., Na^{+}) lead to thicker double layers than divalent ions (e.g., Ca^{2+}) since twice as many of the former are required to balance a given charge (Scott 1980). When the mineral surface is approached, the ionic concentration and holding force in water increase exponentially. The difference in concentration between double layer water and free water gives rise to osmotic suction (van Olphen 1977).

The double layer accounts for the viscous nature of cohesive soils; in conjunction with the small particle and pore sizes it is responsible for the phenomenon of "hydrodynamic lag"; that is, the time required for pore fluid to drain from a loaded cohesive soil. This

phenomenon is intimately related to a second time effect, namely, drained creep. Whereas drained creep involves a slow reorientation of the clay particles themselves (due to slow diffusion mechanisms, viscous effects and breakage of bonds), hydrodynamic time lag is caused mainly by the friction between the particles (surrounded by layers of adsorbed water) and the pore fluid. As a result of this friction, during the process of consolidation the expulsion of excess pore fluid is restrained; macroscopically the clay is said to have a low permeability. There is no consensus whether drained creep actually occurs during the period of hydrodynamic time lag. Some researchers (Šuklje 1957, Barden 1965, Bjerrum 1967) support the notion that the two phenomena occur simultaneously. Others believe that during this time creep is insignificant (Ladd, Foott, Ishihara, Schlosser & Poulos 1977, Leonards 1977, Mesri & Choi 1985). The theoretical development of Janbu (1985) seem to indicate that the true soil behavior may lie somewhere in between the two above extremes.

2.5. Structure and Fabric of Fine-Grained Soils

The geometric arrangement of particles, particle groups and pore spaces (voids) in a soil is referred to as *fabric*. Referring to the fabric scale concept, Mitchell & Soga (2005) further divide soil fabric into the *microfabric*, *minifabric*, and *macrofabric*. The microfabric includes the regular aggregation of particles (i.e., particle clusters) and the very small pores between them called *micropores*. The minifabric contains the aggregation of the microfabric and the pores between them called *minipores*. Finally, the macrofabric is the largest scale, which includes cracks, fissures, root holes, etc., thus, characterizing the in-situ conditions.

In soil mechanics, the term *structure*, or more accurately *microstructure*, is used to describe the fabric along with the interparticle forces present in a soil. Since the microstructure acquired by a clay deposit at the time of formation may have a profound influence on its subsequent engineering properties, an understanding of factors influencing the microstructure is of considerable importance. Compared to the quantification of its macroscopic response, the study of a soil's microstructure is significantly more difficult. Furthermore, since interparticle forces are very difficult, if not impossible to measure, it follows that the fabric is most amenable to study and quantification.

In cohesionless soils (i.e., gravels, sands and silts), the surface activity of the individual particles is very small. The fabric and microstructure of cohesionless soils is thus essentially the same. However, in fine-grained cohesive soils the interparticle forces are relatively large. Consequently, the microstructure of such soils consists of both these forces and the soil fabric. The interaction of individual clay particles through their adsorbed water layers is closely associated with the microstructure of the soil, and has a profound influence on its behavior and engineering properties. Research on clay microstructure suggests that the greatest single factor influencing the final microfabric of a clay is the electrochemical environment existing at the time of sedimentation (Holtz et al. 2011).

2.5.1. Early Studies and Classification

The concept of fabric in soils is traced to the work of Terzaghi (1925), Goldschmidt (1926) and Casagrande (1932). The subsequent work of Lambe (1953) and his students (Mitchell

1956, Martin 1962), of Schofield & Samson (1954), Tan (1957) and van Olphen (1963) significantly advanced the study of microfabric in cohesive soils by establishing models that included consideration of colloidal and electrochemical properties of clays.

The early microfabric studies were primarily concerned with the interaction of individual clay platelets or groups of platelets. Since clay particles are platey, the interparticle contacts may be edge-to-edge, edge-to-face, or face-to-face (Sides & Barden 1971). Terzaghi (1925) assumed a model in which the individual clay mineral grains stick to each other at the points of contact with forces sufficiently strong to allow for the formation of the "honeycomb" arrangement shown in Figure 3. The "honeycomb" arrangements of particles postulated by Casagrande (1932) for sensitive marine soils built on the concepts proposed by Terzaghi (1925). In this model, the particle arrangements located in the smallest gaps between adjacent silt particles were thought to be highly compressed, whereas those in the larger spaces between silt particles had undergone relatively little compression (Figure 4). The former particle groups were referred to as "bond clay", whereas the latter were "matrix clay." The bonds between particles were hypothesized as being quite brittle.

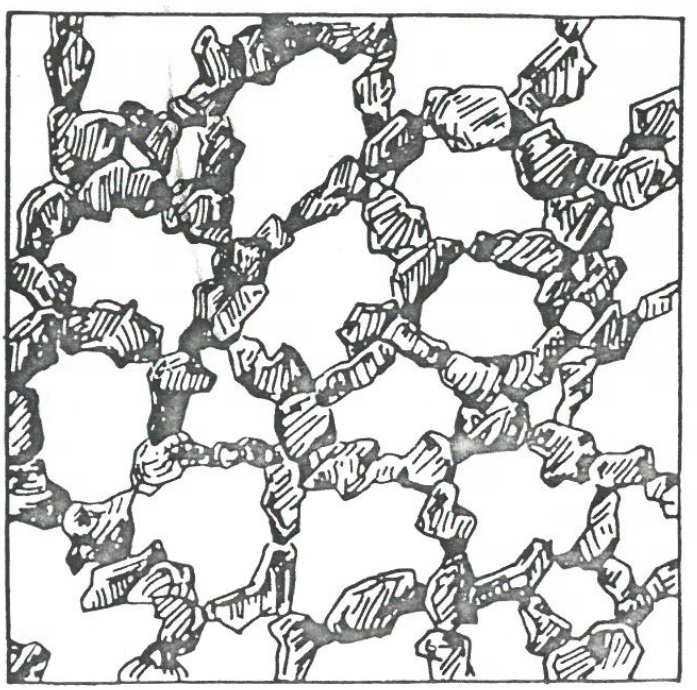

Figure 3. Hypothetical "honeycomb" fabric.
(Terzaghi 1925)

2.5.2. More Refined Studies

In subsequent years the study of clay microstructure involved consideration of the double layer theory and the behavior of clay platelets in dilute colloidal suspensions. Lambe (1953)

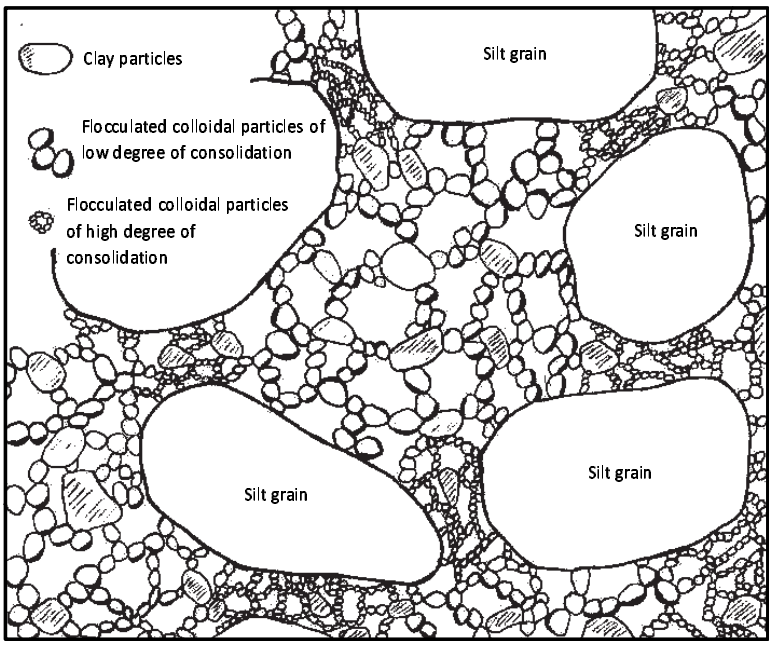

Figure 4. Hypothetical fabric of sensitive clay.
(Casagrande 1932)

considered the microstructure of inorganic soils and presented clay mineral arrangements associated with deposition in a rather wide range of electrochemical environments from fresh water to marine. As previously stated, van der Waals-London attractive forces are independent of the nature of the pore fluid. It follows that, for a given type of clay in suspension, the net force between adjacent particles (as a function of distance between the particles) can be prescribed by the addition of electrolyte to the suspension, since this will only have an influence on the repulsive particle force.

Lambe (1958) found that sedimentation in intermediate electrolyte concentrations, such as that found in brackish water, would lead to *dispersed* microstructure. Indeed, in a dilute suspension with wide particle spacings, the net force will be repulsive. The particles remain separate, the force of gravity upon any particle being negligibly small, and the particles settle out very slowly or remain in suspension exhibiting Brownian (random) movement. The repulsion between the particles as they near each other causes them to assume a configuration having a maximum grain-to-grain distance in a given volume of soil (Sowers & Sowers 1970). The process that takes place under these conditions of settling is known as dispersion, and the microstructure produced is called *dispersed*. This requires a large or expanded double layer, which suggests that clays compacted wet of optimum will have a dispersed microstructure. This dispersion implies a rather closely packed configuration involving essentially face-to-face arrangements. Dispersion can, in general, be increased by adding substances to the suspension that increase the repulsion forces without increasing the attraction.

If electrolyte is added to a soil-water suspension that initially is dispersed, a *flocculent*

microstructure will form. The sudden addition of an electrolyte supplies ions to the soil particles that partially neutralize the negative surface charges and thereby create net attractive forces (Lambe 1958). The particles, even though widely spaced, will then attract each other and will move together and stick (coagulate) in a heterogeneous loose edge-to-edge or edge-to-face arrangement termed a "floc". Such flocs often contain hundreds of individual particles and there may be considerable interparticle contact between the positively charged clay mineral edges and the negative faces, producing strong bonds that resist displacement. Such flocculation requires a small or contracted double layer, which suggests that clays compacted dry of optimum will have a flocculated microstructure (Lambe 1958). Considerable free water is trapped in the large voids between the particles, in addition to the adsorbed water already immobilized by the clay. Sides & Barden (1971) demonstrated that as the particle size is reduced and the colloidal activity increases, chemical additives become more effective in producing dispersed and flocculated microstructures. Thus, such additives have little visible effect on the microstructure of kaolinite clays but their effect is evident for illitic clays.

The flocculation process includes coarser particles so that flocculated clays will exhibit a structure consisting of silt and sand grains. These grains are fairly evenly distributed, except in stratified or varved clays, and the larger grains are not usually in contact with each other (Mitchell 1976). Figure 4 shows such a mixed-grained "honeycomb" soil structure proposed by Casagrande (1932) to account for the sensitivity of marine clays. This structure was confirmed by an electron microscope study of quick clays by Pusch (1966). Dispersion, on the other hand, is selective, and the materials under certain conditions will settle in layers differentiated on the basis of particle size (Scott 1963).

The basis of many of the early studies was that particular fabric models could be associated with certain depositional environments. The inherent assumption was that the dominant factors in the determination of the particle arrangement were 1) the mode of deposition, and 2) the electrochemistry of the pore fluid at the time of deposition. Subsequently, Collins & McGown (1974) showed that the following factors also influence the depositional arrangement of particles: 1) particle size, shape and gradation, 2) clay mineralogy, 3) Exchangeable cations (particularly their valency), 4) acidity, 5) organic content of the soil, 6) concentration of sediment and rate of deposition, 7) state of agitation and depth of water, and 8) seasonal drying.

2.5.3. Studies Employing Enhanced Experimental Techniques

Much of the aforementioned work was rather *speculative* in nature. This changed in the late 1960's with the use of X-ray diffraction, the polarizing microscope, and the electron microscope. Of these, the scanning electron microscope (SEM), with its relatively high level of magnification and large depth of focus (which provides an almost three-dmensional image), is generally viewed as being the most useful for interpreting clay fabric. The work of Gillott (1969), Barden & Sides (1970) and Sides & Barden (1971) is representative of the early use of the SEM in such applications. In recent years, various other techniques such as indirect measurements (electrical resistance or acoustic wave velocity), Magnetic Resonance Imaging (MRI) and X-ray computerized tomography (X-ray CT) have been developed for observing and possibly quantifying the fabric. Unfortunately, some of this work

generated a multiplicity of descriptive terminology that tended to complicate understanding of the subject (Collins & McGown 1974). Mitchell & Soga (2005) give further details pertaining to enhanced experimental techniques.

From electron microscope observations of laboratory prepared clays, it has generally been established that the mineralogy and concentration of clay in the sediment, as well as the salt content of the pore fluid, influence clay particle arrangements. In such studies, the desired microfabric is obtained by mixing dry soil with a suitable pore fluid, subjecting the slurry to a prescribed consolidation pressure, or some combination of the two.

Flocculent soils are light in weight and quite compressible, but are relatively strong and insensitive to vibration because the particles are tightly bound by their edge-to-face attraction. In general, an element of flocculated soil has a higher strength, lower compressibility and higher permeability than the same element of soil at the same void ratio but in a dispersed state (Lambe & Whitman 1979). The higher strength and lower compressibility result from the interparticle attraction and the greater difficulty of displacing particles when they are in a disorderly array. The higher permeability in the flocculated soil results from the larger channels available for flow.

Sachan & Penumadu (2007) studied the compressibility behavior of laboratory prepared samples of kaolin having dispersed and flocculated microfabrics. Since the latter consist of randomly organized clay platelets in contact with each other and thus possess larger micropores, it follows that flocculated microfabrics exhibit higher compressibility than dispersed ones (Figure 5). Pillai, Robinson & Boominathan (2011) compared the permeability of samples having flocculated and dispersed microfabrics. They confirmed previous observations (Lambe & Whitman 1979) that, at the same void ratio, flocculated microfabrics are more pervious than dispersed ones (Figure 6).

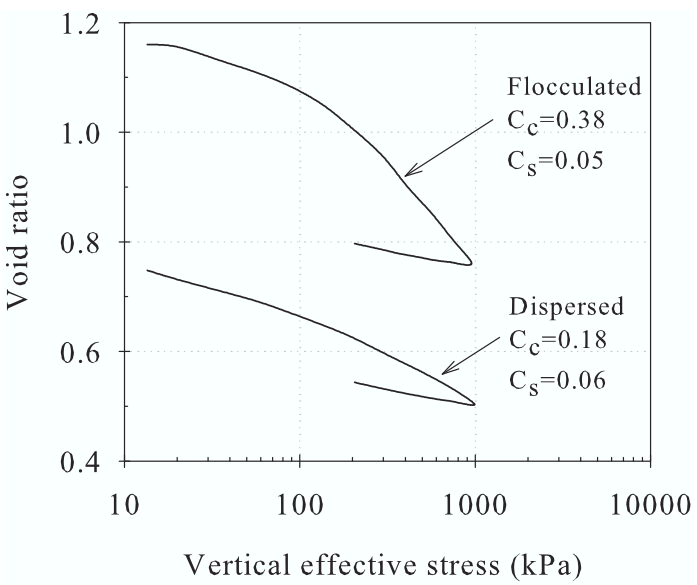

Figure 5. Compressibility of kaolinite clay with flocculated and dispersed microfabric (Sachan & Penumadu 2007).

The response of cohesive soils subjected to various loading conditions has been shown to be slightly different for flocculated and dispersed microfabrics (Sridharan, Narasimha & Venkatappa 1971, Wang & Siu 2006, Sachan & Penumadu 2007, Prashant & Penumadu 2007, Pillai et al. 2011). Due to the fact that clays with flocculated microfabrics have larger micropores, their response under undrained shear loading will be softer than for dispersed samples. In particular, samples with dispersed microfabrics exhibit peak stresses followed by strain softening, while samples with flocculated microfabrics exhibit a plastic strain hardening response. Under drained conditions, flocculated samples will experience larger volumetric strain. In terms of overconsolidation ratio, the response of overconsolidated cohesive soils with flocculated and dispersed microfabric is quite similar (Sachan & Penumadu 2007). Thus, overconsolidation has a stronger influence on shear resistance and volumetric response than does microfabric. At critical state cohesive soils assume a state independent of the sample's initial microfabric (Pillai et al. 2011).

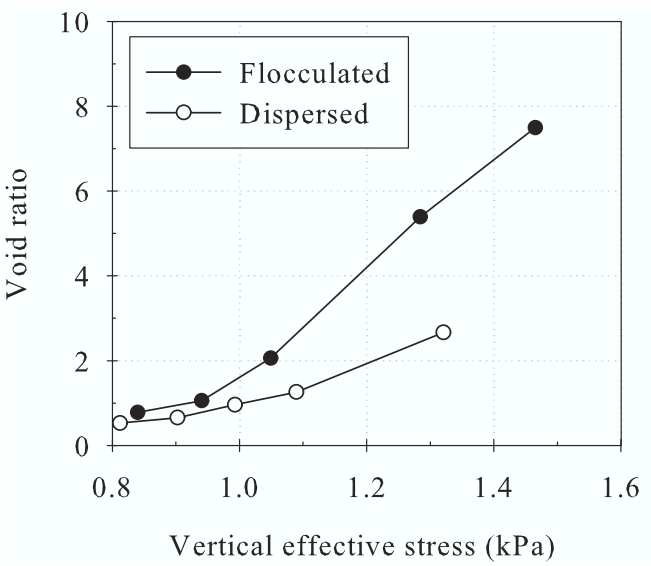

Figure 6. Permeability of kaolinite clay with flocculated and dispersed microfabric (Pillai et al. 2011).

In concluding this section, it is evident that the flocculated and dispersed structures discussed in the previous section represent the two extremes in soil fabric for clay suspensions. Indeed, previous SEM studies of the microfabric of compacted clays (Barden & Sides 1970) have revealed that the generally accepted concepts of flocculated and dispersed microfabrics are *too simplistic*, particularly for the case of flocculated microfabrics. Between these limits there is a large number of intermediate configurations. For mixed-grained soils, the particle arrangements assume a variety of forms. Most of these are, however, related to the flocculent and dispersed configurations discussed previously and reflect the difference in water content between a clay suspension and a denser soil mass.

The feeling of many researchers is that purely dispersed states in cohesive soils are *rare*, occurring only in very dilute natural clay-water systems, in remolded (disturbed) natural

clays, and in ones artificially prepared (Scott 1963, Holtz et al. 2011). In virtually all natural depositional environments (e.g., fresh water, brackish, marine) the presence of electrolytes (dissolved salts) in the pore fluid supplies ions that result in the formation of a flocculated or aggregated fabric. The submicroscopic fabric units consisting of aggregated particles are called *domains*. Domains, in turn, group together to form *clusters*. Finally, clusters group together to form *peds* (aggregates) or groups of peds (Collins & McGown 1974). The fabric thus consists of an irregular three-dimensional arrangement of particles, clusters and peds. The degree of flocculence, and hence, of group formation, depends primarily upon the electrolyte concentration of the pore fluid.

3. Macroscopic Aspects Related to Clays

The physically observed behavior of a loaded soil is a macroscopic manifestation of the mechanisms active at the level of the material microstructure. Since such mechanisms have been discussed in the previous section, attention is turned to the macroscopic time- and temperature-dependent behavior of cohesive soils.

3.1. Time-Dependent Behavior

The effect of time on the strength and deformation characteristics of various materials assumes importance in a variety of engineering problems where a) very rapid, or very long-term response is of concern, or b) in cases where translation of measured behavior is necessary from one time scale to another. In the field of geomechanics, the subject of time-dependent behavior aroused interest early on, being first discussed in detail by Terzaghi (1931). Subsequent to this pioneering work, this subject has been the focal point of numerous investigations, in particular since the early sixties. Although considerable progress has been made, present knowledge of the basic physical mechanisms responsible for the time-dependent behavior of soils is still far from being complete.

In discussing the time-dependent behavior of cohesive soils from a macroscopic point of view, it is convenient to divide the subject into the following categories: a) creep, b) stress relaxation, and c) strain-rate effects. Such a division could be considered rather artificial, but it adequately separates different types of time-dependent behavior under particular loading conditions, is generally how the literature has been delineated, and provides a means to present the material in this section in a logical manner. Indeed, it is the feeling of many researchers that the same physical mechanism may be responsible for all three of the above phenomena.

3.1.1. Creep

Of the categories listed above, creep of soils has been studied more extensively than the other two. Creep is defined as the time-dependent development of shear and/or volumetric deformations under a constant state of total stress. Creep occurs under undrained (constant volume), as well as drained (constant effective stress) conditions, at a rate that either remains constant, or varies with time.

In typical laboratory creep experiments, specimens are first preconsolidated and then sheared to a prescribed deviatoric stress level. This stress is then maintained constant throughout the remainder of the test. During undrained creep tests, shear strains and changes in effective stress (resulting from changes in pore pressure) are induced in the specimen. Since the effective stress relaxes, such tests are true creep tests only with respect to the total stress. Drained creep tests, on the other hand, can induce both deviatoric and volumetric strains in the specimen. The creep response of soils, as measured in such tests, varies widely depending upon the soil type, soil structure, water content, activity, stress history, temperature, drainage conditions, and other factors (Campanella & Vaid 1972, Mitchell 1976, Campanella & Vaid 1974).

The phenomenon of consolidation was first modeled by the classical linear uniaxial theory developed by Terzaghi (1925). This hydrodynamic process, termed *primary consolidation*, first introduced the element of time into soil mechanics. For certain soils significant departures from Terzaghi's theory were observed. In particular, it was found that toward the end of the consolidation process, the rate of settlement decreased less rapidly than predicted by the theory. It is this additional settlement, that is not accounted for by Terzaghi's theory and that takes place at practically constant effective stress, that has been called "secondary". Consequently, in the past, most investigations of drained creep behavior have studied the specific phenomenon of secondary compression; i.e., the drained volumetric creep under uniaxial strain conditions that follows primary consolidation.

The subject of drained creep behavior of cohesive soils under general stress states has received relatively limited attention in the soil mechanics literature. This is somewhat surprising in view of the fact that from a practical standpoint, the problem of drained creep is very pertinent to in situ problems where creep deformations and eventually creep failure may develop as a result of a reduction in shear strength with time. Excavated or natural slopes are prime examples of such conditions; in all these situations, partial or full drainage would be expected, though uniaxial conditions would not necessarily apply. The findings of the limited number of investigations of general drained creep behavior have been rather inconclusive. In some cases the drained creep strength of the cohesive soil was found to coincide with the compressive strength as measured in normal duration drained tests (Shibata & Karube 1969, Finn & Shead 1973, Tavenas, Leroueil, La Rochelle & Roy 1978). Failure of the soil, if it occurred at all, did so after only a few days. Other results show a marked instability of strain rate and subsequent failure, but only after periods of time exceeding about two years (Bishop & Lovenbury 1969). Because the types of clays used in these investigations differed, it is evident that further research is required before an improved understanding of response under conditions of general drained creep can be achieved.

Under uniaxial as well as general conditions, the time permitted for drained creep prior to shear testing is sometimes called the "age" of the sample. Aging greatly influences the strength and compressibility characteristics of cohesive soils. Longer periods of aging result in a reduction of void ratio, in the development of a more stable arrangement of soil particles with a greater number of interparticle bonds (Bjerrum 1967), and in a greater resistance to further consolidation (Whitman 1960, Leonards & Altschaeffl 1964, Ladd & Preston 1965). The process of aging also increases the efficiency of thixotropic time effects, that also contribute to the increase in strength. Since pore water pressure is a measure of the potential structural rearrangement of soil particles (Barden 1969), older samples, that have

a reduced rearrangement potential, will have a lower potential for pore pressure build-up, resulting in higher undrained strength. The above hypotheses have been supported by experimental findings. In particular, for older samples, sizable increases in shear strength and stiffness with a more brittle response (Wissa 1961, Bjerrum & Lo 1963), and reductions in the amount of pore water pressure build-up during subsequent undrained creep (Shen, Arulanandan & Smith 1973) have been noted. This behavior closely resembles that exhibited by overconsoidated clays.

Time-dependent soil behavior under undrained creep conditions has been the subject of numerous investigations. The relation between drained and un-drained creep is generally well understood. The mechanisms that cause volume decrease at constant effective stress in the drained case lead to the development of excess pore pressures for undrained (constant volume) loadings. This applies to both isotropic and deviatoric stresses, though only the latter result in deformations because of the constant volume condition (Ladd et al. 1977).

During undrained creep tests shear strains and changes in pore pressure are induced in the specimen. The changes in pore pressure have been attributed to the arresting of secondary compression (Arulanandan, Shen & Young 1971, Holzer, Höeg & Arulanandan 1973, Shen et al. 1973), and to the magnitude of shearing strain imposed on the specimen (Bonaparte 1981).

3.1.2. Stress Relaxation

In studying the time-dependent behavior of soils, emphasis has primarily been placed on deformation-related phenomena such as the rate of applied strain, drained and undrained creep, secondary consolidation (drained volumetric creep), etc. Such considerations have important applications for the solution of field problems involving the settlement of earth structures where the applied loads are essentially constant. Although stress relaxation represents a complementary phenomenon to creep, relatively few investigations of this phenomenon have been performed.

Relaxation tests attempt to duplicate the behavior of loaded soil masses whose dimensions are held constant in situ. Prime examples of such problems are those involving soil-structure interaction in which the presence of the structure prevents excessive deformation of the soil mass. In such cases, the relaxation of stresses becomes the response quantity of primary interest. Since relaxation behavior involves the soil state "relaxing" to an equilibrium stress level at constant deformation, the relaxed state is quite highly dependent on the existing soil microstructure at the point of relaxation. Thus, in observed macroscopic relaxation behavior there is a close correlation to, and manifestation of a soil's microstructure (Sheahan & Kaliakin 1998, Sheahan & Kaliakin 1999).

Relaxation tests are typically performed under axisymmetric conditions in which the axial stress, radial stress and pore pressure can each be controlled independently. Following a preconsolidation phase, in which a consolidation stress state is applied to the specimen and pore pressure allowed to drain, specimens are typically axially loaded to a desired strain level (with or without further pore pressure drainage), and this level is subsequently held constant. The principal stress difference $(q = \sigma_1 - \sigma_3)$, mean normal effective stress and pore pressure or volumetric strain are all monitored with time. In a properly performed relaxation test, a stable stress state is reached at each strain level before imposing further

strain on the specimen (Sheahan & Kaliakin 1998).

Based on the results of stress relaxation tests performed primarily on hydrostatically consolidated and remolded specimens, the following behavioral trends have been noted: a) following the application of a constant strain, the decay of q is essentially linear with the logarithm of time (Pagen & Jagannath 1967, Lacerda & Houston 1973, Murayama, Sekiguchi & Ueda 1974, Lacerda 1976, Arai 1985, Hicher 1988), b) during undrained relaxation tests, the variation in pore pressure is very small in comparison with the drop in q (Murayama & Shibata 1964, Lacerda & Houston 1973, Lacerda 1976, Arai 1985, Hicher 1988); this is in accord with Lo's hypothesis (Lo 1969a, Lo 1969b) which states that under undrained conditions the magnitude of pore pressure depends almost exclusively upon the amount of strain, c) in stress relaxation tests performed under drained conditions, the volume change during relaxation was negligible; this is in accordance with the observed constancy of pore pressures in the undrained relaxation tests, and d) in contrast with the large effect of anisotropic consolidation on creep, no measurable deviation between the stress relaxation of isotropically and anisotropically consolidated samples of undisturbed clay has been observed (Lacerda & Houston 1973). Thus, unlike in the case of drained creep, experimental findings related to stress relaxation appear to be quite consistent.

Two subsequent testing programs (Silvestri, Soulie, Touchan & Fay 1988, Sheahan, Ladd & Germaine 1994) showed more clearly that a soil's microstructure determines the stabilized stress state during relaxation. At smaller relaxation strains when the soil's inherent microstructure is still intact, a natural soil will reach stabilized stress states along the soil's depositional consolidation line. At higher relaxation strains, when the soil has been destructured, the stabilized relaxation stress states will depend on its new equilibrium microstructure that will typically be indicated by a different line of stabilized strain states. It thus appears that when realistic test methods such as anisotropic consolidation are used, and when the soil retains some of its original microstructure throughout the consolidation process, both the microstructure and anisotropy can affect the observed relaxation (Sheahan & Kaliakin 1998).

3.2. Temperature-Dependent Behavior

Due to the complex, heterogeneous and discontinuous nature of the microstructure and physicochemical constitution of cohesive soils, it is not yet possible to macroscopically account for detailed microscopic aspects in a practical manner. Instead, in order to quantify how microscopic phenomena affect the macroscopic constitutive modeling of the thermomechanical response of saturated cohesive soils, it is necessary to review the findings from pertinent experimental studies in several general areas. Over the past fifty or so years a number of studies have established that the engineering properties of geomaterials can significantly be influenced by temperature variations. In this section the findings of these studies are briefly reviewed.

3.2.1. Compressibility and Preconsolidation Pressure

Several investigators studied the effect of temperature cycling on volume changes for drained tests performed at different levels of (constant) confining stress. Both standard oedome-

ters (Finn 1951, Paaswell 1967, Plum & Esrig 1969, Habibaghi 1973, Tidfors & Sällfors 1989, Towhata, Kuntiwattanakul & Kobayashi 1993) and special triaxial cells (Demars & Charles 1982, Campanella & Mitchell 1968, Del Olmo, Fioravante, Gera, Hueckel, Mayor & Pellegrini 1996, Abuel-Naga, Bergado & Lim 2007) were used in these studies. It was observed that at constant effective stress levels, normally consolidated and lightly overconsolidated specimens subjected to temperature increases consolidate. Decreases in temperature typically cause such specimens to swell; the soil behaves as if it were overconsolidated (Campanella & Mitchell 1968, Hueckel & Baldi 1990, Paaswell 1967, Plum & Esrig 1969). Heating, at constant mean normal effective stress, produces a quasi-preconsolidation behavior similar to the associated with the effects of prolonged consolidation (Campanella & Mitchell 1968, Plum & Esrig 1969, Tidfors & Sällfors 1989, Towhata, Kuntiwattanakul & Kobayashi 1993).

The effect of temperature cycling on the volume change behavior of overconsolidated cohesive soils has also been investigated (Plum & Esrig 1969, Demars & Charles 1982, Baldi et al. 1988, Hueckel & Baldi 1990, Del Olmo et al. 1996, Abuel-Naga et al. 2007). The consensus appears to be that compared to normally consolidated specimens, thermally induced volumetric changes are relatively small. The amount of volume contraction appears to decrease with increasing overconsolidation ratio. For low-porosity clays, the behavior of overconsolidated specimens was found to be thermoelastic (Baldi et al. 1988, Hueckel & Baldi 1990, Del Olmo et al. 1996). Furthermore, when heated, highly overconsolidated specimens of such clays exhibited volume expansion. This is explained in part by the fact that upon heating, the pore fluid in low-porosity clays expands more than the solids. Since the permeability of such soils is low, the fluid cannot readily drain from the pores, resulting in a volume expansion.

The effect of temperature on the preconsolidation pressure has been studied using isothermal oedometer tests performed at various temperatures. Based on the results of these tests, it was determined that at a given value of void ratio, increases in temperature cause the preconsolidation pressure to decrease (Eriksson 1989, Tidfors & Sällfors 1989, Moritz 1995); the change in preconsolidation pressure seems to be larger for soils possessing a higher clay content and for those with higher liquid limits (Tidfors & Sällfors 1989). Finally, the complete temperature cycles were found to be irreversible.

3.2.2. Compression and Swell/Re-Compression Indices

Based on the results of isothermal oedometer tests performed at various temperatures, at low confining pressures (less than $207kPa$) the compression index (C_c) was found to be a function of the temperature and pressure (Plum & Esrig 1969). However, at higher pressures, C_c was found to be essentially independent of temperature (Finn 1951, Campanella & Mitchell 1968, Demars & Charles 1982, Eriksson 1989).

No consensus has been reached on the effect of temperature changes on the swell/recompression index (C_s). Campanella & Mitchell (1968) concluded that the effect of temperature on C_s was insignificant. By contrast, Eriksson (1989) and Graham, Tanaka, Crilly & Alfaro (2001) found that C_s varied with temperature.

3.2.3. Permeability

To better understand the effect of temperature changes on the permeability of clays, the coefficient of permeability (k) commonly used by geotechnical engineers (units of Lt^{-1}) is written in terms of the intrinsic permeability k^d (units of L^2); viz.,

$$k = \left(\frac{\rho^f g}{\eta}\right) k^d \tag{1}$$

where ρ^f is the density of the pore fluid (units of ML^{-3}), g is the gravitational acceleration (units of Lt^{-2}), and η is the dynamic viscosity (units of $FL^{-2}t$). The density of water is a function of pressure and temperature (Khan 2000). Although for most fluids the viscosity shows a rather pronounced variation with temperature, it is relatively insensitive to pressure until rather high pressures have been attained (Bear 1972). For free (non-adsorbed) pore water, η decreases exponentially with temperature (Houwink 1953).

Although the above observations apply for free water, it is less evident that they also apply to saturated clays, as clay-water interactions are known to be sensitive to changes in temperature (Mitchell 1969). In addition, clays exhibit an apparent viscosity that is larger close to the clay particles and decreasing with the clay-water distance. It is thus difficult to clearly separate viscosity effects from those related to clay-water interaction when analyzing the effect of temperature on water flow in cohesive soils. As a consequence, the use of the standard exponential expression giving the change of viscosity of free water with temperature is approximate (Delage, Sultan & Cui 2000).

In previous investigations, the effect of temperature on permeability was determined *indirectly*. Habibagahi (1977) performed isothermal consolidation tests at various temperatures in a rigid ring odometer. He derived permeability values at different temperatures and concluded that they increased with increasing temperatures. This was attributed to the fact that the viscosity of pore water decreases with temperature, thus reducing the internal resistance to flow. Towhata, Kuntiwattanakul, Seko & Ohishi (1993) performed similar tests and confirmed Habibagahi's conclusions.

Delage et al. (2000) concluded that investigations of the effect to temperature changes on the permeability should be made using *direct* isothermal tests at different temperatures. They observed that indirect values, obtained from consolidation for Boom clay, overestimated the permeability by a factor of four. Direct permeability measurements at various temperatures appear to be rather rare. Morin & Silva (1984) performed constant head permeability tests on various ocean sediments at temperatures ranging from 22^oC to 220^oC. Their conclusions regarding the effect of temperature changes on permeability agreed with the aforementioned ones of Habibagahi (1977) and Towhata, Kuntiwattanakul, Seko & Ohishi (1993).

To study the relationship between the intrinsic permeability k^d, porosity and temperature, Delage et al. (2000) performed a series of constant head permeability tests at different temperatures on Boom clay. They concluded that there is a unique and essentially linear relationship between the porosity and the logarithm of k^d that is independent of the thermo-mechanical load path that is applied to a sample. Consequently, since changes in ρ^f for the temperature range used in the tests (20 to 90^oC) were negligible, it was concluded that the increase in permeability of a sample with temperature is only related to the decrease

in viscosity of the pore water. In addition, the water flowing through a sample during a permeability test is free water. These conclusions agree with the earlier ones of Morin & Silva (1984).

3.2.4. Pore Pressure Development

For normally consolidated and lightly overconsolidated cohesive soils tested under undrained conditions at a constant level of total stress, temperature increases, even relatively minor ones, lead to the generation of excess pore pressure and thus to a decrease in effective stress. Decreases in temperature have the reverse effect. The changes in pore pressure are typically attributed to: 1) the difference in thermal expansion of the fluid and solid phases, and 2) physicochemical effects. The *amount* of pore pressure change is thought to be a function of: 1) the thermal path, 2) the temperature increment, 3) the boundary conditions, 4) the soil's compressibility (under drained conditions) attributed to thermally induced physicochemical effects, and 5) The thermal expansion properties of the pore fluid and soil (Houston, Houston & Williams 1985).

The effect of temperature cycling on pore pressure development has also been investigated, typically using a standard triaxial cell. The biggest point of contention appears to be whether residual pore pressures are developed after a temperature cycle. Although Mitchell & Campanella (1964) reported closed hysteresis loops and no build-up of residual pore pressures, a number of other investigators found the pore pressure changes to be irreversible (Henkel & Sowa 1964, Campanella & Mitchell 1968, Plum & Esrig 1969). In light of these findings, it appears safe to conclude that: 1) upon temperature cycling, hysteresis loops shall be formed, though not necessarily always in the first cycle, and 2) the amount of residual excess pore pressure decreases with the number of cycles, for the soil is becoming more overconsolidated. Since the development of residual pore pressure is attributed to irreversible physicochemical phenomena, and since such phenomena vary from soil to soil, it follows that the level of the aforementioned hysteresis will likewise vary.

3.2.5. Elastic Response

The effect of temperature on the elastic response of clay was investigated by Murayama (1969). From the results of experiments performed in oedometer and triaxial cells on undisturbed Osaka clay it was that, provided the axial strain did not exceed a certain critical value (approximately 1.0 percent), the elastic moduli at a given temperature were constant. However, beyond this critical value, temperature increases resulted in a reduction in the elastic moduli. Such behavior was attributed to the fracture in the clay skeleton that proceeds with straining beyond the critical value. In addition, when comparing the constant elastic moduli, it was observed that the relative magnitude of the moduli decreased with increases in temperature. These conclusions were supported by more general findings (Eriksson 1989, Tidfors & Sällfors 1989, Hueckel & Baldi 1990) that showed that the elastic domain of a soil reduces with increased temperature.

3.2.6. Shear Strength and Friction Angle

Many individuals (Lambe 1958, Mitchell 1964, Duncan & Campanella 1965, Campanella & Mitchell 1968, Noble & Demirel 1969, Sherif & Burrous 1969, Houston et al. 1985) have investigated the effects of temperature variations on soil strength. Campanella & Mitchell (1968) noted that an increase in temperature causes a decrease in the shearing strength of individual interparticle contacts. This decrease in bond strength was attributed to the increase in thermal energy that acts in conjunction with the shear force at interparticle contacts to increase the probability of bond slippage or failure. As a consequence, there is a partial collapse of the soil structure and (under drained conditions) a decrease in void ratio until a sufficient number of additional bonds are formed to enable the soil to carry the stress at the higher temperature. This effect was thought to depend only on properties of the soil structure; its rate was considered to be independent of pore pressure considerations, and was thought to be analogous to secondary compression under a stress increase.

Sherif & Burrous (1969) and Noble & Demirel (1969) reported similar results. In the latter study, specimens of a highly plastic alluvial clay were sheared at temperatures lower than the consolidation temperature. It was observed that the higher the consolidation temperature, the greater the shear strength at any given temperature. This observation, which is supported by the results of Laguros (1969), is attributed to the greater decrease in void ratio at higher consolidation temperatures. However, for a given consolidation temperature, the strength decreases in a regular manner with increasing test temperature. For overconsolidated clays, Hueckel & Baldi (1990) showed that besides reducing shear strength, temperature increases also lead to less dilatant volume change behavior. To summarize the above findings, Leroueil & Marques (1996) state that, as a rule of thumb, the undrained shear strength and preconsolidation pressure typically change by 10 percent per 12^oC change in temperature.

Test results presented by Mitchell (1964), Hueckel & Pellegrini (1989) and Hueckel & Baldi (1990) indicate that, for normally consolidated soils, temperature changes have little effect on the friction angle. From tests performed at temperatures below 40^oC, Houston et al. (1985) confirmed these observations. However, at higher temperatures the peak strength (and stiffness) of soils increased significantly. Lingnau, Graham & Tanaka (1995) reported similar results for sand-bentonite mixtures. More recently, Cekerevac & Laloui (2004) showed that the friction angle at the critical state can either slightly increase or decrease with temperature; they thus assumed it to be independent of temperature. To summarize this issue, it appears that the effect of temperature on friction angle is material-specific.

3.2.7. Time Effects

Related to the thermal dependence of soil strength is the influence of temperature on time effects such as the creep and stress relaxation of soils. Although especially pertinent to the present development, this subject has unfortunately not been widely investigated. The general conclusions made should thus be viewed as being somewhat preliminary.

In drained triaxial tests performed by Mitchell, Campanella & Singh (1968) on normally consolidated specimens, temperature increases during testing resulted in increased axial strain and strain rate, combined with a decrease in volume. Virdi & Keedwell (1988) also performed drained creep tests under both constant and transient (two complete cycles)

temperature conditions. They noted that increases in temperature considerably reduced the volume of a specimen and decreased its height; decreases in temperature were found to have the reverse effect. Volume changes associated with a temperature cycle were irreversible. In all the drained creep tests the effects of temperature change on sample height and on axial strain rate were greater at higher levels of deviator stress. Virdi & Keedwell (1988) noted that, due to variations in temperature, the volume of water drained out or absorbed appeared to be proportional to the moisture content of the soil.

Several individuals have investigated the effect of heating on secondary compression (i.e., drained volumetric creep). Plum & Esrig (1969) concluded that, provided that sufficient time is allowed for the volume change associated with the temperature increase to be dissipated, secondary compression rates appear to be only slightly affected by increases in temperature. This conclusion, which is based on the results of a single test conducted at quite high consolidation pressure (loading from 1242 to $1442kPa$), was in rather sharp contrast to those reached by other investigators (Lo 1961, Schiffman, Ladd & Chen 1966, Campanella & Mitchell 1968, Towhata, Kuntiwattanakul & Kobayashi 1993). It is possible, however, that in the latter investigations insufficient time was allowed for thermally induced volume changes to fully manifest themselves. Before leaving this somewhat unresolved subject of secondary compression, it is timely to note that investigators are in agreement with the observation that overconsolidation of soil due to cooling reduces the rate of secondary compression (Campanella & Mitchell 1968, Plum & Esrig 1969).

For normally consolidated and lightly overconsolidated soils tested under undrained conditions, increases in temperature tend to increase the pore pressure and strain, and to thus decrease the effective stress (Murayama & Shibata 1961, Mitchell & Campanella 1964, Mitchell et al. 1968, Houston et al. 1985, Virdi & Keedwell 1988). Decreases in pore pressure generally have the reverse effect. Virdi & Keedwell (1988) performed undrained triaxial creep tests under transient temperature conditions involving two complete cycles. In these tests, four levels of deviator stress (30, 50, 70 and 90% of the failure stress for monotonic loading) were used. During increases in temperature the axial strain increased, but at a decreasing rate, with each cycle. During decreases in temperature, the axial strain did not decrease appreciably, especially at the higher levels of deviator stress. The results was a permanent axial strain almost twice the magnitude of that associated with tests performed on the same material only at constant temperature.

Data concerning the effect of temperature on stress relaxation is quite scarce. The only results of stress relaxation experiments, performed in compression under undrained triaxial conditions, appear to be those presented by Murayama (1969). These show that for a given increment of strain, both the initial and the fully relaxed stress decrease with increasing temperature.

4. Framework for Modeling Time and Temperature-Dependent Clay Behavior

A mathematical framework for a constitutive model to simulate the time and temperature-dependent behavior of cohesive soils is presented in this section. There are two main and, in general, complimentary approaches to developing such a model.

The first approach represents the soil as an assembly of discrete particles (Anandarajah 1994, Anandarajah 2000b, Anandarajah 2000a, Yao & Anandarajah 2003) or clusters of particles (Chang, Hicher, Yin & Kong 2009, Yin, Chang, Hicher & Karstunen 2009, Yin & Chang 2009, Yin, Chang, Hicher & Wang 2011, Yin, Hattab & Hicher 2011). Suitable material characteristics are assumed for the particles or clusters, and are supplemented by proper interparticle or intercluster contact laws. The macroscopic behavior of cohesive soils is then simulated through a collection of such particles or clusters that interact with each other primarily through mechanical forces rather than physicochemical ones (e.g., double-layer repulsive forces and van der Waals attractive forces). Although such discrete particle methods offer insights into the mechanical and physicochemical phenomena controlling macroscopic behavior, they tend to be computationally intensive. More importantly, the scalability of such methods has yet to be proven.

In the second approach, the microscopic and physicochemical phenomena are not of prime concern. Instead, only the behavior of the material as a whole is deemed important. The macroscopic behavior is explained by assuming the material to be a continuum. However, since the physically observed behavior of a material is a macroscopic manifestation of the mechanisms active at the level of the microstructure, a continuum based model cannot be developed without due consideration, either in detail or in concept, of microscopic phenomena. Since the present mathematical framework is continuum based, the following observations are timely.

4.1. The Continuum Approach

As noted at the outset of this chapter, a two-phase continuum, consisting of a coherent solid matrix (skeleton) with fluid-filled pore space, is assumed (Figure 7). The solid matrix is composed of both a solid part and possibly an occluded porosity. The occluded pores may or may not be saturated, but it does *not* affect the storage or transport properties of the porous material because no flow is assumed to take places through these pores (Coussy 2004). The pore space is completely filled by a single fluid that is freely moving. Unless stated otherwise, the pore fluid is assumed to be water. The pore space is assumed to be *fully connected*; it is through this space that the fluid actually flows. The pore space is assumed to remain continuous throughout deformation of the material.

A porous material is commonly treated as the superimposition of *two* continua: the solid matrix continuum and the pore fluid continuum (Coussy 2004). A continuum description of a porous medium that is heterogeneous at the level of the microfabric requires the suitable choice of a macroscopic scale at which the constitution of the material at the micro-level will be ignored in the analysis of physical macroscopic phenomena. The hypothesis of continuity assumes the existence of a representative *elementary volume* that is relevant at the macroscopic scale for all the physical phenomena involved in the intended application (Coussy 2004). The physics of one such elementary volume is assumed to vary continuously to neighboring volumes, giving a continuum for which the densities of mass, momentum, and energy exist in the mathematical sense (Fung 1977).

In concluding the discussion of microstructure and fabric given in Section 2.5., it was noted that in virtually all natural depositional environments the presence of electrolytes in the pore fluid supplies ions that result in the formation of an irregular, three-dimensional ar-

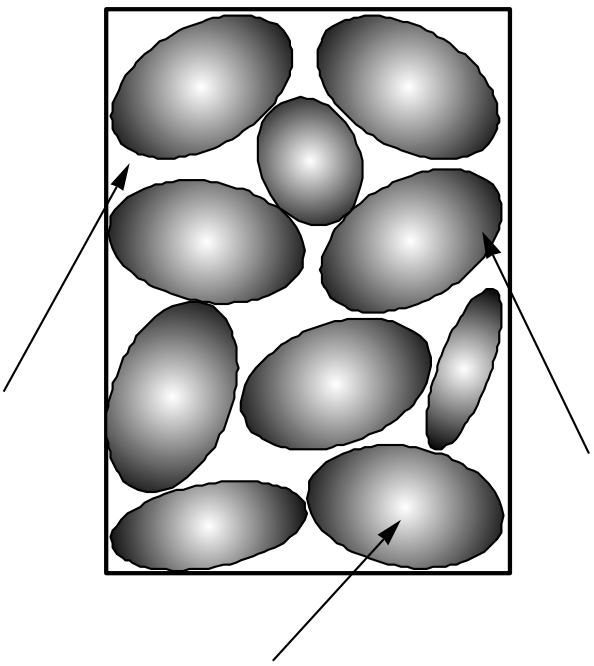

Figure 7. Schematic illustration of a fully saturated porous medium.

rangements of aggregated particles or domains surrounded by micropores. Domains group together to form clusters. Clusters, in turn, group together to form peds or groups of peds that are surrounded by minipores.

Based on the above considerations, an elementary volume is assumed to consist of groups of clusters; i.e., one or more peds. In the case of laboratory prepared soils possessing a primarily dispersed fabric, the elementary volume consists of an assemblage of individual particles and their associated pore space. With the elementary volume defined, attention is turned to the various aspects of material response exhibited by cohesive soils subject to applied mechanical, thermal or thermo-mechanical loads.

4.2. The Instantaneous Response

Within a saturated cohesive soil, very low changes in effective stress under isothermal conditions produce changes in the shear and normal forces at points of interparticle contact. These, in turn, produce an elastic bending of particles within clusters, and an elastic deformation of particle clusters and/or peds. A relaxation of previously bent or distorted particles and/or particle clusters may also occur (Murayama 1969). Both of these phenomena occur without slippage or breakage of interparticle bonds, and result in an instantaneous elastic deformation of the elementary volume.

If the applied mechanical, thermal or thermo-mechanical loading causes a sufficiently large change in effective stress within the soil, the shear forces at intercluster “bridges” or

other points of particle discontinuity become large enough to cause the breakage of bonds. Although the exact manner in which the bonds between individual particles are disrupted in a shearing process is not known (Scott 1963), the result is an instantaneous rearrangement of clusters that occurs simultaneously with the elastic deformations. This, in turn, leads to the formation of localized groups of particles oriented parallel to the direction of shear and causes a translation and rotation of the clusters themselves. In a primarily dispersed fabric this leads to a translation and rotation of the individual particles. In either case, the result is an instantaneous plastic deformation of the elementary volume.

Regardless of the clay's fabric, the simultaneously occurring instantaneous elastic and plastic responses can be modeled macroscopically within the framework of rate-independent thermo-elastoplasticity. Under one-dimensional drained conditions this response is associated with the phenomenon of primary consolidation (with or without deviatoric stress), as excess pore pressure is dissipated by drainage of fluid from the minipores.

The word "instantaneous," as used in the previous discussion, requires some explanation. It is a well-known fact that, due to hydrodynamic time lag, the testing of cohesive soils under drained conditions requires a finite waiting period between the application of load and the measurement of deformations. This is to allow for the aforementioned dissipation of excess pore pressure within the sample, a process that is slowed by the low permeability of the soil and by the fact that drainage occurs only at the boundaries of the test specimen. Were it possible to establish drainage at all points within the sample, the above deformations would indeed appear to occur essentially instantaneously in real time[1]. Thus, if no further deformation of the particles occurs, the constitutive relations for cohesive soils in relation to effective stress can be formulated solely within the framework of rate-independent thermo-elastoplasticity. The analysis in relation to total stress requires consideration of the mechanisms of two-phase materials (i.e., the soil skeleton and pore fluid) (Biot 1956).

4.3. The Delayed Response

The deformation is, however, known to continue past the instantaneous phase. In cohesive soils possessing a dispersed fabric, and in the particles comprising the relatively weak intercluster bridges in aggregated fabrics, this additional deformation consists primarily of the re-orientation of particles caused by the further breaking of interparticle bonds. The partial equilibrium achieved during the instantaneous phase of deformation is slowly changed by the motion of ions, water molecules, and other slow diffusion processes (Scott 1963). If, as a result of this change in equilibrium, the shear force at a point of interparticle contact is of sufficient magnitude, it causes the bond at this location to break.

This, in turn, further disrupts the equilibrium among contact forces and results in further displacement of clusters and particles as they seek new equilibrium configurations in which interparticle bonds can once again be formed. This displacement (and thus the subsequent re-formation of bonds) is greatly retarded by the layers of highly viscous adsorbed water that surround the particles. The rate of this retardation depends primarily on the applied stress level, the change in temperature, or both. Macroscopically, these processes

[1]These instantaneous deformations would not, however, occur with sufficient rapidity to warrant consideration of inertia forces.

produce a delayed viscoplastic deformation of the elementary volume, which occurs with negligible change in pore pressure (under undrained conditions) or volume (under drained conditions). Such deformation is expected to continue until the shear forces at particle contacts are transformed to normal forces at different contacts as a result of particle movements (Mitchell 1976).

In cohesive soils with an aggregated fabric, the delayed deformation tends to be even more pronounced than in those possessing a relatively dispersed one. In the former case it is not only the above viscous and physicochemical processes that affect the intercluster contact forces and cause cluster rearrangement with time, but also the clusters themselves undergo time-dependent deformation as pore fluid is slowly forced from the micropores. However, because of the small interparticle spacing and larger number of bonds in a cluster due to the close proximity of diffuse double layers, these intracluster deformations are much smaller than the intercluster ones associated with the instantaneous deformation. As a result, the highly viscous intracluster pore fluid drains from the micropores into the minipores at a much slower rate than the intercluster fluid drains during the instantaneous phase of deformation.

During the process of cluster deformation, the reduction in cluster volume is exactly balanced by the increase of the minipores due to the transfer of incompressible pore fluid from the micropores. Thus, the relatively small cluster deformations alone cannot account for the delayed volumetric strain (under drained conditions) or pore pressure increase (under undrained conditions) in the elementary volume. Instead, it is the perturbation of contact force equilibrium (due to the aforementioned physicochemical diffusion processes) that facilitates further cluster rearrangement and, consequently, further deformation of the elementary volume. Under drained conditions, as the clusters change orientation, the perturbed intercluster contact forces are continuously restored to some average value and the excess pore pressure remains negligible. As a result, the macroscopically measured effective stress remains essentially constant. Under undrained conditions no change in volume is permitted; as a result, the pore pressure increases, causing a decrease in effective stress.

Regardless of the soil fabric, the delayed deformation mechanisms can be macroscopically modeled in a unified manner within the framework of *viscoplasticity*. Although both instantaneous (elastoplastic) and delayed (viscoplastic) deformations occur simultaneously, the development rate of the latter is typically slow enough to exhibit measurable effects only after considerable time has elapsed.

4.4. Brief Note on Unification of Macroscopic Time-Dependent Phenomena

Before proceeding further with the discussion, it is timely to unify some of the commonly observed macroscopic time-dependent phenomena in light of the viscous mechanism discussed above. By retarding the rearrangement of particles, the viscous adsorbed water layers delay changes in pore pressure. These viscous layers are thus primarily responsible for the rate dependence of the material response; i.e., for the so-called "strain-rate effect." The same delayed deformation mechanism is also responsible for the long term time-dependent behavior of clays. More precisely, under uniaxial drained conditions, the delayed deformation is associated with the phenomenon of secondary compression (drained volumetric creep). If, on the other hand, drainage is prevented and the applied stress level maintained

constant, the resulting response is known as undrained creep. Finally, if the applied level of deformation remains unchanged, the resulting decrease in stress is termed stress relaxation. Thus, the common classifications of "rate dependent response" and "time effects" are both macroscopic manifestations of the *same* microstructural process.

4.5. The Combined Elastoplastic - Viscoplastic Response

Based upon the above considerations, it is evident that a general description of material response for clays cannot realistically be obtained by means of elastoplasticity alone, nor by viscoplasticity alone. Instead, cohesive soils, regardless of the fabric they possess, must be modelled within the general framework of *combined* and *coupled* elastoplasticity-viscoplasticity. Dafalias (1982) first introduced such a combined formulation in the field of soil mechanics. Kaliakin (1985) subsequently refined, implemented and verified the formulation. Kaliakin & Dafalias (1990a) presented further details pertaining to the elastoplastic-viscoplastic bounding surface model for cohesive soils under isothermal conditions, swell as its verification (Kaliakin & Dafalias 1990b). Kaliakin (1994) extended the formulation to a thermo-elastoplastic-viscoplastic one, suitable for isotropic cohesive soils. In this section, the latter formulation is extended to include the effect of anisotropy.

4.6. Overview of Proposed Framework

Having established the applicability of a combined and coupled thermo-elastoplastic-viscoplastic formulation for modeling the anisotropic, time, rate and temperature-dependent behavior of cohesive soils, a general mathematical framework for developing an associated bounding surface constitutive model is now presented.

Although in its most general form, soil consists of solid, liquid, and gaseous phases, in discussing the constitutive relations for soils, reference is made specifically to the deformation of the soil skeleton. In view of this fact, the material state is defined in terms of external variables, identified as the *effective* stress tensor σ'_{ij}, temperature θ, and n scalar or tensor internal variables q_n that account for the nonconservative nature of soil by keeping track of the past loading history. In the subsequent development *compressive* stresses and strains are considered as positive. The effective stress σ'_{ij} is related to the total stress σ_{ij} and the pore fluid pressure u by

$$\sigma_{ij} = \sigma'_{ij} + \delta_{ij} u \tag{2}$$

where δ_{ij} is the Kronecker delta. Hueckel & Pellegrini (1992) ascertained the applicability of the effective stress principle to the thermo-mechanical modeling of saturated cohesive soils.

From the point of view of the microstructure, the effective stress represents the inelastic forces acting over the total intercluster contact area. The effective stress represents a means by which to quantify the elastic and inelastic response that occurs instantaneously upon loading of the soil, and that remains essentially constant with time. However, also present during (and subsequent to) this loading is the delayed viscoplastic deformation. In clays possessing a dispersed fabric, and in the particles comprising the intercluster bridges

in aggregated fabrics, this delayed deformation is due to the evolution of slow diffusion processes of a physicochemical nature. In the case of aggregated fabrics, additional delayed deformation occurs as a result of the mechanical process of pore fluid drainage from the micropores to the minipores. As a result of this drainage, the effective stress associated with the interparticle contact forces within a cluster or ped increases, tending toward some equilibrium value. Following the approach of Dafalias (1982), regardless of the clay fabric, the delayed deformation is represented by one of the microscopic internal variables q_n.

Anisotropy of cohesive soils is attributed to the preferred orientation of particles and the development of residual stresses. Preferred microstructural orientations cause both elastic and plastic anisotropy. Since cohesive soils are soft materials, they develop anisotropic characteristics in the course of inelastic loading as easily as they may loose them. Consequently, the inclusion of initial anisotropy alone without providing for its evolution and possible demise, is only marginally better than not including it at all (Dafalias 1986). Stress-induced anisotropy is mathematically accounted for through rotational hardening of the bounding surface. As such, the material state is not determined solely by the state of σ'_{ij}, but also requires a measure of stress-induced anisotropy.

The dependence of the bounding surface on σ'_{ij} is expressed in terms of three stress invariants, namely (Ling, Yue, Kaliakin & Themelis 2002)

$$I_1 = \sigma'_{ij}\delta_{ij} \tag{3}$$

$$J^a = \sqrt{\frac{1}{2}s^a_{ij}s^a_{ij}} \tag{4}$$

$$\alpha^a = \frac{1}{3}\sin^{-1}\left[\frac{3\sqrt{3}}{2}\left(\frac{S^a}{J^a}\right)^3\right] \quad , \quad -\frac{\pi}{6} \le \alpha^a \le \frac{\pi}{6} \tag{5}$$

The quantities J^a and α^a are the second *reduced* deviatoric stress invariant and the*reduced* Lode angle, respectively, and α_{ij} is the symmetric second-order *anisotropic tensor* that provides the aforementioned measure of stress-induced anisotropy. The values of $\alpha = \pm\pi/6$ correspond to to conditions of axisymmetric triaxial compression and extension, respectively. Finally, s_{ij} is the deviatoric stress tensor as defined by $s_{ij} = \sigma'_{ij} - \delta_{ij}\sigma'_{kk}/3$.

A section of the elliptical bounding surface, for a given value of α^a, is shown in Figure 8. Analytically, the bounding surface is defined by

$$F\left(\bar{I}_1, \bar{J}^a, \bar{\alpha}^a, \theta, q_n\right) = 0 \tag{6}$$

where a bar indicates an "image" point on the surface.

The prominent feature of the bounding surface concept is the prediction of inelastic deformations for points $(I_1, J^a, \alpha^a, \theta)$ within or on the surface at a pace depending on the proximity (δ) of $(I_1, J^a, \alpha^a, \theta)$ to a unique "image" point $(\bar{I}_1, \bar{J}^a, \bar{\alpha}^a, \theta)$ on the surface. The latter is uniquely assigned by the "radial" mapping rule (Dafalias & Herrmann 1986)

$$\bar{I}_1 = b\left(I_1 - CI_o\right) + CI_o \quad ; \quad \bar{J}^a = bJ^a \quad ; \quad \bar{\alpha}^a = \alpha^a \tag{7}$$

where b $(b \ge 1)$ is from an explicit expression for the bounding surface, I_o represents a measure of the pre consolidation history, and C $(0 \le C < 1)$ is a model parameter (Figure

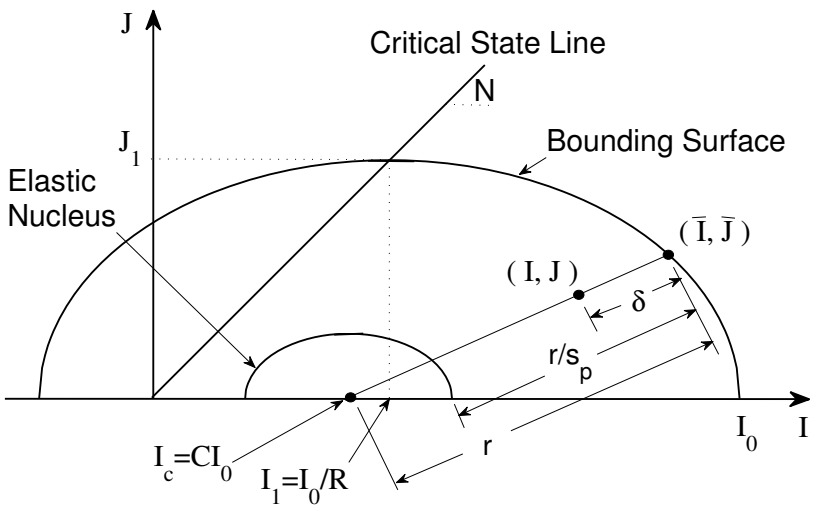

Figure 8. Schematic illustration of elliptical bounding surface and radial mapping rule in stress invariants space.

8). Unlike previous isothermal formulations (Kaliakin & Dafalias 1990a), the bounding surface and I_o must now be functions of temperature.

The direction of inelastic loading-unloading is defined as the gradient of F at the "image" point. To complete the formulation, a relation between the plastic modulus K_p (associated with the actual stress point) and a "bounding" plastic modulus $\bar{K}_p$ (associated with the the "image" point) is established as a function of the Euclidean distance δ between $(I_1, J^a, \alpha^a, \theta)$ and $(\bar{I}_1, \bar{J}^a, \bar{\alpha}^a, \theta)$; i.e.,

$$K_p = \bar{K}_p + \hat{H}\frac{\delta}{\langle r - s_p\delta\rangle} = \bar{K}_p + \hat{H}\frac{1}{\left\langle \dfrac{b}{b-1} - s_p \right\rangle} \tag{8}$$

where $\hat{H}$ denotes a proper scalar hardening function of the state, $s_p\,(\geq 1)$ is a model parameter, r represents the Euclidean distance between the points CI_o and $(\bar{I}_1, \bar{J}^a, \bar{\alpha}^a, \theta)$, and the symbols $< >$ denotes Macaulay brackets.

The bounding surface undergoes isotropic hardening. In addition, simulation of stress induced anisotropy of the material requires that the surface also undergo kinematic hardening that is realized through rotation of the surface. In both cases the hardening is dependent on temperature.

In light of the discussion presented in Section 2.5., it is timely to note that at the microscopic level, soil anisotropy is largely attributed to a soil's fabric. It follows that stress induced anisotropy will be a macroscopic manifestation of the *evolution* of the fabric. This evolution has largely inferred from the results of studies involving X-ray diffraction, scanning electron microscopy, electrical measurements, and assemblies of discrete particles. Based on such results, it has been postulated that the minifabric (i.e., the assembly or aggregation of clusters) governs the behavior of cohesive soils (Delage & Lefebre 1984,

Anandarajah 2000b, Hattab, Bouziri-Adrouche & Fleureau 2010). In particular, in a loaded cohesive soil the minipores compress and the minifabric reorients into a preferred configuration. At high stress levels, the compression of the micropores becomes more pronounced, thus placing the microfabric into a preferred configuration as well.

The infinitesimal strain rate tensor ε_{ij} is additively decomposed as follows

$$\dot{\varepsilon}_{ij} = \dot{\varepsilon}^e_{ij} + \dot{\varepsilon}^v_{ij} + \dot{\varepsilon}^p_{ij} + \dot{\varepsilon}^\theta_{ij} + \dot{\varepsilon}^s_{ij} \tag{9}$$

where ε^e_{ij}, ε^p_{ij}, and ε^p_{ij} are the elastic, viscoplastic and plastic components, respectively, and a superposed to denotes a material time derivative or rate. The quantity ε^θ_{ij} represents the reversible part of the thermal strain, and ε^s_{ij} represents the overall volumetric strain caused by the uniform compression of the solid phase by the pore fluid pressure.

The elastic response is assumed to be isotropic, and to be independent of the rate of loading and to be unaltered by inelastic deformation. It is expressed in terms of the elastic bulk and shear moduli K and G, respectively. Thermal effects enter into the elastic strain ε^θ_{ij} via a suitable coefficient of thermal expansion for the soil skeleton (Campanella & Mitchell 1968).

The rate equation for $\dot{\varepsilon}^v_{ij}$ is based on a generalization of the viscoplastic theory of Perzyna (1966). According to this theory, $\dot{\varepsilon}^v_{ij}$ is a function of the "distance" between the current stress and that on the boundary of a "quasi-static" elastic domain. For the present development the normalized overstress

$$\Delta\hat{\sigma} = \frac{\hat{\delta}}{r - \dfrac{r}{s_v}} = \frac{s_v}{b(s_v - 1)} - 1 \tag{10}$$

constitutes this distance. The elastic domain is represented by the implicitly defined "elastic nucleus", whose size is defined by the model parameter s_v. Although the boundary of the nucleus is equivalent to the concept of a yield surface, it is not identical since the stress point $(I_1, J^a, \alpha^a, \theta)$ can cross this boundary and move outside with a smooth inelastic transition at $\delta = r/s_v$. Assuming an associative flow rule, it follows that

$$\dot{\varepsilon}^v_{ij} = \langle \phi \rangle \frac{\partial F}{\partial \bar{\sigma}'_{ij}} \tag{11}$$

where ϕ represents a scalar "overstress function." Kaliakin & Dafalias (1990b) give explicit expressions for ϕ that are suitable for simulating the time-dependent response of cohesive soils.

The plastic strain rate is given by

$$\dot{\varepsilon}^p_{ij} = \langle L \rangle \frac{\partial F}{\partial \bar{\sigma}'_{ij}} \tag{12}$$

where the scalar loading index L accounts for the coupling of plastic-viscoplastic hardening for states on and within the bounding surface (Kaliakin & Dafalias 1990a). Loading, unloading and neutral loading is denoted by $L > 0$, $L < 0$ and $L = 0$, respectively.

From the above discussion it is evident that the present model differs from classical yield surface thermo-elastoviscoplastic formulations in that the stress is continuously at an

inelastic state, with the possibility of plastic-viscoplastic coupling either within or on the bounding surface. The abrupt transition between elastic and inelastic response, which is not exhibited by actual soils, is thus avoided.

Based on equations (9), (11) and (12), the constitutive relations, in inverse form, are given by

$$\begin{aligned}\dot{\sigma}_{ij} &= E_{ijkl}\left(\dot{\varepsilon}_{ij} - \dot{\varepsilon}^{v}_{ij} - \dot{\varepsilon}^{p}_{ij} - \dot{\varepsilon}^{\theta}_{ij} - \dot{\varepsilon}^{s}_{ij}\right) \\ &= E_{ijkl}\left(\dot{\varepsilon}_{ij} - \langle\phi\rangle\frac{\partial F}{\partial \bar{\sigma}'_{ij}} - \langle L\rangle\frac{\partial F}{\partial \bar{\sigma}'_{ij}} - \dot{\varepsilon}^{\theta}_{ij} - \dot{\varepsilon}^{s}_{ij}\right)\end{aligned} \tag{13}$$

where E_{ijkl} is a tensor of elastic moduli expressed in terms of K and G. Kaliakin (1994) gives explicit expressions for $\dot{\varepsilon}^{\theta}_{ij}$ and $\dot{\varepsilon}^{s}_{ij}$ for the case of isotropic cohesive soils.

To complete the development of a constitutive model within the above framework requires explicit expressions for the a) bounding surface (recall equation 6), b) isotropic hardening rule, c) kinematic (rotational) hardening rule, d) shape hardening function $\hat{H}$, and e) evolution of $\varepsilon^{\theta}_{ij}$. Details pertaining to such development are beyond the scope of the present chapter. It is, however, timely to note that Kaliakin & Nieto-Leal (2013) present an overview of a generalized bounding surface model for cohesive soils.

Conclusion

Thermal-mechanical analyses of soils are complicated by the nature of these materials. Macroscopically such materials exhibit an anisotropic, inelastic, path-dependent, strain hardening (and softening), time-, rate- and temperature- dependent behavior. To further complicate matters, the thermal properties of such materials are not as well known as those for other materials such as metals. Several important problems have arisen that necessitate the realistic simulation of thermal-mechanical behavior of cohesive soils. The analysis of such problems requires a general but practical analytical framework that accounts for not only material non-lineariltes and thermo-mechanical coupling, but also for the time- and rate-dependent characteristics of cohesive soils.

Since the behavior of a cohesive soil loaded by mechanical, thermal or thermo-mechanical loads is a macroscopic manifestation of the mechanisms active at the level of the material microstructure, a brief discussion of rudimentary microscopic and physicochemical aspects associated with saturated cohesive soils has been presented at the outset of this chapter. This was followed by a discussion of the macroscopically observed time- and temperature-dependent behavior of such soils. Finally, a combined and coupled thermo-elastoplastic-viscoplastic framework for modeling the anisotropic, time-, rate- and temperature-dependent behavior of cohesive soils in the context of a bounding surface formulation was proposed.

References

Abuel-Naga, H. M., Bergado, D. T. & Lim, B. F. (2007). Effect of temperature on shear strength and yielding behavior of soft Bangkok clay, *Soils and foundations* 47(3): 423–436.

Anandarajah, A. (1994). Discrete element method for simulating behavior of cohesive soil, *Journal of Geotechnical Engineering, ASCE* 120(9): 1593–1613.

Anandarajah, A. (2000a). Numerical Simulation of One-Dimensional Behaviour of a Kaolinite, *Géotechnique* 50(5): 509–519.

Anandarajah, A. (2000b). On Influence of Fabric Anisotropy on the Stress-Strain Behavior of Clays, *Computers and Geotechnics* 27(1): 1–17.

Arai, K. (1985). Representation of soft clay behavior based on minimization of dissipated energy, *in* T. Kawamoto & Y. Ichikawa (eds), *Proceedings of the Fifth International Conference on Numerical Methods in Geomechanics*, Balkema, Rotterdam, pp. 277–284.

Arulanandan, K., Shen, C. K. & Young, R. B. (1971). Undrained creep behaviour of a coastal organic silty clay, *Géotechnique* 21(4): 359–375.

Baldi, G., Hueckel, T. & Pellegrini, R. (1988). Thermal volume changes of the mineral-water system in low-porosity clay soils, *Canadian Geotechnical Journal* 25(4): 807–825.

Barden, L. (1965). Consolidation of clay with non-linear viscosity, *Géotechnique* 15(4): 345–362.

Barden, L. (1969). Time dependent deformation of normally consolidated clays and peats, *Journal of the Soil Mechanics and Foundations Division, ASCE* 95(SM1): 1–32.

Barden, L. & Sides, G. R. (1970). The engineering behavior of compacted clay, *Journal of the Soil Mechanics and Foundations Division, ASCE* 96(SM4): 1171–1200.

Bear, J. (1972). *Dynamics of Fluids in Porous Media*, American Elsevier Publishing Company, New York, NY.

Biot, M. A. (1956). General solutions of the equations of elasticity and consolidation for a porous material, *Journal of Applied Mechanics, Transactions of ASME* 78: 91–96.

Bishop, A. W. & Lovenbury, H. T. (1969). Creep characteristics of two undisturbed clays, *Proceedings of the Seventh International Conference on Soil Mechanics and Foundation Engineering*, Mexico City, pp. 29–37.

Bjerrum, L. (1967). Engineering geology of norwegian normally consolidated marine clays as related to settlements of buildings, *Géotechnique* 17(2): 81–118.

Bjerrum, L. & Lo, K. Y. (1963). Effect of aging on the shear strength properties of a normally consolidated clay, *Géotechnique* 13(2): 147–157.

Bonaparte, R. (1981). *A Time-Dependent Constitutive Model for Cohesive Soils*, PhD thesis, University of California, Berkeley, Department of Civil Engineering.

Campanella, R. G. & Mitchell, J. K. (1968). Influence of temperature variations on soil behavior, *Journal of the Soil Mechanics and Foundations Division, ASCE* 94(SM3): 709–734.

Campanella, R. G. & Vaid, Y. P. (1972). Creep rupture of a saturated natural clay, *Proceedings of the Sixth International Congress on Rheology*, Lyon, France, pp. 1–18. also Soil Mechanics Series No. 16, University of British Columbia, Civil Engineering Department Report.

Campanella, R. G. & Vaid, Y. P. (1974). Triaxial and plane strain creep rupture of an undisturbed clay, *Canadian Geotechnical Journal* 11(1): 1–10.

Casagrande, A. (1932). The structure of clay and its importance in foundation engineering, *Journal of the Boston Society of Civil Engineers* 19(3): 168–208.

Cekerevac, C. & Laloui, L. (2004). Experimental study of thermal effects on the mechanical behaviour of a clay, *International Journal for Numerical and Analytical Methods in Geomechanics* 28(3): 209–228.

Chang, C., Hicher, P., Yin, Z. & Kong, L. (2009). Elastoplastic Model for Clay with Microstructural Consideration, *Journal of Engineering Mechanics, ASCE* 135(9): 917–931.

Collins, K. & McGown, A. (1974). The form and function of microfabric features in a variety of natural soils, *Géotechnique* 24(2): 223–254.

Coussy, O. (2004). *Poromechanics*, John Wiley and Sons, Chichester, UK.

Dafalias, Y. F. (1982). Bounding surface elastoplasticity-viscoplasticity for particulate cohesive media, *in* P. A. Vermeer & H. J. Luger (eds), *Deformation and Failure of Granular Materials, IUTAM Symposium on Deformation and Failure of Granular Materials*, A. A. Balkema, Rotterdam, Delft, the Netherlands, pp. 97–107.

Dafalias, Y. F. (1986). On elastoplastic-viscoplastic constitutive modelling of cohesive soils, *in* R. Dungar & J. A. Studer (eds), *Geomechanical Modelling in Engineering Practice*, A. A. Balkema, Amsterdam, chapter 13, pp. 313–330.

Dafalias, Y. F. & Herrmann, L. R. (1986). Bounding surface plasticity ii: Application to isotropic cohesive soils, *Journal of Engineering Mechanics, ASCE* 112(12): 1263–1291.

Del Olmo, C., Fioravante, V., Gera, F., Hueckel, T., Mayor, J. C. & Pellegrini, R. (1996). Thermomechanical properties of deep argillaceous formations, *Engineering Geology* 41(1-4): 87–102.

Delage, P. & Lefebre, G. (1984). Study of the structure of a sensitive Champlain clay and of its evolution during consolidation, *Canadian Geotechnical Journal* 21(1): 21–35.

Delage, P., Sultan, N. & Cui, Y. J. (2000). On the thermal consolidation of Boom clay, *Canadian Geotechnical Journal* 37(2): 343–354.

Demars, K. R. & Charles, R. D. (1982). Soil volume changes induced by temperature cycling, *Canadian Geotechnical Journal* 19(2): 188–194.

DeWit, C. T. & Arens, C. T. (1950). Moisture content and density of some clay minerals and some remarks on the hydration pattern of clay, *in* F. A. e. a. Van Baren (ed.), *Transactions, 4th International Congress on Soil Science*, Hoitsema Brothers, Groningen, The Netherlands, pp. 59–62.

Duncan, J. M. & Campanella, R. G. (1965). The effect of temperature changes during undrained tests, report to the U. S. Army Corps of Engineers Waterways Experiment Station, *Technical Report TE-65-10*, University of California, Berkeley, Berkeley, CA. Soil Mechanics and Bituminous Materials Research Lab.

Eriksson, L. G. (1989). Temperature Effects on Consolidation Properties of Sulphide Clays, *in* Publications Committee of the XII ICSMFE Staff (ed.), *Proceedings of the 12th International Conference on Soil Mechanics and Foundation Engineering*, Taylor & Francis, Rio De Janeiro, pp. 2087–2090.

Finn, F. N. (1951). The effect of temperature on the consolidation characteristics of remolded clay, *ASTM Symposium on Consolidation Testing of Soils* ASTM STP 126: 65–71.

Finn, W. D. L. & Shead, D. (1973). Creep and creep rupture of an undisturbed sensitive clay, *Proceedings of the Eighth International Conference on Soil Mechanics and Foundation Engineering*, Moscow, pp. 135–142.

Fung, Y. C. (1977). *A First Course in Continuum Mechanics*, second edn, Prentice Hall, Englewood Cliffs, NJ.

Gillott, J. E. (1969). Study of the fabric of fine grained sediments with the scanning electron microscope, *Journal of Sedimentary Petrology* 39(1): 90–105.

Goldschmidt, V. M. (1926). Undersokelser over lersedimenter, *Nordisk jordbrugsforskning* 4-7: 434–445.

Graham, J., Tanaka, N., Crilly, T. & Alfaro, M. (2001). Modified Cam-Clay modelling of temperature effects in clays, *Canadian Geotechnical Journal* 38(3): 608–621.

Grim, R. E. (1959). Physico-chemical properties of soils: Clay minerals, *Journal of the Soil Mechanics and Foundations Division, ASCE* 85(SM2): 1–17.

Grim, R. E. (1968). *Clay Mineralogy*, 2nd edn, McGraw-Hill Book Company, New York, NY.

Habibagahi, K. (1977). Temperature effect and the concept of effective void ratio, *Indian Geotechnical Journal* 7(1): 14–34.

Habibaghi, K. (1973). Temperature effects on consolidation behavior of overconsolidated soils, *Proceedings of the 8th International Conference on Soil Mechanics and Foundation Engineering*, Moscow, USSR, pp. 159–163.

Hattab, M., Bouziri-Adrouche, S. & Fleureau, J. (2010). Évolution de la microtexture d'une matrice kaolinitique sur chemin triaxial axisymétrique, *Canadian Geotechnical Journal* 47(1): 34–48.

Henkel, D. J. & Sowa, V. A. (1964). Discussion on symposium on laboratory shear testing of soils, *ASTM-NRC Symposium on Laboratory Shear Testing of Soils* ASTM STP 361.

Hicher, P. Y. (1988). The viscoplastic behavior of bentonite, *in* M. J. Keedwell (ed.), *Rheology and Soil Mechanics*, Elsevier, London, UK, pp. 89–107.

Hogentogler, C. A. (1937). *Engineering Properties of Soil*, McGraw-Hill Book Company, New York, NY.

Holtz, R. D., Kovacs, W. D. & Sheahan, T. C. (2011). *An Introduction to Geotechnical Engineering*, Pearson Education, Inc., Upper Saddle River, NJ.

Holzer, T. L., Höeg, K. & Arulanandan, K. (1973). Excess pore pressures during undrained clay creep, *Canadian Geotechnical Journal* 10(1): 12–24.

Houston, S. L., Houston, W. N. & Williams, N. D. (1985). Thermo-mechanical behavior of seafloor sediments, *Journal of Geotechnical Engineering, ASCE* 111(11): 1249–1263.

Houston, S. L. & Lin, H.-D. (1987). A thermal consolidation model for pelagic clays, *Marine Geotechnology* 7(2): 79–98.

Houwink, R. (1953). *Elasticity, Plasticity and Structure of Matter*, Harren Press, Washington, D. C.

Hueckel, T. & Baldi, G. (1990). Thermoplasticity of saturated clays: Experimental constitutive study, *Journal of Geotechnical Engineering, ASCE* 116(12): 1778–1796.

Hueckel, T. & Pellegrini, R. (1989). Modelling of thermal failure of saturated clays, *in* S. Pietruszczak & G. N. Pande (eds), *Numerical Models in Geomechanics*, Elsevier, Amsterdam, pp. 81–90.

Hueckel, T. & Pellegrini, R. (1992). Effective stress and water pressure in saturated clays during heating-cooling cycles, *Canadian Geotechnical Journal* 29(6): 1095–1102.

Iler, R. H. (1955). *The Colloid Chemistry of Silica and Silicates*, Cornell University Press, Ithaca, NY.

Janbu, J. (1985). Soil models in offshore engineering, *Géotechnique* 35(3): 241–281.

Kaliakin, V. N. (1985). *Bounding Surface Elastoplasticity-Viscoplasticity for Clays*, PhD thesis, University of California, Davis, Davis, CA.

Kaliakin, V. N. (1994). Numerical implementation and solution strategies for a thermo-elastoplastic-viscoplastic model for cohesive soils, *Computing Systems in Engineering* 5(2): 203–214.

Kaliakin, V. N. & Dafalias, Y. F. (1990a). Theoretical aspects of the elastoplastic-viscoplastic bounding surface model for cohesive soils, *Soils and Foundations* 30(3): 11–24. Japanese Society of Soil Mechanics and Foundation Engineering.

Kaliakin, V. N. & Dafalias, Y. F. (1990b). Verification of the elastoplastic-viscoplastic bounding surface model for cohesive soils, *Soils and Foundations* 30(3): 25–36. Japanese Society of Soil Mechanics and Foundation Engineering.

Kaliakin, V. N. & Nieto-Leal, A. (2013). Towards a generalized bounding surface model for cohesive soils, *in* C. Hellmich, C. B. Pichler & C. Adam (eds), *Proceedings of the 5th Biot Conference on Poromechanics (BIOT-5)*, Vienna, Austria, pp. CD–ROM.

Kèzdi, A. (1974). *Handbook of Soil Mechanics*, Elsevier, Amsterdam, The Netherlands.

Khan, A. (2000). A liquid water model: Density variation from supercooled to superheated states, prediction of H-bonds, and temperature limits, *Journal of Physical Chemistry B* 104: 11268–11274.

Lacerda, W. A. (1976). *Stress-Relaxation and Creep Effects on Soil Deformation*, PhD thesis, University of California, Berkeley, Department of Civil Engineering.

Lacerda, W. A. & Houston, W. N. (1973). Stress relaxation in soils, *Proceedings of the 8th International Conference on Soil Mechanics and Foundation Engineering*, Moscow, USSR, pp. 221–227.

Ladd, C. C., Foott, R., Ishihara, K., Schlosser, F. & Poulos, H. G. (1977). Stress-deformation and strength characteristics, *Proceedings of the 9th International Conference on Soil Mechanics and Foundation Engineering*, Tokyo, pp. 421–494.

Ladd, C. C. & Preston, W. B. (1965). On the secondary compression of saturated clays, *Technical Report R65-59*, MIT, Department of Civil Engineering. Research in Earth Physics, Phase Report No. 6.

Laguros, J. G. (1969). Effect of temperature on some engineering properties of clay soils, *Proceedings of International conference on the Effects of Temperature and Heat on Engineering Behaviour of Soils*, Highway Research Board, National Research Council, Special Report 103, Washington, DC, pp. 186–193.

Lambe, T. W. (1953). The structure of inorganic soils, *Proceedings of ASCE* 79: 1–49. Separate 315.

Lambe, T. W. (1958). The structure of compacted clay, *Journal of the Soil Mechanics and Foundations Division, ASCE* 84(SM2): 1–34.

Lambe, T. W. & Whitman, R. V. (1979). *Soil Mechanics, SI Version*, John Wiley and Sons, New York, NY.

Leonards, G. A. (1977). Panel discussion, *Proceedings of the 9th International Conference on Soil Mechanics and Foundation Engineering*, Tokyo, pp. 384–386.

Leonards, G. A. & Altschaeffl, A. G. (1964). Compressibility of clay, *Journal of the Soil Mechanics and Foundations Division, ASCE* 90(SM5): 133–156.

Leroueil, S. & Marques, M. E. S. (1996). State of the art: Importance of strain rate and temperature effects in geotechnical engineering, *in* T. C. Sheahan & V. N. Kaliakin (eds), *Measuring and Modeling Time Dependent Soil Behavior, ASCE Geotechechnical Special Technical Publication*, ASCE, New York, NY, pp. 1–60.

Ling, H. I., Yue, D., Kaliakin, V. N. & Themelis, N. J. (2002). An anisotropic elasto-plastic bounding surface model for cohesive soils, *Journal of Engineering Mechanics, ASCE* 28(7): 748–758.

Lingnau, B. E., Graham, J. & Tanaka, N. (1995). Isothermal modeling of sand-bentonite mixtures at elevated temperatures, *Canadian Geotechnical Journal* 32(1): 78–88.

Lo, K. Y. (1961). Secondary compression of clays, *Journal of Soil Mechanics and Foundation Division, ASCE* 87(SM4): 61–66.

Lo, K. Y. (1969a). The pore pressure-strain relationships of normally consolidated undisturbed clays - part i. theoretical considerations, *Canadian Geotechnical Journal* 7(4): 383–394.

Lo, K. Y. (1969b). The pore pressure-strain relationships of normally consolidated undisturbed clays - part ii. experimental investigation and practical applications, *Canadian Geotechnical Journal* 7(4): 395–412.

Martin, R. T. (1960). Adsorbed water on clay: A review, *Clays and Clay Minerals* 9(1): 28–70.

Martin, R. T. (1962). Adsorbed water on clay, *in* A. Swineford (ed.), *Proceedings of the Ninth National Congress on Clays and Clay Minerals*, Pergamon Press, New York, NY, pp. 28–70.

Mesri, G. & Choi, Y. K. (1985). The uniqueness of the end-of-primary (eop) void ratio-effective stress relationship, *Proceedings of the Eleventh International Conference on Soil Mechanics and Foundation Engineering*, San Francisco, CA, pp. 587–590.

Michaels, A. S. (1959). Discussion of physico-chemical properties of soils: Soil water systems, *Journal of the Soil Mechanics and Foundations Division, ASCE* 85(SM2): 91–92.

Mitchell, J. K. (1956). The fabric of natural clays and its relation to engineering properties, *Highway Research Board Proceedings* 35: 693–713.

Mitchell, J. K. (1964). Shearing resistance of soils as a rate process, *Journal of the Soil Mechanics and Foundations Division, ASCE* 90(SM1): 29–61.

Mitchell, J. K. (1969). Temperature effects on the engineering properties and behavior of soils, *Proceedings of International conference on the Effects of Temperature and Heat on Engineering Behaviour of Soils*, Highway Research Board, National Research Council, Special Report 103, Washington, DC, pp. 9–28.

Mitchell, J. K. (1976). *Fundamentals of Soil Behavior*, John Wiley and Sons, New York, NY.

Mitchell, J. K. & Campanella, R. G. (1964). Creep studies on saturated clays, *ASTM-NRC Symposium on Laboratory Shear Testing of Soils* ASTM 361: 90–103. Special Technical Publication, Ottawa, Canada.

Mitchell, J. K., Campanella, R. G. & Singh, A. (1968). Soil creep as a rate process, *Journal of the Soil Mechanics and Foundations Division, ASCE* 94(SM1): 231–253.

Mitchell, J. K. & Soga, K. (2005). *Fundamentals of Soil Behavior*, 2nd edn, John Wiley and Sons, New York, NY.

Mooney, R. W., Keenan, A. G. & Wood, L. A. (1952). Adsorption of water vapor on montmorillonite, ii., *Journal of the American Chemical Society* 74: 1371–1374.

Morin, R. & Silva, A. J. (1984). The effects of high pressure and high temperature on some physical properties of ocean sediments, *Journal of Geophysical Research* 89(B1): 511–526.

Moritz, L. (1995). Geotechnical properties of clay at elevated temperatures, *in* Y. Hiroshi & O. Kusakabe (eds), *International Symposium on Compression and Consolidation of Clayey Soils - IS-Hiroshima 95*, Balkema Publishers, The Netherlands, pp. 267–272.

Murayama, S. (1969). Effect of temperature on elasticity of clays, *Highway Research Board Special Report* 103: 194–203.

Murayama, S., Sekiguchi, H. & Ueda, T. (1974). A study of the stress-strain-time behavior of saturated clays based on a theory of nonlinear viscoelasticity, *Soils and Foundations* 14(2): 19–33.

Murayama, S. & Shibata, T. (1961). Rheological properties of clays, *Proceedings of the 5th International Conference on Soil Mechanics and Foundation Engineering*, Paris, France, pp. 269–273.

Murayama, S. & Shibata, T. (1964). Flow and stress relaxation of clays (theoretical studies on the rheological properties of clay - part I), *in* P. M. Sirieys & J. Kravtchenko (eds), *Proceedings of the IUTAM Symposium on Rheology and Soil Mechanics*, Springer-Verlag, Berlin, Grenoble, France, pp. 99–129.

Noble, C. A. & Demirel, T. (1969). Effect of temperature on the strength behavior of cohesive soil, *Proceedings of International conference on the Effects of Temperature and Heat on Engineering Behaviour of Soils*, Highway Research Board, National Research Council, Special Report 103, Washington, DC, pp. 204–219.

Paaswell, R. E. (1967). Temperature effects on clay soil consolidation, *Journal of Soil Mechanics and Foundation Engineering, ASCE* 93(SM3): 9–22.

Pagen, C. A. & Jagannath, B. N. (1967). Evaluation of soil compaction by rheological techniques, *Highway Research Record* 177: 22–43.

Perzyna, P. (1966). Fundamental problems in viscoplasticity, *Advances in Applied Mechanics* 9: 243–377.

Pillai, R., Robinson, R. & Boominathan, A. (2011). Effect of Microfabric on Undrained Static and Cyclic Behavior of Kaolin Clay, *Journal of Geotechnical and Geoenvironmental Engineering, ASCE* 137(4): 421–429.

Plum, R. L. & Esrig, M. I. (1969). Some temperature effects on soil compressibility and pore water pressure, *Proceedings of International conference on the Effects of Temperature and Heat on Engineering Behaviour of Soils*, Highway Research Board, National Research Council, Special Report 103, Washington, DC, pp. 231–242.

Prashant, A. & Penumadu, D. (2007). Effect of microfabric on mechanical behavior of kaolin clay using cubical true triaxial testing, *Journal of Geotechnical and Geoenvironmental Engineering, ASCE* 133(4): 433–444.

Pusch, R. (1966). Quick clay microstructure, *Engineering Geology* 1(6): 433–443.

Rosenqvist, I. T. (1959). Physico-chemical properties of soils: Soil water systems, *Journal of the Soil Mechanics and Foundations Division, ASCE* 85(SM2): 31–54. also in Norwegian Geotechnical Institute, 37: 1–14 (1960).

Sachan, A. & Penumadu, D. (2007). Effect of microfabric on shear behavior of kaolin clay, *Journal of Geotechnical and Geoenvironmental Engineering, ASCE* 133(3): 306–318.

Schiffman, R. L., Ladd, C. C. & Chen, A. T. (1966). Secondary consolidation of clay, *in* J. Kravtchenko & P. M. Sirieys (eds), *Proceedings of the Rheology and Soil Mechanics Symposium, IUTAM*, Springer-Verlag, Grenoble, pp. 273–304.

Schofield, R. K. & Samson, H. R. (1954). Flocculation of kaolinite due to the attraction of oppositely charged crystal faces, *Faraday Society, London* 18: 135–145. Discussion.

Scott, C. R. (1980). *An Introduction to Soil Mechanics and Foundations*, Applied Science Publishers, Ltd., London, UK.

Scott, R. F. (1963). *Principles of Soil Mechanics*, Addison-Wesley Publishing Co., Inc., Reading, MA.

Sheahan, T. C. & Kaliakin, V. N. (1998). Integrating micromechanics in modeling relaxation behavior of cohesive soils, *in* J.-F. Thimus, Y. Abousleiman, A. H.-D. Cheng, O. Coussy & E. Detournay (eds), *Poromechanics, A Tribute to Maurice A. Biot, Proceedings of the Biot Conference on Poromechanics*, Balkema, Rotterdam, Université catholique de Louvain, Louvain-la-Neuve, Belgium, pp. 147–152.

Sheahan, T. C. & Kaliakin, V. N. (1999). Microstructural considerations and validity of the correspondence principle for cohesive soils, *in* N. Jones & R. Ghanem (eds), *Proceedings of the 13th ASCE Engineering Mechanics Conference*, ASCE, Baltimore, MD, pp. CD–ROM.

Sheahan, T. C., Ladd, C. C. & Germaine, J. T. (1994). Time-dependent triaxial relaxation behavior of a resedimented clay, *ASTM Geotechnical Testing Journal* 17(4): 444–452.

Shen, C. K., Arulanandan, K. & Smith, W. S. (1973). Secondary consolidation and strength of a clay, *Journal of the Soil Mechanics and Foundations Division, ASCE* 99(SM1): 95–110.

Sherif, M. A. & Burrous, C. M. (1969). Temperature effects on the unconfined shear strength of saturated, cohesive soil, *Proceedings of International conference on the Effects of Temperature and Heat on Engineering Behaviour of Soils*, Highway Research Board, National Research Council, Special Report 103, Washington, DC, pp. 267–272.

Shibata, T. & Karube, D. (1969). Creep rate and creep strength of clays, *Proceedings of the 7th International Conference on Soil Mechanics and Foundation Engineering*, Mexico City, pp. 361–367.

Sides, G. & Barden, L. (1971). The microstructure of dispersed and flocculated samples of kaolinite, illite, and montmorillonite, *Canadian Geotechnical Journal* 8(3): 391–399.

Silvestri, V., Soulie, M., Touchan, Z. & Fay, B. (1988). Triaxial relaxation tests on a soft clay, *in* R. T. Donaghe, R. C. Cheney & M. L. Silver (eds), *Advanced Triaxial Testing of Soil and Rock*, ASTM, pp. 321–337. ASTM Special Technical Publication.

Sowers, G. B. & Sowers, G. F. (1970). *Introductory Soil Mechanics and Foundations*, Macmillan Publishing Co., Inc., New York, NY.

Sridharan, A., Narasimha, R. S. & Venkatappa, R. G. (1971). Shear Strength Characteristics of Saturated Montmorillonite and Kaolinite Clays, *Soils and Foundations* 11(3): 1–22.

Šuklje, L. (1957). The analysis of the consolidation process by the isotaches method, *Proceedings of the Fourth International Conference on Soil Mechanics and Foundation Engineering*, London, UK, pp. 200–206.

Tan, T. K. (1957). Discussion on: Soil properties and their measurement, *Proceedings of the 4th International Conference on Soil Mechanics and Foundation Engineering*, London, UK, pp. 87–89.

Tavenas, F., Leroueil, S., La Rochelle, P. & Roy, M. (1978). Creep behaviour of an undisturbed lightly overconsolidated clay, *Canadian Geotechnical Journal* 15(3): 402–423.

Terzaghi, K. (1925). *Erdbaumechanik auf Bodenphysikalischer Grundlage*, Franz Deuticke, Vienna.

Terzaghi, K. (1931). The static rigidity of plastic clays, *Journal of Rheology* 2(3): 253–262.

Terzaghi, K. (1941). Undisturbed clay samples and undisturbed clays, *Journal of the Boston Society of Civil Engineers* 28(3): 211–231.

Terzaghi, K. & Peck, R. B. (1967). *Soil Mechanics in Engineering Practice*, 2nd edn, John Wiley and Sons, New York, NY.

Tidfors, M. & Sällfors, G. (1989). Temperature effect on preconsolidation pressure, *ASTM Geotechnical Testing Journal* 12(1): 93–97.

Towhata, I., Kuntiwattanakul, P. & Kobayashi, H. (1993). A preliminary study of heating of clays to examine possible effects of temperature on soil-mechanical properties, *Soils and Foundations* 33(4): 184–190.

Towhata, I., Kuntiwattanakul, P., Seko, I. & Ohishi, K. (1993). Volume change of clays induced by heating as observed in consolidation tests, *Soils and Foundations* 33(4): 170–183.

Tschebotarioff, G. P. (1952). *Soil Mechanics, Foundations and Earth Structures*, McGraw-Hill Book Co., Inc., New York, NY.

van Olphen, H. (1963). *An Introduction to Clay Colloid Chemistry*, 1st edn, Wiley Interscience, New York, NY.

van Olphen, H. (1977). *An Introduction to Clay Colloid Chemistry*, 2nd edn, John Wiley and Sons, New York, NY.

Virdi, S. P. S. & Keedwell, M. J. (1988). Some observed effects of temperature variation on soil behaviour, *in* M. J. Keedwell (ed.), *International Conference on Rheology and Soil Mechanics*, Elsevier Applied Science, Coventry, UK, pp. 336–354.

Wang, Y. & Siu, W. (2006). Structure Characteristics and Mechanical Properties of Kaolinite Soils II. Effects of Structure on Mechanical Properties, *Canadian Geotechnical Journal* 43(6): 601–617.

Whitman, R. V. (1960). Some considerations and data regarding the shear strength of clays, *Proceedings of the ASCE Research Conference on the Shear Strength of Cohesive Soils*, ASCE, Boulder, CO, pp. 581–614.

Wissa, A. E. Z. (1961). *A Study of the Effects of Environmental Changes on the Stress-Strain Properties of Kaolinite*, PhD thesis, MIT, Cambridge, MA. Department of Civil Engineering.

Yao, M. & Anandarajah, A. (2003). Three-dimensional discrete element method of analysis of clays, *Journal of Engineering Mechanics, ASCE* 129(6): 585–596.

Yin, Z. & Chang, C. (2009). Microstructural modelling of stress-dependent behaviour of clay, *International Journal of Solids and Structures* 46(6): 1373–1388.

Yin, Z., Chang, C., Hicher, P. & Karstunen, M. (2009). Micromechanical analysis of kinematic hardening in natural clay, *International Journal of Plasticity* 25(8): 1413–1435.

Yin, Z., Chang, C., Hicher, P. & Wang, J. (2011). Micromechanical analysis of the behavior of stiff clay, *Acta Mechanica Sinica* 27(6): 1013–1022.

Yin, Z. Y., Hattab, M. & Hicher, P. (2011). Multiscale modeling of a sensitive marine clay, *International Journal for Numerical and Analytical Methods in Geomechanics* 35(15): 1682–1702.

Yong, R. N. & Warkentin, B. R. (1975). *Soil Properties and Behaviour*, Elsevier, Amsterdam, The Netherlands.

In: Clays and Clay Minerals
Editor: Liam R. Wesley
ISBN: 978-1-63117-779-8

Chapter 2

ESTIMATION OF DIFFUSION COEFFICIENTS FOR ORGANIC SOLUTES OF ENVIRONMENTAL CONCERN IN SATURATED CLAY-SILT MIXTURES

Derya Ayral [*] ***and Avery Demond***
Department of Civil and Environmental Engineering,
University of Michigan, Ann Arbor, MI, US

ABSTRACT

Clay-rich soil lenses and layers in the subsurface play an important role in determining the efficiency of remediation of waste sites contaminated with hazardous organic compounds. Often organic solvents, such as trichloroethylene or tetrachloroethylene, are spilled or disposed of in such a manner that they enter the subsurface. There they dissolve in the groundwater and accumulate over time in the clayey lenses and layers located in the saturated zone. During the remediation of these waste sites, the contaminants are then slowly released, contributing to elevated concentrations in groundwater over an extended period of time. Because of the low permeability of the clayey lenses and layers, the main transport process into and out of these locations is considered to be diffusion. Thus, estimating the rates of diffusion in clayey soil materials is key to determining the rates at which these hazardous compounds may be released during clean-up activities.

Correlations have been developed to estimate diffusion coefficients in soil media based on the diffusion coefficient of the compound in water and the porosity of the soil. However, the use of these methods may be limited as they suggest an increase in the diffusion coefficient with an increasing porosity whereas lower diffusion coefficients are usually measured in clay materials despite their higher porosity. Furthermore, the flexibility of the structure of smectitic clay minerals can result in variable porosities. Because remediation time frames depend on the diffusional rate of release of hazardous organic solutes from clayey soils, this study quantitatively assessed the performance of commonly-used methodologies to estimate the diffusion coefficient of organic solutes in saturated clay-silt mixtures. The results suggest that the performance of these methodologies is acceptable (average relative error of 61%) if the soil contains less than

[*] Corresponding author: ayrald@umich.edu.

25% clay, whereas high relative errors (> 151%) may occur for soils containing more than 25% clay. To improve predictions for the materials with high clay contents, two methodologies were developed from literature data to estimate the effective diffusion coefficient as a function of dry bulk density, which yielded relative errors of 83% and 48%. Consequently, these methods are recommended as alternatives to those commonly used to estimate effective diffusion coefficients of organic solutes in saturated clayey soils.

1. INTRODUCTION

Two of the most common organic contaminants found at hazardous waste sites in the United States are trichloroethylene (TCE) and tetrachloroethylene (PCE) (SERDP, 2006). These chemicals are used extensively as cleaning solvents in processes like degreasing and dry cleaning because of their ability to dissolve oil, dirt, and stains (ATSDR, 1997). Unfortunately, their improper disposal has resulted in the introduction of these solvents into the subsurface environment. As a consequence, these contaminants are frequently found in groundwater at concentrations above the maximum contaminant levels that are permitted in drinking water.

TCE and PCE belong to a group of organic solvents that are sometimes referred to as dense non-aqueous phase liquids (DNAPLs) (Cohen et al., 1993) as their density is greater than that of water. They also have a low solubility in water, resulting in the fact that they can persist as a separate liquid phase in the subsurface. Because they are denser than water, DNAPLs travel through the groundwater column under the force of gravity. Due to their low permeability, layers and lenses that contain silt and clay may limit the downward vertical movement of such contaminants, with the result that the DNAPLs form pools on top of these surbsurface strata. These pools then slowly dissolve, allowing transport into these strata via diffusion.

Once contaminants enter the low permeability layers, they cannot be flushed out easily. As a result, these zones become contaminant storage areas (Chapman and Parker, 2005). Studies such as that by Parker et al. (2008) show that even a thin clay layer can result in groundwater concentrations above permissible levels for decades after the original source is isolated or removed. Thus, these strata that have accumulated a significant mass of contaminants over time can be regarded as long-term secondary contamination sources (Sale et al., 2008; Stroo et al., 2012).

The process of the accumulation in and the release from low permeability geologic materials of hazardous compounds is thought to be dominated by diffusion (Mackay and Cherry, 1989; Ball et al., 1997; Wilson, 1997; Chapman and Parker, 2005; Parker et al., 2008). Thus, calculations of accumulated mass and the efficiency of remediation are highly dependent on estimated diffusion rates. Since there are limited experimental studies providing measurements of the diffusion coefficients for organic contaminants in geologic media, particularly unconsolidated materials which contain appreciable quantities of clay, this study examined the available data, and analyzed the ability of established correlations to estimate these coefficients.

2. DIFFUSION IN POROUS MEDIA

Effective Diffusion Coefficient

Diffusion is defined as the transport arising from the Brownian motion of molecules due to their relative kinetic energy (Weber and Digiano, 1996). Diffusion is governed by Fick's first law, written here in one dimension for solutes in bulk water:

$$J_D = -D_{aq}\frac{dC}{dx} \tag{1}$$

where J_D is the diffusional flux $\left(\frac{M}{L^2T}\right)$, D_{aq} is the diffusion coefficient in bulk water $\left(\frac{L^2}{T}\right)$, C is the aqueous phase concentration of the diffusing species $\left(\frac{M}{L^3}\right)$, and x is the spatial coordinate (L).

When considering diffusion in porous media, the cross section area available for the movement of molecules is reduced due to the presence of a solid phase. If the pores can be modeled as straight capillary tubes, a continuity of flux between that measured external to the porous medium (Figure 1A) and that in the porous medium (Figure 1B) dictates the following relation (Weber and Digiano, 1996):

$$D_{aq}\frac{dC}{dx}\Big|_{surface} = \varepsilon D_c \frac{dC}{dx}\Big|_{within\ pore} \tag{2}$$

where D_c is the diffusion coefficient in the pores $\left(\frac{L^2}{T}\right)$, and ε is the porosity of the porous medium (volume of pores/total volume, or $\left(\frac{L^3}{L^3}\right)$).

In addition to the reduced volume available for transport, the modification of the description of diffusion for porous media must account for the increase in path length that the solute molecules must travel (Figure 1C). Dullien (1992) compared two models of porous media, one with straight capillary tubes and one with tortuous tubes. He defined tortuosity, τ, as the ratio of the path length travelled by the solute molecules, L_e to the linear path length, L:

$$\tau = \frac{L_e}{L} \tag{3}$$

In order to correct for the increase in travel distance, the diffusion coefficient for the straight pore system, D_c, needs to be divided by the tortuosity, τ. Furthermore, if the number of capillary tubes is held constant in moving from the system in Figure 1B to that in Figure 1C, then the porosity increases by a factor of L_e/L. Thus, it is necessary to divide the porosity by this ratio in order to maintain the same porosity as in the straight capillary tube system. As a result, the square of L_e/L appears in the diffusive flux equation for the tortuous capillary tube system:

$$J_D = -D_{aq} * \frac{\varepsilon}{\frac{L_e}{L}} * \frac{dC}{dx * \frac{L_e}{L}} = -D_{aq} * \frac{\varepsilon}{\left(\frac{L_e}{L}\right)^2} * \frac{dC}{dx} \tag{4}$$

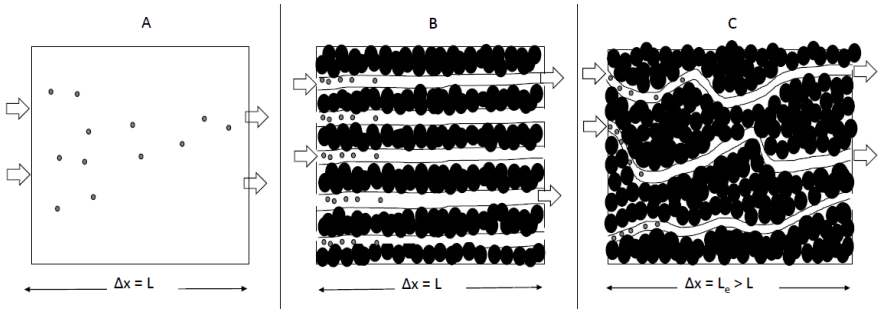

Figure 1. Diffusion in (A) bulk aqueous phase, (B) porous medium with straight pores and (C) porous medium with tortuous pores.

Table 1. Various definitions of the effective diffusion coefficient

D_e	Explanation	Studies Using the Definition
$D_{aq}\,\varepsilon\,\tau$	τ defined by Eqn. 8; ε included.	Oscarson et al. (1992); Oscarson and Hume (1994).
$\frac{D_{aq}\,\varepsilon}{\tau_f}$	τ_f defined by Eqn. 5; ε included.	Grathwohl (1998); Boving and Grathwohl (2001); García-Gutiérrez et al. (2006).
$\frac{D_{aq}}{\tau}$	τ defined by Eqn. 3; ε excluded.	Ball et al. (1997); Young and Ball (1998).
$D_{aq}\,\tau$	τ defined by Eqn. 8; ε excluded.	Johnson et al. (1989); Shackelford et al. (1989); Barone et al. (1992); Cho et al. (1993); Sawatsky et al. (1997); Roehl and Czurda, (1998).

The square of L_e/L is sometimes termed the tortuosity factor, denoted τ_f (Epstein, 1989):

$$\tau_f = \left(\frac{L_e}{L}\right)^2 \tag{5}$$

Based on the conceptualization outlined here, the effective diffusion coefficient, D_e, for diffusion in a porous medium is then (Grathwohl, 1998):

$$D_e = \frac{D_{aq}\,\varepsilon}{\tau_f} \tag{6}$$

and the diffusive flux (per unit bulk area) in a porous medium is given by:

$$J_D = -D_e \frac{dC}{dx} \tag{7}$$

The porosity in Eqn. 6 is the effective porosity, which may be less than the overall porosity of the porous medium if there are pores that do not contribute to the overall diffusive flux such as dead-end pores (Lever et al., 1985). If the pores are sufficiently small that their diameter is on the same order as that of the diffusing solute, an additional factor, the constrictivity, δ, may be applied.

Table 1 provides a summary of definitions for the effective diffusion coefficient. A summary was also recently included in Shackelford and Moore (2013). A number of the variations stem from the way in which tortuosity and the tortuosity factor are defined. Sometimes tortuosity is defined as the inverse of that in Eqn. 3 (Porter et al., 1960; Bear, 1972; Johnson et al., 1989; Shackelford et al., 1989; Oscarson et al., 1992), or:

$$\tau = \frac{L}{L_e} \tag{8}$$

yielding a factor that is smaller than 1 rather than greater. To add to the confusion, the terms tortuosity and the tortuosity factor are sometimes used interchangeably, as Epstein (1989) pointed out. Some studies do not utilize the terminology of tortuosity or tortuosity factor, but talk instead of hindrance factors (Mott and Weber, 1991; Khandelwal et al., 1998). In addition, some studies describe effective diffusion coefficients that include porosity (Oscarson et al., 1992; Oscarson and Hume, 1994) whereas others exclude it (Johnson et al., 1989; Shackelford et al., 1989; Ball et al., 1997), as this is a parameter that can be determined independently (Shackelford, 1991).

Apparent Diffusion Coefficient

Fick's first law for a porous medium given in Eqn. 7 defines the diffusive flux at steady state. When the Fick's first law is combined with a mass balance, Fick's second law is obtained (Crank, 1975), written here for diffusion in a porous medium:

$$\frac{dC}{dt} = D_{app}\frac{d^2C}{dx^2} \tag{9}$$

where D_{app} is the diffusion coefficient observed under nonsteady-state conditions in a porous medium. D_{app} is called by various names, including the apparent diffusion coefficient (Grathwohl, 1998), the reactive diffusion coefficient (Myrand et al., 1992) and the effective diffusion coefficient of a reactive solute (Shackelford et al., 1989). The primary difference between D_e and D_{app} is that D_{app} is a function of sorption characteristics of the porous medium whereas D_e is considered to be independent of sorption, and dependent only on the geometry of the porous medium.

Since sorption implies a partitioning of the solute to the solid phase, the transient diffusive flux is reduced, thus:

$$D_{app} = \frac{D_e}{R} \tag{10}$$

where R is the retardation factor. The form of R depends on how the sorption relationship is described. Two common forms are a linear relationship and the nonlinear Freundlich isotherm, both of which assume local equilibrium. If the sorption isotherm is linear, then:

$$R = 1 + \frac{K_d\rho_b}{\varepsilon} \tag{11}$$

where ρ_b is the bulk density of the porous medium $\left[\frac{M}{L^3}\right]$ and K_d is the distribution coefficient $\left[\frac{L^3}{M}\right]$. In the case of the Freundlich isotherm, R will have the form of:

$$R = 1 + \frac{K_F C^{\frac{1}{n}-1}\rho_b}{\varepsilon} \tag{12}$$

where K_F and n are characteristic parameters of the isotherm, and C is the equilibrium concentration in the aqueous phase.

Apparent diffusion coefficients have also been defined by the following relation:

$$D_{app} = \frac{D_e}{\frac{\alpha}{\varepsilon}} \tag{13}$$

where α is called the capacity factor (Grathwohl, 1998), and $\alpha = \varepsilon R$. Since, the calculation of D_e from measurements of D_{app} depends on how the isotherm relationship is described, it is critical to report the form of the sorption relationship when calculating values of D_e from measurements of D_a (Shackelford, 1991) and to recognize that the values may change depending on how the sorption relationship is modeled.

Measurement of the Effective Diffusion Coefficient

Measurements of diffusion coefficients of organic solutes in geologic media have been made using both steady state and nonsteady methods. The main advantage of steady-state methods is that measured diffusion coefficients are theoretically independent of the retardation factor. But, in order to achieve a constant flux and evaluate the diffusion coefficient from Fick's first law (Eqn. 7), the concentration gradient must be maintained constant, thus requiring the construction of an experimental system in which the influent and effluent concentrations are essentially maintained at the same value (Grathwohl, 1998). Furthermore, the time to establish this condition could be considerable especially for sorbing solutes or reactive soils, as Garcia-Gutierrez et al. (2006) determined a time to steady-state of five years for tracer diffusion through a bentonite (>90% smectites) plug with a thickness of two cm.

To avoid the long times that may be necessary to reach steady state, transient state experiments may be preferred. Another advantage of transient methods is the concentration gradient across the domain does not need to be maintained at a constant value. However, obtaining the concentration profile along the column may require destructively slicing the column or the extraction and analysis of pore water concentrations (Mott and Weber, 1991; Parker, 1996; Donahue et al., 1999), both of which may be problematic in the case of volatile organic solutes. Furthermore, the diffusion coefficient obtained by analyzing the concentration profile is the apparent diffusion coefficient, so sorption characteristics of the soil have to be determined independently to obtain the effective diffusion coefficient (Shackelford, 1991).

Table 2 presents a summary of measurements of diffusion coefficients for organic solutes in saturated soils containing clay. As the table shows, the procedures vary considerably from

one study to another. Nonsteady state experiments are preferred. Most of these measurements involve the fitting of solutions to the nonsteady-state diffusion equation (Eqn. 9) to concentrations measured in the source and/or collection reservoirs (Barone et al., 1992; Myrand et al., 1992; Headley et al., 2001; Itakura et al., 2003), or alternatively, solutions to the advection-dispersion equation (Khandelwal et al., 1998; Young and Ball, 1998).

The reported clay content ranges from 14-87%, with the mineralogy primarily consisting of non-expansive clays. However, some studies did use appreciable percentages of expansive clays (e.g., Sawatsky et al., 1997; Donahue et al. 1999). These studies restricted the swelling using different pressures, but the impact of swelling on the diffusion coefficient was not discussed.

3. ESTIMATION OF RELATIVE DIFFUSIVITY

Because of the paucity of experimental measurements, many studies examining the accumulation of organic solutes in clayey zones in the subsurface use estimated diffusion coefficients (e.g., Ball et al., 1997; Parker et al., 2004). Based on Eqn. 6, estimating the effective diffusion coefficient requires the diffusion coefficient in water, the tortuosity factor and the porosity available for diffusion. The aqueous diffusion coefficient for a number of organic contaminants can be obtained from the literature (Poling et al., 2001) or can be estimated using estimation techniques such as Hayduk and Laudie (1974) (as in Montgomery, 2000). However, independent assessments of the tortuosity factor can be challenging and, as a result, empirical methods have been developed to estimate the ratio of the effective diffusion coefficient to the aqueous diffusion coefficient, or the relative diffusivity, as a function of porosity:

$$\frac{D_e}{D_{aq}} = \frac{\varepsilon}{\tau_f} = f(\varepsilon) \tag{14}$$

Since the presence of the pore structure influences more than just solute diffusion through a porous medium, the reduction in the diffusion coefficient can be estimated in analogy with other properties. The formation resistivity factor, F, is defined as the ratio of the electrical resistance of the porous medium saturated with an electrolyte (e.g., water), R_o, to the electrical resistance of the electrolyte itself, R_w. According to Archie (1942):

$$\frac{R_o}{R_w} = \varepsilon^{-m} \tag{15}$$

where m is an empirical exponent whose value ranges from 1.3 to 2 for sand and sandstone (Archie, 1942). Similar to Eqn. 15, many of the models for estimating the relative diffusivity in soils present it as a function of porosity only, and state that it is not affected by parameters like sorption characteristics of porous medium, type of solute (Petersen et al., 1994; Jin and Jury, 1996) or temperature (Grathwohl, 1998).

Table 2. Summary of measured diffusion coefficients for organic solutes in saturated clayey soils

Solute[a]	Soil	Type of measurement	Porosity (ε)	D_e; D_{aq}; $[D_e/D_{aq}]^b$	$D_{app}{}^b$	R; $K_d{}^b$	Notes	Reference
1,4-DCB 4-CP	Synthetic soil mixture containing silica sand, kaolinite, and Na-bentonite; L = 0.3 - 0.5 cm.	"Quasi steady state" (source and collection reservoirs sampled at 10 and 20 days after an equilibration time of two weeks).	0.40 (2% bent.) 0.43 (4% bent.) 0.48 (4% bent.)	2.41; *8* [0.301] (DCB) 2.34; *8.9* [0.263] (CP) 2.65; *8* [0.331] (DCB) 2.59; *8.9* [0.291] (CP) 3.05; *8* [0.381] (DCB) 3.05; *8.9* [0.343] (CP)			Confining pressure is 4 psi. Study reported hindrance factor (H) which is defined as D_{aq}/D_e. D_e is calculated as D_{aq}/H.	Mott and Weber (1991)
Lindane	Synthetic soil mixture containing silica sand, kaolinite, and Na-bentonite; L = 0.3 - 0.5 cm.	Non-steady state (columns sectioned at 8, 16 and 32 days).	0.46 (avg. of 4% bentonite values is assumed)	2.4; 5.6 [0.429]		K_F = 3.84 x 10-4 ; 1/n = 1.17	Sorption of lindane is described by Freundlich isotherm, parameter values compatible with units of mg/g and mg/L; Confining pressure = 4 psi. Study reported D_e.	Mott and Weber (1991)
Acetone 1,4-Dioxane Aniline	Grey clay soil from Sarnia, ON, Canada (45% clay, mainly chlorite and illite); L = 1.6 cm.	Non-steady state (source and collection reservoirs sampled at two-day intervals over 14 days).	0.39 ρ_s = 2.73 g/cm^3 ρ_b = 1.68 g/cm^3	2.2; *12.8* [0.172] 1.6; *9.7* [0.165] 2.7; *10.5* [0.257]	1.20 0.90 0.40	1.8; [0.19] 1.7; [0.17] 6.6; [1.3]	Soil was placed in the cell saturated. Study reported D_e. εD_e is reported here in accordance with Eqn. 6. Batch tests indicated linear isotherms. R is calculated from	Barone et al. (1992) Barone et

Solute[a]	**Soil**	**Type of measurement**	**Porosity (ε)**	**D_e; D_{aq}; $[D_e/D_{aq}]$**[b]	**D_{app}**[b]	**R; K_d**[b]	**Notes**	**Reference**
Chloroform Toluene				4.3; *10* [0.430] 5.4; *8.5* [0.635]	0.16 0.05	26.8; [6.0] 113.0; [26]	reported values of ρ_b, K_d (fitted to data) and ε. using Eqn. 11. D_{app} is calculated as D_e/R.	al. (1992)
Benzene TCE Toluene CB	Glaciolacustrine clay from Sarnia, ON, Canada (40% clay, mostly chlorite and illite); L = 10 cm.	Non-steady state (source reservoir is sampled over 23 days).	0.34 ρ_b= 1.77 g/cm^3	3.5; *10.9* [0.321] 3.5; *9.4* [0.372] 3.0; *8.5* [0.353] 2.9; *8.7* [0.333]	0.11 0.06 0.04 0.03	32.3 58.4 74 98.4	Soil used directly from soil sampler. Study reported D_{app} and R. Batch tests indicated linear isotherms. D_e is calculated from D_{app}*R (fitted to data).	Myrand et al. (1992)
DCM	Silty-clay glacial till from Sarnia, ON, Canada (38% clay, mainly chlorite and muscovite); L = 9 cm.	Non-steady state (column sectioned at two weeks).	0.34 ρ_b= 1.71 g/cm^3	3.5; *11.5* [0.304]	2.94	1.19	Soil used directly from soil sampler. Study reported D_e and R. D_{app} was calculated from D_e /R.	Parker (1996)
1-Naphthol	Weathered shale (43 % clay, mainly montmorillonite); L = 0.4 cm.	Steady state (collection reservoir sampled over about 30 days; steady-state reached in 21 days).	(avg) ρ_b =1.26 g/cm^3 ρ_b =1.40 g/cm^3 ρ_b =1.57 g/cm^3	(avg) 0.17; *7.5* [0.023] 0.20; *7.5* [0.027] 0.067; *7.5* [0.009]	(avg) 0.0019 0.0017 0.00044	(avg) 94 [39] 116 [39] 151 [39]	Sample was partially saturated, compacted to a particular ρ_b, and then fully saturated. Batch tests indicated linear isotherms. Study reported D_e and R. Reported values of D_{es} were taken as D_e, based on Eqn. 3 in the reference.	Sawatsky et al. (1997)

Table 2. (Continued)

Solute[a]	Soil	Type of measurement	Porosity (ε)	D_e; D_{aq}; $[D_e/D_{aq}]$[b]	D_{app}[b]	R; K_d[b]	Notes	Reference
Naphthalene	Weathered shale (43 % clay, mainly montmorillonite); L = 0.4 cm.		ρ_b =1.49 g/cm^3	0.024; *7* [0.003]	0.00025	94 [27]	D_{app} is calculated from D_{es} and R.	Sawatsky et al. (1997)
Naphthalene	Montmorillonite (reference clay from Source Clay Repository, Columbia, MS; all cations were replaced with Ca^{2+} prior to use); L = 0.4 cm.		ρ_b =1.45 g/cm^3	0.069; *7* [0.010]	0.069	1 [27]		
TCE	Jurassic clay from Frommern, Germany (52% clay);	Steady state (collection reservoir sampled up to 20 days).	(avg) 0.45; ρ_s =2.67	(avg) 0.89; *9.4* [0.095]	(avg) 0.27	(avg) 3.3	Material was pressed tightly into the diffusion cell ring. Study reported D_e, D_{app} and α. R is calculated from α/ε. $D_{app.}$ is calculated from D_e and R using Eqn. 11.	Grathwohl (1998)
	Jurassic clay from Lustnau, Germany (41% clay);		0.41; ρ_s =2.65	1.37; *9.4* [0.146]	0.24	5.8		
	Triassic clay from Haigerloch Germany, (55% clay);		0.46 ρ_s =2.7	0.72; *9.4* [0.077]	0.73	1.0		

Solute[a]	Soil	Type of measurement	Porosity (ε)	D_e; D_{aq}; $[D_e/D_{aq}]$[b]	D_{app}[b]	R; K_d[b]	Notes	Reference
	Activated Na-bentonite from Friedland, Germany (87% clay); Silt-clayey soil from Darmstadt, Germany (6% clay); L = 1 cm.		0.55; ρ_s =2.65 0.34; ρ_s =2.65	0.21; *9.4* [0.022] 1.25; *9.4* [0.133]	0.52 1.08	0.4 1.2		Grathwohl (1998)
TCE Aniline	Mixture of "backfill soil from local source" (45% < 75 μm) and 6% Na-bentonite; L = 11.8 cm (avg).	Non-steady state (diffusion coefficient determined by fitting the adv-dispersion equation to column exp'ts which last 25-49 days).	0.33 (avg)	1.27; *9.4* [0.135] (avg) 0.81; *10.5* [0.077] (avg)	0.99 0.62	1.28; [0.051] 1.25; [0.044]	Soil was wet uniformly and placed into cell and saturated by increasing the pressure from 28 to 315 kPa. Study reported D_e/ε. D_e is calculated from D_e/ε and ε. R is calculated from K_d (fitted to data), ρ_b and ε using Eqn. 11.	Khandelwal et al. (1998)
PCE 1,2,4-TCB	Silty clay loam from Dover AFB, DE (35% clay, clay minerals identified were kaolinite and chlorite); L = 25 cm, diffusion distance = 0.59 cm	Non-steady state (diffusion coefficient determined by fitting a dual domain model to breakthrough experiments lasting 11 to 112 days).	0.43 ρ_b= 1.51 g/cm^3	1.8; *8.7* [0.207] 2.0; *6.7* [0.299]	0.918 0.344	1.96 5.82	Material moistened at 20%, packed and then saturated for three weeks. Study reported D_e and R (fitted to data). D_{app} is calculated from D_e/R.	Young and Ball (1998)

Table 2. (Continued)

Solute[a]	Soil	Type of measurement	Porosity (ε)	D_e; D_{aq}; $[D_e/D_{aq}]$[b]	D_{app}[b]	R; K_d[b]	Notes	Reference
Benzene	Silty clay from Regina, Saskatchewan, Canada (70 % clay, mainly smectite); L = approx. 3 cm.	Non-steady state (source and collection reservoirs sampled over 36 days; column sectioned at end of exp'ts).	0.57 (avg) ρ_s =2.81 g/cm^3	1.8; *10.9* [0.165]	0.577	3.12 [1.0]	Soil was saturated and consolidated. Batch tests indicated linear isotherms. Study reported D_e. εD_e is reported here in accordance with Eqn. 6. R is calculated from K_d (fitted to data), ρ_b and ε using Eqn. 11. D_{app} is calculated from D_e/R.	Donahue et al. (1999)
Benzene Toluene 2-FT	Synthetic soil mixture (85% sand, 12% Na-bentonite, 3% organophilic clay); L = approx. 3 cm	Non-steady state (source reservoir sampled daily for the first two weeks and then twice weekly up to 56 or 72 days).	0.34 ρ_b= 1.74 g/cm^3	1.6; *10.9* [0.144] 0.8; *8.5* [0.093] 1.1; *8.3* [0.133]	0.0076 0.0011 0.0015	206 [40] 717 [140] 717 [140]	Soil was compacted at a water content of 15% and vacuum-saturated at 70 kPa for three days. Study reported D_e. D_e for toluene and 2-fluorotoluene measured in a three-component mixture. R is calculated from K_d (fitted to data), ρ_b and ε using Eqn. 11 D_{app} is calculated as εD_e /R.	Headley et al. (2001)

Solute[a]	Soil	Type of measurement	Porosity (ε)	D_e; D_{aq}; $[D_e/D_{aq}]$[b]	D_{app}[b]	R; K_d[b]	Notes	Reference
MEK TCE Toluene	Reconstituted clay (Londonderry clay from Sydney, New South Wales, Australia) (95% finer than 75 μm, mainly kaolinite and illite); L = 1.25 – 2.97 cm. Undisturbed clay (50% finer than 75 μm, mainly kaolinite and illite); L= 1.25 cm.	Non-steady state (source and collection reservoirs sampled over 15-27 days).	Reconst. 0.41 (avg) ρ_b= 1.51 g/cm^3 (avg) Undist. 0.36 (avg) ρ_b= 1.68 g/cm^3 (avg)	1.02; *9.4* [0.109] (MEK) 0.83; *9.4* [0.088] (TCE) 0.88; *8.5* [0.104] (Toluene) 1.02; *9.4* [0.108] (MEK) 0.91; *9.4* [0.097] (TCE) 1.19; *8.5* [0.140] (Toluene)	1.02 0.53 0.57 0.70 0.54 0.61	1 [0] 1.5 [0.15] 1.5 [0.15] 1.46 [0.10] 1.69 [0.15] 1.92 [0.2]	Reconstituted sample mixed with distilled water at a moisture content of 40%, then placed in cell and compressed at 100 kPa to achieve field densities. Undisturbed samples used directly from corers. Study reported D_e. εD_e is reported here in accordance with Eqn. 6. R is calculated from K_d (fitted to data), ρ_b and ε using Eqn. 11. D_{app} is calculated as εD_e /R.	Itakura et al. (2003)

[a]CB: Chlorobenzene, 4-CP: 4-Chlorophenol, 1,4-DCB: 1,4-Dichlorobenzene, DCM: Dichloromethane, 2-FT: 2-Fluorotoluene, MEK: Methylethyl ketone, 1,2,4-TCB: 1,2,4-Trichlorobenzene, TCE: Trichloroethylene, PCE: Tetrachloroethylene.

[b]D_e: Effective diffusion coefficient ($cm^2/s * 10^6$); D_{aq}: Aqueous diffusion coefficient ($cm^2/s * 10^6$) (values from Montgomery, 2000); D_{app} : Apparent diffusion coefficient ($cm^2/s * 10^6$); R: Retardation factor; K_d : Distribution coefficient, K_F and n: Freundlich isotherm fitting parameters.

L: Thickness of sample; ρ_s: Soil particle density; ρ_b: Dry bulk density.

Table 3 summarizes methods proposed in the literature to estimate the relative diffusivity. Many of these methods are from the field of soil science where the concern is the diffusion of oxygen, for example, in the gas phase in unsaturated sandy soils. These models have been examined for their ability to predict diffusion in such systems: the Millington and Quirk (1960) and Penman (1940) models are reported to overestimate gas diffusion in unsaturated soils, whereas the Millington and Quirk (1961) model is said to provide underestimates (Sallam et al., 1984; Schaefer et al., 1995; Jin and Jury, 1996; Moldrup et al., 2000; Saripalli et al., 2002). On the other hand, the diffusion of inorganic solutes in unsaturated soil is overestimated by Millington and Quirk (1961). To provide better estimates of relative diffusivity, later methods added soil-dependent fitting parameters (Troeh et al., 1982; Shimamura, 1992; Olesen et al., 1999; Moldrup et al., 2000). However, these methods have as a drawback the necessity of determining the values of empirical parameters, for which there are not adequate means to do so independently.

To adapt these models originally developed for gas or inorganics in unsaturated soils to the transport of organic solutes in saturated soils, the total pore volume can be assumed to be filled with water; thus, $a = \theta = \varepsilon$. Under these conditions, both Millington and Quirk models yield:

$$\frac{D_e}{D_{aq}} = \varepsilon^{4/3} \tag{16}$$

The exponent has a value of 1.33, the same magnitude as the exponent given by Archie (1942) for sand. Thus, this method suggests an increase in effective diffusion coefficient with increasing porosity. However, it is observed that soils with a higher porosity such as clayey soils often have a lower diffusion coefficient (Grathwohl, 1998; Itakura et al., 2003). So, the possible overestimation of the effective diffusion coefficient for clay-containing soils may be inherent to this type of estimation method despite the report by some that Eqn. 16 gives the best agreement with experimental data (e.g., Mott and Weber, 1991; Jin and Jury, 1996).

The issues arising with methods that extrapolate from sandy soils for calculating relative diffusivities in clays have been recognized by, for example, Olesen et al. (1999) who pointed out that the goodness of the Millington and Quirk (1961) method appeared to depend on the clay content of the soil. As the clay content increased over 21%, the method gave increasingly large overestimates for solutes such as chloride in unsaturated soils. There may be a number of reasons for this increase. Clay soils that contain clay minerals such as smectites (e.g., montmorillonite and bentonite) include macropores or interparticle void volume, and micropores or interlayer void volume (Bourg et al., 2003).As Shackelford and Moore (2013) point out, the total porosity does not reflect the porosity available for diffusion for clayey soils because the water in the micropores and some fraction of that in the macropores are not available for diffusion; thus, the total porosity is not the "diffusion-accessible porosity." Additionally, diffusion-accessible porosity depends on the charge of the solute. Through experiments using uncharged species such as tritiated water (HTO), researchers have suggested that the diffusion-accessible porosity is equal to the total porosity for uncharged species even in expanding clays with large fractions of interlayer water (Garcia-Gutierrez et al., 2004; Montavon et al., 2009). However, because of the negative charge of the clay surfaces, anions may be excluded from some pores due to the repulsive force between the negatively-charged solute and the surface (Garcia-Gutierrez et al., 2004; Shackelford and

Moore, 2013). As a result, the diffusion-accessible porosity for anions may be much smaller than the total porosity (Garcia-Gutierrez et al., 2004; Shackelford and Moore, 2013).

Table 3. Methods for the determination of relative diffusivity, D_e/D_{aq}

Method	Reference
0.66a	Penman (1940)
$a^{3/2}$	Marshall (1959)
$\frac{a^2}{\varepsilon^{2/3}}$	Millington and Quirk (1960)
$\frac{a^{10/3}}{\varepsilon^2}$	Millington and Quirk (1961)
$\left(\frac{a-u}{1-u}\right)^v$	Troeh et al. (1982)
$\frac{a^{3.1}}{\varepsilon^2}$	Sallam et al. (1984)
$\alpha(a-\beta)$	Shimamura (1992)
$0.45\left(\frac{\theta-0.022b}{\varepsilon-0.022b}\right)$	Olesen et al. (1999)
Suggested θ/ε as a coefficient in Penman, Marshall and Millington-Quirk models	Moldrup et al. (2000)

ε: total porosity; a: volumetric air content; θ: volumetric water content; u, v, α and β: soil dependent empirical parameters; b: Campbell soil moisture characteristic parameter (Campbell, 1974).

Although the diffusion accessible porosity may be equal to the total porosity for uncharged species, clay pore morphology may differ from that of sand. Yang and Aplin (2010) emphasized that the relation between porosity and permeability needs to be adjusted to include the clay content as a parameter since the pore radii are smaller at higher clay contents, implying a hindrance to diffusion despite the higher porosities. In addition, expansive clays may have variable porosities depending on their degree of compaction. A number of studies have addressed the relationship between the bulk density of clay materials and the relative diffusivity for inorganic species. Figure 2 shows the data from three studies (Miyahara et al., 1991; Sato et al., 1992; Garcia-Gutierrez et al., 2004) for HTO diffusion in montmorillonite compacted to different bulk densities. These data show that relative diffusivity decreases with increasing bulk density and that the relationship between the relative diffusivity and the bulk density is log-linear. Fitting such a functional form to the combined data yields:

$$\log\left(\frac{D_e}{D_{aq}}\right) = -0.8549\rho_b - 0.0868 \tag{17}$$

Eqn. 17 provides an alternative method for estimating relative diffusivities.

Also, Bourg et al. (2006) proposed a method to calculate relative diffusivities, based on a weighted average of the relative diffusivities in macropores and interlayer space. Assuming that the constrictivity of macropores equals one and the geometric factor for the macropores and interlayer space is the same, they proposed for montmorillonite:

$$\frac{D_e}{D_{aq}} = \frac{(1-f_{interlayer})+\delta_{interlayer}f_{interlayer}}{G} \tag{18}$$

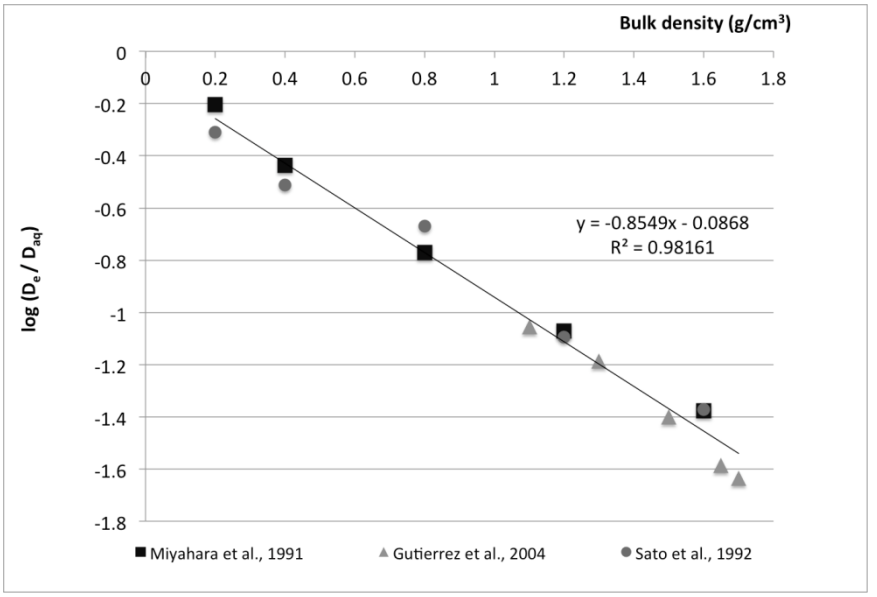

Figure 2. Relative diffusivity of tritiated water (HTO) in montmorillonite as a function of bulk density.

where G is a geometric factor that has a value of 4.0, δ, the constrictivity, has a value of 0.3, and $f_{interlayer}$ is the fraction of porosity in the interlayers, and is a function of ρ_b. Values of $f_{interlayer}$ are given in tabular form in Bourg et al. (2006) and are plotted here in Figure 3. Fitting linear models to these data yields:

$$f_{interlayer} = 0.87\rho_b - 0.348, \text{ for } 1 < \rho_b < 1.3 \text{ g/cm}^3 \quad (19)$$

$$f_{interlayer} = 0.78 \text{ for } 1.3 < \rho_b < 1.5 \text{ g/cm}^3 \quad (20)$$

$$f_{interlayer} = 0.9\rho_b - 0.58 \text{ , for } 1.5 < \rho_b < 1.7 \text{ g/cm}^3 \quad (21)$$

The models in Table 3 and in Eqns. 17 and 18 were developed for the diffusion of inorganic solutes in soil. In order to evaluate their performance for estimating the effective diffusion coefficient for organic solutes in saturated clayey soils, values of the relative diffusivity were calculated with those models where estimates could be made using independently determined parameters (e.g., the Marshall, Millington and Quirk, Penman, and Sallam models [the coefficient suggested by Moldrup et al. (2000) is equal to one in the case of saturated soils] and Eqns. 17 and 18) and compared with values of relative diffusivity compiled in Table 2. The measurements of Sawatsky et al. (1997) were not included in this assessment, due to the difference in orders of magnitude of their reported values relative to the others.

The average relative errors for the various methods are given in Table 4. Among the models considered, Penman's model produced the lowest overall percent relative error (130%) whereas Sallam's model's estimates are the worst (200% relative error). If the experimental results are divided into two categories, soils with a clay content lower than 25% versus those with a clay content higher than 25%, the relative errors change dramatically. For

soils with a low clay content (<25%), the percent relative error range decreased to 42 – 93% with Marshall's model having the least amount of error. However, for soils with a high clay content, the smallest percent relative error for the established models is 151% for the Penman model. These results support the observation of Olesen et al. (1999) that these estimation techniques give poor estimates for soil media containing more than 25% clay.

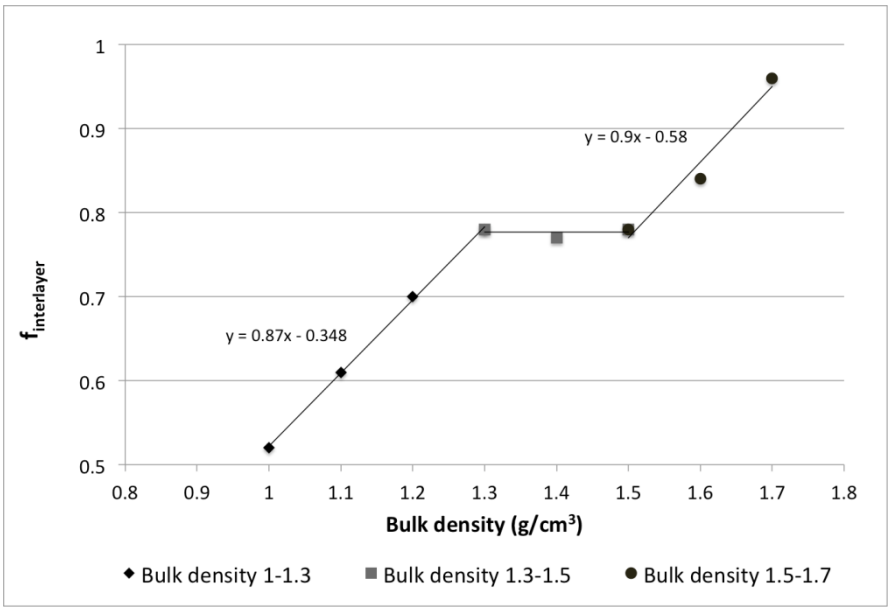

Figure 3. Fraction of porosity in the interlayers as a function of bulk density. Values are from Bourg et al. (2006).

Table 4. Average percent relative errors for calculating relative diffusivity, D_e/D_{aq}

Method	Percent Average Relative Error		
	Over all	Soil clay content <25%	Soil clay content >25%
Penman (1940) (Table 3)	130	54	151
Marshall (1959) (Table 3)	132	42	157
Sallam et al. (1984) (Table 3)	200	93	229
Millington and Quirk (1960, 1961) (Table 3)	156	58	184
Log-linear fit to data in Figure 2 (Eqn. 17)	83	82	83
Piece-wise linear fit to data in Figure 3 (Eqns. 19-21)	60	48	63

However the models listed in Table 3 were not developed specifically for clayey soils. The log-linear relationship (Eqn. 17) improved the estimations for the soils with high clay content as the error decreased to 83%. On the other hand, its performance is worse than the other methods for soils with low clay content as the relative error was 82%. The equations based on the data of Bourg et al. (2006) (Eqns. 19-21) were also used to calculate relative

diffusivity and yielding an error of 63% in soils with a high clay content and a surprisingly low error of 48% for the soils with a low clay content. Consequently, this method appears to be the most accurate for estimating effective diffusion coefficients for organic solutes in clayey soils.

CONCLUSION

Remediation of contaminated sites is a major environmental concern, with recent research tying the lack of closure at hazardous wastes sites in part to back diffusion from clay lenses and layers that have accumulated contaminants over decades (Stroo et al., 2013). Calculations of the efflux from these low permeability zones are based on estimates of the effective diffusion coefficient and are key to determining remediation time frames. Despite this need for accurate estimates of the effective diffusion coefficient, few experimental measurements exist for organic solutes in clayey soils. Because of the paucity of measurements, these coefficients are often estimated. However, the results presented here show that commonly used estimation methods overestimate the effective diffusion coefficient considerably and are only appropriate for clay soils with less than 25% clay content. Two estimation techniques, one developed in this study based on a regression analysis of published data for tritiated water diffusion in montmorillonite and another based on a semi-empirical correlation presented in Bourg et al. (2006) proved to provide better estimates. In fact, the equations derived from the information from Bourg et al. (2006) provided almost as good an estimate as the Marshall (1959) model for low clay content soils. Although the equations based on Bourg et al. (2006) would involve slightly more work to implement in numerical models, its ability to produce more accurate estimates across all clay contents might justify the additional effort. This assessment of the ability of these methods to predict relative diffusivity was based on experimental measurements available in the literature for effective diffusion coefficients of organic solutes in clayey soils, of which there are relatively few. Additional measurements are needed to determine whether the conclusions reached here based on the currently available data can be applied more broadly.

ACKNOWLEDGMENT

Financial support was provided by the Strategic Environmental Research and Development Program (SERDP). This paper has not been subject to review by the funding agency; it, therefore, does not necessarily reflect the sponsor's views, and no official endorsement should be inferred.

REFERENCES

Archie, G. E. (1942). The electrical resistivity log as an aid in determining some reservoir characteristics. *Trans. Am. Inst. Min. Metall. Pet. Eng., 146*, 54-62.

ATSDR (Agency for Toxic Substances and Disease Registry) (1997). *Toxicological Profile for Trichloroethylene*. U.S. Department of Health and Human Services, Atlanta, GA.

Ball, W. P., Liu, C., Xia, G. & Young, D. F. (1997). A diffusion-based interpretation of tetrachloroethene and trichloroethene concentration profiles in a groundwater aquitard. *Water Resour. Res.*, *33*, 2741-2757.

Barone, F. S., Rowe, R. K. & Quigley, R. M. (1992). A laboratory estimation of diffusion and adsorption coefficients for several volatile organics in a natural clayey soil. *J. Contaminant Hydrol.*, *10*, 225-250.

Bear, J. (1972). *Dynamics of Fluids in Porous Media.* New York, NY: American Elsevier.

Bourg, I. C., Bourg, A. & Sposito, G. (2003). Modeling diffusion and adsorption in compacted bentonite: a critical review. *J. Contaminant Hydrol.*, *61*, 293-302.

Bourg, I. C., Sposito, G. & Bourg, A. C. M. (2006). Tracer diffusion in compacted, water-saturated bentonite. *Clays and Clay Minerals, 54*, 363-374.

Boving, T. B. & Grathwohl, P. (2001). Tracer diffusion coefficients in sedimentary rocks: Correlation to porosity and hydraulic conductivity. *J. Contaminant Hydrol.*, *53*, 85-100.

Campbell, G. (1974). A simple method for determining unsaturated conductivity from moisture retention data. *Soil Sci.*, *117*, 311-314.

Chapman, S. W. & Parker, B. L. (2005). Plume persistence due to back diffusion following dense non-aqueous phase liquid source removal or isolation. *Water Resour. Res.*, *41*, 1-16.

Cho, W. J., Oscarson, D. W. & Hahn, P. S. (1993). The measurement of apparent diffusion coefficients in compacted clays: An assessment of methods. *Applied Clay Science, 8*, 283–294.

Cohen, R. M. & Mercer, J. W. (1993). *DNAPL Site Evaluation*. Boca Raton, FL: C.K. Smoley.

Crank, J. (1975). *Mathematics of Diffusion.* Oxford: Clarendon Press.

Donahue, R. B., Barbour, S. L. & Headley, J. V. (1999). Diffusion and adsorption of benzene in Regina clay. *Canadian Geotech. J.*, *36*, 430-442.

Dullien, F. A. (1992). *Porous Media: Fluid Transport Pore Structure,* 2nd ed. New York, NY: Academic Press.

Epstein, N. (1989). On tortuosity and tortuosity factor in flow and diffusion through porous media. *Chem. Engineering Sci.*, *44*, 777-779.

Garcia-Gutierrez, M., Cormenzana, J.L., Missana, T., Mingarro, M. & Molinero, J. (2006). Overview of laboratory methods employed for obtaining diffusion coefficients in FEBEX compacted bentonite. *J. Iberian Geol.*, *32*, 37-53.

Garcia-Gutierrez, M., Cormenzana, J. L., Missana, T. & Mingarro, M. (2004). Diffusion coefficients and accessible porosity for HTP and ^{36}Cl in compacted FEBEX bentonite. *Applied Clay Science, 26*, 65-73.

Grathwohl, P. (1998). *Diffusion in Natural Porous Media*. Dordrecht, Netherlands: Kluwer Academic.

Hayduk, W. & Laudie, H. (1974). Prediction of diffusion coefficients for nonelectrolytes in dilute aqueous solution. *Am. Inst. Chem. Eng.*, *20*, 611-615.

Headley, J. V., Boldt-Leppin, B. E., Haug, M. D. & Peng, J. (2001). Determination of diffusion and adsorption coefficients for volatile organics in an organophilic clay-sand-bentonite liner. *Canadian Geotech. J.*, *38*, 809-817.

Itakura, T., Airey, D. W. & Leo, C. J. (2003). The diffusion and sorption of volatile organic compounds through kaolinitic clayey soils. *J. Contaminant Hydrol.*, *65*, 219-243.

Jin, Y. & Jury, W. A. (1996). Characterizing the dependency of gas diffusion coefficient on soil properties. *Soil Sci. Soc. Am. J.*, *60*, 66–71.

Johnson, R. L., Cherry, J. A. & Pankow, J. F. (1989). Diffusive contaminant transport in natural clay: A field example and implications for clay-lined waste disposal sites. *Environ. Sci. Technol.*, *23*, 340-349.

Khandelwal, A., Rabideau, A. J. & Shen, P. (1998). Analysis of diffusion and sorption of organic solutes in soil-bentonite barrier materials. *Environ. Sci. Technol.*, *32*, 1333-1339.

Lever, D. A., Bradbury, M. H. & Hemingway, S. J. (1985). The effect of dead-end porosity on rock matrix diffusion. *J. Hydrology*, *80*, 45-76.

Mackay, D. M. & Cherry, J. A. (1989). Groundwater contamination: Pump-and-treat remediation. *Environ. Sci. Technol.*, *23*, 630-636.

Marshall, T. J. (1959). The diffusion of gases through porous media. *J. Soil Sci., 10*, 79-82.

Millington, R. J. & Quirk, J. P. (1960). Transport in porous media. In: van Beren, F. A., et al. (Eds.), *7th Int. Cong. Soil Sci.*, (97-106). Amsterdam: Elsevier.

Millington, R. J. & Quirk, J. P. (1961). Permeability of porous solids. *Trans. Faraday. Soc.*, *57*, 1200-1207.

Miyahara, K., Ashida, T., Kohara, Y., Yusa, Y. & Sasaki, N. (1991). Effect of bulk density on diffusion for cesium in compacted sodium bentonite. *Radiochimica Acta*, *52(53)*, 293-297.

Moldrup, P., Olesen, T., Gamst, J., Schjønning, P., Yamaguchi, T. & Rolston, D. E. (2000). Predicting the gas diffusion coefficient in repacked soil: Water-induced linear reduction model. *Soil Sci. Soc. Am. J.*, *64*, 1588-1594.

Montavon, G., Guo, Z., Tournassat, C., Grambow, B., Le Botlan, D. (2009). Porosities accessible to HTO and iodide on water-saturated compacted clay materials and relation with the forms of water: A low field proton NMR study. *Geochimica and Cosmochimica Acta*, *73*, 7290-7302.

Montgomery, J. H. (2000). *Groundwater Chemicals Desk Reference*. Boca Raton, FL: CRC Press.

Mott, H. V. & Weber, W. J. (1991). Factors influencing organic contaminant diffusivities in soil-bentonite cutoff barriers. *Environ. Sci. Technol.*, *25*, 1780-1715.

Myrand, D., Gillham, R. W., Sudicky, E. A., O'Hannesin, S. F. & Johnson, R. L. (1992). Diffusion of volatile organic compounds in natural clay deposits: Laboratory tests. *J. Contaminant Hydrol.*, *10*, 159-177.

Olesen, T., Moldrup, P. & Gamst, J. (1999). Solute diffusion and adsorption in six soils along a soil texture gradient. *Soil Sci. Soc. Am. J.*, *63*, 519-524.

Oscarson, D. W., Hume, H. B., Sawatsky, N. G. & Cheung, S. C. (1992). Diffusion of iodide in compacted bentonite. *Soil Sci. Soc. Am. J.*, *56*, 1400-1406.

Oscarson, D. W. & Hume, H. B. (1994). Diffusion of 14C in dense saturated bentonite under steady-state conditions. *Trans. Porous Media*, *14*, 73-84.

Parker, B. L. (1996), Effects of molecular diffusion on the persistence of dense, immiscible phase organic liquids in fractured porous geologic media, Ph.D. thesis, 191 pp., Univ. of Waterloo, Waterloo, ON, Canada.

Parker, B. L., Cherry, J. A. & Chapman, S. W. (2004). Field study of TCE diffusion profiles below DNAPL to assess aquitard integrity. *J.f Contaminant Hydrol.*, *74*, 197-230.

Parker, B. L., Chapman, S. W. & Guilbeault, M. A. (2008). Plume persistence caused by back diffusion from thin clay layers in a sand aquifer following TCE source-zone hydraulic isolation. *J. Contaminant Hydrol.*, *102*, 86-104.

Penman, H. L. (1940). Gas and vapor movements in soil: The diffusion of vapors through porous solids. *J. Agric. Sci*., *30*, 437-462.

Petersen, L. W., Rolston, D. E., Moldrup, P. & Yamaguchi, T. (1994). Volatile organic vapor diffusion and adsorption in soils. *J. Environ. Qual.*, *23*, 799-805.

Poling, B. E., Prausnitz, J. M. & O'Connell, J. P. (2001). *The Properties of Gases and Liquids*, *5th ed.* New York, NY: McGraw-Hill.

Porter, L. K., Kemper, W. D., Jackson, R. D. & Steward, B. A. (1960). Chloride diffusion in soils as influenced by moisture content. *Proc. Soil Sci. Soc. Am.*, *24*, 460-463.

Roehl, K. E. & Czurda, K. (1998). Diffusion and solid speciation of Cd and Pb in clay liners. *Applied Clay Science*, *12*, 387-402.

Sale, T. C., Zimbron, J. A. & Dandy, D. S. (2008). Effects of reduced contaminant loading on downgradient water quaility in an idealized two layer granular porous media. *J. Contaminant Hydrol.*, *102*, 72-85.

Sallam, A., Jury, W. A. & Letey, J. (1984). Measurements of gas diffusion coefficient under relatively low air-filled porosity. *Soil Sci. Soc. Am. J.*, *48*, 3-6.

Saripalli, K., Serne, R., Meyer, P. & McGrail, B. (2002). Prediction of diffusion coefficients in porous media using tortuosity factors based on interfacial areas. *Ground Water*, *40*, 346-352.

Sato, H., Ashida, T., Kohara, Y., Yui, M. & Sasaki, N. (1992). Effect of dry density on diffusion of some radionuclides in compacted sodium bentonite. *J. Nuclear Sci. Technol.*, *29*, 873-882.

Sawatsky, N., Feng, Y. & Dudas, M. J. (1997). Diffusion of 1-naphthol and naphthalene through clay materials: Measurement of apparent exclusion of solute from the pore space. *J. Contaminant Hydrol.*, *27*, 25-41.

Schaefer, C. E., Arands, R. R., van der Sloot, H. A. & Kosson, D. S. (1995). Prediction and experimental validation of liquid phase diffusion resistance in unsaturated soils. *J. Contaminant Hydrol.*, *20*, 145-166.

SERDP (Strategic Environmental Research and Development Program) (2006). Expert Panel Workshop on Reducing the Uncertainty of DNAPL Source Zone Remediation, March 7-8, 2006, Baltimore, MD.

Shackelford, C. D., Daniel, D. E. & Liljestrand, H. M. (1989). Diffusion in inorganic chemical species in compacted clay soil. *J. Contaminant Hydrol.*, *4*, 241-273.

Shackelford, C. D. (1991). Laboratory diffusion testing for waste disposal—A review. *J. Contaminant Hydrol.*, *7*, 177-217.

Shackelford, C. D. & Moore, S. M. (2013). Fickian diffusion of radionuclides for engineered containment barriers: Diffusion coefficients, porosities & complicating issues. *Engineering Geology*, *152(1)*, 133-147.

Shimamura, K. (1992). Gas diffusion through compacted sands. *Soil Sci.*, *153*, 274-279.

Stroo, H. F., Leeson, A., Marqusee, J. A., Johnson, P. C., Ward, C. H., Kavanaugh, M. C., Sale, T. C., Newell, C. J., Pennell, K. D., Lebron, C. A. & Unger, M. (2012). Chlorinated ethene source remediation: Lessons learned. *Environ. Sci. Technol.*, *46*, 6438-6447.

Troeh, F. R., Jabro, J. D. & Kirkham, D. (1982). Gaseous diffusion equations for porous materials. *Geoderma*, *27*, 239-253.

Weber, W. J. & Digiano, F. A. (1996). *Process Dynamics in Environmental Systems.* New York, NY: Wiley Interscience.

Wilson, J. L. (1997). Removal of aqueous phase dissolved contamination: Non-chemically enhanced pump-and-treat. In: Ward, B. S., Cherry, J. A., Scalf, M. R. (Eds.), *Subsurface Restoration*, (271-285). Boca Raton, FL: CRC Press.

Yang, Y., & Aplin, A. C. (2010). A permeability–porosity relationship for mudstones. *Mar. Petrol. Geology, 27*, 1692-1697.

Young, D. F. & Ball, W. P. (1998). Estimating diffusion coefficients in low-permeability porous media using a macropore column. *Environ. Sci. Technol.*, *32*, 2578-2584.

In: Clays and Clay Minerals
Editor: Liam R. Wesley
ISBN: 978-1-63117-779-8

Chapter 3

MECHANOCHEMICAL TREATMENT OF CLAY MINERALS BY DRY GRINDING: NANOSTRUCTURED MATERIALS WITH ENHANCED SURFACE PROPERTIES AND REACTIVITY

L. Pérez-Villarejo[1,*], S. Martínez-Martínez[1], D. Eliche-Quesada[1], B. Carrasco-Hurtado[2] and P. J. Sánchez-Soto[3]

[1]Department of Chemical, Environmental and Materials Engineering. Higher Polytechnic School of Linares. University of Jaén, Jaén, Spain

[2]Department of Engineering Graphics, Design and Projects. Higher Polytechnic School of Linares. University of Jaén, Jaén, Spain

[3]Materials Science Institute of Sevilla (ICMS), Joint Center National Research Council (CSIC)-University of Sevilla, Structural Unit "Mechanochemistry of Solids and Reactivity", Sevilla, Spain

ABSTRACT

Physico-chemical changes during the dry grinding of clays produce mechanochemical effects, as in other solids subjected to mechanical stress by impact and friction forces among particles, such as planetary mills. Thus, the reactivity of ground materials is enhanced and, therefore, it leads to mechanochemical reactions. The effects of dry grinding on clays and clay minerals have been extensively studied. It is associated to their relevant importance in some industrial applications as ceramic raw materials and processing of advanced ceramics.

In the present research, kaolinite (1:1 layer silicate), pyrophyllite and talc (2:1) and raw clay materials have been selected. Dry grinding experiments using planetary milling have been performed using selected samples. Several techniques have been used to follow the evolution of the layer silicates, mainly XRD, surface area (nitrogen

[*] Corresponding author: Tel.: +34 953648633; Fax: +34 953648623;
Email address: lperezvi@ujaen.es

adsorption), SEM, TEM, MAS-NMR, FTIR, particle size analysis and thermal methods (DTA-TGA).

The mechanical stress during grinding clays are quite diverse, producing important changes such as lattice distortions, amorphization, decrease in particle size, formation of nanostructures and an increase in surface area. Modifications of surface area, particle size and shape of short and prolonged grinding on the crystal structure of the layer silicates have been evaluated. These observed changes have been related to a progressive delamination and structural breakdown during grinding, with final formation of a turbostratic-type structure. Short grinding times resulted in the breakdown and drastic size reduction of relatively thin particles. It has been found an inverse relationship between coherent X-ray domain and lattice microstrains in the ground powders. It can be also observed an increasing in amorphization as a consequence of the loss of long-range order. On the other hand, the rate of size reduction decreased with time and a limit was reached for each layer silicate producing more rounded particles and aggregates, with a decrease of surface area. Grinding produced a loss of periodicity perpendicular to the layer silicate plane, and the dimensions of the crystallites along the c-direction resulted too small to produce coherent X-ray scattering. Microscopy techniques (TEM and SEM) allowed to observe the formation of nanometer size ground powders and further particle agglomeration. Modifications in the coordination of Si and Al nuclei have been also deduced from MAS-NMR spectroscopy, demonstrating a short-range order.

The present results are interesting in clay research to analyze the formation of nanostructured powders, with enhanced surface properties and reactivity, when grinding clays and to compare the effects of grinding on 1:1 and 2:1 layer silicates, the modifications of tetrahedral and octahedral sheets, the mechanochemical effects induced by grinding and the influence of experimental conditions.

Keywords: clay minerals, mechanochemical, grinding, reactivity, surface area, nanostructures

1. INTRODUCTION

First of all, it is important in this chapter to describe some structural features of layer silicates or phyllosilicates that constitute the clay minerals. The terms “planes”, “sheet” and “layer” refer to specific parts of the structure [1-7]. A “plane” can occur consisting of one or more types of atoms (e.g., a plane of Si and Al atoms, a plane of basal oxygen atoms). A “tetrahedral sheet” is composed of continuous corner-sharing tetrahedral like a “octahedral sheet” is composed of the edge-sharing octahedral. A “layer” contains one or more tetrahedral sheets and an octahedral sheet. The so-called “interlayer material” separates the layers and generally may consist of cations, hydrated cations, organic materials, and/or hydroxide octahedral sheets. In certain cases (e.g., pyrophyllite, talc) there is no interlayer material, and thus an empty interlayer separates the layers [1-7].

Two types of layers, depending of the component sheets are a “1:1 layer” consisting of one tetrahedral sheet and one octahedral sheet, and a “2:1 layer” containing an octahedral sheet between two opposite tetrahedral sheets. The theoretical formula of kaolinite is $Al_2Si_2O_5(OH)_4$ and the formula of pyrophyllite is $Al_2Si_4O_{10}(OH)_2$ being $M_3Si_4O_{10}(OH)_2$ for talc. Thus, kaolinite is a 1:1 layer silicate and pyrophyllite and talc 2:1 [7]. The structure of 2:1 layer silicates is composed of tetrahedral (T) and octahedral (O) sheets. For instance, the general basic structural unit cell of 2:1 layer silicates as found in pyrophyllite and talc

(Figure 1) is constituted by octahedra containing Al (in pyrophyllite) or Mg cations (in talc) linked with OH groups. Al cations are trivalent and Mg cations are divalent. Hence, talc is a trioctahedral 2:1 layer clay mineral, characterized by three octahedral Mg positions per four tetrahedral Si positions, and pyrophyllite is a dioctahedral 2:1. The octahedra are perfectly sandwiched by two tetrahedral silica layers. In contrast, 1:1 layer silicates, such as kaolinite, contain more OH groups linked directly to the cation. Kaolinite is a 1:1 layer silicate with a single sheet of OH octahedrally coordinated to Al cations linked through oxygens to a single layer of silicon tetrahedra. It should be noted that kaolinite crystals have a siloxane-like sheet only on one basal plane, with a hydrophylic gibbsite-type Al-OH sheet on the other side, whereas talc and pyrophyllite have siloxane-like sheets on both basal planes. The layer silicates may be considered as natural nanostructured materials with "nanomorphology" since their physical and technological properties are nanosize-dependent [8-10].

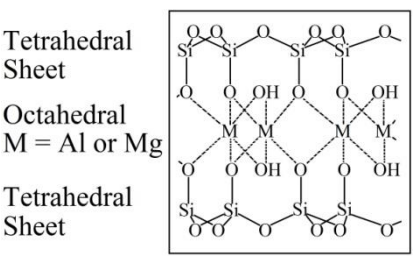

Figure 1. Structural basic unit cell of 2:1 layer silicates.

Concerning the effects of grinding on clay minerals, they have been extensively studied along years as described and reviewed in the present chapter. These studies are associated to the relevant importance of clay minerals in some industrial applications as ceramic raw materials, processing of advanced ceramics, catalysts, adsorbents, paints, paper manufacturing, pharmaceuticals, cosmetics and fillers in nanocomposite polymers [4-6, 10]. In general, two procedures, wet or dry grinding, are commonly used for the preparation of fine and reactive powders and further processing steps [11-17]. In general, physico-chemical changes during the grinding of a material produce the so-called mechanochemical effects. They are more frequently observed when grinding is carried out in equipment using impact and friction forces among particles, such as vibratory, oscillating and planetary mills [16-23]. Deagglomeration and elimination of soft aggregates during processing are produced by wet grinding. In contrast, dry grinding is most intensive when acting on solids. It originates mechanical stress which are quite diverse, producing important changes such as changes in the solid-state properties, defects in solids, lattice distortions, amorphization, decrease in particle size by disintegration of solids, creating interphases, generation of new solid surfaces, decrease in crystal size, increase in specific surface area and formation of nanostructures, besides the formation of new phases by mechanical alloying and time-convenient one-step syntheses [17, 21-23]. Thus, the reactivity of ground solids is enhanced and, therefore, it leads to mechanochemical reactions. Mechanochemical reaction is defined as a "chemical reaction that is induced by mechanical energy" [23]. For these reasons, there is a general interest along years on this kind of studies on the important physical and chemical induced effects by grinding in solids [11-23].

As pointed out above, the effects of grinding on several clay minerals have been extensively studied but mainly for kaolinite and montmorillonite or bentonite due to their importance as industrial raw materials. Talc, pyrophyllite, muscovite, illite and vermiculite have been also studied, although in less extension despite their relative great industrial importance. Some attention has been devoted to other silicates such as chrysotile, sepiolite and palygorskite (attapulgite), but they are fibrous silicates [4-7]. An extensive literature review on grinding clay minerals will be provided in the next sections of this chapter. Furthermore, several works have been published to compare the grinding behaviour of layer silicates [5, 10, 17, 23-28]. The more recent review paper titled "Hallmarks of mechanochemistry: from nanoparticles to technology" by Baláž et al. [23] includes silicates, such as kaolinite, with a few references and scarce references to montmorillonite, illite, talc, mica, etc., under the subject of 'mechanochemical effects in the presence of water'. As hydroxides and oxyhydroxides, these silicates undergo mechanically induced dehydroxylation.

In the present chapter, dry grinding using planetary ball milling has been studied for kaolinite, pyrophyllite, talc and raw clay materials. Several techniques have been used to follow the evolution of the layer silicates. The changes of surface area, particle size and shape of short and prolonged grinding on the crystal structure and reactivity of these clays have been evaluated.

Consequently, the aim of this research was: (a) to compare the mechanochemical effects by grinding on 1:1 (kaolinite) and 2:1 (pyrophyllite and talc) layer silicates because these clay minerals are present in raw clays, and (b) to analyze the formation of nanostructured powders, with enhanced surface properties and reactivity, when grinding these clays.

2. EXPERIMENTAL

2.1. Materials

Kaolinite (1:1 layer silicate), pyrophyllite and talc (2:1 layer silicates) as clay materials have been selected. The theoretical formula are as follows: kaolinite $Al_2Si_2O_5(OH)_4$; pyrophyllite $Al_2Si_4O_{10}(OH)_2$ and talc $Mg_3Si_4O_{10}(OH)_2$.

Two reference kaolinite samples both from Georgia (USA) have been used: well-crystallized kaolinite (KGa-1) from Washington County and poorly crystallized kaolinite (KGa-1) from Warren County. They are reference kaolinite samples certified by The Clay Minerals Society (Source Clays Repository, University of Missouri, Columbia). These two kaolinite samples have been extensively characterized [29, 30]. An industrial kaolin from Vimianzo (A Coruña, Spain) has been also considered for grinding experiments. The commercial sample is the washed product of alteration of granitic rocks [31], with > 90 wt % purity of well-crystallized kaolinite and minor amounts of quartz and muscovite. It is applied for porcelain formulations, preparation of ceramics and refractories and paper industry. The sample was used as-received.

Raw industrial pyrophyllite from a deposit located near Zalamea de la Serena (Badajoz, Spain) was used for this study. The sample is considered an aluminum shale and the bed was previously studied [32, 33]. This is a natural mixture of pyrophyllite, kaolinite, illite and

mixed-layer illite-smectite with a small content of rutile (TiO_2) and iron oxides. The raw sample was purified by a chemical procedure using acids (nitric-hydrochloric-hydrofluoric) because pyrophyllite is not dissolved [34]. As a result of this chemical treatment, all the extraneous phases were eliminated except for a small amount of rutile (~ 5 wt %). Thus, the pyrophyllite content is ~ 95 wt %.

A raw talc rock sample from Puebla de Lillo (León, Spain) was used. The talc bed was previously studied [35]. The aggregate was gently ground using an automatic agate mortar and used in this form for grinding experiments. This sample belongs to fine grained steatite. A steatite is the non-platty, granular variety of talc according to Schüller and Kromer [36]. Industrial commercial talc sample from Fuengirola (Málaga, Spain), provided by Talcs of Luzenac, has been also used for the grinding experiments. It is applied for paints, adhesives, fillers, cosmetics, plastics and ceramics. The platty sample (> 80 wt % of talc) contains minor proportions of quartz (< 10 wt %) and chlorite (< 10 wt %). It was used as-received in ground powdered form.

2.2. Grinding Procedures

Dry grinding experiments in air using planetary milling have been performed. A Retsch planetary ball mill, model S-1, at a rate of 250 rpm was used. The grinding vessel of 350 mL was hard porcelain and contained 10 balls, 20 mm in diameter, of the same material with grinding time up to 325 min. Samples of 2.200 g were used for each experiment, as in previous papers [37-39]. Thus, a balls:powder weight ratio of 1:0.22 was used. Samples of 60 g were also used for other grinding experiments using vessels of hard porcelain of the same volume but at a rate of 400 rpm. In this case, 7 balls of 17 mm in diameter and 7 balls of 15 mm were introduced. Thus, the balls:powder weight ratio of 1:4.28 was used. Under these conditions, the grinding time was prolonged up to 80 h (4800 min.).

The purpose was to compare the effects of different conditions of grinding on these clay minerals.

2.3. Techniques

Several techniques have been applied to follow the evolution of the layer silicates by dry grinding.

First of all, X-Ray powder Diffraction (XRD) of original and ground samples were obtained using a Siemens Kristalloflex D-501 diffractometer equipment with Ni-filtered CuKα radiation and goniometer speed of 1º 2θ/min. To avoid prefered orientation, quasi-randomly oriented samples were prepared using a side-packed holder with an opened window. The holder was tapped gently with a glass slide to consolidate the powder, as suggested previously for layer silicates [40], and covered with a piece of filter paper between the sample and the glass slide, both being removed before X-raying. Ground and heated samples were examined by XRD as oriented aggregates on glass slides.

The breadths (B in degrees 2θ) for selected diffractions were obtained from the diffractometer profiles at a continuous scan at 0.1º 2θ/min by measuring the peak full widths at half-maximum (FHWM). A microprocessor DACO MP-8 and a personal computer PC

Siemens model 16-20 were used. The instrumental broadening was measured with a sample of quartz (> 100 mm), "pro analisi" quality, supplied by Merck (Germany). Corrected FHWM of each diffraction peak were calculated using a computer program based on the Jones correction of the instrumental broadening, peak stripping of Cu Kα radiation and elimination of instrumental background [41, 42]. The mean crystallite size (D) and the mean lattice strain (e) were obtained from the corrected B values according to the Scherrer and Williamson-Hall equations, as described by Klug and Alexander [41].

The Infrared (IR) spectra were recorded in the range of 250 to 4000 cm^{-1} for samples in KBr pellet form (2 mg of sample in 300 mg of dried KBr), using a Fourier Transform FTIR apparatus (Nicolet model 510P).

High-resolution solid-state Magic Angle Spinning (MAS)-Nuclear Magnetic Resonance (NMR) spectra of 29-Si and 27-Al nuclei using powdered samples were recorded at 79.49 and 104.26 MHz, respectively, by spinning the samples at the magic angle (54º 44') in a Bruker MSL-400 spectrometer equipped with a Fourier Transform unit. The spinnig frequency was in the range 4000-5000 cps. 29-Si and 27-Al NMR spectra were recorded after 2.6 μs and 2 μs pulses, respectively. Intervals between successive acumulations (8 and 2 s.) were selected to avoid saturation effects. Measurements were conducted at room temperature with Tetramethylsilane (TMS) and $[Al(H_2O)_6]^{3+}$ as external references. The mean error in the measured chemical shifts was ≤ 1 ppm.

The surface area determinations were carried out using two automatic system Micromeritics equipments: 2200A model for direct measurement of the value of surface area (estimation by the point "b" method) and ASAP 2010 model for the complete adsorption-desorption isotherm, with nitrogen gas (N-45, 99.99 % of purity) as the adsorbate at liquid nitrogen temperature. Samples were degassed over two hours at 150 ºC prior to analysis, and the Brunauer-Emmett-Teller (BET) method was used to calculate the nitrogen surface area [43].

Particle-size distribution analysis was performed by sedimentation in water using a Micromeritics Sedigrap apparatus, model 5100 VI-02 based on the Stokes´ Law and sodium hexametaphosphate (5 wt %) as dispersant, a previous sonication treatment and magnetic stirring. In some cases, it was also used a Mastersizer X Laser equipment of Malvern Instruments for particle size determinations. For these determinations, homogenous diluted aqueous suspensions of the original and ground samples were prepared and dispersed with aqueous solution of sodium silicate (10 wt %) and sonicated.

The particle morphology of original and ground samples was examined by Scanning Electron Microscopy (SEM) using a ISI equipment, model SS-40, and a JEOL equipment, model JSM 5400, following the same procedure as in previous papers [37-39, 44].

Dispersed samples in deionized water and sonicated were prepared. A drop of the diluted suspension was deposited on Cu grids covered with collodion membrane and dried at 40 ºC. The preparations were examined by Transmission Electron Microscopy (TEM) using a Hitachi H-800 electron microscope at 200 kV.

To investigate the thermal behaviour of mechanochemically treated samples by grinding, simultaneous thermal methods were used. Differential Thermal and Thermogravimetric Analyses (DTA-TGA) were performed using a thermal analyzer Setaram 92-16, 18 in static air, heating rate of 10 ºC/min and Pt-Pt/Rh (13 %) thermocouples. About 40 mg of samples was gently packed each time in a Pt holder and thermally treated. Calcined alumina at 1400

ºC was used as reference material for DTA runs. The temperatures of the thermal events were estimated from their positions at the top or bottom of the DTA-TGA diagrams.

3. RESULTS AND DISCUSSION

3.1. Structural Alteration by Dry Grinding

3.1.1. The Effects of Grinding on Kaolinite (1:1 Layer Silicate)

The effect of grinding on different kaolinite samples has been a research subject during a long time. The use of different grinding devices (ball milling, planetary milling, jet mill, ring-mill, oscillating mill, etc.), wet and dry grinding, and non-reference kaolinite samples have produced different and contradictory reported results, in particular on structural alteration and degradation time, as studied mainly by XRD, fisisorption of nitrogen gas, several spectroscopic and microscopic techniques, particle size analysis and thermal methods.

However, earlier studies on grinding kaolinite considered this layered silicate as a soil component and grinding experiments were performed for several days. A few authors have summarized these first investigations [5, 17, 24-28, 44]. In a sistematic work on grinding kaolinite minerals, Takahashi [45] ground a kaolinite sample using a mechanical mortar during 48 hours. He reported the destruction of crystal structure of kaolinite and a reduction of particle size, although with prolonged grinding time the powder is reaggregated in spherical particles. Haase and Winter [46] studied the influence of grinding on the ceramic properties of a sample of kaolin. Several years later, Miller and Oulton [47] studied a water-washed kaolinite sample of unknown origin and the grinding was performed by percussive grinding. These authors suggested a prototropy-effect in ground kaolinite or transfer of protons from bound water of the remained unaltered kaolinite structure to broken bonds of the altered kaolinite structure. This effect will be discussed on the next section. Some effects of grinding kaolinite with KBr have been also reported [48]. Hlavay et al. [49] studied the effect of crystallinity, particle size and structural water variation on grinding two kaolin samples. Yariv and Cross [50] classified the reactions occurring during the grinding of kaolinite in four groups: delamination, layer breakdown, sorption of water and thermal difussion.

Juhász [24] reviewed the previous literature reports on grinding kaolinite, as described above. This author studied the processes during intensive grinding (supergrinding) of kaolinite minerals and developed some tests to study them. It is interesting to remark that the existence of multiple well-crystallized kaolinite phases, that influence the changes caused by grinding, has been demonstrated using a crystallized kaolinite sample [51]. A model based on these XRD results has been also proposed [51]. The ‘mechanochemical effects’ (structural and textural) produced by grinding kaolinite have been reported by Aglietti et al. [52, 53]. Using XRD and other techniques, even chemical dissolution analyses, Kodama et al. [54] quantified the crystalline and non-crystalline material in a ground kaolinite sample.

Industrial kaolin samples have been considered for grinding experiments [10, 28, 55-58]. Kristóf et al. [56] studied the effect of mechanical treatment on the crystal structure and thermal behavour of kaolinite. They summarized the previous contributions to the study of mechanochemical amorphization of kaolinite and the discussion by several authors on this mechanism. Suraj et al. [57] studied the effect of micronization on kaolinite clay mineral

using ball milling and oscillatory milling during dry and wet conditions. These authors discussed the previous findings on mechanochemical activation in relation to the behaviour of kaolin and clay minerals. As most studies devoted interest to investigate only one type of grinding device, they compared these two grinding procedures. Mendelovici [5, 27] has reported: (1) a comparative review of the effects of thermal and mechanical treatments on the structure of clay minerals, and (2) a research on the selective mechanochemical reactions on dry grinding structurally different silicates. Baudet et al. [58] studied the comminution of kaolinite using attrition milling and pug milling to produce delamination and transverse breakage of kaolin platelets.

XRD analysis, thermal methods and Diffuse Reflectance IR Fourier Transform (DRIFT) spectroscopy analysis have been also used to study the mechanochemical activation of kaolinite by grinding [59-69]. Kristóf et al. [63] detected four different OH groups in ground kaolinite using Controlled-Rate Thermal Analysis. The modification of low- and high-defect kaolinite surfaces by mechanical activation has been studied by Frost et al. [66]. These authors reported the implications for kaolinite mineral processing. Stepkowska et al. [62] studied the effect of grinding (using an oscillatory mill) and water vapour on the particle size of kaolinite using the reference well-crystallized kaolinite (KGa-1). In this sense, it is remarkable that the reference kaolinite samples (KGa-1 and KGa-2) are more used in this kind of studies on mechanochemical effects of kaolinite, as it was previously proposed [44]. Sánchez-Soto et al. [44] studied the effects of dry grinding on the structural changes of kaolinite powders using well-crystallized and poorly crystallized reference kaolinite samples. The evolution of theses kaolinite samples was followed by several techniques, in particular XRD, SEM and DTA-TGA. DTA-TGA methods have been also applied to study some physico-chemical alterations caused by mechanochemical treatments in kaolinites of different structural order [68].

It is interesting to note that Kameda et al. [67] reported a hydrogen release during dry milling of kaolinite: H_2 is formed by the reaction between surface water molecules and mechanoradicals created by the rupture of Si-O or Al-O-Si bonds. The study of industrial kaolin by ball-milling under vacuum allowed to find a linear relationship between thermo-dehydroxylation and induced strain by mechanical processing [70]. The reference well-crystallized kaolinite sample KGa-1 has been studied using two vibrating dry milling procedures [71]. XRD and electron microscopy methods have been used to evaluate the microstructural alteration of kaolinite, comparing the results and analyzing the correlations between them [71]. It was also reported the surface modification of mechanochemically activated kaolinites by selective leaching [72]. The well-crystallized kaolinite sample and the poorly-crystallized kaolinite sample (KGa-2) have been also considered for grinding experiments using a laboratory planetary mill [73]. The ground samples were studied by XRD, thermal methods, IR and specific surface measurement, although the purpose was to activate the ground kaolinites with acids and to assess the intercalation ability with urea. Tang et al. [74] studied the effect of dry grinding on the physicochemical properties of silica material prepared from kaolin residue. Recently, Dellisanti and Valdré [75] have investigated the role of microstrain on the thermostructural behaviour of industrial kaolin deformed by ball-milling at low mechanical load.

3.1.2. X-Ray Powder Diffraction of Kaolinite After Grinding

The industrial kaolin sample is considered in this section. The kaolinite content of this sample is > 90 wt %. Grinding treatment produces a strong structural alteration and deterioration of the structure of this 1:1 layer silicate, with formation of an amorphous material. This is illustrated in Figure 2 for this sample of industrial kaolin, showing the evolution observed in the XRD powder diagrams of the kaolinite reflections after dry grinding at different times, from 0 to 80 h. It should be emphasized that a complete degradation of the kaolinite crystal structure in this sample after 80 h of grinding is not reached. However, changing the grinding conditions and studying the reference kaolinite sample (well-crystallized KGa-1 sample), a total degradation of the crystal structure can be reached after 120 min of grinding, as demonstrated in a previous paper [44]. This industrial kaolin sample, with high proportion of kaolinite > 90 wt %, can be considered a well-crystallized sample with similar characteristics as the reference kaolinite sample.

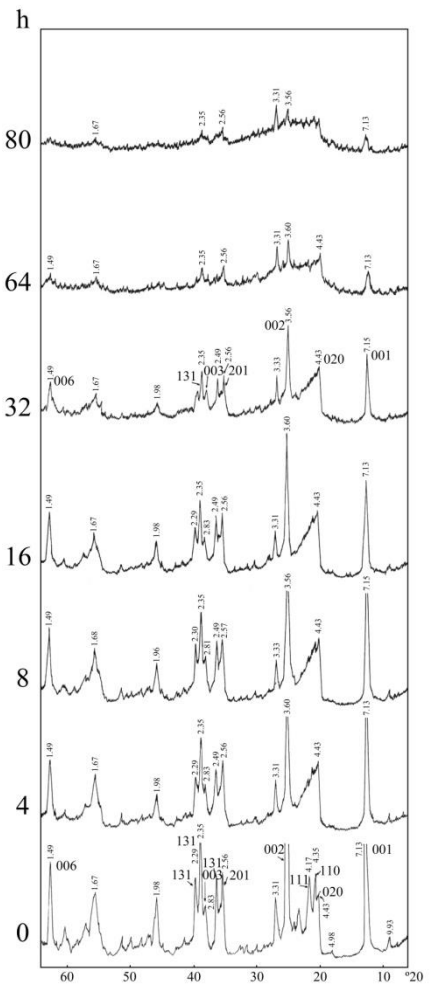

Figure 2. XRD diagrams of original (0 h) and dry ground (4-80 h) industrial kaolin sample (h=hours).

Considering the 1:1 layer silicates, the well-crystallized kaolinite sample after short grinding times produced the formation of a disordered material or "poorly-crystallized" kaolinite, which seems the original KGa-2 (poorly crystallized kaolinite) at the starting of the grinding experiments. The progressive grinding treatment produced disordered and highly disordered kaolinite crystals, as described in natural samples [76]. In this sense, some previous works [52, 53, 55] suggested that the disorder induced by dry grinding kaolinite occurs mainly in the direction of the c-axis but that, within the randomness of the layer displacement, some of these displacements are similar to the disorders existing in natural kaolinites. In fact, changes in the (02*l*) and (11*l*) reflections are significative, which are associated to the abundance of translations defects consisting in random and specific interlayer displacements, as pointed out by Aglietti et al. [52, 53]. In contrast, minor modifications are observed in the (20*l*) and (13*l*) reflections, also affected by small random displacements [77]. The disordered structure is associated with either the displacement of the b-axis or rotations of the layers among themselves, which cause a change in the sequence of octahedral vacancies along the c-axis. Consequently, the variability of XRD results concerning the grinding of several kaolinite samples, as described in the literature [5, 24, 27, 28, 45-75], is associated to the study of samples of different crystalinities and/or disordered structures.

As example of such works, not to mention too many, the study of De Luca and Slaughter [51]. These authors investigated by XRD the effects of dry grinding on a crystallized sample of kaolinite, showed the existence of multiple well-crystallized kaolinite phases that influence the changes caused by grinding. Reynolds and Bish [64] reported that grinding of kaolinite does not produce a progressive increase in disorder for all of the cristalites present in a sample. Grinding apparently creates increased amounts of disordered kaolinite that coexists with relatively unaffected material. They claimed that there is no evidence for the occurrence of an intermediate disordered phase. Even small kaolinite crystals (produced by dry grinding), protected by an amorphous matrix, remained in the final product after a chemical attack of highly ground material, as found in a previous research [54].

On the other hand, dry grinding breaks the hydrogen bond between adjacent kaolinite layers, as proposed first by Yariv and Cross [50] and later by several authors [5, 52, 53, 60, 61, 66, 71, 73]. Thus, this effect produces the delamination of the original kaolinite packets. The delamination depends of the characteristics of the particular kaolinite sample, as evidenced, for example, by Frost et al. [66].

3.1.3. The Effects of Grinding on Talc and Pyrophyllite (2:1 Layer Silicates)

3.1.3.1. Talc and Raw Materials Containing Talc

Earlier research works on grinding talc were performed by Farmer [78], who studied the influence of grinding on IR spectra of talc, and Takahashi [79]. Okuda et al. [80] have studied the density of charges on the edge and basal surfaces of dry- and wet-ground talc and pyrophyllite. Other authors [81] studied the grinding of talc and its influence on the cationic exchange capacity (CEC). Yvon et al. [82] investigated the effects of grinding on chlorite and talc because these minerals can be associated in several mineral beds. They proposed a model to explain the changes of CEC and the structural and textural modifications by grinding under different experimental conditions. Heller-Kallai et al. [83] studied by thermal and IR methods the interaction of talc with stearic acid by grinding.

A structural analysis by XRD of talc under dry atmospheric conditions for different grinding times has been reported by Sugiyama et al. [84]. These authors confirmed that an increase of the grinding time produced a change in oxygen coordination number around Mg, this variation being attributed to the change of an OH induced by the prolonged grinding. Liao and Senna [85] indicated that the mechanical activation of talc shows specific features related to the change in state of H_2O or OH during structure degradation under mechanical stress, with important variations in thermal behaviour (DTA-TGA). Aglietti and Porto López [86] and Aglietti [87] reported on the structural, physico-chemical and textural effects on talc by XRD and other methods and its influence on thermal behaviour. Even more, Aglietti [87] described these progressive changes on talc during dry grinding using oscillating and ball mills. Filio et al. [88] performed a study on talc ground by tumbling and planetary ball mills comparing the effects of these two grinding devices on talc. They used XRD, SEM, DTA-TGA, surface area and density measurements, particle size analysis and compressive strength. Mendelovici [5] has reviewed the main changes observed on talc after grinding. In all these previous papers, it has been generally agreed that dry grinding is a complex mechanochemical process involving, among others, a mechanical activation which is related to the state of the OH groups in the structure.

For a more profound investigation, Wiéwiora et al. [89] and Sánchez-Soto et al. [90], following previous experiments on grinding pyrophyllite [39], studied the effects of dry grinding by ball milling of talc. They used XRD and other methods (SEM, IR, DTA-TGA, nitrogen adsorption), showing the structural changes and the effect of dry grinding on particle size and shape. These authors reported an initial delamination by grinding, with reduction of particle thickness due to crystallite degradation along (00l), and a crystal structure breakdown and amorphization to the X-rays as increasing grinding time. A correlation of powder characteristic of talc during planetary ball milling has been proposed [91]. Kano et al. [92] performed a ball mill simulation and powder characteristics of ground talc in various types of mill.

Zbik and Smart [9] studied the dispersion of talc in aqueous solution showing the nano-morphology and nano-bubble entrapment. The physico-chemical properties and surface free energy of ground talc have been also reported [93, 94]. Christidis et al. [95] studied the influence of dry grinding on the structure and colour properties of talc, bentonite and calcite white fillers. Yang et al. [96] have prepared a porous material from talc by mechanochemical treatment by planetary ball milling and subsequent leaching. The presence of negative charge on the basal planes of ground talc, a subject previously studied by Okuda et al. [80], has been also investigated recently by Burdukova et al. [97]. The effect of dry grinding of 1:1 and 2:1 clay minerals using vacuum conditions has been also investigated. Dellisanti and Valdré [10] have found a linear relationship between termo-dehydroxylation and induced strain by mechanical processing of talc and other clay minerals using a ball mill working although at room temperature and under a medium/high vacuum. In a next paper, Dellisanti et al. [98] examined the main physical and technological properties of talc due to induced progressive mechanical stress by planetary ball milling.

Although it is clear that different talc samples and grinding devices have been used by all these authors, the main effects on grinding talc could be summarized. The previous paper reported a progressive structural disorder of this 2:1 layer silicate and a subsequent amorphization, as studied by XRD methods, and the ground products show important changes in textural, physical and thermal properties. A delamination process (along ab planes) takes

place in the initial stage of the grinding, following by a drastic reduction of particle sizes with an increasing of specific surface areas. Prolonged grinding produces an agglomeration and re-agregation of the fine ground talc particles which show and increased reactivity. The change in reactivity of talc after grinding is relevant. For instance, the research work of Yang et al. [96] on porous material from ground and leached talc. Furthermore, a simple synthesis and characterization of nanoporous materials obtained from ground talc and chemical treatments have been proposed [99]. In this sense, grinding played an important role in the whole synthesis process because the reduction of particle size of the talc and weakening the Mg-OH bonds [84, 88] facilitated the subsequent leaching for this synthesis. Talc containing dolomite has been also studied. Mahadi and Palaniandy [100] reported the mechanochemical effect of dolomitic talc during wet grinding process using a mortar mill by varying the milling time, solid content and vertical stress. Finally, to increase the reactivity of talc, Tavangarian et al. [101] ground talc and magnesium carbonate. The aim was to achieve the synthesis of the high-temperature phase forsterite at lower temperatures.

3.1.3.2. Pyrophyllite and Raw Clays Containing Pyrophyllite

Pyrophyllite and talc are 2:1 layer silicates. The crystal structures are analogous and, hence, their physical properties are so close to each other [1-4]. For instance, the hardness of talc (according to Mohs scale) is 1 and that of pyrophyllite between 1 and 2. The wettability of both minerals is the lowest among all phyllosilicates [4]. However, talc contains Mg in its structure and pyrophyllite Al. The high alumina content of pyrophyllite and physico-chemical properties make it useful in several industries, such as refractories, ceramics and sundry uses [102-104].

Levine and Joffé [105] described in a pioneering work some grinding experiments using pyrophyllite. Later, researchers in Japan performed studies on pyrophyllite grinding. For instance, Hayashi et al. [106] studied the continued grinding of pyrophyllite and its effect on toxicity of the cell. Shiraki and Inoue [107] studied the wet and dry grinding of pyrophyllite using ball milling. Okuda et al. [80] studied the density of charges on the edge and basal surfaces of dry- and wet-ground pyrophyllite.

Industrial grinding of pyrophyllite materials has also been examined to determine the efficiency of the method [108] and to separate pyrophyllite from other minerals [109]. Juhász [110] suggested that destruction of pyrophyllite during mechanochemical activation by intensive dry grinding may be accelerated by cations and adsorbed water. Attrition milling of pyrophyllite has been also studied [111]. Rosenberg and Cliff [112] studied the formation of pyrophyllite solid solutions. They started from a lightly ground natural pyrophyllite (Glendon, NC, USA), milled pyrophyllite and pyrophyllite gel [113]. These authors claimed that grinding pyrophyllite using a vibratory mill for 60 minutes produced a rapid structural degradation: X-ray reflections began to deteriorate almost inmediately and completely disappeared after 60 minutes of grinding. However, no more experimental details were given. Nemecz [114] reported that triclinic pyrophyllite (1Tc) is transformed into a monoclinic modification as a result of dry grinding for up to 60 minutes.

These previous contributions aimed to study the problems of the identification of pyrophyllite occurring in natural multiphase samples and the effects of chemical treatments in acid solutions [32-34]. It was of special interest to investigate further the effects of dry and wet grinding using several grinding devices and experimental conditions [37, 38]. Pérez-Rodríguez et al. [37, 38] studied the effects of dry grinding on pyrophyllite using a pure

sample (Hillsboro, NC, USA). Delamination, gliding and folding of the layers, and a decrease in particle size were detected by SEM. An increase in the background, broadening of the diffraction bands and an increase in the degree of disorder was also reported, resulting in a large increase in specific surface area. Longer grinding times than 32 minutes decreased the surface area due to particle aggregation and agglomeration and an amorphous powder is produced. Sánchez-Soto and Pérez-Rodríguez [115] demonstrated the formation of the high-temperature phase mullite at lower temperatures than in the unground pyrophyllite.

The crystallite size and lattice distortion of ground prophyllite was studied by X-Ray methods [116, 117]. González-García et al. [118] studied the effects of dry grinding on a sample containing pyrophyllite, kaolinite and illite. These authors discussed the behaviour of this natural multiphase sample after grinding with those previous results on grinding pyrophyllite [37]. The effects of dry grinding on X-ray diffraction line broadening in pyrophyllite were also reported [119]. The mechanical treatment by dry grinding of pyrophyllite strongly influenced the thermal behaviour with an increase of reactivity [38]. The formation mullite at lower temperatures than in the unground pyrophyllite was firstly reported [115]. Later, the influence of dry grinding on mullite and cristobalite formation was also studied by high-temperature DTA [120]. An interesting research was the comparative study of wet and dry grinding on pyrophyllite and their effects on the microstructure of the resultant powders [121]. The structural alteration of pyrophyllite by dry grinding was also studied by IR spectroscopy and XRD using thin oriented films [122]. Sánchez-Soto et al. [123] studied the grinding effect on kaolinite-pyrophyllite-illite natural mixtures and its influence on mullite formation.

Thus, the knowledge of the mineralogical and chemical composition of natural pyrophyllite materials and these previous research papers on dry grinding pyrophyllite aimed to approach the study of structural alteration with the point of view of polytypism. Wiéwiora et al. [39] studied several pyrophyllite samples and the effects of dry grinding and acid leaching on polytypic structure of pyrophyllite. These authors discussed the polytypism of pyrophyllite and concluded that the formation of a one-layer triclinic polytype of pyrophyllite or disordered forms is more likely than the formation of the two-layer monoclinic variety by grinding. In a later research, Wiéwiora and Hida [124] reported the X-ray determination of superstructure of pyrophyllite studying a sample from Japan.

The structural alteration of pyrophyllite by dry grinding was also studied by IR spectroscopy [122]. In particular, a prototropy effect by grinding pyrophyllite, as occurs in kaolinite, was discussed. This first spectroscopy study was completed by a MAS-NMR spectroscopy investigation on the influence of thermal and combined mechanical, by dry grinding, and thermal treatments in pyrophyllite-mullite thermal transformation [125]. The diffusion of Al-ions and formation of Si-poor nuclei of mullite at 1000 ºC is favoured by grinding and the exothermic DTA effect, detected at 1000 ºC, is ascribed to transformation of pentahedral coordination of Al in tetra- and octahedral Al in mullite. These results were compared with those obtained in kaolinite-mullite transformation, which were previously analyzed [126]. An invited paper [127] reviewed these previous studies on the influence of mechanical and thermal treatments on raw materials containing pyrophyllite. Other authors reported the evolution of pyrophyllite particle sizes during dry grinding as studied by TEM methods [128].

The influence of dry grinding of pyrophyllite using an oscillatory mill (at 1500 rpm) on water sorption has been studied by Stepkowska et al. [62]. These authors reported the effects

of grinding by delamination and structural degradation by the action of water molecules on the size of pyrophyllite and kaolinite particles, showing interesting results on the evolution of both 1:1 and 2:1 layer silicates previously ground. Thus, the storage in water or water vapour for 20 days may improve the technological properties of these clays, in particular the rheology of water suspensions [62].

The effect of dry grinding on pyrophyllite flotation were also studied [129]. It was concluded that dry grinding for longer times affects the flotation recovery of pyrophyllite, since the crystal structure is distorted by mechanical treatment, in accordance with previous reports [37, 39, 122]. The effect of grinding on the leaching behaviour of pyrophyllite has been also studied by Temuujin et al. [130]. These authors reported the presence of significant numbers of micropores in ground samples after leaching. In this sense, it was interesting the study of the textural properties of dry ground pyrophyllite. The pore size distribution of ground pyrophyllite samples was reported [131]. This textural study showed that the fisisorption of nitrogen gas is produced by multilayers and the absence of micropores in the ground powders.

3.1.4. X-Ray Powder Diffraction of Talc After Grinding

As in 1:1 layer silicates, grinding treatment produces a strong structural alteration and deterioration of the structures of 2:1 layer silicates, with formation of an amorphous material. Figure 3 shows the XRD powder diagrams of industrial talc ground from 0 to 80 h.

The crystal structure of talc (platty sample) is completely degraded after 32 h under the same conditions of grinding the industrial sample of kaolin. In contrast, in the talc sample (fine grained esteatite) ground from 0 to 325 min, the crystal structure is degraded after 60 min (Figure 4), as demonstrated in a previous paper [90]. The series of XRD diagrams allow to observe an important change in the X-ray patterns after grinding talc from 20-30 min. In the case of purified pyrophyllite, this change can be observed from 30 min, with disappearance of (00*l*) reflections and an increase of line broadening of remaining reflections. In previous works grinding other pyrophyllite sample under the same conditions, this change was observed between 30-32 min [37, 38, 115, 119].

Grinding of the natural mixture of pyrophyllite, kaolinite, illite and mixed-layer illite-smectite revealed that this treatment gradually destroys the pyrophyllite, kaolinite and illite structures. The use of different grinding conditions produces some differences in the structural alteration of pyrophyllite and kaolinite in the mixture. If a ball:sample ratio of 1:4.28 is used, pyrophyllite seems to have less mechanical strength to be destroyed than kaolinite, a result that coincides with a previous report [118]. However, if a ball:sample mass ratio of 1:0.22 is used, the effect is opposite, as is demonstrated in a previous paper using XRD of thin oriented films [122]. After 32 min of grinding, basal reflections of pyrophyllite, kaolinite and illite have almost disappeared and the (110) reflection of pyrophyllite remained.

In general, although previous studies indicated the variety of samples, grinding devices and different experimental conditions, for both 1:1 and 2:1 layer silicates (Figures 2 and 3) the intensities of the general (*hkl*) reflections change less than that the basal (00*l*) reflections, with a progressive increase of line broadening. The reason is that the alteration caused by dry grinding is greater along the c-axis of the silicate structures. This is a general result of the pronounced propensity of these layered silicates toward cleavage perpendicular to this c-axis. Consequently, there is a loss of periodicity perpendicular to the layer silicate plane and the dimensions of the crystallites along the c direction become too small to produce coherent X-

ray scattering with an increasing in amorphization. This is in accordance with previous research works, as reviewed in previous sections. However, Temuujin et al. [130] studied the grinding of a pyrophyllite sample and observed the retention of the basal (00*l*) reflections in samples ground for 3-18 hours using a planetary pot mill. These authors suggested that the basal reflection may also be stable to dry grinding and the structural alteration produced by mechanical treatment does not necessarily occur readily along the c-axis of the crystal structure.

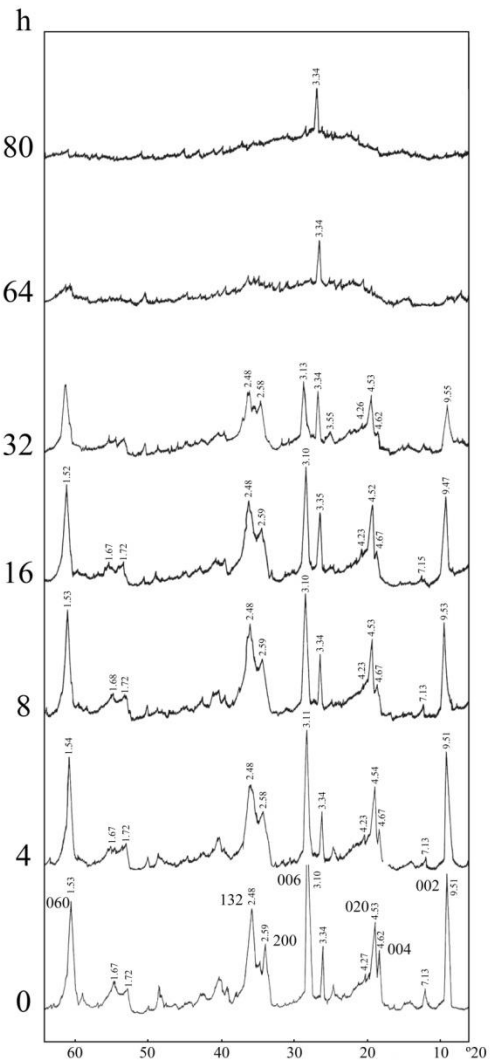

Figure 3. XRD diagrams of original (0 h) and dry ground (4-80 h) industrial talc sample.

A detailed structural examination of the powder XRD diagrams (Figures 2 and 3) have shown that, in fact, there are random translations along b-axis induced at the first grinding stages. This process caused a partial ortogonalization of the structures. Although these kinds of studies by XRD are complex, it was confirmed using quasi-randomly oriented samples of pyrophyllite and talc examined by X-ray diffraction transmission techniques [39, 89, 90]. In

other words, relative short times of dry grinding treatments induced only limited layer translations, changing regular stackings modes of the layer silicates into more random and thus the structure became more disordered.

However, for a study by XRD of the grinding effects with care, it was necessary to prepare an aggregate cut out directly from the raw talc rock sample. It was subsequently polished slightly using a fine grained glass paper to remove the surface layer, possibly affected by stress and heat treated by mechanical shear during cutting. The XRD of this prepared sample demonstrated that the original unground sample belongs to fine grained steatite [89]. Steatite is a non-platty, granular variety of talc according to Schüller and Kromer [36]. Moreover, the XRD recorded on the polished surface of the natural talc rock, after structural analysis and determination of unit cell parameter refined by a computer program, allowed to study this sample in a profound extension [89]. According to these previous results, this sample is characterized by random translations, that is, random stacking of the layer along the Y axis and the determination of the polytype was not possible. Dry grinding produces a profound structural alteration, with progressive smearing of (00l) basal reflections as suggested before, being (004) the most affected. Other (*hkl*) planes are less affected by dry grinding (Figure 3). The polytypes and polytypism of pyrophyllite and talc and the structural disorder have been already studied by XRD methods in previous papers [39, 89]. It could be very complex in the case of kaolinite, according to previous studies [51, 64]. On the other hand, as in kaolinite, several authors reported a delamination effect in talc after grinding. For instance, Christidis et al. [95] considered delamination due to the decrease of crystallite thickness. Studying (002) and (104) planes of ground talc, Mahadi and Palaniandy [100] reported a reduction in XRD peak intensity, peak base broadening, increase in background, and even peak shift. Terada and Yonemochi [94] studied the physicochemical properties of surface free energy of ground talc. They found a selective destruction of (00*l*) planes, in accordance with the present results (Figure 3). Thus, the hydrophobic property of talc surface was significantly changed to the hydrophilic property by the grinding treatment, with an improvement of surface property of talc by the grinding.

On the basis of delamination effects observed in pyrophyllite after grinding, as previously reported by Pérez-Rodríguez et al. [37], a mechanism of pyrophyllite particle degradation by grinding has been proposed by Uhlik et al. [128]. These authors considered the shape of the crystallite and the particle size distributions obtained by XRD analysis of 001 peak intensities (mean crystallite thickness and crystallite thickness distribution) and HRTEM images. The particles are first delaminated randomly, then some are delaminated preferentially and, finally, all particles undergo delamination.

In summary, the stages of degradation by dry grinding of the 1:1 and 2:1 layer silicates are directly related to a state of increasing structural disorder. Short grinding time induces only limited layer translations, changing the regular stacking mode of layers into a more random one. The process starts along the b-axis and subsequently along the b and a-axes, which results in the formation of a turbostratic structure, although it is influenced by the experimental conditions according to previous studies on kaolinite, talc and pyrophyllite. This is common for the finest particles. Thus, the prolonged grinding produces a near turbostratic structure [132] characterized by the presence of 00*l* and *hk* diffraction effects (Figures 2 and 3), with disappearance of (0*kl*) reflections such as (02*l*) and (11*l*).

3.1.2. IR Spectroscopy

Structural information can be also deduced studying the 1:1 and 2:1 layer silicates by IR spectroscopy. Figure 4 shows selected IR spectra of pyrophyllite. Detailed analysis can be performed studying different zones in the IR spectra: OH stretching, OH bending and lattice vibrations. The IR band at 3670 cm^{-1} is associated to structural OH groups bonded directly to Al cations within the structure and perpendicular to pyrophyllite layer planes [109, 122, 130]. This band decreases in intensity along grinding. The disappearance of this sharp band is explained considering that the loss of structural regularity takes place mainly along the c-axis direction. This fact is in accordance with the above X-ray results. In the case of kaolinite, the IR bands due to OH stretching at 3696, 3670, 3653 and 3620 cm^{-1} are rapidly altered by grinding, showing a noticeable reduction in their intensities, in accordance with previous reports [5, 47, 48, 52, 53, 56, 59, 66, 73]. At the same time, a broad band increases at ~ 3400 cm^{-1} and being at 3440 cm^{-1} in the case of pyrophyllite. They are both associated to randomly attached OH ions and adsorbed water.

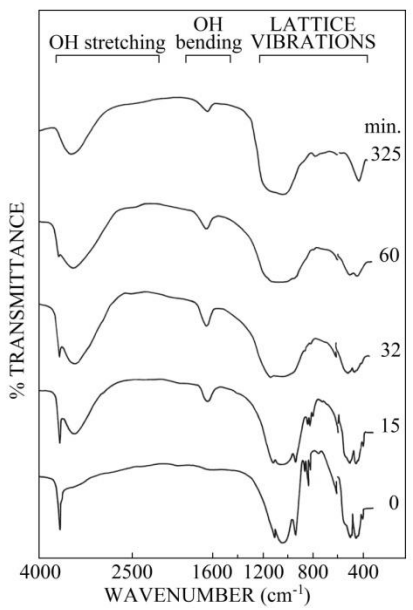

Figure 4. Selected IR spectra of original (0 min) and ground (15-325 min) pyrophyllite sample (min=minutes).

It can be also observed for pyrophyllite an important reduction of the intensity of the IR bands from 30 to 32 minutes. Thus, OH bending at 940 cm^{-1} from Al-OH groups markedly decreases, in a similar way to the band associated to OH structural groups at 3670 cm^{-1}, as well as the band at 545 cm^{-1} associated to Si-O-Al vibrations. Longer grinding times produce a drastic reduction of all these IR bands. These observations indicate total decomposition of 2:1 layer silicate with loss of periodicity perpendicular to the layer plane and a greated rupture degree between the octahedral (Al or Mg in the case of talc) and tetrahedral (Si) layers as grinding increases.

The IR bands in the region of lattice vibrations at 1115-1120 cm^{-1} and 1060-1050 cm^{-1} associated with Si-O stretching vibrations [109, 122, 130] decrease in intensity as increasing

grinding time. This band is originated from the vibrations of oxygen common to tetrahedra and octahedra, and the Si-O vibration is perpendicular to the silicate layers, i.e., to the (00*1*) plane. A progressive disappearance during grinding indicates that the structural alteration occurs mainly along the c-axis, as deduced by XRD. Detailed study of the IR spectra revealed that after 60 minutes of grinding, the band at 1120 cm^{-1} appeared slightly shifted at higher wavenumbers. A broader IR band centered at ca. 1100 cm^{-1} was observed after 90 minutes, which would indicate formation of amorphous silica after pyrophyllite decomposition by grinding. The same process occurs when grinding the well-crystallized sample of kaolinite, but after 60 minutes under the same experimental conditions. A similar fact was deduced by IR spectroscopy in previous reports when grinding kaolinite [5, 47, 52, 53, 59, 66].

At longer grinding times than 60 minutes, broader IR bands are detected at 1100 and 435 cm^{-1} associated to the formation of amorphous silica with an intense deformation of SiO_4 tetrahedra from the silicate. Modifications of the band at 1098 cm^{-1} (band SiO_2) has been also related to delamination effects during grinding kaolinite [48, 50].

On the other hand, IR broad bands are detected at ca. 3440 cm^{-1} and 1620 cm^{-1} being both associated to adsorbed or extrastructural water. Both bands increase in intensity as increasing grinding time. The disappearance of 913 and 937 cm^{-1} IR bands by grinding kaolinite is associated to the breakage of Al-OH bonds.

Finally, the alteration of Si-O stretching and the disappearance of the Si-O-Al band suggest an increase of the alteration of tetrahedral and octahedral layer.

In general, analogous observations for pyrophyllite can be deduced for kaolinite and talc after grinding, demonstrating: a) the OH groups are displaced irreversibly during grinding treatment, and b) the rupture of the O-H, Al-OH, Mg-OH, Al-O-Si, Mg-O-Si and Si-O bonds during grinding, as reported in previous papers [5, 47, 56, 59, 96].

Grinding the reference kaolinite sample KGa-1, Pardo et al. [71] suggested that dry grinding breaks the hydrogen bond between adjacent kaolinite layers, leading to the delamination of the material in accordance with previous results on dry grinding kaolinite [59, 61]. This can be the same mechanism of delamination grinding other layer silicates.

It is also possible a transfer or migration of protons from one phase (bound water of the remained unaltered 2:1 and 1:1 silicate structure) to another (broken bonds of the altered structure). This is a ‘prototropy effect’ as proposed in previous investigations on grinding kaolinite [5, 26, 47]: migrated protons interacting with OH groups and generate water molecules that can be lost at lower temperatures. Horváth et al. [65] considered this effect under the concept of ‘proton migration through grinding and their combination with OH units’. In a next paper of the same research group [66], they proposed that another mechanochemical effect on grinding kaolinite is the dehydroxylation of basal surfaces by the coalescence of two OH groups to form H_2O leaving a chemically bonded oxygen as an oxide anion in the lattice. Thus, grinding produces a mechanochemical effect of dehydroxylation at lower temperatures than that unground samples.

In a recent review, Baláž et al. [23] studied the mechanochemical effects in the presence of water. These authors considered kaolinite under this subject and indicated that amorphization by grinding is often accompanied by a condensation process within the crystal lattice, which is typical for kaolinite, and the surface OH groups lost during milling were replaced with coordinated and adsorbed water on the surface of the octahedral sheet, following the previous findings of Frost et al. [60].

However, there is also a possibility of partial rehydroxylation by activated and reactive ground powder with atmospheric water molecules. Consequently, it would be originated a weight loss by heating due to adsorbed water and, in part, weight loss of dehydroxylation associated to weakly bound OH groups. In this sense, when grinding lepidocrocite (γ-FeOOH) the OH groups are affected by the close vicinity of the positively charged Fe ions. They are polarized with the change arranged in a tetrahedral configuration and, by *prototropic interaction* with neighbour OH ions, bound water molecules are formed, resulting in a weak zone in the layered structure which facilitates delamination fracture [133]. A similar mechanism is suggested for the delamination effects during dry grinding 1:1 and 2:1 layer silicates, as discussed above.

3.1.3. Solid-State ^{29}Si and ^{27}Al MAS-NMR Spectroscopies

For this section of the present chapter, pyrophyllite was selected. The ^{29}Si MAS-NMR spectrum of the sample (Figure 5) shows a narrow resonance peak at -95.1 ppm from TMS. This is associated with Si surrounded by three Si in a Q^3 configuration or polymerization state: three Si atoms bonded to a SiO_4 tetrahedron [134-136]. The ^{29}Si MAS-NMR spectra of ground pyrophyllite samples produce a progressive broadening of the -95.1 ppm peak as increasing grinding time. A new ^{29}Si broad band, centered at -100 ppm, appears after 32 minutes of grinding. This band increased in intensity for prolonged grinding treatments, overlapping with the -95 ppm peak. At longer grinding times, a single broad band can be only observed centered at -101 ppm which was overlapped with the peak at -95 ppm. The formation of this new signal is associated to Q^4 environments in which Si is surrounded by four tetrahedra of Si and Al [134-136].

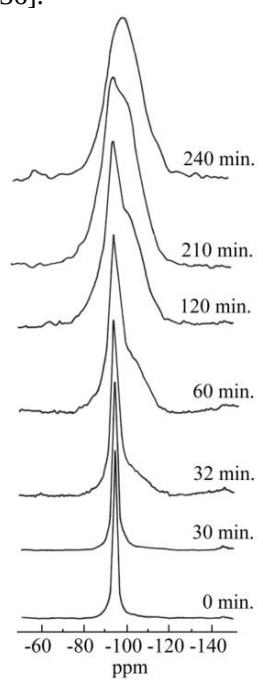

Figure 5. ^{29}Si MAS-NMR spectra of original (0 min) and ground (30-240 min) pyrophyllite.

The ^{27}Al MAS-NMR spectrum of pyrophyllite shows several peaks: a sharp peak at 4 ppm, which is ascribed to octahedral Al coordination [134-136], and four small peaks or sidebands (SB) associated with the sample spinning. The ^{27}Al MAS-NMR spectra of ground pyrophyllite show the single peak at 4 ppm and below 32 minutes of grinding, additional bands between 30-60 ppm are detected. Their intensities increase as grinding times is longer. These new bands can be associated to tetrahedral and possible pentahedral Al coordination [126, 135-137], which are being generated during grinding. The progresive grinding produces an increase of tetrahedral Al coordination and confirmed the asignation of Si surrounded by four tetrahedra of Si and Al, as described above. The ^{27}Al MAS-NMR spectrum of a pyrophyllite sample heated at 300 ºC and previously ground for 240 minutes showed signals at 50, 35 and -1.6 ppm. They have been ascribed to tetra-, penta- and octahedral coordination of Al [125, 126]. Thus, the heating at temperatures lower than 300 ºC leads to the formation of less distorted pentahedral Al than that detected in unground heated pyrophyllite samples. These different Al coordinations can be detected as MAS-NMR signals associated to the structural alteration of the 2:1 layer silicate by dry grinding.

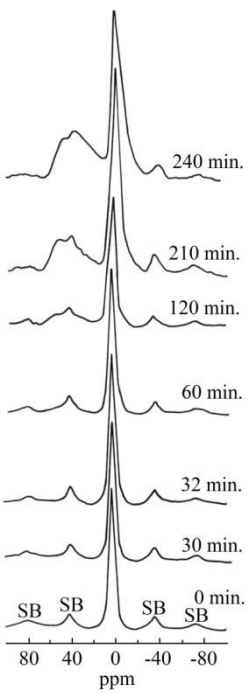

Figure 6. ^{27}Al MAS-NMR spectra of original (0 min) and ground (30-240 min) pyrophyllite.

This result is explained taking into account a dehydroxylation of the mechanochemically activated pyrophyllite at lower temperatures as compared with the unground sample. It should be emphasized that the characteristics peaks of ^{27}Al MAS-NMR spectra are affected by the local environment: sharp resonances usually indicate short-range order while broad resonances indicate short-range disorder in the structure [138, 139].

After comparison of both set of MAS NMR spectra (Figures 5 and 6), it can be deduced that a considerable tetrahedral structural breakdown is produced after 32 minutes of grinding. It is concluded from these results that the structure of this 2:1 layer silicate is progressively

destroyed by dry grinding, in accordance with IR results (Figure 4), where the crystal structure is progressively disordered and altered by this treatment, as above described. Taking into account these MAS-NMR results, it is also very important to note the structural modifications detected in tetrahedral sheets of pyrophyllite, with theoretical formula $Al_2Si_4O_{10}(OH)_2$ because the original octahedral Al coordination, with Al bonded to OH groups, changed to tetrahedral Al coordination, with a vacancy due to the loss of a ligand. Water is eliminated by dehydroxylation because the octahedral Al-O(OH) sheet is affected, being in connection with the structural breakdown and formation of an amorphous material as deduced by XRD [37, 115-117, 119]. Kaolinite is a 1:1 layer aluminium silicate with OH groups, whereas pyrophyllite is 2:1 containing originally aluminium octahedra bonded with OH groups perfectly sandwiched between silica tetrahedra. Structural breakdown is facilitated a priori in kaolinite by grinding, but does not in pyrophyllite. In other words, taking into account the structure of 2:1 silicates (Figure 1), the breakdown of tetrahedral sheet produced a looser environment coordination structure around the Al cations and thus it is affected by the progressive grinding.

The structural changes of kaolinite are consistent with those previous results on quantification of crystalline and noncrystalline material in ground kaolinite analyzed by several techniques, including solid-state MAS-NMR [54]. The ^{29}Si MAS-NMR spectrum of unground kaolinite showed a sharp resonance peak at -91.8 ppm from TMS. This is associated with Si surrounded by three Si in a Q^3 configuration or polymerization state [126, 134-139]. Grinding kaolinite showed an increase in breadth of this resonance and the formation af a broad band, as in the case of pyrophyllite, being observed at ca. -95 ppm which was overlapped with the peak at -91.8 ppm. The formation of this new signal is associated to Q^4 environments in which Si is surrounded by four tetrahedra of Si [126, 134-139], as point out above. Using ^{29}Si NMR spectroscopy at 60 MHz, Suraj et al. [57] reported that an unground kaolinite shows a single sharp peak at -92.213 ppm. When the sample is ground for 30 minutes in a disc mill, the Si resonance was broadened and shifted towards upfield to ~ -100 ppm, atributable to the presence of a number of Si sites of different bond lengths, bond angles or cation-oxygen bond strengths [140]. Suraj et al. [57] suggested that this observation reflects a decrease in the number of aluminum groups bonded to SiO_4 groups. These authors concluded that silica is being separated from the aluminosilicate phase. The study of ground kaolinite by ^{29}Si MAS-NMR spectroscopy suggested that SiO_4 tetrahedra were considerably distorted in the structure ground in an agate mortar for $\geq$ 30 hours [54]. It is clear that when grinding time is increased for kaolinite, the structural alteration and disorder became more pronounced, as in pyrophyllite (Figures 5 and 6).

The ^{27}Al MAS-NMR spectra of kaolinite ground at several times are similar to those presented for pyrophyllite. For a complete discussion, the previous results of Kodama et al. [54] grinding kaolinite up to 150 hours are interesting.

The original kaolinite sample shows a single peak of octahedral Al coordination at -4.1 ppm. Grinding kaolinite produced the detection of extra resonance bands near 30 ppm (it appeared from 30 hours of grinding) and near 56-60 ppm, characteristic of tetrahedral Al coordination [126, 134-139]. They attributed that the weak resonance at 30 ppm that may be due to separate tetrahedral species [141], as previously observed in the spectra of heated kaolinite after dehydroxylation (metakaolinite). However, the ^{27}Al MAS-NMR spectra of several samples of kaolinite treated at different temperatures indicated that, after heating, the

intensity of the peak at 3 ppm (assigned to octahedral Al) decreases and two additional peaks appeared near 57 and 27 ppm [139].

The first one of these additional peaks corresponded to pentahedral coordinated Al and the second one to tetrahedral coordinated Al [134-139]. It should be noted that the octahedral Al coordination signals appeared shifted from -4.1 ppm to 2.0 ppm, and the tetrahedral signals shifted from 56 to 60 ppm as grinding time increased. According to Kodama et al. [54], the ^{29}Si and ^{27}Al MAS-NMR spectra of the sample of ground kaolinite studied in their work showed a remarkable similarity to those reported for metakaolinite [141, 142].

Table 1. Specific surface areas (m^2/g) of the two kaolinite samples (KGa-1 and KGa-2), purified Pyrophyllite (P), Talc (T) and Pyrophyllite Raw Clay sample (PRC), original (0 minutes) and ground in a planetary ball mill using a ball:powder ratio of 1:0.22 at a rate of 250 rpm

Grinding time (min)	KGa-1 (m^2/g)	KGa-2 (m^2/g)	P (m^2/g)	T (m^2/g)	PRC (m^2/g)
0	10.20	19.81	1.17	3.20	12.44
5	-	-	14.01	11.41	-
10	-	38.63	21.02	24.62	-
15	18.31	-	41.52	-	24.73
20	-	-	-	47.71	-
30	-	50.27	51.60	109.72	-
32	17.73	-	38.21	-	39.35
60	13.01	37.00	19.13	28.74	34.14
120	11.35	-	-	-	-
180	-	9.49	-	-	-
210	-	-	-	2.82	-
240	-	-	5.26	-	8.41

Table 2. Specific surface areas (m^2/g) of the industrial kaolin (IK), industrial talc (IT) and Pyrophyllite Raw Clay sample (PRC) original (0 hours) and ground in a planetary ball mill using a ball:powder ratio of 1:4.28 at a rate of 400 rpm

Grinding time (hours)	IK	IT	PRC pyrophyllite
0	14.7	8.4	14.0
4	30.6	42.9	43.5
8	35.7	44.7	51.2
16	41.2	52.6	50.0
32	46.6	59.1	70.1
64	44.9	30.3	38.7
80	38.5	10.8	22.2

Following the above discussion, and taking into account the formation of metakaolinite by heating kaolinite [126, 137, 139-142], the dry grinding of kaolinite, and pyrophyllite and talc, produced the mechanochemical effect of dehydroxylation by intense local heating and impact of the particles and the grinding media, as well as the mechanism proposed in the above section of OH basal groups. In the present case, the grinding media are balls and the

planetary milling. Then, the original octahedral Al coordination in kaolinite bonded to OH groups changed to tetrahedral Al coordination with a vacancy due to the loss of a ligand and water is eliminated by dehydroxylation. Due to the loss of OH groups, and considering that the theoretical formula of kaolinite is $Al_2Si_2O_5(OH)_4$ the octahedral Al-O(OH) sheets appeared to be more directly affected than the SiO_4 sheets, as deduced from the MAS NMR spectra. This is in accordance with previous IR results, as above discussed, and the plausible mechanism of structural alteration of 1:1 and 2:1 layer silicates by dry grinding.

3.2. Textural Properties of Ground Layer Silicates: Specific Surface Areas, Particle Sizes, Crystal Sizes (Coherent Diffraction Domains), Lattice Microstrains and Morphologies

3.2.1. Specific Surface Areas and Particle Sizes

Tables 1 and 2 show the BET specific surface areas determined for all the samples ground using two different balls:powder weight ratios, as studied in this chapter.

From these values, the average diameter of the particles assuming a spherical shape (equivalent spherical diameter) was calculated using the equation S=F/(ρD) where F is a shape factor (6.0 considering a particle's shape as a sphere); S is the specific surface area (m^2/g); ρ the density of the clay sample (theoretical kaolinite, talc, pyrophyllite and an estimation for the pyrophyllite raw clay) and D the diameter (in μm). The obtained values are included in Tables 3 and 4.

The specific surface areas of the samples increase with grinding time in the first minutes (Table 1) and hours (Table 2) up to a maximum value different for each clay sample. Differences are observed considering the two kaolinite samples comparing the ordered or well-crystallized (KGa-1) and the disordered or poorly crystallized kaolinite (KGa-2), with a maximum of 50.27 m^2/g in the second one at 30 min starting with powders of different surface areas. In this case, the balls:powder weight ratio is of 1:0.22.

Table 3. Average particle sizes of the clay samples estimated from specific surface area values (Table 1)

Grinding time (min)	KGa-1 (μm)	KGa-2 (μm)	P (μm)	T (μm)	PRC (μm)
0	0.22	0.11	1.83	0.73	0.17
5	-	-	0.15	0.20	-
10	-	0.05	0.10	0.10	-
15	0.12	-	0.05	-	0.08
20	-	-	-	0.05	-
30	-	0.04	0.04	0.02	-
32	0.12	-	0.05	-	0.05
60	0.17	0.06	0.11	0.08	0.06
120	0.20	-	-	-	-
180	-	0.24	-	-	-
210	-	-	-	0.83	-
240	-	-	0.40	-	0.26

Table 4. Average particle sizes (μm) of the industrial kaolin (IK), industrial talc (IT) and Pyrophyllite Raw Clay sample (PRC) estimated from specific surface area values (Table 2)

Grinding Time (hours)	IK	IT	PRC pyrophyllite
0	0.15	0.34	0.16
4	0.07	0.06	0.05
8	0.06	0.06	0.04
16	0.05	0.05	0.04
32	0.04	0.04	0.03
64	0.05	0.09	0.05
80	0.06	0.27	0.10

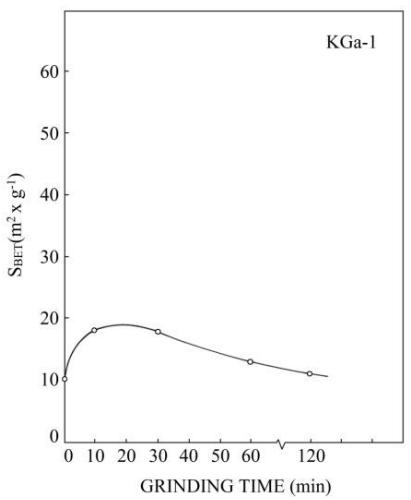

Figure 7. Specific surface areas of original well-crystallized kaolinite (KGa-1 sample) and ground by ball-milling using a balls:powder ratio of 1:0.22, as a function of grinding time (min).

Figures 7 to 10 include illustrative graphical representations of the evolution of specific surface areas of these clay samples as increasing grinding times (min or h). Figures 11 and 12 show the evolution of calculated average particle sizes (equivalent spherical diameter) for industrial kaolin and talc after grinding. It can be observed that the rate of size reduction decreased with time and a limit is reached for each clay sample, producing particles of average sizes higher than 0.02 μm (talc sample, Table 1).

In accordance with previous reports grinding layer silicates and from a point of view of mineral processing [5, 12, 16, 17, 23], there is an optimum time for grinding to produce an increase of specific surface areas, i.e., to decrease the particle size, beyond which any further grinding will be of no benefit. Taking into account the present results (Tables 3 and 4), after the lower limits of particle size reduction of these clay samples are reached, the particle sizes remains almost constant. The evolution is similar to those found after grinding other solids [23] and layer silicates in previous works [10, 14-17, 21-28, 37-39, 44-75, 79-101, 103-127].

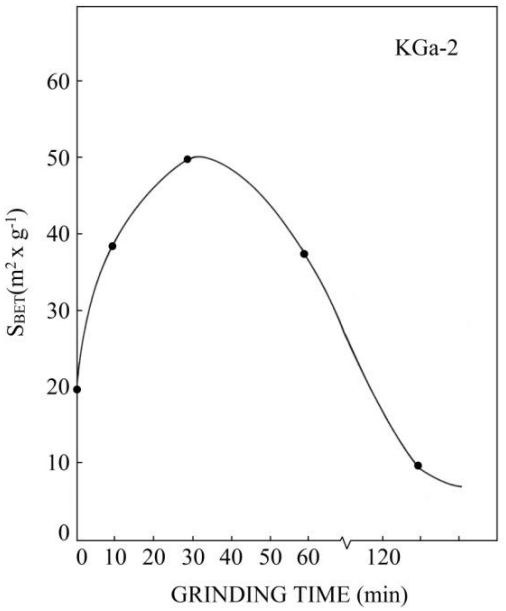

Figure 8. Specific surface areas of original poorly-crystallized kaolinite (KGa-2 sample) and ground by ball-milling using a balls:powder ratio of 1:0.22 milling, as a function of grinding time (min).

However, the values of maxima of specific surface areas could be different according to the characteristic of the starting clay samples and experimental grinding conditions, as pointed out in previous sections.

The industrial kaolin sample ground using a balls:powder weight ratio of 1:4.28, and grinding time prolonged up to 80 h, shows a maximum of 46.6 m^2/g at 32 h of grinding time (Table 2 and Figure 9), with minimum particle size of 0.04 μm (Table 4 and Figure 11). Pyrophyllite shows a maximum of 51.60 m^2/g and 39.35 m^2/g in the pyrophyllite raw sample (Table 1), although the maximum value of this sample is 70.1 m^2/g at 32 h (Table 2) using different experimental conditions of grinding. Talc shows the maximum relative value of 109.72 m^2/g at 30 min (Table 1), as compared with the other samples. Changing the experimental conditions, the pyrophyllite raw clay sample is the higher (Table 2). It should be noted that these features for each clay sample coincide with the strong estructural alteration and amorphization, as observed by XRD, IR and MAS-NMR (Figures 2-6) in the previous section of this chapter. In fact, grinding produces that primary particles tend to adhere to each other because of the increased energy and the action of the amorphous surface layers formed during grinding, as previously proposed [54, 57].

González-García et al. [55] found a maximum value of 40 m^2/g by ball milling an industrial kaolinite sample under the same experimental conditions of balls:powder weight ratio of 1:4.28, and grinding time prolonged up to 80 h. Grinding several high-grade natural kaolinites, Frost et al. [66] suggested that the effectiveness of the mechanochemical treatment depends on the crystallinity of kaolinite, in accordance with the present results. These authors

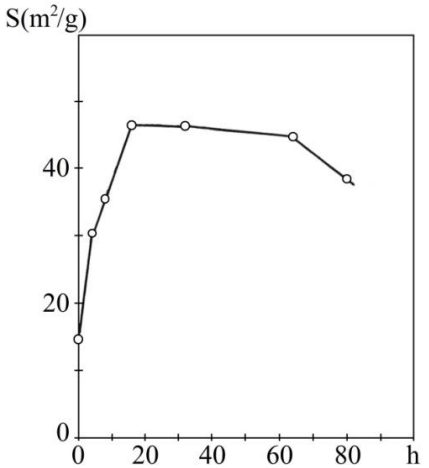

Figure 9. Specific surface areas of industrial kaolin samples, original and ground by ball-milling using a balls:powder ratio of 1:4.28, as a function of grinding time (h).

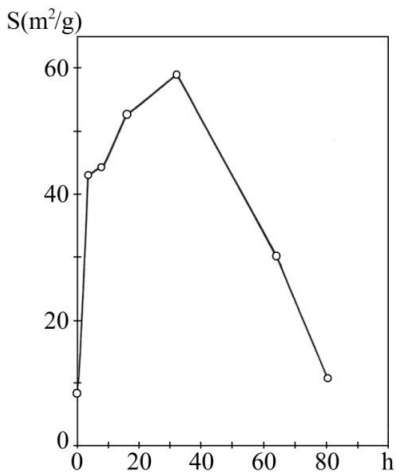

Figure 10. Specific surface areas of industrial talc samples, original and ground by ball-milling using a balls:powder ratio of 1:4.28, as a function of grinding time (h).

identified two processes in the mechanochemical activation of kaolinite. First of all, the delamination process of kaolinite appears to takes place at the first hour of grinding (under their experimental conditions), and second a recombination process results in the reaggregation of the ground crystals. Taking into account previous reports [17, 23, 66, 68, 69], the changes in the surface areas can be used to identify different stages or steps of the grinding process: (I) the produced new surface areas by breaking the original particles, with delamination in the case of layer silicates, is approximately proportional to the grinding time; (II) aggregation section with a monotonic decrease in the specific surface areas, and (III) agglomeration section, when the specific surface areas decrease.

The increasing of specific surface areas of the clay samples is interpreted due to an important reduction of particle sizes (Tables 3 and 4 and Figures 11 and 12) as a consequence of grinding treatment. This is produced very fast at the first minutes (or hours) of grinding treatment up to reach a maximum value (see Tables 1-2 and Figures 9-10). Consequently, a

limit in particle size reduction is reached by grinding and mechanochemical effects are operating and generating particles with high surface energy partially compensated by a size increase. The activated ground particles with enhanced surface reactivity start a reaggregation, agglomeration or "cold-welding" process [11-13]. Mechanochemical effects are manifested with formation of reduced particles with high surface energy, which is partially compensated by the size increase by re-aggregation forming aggregates and agglomerates. These features are similar to thoser found after grinding silicates and other inorganic solids [16-23]. This is a general behaviour of solids submitted to grinding and considered mechanochemical reactions [23]. It is interesting to mention a recent paper by Li et al. [143]. These authors discussed the formation of aggregates and agglomerates in a dry ground sample. They suggested that as a result of the low thermal conductivity of most of non-metallic solids, the energy delivered by the mill is not totally stored in the particle as thermal energy but is also applied to the bending and/or breaking of the crystalline solid, following the previous work on grinding kaolinite by Aglietti et al. [53]. Many broken bonds are formed in the process of fragmentation; these create new surfaces to take more charge and to enhance surface activity. Consequently, there is a tendency for particles to aggregate spontaneously to reduce the enthalpy of the system [143].

On the other hand, the previous studies on a pyrophyllite sample (Hillsboro, North Carolina, USA) by fisisorption of nitrogen have demonstrated a maximum of specific surface area of 60 m^2/g at 30 minutes of grinding [37-39, 131]. The adsorption of nitrogen gas by multilayers and the absence of micropores have been reported [131]. The pore size distribution analysis of these ground pyrophyllite samples has proved a contribution of sizes ranging between 2-5 nm to the increase of surface area. Above 30 minutes of grinding, this contribution decreases progressively by the re-aggregation or agglomeration process of the ground particles due to their high surface energy, with an important contribution of size pores lower than 4 nm [131]. However, Temuujin et al. [130] reported the presence of significant numbers of micropores in ground pyrophyllite samples but after leaching.

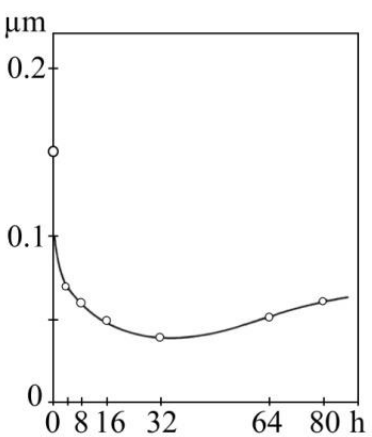

Figure 11. Average particle sizes (equivalent specific surface diameters) of original industrial kaolin sample and ground by ball-milling (balls:powder ratio of 1:4.28), as a function of grinding time (h).

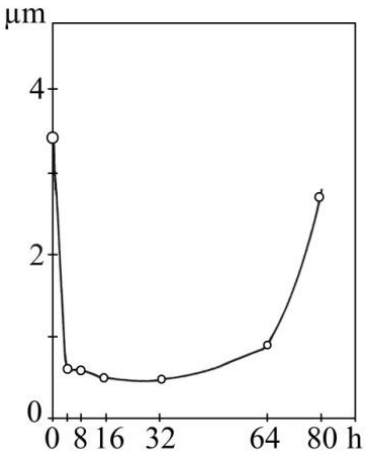

Figure 12. Average particle sizes (equivalent specific surface diameters) of original industrial talc sample and ground by ball-milling (balls:powder ratio of 1:4.28), as a function of grinding time (h).

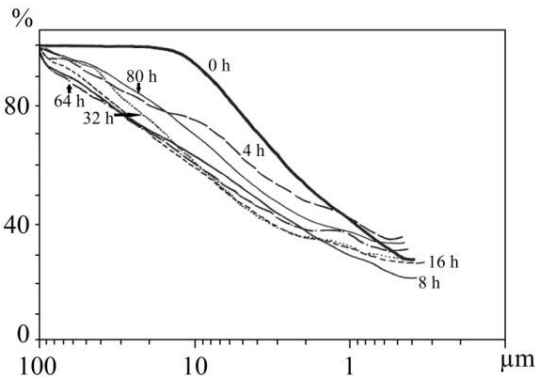

Figure 13. Cumulative curves of particle size distribution analysis (Sedigraph) for original industrial kaolin sample and samples ground by ball-milling (balls:powder ratio of 1:4.28).

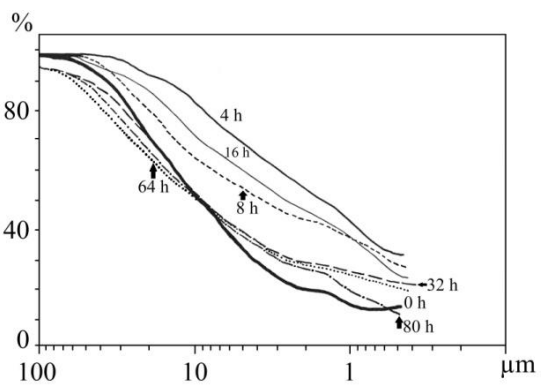

Figure 14. Cumulative curves of particle size distribution analysis (Sedigraph) for original industrial talc sample and samples ground by ball-milling (balls:powder ratio of 1:4.28).

Particle size distribution analysis of selected original and ground samples has been studied using two methods after dispersion in water: Laser scattering and sedimentation using

X-ray methods (Sedigraph). The size distribution of particles is affected by the mechanochemical agglomeration process, as described above.

To illustrate this behaviour, Figures 13 and 14 are presented. They show the cumulative curves of particle size distribution analysis (by Sedigraph) of industrial kaolin (Figure 13) and talc (Figure 14) samples, respectively. These samples were ground by ball-milling using a balls:powder weight ratio of 1:4.28 and grinding time was prolonged up to 80 h.. In general, the measured size distributions of the ground powders (4-80 h) dispersed in water contained particles that seemed larger than those of the starting samples. These agglomerated particles seem to be rather hard and the dispersion treatment using chemicals and sonication before particle size analysis using both techniques is not so effective. This observation is in accordance with previous results grinding layer silicates [52, 53, 55, 57, 88]. For instance, agglomerates produced by dry-grinding kaolinite can be of sizes in the range 15-20 μm and larger, even up to 40 μm in diameter [52, 53, 55]. Dellisanti and Valdré [75] reported particles larger than 100 μm by grinding kaolinite during 20 hours, the particles dispersed in water and laser scattering measurements.

Agglomeration of the fine particles increases with the progress of grinding. Thus, the mean size calculated from the cumulative size distribution curve is significantly larger than the average particle size diameter (equivalent spherical diameter), as estimated from specific surface areas (Tables 3 and 4). This discrepancy is explained considering the agglomeration of the very fine particles produced by ball milling. A microscopy study will be presented in a next section to study the formation of agglomerates in these ground clay samples.

If it is considered the particle size distribution analysis (Figures 13 and 14), the mean particle diameter can be calculated in each case for kaolinite and talc. Figures 15 and 16 show the determined values. The observations of Figures 15 and 16 are in agreement with the above: the particles seemed larger than those of the starting samples and this behaviour is associated to the agglomeration process. Starting from average particle size of 2μm in the case of kaolinite, the maximum agglomerated particles reached ~ 6 μm at 16-32 hours and slightly decreased as increasing grinding time. For the industrial talc sample, the rapid decrease of average particle size at 4 hours (1.45 μm) starts to increase with grinding time up to a similar average particle sizes of the original (unground) talc sample at 32 hours, with average particle sizes of ~ 9 μm at 80 hours.

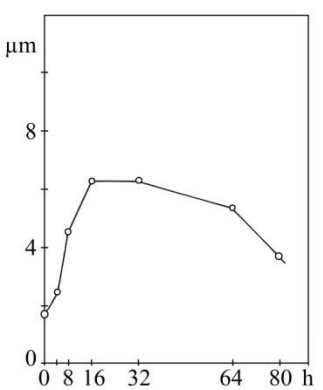

Figure 15. Average particle sizes (μm) determined by particle size distribution analysis (Sedigraph, Figure 13) for original industrial kaolin samples and ground for different times.

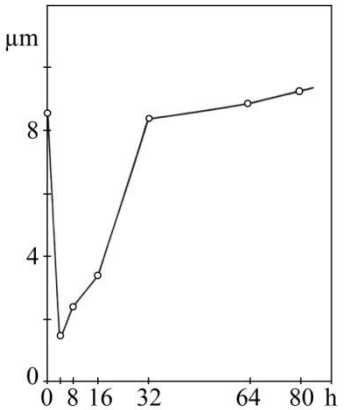

Figure 16. Average particle sizes (μm) determined by particle size distribution analysis (Sedigraph, Figure 13)) for original industrial talc samples and ground for different times.

3.2.2. Crystal Sizes (Coherent Diffraction Domains) and Lattice Microstrains

Crystal sizes and lattice microstrains are two parameters obtained from XRD profiles to evaluate the progress of mechanical treatments by dry grinding. In the present chapter they are also interesting to compare the evolution of 1:1 and 2:1 layer silicates by dry grinding. The XRD diagrams (Figures 2 and 3) of industrial kaolin and talc samples, original and ground from 4 to 80 h, are considered in this part of the chapter. Taking into account the pronounced propensity of layered silicates toward cleavage perpendicular to this c-axis, the alteration caused by dry grinding is greater along the c-axis of the silicate structures and the (00*l*) reflections are the most affected. Hence, there is a loss of periodicity perpendicular to the layer silicate plane and the dimensions of the crystallites along the c direction become too small to produce coherent X-ray scattering, with an increasing in amorphization.

The results of XRD (Figures 2 and 3) show that the intensities of the general (*hkl*) reflections change less than that the basal (00*l*) reflections, with a progressive increase of line broadening which leads to an amorphous material. The increase in line broadening and the decrease in intensity of the XRD peaks become marked. The characteristic kaolinite and talc XRD peaks finally disappear at long grinding times since the original crystal structure is destroyed under the mechanical action of the ball milling. Thus, grinding produces a reduction in the number of layers in individual particles and a profound distortion of the crystal lattice. The crystalline disorder, defects, particle size diminution and microstrains cause the broadening of the XRD peaks and the ground material become more amorphous to X-rays. The contribution of crystallite size and lattice microstrains can be analyzed from X-ray line broadening.

The line breadths for selected (00*l*) diffractions have been obtained from the diffractometer profiles by measuring their respective FHWM and performing the corrections (see experimental section). From these FHWM corrected values, the mean crystallite size (D) or coherent domain and the mean lattice microstrain (e) have been estimated. Figures 17 and 18 show the results of D considering the (001) peak for kaolinite and the (002) peak for talc as a function of grinding time.

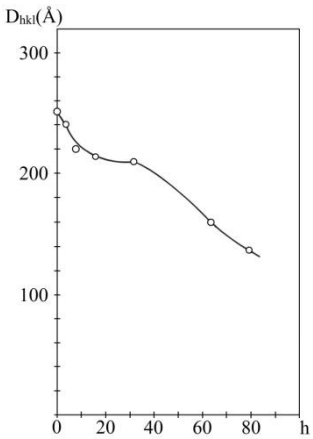

Figure 17. Crystallite size (coherent diffraction domain) for (001) reflection of kaolinite as a function of grinding time (balls:powder ratio of 1:4.28), as determined for the sample of industrial kaolin (Figure 2). 1 A = 0.1 nm

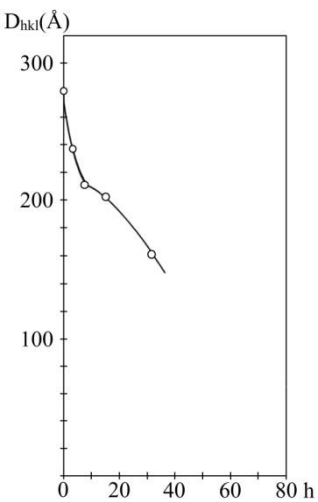

Figure 18. Crystallite size (coherent diffraction domain) for (002) reflection of talc as a function of grinding time (balls:powder ratio of 1:4.28), as determined for the sample of industrial talc (Figure 3). 1 A = 0.1 nm

Figures 19 and 20 show the corresponding evolution of the e values. According to these results, the crystallite sizes decrease and lattice microstrains increase as grinding time increases. The values of D in kaolinite decrease from 25 nm (original) to 14 nm at 80 hours of grinding. For instance, Pardo et al. [71] found variations for kaolinite (well-crystallized sample) from ~ 40 nm to 31.7 nm and from to 37 nm to 8.5 nm using two procedures of dry grinding.

Concerning the sample of industrial talc, the values decrease from 28 nm (original) to 16 nm at 32 hours because longer grinding times produced the disappearance of (002) peak. As pointed out before, the coherent domain size or "crystallite size" and the grain size or "particle size" of materials are two features which are theoretically independent [119]. However, it is clear that there may be some indirect relationships between both parameters.

Thus, there is small grain size and small domain size in the "clay fraction" or fraction below 2 μm of layer silicates and natural mixtures of them.

On the other hand, the values of lattice microstrains for both layer silicates increase as increasing grinding time, although the relative values are higher for talc (Figure 20) as compared with kaolinite at the same grinding time (Figure 19).

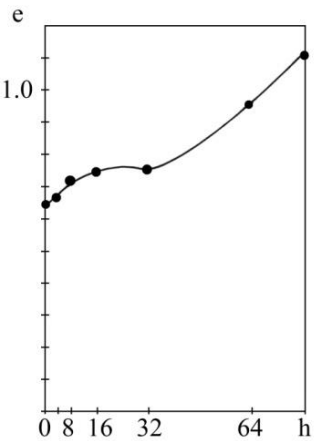

Figure 19. Values of mean lattice microstrains for the industrial kaolin sample determined by (001) reflection analysis of kaolinite as a function of grinding time (h).

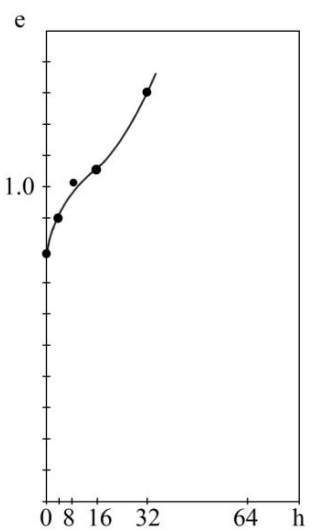

Figure 20. Values of mean lattice microstrains for the industrial talc sample determined by (002) reflection analysis of talc as a function of grinding time (h).

These observations could be in connection with the differences in the crystal structures of 1:1 and 2:1 layer silicates, although there is not a plausible explanation. Efforts have been previously performed to study samples of talc and pyrophyllite by grinding and using other X-ray methods [39, 89, 90]. For instance, in a previous paper studying two pyrophyllite samples, the X-ray variance method was used to determine D and e after mechanical treatment by dry grinding [116, 117].

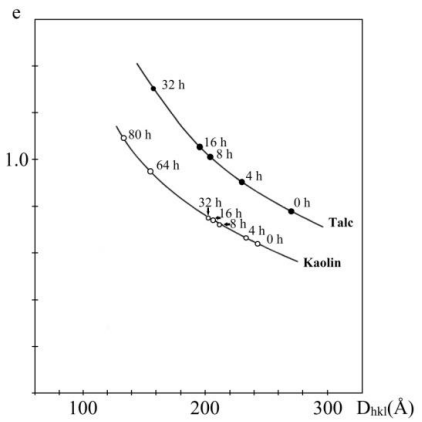

Figure 21. Mean lattice microstrains plotted as a function of crystallite sizes (coherent diffraction domain) for original and ground industrial kaolin and talc samples.

However, the basal reflections were not considered. The (131) diffraction profiles of the samples were analyzed by this method and assuming octahedral and tetrahedral crystallite shape. A size limit of ~ 10 nm of D at 30 minutes of grinding time was reached. The strain increased up to a maximum of $4.8x10^{-3}$. In the case of talc, in a previous study using the Scherrer equation and MudMaster software, both applied to talc samples after grinding, the reduction in particles size was as low as 0.009 μm, with equivalent spherical diameter of 0.021 μm [89, 90]. However, in the present investigation different experimental conditions have been considered: a balls:powder weight ratio of 1:4.28 and prolonged times up to 80 hours (Figures 2 and 3).

Finally, Figure 21 shows a plot of these D and e values to show the relation between both parameters. It is observed an inverse relationship between mean lattice microstrains and crystallite size considering the (001) peak for kaolinite and (002) for talc. The microstrain content increases proportionally with the reciprocal of crystallite size, as occurs in other materials [144-147]. This kind of relationship was also found for pyrophyllite samples after grinding [116, 117, 119]. Grinding produces an increase in X-Ray line broadening and a decrease in crystallite size (Figures 17 and 18). The small crystals produced by grinding have a high content of lattice microstrains as the crystal structure is altered and degraded by impact of the grinding media. The particles of ground samples are formed by small crystallites welded together in a mosaic structure, as has been assumed grinding other solids [146]. According to Criado et al. [146], the grain boundaries constitute the main contribution to the lattice microstrains. Therefore, the higher the number of grain boundaries in a particle, the smaller the size of the crystallites. Through mechanical treatment by dry grinding, the number of grain boundaries increase substantially within a more defective structure. A previous study on crystal imperfections with respect to crystal orientation in kaolinite minerals by XRD and TEM concluded that there is a mosaic structure in the crystalline surface, with imperfections being more important in [111] and [002] directions [148]. This fact significantly influences the properties of the silicate.

3.2.3. Morphological Changes by SEM and TEM

Morphological changes and size reduction with grinding have been studied by SEM and TEM. In general, SEM and TEM examination of original and ground clay minerals treated at

short grinding times allow to observe that the layered particles are delaminated. Prolonged grinding resulted in the breakdown and drastic size reduction of relatively thin particles. Progressively, they lose their original shape reaching more isometric particles with nanometer size as increasing grinding time. For the sake of simplicity, in this section only the SEM results are presented and discussed.

The evolution of a ground clay sample is illustrated in Figure 22 for purified pyrophyllite. At the first stages of grinding, SEM observations indicate that the original pyrophyllite plates experiment a morphological evolution changing the layered aspect. Thus, it can be observed delamination of the stacking layers, some gliding, folding of the layers and reduction of the layers in smaller particles (Figure 22 a, b, c, d). This is a contribution to the relative rapid increase of specific surface area (Tables 1 and 2). Progressive grinding produces a decrease in particle size (Figure 22 e, f), and the surface area can reach a maximum, as pointed out above. However, agglomeration of the particles starts to be observed by SEM (Figure 22 f, g, h), with degradation of the original material and formation of an amorphous product, and specific surface areas decrease. The agglomeration or re-aggregation process increases with grinding time. It can be observed by SEM that the agglomerates gradually became almost rounded in shape with a rugged surface. At longer grinding times, larger agglomerates are present, as observed by SEM. They contain very smaller particles and appeared welded (Figure 22 g, h). Then, SEM allows to observe the formation of nanometer size ground powders and further particle agglomeration with an increase of amorphization as a consequence of long grinding times.

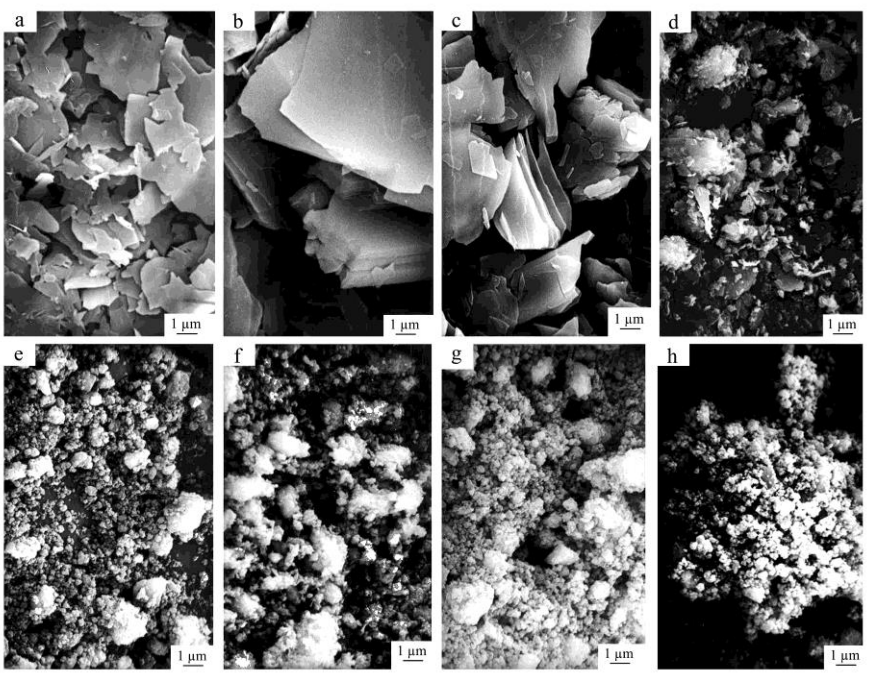

Figure 22. Selected SEM microphotographs of original pyrophyllite sample (a, b) and after grinding (balls:powder ratio of 1:0.22) at several times (min): c) 5 min; d) 15 min; e) 30 min; f) 60 min; g) 120 min and h) 240 min.

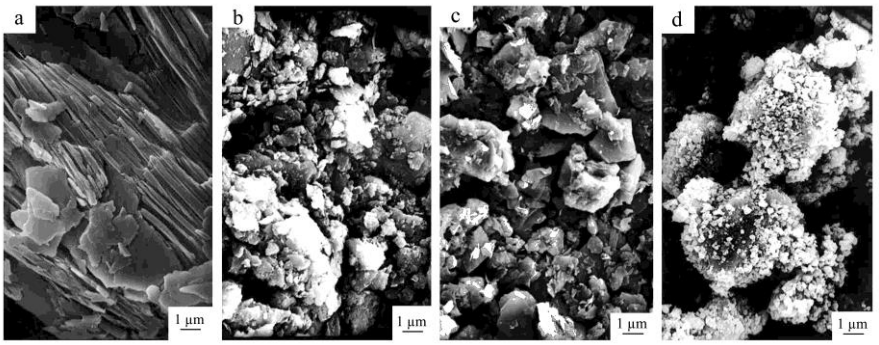

Figure 23. Selected SEM microphotographs of original Pyrophyllite Raw Clay sample (a) and after grinding (balls:powder ratio of 1:0.22) at several times (min): b) 15 min; c) 32 min; d) 240 min.

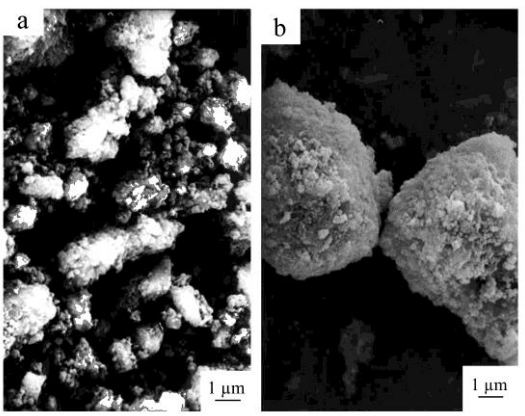

Figure 24. Selected SEM microphotographs of industrial talc sample after grinding (balls:powder ratio of 1:4.28) at several times (min): a) 64 h; b) 80 h.

SEM observations of the original and ground pyrophyllite raw clay show similar features to the above described for the purified pyropyllite sample (Figure 23). The original stacking layers of the mixtures of silicates are delaminated and these particles are broken by mechanical impact of the balls, producing a decrease in particle size (Figure 23 a, b, c) and an increase in specific surface area (Table 1). As grinding progresses, the agglomeration and re-aggregation process can be observed by SEM (Figure 23 d). It is important to note that the agglomerates are constituted by smaller particles.

Figure 24 shows selected SEM micrographs of the industrial talc sample after grinding to show the formation of agglomerates. These are samples where the reduction of specific surface area is very important (Figure 10). The change of greasy feel of the original platy particles of talc into a gritty feel of the ground material is noteworthy, as pointed out by Filio et al. [88]. However, wet milling of a dolomitic talc produced particles that exhibited delaminated talc in nanosheets [100].

Grinding the industrial kaolin sample under the same experimental conditions allows to observe the delamination of the original booklets. The layered particles, with well-formed faces, are broken by grinding. Dry grinding produces a decrease in particle size and an increase of specific surface area (Figures 9, 11 and 15). In this case, formation of amorphous

agglomerates by grinding can be observed by SEM (Figure 25), although it is not so extended as compared with the other clay samples.

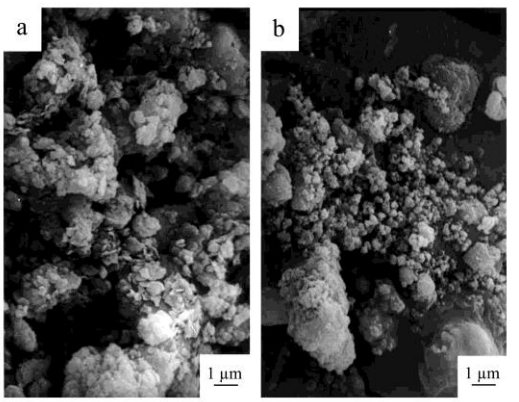

Figure 25. Selected SEM microphotographs of industrial kaolin sample after grinding (balls:powder ratio of 1:4.28) at several times (min): a) 60 h; b) 80 h.

Thus, the evolution of specific surface area of this sample shows that the maximum of surface area reached a plateau from 20 to 60 hours of grinding, decreasing at 80 hours but no so fast as in ground talc (Table 2 and Figure 10). The ball-milling conditions have not produced the intense effect as in the others clay samples.

The agglomerates can be of several sizes depending of the kaolinite sample and the experimental grinding conditions. For instance, Aglietti et al. [52, 53] observed a size up to 40 μm of diameter. These authors also reported that the ground kaolinite agglomerates are not disintegrated by the use of chemical dispersants or sonication before size analysis, as pointed out in a precedent section (Figures 13-16). This is an indication of the high energy involved in the bond of the solid broken particles produced by milling. González-García et al. [55], grinding two industrial kaolins of different degree of crystalinity, observed the formation of large spheroidal aggregates of fine particles produced by ball milling. As noted before, these authors used the same grinding conditions as in the present case for the industrial kaolin and talc (Figures 2 and 3). They reported a size of 15-20 μm by SEM for these tightly bound particles. Grinding other sample of kaolinite, Suraj et al. [57] reported the agglomeration of formed platelets produced by oscilatory milling into small balls, with a size of agglomerates of 5 μm in diameter, which tends to increase with milling time. Frost et al. [66] indicated that SEM images of ground kaolinite particles agglomerate to take on a spherical shape.

In consequence, ball milling of these clay minerals during long time produces, as a mechanochemical effect, the change of platy morphology to a new particle structure, as it was previously found [9, 28, 37, 44, 52, 53, 57, 62, 73, 86, 96, 100, 118, 123].

Agglomerates are very common in many finely divided powders. Its formation is due to a tendency of the starting particles to reduce their surface free energy [11-16]. An “aglomerate” is defined as a limited arrangement of primary particles, which forms a network of interconnective pores. The primary particles in “hard agglomerates” or “aggregates” are bonded by solid bridges or grain boundaries. It is the behaviour when the clay samples are ground at longer times above the limit of mechanochemical reduction of the particles (Tables 1-4 and Figures 7-10). Even this can justify the problems found when the particle size

analyses are performed (see section 3.2.1). In "soft agglomerates", the fine particles are held together by short-range surface forces, such as van der Waals attractions, electrostatic, etc.), as seem to occur in the studied clay samples at short grinding times depending of the experimental conditions. It is clear that the formation of reduced particles by grinding of the parent clay minerals is mechanochemically activated because progressively they reached a high surface energy. After a limit, they start a reaggregation process in which adhesion forces act that leads to a decrease in surface areas with an apparent increase of the particle size. It seems also possible that the solid residues from grinding became cemented together by highly reactive amorphous material (generated by grinding) that act as a coating as grinding progresses, producing the reaggregation as seen by the changes in surface areas [149, 150]. Baláž et al. [23] considered that agglomeration can be attributed to capillary pressure and/or chemihesion (the presence of chemical bonds exactly at the places of contact among solids), although the overall stability of the dispersed system may be influenced by the interplay of several phenomena occurring simultaneously (adhesion, chemihesion, capillary pressure, etc.).

Figure 26 shows a plot of average particle sizes, as estimated by SEM (Figure 22) considering the particles which form the agglomerates, and specific surface areas of original and dry ground purified pyrophyllite (Table 1) after ball-milling (balls:powder weight ratio of 1:0.22). It can be observed that the average particle size estimated by SEM decrease as opposite to the increase and evolution of specific surface areas. According to the results of specific surface areas (Table 1), the equivalent spherical diameter range from 1.83 μm (unground) to 0.04 μm at the maximum (30 minutes), reaching 0.40 μm at 240 minutes of grinding (Table 3) when agglomeration is more intense. The irregular agglomerates, progressively denser, are formed by intensive grinding (Figure 22), with destruction of the layered shape initially present.

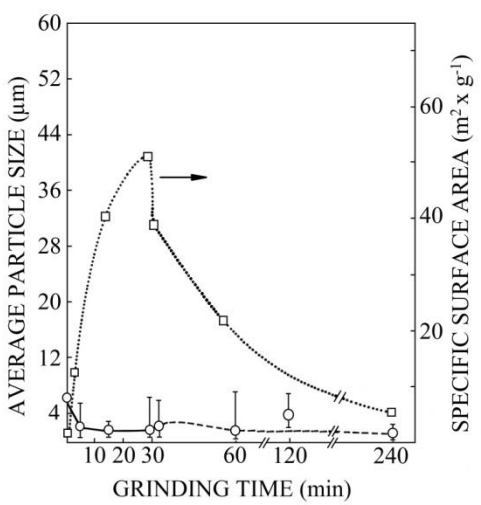

Figure 26. Plot of average "particle sizes" estimated by SEM (Figure 22) and specific surface areas of original pyrophyllite sample and ground by ball-milling (balls:powder ratio 1:0.22) as a function of grinding time.

The limit in particle size reduction is reached and mechanochemical effects are operating: the particles with high surface energy start to be aggregated forming the agglomerates and,

hence, the specific surface areas decrease as pointed out above. However, the agglomerates are constituted by very small particles aggregated between them and intimely mixed. For this reason, an estimation of "particle size" inside the agglomerates as observed by SEM could be performed (Figure 26).

Concluding this part of the present chapter, it is emphasized that the mechanical stress in these ground clays are quite diverse, producing important mechanochemical changes such as structural alteration, lattice distortions, amorphization, decrease in particle size, formation of nanostructures and an increase in surface area. Modifications of surface area, particle size and shape of short and prolonged grinding on the crystal structures of 1:1 and 2:1 layer silicates have been also evaluated.

3.3. Thermal Analysis by DTA-TGA

Thermal evolution of original and ground clay samples as increasing grinding times has been studied by DTA-TGA. Figure 27 shows the DTA diagrams of original industrial kaolin and after grinding up to 80 hours, using a balls:powder weight ratio of 1:4.28. The original kaolin sample shows the characteristic endothermic DTA peak of kaolinite dehydroxylation, with loss of structural OH groups, at ~ 538 ºC. The exothermic DTA peak is observed at ~ 985 ºC. These two features are in accordance with well-known previous DTA studies on thermal analysis of kaolinite samples [29, 151, 152]. The endothermic DTA peak is shifted to lower temperatures as grinding time increases, changing to 520 ºC at 32 hours of grinding. The plot of Figure 28 shows this evolution. This endothermic DTA effect appears as low as 490 ºC at 80 hours. At the same time, it is also observed a decrease in intensity of this peak as increasing grinding time, although it does not disappear at 80 hours.

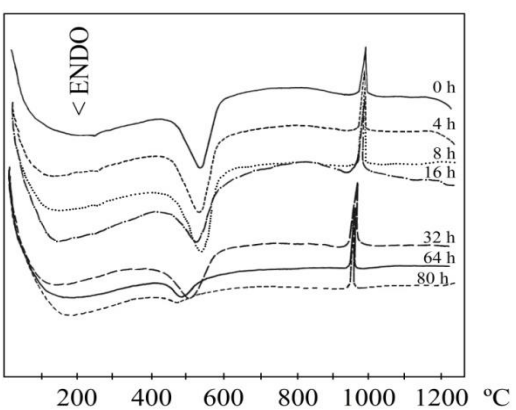

Figure 27. DTA diagrams of the original industrial kaolin sample and of samples ground by ball-milling (ratio balls:powder 1:4.28) for different times (h).

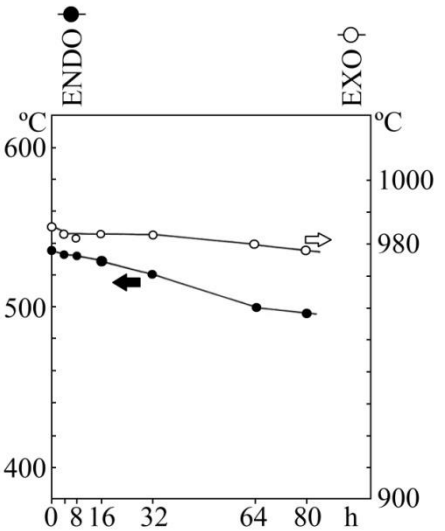

Figure 28. Evolution of peak temperatures of endothermic and exothermic DTA effects observed in original industrial kaolin sample and in those ground for different times (h).

The exothermic DTA peak is affected only after longer grinding times, with a change from 985 ºC to 980 ºC at 64 and 80 hours. These observations are in accordance with previous reports on grinding kaolinite, being a mechanochemical effect [5, 24-28, 52-57, 59-63, 65-75]. However, the use of different kaolinite samples, several grinding devices and distinct experimental conditions, influence on the reported variations in DTA thermal effects and TGA diagrams after grinding the samples, as it was mentioned in a previous section. For instance, González-García et al. [55] used the same grinding experimental conditions as described here for the industrial kaolin sample. These authors found changes from 540 ºC to 485 ºC (at a heating rate of 10 ºC/min) in the DTA endotherm of one kaolinite sample similar to the industrial kaolin (Figure 27), with variation of the DTA exothermic from 988 ºC to 979 ºC.

Grinding kaolinite, Kristóf et al. [56] reported variations in endothermic and exothermic DTA peaks, although the peak temperatures were not provided. Suraj et al. [57] found variations from 538.1 ºC (original) to 470.9 ºC at 30 minutes grinding using a disc mill, although with a slight increase of the exothermic DTA peak from 999.6 ºC (original) to 1002.5 ºC. It was already mentioned that Frost et al. [66] suggested that an effect of dry grinding in kaolinite is the dehydroxylation of basal surfaces by the coalescence of two OH groups to form H_2O, leaving a chemically bonded oxygen as an oxide anion in the lattice. Dellisanti and Valdré [57] reported similar results on DTA evolution of a sample of kaolinite, although this sample contained dickite.

The main cause of the DTA exothermic in kaolinite has been controversial in the literature [5, 52, 53, 75, 115, 123, 125, 126, 151, 153-156]. The observation of the DTA exothermic effect at ~ 980 ºC in kaolinite has been attributed to the formation of either mullite nuclei or a transient alumina-type spinel (γ-alumina solid solution or cubic phase) or both, because at DTA heating rates both mullite and spinel have the possibility of forming concurrently [156]. In this sense, it must be noted that the lower limit of composition for the formations of Al-Si spinel is 30 wt % Al_2O_3 according to Okada and Otsuka [154]. This value

is the maximum amount of Al_2O_3 that is present in the theoretical chemical composition of pyrophyllite. The theoretical chemical composition of kaolinite is 45 wt % Al_2O_3. Consequently, the formation of spinel phase is not possible in pyrophyllite after thermal treatment although it is possible in kaolinite. Evidences by MAS-NMR indicated that the formation of such an exothermic peak is most likely due to a release of energy, associated with the Al ion transformation to a more stable octahedral coordination, facilitating the formation of mullite with segregation of amorphous silica [125, 126].

Figure 29 shows selected DTA-TGA diagrams corresponding to a purified pyrophyllite and samples ground by ball milling using a balls:powder weight ratio of 1:0.22. It can be observed that the broad DTA endotherm, associated to the elimination of structural OH groups between 600-800 ºC, becomes sharper and appears progressively shifted at lower temperatures, with disappearance at higher grinding times. When the sample is ground for 30 minutes, the DTA diagram is similar to that of unground kaolinite (Figure 27). The structural OH groups in pyrophyllite (and talc), as 2:1 layer silicate, need higher temperature than kaolinite (1:1 layer silicate) for dehydroxylation [3, 151, 152]. Grinding for more than 30 minutes does not cause any further change in the temperature of the endothermic peak, as it was previously found studying by thermal analysis other sample of pyrophyllite [38, 115]. These observations are in connection to two factors: 1) the decrease in bond energy of OH groups in a more stressed structure produced by the mechanical treatment by grinding, and 2) the particle size reduction which produces dehydroxilation at lower temperatures than in unground clay sample. As a consequence, thermal decomposition occurs at lower temperatures in 2.1 layer silicates after grinding. The dehydroxylation of basal surfaces by the coalescence of two OH groups, as suggested by Frost et al. [66], must be also considered.

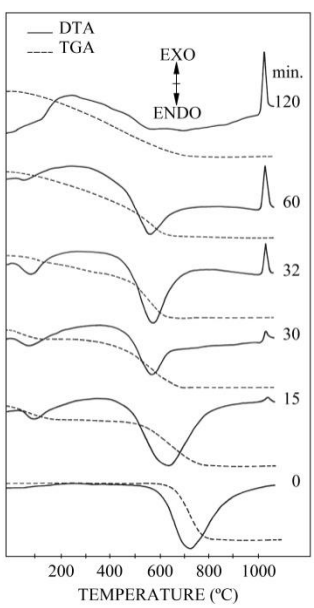

Figure 29. DTA-TGA diagrams of original (0 min) and ground (15-120 min) pyrophyllite samples by ball-milling (balls:powder ratio 1:0.22).

A sharp exothermic DTA peak which increases in intensity is observed from 32 minutes to higher grinding times, when disruption between tetrahedral and octahedral layers of the pyrophyllite structure is being more important, as demonstrated by spectroscopy techniques (Figures 4-6). The shape of the DTA diagram of the ground pyrophyllite sample for 32 minutes and higher is very similar to that of unground kaolinite (Figure 27). As a difference with DTA diagram of kaolinite, the exothermic DTA peak observed in pyrophyllite is associated to the formation of mullite by combined mechanical by grinding and thermal treatments. It has been already reported the formation of mullite from ground pyrophyllite grinding other sample [38, 119]. In this sense, ground pyrophyllite samples as amorphous materials are interesting as mullite precursors.

Grinding talc (industrial talc sample and the other talc sample) produces a slight shift in the main endothermic DTA peak of dehydroxylation (800-1100 ºC) as indicated also by TGA. It has been also detected an increase of weight loss on heating at lower temperatures than those observed in unground talc samples. An exothermic DTA effect appears on grinding talc, being detected from 10 minutes (grinding using a balls: powder weight ratio of 1:0.22) and from 8 hours (grinding using a balls:powder weight ratio of 1:4.28). This effect is not detected in ungroud samples of talc and appears at 830 ºC. It increases markedly in intensity during grinding, especially when structural breakdown is very important and an amorphous and reactive solid is produced. The present results and previous reports on grinding talc agree that crystallization of ortho-rhombic enstatite is produced at ~ 830 ºC by combined grinding and thermal treatments [85-90]. Previous studies suggested that the lower temperature dehydroxylation on grinding talc, and the formation of this new exothermic DTA effect, could be closely related to the environmental change around Mg ions [84, 88]. Talc is a 2:1 layer silicate whereas enstatite is a chain silicate. However, other authors interpreted the formation of such as exothermic DTA in ground talc samples as a result of the liberation of energy stored during mechanical activation in the form of ‘excess enthalpy’ [85]. In this sense, Li et al. [143] suggested enthalpy reduction changes produced by grinding.

It should be noted that in the case of pyrophyllite and talc, exothermic DTA effects detected in these samples after grinding are characteristic of the formation of high-temperature phases, as identified by XRD, but at lower temperatures than in unground samples: (1) mullite from ground pyrophyllite and (2) enstatite from ground talc. In contrast, the case of kaolinite (1:1 silicate) is different because: (1) grinding did not seem to influence the formation of a phase with a spinel-type structure (silicon-aluminum spinel), and (2) the transformation of the amorphous mechanically activated phase to low-crystalline mullite nuclei occurred at relatively lower temperatures than in the original (unground) kaolinite, in particular when the starting material is a disordered or poorly-crystallized sample (KGa-2), as it was previously demonstrated [44]. Mullite formation requires previous Al rearrangement, which is hindered by the existence of the two tetrahedral silica sheets that surrounds the octahedral one (Al) and that impedes Al atomic diffusion in pyrophyllite. For this reason, no exothermic DTA effect can be observed in unground pyrophyllite (Figure 29). Destruction of the tetrahedral network by grinding eliminates this restriction, decreasing the temperature of formation of mullite nuclei to ~ 1000 ºC (Figure 29), when the ground pyrophyllite samples are dynamically heated (DTA).

Tetrahedral sheet destruction by grinding favours also the incorporation of Si in Al-rich mullite nuclei during thermal treatment of ground samples above 1000 ºC. It is concluded that dry grinding affects kaolinite and pyrophyllite structures and, in turn, affects the

characteristics of the kaolinite-mullite and pyrophyllite.mullite reaction series [125, 126]. These all results are interesting in clay research because the formation of high-temperature phases is enhanced at lower temperatures by a previous intensive mechanical treatment of the 1:1 and 2:1 layer silicates by dry grinding.

Finally, the weight losses calculated from the TGA curves (Figure 29) are presented in Figure 30. These results are interesting for an additional discussion considering both 1:1 and 2:1 layer silicates by grinding. The weigh losses are assumed that they are due entirely to loss of water by heating, although evidently a part is from dehydroxylation of structural OH groups. Concerning these results, grinding increases the weight loss on heating at temperatures lower than 110 ºC or "free moisture". Grinding also increases the weight loss between 110 and 250 ºC and lowers slightly the loss of structural OH groups in the region of thermal dehydroxylation.

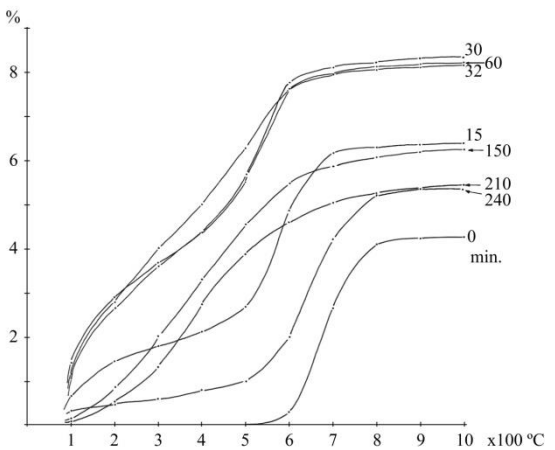

Figure 30. TGA plots (wt %) of original (0 min) and ground (15-120 min) pyrophyllite samples by ball-milling (balls:powder ratio 1:0.22) calculated by TGA diagrams (Figure 29).

In other words, dry grinding of pyrophyllite produces dehydroxylation at lower temperatures, as would be expected from IR spectroscopic observations that protons move to their original positions of stable attachment to oxygen ions, with detection of IR bands at ca. 3440 cm^{-1} and ~ 1620 cm^{-1} (Figure 4). However, weight losses observed after grinding are also in accordance with the possibility of some dehydroxylation even during initial grinding.

The evidence of a prototropy effect in these 1:1 and 2:1 layer silicates, as pointed out studying the IR results of pyrophyllite (Figure 4), must be considered. This mechanism of transfer of protons, from one plane to another within the structure, generates water molecules (detected by IR spectroscopy) when interacting the protons with OH groups. These water molecules can be lost at lower temperatures, as confirmed by thermal analysis (Figure 30).

However, as grinding proceeds, it is also possible a rehydroxylation process of the reactive ground powder with atmospheric water molecules or moisture in the atmosphere. Then, this would suggest further that weight losses are not due entirely to loss of adsorbed water but are, at least in part, due to dehydroxylation of extremely weakly bound OH groups. The increasing of specific surface areas (Table 1) and the smaller particle size of the ground clay powder favour this interpretation. The formation of broad endothermic DTA effects at low temperatures (< 200 ºC) in ground samples (Figures 27 and 29) is in accordance with the

above. Then, after a limit of mechanochemical reduction (Tables 1-4), the process seems to be inverted, although the ground product still become dehydroxylated at lower temperatures than in the unground sample (Figure 30).

CONCLUSION

In the present research, kaolinite (1:1 layer silicate), pyrophyllite and talc (2:1) and raw clay materials have been considered. The previous research works on grinding these layer silicates have been reviewed and updated. Dry grinding experiments using planetary ball milling have been performed using selected samples. Several techniques have been used to follow the evolution of the layer silicates, mainly XRD, surface area (nitrogen adsorption), SEM, TEM, MAS-NMR, FTIR, particle size analysis and thermal methods (DTA-TGA).

The mechanical stress in ground clays are quite diverse, producing important changes such as lattice distortions, amorphization, decrease in particle size, formation of nanostructures and an increase in surface area. Modifications of surface area, particle size and shape of short and prolonged grinding on the crystal structure of the layer silicates have been evaluated. These observed changes have been related to a progressive delamination and structural breakdown during grinding, with final formation of a turbostratic-type structure. Short grinding times resulted in the breakdown and drastic size reduction of relatively thin particles. It has been found an inverse relationship between coherent X-ray domain and lattice microstrains in the ground powders.

It was found that the rate of size reduction decreased with time and a limit is reached for each layer silicate producing more rounded particles and aggregates, with a decrease of surface area because mechanochemical effects are operating. It can be also observed an increasing in amorphization as a consequence of the loss of long-range order. It is explained considering that grinding produces a loss of periodicity perpendicular to the layer silicate plane, and the dimensions of the crystallites along the c-direction resulted too small to produce coherent X-ray scattering. SEM allows to observe the formation of nanometer size ground powders and further particle agglomeration. Modifications in the coordination of Si and Al nuclei have been also deduced from MAS-NMR spectroscopy, demonstrating a short-range order.

The present results evidenced the influence of experimental grinding conditions and characteristics of the clay samples with the structure of 1:1 and 2:1 layer silicates. In particular, the rupture of the tetrahedral and octahedral sheets led to important modifications. These results are interesting in clay research to analyze the formation of nanostructured powders, with enhanced surface properties and reactivity, when grinding clays and further to compare the effects of grinding on 1:1 and 2:1 layer silicates, in particular when the ground mechanochemical activated samples are thermally treated.

ACKNOWLEDGMENTS

The financial supports of Research Group TEP 204 and Research Project MAT2011-22981, in part financed with Feder, are acknowledged.

REFERENCES

[1] Brindley, G.W.; Pedro, G. *AIPEA Newsletter*, 1972, 7, 8-13.
[2] Newman, A.C.D.; Brown, G. In Chemistry of Clays and Clay Minerals; Editor, A.C.D. Newman; Monograph 6; Mineralogical Society: London, 1987.
[3] Bailey, S.W. Hydrous Phyllosilicates; Reviews in Mineralogy 19; Mineralogical Society of America: Wahinghton D.C., 1988.
[4] Konta, J. *Appl. Clay Sci*., 1995, 10, 275-335.
[5] Mendelovici, E. *J. Therm. Anal.*, 1997, 49, 1385-1397.
[6] Murray, H.H. *Appl. Clay Sci.*, 2000, 17, 297-221.
[7] Guggenheim, S.; Adams, J.M.; Bain, D.C.; Bergaya, F.; Bigatti, M.F.; Drits, V.A.; Formoso, M.L.L.; Galán, E.; Kogue, T.; Stanjek, H. *Clays Clay Miner.*, 2006, 54, 761-772.
[8] Zbik, M.; Smart, R.S.C. *Clays Clay Miner.*, 1998, 46, 153-160.
[9] Zbik, M.; Smart, R.S.C. *Miner. Eng.*, 2002, 15, 277-286.
[10] Dellisanti, F.; Valdré, G. *Int. J. Miner. Process.*, 2008, 88, 94-99.
[11] Gregg, S.J. *Chem. Ind.*, 1968, 11, 611-617.
[12] Somasundaran, M. In Ceramic Processing before Firing; Editors G. Onoda and L.L. Hench; Wiley and Sons: New York, 1978.
[13] Glasson, D.R. *Thermochim. Acta*, 1981, 51, 45-52.
[14] Boldyrev, V.V. *Thermochim. Acta*, 1987, 110, 303-317.
[15] Mendelovici, E. *Thermochim. Acta*, 1989, 148, 205-218.
[16] Tkácová, K. Mechanical Activation of Minerals; Elsevier: Amsterdam, 1989.
[17] Juhász, A.Z.; Opoczky, L. Mechanical Activation of Minerals by Grinding: Pulverizing and Morphology of Particles; Ellis Horwood Ltd. Chichester; Akademiai Kiado: Budapest, 1990.
[18] Ban, T.; Okada, K.; Hayashi, T.; Otsuka, N. *J. Mater. Sci.*, 1992, 27, 465-471.
[19] Baláž, P. Extractive Metallurgy of Activated Minerals; Elsevier: Amsterdam, 2000.
[20] Cho, H.; Lee, H.; Lee, Y. *Int. J. Miner. Process*, 2006, 78, 250-261.
[21] Baláž, P., Mechanochemistry in Nanoscience and Minerals Engineering; Springer-Verlag: Berlin, 2008.
[22] Knieke, C.; Sommer, M.; Penkert, W. *Powder Technol.*, 2009, 195, 25-30.
[23] Baláž, P., Achimovičová M., Baláž, M.; Billik, P.; Cherkezova-Zheleva, Z.; Criado, J.M.; Delogu, F.; Dutková, E.; Gaffet, E.; Gotor, F.J.; Kumar, R.; Mitov, I.; Rojac, T.; Senna, M.; Streletskii, A.; Wieczorek-Ciurowa, K. *Chem. Soc. Rev.*, 2013, 42, 7571-7637.
[24] Juhász, Z. *Acta Mineralogica-Petrographica*, 1980, 24, 121-145.
[25] Čičel, B.; Kranz, G. *Clay Miner.*, 1981, 16, 151-162.
[26] Yariv, S.; Lapides, I.J. *J. Mater. Synth. Process*, 2000, 8, 223-233.
[27] Mendelovici, E. *J. Mater. Sci. Letters*, 2001, 20, 81-83.
[28] Vdovic, N.; Jurina, I.; Skapin, S.D.; Sondi, I. *Appl. Clay Sci.*, 2010, 48, 575-580.
[29] Olphen, H. van; Fripiat, J.J., Data Handbook for Clay Materials and Other Non-Metallic Minerals; Pergamon Press: Oxford, 1979.
[30] Carty, W.M.; Senapati, U. *J. Am. Ceram. Soc.*, 1998, 81, 3-20.

[31] González Peña, J.Mª; Rodríguez Pascual, C.; Oteo Mazo, J.L.; Sandoval, F.; Lacaba Velasco, M. *Bol. Soc. Esp. Ceram. V,* 1984, 23, 315-324.
[32] García Ramos, G.; González García, F.; Sánchez-Soto, P.J.; Ruiz Abrio, M.T. *Bol. Soc. Esp. Ceram. V,* 1985, 24, 67-79.
[33] Pérez-Rodríguez, J.L.; Maqueda, C.; Justo, A. *Clays Clay Miner.*, 1985, 33, 563-566.
[34] Maqueda, C.; Pérez-Rodríguez, J.L.; Justo, A. *Analyst.*, 1986, 111, 1107-1108.
[35] Galán Huertos, E.; Rodas, M. *Bol. Geol. Min.*, 1973, 84-85, 347-365.
[36] Schüller, K.H.; Kromer, H. In Proceedings of the International Clay Conference Denver 1985; Editors Schultz L.G., van Olphen H., Mumpton F.A.; The Clay Minerals Society: Bloomington, IN, 1985, pp. 396-399.
[37] Pérez-Rodríguez, J.L.; Madrid, L.; Sánchez-Soto, P.J. *Clay Miner.*, 1988, 23, 399-410.
[38] Pérez-Rodríguez, J.L.; Sánchez-Soto, P.J. *J. Therm. Anal.*, 1991, 37, 1401-1413.
[39] Wiéwiora, A.; Sánchez-Soto, P.J.; Avilés, M.A.; Justo, A.; Pérez-Rodríguez, J.L. *Appl. Clay Sci.*, 1993, 8, 261-282.
[40] Niskanen, E. *Am. Mineral.*, 1964, 49, 705-714.
[41] Klug, H.P.; Alexander, L.E. X-ray Diffraction Procedures for Polycrystalline and Amorphous Materials; 2nd Edition; John Wiley and Sons: New York, 1974.
[42] Edwards, H.J.; Toman, K. *J. Appl. Crystallogr.*, 1971, 4, 319-321.
[43] Brunauer, S.; Emmett, P.H.; Teller, E. *J. Am. Chem. Soc.*, 1938, 60, 309-319.
[44] Sánchez-Soto, P.J.; Jiménez de Haro, M.C.; Pérez-Maqueda, L.A.; Varona, I.; Pérez-Rodríguez, J.L. *J. Am. Ceram. Soc.*, 2000, 83, 1649-1657.
[45] Takahashi, H. *Bull. Chem. Soc. Jap.*, 1959, 32, 235-245.
[46] Haase, T.; Winter, K. *Bull. Soc. Fr. Ceram.*, 1959, 44, 13-19.
[47] Miller, J.G.; Oulton, T.D. *Clays Clay Miner.*, 1970, 18, 313-323.
[48] Yariv, S. *Clays Clay Miner.*, 1975, 23, 80-82.
[49] Hlavay, J.; Jonas, K.; Elek, S.; Inczedy, J. *Clays Clay Miner.*, 1977, 25, 451-456.
[50] Yariv, S.; Cross, H. Geochemistry of Colloid Systems for Earth Scientists; Springer-Verlag: Berlin, 1979.
[51] De Luca, S.; Slaughter, M. *Am. Miner.*, 1985, 70, 149-158.
[52] Aglietti, F.; Porto-López, J.M.; Pereira, E. *Int. J. Miner. Process*, 1986, 16, 125-133.
[53] Aglietti, F.; Porto-López, J.M.; Pereira, E. *Int. J. Miner. Process*, 1986, 16, 135-146.
[54] Kodama, H.; Kotliar, L.S.; Ripmeester, J.A. *Clays Clay Miner.*, 1989, 37, 364-370.
[55] González-García, F.; Ruiz-Abrio, M.T.; González-Rodríguez, M. *Clay Miner.*, 1991, 26, 549-565.
[56] Kristóf, E.; Juhász, A.Z.; Vassányi, I. *Clays Clay Miner.*, 1993, 41, 608-612.
[57] Suraj, G.; Iyer, C.S.P.; Rugmini, S.; Lalithambika, M. *Appl. Clay Sci.*, 1997, 12, 111-130.
[58] Baudet, G.; Perrotel, V.; Seron, A.; Stellatelli, M. *Powder Technol.*, 1999, 105, 125-134.
[59] Frost, R.L.; Makó, E.; Kristóf, J.; Horváth, E.; Kloprogge, J.T. *Langmuir* 2001, 17, 4731-4738.
[60] [60] Frost, R.L.; Makó, E.; Kristóf, J.; Horváth, E.; Kloprogge, J.T. *J. Colloid Interface Sci.*, 2001, 239, 458-466.
[61] Makó, E.; Frost, R.L.; Kristóf, J.; Horváth, E. *J. Colloid Interface Sci.*, 2001, 244, 359-364.

[62] Stepkowska, E.; Pérez-Rodríguez, J.L.; Jiménez de Haro, M.C.; Sánchez-Soto, P.J.; Maqueda, C. *Clay Miner.*, 2001, 36, 105-114.
[63] Kristóf, J.; Frost, R.L.; Kloprogge, J.T.; Horváth, E.; Makó, E. *J. Therm. Anal. Cal.*, 2002, 69, 77-83.
[64] Reynolds, R.C.; Bish, D.L. *Am. Miner.*, 2002, 87, 1626-1630.
[65] Horváth, E.; Frost, R.L.; Makó, E.; Kristóf, J.; Cseh, T. *Thermochim. Acta*, 2003, 227-234.
[66] Frost, R.L.; Horváth, E.; Makó, E.; Kristóf, J. *J. Colloid Interface Sci.*, 2004, 270, 337-346.
[67] Kameda, J.; Saruwatari, K.; Tanaka, H.J. *J. Colloid Interface Sci.*, 2004, 275, 225-230.
[68] Vizcayno, C.; Castelló, R.; Ranz, I.; Calvo, B. *Thermochim. Acta*, 2005, 428, 173-183.
[69] Makó, E.; Senkár, Z.; Kristóf, J.; Vágvölgyi, V. *J. Colloid Interface Sci.*, 2006, 294, 362-370.
[70] Dellisanti, F.; Valdré, G. *Int. J. Miner. Process*, 2008, 88, 94-99.
[71] Pardo, P.; Bastida, J.; Serrano, F.J.; Ibáñez, R.; Kojdecki, M. *Clays Clay Miner.*, 2009, 57, 25-34.
[72] Tang, A.; Su, L.; Li, C.; Wei, W. *Appl. Clay Sci.*, 2010, 48, 296-299.
[73] Valasková, M.; Barabaszová, K.; Hundáková, M.; Ritz, M.; Plevová, E. *Appl. Clay Sci.*, 2011, 54, 70-76.
[74] Tang, A.; Su, L.; Li, C. *Powder Technol.*, 2012, 218, 86-89.
[75] Dellisanti, F.; Valdré, G. *Int. J. Mineral Process*, 2012, 102-103, 69-77.
[76] Plançon, A.; Tchoubar, C. *Clays Clay Miner.*, 1977, 25, 430-450.
[77] Plançon, A.; Zacharie, C. *Clay Miner.*, 1990, 25, 249-260.
[78] Farmer, V.C. *Miner. Mag.*, 1958, 31, 829-845.
[79] Takahashi, H. *Bull. Ceram. Soc. Japan*, 1959, 32, 378-380.
[80] Okuda, S.; Inoue, K. ; Williamson, W.O. In Proceedings International Clay Conference Tokyo; Editor Heller-Kallai, L.; Israel University Press: Jerusalem, 1969, pp. 31-41.
[81] Mukherjee, D.K.; Roy, S. *Ind. Ceram.*, 1973, 10, 215-219.
[82] Yvon, J.; Cases, J.M.; Mercier, R.; Delon, J.F. In Proceedings of the International Clay Conference Denver 1985; Editors Schultz L.G., van Olphen H., Mumpton F.A.; The Clay Minerals Society: Bloomington, IN, 1985, pp. 257-260.
[83] Heller-Kallai, L.; Yariv, S.; Friedman, I. *J. Therm. Anal.*, 1986, 31, 95-106.
[84] Sugiyama, K.; James, P.F.; Saito, F.; Waseda, Y. *J. Mater. Sci.*, 1991, 26, 5297-5300.
[85] Liao, J.; Senna, M. *Thermochim. Acta*, 1992, 197, 295-306.
[86] Aglietti, E.F.; Porto López, J.M. *Mater. Res. Bull.*, 1992, 27, 1205-1216.
[87] Aglietti, E.F. *Appl. Clay Sci.*, 1994, 9, 139-147.
[88] Filio, J.M.; Sugiyama, K.; Saito, F.; Waseda, Y. *Powder Technol.*, 1994, 78, 121-127.
[89] Wiéwiora, A.; Sánchez-Soto, P.J.; Avilés, M.A.; Justo, A.; Pérez-Maqueda, L.A.; Pérez-Rodríguez, J.L.; Bylina, P. *Appl. Clay Sci.*, 1997, 12, 233-245.
[90] Sánchez-Soto, P.J.; Wiéwiora, A.; Avilés, M.A.; Justo, A.; Pérez-Maqueda, L.A.; Pérez-Rodríguez, J.L.; Bylina, P. *Appl. Clay Sci.*, 1997, 12, 297-312.
[91] Kano, J.; Saito, F. *Powder Technol.*, 1998, 98, 166-170.
[92] Kano, J.; Miyazaki, M.; Saito, F. *Adv. Powder Technol.*, 2000, 11, 333-342.
[93] Godet-Morand, L.; Chamayou, A.; Dodds, J. *Powder Technol.*, 2002, 128, 306-313.
[94] Terada, K.; Yonemochi, E. *Solid State Ionics*, 2004, 172, 459-462.
[95] Christidis, G.E.; Makri, P.; Perdikatsis, V. *Clay Miner.*, 2004, 39, 163-175.

[96] Yang, H.; Du, C.; Hu, Y.; Jin, S.; Yang, W.: Tang, A.; Avvakumov, E.G. *Appl. Clay Sci.*, 2006, 31, 290-297.
[97] Burdukova, E.; Becker, M.; Bradshaw, D.J.; Laskowski, J.S. *J. Colloid Interface Sci.*, 2007, 315, 337-342.
[98] Dellisanti, F.; Valdré, G.; Mondonico, M. *Appl. Clay Sci.*, 2009, 42, 398-404.
[99] Du, C.; Yang, H. *Clays Clay Miner.*, 2009, 57, 290-301.
[100] Mahadi, M.I.; Palaniandy, S. *Int. J. Miner. Process.*, 2010, 94, 172-179.
[101] Tavangarian, F. ; Emadi, R.; Shafyei, A. *Powder Technol.*, 2010, 198, 412-416.
[102] Harben, P.W. In Industrials Minerals Consumer Survey; Editor, B.M. Coope and E.M. Dickson; Metal Bulletin Ltd: London, 1981.
[103] Sánchez-Soto, P.J.; Pérez-Rodríguez, J.L. *Bol. Soc. Esp. Ceram. Vidr.*, 1998, 37, 285-289.
[104] Sánchez-Soto, P.J.; Pérez-Rodríguez, J.L. *Bol. Soc. Esp. Ceram. Vidr.*, 1998, 37, 359-368.
[105] Levine, A.K.; Joffe, J.S. *Soil Sci.*, 1947, 63, 407-416.
[106] Hayashi, H.; Koshi, K.; Hamada, A.; Sakabe, H. *Clay Sci.*, 1962, 1, 99-108.
[107] Shiraki, Y.; Inoue, A. *J. Ceram. Assoc. Jap.*, 1965, 73, 187-195.
[108] Kuwahara, Y. *J. Chem.Eng. Jap.*, 971, 4, 359-363.
[109] Hayashi, T., Inoue, A.; Ogihara, M.; Otsuka, N. *Yogyo Kyokai Shi*, 1979, 87, 623-632.
[110] Juhász, Z. *Kémiai Közlemények*, 1977, 48, 167-187.
[111] Stanczyk, M.H.; Feld, I.L. US Bureau of Mines 1980, Bulletin No. 670.
[112] Rosenberg, P.E.; Cliff, G. *Am. Miner.*, 1980, 65, 1217-1219.
[113] Rosenberg, P.E. *Am. Miner.*, 1980, 59, 254-260.
[114] Nemecz, E. *Acta Geol. Hung.*, 1984, 27, 191-202.
[115] Sánchez-Soto, P.J.; Pérez-Rodríguez, J.L. *J. Am. Ceram. Soc.*, 1989, 72, 154-157.
[116] Sánchez-Soto, P.J.; Macías, M.; Pérez-Rodríguez, J.L. *Br. Ceram. Trans. J.*, 1991, 90, 192-194.
[117] Sánchez-Soto, P.J.; Macías, M.; Pérez-Rodríguez, J.L. *Br. Ceram. Trans. J.*, 1992, 91, 15-19.
[118] González-García, F.; González-Rodríguez, M.; González-Vilchez, C.; Raigón-Pichardo, M. *Bol. Soc. Esp. Ceram. Vidr.*, 1992, 7, 297-304.
[119] Sánchez-Soto, P.J.; Macías, M.; Pérez-Rodríguez, J.L. *J. Am. Ceram. Soc.*, 1993, 76, 180-184.
[120] Pérez-Maqueda, L.A.; Pérez-Rodríguez, J.L.; Scheiffele, G.W.; Justo, A.; Sánchez-Soto, P.J. *J. Therm. Anal.*, 1993, 39, 1055-1067.
[121] Sánchez-Soto, P.J.; Justo, A.; Pérez-Maqueda, L.A.; Pérez-Rodríguez, J.L. *Mater. Eng.*, 1993, 4, 5-21.
[122] Sánchez-Soto, P.J.; Justo, A.; Pérez-Rodríguez, J.L.; Morillo, E. *J. Mater. Sci. Lett.*, 1994, 13, 915-918.
[123] Sánchez-Soto, P.J.; Justo, A.; Pérez-Rodríguez, J.L. *J. Mater. Sci.*, 1994, 29, 1276-1283.
[124] Wiéwiora, A.; Hida, T. *Clay Sci.*, 1996, 10, 15-35.
[125] Sánchez-Soto, P.J.; Pérez-Rodríguez, J.L.; Sobrados, I.; Sanz, *J. Chem. Mater.*, 1997, 677-684.
[126] Sanz, J.; Madani, A.; Serratosa, J.M.; Moya, J.S.; De Aza, S. *J. Am. Ceram. Soc.*, 1988, 71, C418-C421.

[127] Sánchez-Soto, P.J.; Jiménez de Haro, M.C.; Pascual Cosp, J., Raigón Pichardo, M.; Pérez-Rodríguez, J.L. *Bol. Soc. Esp. Ceram. Vidr.*, 2000, 39, 119-134.
[128] Uhlik, P; Šucha, V.; Eberl, D.D.; Puskelova, L.; Čaplovičová, M. *Clay Minerals*, 2000, 35, 423-432.
[129] Erdemoğlu, M.; Sarikaya, M. *Miner. Eng.*, 2002, 15, 723-725.
[130] Temuujin, J.; Okada, K.; Jadambaa, T.; MacKenzie, K.J.D.; Amarsanaa, J. *J. Eur. Ceram. Soc.*, 2003, 23, 1277-1282.
[131] Sánchez-Soto, P.J. *Bol. Soc. Esp. Ceram. Vidr.*, 2009, 48, 59-68.
[132] Ehlissen. K.T.; Delahaye-Vidal, A.; Genin, P.; Figlarz, M.; Willmann, P. *J. Mater. Chem.*, 1993, 3, 883-888.
[133] Lin, I.J.; Nadiv, S. *Mater. Sci. Eng.*, 1979, 39, 193-197.
[134] Kinsey, R.A.; Kirkpatrick, R.J.; Hower, J.; Smith, K.A.; Oldfield, E. *Am. Miner.*, 1985, 70, 537-548.
[135] Engelhardt, G.; Michel, D. High-Resolution Solid-State NMR of Silicates and Zeolites; John Wiley and Sons: New York, 1987.
[136] Sanz, J.; Sobrados, I.; Cavalieri, A.L.; Pena, P.; De Aza, S.; Moya, J.S. *J. Am. Ceram. Soc.*, 1991, 74, 2398-2403.
[137] He, H.P. Guo, J.G.; Zhu, J.X.; Hu, C. *Clay Miner.* 2003, 38, 551-559.
[138] Fyfe, C.A.; Thomas, J.M.; Klinowski, J.; Gobbi, G.C. *Angew. Chem. (Eng. Ed.)*, 1983, 22, 259-336.
[139] Barreto Maia, A.A.; Angélica, R.S.; Neves, R.F.; Pöllman, H.; Straub, C.; Saalwächter, K. *Appl. Clay Sci.*, 2014, 87, 189-196.
[140] Meinhold, R.H.; MacKenzie, K.J.D.; Brown, I.W.M. *J. Mater. Sci. Lett.* 1985, 4, 163-166.
[141] MacKenzie, K.J.D.; Beown I.W.M.; Meinhold, R.H.; Bowden, M.E. *J. Am. Ceram. Soc.*, 1985, 68, 293-297.
[142] Watanabe, T.; Shimizu, H.; Nagasawa, K.; Masuda, A.; Saito, H. *Clay Miner.*, 1987, 22, 37-48.
[143] Li, T.; Sui, F.; Li, F.; Cai, Y.; Jin, Z. *Powder Technol.*, 2014, 254, 338-343.
[144] Brett, N.H.; González, M.; Bouillot, J.; Niepce, J.C. *J. Mater. Sci.* 1984, 19, 1349-1358.
[145] Nagao, H.; Aikawa, N. *J. Am. Ceram. Soc.*, 1988, 71, C421-C423.
[146] Criado, J.M; González, M.; Real, C. *J. Mater. Sci. Lett.*, 1986, 5, 467-469.
[147] Lin, J.D.; Duh, J.G. *J. Mater. Sci.*, 1997, 32, 5779-5790.
[148] Williams, D.G.; Garey, C.L. *Clays Clay Miner.*, 1974, 22, 117-125.
[149] Papirer, E.; Roland, P. *Clays Clay Miner.*, 1981, 29, 161-170.
[150] Cornejo, J.; Hermosín, M.C. *Clay Miner.*, 1988, 23, 391-398.
[151] Mackenzie, R.C. Differential Thermal Analysis; Academic Press: London and New York, 1970.
[152] Guggenheim, S.; van Groos, A.F.K. *Clays Clay Miner.*, 2001, 49, 433-443.
[153] Chakravorty, A.K.; Ghosh, D.K. *J. Am. Ceram. Soc.*, 1978, 61, 170-173.
[154] Okada, K.; Otsuka, N. *J. Am. Ceram. Soc.* 1986, 69, 652-656.
[155] Aksay, I.A.; Dabbs, D.M.; Sarikaya, M. *J. Am. Ceram. Soc.*, 1991, 74, 2343-2354.
[156] Pask, J.A.; Tomsia, A.P. *J. A. Ceram. Soc.*, 1991, 74, 2367-2373.

In: Clays and Clay Minerals
Editor: Liam R. Wesley
ISBN: 978-1-63117-779-8

Chapter 4

APPLICATIONS OF CLAY MATERIALS FOR THE REMOVAL OF ORGANIC XENOBIOTICS FROM CONTAMINATED WATERS

***A. Dordio*[*1,2] *and A. J. P. Carvalho*[1,3]**
[1] Chemistry Department, University of Évora, Évora, Portugal
[2]IMAR – Marine and Environmental Research Centre,
University of Évora, Évora, Portugal
[3]CQE – Évora Chemistry Centre, University of Évora, Évora, Portugal

ABSTRACT

The peculiar characteristics of clays (namely, among others, the silicates' sheet structure that makes a large surface area accessible for adsorption; the usually significant surface charge that can be responsible for strong electrostatic interactions; and clays' swelling properties and presence of exchangeable surface cations that facilitate ion-exchange mechanisms) provide these materials with very interesting adsorption qualities, especially for polar or ionizable molecules. Added to their wide availability and associated low cost, these characteristics have motivated in recent years an increasing interest in utilizing natural, processed or chemically-modified clays for the removal of organic contaminants from aqueous solutions. In fact, organic xenobiotic compounds have been emerging in the latest years as a serious environmental concern, as many of these pollutants have a proven ecotoxicity and may even be a threat to human health. Associated to the fact that many such substances are not efficiently removed from wastewaters by conventional wastewater treatment processes (which has resulted in many reports of the detection of organic xenobiotics presence in treated wastewaters, natural waters and even drinking waters) urges for the development and implementation of alternative or complementary water and wastewater treatment technologies, of which adsorption-based processes have been recognized as one of the most economic possibilities (depending on the cost of the adsorbent materials). The aim of this work is to present a review on the extensive amount of studies on the adsorption of organic compounds to several clay-based materials. The discussion is focused on the

[*] Corresponding author: Tel: +351 - 266 745343; E-mail address: avbd@uevora.pt

environmental applications, specifically for the decontamination of water and wastewater polluted with organic xenobiotics, and with the aim of highlighting the possibilities presented by this type of generally cheap materials, and to provide resources for the screening of prospective adsorbents with potential to be used as efficient and economic water and wastewater treatment alternatives.

1. INTRODUCTION

The enormous and rapid development of chemical and agrochemical industries during the last century has resulted in the release of a large number of chemical compounds into the environment. In fact, a lot of different organic substances are currently used in the daily life of human beings or result from human activities and many of these are frequently being detected in numerous environmental monitoring studies (Bourg et al., 1992; Jones and de Voogt, 1999; Gavrilescu, 2005; Doble and Kumar, 2005; Fent et al., 2006; Pal et al., 2010; El Shahawi et al., 2010; Bell et al., 2011; Haarstad et al., 2011; Kosjek et al., 2012; Lapworth et al., 2012; Verlicchi et al., 2012; Ratola et al., 2012; Rivera-Utrilla et al., 2013; Michael et al., 2013; Luo et al., 2014). Pollution of soils and surface or ground waters, both from point and diffuse sources, occurs as a result of the improper use and disposal or accidental release of chemicals into the environment.

Aquatic ecosystems are especially vulnerable because water bodies are frequently used, directly or indirectly, as recipients of potentially toxic liquids and solids from domestic, agricultural and industrial wastes and wastewaters (Safe, 1994; Jones and de Voogt, 1999; Gavrilescu, 2005; Doble and Kumar, 2005; Fent et al., 2006; Demirezen et al., 2007; Peng et al., 2008; Aga, 2008; Kümmerer, 2009; Pal et al., 2010; Michael et al., 2013). Some of the primary classes of pollutants which may accumulate in surface waters, ground water, soil and sediments are nutrients, organic contaminants (in particular xenobiotic compounds) and metals and metalloids.

Over the last decades, increasing attention is being turned to a set of harmful organic chemicals mostly composed of xenobiotics (Tyler et al., 1998; Jones and de Voogt, 1999; Gavrilescu, 2005; Fent et al., 2006; Barceló and Petrovic, 2008; El Shahawi et al., 2010; Bell et al., 2011; Lapworth et al., 2012; Luo et al., 2014). Most of these pollutants persist in the environment, can bioaccumulate throughout the food chain, and may be toxic to biotic communities, thus posing a risk to human health and the environment (Safe, 1994; Jones and de Voogt, 1999; Gavrilescu, 2005; Fent et al., 2006; Crane et al., 2006; Barceló and Petrovic, 2008; Pal et al., 2010; El Shahawi et al., 2010; Bell et al., 2011; Escher et al., 2011; Verlicchi et al., 2012; Michael et al., 2013). Many of these substances can be transported over long distances, can be distributed into different compartments of the environment, and also undergo a variety of reactions and transformations (El Shahawi et al., 2010). Because of the many competing interactions, the fate of such pollutants is not easy to predict and in many cases their ecotoxicological effects are difficult to assess (El Shahawi et al., 2010). Nevertheless, possible synergistic effects that may potentiate their toxicity and the established possibility of long-range transport of these substances to regions where they have never been used or produced, with all the consequent threats they may pose to the environment of the whole globe, has motivated the international community to call, at several occasions, for urgent global actions to be taken with the aim of reducing the release of these chemicals.

Optimizations of the conventional water and wastewater treatment processes have been attempted but in many cases the increases in efficiency that have been achieved were not considered satisfactory (Tauxe-Wuersch et al., 2005; Fent et al., 2006; Maurer et al., 2007; Aga, 2008; Miège et al., 2009; Verlicchi et al., 2012; Rivera-Utrilla et al., 2013; Luo et al., 2014).

In recent years, numerous strategies and technologies have been developed for water and wastewater treatment that are targeted specifically for the removal of organic xenobiotics. Some of the water and wastewater treatment technologies that have been evaluated for the removal of organic xenobiotics include advanced oxidative processes, membrane processes, ozonization, irradiation and membrane bioreactors (UNEP, 1998; Fent et al., 2006; Crini, 2006; Radjenovic et al., 2007; Kim et al., 2007; Esplugas et al., 2007; Snyder et al., 2007; Aga, 2008; Benner et al., 2008; Gupta and Suhas, 2009; Wang and Xu, 2011; UNEP, 2013; Nidheesh et al., 2013). Despite the sometimes high removal efficiencies attained, most of these processes are not, however, widely used mainly for the high costs involved in its implementation and maintenance (Zodrow, 1999; Susarla et al., 2002; Doble and Kumar, 2005; Fent et al., 2006; Aga, 2008; Benner et al., 2008; Gan et al., 2009). Consequently, there is a growing need for alternative or complementary treatment processes for removing organic xenobiotics from waters and wastewaters that have higher efficiencies at reasonable costs of operation/maintenance.

Adsorption processes have been found to be relatively effective for the removal of organic compounds from water and wastewater. These processes are in general superior to other technologies for water decontamination in terms of the flexibility and simplicity of design, ease of operation and insensitivity to toxic pollutants. Treatment by adsorption also does not result in the formation of harmful substances. Its cost of implementation, however, is primarily related with the cost of the adsorbents used and of their regeneration. Therefore, much attention has been given in recent years to the research of low cost and easily available natural materials such as clays or zeolites, certain agricultural wastes such as almond shell, pine bark, rice husk and cork, and other industrial wastes and by-products such as fly ash, red mud and sludges (see Dordio and Carvalho (2013b) for a general review).

In particular clay materials have been studied extensively due to their wide availability worldwide and their interesting properties such as high cation-exchange capacities, surface areas, pore volumes and porosities (associated in many cases with swelling phenomena) which are responsible for generally large adsorption capacities.

2. ORGANIC XENOBIOTIC POLLUTANTS

One of the challenges of dealing with organic pollutants is their great diversity. The number of organic molecules generated by different industries increases every day. The list of such organic xenobiotics includes polycyclic aromatic hydrocarbons, petroleum hydrocarbons, clorinated solvents, explosives, dyes, pesticides, pharmaceuticals, etc.

Many of these substances have been released in increasing amounts in the environment since decades, and, due to the low degradation rate of many of these compounds, a significant increase of their background concentrations has been observed in the different environmental compartments (Bourg et al., 1992; Tyler et al., 1998; Jones and de Voogt, 1999; Skakkebaeck

et al., 2000; Gavrilescu, 2005; Doble and Kumar, 2005; Barceló and Petrovic, 2008; Aga, 2008; Pal et al., 2010; El Shahawi et al., 2010; Bell et al., 2011; Lapworth et al., 2012; UNEP, 2013; Luo et al., 2014). A growing environmental concern has been emerging in recent years because of the high toxicity and high persistence of most of these substances in the environment and in biological systems. Even though they occur only at very low concentrations in the environment, and their threats to aquatic life and public health are still not completely understood, nevertheless, sub-lethal effects of these compounds over long-term exposure may cause significant damage to aquatic life, particularly considering that some of these compounds potentially cause significant endocrine disruption, impair reproduction functions of animals or even be carcinogenic, mutagenic or teratogenic (Safe, 1994; Wu, 1999; Mason, 2002; Fent et al., 2006; Crane et al., 2006; Pal et al., 2010; El Shahawi et al., 2010; Escher et al., 2011). Furthermore, the high lipophilicity of many of these xenobiotics greatly enhances their biomagnification, thereby posing potential health hazards on predators at higher trophic levels (including human beings).

The major ecological concern of xenobiotics is their ability to impair reproductive functions and subsequently threaten survival of the species. In fact, there is growing evidence from laboratory and field studies showing that exposure to trace amounts (μg L^{-1} – ng L^{-1} level) of certain xenobiotic organic compounds (e.g., halogenated hydrocarbons, PCBs, DDT, TBT) may cause reduced gonad development, disruption of normal metabolism of sex hormones (including gonadotropins), arrest of sperm maturation and block a variety of "oestrogen-like" effects on female reproductive systems in fish, birds, reptiles and mammals (Safe, 1994; Jones and de Voogt, 1999; Wu, 1999; Barceló and Petrovic, 2008; Pal et al., 2010; El Shahawi et al., 2010). This in turn, may lead to reproductive dysfunction such as delayed sex maturity, reduced fertility and hatch rate, depression in secondary sexual characteristics, alternation of sex behavior and viability of offspring (Wu, 1999).

Due to long environmental and biological half-lives, recovery from the effects of many xenobiotic compounds is expected to be slow.

The presence of organic xenobiotics in the environment may be attributed to several sources. A number of organic xenobiotic classes (chlorinated solvents, pesticides, pharmaceuticals, dyes, phenolic compounds, etc.) are ubiquitous pollutants as they are industrial products used worldwide in a variety of applications. One of the main sources of these xenobiotics contamination are the effluents of wastewater treatment plants, which frequently contain significant amounts of various recalcitrant organics that are not efficiently removed by the conventional wastewater treatment processes (Neumann et al., 2002; Fent et al., 2006; Maurer et al., 2007; Barceló and Petrovic, 2008; Miège et al., 2009; Pal et al., 2010; Verlicchi et al., 2012; Ratola et al., 2012; Michael et al., 2013; Luo et al., 2014). Other kinds of compounds (dioxins and PAHs) are not commercial products, but are formed as by-products of industrial and combustion processes and ultimately are transported from atmosphere to soil and water bodies by the atmospheric runoff or deposited on the soil during the dry period and then go through the water cycle by land runoff (Birkett and Lester, 2003).

A brief description of the main classes of typical organic xenobiotic pollutants follows.

a.) Polycyclic Aromatic Hydrocarbons

Polycyclic aromatic hydrocarbons (PAHs) consist of a large group of several hundred organic compounds characterized by containing two or more fused aromatic rings. These compounds are important pollutants because of their ubiquitous presence in the environment and the fact that some of them are considered as dangerous substances due to their toxic and mutagenic or carcinogenic potential (Kadlec and Wallace, 2009; Haritash and Kaushik, 2009; Perelo, 2010). For this reason, several of these which are considered especially harmful are included in the European Union's and United States Environmental Protection Agency's (EPA) priority pollutants list (Parrish et al., 2004; Gan et al., 2009; Perelo, 2010).

Both natural and anthropogenic sources contribute PAHs to the environment. Those compounds are formed during the incomplete combustion of almost any organic material (combustion of fossil fuels, forest fires, volcanic activities, automobile exhausts, etc.) but other sources are their synthesis by microorganisms, fungi, plants, and animals. Crude oil and other petroleum based products also contribute significant amounts of PAHs to the environment (Gan et al., 2009; Haritash and Kaushik, 2009).

b.) Petroleum Hydrocarbons

Crude oil is a lipophilic mixture that consists of more than 17000 organic compounds and is regarded as the most complex, naturally occurring mixture of organic substances. It mainly consists of alkanes, cycloalkanes, and PAHs. Contamination of the environment by total petroleum hydrocarbons (TPHs) arises from natural as well as anthropogenic sources and is potentiated by the widespread use of so many petroleum-based products in the modern society. Human-mediated sources of TPHs include offshore oil production, marine transportation, atmospheric or aerial depositions from combustion of coal and gas flaring, direct ocean dumping, coastal, municipal and industrial wastes, and runoff (Knight et al., 1999; Doble and Kumar, 2005).

Only a relatively small number of TPHs is well characterized for toxicity. The health effects of some fractions can be well characterized based on their components or representative compounds, for example the fraction of light aromatics and, in particular, the BTEX (benzene, toluene, ethylbenzene, and xylenes) fraction. These monoaromatic hydrocarbons, which are typical constituents of TPHs wastewaters, are commonly found in some petroleum-based fuels. Of all of the BTEX compounds, benzene is of most concern, because it is the most toxic one and a well-known human carcinogen. The benzene ring is a chemical structure that is very common in nature, which together with its high thermodynamic stability, provides for a significant persistence in the environment. Therefore, many aromatic compounds are major environmental pollutants and benzene contamination in particular is, thus, a significant problem. This hydrocarbon is very soluble and mobile, especially in ground and surface waters and it is poorly biodegraded in the absence of oxygen.

c.) Chlorinated Solvents

The term chlorinated solvents refers to a family of organics containing one or more chlorine atoms, which include derivatives of methane, ethane, and ethene but also polychlorinated biphenyls (PCBs). Common uses of chlorinated solvents include dry cleaning, degreasing operations, polymer manufacturing and as a chemical intermediate (Susarla et al., 2002; USEPA, 2004; Amon et al., 2007; Perelo, 2010; Aken et al., 2010).

Trichloroethylene (TCE), perchloroethylene (PCE) and polychlorinated biphenyls (PCBs) are among the most predominant chlorinated solvents which are present in the environment as contaminants (Bourg et al., 1992; Susarla et al., 2002; USEPA, 2004; Amon et al., 2007; Perelo, 2010). TCE, mainly used as a metal cleaning agent and in specialty adhesives, is a probable carcinogen and can affect kidneys, liver, lungs, and heart rate. PCE, which is also used as a metal cleaning agent and in dry cleaning, on the other hand is not classified as a carcinogen but has been known to affect the central nervous system and to cause irritation of the skin, eyes, and upper respiratory system (USEPA, 2004). PCBs are synthetic oils that do not readily react at room temperature and are primarily used as coolants and/or insulators. They are classified as probable carcinogens by the EPA and the International Agency for Research on Cancer. PCB contamination is an ecological concern, because some by-products from their combustion at low temperatures (e.g., dioxins) are highly toxic and carcinogenic (USEPA, 2004; Perelo, 2010).

Most chlorinated solvents are only slightly soluble in water and, with the exception of vinyl chloride, have densities greater than that of water. This combination leads to the formation of dense non-aqueous phase liquid deposits which act as a slow releasing, continuous source of chlorinated solvents (Amon et al., 2007). For this reason they tend to remain in the environment for long periods of time and take a long time to remediate.

d.) Explosives

There are three main classes of explosives: nitroaromatics, nitramines and nitrate esters. The contamination of the environment by explosives, especially by nitroesters and nitroaromatics, is a worldwide environmental problem. Contamination of soil and waters with explosives is largely due to manufacturing, storage, testing and inappropriate waste disposal of explosive chemicals and, therefore, most contaminated sites are located at ammunition factories and other places where these compounds are handled (Hannink et al., 2002).

The primary explosives typically found at hazardous waste sites are 2,4,6-trinitrotoluene (TNT), hexahydro-1,3,5-trinitro-1,3,5-triazine (Royal Demolition eXplosive-RDX) and octahydro-1,3,5,7-tetranitro-1,3,5,7-tetrazine (High Melting eXplosive-HMX). TNT and RDX are listed as priority pollutants and possible human carcinogens by the U.S. Environmental Protection Agency (EPA) (Etnier, 1989; Hannink et al., 2002; Aken et al., 2010). TNT is a nitroaromatic constituent of many explosives. In a refined form, TNT is stable and can be stored over long periods of time. It is relatively insensitive to blows or friction. It is readily acted upon by alkalis to form unstable compounds that are very sensitive to heat and impact. Health effects due to exposure to TNT include anemia, abnormal liver function, skin irritation, and cataracts (Hannink et al., 2002; USEPA, 2004; Aken et al., 2010). RDX is a nitramine widely used as an explosive and as a constituent in plastic

explosives. RDX can cause seizures when large amounts are inhaled or eaten (Etnier, 1989; Hannink et al., 2002; USEPA, 2004). Long-term health effects on the nervous system due to low-level exposure to RDX are not known. HMX is a nitramine that explodes violently at high temperatures. It is used in nuclear devices, plastic explosives and rocket fuels. Insufficient studies have been performed so far on the effects of HMX to the health of humans and animals (USEPA, 2004).

e.) Dyes

Dye molecules comprise two key components: the chromophore, which is the part of the molecule (in particular, the relevant functional groups) responsible for producing colour, and the auxochrome, which can not only supplement the chromophore's action (i.e. intensify the color) but also provide water solubility to the dye molecule and/or enhance its affinity (to attach) toward the fibers (Gupta and Suhas, 2009).

There are an enormous number of commercially available dyes to date and the annual production ranges the 10^5-10^6t per year (McMullan et al., 2001; Pearce et al., 2003; Nidheesh et al., 2013). According to Chakrabarti et al. (1988), nearly 40,000 dyes and pigments were listed by the end of the 1980's which consisted of over 7000 different chemical structures. In regard to the pollution produced by this industry, it is estimated that up to 15% of the total world production of dyes is lost during the dyeing process and is released in the textile effluent (Zollinger, 2003).

Most dyes are toxic (many of them contain metals), mutagenic, and/or carcinogenic. Therefore, there is potentially a grave risk of ecotoxicity for aquatic ecosystems and even lethal levels for the associated flora and fauna may be easily reached (Gupta et al., 2007). Moreover, these compounds are unusually resistant to degradation due to their complex chemical structures (synthetic dyes are purposely designed to resist fading on exposure to sweat, soap, water, light and oxidizing agents). As a result, wastewaters containing dyes are difficult to treat by conventional means since dyes are resistant to conventional biological treatment, particularly by aerobic digestion, and also stable to oxidizing agents, light and heat (Crini, 2006; Gupta and Suhas, 2009; Nidheesh et al., 2013).

f.) Pesticides

Heavy usage of pesticides over the years has resulted in their ubiquitous dispersal, most typically in aquatic environments (Chaudhry et al., 2002). The intensive use of pesticides has been a public concern for decades owing to their potential risk to human health and the environment.

Pesticides can enter the water bodies via diffuse sources or via point sources. Diffuse source pesticide inputs result from field applications of pesticides and can arise not only from agricultural practices but also from some non-agricultural practices as well, affecting both surface and ground waters. Such type of sources include tile drain overflow, baseflow seepage, surface and subsurface runoff, erosion, spray drift, deposition after volatilization, leaching through the soils and infiltration through river banks and beds (Reichenberger et al., 2007). Major point sources of pesticides and their treatment-resistant metabolites are WWTP

effluents, farmyard runoff (either directly into streams or into the sewer system) and accidental spills (Neumann et al., 2002; Gerecke et al., 2002; Bailey et al., 2005; Reichenberger et al., 2007; Gomez et al., 2007; Köck-Schulmeyer et al., 2013).

g.) Pharmaceutical Compounds

Pharmaceuticals comprise a wide ranging class of bioactive compounds with substantial variability in chemical structures, functions, behavior and activity. Their development and use aims specific biological effects and most of them are polar compounds because they are supposed to be transported within organisms through an aqueous medium.

Despite being consumed worldwide in increasing quantities, there are still not enough data available on the total use of pharmaceuticals. The consumption and application of human pharmaceuticals may vary considerably from country to country due to differences in the prevalence of diseases, treatment habits and options, or simply for market reasons. For instance, some pharmaceuticals are, in some countries, sold over the counter without prescription, while in others they are only available by prescription. Pharmaceutically active substances used in human medicine can be divided in several pharmacological classes such as analgesics and anti-inflammatory drugs, beta-blockers, lipid regulators, neuroactive compounds and antibiotics, which reflects the wide variety of compounds comprising this pollutant class.

Many of these pharmaceuticals, from all classes, are frequently detected in monitoring studies worldwide (Heberer, 2002; Fent et al., 2006; Hernando et al., 2006; Barceló and Petrovic, 2008; Aga, 2008; Miège et al., 2009; Kümmerer, 2009; Pal et al., 2010; Lapworth et al., 2012; Verlicchi et al., 2012; Ratola et al., 2012; Rivera-Utrilla et al., 2013; Luo et al., 2014), although typically present at trace levels, from low $\mu g\ L^{-1}$ to $ng\ L^{-1}$. Such low concentration levels, which were attainable by sufficiently sensitive methods of chemical analysis only in the most recent decades, is the main reason for pharmaceutical contamination passing without much concern until recently, but these pollutants may have been contaminating many water bodies for already quite a long time (Garrison et al., 1976; Hignite and Azarnoff, 1977).

Pharmaceuticals are being continuously introduced in the environment, mainly due to improper disposal of unused or expired drugs, through metabolic excretion and manufacturing processes. Some of these residues are discharged directly in the environment without going through suitable treatment, but even those receiving appropriate disposal in WWTPs in many cases are not effectively removed by the conventional wastewater treatment processes (Halling-Sørensen et al., 1998; Heberer, 2002; Verlicchi et al., 2012; Ratola et al., 2012; Rivera-Utrilla et al., 2013; Michael et al., 2013; Luo et al., 2014). Despite the trace level concentrations of pharmaceutical residues, such low amounts can sometimes be large enough to induce toxic effects on organisms (Ferrari et al., 2003; Fent et al., 2006; Crane et al., 2006; Hernando et al., 2006; Pal et al., 2010; Santos et al., 2010; Escher et al., 2011; Verlicchi et al., 2012; Michael et al., 2013; Tijani et al., 2013). A major problem is caused by the very nature of pharmaceuticals since these compounds are designed to have very specific modes of action and biological effects, and many are persistent in the body. Because of their physicochemical and biological properties, when released into environment, it may be possible that they cause serious impacts on non-target species, e.g., aquatic and terrestrial organisms. Concern has

been mostly focused on antibiotics that may cause resistance among bacteria or steroids that can induce estrogenic effects on aquatic species (Halling-Sørensen et al., 1998; Fent et al., 2006; Michael et al., 2013).

Besides toxicity, the element of persistence is of particular importance when considering the environmental significance of pharmaceuticals. Unlike persistent organic pollutants like pesticides, many pharmaceuticals are not lipophilic, so they do not bioaccumulate in the environment. However, some of those are "pseudo persistent pollutants" due to their continuous introduction in the environment. In fact, while not truly "persistent" in terms of a "long half-life", these chemicals are constantly entering the environment, still resulting in long-term exposure for the aquatic ecosystem. Potential synergetic and chronic effects have been mostly overlooked in the past, but recent ecotoxicological studies indicate that pharmaceutical residues pose a major threat especially for the aquatic species due to the continuous life-long exposure to which they are subjected (Fent et al., 2006; Tijani et al., 2013). The possible development of antibiotic-resistant bacteria, the genotoxic effects of some drugs, and endocrine disruption by therapeutically administered synthetic and natural hormones have all been discussed (Halling-Sørensen et al., 1998; Tyler et al., 1998; Fent et al., 2006; Pal et al., 2010; Santos et al., 2010; Verlicchi et al., 2012; Michael et al., 2013), but very little is known about possible long-term subtle effects on non-target organisms.

3. Water and Wastewater Treatment Processes for Organic Xenobiotic Pollutants Removal

Several studies have shown that a wide range of xenobiotic compounds are present in the effluents from domestic and industrial conventional wastewater treatment plants (Fent et al., 2006; Kim et al., 2007; Barceló and Petrovic, 2008; Aga, 2008; Miège et al., 2009; Pal et al., 2010; Bell et al., 2011; Verlicchi et al., 2012; Ratola et al., 2012; Clara et al., 2012; Michael et al., 2013; Köck-Schulmeyer et al., 2013; Luo et al., 2014), in natural (surface and subsurface) water (Gerecke et al., 2002; Heberer, 2002; Kabzinski et al., 2002; Kim et al., 2007; Zhang et al., 2007; Kasprzyk-Hordern et al., 2008; Bell et al., 2011; Lapworth et al., 2012; Moliner-Martínez et al., 2013; Menzies et al., 2013) and even in drinking water (Kabzinski et al., 2002; Kim et al., 2007; Huerta-Fontela et al., 2011; Qiao et al., 2011; Nam et al., 2014) which indicates that conventional water and wastewater treatment processes are not efficient to remove most of these pollutants and can not prevent contamination of the receiving water bodies or guarantee the production of safe drinking water.

In fact, the conventional water and wastewater treatment plants are designed and optimized to remove bulk substances that arrive regularly in large quantities (suspended solids, dissolved biodegradable organic matter, pathogens and nutrients). However, organic xenobiotics are present in wastewaters as a wide variety of chemical substances, which exihibit diverse and very particular physical/chemical properties and behaviors and are typically present at low concentrations, thus comprising a combination of features for which the conventional treatment processes are not well-suited.

Several attempts have been made to optimize conventional processes for more efficient xenobiotics removal, but such efforts have not been successful in general. Nevertheless, as more information has become available in the latest years on the environmental hazards that

potentially may be caused by many of these organic xenobiotic pollutants, it becomes increasingly evident that there is an urgent need for alternative/complementary processes which can achieve substantially larger removal efficiencies of persistent, xenobiotic organics from domestic, industrial and agricultural wastewater, as well as from drinking water.

Up to now there is already a wide range of physical and chemical processes which have been studied, such as advanced oxidation processes (Esplugas et al., 2007; Wang and Xu, 2011; Saien et al., 2011; Khulbe et al., 2012; Nidheesh et al., 2013; Tijani et al., 2013; De Luca et al., 2013; Prieto-Rodriguez et al., 2013), membrane processes (Yoon et al., 2006; Snyder et al., 2007; Acero et al., 2010; Srivastava et al., 2011; Ellouze et al., 2011; Al Rifai et al., 2011; Khulbe et al., 2012), ozonation (Esplugas et al., 2007; Naddeo et al., 2009a; Tizaoui and Grima, 2011; Derco et al., 2013; Derrouiche et al., 2013), irradiation (Naddeo et al., 2009a; Naddeo et al., 2009b), coagulation/ flocculation (Chafi et al., 2011; Ellouze et al., 2011; Alexander et al., 2012) and electro chemical methods (Gupta et al., 2007; Balla et al., 2010; Chafi et al., 2011; Nidheesh and Gandhimathi, 2012; Feng et al., 2013).

Despite the sometimes high removal efficiencies attained, most of these processes are not, however, widely used mainly for reasons of cost effectiveness, difficulties of large-scale implementations and, in some, cases additional environmental problems caused by yield of hazardous by-products (Fent et al., 2006; Crini, 2006; Aga, 2008; Ahmaruzzaman, 2008; Miège et al., 2009; Gupta and Suhas, 2009; Homem and Santos, 2011; Lofrano et al., 2013).

In regard to biological processes for removal of organic xenobiotics, several types of reactors have been studied such as membrane reactors, rotating biological contactor, enzyme membrane reactors, fluidized bed reactor, etc. (Modin et al., 2008; Sipma et al., 2010; Pakshirajan and Singh, 2010; Abargues et al., 2012; Potvin et al., 2012; Pakshirajan and Kheria, 2012; Andleeb et al., 2012; Novotny et al., 2012; Maeng et al., 2013; Zhu and Li, 2013; Jafari et al., 2013; Lin et al., 2013). Relatively to the microbial populations, species like fungi, yeasts, bacterial and fungal–bacterial consortia (Chakrabarti et al., 1988; Haritash and Kaushik, 2009; Novotny et al., 2012; Lade et al., 2012; Si et al., 2013; Hadibarata et al., 2013; Sadaf et al., 2013; Chengalroyen and Dabbs, 2013; Khan et al., 2013; Cruz-Morato et al., 2013; Garcia-Diaz et al., 2013; Usharani and Muthukumar, 2013; Langenhoff et al., 2013) have been tested and characterized. In comparison with other (physical and chemical) processes, biological treatment is frequently the most economical alternative and is, in fact, commonly used in conventional treatment for removal of some bulk pollutants. However, biological processes are slow and often ineffective in removing some complex organic molecules with low biodegradability or in cases (e.g., most industrial wastewaters) where such molecules present toxicity to the organisms used in the processes (Fent et al., 2006; Crini, 2006; Zaroual et al., 2006; Aga, 2008; Ahmaruzzaman, 2008; Gupta and Suhas, 2009; Homem and Santos, 2011; Michael et al., 2013; Tijani et al., 2013; Lofrano et al., 2013; Luo et al., 2014).

Among the alternatives, adsorption has been one of the processes with better acceptance in result of the generally high efficiencies, simplicity of implementation and maintenance, and versatility for the removal of a wide variety of organic pollutants from contaminated water (Crini, 2006; Ahmaruzzaman, 2008; Gupta and Suhas, 2009; Ali et al., 2012; Park et al., 2013; Tahar et al., 2013; Dordio and Carvalho, 2013b). Activated carbon is one of the most popular adsorbents and with widest and longest-standing use in various domains ((Ramakrishna and Viraraghavan, 1997; Derbyshire et al., 2001; Babel and Kurniawan, 2003; Ahmaruzzaman, 2008; Gupta and Suhas, 2009). Its capacity and versatility is mainly due to

its porous texture which provides it with a large surface area, its controllable pore structure and its thermo-stability (Chen et al., 2011). Its chemical nature can also be easily modified by chemical treatment in order to enhance its properties. Activated carbon has been proven to be an effective adsorbent for the removal of a wide variety of organic pollutants from aqueous media or gaseous environments (Behera et al., 2012; Hindarso et al., 2001; Mestre et al., 2007; Beninati et al., 2008; Nabais et al., 2009; Salman and Hameed, 2010; Lu et al., 2011; Jusoh et al., 2011; Serrano et al., 2013). In fact, the major barrier to the general use of activated carbon is its cost and the difficulties associated with regeneration (Babel and Kurniawan, 2003; Ahmaruzzaman, 2008; Gupta and Suhas, 2009; Chen et al., 2011). Activated carbon is quite expensive and the higher the quality, the greater the cost. The use of carbons based on relatively expensive starting materials is unjustified for most pollution control applications (Streat et al., 1995; Gupta and Suhas, 2009). Also, both chemical and thermal regeneration of spent carbon is expensive, impractical on a large scale, produces additional effluent and results in considerable loss of the adsorbent.

All these shortcomings have led many researchers to look for more economic adsorbents, especially for water pollution control, where cost factors play a major role. In recent years, inexpensive widely available materials have been investigated for the selection of efficient adsorbents that can make adsorption processes an attractive solution at reasonable costs. Among some of the adsorbents studied, clay-based materials have received some attention (Choi and Cho, 1996; Shen et al., 2004; Peng et al., 2009; Dordio et al., 2009a; Kyziol-Komosinska et al., 2010; Dordio et al., 2010; Park et al., 2011; Nourmoradi et al., 2012; Park et al., 2013; Dordio and Carvalho, 2013b; Park et al., 2014) due to their interesting properties such as the high cation exchange capacity, swelling properties and high specific surface areas.

4. Application of Clay-Based Materials for Removal Organic Xenobiotic Pollutants

Clay minerals are one of the most common constituents of soils. Its ubiquity in nature makes this class of materials unsurprisingly one of the most extensively studied groups of adsorbents.

Its adsorption properties are related with several characteristics of clays which are rather relevant for the type of surface interactions established with organic molecules (especially polar and ionizable ones). One of the most salient features of the structure of these minerals is the net negative charge due to isomorphous substitutions which is balanced by exchangeable cations on the surface of the silicate layers and in the interlayer space. These ions can be easily exchanged with some cations (with appropriate size to fit in the interlayer spaces) from the liquid media (Bhattacharyya and Sen Gupta, 2008; Rafatullah et al., 2010). In addition, the amphiprotic character of silanol and aluminol groups in clays surfaces is responsible for a pH-dependent surface charge in these materials (however, water molecules associated with exchangeable cations and clay surfaces may obscure these charged adsorption sites; such effect is dependent on the hydration strength of the exchangeable ions (Boyd et al., 2001; Johnston et al., 2001; Sheng et al., 2002; Li et al., 2004; Wang et al., 2009; Zhang et al., 2010)). Electrostatic interactions with the surface and mechanisms such as cation exchange, cation bridging with the surface, surface complexation, and hydrogen bonding seem to be

involved in the capture of ionic and polar species from aqueous media (Tolls, 2001; Figueroa et al., 2004; Pereira et al., 2007; Kyziol-Komosinska et al., 2010; Klika et al., 2011; Pei et al., 2012). In addition, the interlayer expandability of many of these minerals and the presence of water molecules associated with exchangeable cations in these interlayers allows the exchange of these hydrated ions with much larger organic molecules and their intercalation between the aluminosilicate layers (Klika et al., 2011; Li et al., 2011; Sanchez et al., 2011).

Because of this high potential for ion exchange and surface interactions, in addition to the extensive sorption capacities resulting from their large surface areas (due to the sheet structure of these minerals) clays act as natural scavengers of pollutants. For such reasons, and adding to their wide availability and associated low cost, in recent years there has been an increasing interest in utilizing natural clays for the removal of organic contaminants from aqueous solutions (Table 1).

Notwithstanding, due to the hydrophilic characteristics of their surfaces and charges, naturally occurring clays seem less effective for the adsorption of anionic contaminants and hydrophobic or non-polar organic pollutants (Park et al., 2011). Therefore, in order to increase the ability of mineral clays to remove non-polar and anionic water pollutants, clays, like many other natural materials can also be modified to improve their sorption properties. This modification commonly consists of a simple ion exchange of the natural inorganic interlayer cations with certain organic cations such as quaternary ammonium cations of long hydrocarbon chains. By introducing cationic surfactant molecules into the interlamellar space through ion exchange, the properties of clay minerals are enhanced to those of organoclays (Boyd et al., 1988; Zhou et al., 2007; Park et al., 2011). The intercalation of a cationic surfactant between the clay layers changes the surface properties from highly hydrophilic to increasingly hydrophobic. At sufficient loading, the surfactant forms a bilayer which results in a reversal of the charge on the external surface of the clay that is adequate for retention of anions, while neutral species can partition into the hydrophobic core. In addition, modification of a swelling clay with a cationic surfactant results in an increase of the basal spacing of the layer and exposure of new adsorption sites. These organoclays have been extensively investigated in recent years for a wide variety of environmental applications (Table 1).

As an alternative to the chemical modification of clay surfaces, some studies have employed lightweight clay materials that are based on processed natural clays. The typical form of processing consists of some thermal treatment that has the effect of causing interlayer hydration water to quickly vaporize (sometimes complemented with an additional effect of the thermal expansion of injected gases such as CO_2) with a consequent expansion of the sheet structure of the minerals and formation of pores and channels as the gases escape the softened heated materials. This process yields highly porous materials, with an increased accessible surface area, which can substantially improve the sorbent capacity. Some of the most common processed clay materials that have been used are light expanded clay aggregates (LECA), expanded shale, expanded slate and exfoliated vermiculite (Table1).

In terms of hydraulic conductivity requirements for applications as filter materials in water and wastewater treatment, particle sizes of these materials can in general be obtained in adequate distributions which allow some control of the hydraulic properties of the media.

Table 1. Studies of organic xenobiotics sorption by several natural, modified and synthetic clay materials

Material	Pollutants	Study type (assay type/mixture type/solvent)	Removal efficiency/ Sorption capacity	Reference
Bentonite	Dyes	BSS/MCS/PW	430 mg g^{-1}	(Zhu and Zhu, 2011)
"	PAHs	BSS/MCS/PW	94% – 95%	(Zhu and Zhu, 2011)
"	Pharmaceuticals	BSS/SCS/PW	47 mg g^{-1}	(Putra et al., 2009)
Bentonite modified	Pharmaceuticals	BSS/SCS/PW	2.69 μmol g^{-1} 5.55 μmol g^{-1}	(Rivera-Jimenez et al., 2011)
bentonite (surfactant modified)	Phenol	BSS/SCS/PW	333 mg g^{-1}	(Senturk et al., 2009)
Organo - bentonite	BTEX	BSS/SCS/PW	K_d = 22.1 – 272 L g^{-1}	(Shen et al., 2004)
Organo - bentonite	Dyes	BSS/MCS/PW	>99%; 868.1 mg g^{-1}	(Zhu and Ma, 2008)
"	Surfactants	BSS/MCS/PW	>99%; 980.8 mg g^{-1}	(Zhu and Ma, 2008)
Several organo - bentonite	PAHs	BSS/SCS/PW	$K_{d\ max}$ = 1.7 – 36.2 L g^{-1}	(Changchaivong and Khaodhiar, 2009)
Organo - bentonite (surfactant-modified)	Phenolic compounds	BSS/SCS/PW	K_L = 0.098 – 4.68 L g^{-1} K_F = 0.62 – 11.88 L g^{-1}	(Rawajfih and Nsour, 2006)
Ilite	Explosives	BSS/SCS/PW	0.0025 – 12.5 L g^{-1}	(Haderlein et al., 1996)
"	Pesticides	BSS/SCS/PW	16 L g^{-1}	(Haderlein et al., 1996)
Kaolinite	Explosives	BSS/SCS/PW	0.0003 – 1.8 L g^{-1}	(Haderlein et al., 1996)
"	Pesticides	BSS/SCS/PW	0.0064 – 2.7 L g^{-1}	(Haderlein et al., 1996)
"	Pesticides	BSS/MCS/PW	K_d = 0.039 – 0.052 L g^{-1}	(Hengpraprom et al., 2006)
"	Pesticides	BSS/SCS/PW	K_d = 0.21 L g^{-1}	(Peng et al., 2009)
"	Pesticides	BSS/SCS/PW	K_d = 0.009 – 0.041 L g^{-1}	(Polati et al., 2006a)
"	Pharmaceuticals	BSS/SCS/PW	3.1 mg g-1	(Behera et al., 2012)
"	Pharmaceuticals	BSS/MCS/PW	Poor fit of the Langmuir model	(Figueroa et al., 2004)
"	Phenolic compounds	BSS/SCS/PW	0.11 – 2.16 mg g-1	(Polati et al., 2006b)

Table 1. (Continued)

Material	Pollutants	Study type (assay type/mixture type/solvent)	Removal efficiency/ Sorption capacity	Reference
Montmorillonite	Aromatic compounds	BSS/SCS/PW	K_d = 1.48 – 213 L g^{-1}	(Johnston et al., 2001)
“	Aromatic compounds	BSS/MCS/PW	K_d = 0.03 – 4 L g^{-1}	(Pei et al., 2012)
“	Explosives	BSS/SCS/PW	0.0042 – 21.5 L g^{-1}	(Haderlein et al., 1996)
Montmorillonite (modified)	PAHs	BSS/SCS/PW	~ 99%	(Rytwo et al., 2007)
	Pesticides	BSS/SCS/PW	0.064 – 37.0 L g^{-1}	(Haderlein et al., 1996)
“	Pesticides	BSS/MCS/PW	K_d = 67 – 119 L g^{-1}	(Hengpraprom et al., 2006)
“	Pesticides	BSS/SCS/PW	K_d = 0.18 L g^{-1}	(Peng et al., 2009)
“	Pesticides	BSS/SCS/PW	K_d = 0.005 – 0.014 L g^{-1}	(Polati et al., 2006a)
Montmorillonite (modified)	Pesticides	BSS/SCS/PW	90-99%	(Zadaka et al., 2009)
“	Pharmaceuticals	BSS/SCS/PW	6.1 mg g^{-1}	(Behera et al., 2012)
“	Pharmaceuticals	BSS/MCS/PW	Poor fit of the Langmuir model	(Figueroa et al., 2004)
“	Pharmaceuticals	BSS/SCS/PW	0.88 mmol g^{-1}	(Li et al., 2011)
Montmorillonite (cation-saturated and with surfactants)	Pharmaceuticals	BSS/SCS/PW	K_d = 0.048 – 0.073 L g^{-1} (K^+ and Ca^{2+} saturated), K_d = 0.705 L g^{-1} (with surfactant)	(Zhang et al., 2010)
Montmorillonite	Phenolic compounds	BSS/SCS/PW	0.07 – 0.62 mg g-1	(Polati et al., 2006b)
Sepiolite	Dyes	BSS/SCS/PW	2.82 – 13.5 μmol g-1	(Alkan et al., 2004)
Sepiolite (raw and calcined)	Dyes	BSS/SCS/PW	12.1 μmol g-1 (raw), 9.8 – 16.2 μmol g-1 (calcined)	(Alkan et al., 2005)
Sepiolite (raw and activated)	Dyes	BSS/SCS/PW	0.18 mmol g-1 (raw), 0.41 mmol g-1 (activated)	(Eren and Afsin, 2007)
Sepiolite	Dyes	BSS/SCS/PW	155.5 mg g-1	(Karagozoglu et al., 2007)
“	Dyes	BSS/SCS/PW	70.6 – 110.2 mg g^{-1}	(Rodriguez et al., 2010)
Activated sepiolite	Dyes	BSS/SCS/PW	4.0 – 6.5 mg g^{-1}	(Ugurlu, 2009)
Sepiolite	Pharmaceuticals	BSS/SCS/PW	36% – 43%	(Dordio et al., 2009a)
Smectite (calcined)	Dyes	CS/SCS/PW	10.36 mg g^{-1}	(da Silva et al., 2009)
Smectites (saturated with K^+ and Ca^{2+})	Phenolic compounds	BSS/SCS/PW	31% – 62% (K^+), 12% – 18% (Ca^{2+})	(Pereira et al., 2007)

Material	Pollutants	Study type (assay type/mixture type/solvent)	Removal efficiency/ Sorption capacity	Reference
Vermiculite	Dyes	BSS/SCS/SWW	72 – 106 mg g^{-1}	(Choi and Cho, 1996)
Expanded vermiculite	Pharmaceuticals	BSS/SCS/PW	51% – 60%	(Dordio et al., 2009a)
Expanded clay	Pesticides	BSS/SCS/PW	0.0099 – 0.0278 mg g^{-1}	(Dordio et al., 2007)
"	Pesticides	CWS/SCS/PW	52.4% – 96.7% (unplanted) 89.3% – 99.1% (planted)	(Dordio and Carvalho, 2013a)
"	Pharmaceuticals	BSS/SCS/PW	0.0045 – 0.0123 mg g^{-1}	(Dordio et al., 2007)
"	Pharmaceuticals	BSS/SCS/PW, BSS/MCS/PW, BSS/MCS/WW	58% – 95% (SCS/PW), 51% – 93% (MCS/WW) 0.023 – 0.033 mg g-1 (SCS/PW), 0.014 – 0.030 mg g-1(MCS/PW), 0.011– 0.027 mg g-1(MCS/WW)	(Dordio et al., 2009a)
"	Pharmaceuticals	CWS/SCS/WW	82.0% (unplanted) 92.5% – 94.5% (planted)	(Dordio et al., 2009b)
"	Pharmaceuticals	CWS/MCS/WW	43%– 91% (unplanted, summer) 41% – 87% (unplanted, winter) 75% – 97% (planted, summer) 48% – 88% (planted, winter)	(Dordio et al., 2010)
"	Pharmaceuticals	CWS/MCS/WW	89% – 99% (unplanted) 97% – 100% (planted)	(Dordio and Carvalho, 2013a)
"	Polyphenols	CWS/MCS/WW	57.7% – 64.1% (unplanted) 71.2% – 80.3% (planted)	(Dordio and Carvalho, 2013a)
Organovermiculite	Pesticides	BSS/SCS/PW	Kd = 0.015 – 0.355 L g-1	(Abate and Masini, 2005)
Organoclays (various)	Explosives	BSS/SCS/PW	K = 0.30 – 0.99 L g^{-1}	(Upson and Burns, 2006)
Organoclays (various)	Pesticides	BSS/SCS/PW, CS/SCS/PW	66% – 100%	(Baglieri et al., 2009)

BSS – Batch sorption studies; CS – column studies; CWS – constructed wetlands systems; SCS – single-component solutions; MCS – multi-component solutions; PW –pure water; WW – wastewater; SWW – synthetic wastewater; NW – natural water

Some of the most popular types of clay minerals (kaolinite, illite, montmorillonite, vermiculite, sepiolite, bentonite) have been tested for the removal by adsorption of a variety of organic pollutants such as dyes (Choi and Cho, 1996; Alkan et al., 2004; Alkan et al., 2005; Karagozoglu et al., 2007; Eren and Afsin, 2007; Zhu and Ma, 2008; Ugurlu, 2009; da Silva et al., 2009; Rodriguez et al., 2010; Zhu and Zhu, 2011), pesticides (Abate and Masini, 2005; Hengpraprom et al., 2006; Polati et al., 2006b; Dordio et al., 2007; Peng et al., 2009; Baglieri et al., 2009; Zadaka et al., 2009; Dordio and Carvalho, 2013a), PAHs (Rytwo et al., 2007; Changchaivong and Khaodhiar, 2009; Zhu and Zhu, 2011; Pei et al., 2012), explosives (Haderlein et al., 1996; Upson and Burns, 2006), pharmaceuticals (Behera et al., 2012; Li et al., 2004; Figueroa et al., 2004; Dordio et al., 2007; Putra et al., 2009; Dordio et al., 2009a; Dordio et al., 2009b; Zhang et al., 2010; Dordio et al., 2010; Rivera-Jimenez et al., 2011; Dordio and Carvalho, 2013a), phenolic compounds (Johnston et al., 2001; Polati et al., 2006b; Pereira et al., 2007; Senturk et al., 2009; Dordio and Carvalho, 2013a) and other aromatics (Johnston et al., 2001; Polati et al., 2006a; Zhu and Zhu, 2011; Pei et al., 2012).

From the sample of published works presented above, it is clear that a large amount of research has been produced on the adsorption of organic pollutants by a variety of clay minerals or clay-based materials over the latest years. However, a shortcoming of many of these studies is that most of them have been conducted in very ideal conditions. Typically, many studies have been conducted as batch assays under controlled laboratory conditions, like controlled temperature, focusing on single-component solutions prepared in pure water or, at best, using synthetically prepared wastewater.

The difference between batch feed and continuous flow hydraulics is an essential one as effects such as clogging of the filter medium cannot be properly assessed from a batch assay and the kinetics of the adsorption process may also substantially differ in the two conditions.

Evaluation of multicomponent adsorption is also very important since wastewaters are typically very complex in their composition and, in such systems, the adsorbed amounts of a particular substance will unavoidably depend on the equilibrium resulting from the adsorption competition of all other substances. In addition, pollutant concentrations in these assays are frequently well above those typical of real environmental samples. Other far-from-real conditions include the stirring of the solutions (whereas in realistic systems flow is very slow) and the very low ratio of adsorbent mass-to-volume of solution in comparison to typical ratios of real systems.

In many studies a single substance is often used to represent or model the behavior of a whole family of chemically related substances (or of a big part of it). While in some cases such akin behavior may be observed and assumed, the validity of this assumption should in general be assessed as some traditional “family” denomination (e.g., pharmaceuticals) refer in fact to substances that vary considerably in structure and properties. Even when the chemical structures of the compounds present some similarity, it does not necessarily imply a similar behavior in a particular physical or chemical process such as adsorption.

These batch experiments are useful, nevertheless, to highlight the potential applicability and selectivity of the materials, determine their adsorptive capacities and characterize the mechanisms. However, once these are established, research work must be conducted at larger scale under more realistic conditions to verify their viability in fully operational treatment systems.

An important aspect to consider when assessing the viability of a filter system is the lifetime of the adsorbent and the option between disposal or regeneration of the saturated material.

Sorption studies conducted so far have revealed various options for materials (of very diverse nature and characteristics) with very similar adsorption capacities for the main groups of organic pollutants. Within a set of equivalently performing sorbents, it should be recalled however that the selection of materials is also based on other criteria as well, as has already been enunciated, including among others the hydraulic properties, ability for desorption/regeneration and, of course, the cost of the materials.

CONCLUSION

Pollution caused by organic xenobiotics is a matter of considerable concern as many of these substances have significant ecotoxicity and thus may negatively impact the environment and even present risks to human health. However, as awareness to the problem has arisen during the last decades, the realization that the conventional water and wastewater treatment processes were inefficient to deal with these type of pollutants has led to a search for alternative or complementary processes and technologies that could adequately reduce the release of most of these substances to the environment and eliminate these contaminants in drinking water resources. Some of the more efficient or traditionally used technologies that have been available have high costs which limit their application in most situations. Among the alternatives, adsorption processes can be one of the most cost-effective possibilities, depending on the type of adsorbents used. Clays have been gathering significant attention among the most accessible and cheap materials due to their interesting qualities as adsorbents and filtering media, which is evidenced by the large number of publications on the adsorption studies concerning clays or clay-based materials, either natural, processed or modified. Most studies have been conducted in batch and column studies at a laboratory scale and only very few have highlighted results on pilot or full-scale systems. Therefore, this active area of research does still require work to be carried out on large-scale systems to evaluate scaling-up effects on the efficiency and the kinetics, the behavior over longer periods of operation, the kinetics in different flow regimes, identification of problems such as clogging, etc. This type of study may be one of the most important lines of research to be pursued in the future in this area. Nevertheless, the laboratory scale experiments reported so far point to a variety of clay materials as potentially viable options to be used as filter media.

REFERENCES

Abargues, M.R., Robles, A., Bouzas, A., Seco, A., 2012. Micropollutants Removal In An Anaerobic Membrane Bioreactor And In An Aerobic Conventional Treatment Plant. *Water Sci. Technol.* 65, 2242-2250.

Abate, G., Masini, J.C., 2005. Sorption Of Atrazine, Propazine, Deethylatrazine, Deisopropylatrazine And Hydroxyatrazine Onto Organovermiculite. *J. Braz. Chem. Soc*. 16, 936-943.

Acero, J.L., Benitez, F.J., Teva, F., Leal, A.I., 2010. Retention Of Emerging Micropollutants From UP Water And A Municipal Secondary Effluent By Ultrafiltration And Nanofiltration. *Chem. Eng. J.* 163, 264-272.

Aga, D.S., 2008. *Fate Of Pharmaceuticals In The Environment And In Water Treatment Systems.* CRC Press, Boca Raton, FL.

Ahmaruzzaman, M., 2008. Adsorption Of Phenolic Compounds On Low-Cost Adsorbents: A Review. *Adv. Colloid Interface Sci.* 143, 48-67.

Aken, B.V., Correa, P.A., Schnoor, J.L., 2010. Phytoremediation Of Polychlorinated Biphenyls: New Trends And Promises. *Environ. Sci. Technol*. 44, 2767-2776.

Al Rifai, J.H., Khabbaz, H., Schafer, A.I., 2011. Removal Of Pharmaceuticals And Endocrine Disrupting Compounds In A Water Recycling Process Using Reverse Osmosis Systems. *Sep. Purif. Technol*. 77, 60-67.

Alexander, J.T., Hai, F.I., Al Aboud, T.M., 2012. Chemical Coagulation-Based Processes For Trace Organic Contaminant Removal: Current State And Future Potential. *J. Environ. Manage*. 111, 195-207.

Ali, I., Asim, M., Khan, T.A., 2012. Low Cost Adsorbents For The Removal Of Organic Pollutants From Wastewater. *J. Environ. Manage*. 113, 170-183.

Alkan, M., Celikcapa, S., Demirbas, O., Dogan, M., 2005. Removal Of Reactive Blue 221 And Acid Blue 62 Anionic Dyes From Aqueous Solutions By Sepiolite. *Dyes Pigment*. 65, 251-259.

Alkan, M., Demirba, Ö., Çelikçapa, S., Dogan, M., 2004. Sorption Of Acid Red 57 From Aqueous Solution Onto Sepiolite. *J. Hazard. Mater*. 116, 135-145.

Amon, J.P., Agrawal, A., Shelley, M.L., Opperman, B.C., Enright, M.P., Clemmer, N.D., Slusser, T., Lach, J., Sobolewski, T., Gruner, W., Entingh, A.C., 2007. Development Of A Wetland Constructed For The Treatment Of Groundwater Contaminated By Chlorinated Ethenes. *Ecol. Eng*. 30, 51-66.

Andleeb, S., Atiq, N., Robson, G.D., Ahmed, S., 2012. An Investigation Of Anthraquinone Dye Biodegradation By Immobilized Aspergillus Flavus In Fluidized Bed Bioreactor. *Environ. Sci. Pollut. Res.* 19, 1728-1737.

Babel, S., Kurniawan, T.A., 2003. Low-Cost Adsorbents For Heavy Metals Uptake From Contaminated Water: A Review. *J. Hazard. Mater*. 97, 219-243.

Baglieri, A., Borzi, D., Abbate, C., Negre, M., Gennari, M., 2009. Removal Of Fenhexamid And Pyrimethanil From Aqueous Solutions By Clays And Organoclays. J. Environ. Sci. Health Part B-Pestic. Contam. *Agric. Wastes* 44, 220-225.

Bailey, H.C., Elphick, J.R., Krassoi, R., Mulhall, A.M., Lovell, A.J., Slee, D.J., 2005. Identification Of Chlorfenvinphos Toxicity In A Municipal Effluent In Sydney, New South Wales, Australia. *Environ. Toxicol. Chem*. 24, 1773-1778.

Balla, W., Essadki, A.H., Gourich, B., Dassaa, A., Chenik, H., Azzi, M., 2010. Electrocoagulation/Electroflotation Of Reactive, Disperse And Mixture Dyes In An External-Loop Airlift Reactor. *J. Hazard. Mater*. 184, 710-716.

Barceló, D., Petrovic, M., 2008. Emerging Contaminants From Industrial And Municipal Waste. *Ocurrence, Analysis And Effects*. Springer-Verlag, Berlin, Germany.

Behera, S.K., Oh, S.Y., Park, H.S., 2012. Sorptive Removal Of Ibuprofen From Water Using Selected Soil Minerals And Activated Carbon. *Int. J. Environ. Sci. Technol*. 9, 85-94.

Bell, K.Y., Wells, M.J.M., Traexler, K.A., Pellegrin, M.L., Morse, A., Bandy, J., 2011. Emerging Pollutants. *Water Environ. Res.* 83, 1906-1984.

Beninati, S., Semeraro, D., Mastragostino, M., 2008. Adsorption Of Paracetamol And Acetylsalicylic Acid Onto Commercial Activated Carbons. *Adsorpt. Sci. Technol*. 26, 721-734.

Benner, J., Salhi, E., Ternes, T., Von Gunten, U., 2008. Ozonation Of Reverse Osmosis Concentrate: Kinetics And Efficiency Of Beta Blocker Oxidation. *Water Res.* 42, 3003-3012.

Bhattacharyya, K.G., Sen Gupta, S., 2008. Adsorption Of A Few Heavy Metals On Natural And Modified Kaolinite And Montmorillonite: A Review. *Adv. Colloid Interface Sci.* 140, 114-131.

Birkett, J.W., Lester, J.N., 2003. *Endocrine Disruptors In Wastewater And Sludge Treatment Processes.* CRC Press, Boca Raton, FL, USA.

Bourg, A.C., Mouvet, C., Lerner, D.N., 1992. A Review Of The Attenuation Of Trichloroethylene In Soils And Aquifers. Q. *J. Eng. Geol. Hydrogeol.* 25, 359-370.

Boyd, S.A., Shaobai, S., Lee, J.F., Mortland, M.M., 1988. Pentachlorophenol Sorption By Organo-Clays. *Clay Clay Min*. 36, 125-130.

Boyd, S.A., Sheng, G.Y., Teppen, B.J., Johnston, C.J., 2001. Mechanisms For The Adsorption Of Substituted Nitrobenzenes By Smectite Clays. *Environ. Sci. Technol.* 35, 4227-4234.

Chafi, M., Gourich, B., Essadki, A.H., Vial, C., Fabregat, A., 2011. Comparison Of Electrocoagulation Using Iron And Aluminium Electrodes With Chemical Coagulation For The Removal Of A Highly Soluble Acid Dye. *Desalination* 281, 285-292.

Chakrabarti, T., Subrahmanyam, P.V.R., Sundaresan, B.B., 1988. Biodegradation Of Recalcitrant Industrial Wastes, In: Wise, D.L. (Ed.), *Biotreatment Systems.* CRC Press, Inc., Boca Raton, FL, Pp. 171-234.

Changchaivong, S., Khaodhiar, S., 2009. Adsorption Of Naphthalene And Phenanthrene On Dodecylpyridinium-Modified Bentonite. *Appl. Clay Sci.* 43, 317-321.

Chaudhry, Q., Schröder, P., Werck-Reichhart, D., Grajek, W., Marecik, R., 2002. Prospects And Limitations Of Phytoremediation For The Removal Of Persistent Pesticides In The Environment. *Environ. Sci. Pollut. Res*. 9, 4-17.

Chen, Y., Zhu, Y., Wang, Z., Li, Y., Wang, L., Ding, L., Gao, X., Ma, Y., Guo, Y., 2011. Application Studies Of Activated Carbon Derived From Rice Husks Produced By Chemical-Thermal Process-A Review. Adv. *Colloid Interface Sci.* 163, 39-52.

Chengalroyen, M.D., Dabbs, E.R., 2013. The Microbial Degradation Of Azo Dyes: Minireview. *World J. Microbiol. Biotechnol.* 29, 389-399.

Choi, Y.S., Cho, J.H., 1996. Color Removal From Dye Wastewater Using Vermiculite. *Environ. Technol.* 17, 1169-1180.

Clara, M., Windhofer, G., Weilgony, P., Gans, O., Denner, M., Chovanec, A., Zessner, M., 2012. Identification Of Relevant Micropollutants In Austrian Municipal Wastewater And Their Behaviour During Wastewater Treatment. *Chemosphere* 87, 1265-1272.

Crane, M., Watts, C., Boucard, T., 2006. Chronic Aquatic Environmental Risks From Exposure To Human Pharmaceuticals. Sci. Total Environ. 367, 23-41.

Crini, G., 2006. Non-Conventional Low-Cost Adsorbents For Dye Removal: A Review. *Bioresour. Technol.* 97, 1061-1085.

Cruz-Morato, C., Ferrando-Climent, L., Rodriguez-Mozaz, S., Barcelo, D., Marco-Urrea, E., Vicent, T., Sarra, M., 2013. Degradation Of Pharmaceuticals In Non-Sterile Urban

Wastewater By Trametes Versicolor In A Fluidized Bed Bioreactor. *Water Res.* 47, 5200-5210.

Da Silva, G.L., Silva, V.L., Vieira, M.G.A., Da Silva, M.G.C., 2009. Solophenyl Navy Blue Dye Removal By Smectite Clay In A Porous Bed Column. Adsorpt. *Sci. Technol.* 27, 861-875.

De Luca, A., Dantas, R.F., Simões, A.S.M., Toscano, I.A.S., Lofrano, G., Cruz, A., Esplugas, S., 2013. Atrazine Removal In Municipal Secondary Effluents By Fenton And Photo-Fenton Treatments. *Chem. Eng. Technol*. 36, 2155-2162.

Demirezen, D., Aksoy, A., Uruç, K., 2007. Effect Of Population Density On Growth, Biomass And Nickel Accumulation Capacity Of *Lemna Gibba* (Lemnaceae). *Chemosphere* 66, 553-557.

Derbyshire, F., Jagtoyen, M., Andrews, R., Rao, A., Martin-Gullon, I., Grulke, E.A., 2001. Carbon Materials In Environmental Applications. Chem. Phys. Carb. 27, 1-66.

Derco, J., Valickova, M., Silharova, K., Dudas, J., Luptakova, A., 2013. Removal Of Selected Chlorinated Micropollutants By Ozonation. *Chem. Pap*. 67, 1585-1593.

Derrouiche, S., Bourdin, D., Roche, P., Houssais, B., Machinal, C., Coste, M., Restivo, J., Orfao, J.J.M., Pereira, M.F.R., Marco, Y., Garcia-Bordeje, E., 2013. Process Design For Wastewater Treatment: Catalytic Ozonation Of Organic Pollutants. *Water Sci. Technol.* 68, 1377-1383.

Doble, M., Kumar, A., 2005. Petroleum Hydrocarbon Pollution, Biotreatment Of Industrial Effluents. Butterworth-Heinemann, Burlington, Pp. 241-253.

Dordio, A., Carvalho, A.J.P., 2013a. Constructed Wetlands With Light Expanded Clay Aggregates For Agricultural Wastewater Treatment. *Sci. Total Environ.* 463, 454-461.

Dordio, A.V., Candeias, A.J.E., Pinto, A.P., Da Costa, C.T., Carvalho, A.J.P., 2009a. Preliminary Media Screening For Application In The Removal Of Clofibric Acid, Carbamazepine And Ibuprofen By SSF-Constructed Wetlands. *Ecol. Eng.* 35, 290-302.

Dordio, A.V., Carvalho, A.J.P., 2013b. Organic Xenobiotics Removal In Constructed Wetlands, With Emphasis On The Importance Of The Support Matrix. *J. Hazard. Mater*. 252-253, 272-292.

Dordio, A.V., Teimao, J., Ramalho, I., Palace Carvalho, A.J., Estevao Candeias, A.J., 2007. Selection Of A Support Matrix For The Removal Of Some Phenoxyacetic Compounds In Constructed Wetlands Systems. *Sci. Total Environ.* 380, 237-246.

Dordio, A., Carvalho, A.J.P., Teixeira, D.M., Dias, C.B., Pinto, A.P., 2010. Removal Of Pharmaceuticals In Microcosm Constructed Wetlands Using *Typha* Spp. And LECA. *Bioresour. Technol*. 101, 886-892.

Dordio, A., Pinto, J., Pinto, A.P., Da Costa, C.T., Carvalho, A., Teixeira, D.M., 2009b. Atenolol Removal In Microcosm Constructed Wetlands. Intern. J. Environ. *Anal. Chem.* 89, 835-848.

El Shahawi, M.S., Hamza, A., Bashammakh, A.S., Al Saggaf, W.T., 2010. An Overview On The Accumulation, Distribution, Transformations, Toxicity And Analytical Methods For The Monitoring Of Persistent Organic *Pollutants. Talanta* 80, 1587-1597.

Ellouze, E., Ellouze, D., Jrad, A., Ben Amar, R., 2011. Treatment Of Synthetic Textile Wastewater By Combined Chemical Coagulation/Membrane Processes. Desalin. *Water Treat.* 33, 118-124.

Eren, E., Afsin, B., 2007. Investigation Of A Basic Dye Adsorption From Aqueous Solution Onto Raw And Pre-Treated Sepiolite Surfaces. *Dyes Pigment.* 73, 162-167.

Escher, B.I., Baumgartner, R., Koller, M., Treyer, K., Lienert, J., Mcardell, C.S., 2011. Environmental Toxicology And Risk Assessment Of Pharmaceuticals From Hospital Wastewater. *Water Res.* 45, 75-92.

Esplugas, S., Bila, D.M., Krause, L.G., Dezotti, M., 2007. Ozonation And Advanced Oxidation Technologies To Remove Endocrine Disrupting Chemicals (Edcs) And Pharmaceuticals And Personal Care Products (Ppcps) In Water Effluents. *J. Hazard. Mater.* 149, 631-642.

Etnier, E.L., 1989. Water Quality Criteria For Hexahydro-1,3,5-Trinitro-1,3,5-Triazine (RDX). *Regul. Toxicol. Pharmacol.* 9, 147-157.

Feng, L., Van Hullebusch, E.D., Rodrigo, M.A., Esposito, G., Oturan, M.A., 2013. Removal Of Residual Anti-Inflammatory And Analgesic Pharmaceuticals From Aqueous Systems By Electrochemical Advanced Oxidation Processes. A Review. *Chem. Eng. J.* 228, 944-964.

Fent, K., Weston, A.A., Caminada, D., 2006. Ecotoxicology Of Human Pharmaceuticals. *Aquat. Toxicol.* 76, 122-159.

Ferrari, B., Paxéus, N., Lo Giudice, R., Pollio, A., Garric, J., 2003. Ecotoxicological Impact Of Pharmaceuticals Found In Treated Wastewaters: Study Of Carbamazepine, Clofibric Acid, And Diclofenac. *Ecotox. Environ. Safe.* 55, 359-370.

Figueroa, R.A., Leonard, A., Mackay, A.A., 2004. Modeling Tetracycline Antibiotic Sorption To Clays. *Environ. Sci. Technol.* 38, 476-483.

Gan, S., Lau, E.V., Ng, H.K., 2009. Remediation Of Soils Contaminated With Polycyclic Aromatic Hydrocarbons (Pahs). *J. Hazard. Mater.* 172, 532-549.

Garcia-Diaz, C., Ponce-Noyola, M.T., Esparza-Garcia, F., Rivera-Orduna, F., Barrera-Cortes, J., 2013. PAH Removal Of High Molecular Weight By Characterized Bacterial Strains From Different Organic Sources. *Int. Biodeterior. Biodegrad.* 85, 311-322.

Garrison, A.W., Pope, J.D., Allen, F.R., 1976. GC/MS Analysis Of Organic Compounds In Domestic Wastewaters, In: Keith, L.H. (Ed.), *Identification And Analysis Of Organic Pollutants In Water.* Ann Arbor Science Publishers, Ann Arbor, MI, USA, Pp. 517-556.

Gavrilescu, M., 2005. Fate Of Pesticides In The Environment And Its Bioremediation. *Eng. Life Sci.* 5, 497-526.

Gerecke, A.C., Scharer, M., Singer, H.P., Muller, S.R., Schwarzenbach, R.P., Sagesser, M., Ochsenbein, U., Popow, G., 2002. Sources Of Pesticides In Surface Waters In Switzerland: Pesticide Load Through Waste Water Treatment Plants--Current Situation And Reduction Potential. *Chemosphere* 48, 307-315.

Gomez, M.J., Martinez Bueno, M.J., Lacorte, S., Fernandez-Alba, A.R., Aguera, A., 2007. Pilot Survey Monitoring Pharmaceuticals And Related Compounds In A Sewage Treatment Plant Located On The Mediterranean Coast. *Chemosphere* 66, 993-1002.

Gupta, V.K., Jain, R., Varshney, S., 2007. Electrochemical Removal Of The Hazardous Dye Reactofix Red 3 BFN From Industrial Effluents. *J. Colloid Interface Sci.* 312, 292-296.

Gupta, V.K., Suhas, 2009. Application Of Low-Cost Adsorbents For Dye Removal - A Review. *J. Environ. Manage.* 90, 2313-2342.

Haarstad, K., Bavor, H.J., Maehlum, T., 2011. Organic And Metallic Pollutants In Water Treatment And Natural Wetlands: A Review. Water Sci. Technol. 65, 76-99.

Haderlein, S.B., Weissmahr, K.W., Schwarzenbach, R.P., 1996. Specific Adsorption Of Nitroaromatic Explosives And Pesticides To Clay Minerals. *Environ. Sci. Technol.* 30, 612-622.

Hadibarata, T., Adnan, L.A., Yusoff, A.R.M., Yuniarto, A., Rubiyatno, Zubir, M.M.F.A., Khudhair, A.B., Teh, Z.C., Abu Naser, M., 2013. Microbial Decolorization Of An Azo Dye Reactive Black 5 Using White-Rot Fungus Pleurotus Eryngii F032. *Water Air Soil Pollut.* 224, 1595-1603.

Halling-Sørensen, B., Nors Nielsen, S., Lanzky, P.F., Ingerslev, F., Holten Lützhøft, H.C., Jørgensen, S.E., 1998. Occurrence, Fate And Effects Of Pharmaceutical Substances In The Environment- A Review. *Chemosphere 36*, 357-393.

Hannink, N.K., Rosser, S.J., Bruce, N.C., 2002. Phytoremediation Of Explosives. *Crit. Rev. Plant Sci.* 21, 511-538.

Haritash, A.K., Kaushik, C.P., 2009. Biodegradation Aspects Of Polycyclic Aromatic Hydrocarbons (Pahs): A Review. *J. Hazard. Mater.* 169, 1-15.

Heberer, T., 2002. Occurrence, Fate, And Removal Of Pharmaceutical Residues In The Aquatic Environment: A Review Of Recent Research Data. *Toxicol. Lett.* 131, 5-17.

Hengpraprom, S., Lee, C.M., Coates, J.T., 2006. Sorption Of Humic Acids And Alpha-Endosulfan By Clay Minerals. *Environ. Toxicol. Chem*. 25, 11-17.

Hernando, M.D., Mezcua, M., Fernández-Alba, A.R., Barceló, D., 2006. Environmental Risk Assessment Of Pharmaceutical Residues In Wastewater Effluents, Surface Waters And Sediments. *Talanta* 69, 334-342.

Hignite, C., Azarnoff, D.L., 1977. Drugs And Drug Metabolites As Environmental Contaminants - Chlorophenoxyisobutyrate And Salicylic-Acid In Sewage Water Effluent. *Life Sci.* 20, 337-341.

Hindarso, H., Ismadji, S., Wicaksana, F., Mudjijati, Indraswati, N., 2001. Adsorption Of Benzene And Toluene From Aqueous Solution Onto Granular Activated Carbon. *J. Chem. Eng. Data* 46, 788-791.

Homem, V., Santos, L., 2011. Degradation And Removal Methods Of Antibiotics From Aqueous Matrices - A Review. *J. Environ. Manage.* 92, 2304-2347.

Huerta-Fontela, M., Galceran, M.T., Ventura, F., 2011. Occurrence And Removal Of Pharmaceuticals And Hormones Through Drinking Water Treatment. *Water Res*. 45, 1432-1442.

Jafari, J., Mesdaghinia, A., Nabizadeh, R., Farrokhi, M., Mahvi, A.H., 2013. Investigation Of Anaerobic Fluidized Bed Reactor/Aerobic Moving Bed Bio Reactor (AFBR/MMBR) System For Treatment Of Currant Wastewater. Iran *J. Public Health* 42, 860-867.

Johnston, C.T., De Oliveira, M.F., Teppen, B.J., Sheng, G.Y., Boyd, S.A., 2001. Spectroscopic Study Of Nitroaromatic-Smectite Sorption Mechanisms. *Environ. Sci. Technol.* 35, 4767-4772.

Jones, K.C., De Voogt, P., 1999. Persistent Organic Pollutants (Pops): State Of The Science. *Environ. Pollut.* 100, 209-221.

Jusoh, A., Hartini, W.J.H., Ali, N., Endut, A., 2011. Study On The Removal Of Pesticide In Agricultural Run Off By Granular Activated Carbon. *Bioresour. Technol.* 102, 5312-5318.

Kabzinski, A.K.M., Cyran, J., Juszczak, R., 2002. Determination Of Polycyclic Aromatic Hydrocarbons In Water (Including Drinking Water) Of Lodz. Pol. *J. Environ. Stud.* 11, 695-706.

Kadlec, R.H., Wallace, S.D., 2009. *Treatment Wetlands*. CRC Press, Boca Raton, FL, USA.

Karagozoglu, B., Tasdemir, M., Demirbas, E., Kobya, M., 2007. The Adsorption Of Basic Dye (Astrazon Blue FGRL) From Aqueous Solutions Onto Sepiolite, Fly Ash And

Apricot Shell Activated Carbon: Kinetic And Equilibrium Studies. *J. Hazard. Mater.* 147, 297-306.

Kasprzyk-Hordern, B., Dinsdale, R.M., Guwy, A.J., 2008. The Occurrence Of Pharmaceuticals, Personal Care Products, Endocrine Disruptors And Illicit Drugs In Surface Water In South Wales, UK. *Water Res.* 42, 3498-3518.

Khan, R., Bhawana, P., Fulekar, M.H., 2013. Microbial Decolorization And Degradation Of Synthetic Dyes: A Review. *Rev. Environ. Sci. Bio-Technol.* 12, 75-97.

Khulbe, K.C., Feng, C.Y., Matsuura, T., Ismail, A.F., 2012. Progresses In Membrane And Advanced Oxidation Processes For Water Treatment. Membr. *Water Treat.* 3, 181-200.

Kim, S.D., Cho, J., Kim, I.S., Vanderford, B.J., Snyder, S.A., 2007. Occurrence And Removal Of Pharmaceuticals And Endocrine Disruptors In South Korean Surface, Drinking, And Waste Waters. *Water Res.* 41, 1013-1021.

Klika, Z., Pustkova, P., Dudova, M., Capkova, P., Klikova, C., Matys Grygar, T., 2011. The Adsorption Of Methylene Blue On Montmorillonite From Acid Solutions. *Clay Min.* 46, 461-471.

Knight, R.L., Kadlec, R.H., Ohlendorf, H.M., 1999. The Use Of Treatment Wetlands For Petroleum Industry Effluents. *Environ. Sci. Technol.* 33, 973-980.

Köck-Schulmeyer, M., Villagrasa, M., López De Alda, M., Céspedes-Sánchez, R., Ventura, F., Barceló, D., 2013. Occurrence And Behavior Of Pesticides In Wastewater Treatment Plants And Their Environmental Impact. *Sci. Total Environ.* 458-460, 466-476.

Kosjek, T., Perko, S., Zupanc, M., Zanoški Hren, M., Landeka Dragicevic, T., Žigon, D., Kompare, B., Heath, E., 2012. Environmental Occurrence, Fate And Transformation Of Benzodiazepines In Water Treatment. *Water Res*. 46, 355-368.

Kümmerer, K., 2009. The Presence Of Pharmaceuticals In The Environment Due To Human Use - Present Knowledge And Future Challenges. *J. Environ. Manage.* 90, 2354-2366.

Kyziol-Komosinska, J., Rosik-Dulewska, C., Pajak, M., Jarzyna, M., 2010. Removal Of Direct Dyes From Wastewater By Sorption Onto Smectite-Clay. *Arch. Environ. Prot.* 36, 3-14.

Lade, H.S., Waghmode, T.R., Kadam, A.A., Govindwar, S.P., 2012. Enhanced Biodegradation And Detoxification Of Disperse Azo Dye Rubine GFL And Textile Industry Effluent By Defined Fungal-Bacterial Consortium. Int. Biodeterior. *Biodegrad*. 72, 94-107.

Langenhoff, A., Inderfurth, N., Veuskens, T., Schraa, G., Blokland, M., Kujawa-Roeleveld, K., Rijnaarts, H., 2013. Microbial Removal Of The Pharmaceutical Compounds Ibuprofen And Diclofenac From Wastewater. *Biomed Research International 2013,* Article ID 325806.

Lapworth, D.J., Baran, N., Stuart, M.E., Ward, R.S., 2012. Emerging Organic Contaminants In Groundwater: A Review Of Sources, Fate And Occurrence. *Environ. Pollut.* 163, 287-303.

Li, H., Teppen, B.J., Johnston, C.T., Boyd, S.A., 2004. Thermodynamics Of Nitroaromatic Compound Adsorption From Water By Smectite Clay. *Environ. Sci. Technol.* 38, 5433-5442.

Li, Z.H., Chang, P.H., Jiang, W.T., Jean, J.S., Hong, H.L., Liao, L.B., 2011. Removal Of Diphenhydramine From Water By Swelling Clay Minerals. *J. Colloid Interface Sci.* 360, 227-232.

Lin, Y.H., Lin, W.F., Jhang, K.N., Lin, P.Y., Lee, M.C., 2013. Adsorption With Biodegradation For Decolorization Of Reactive Black 5 By Funalia Trogii 200800 On A Fly Ash-Chitosan Medium In A Fluidized Bed Bioreactor-Kinetic Model And Reactor Performance. *Biodegradation* 24, 137-152.

Lofrano, G., Meric, S., Zengin, G.E., Orhon, D., 2013. Chemical And Biological Treatment Technologies For Leather Tannery Chemicals And Wastewaters: A Review. *Sci. Total Environ.* 461, 265-281.

Lu, G.C., Hao, J., Liu, L., Ma, H.W., Fang, Q.F., Wu, L.M., Wei, M.Q., Zhang, Y.H., 2011. The Adsorption Of Phenol By Lignite Activated Carbon. *Chin. J. Chem. Eng.* 19, 380-385.

Luo, Y., Guo, W., Ngo, H.H., Nghiem, L.D., Hai, F.I., Zhang, J., Liang, S., Wang, X.C., 2014. A Review On The Occurrence Of Micropollutants In The Aquatic Environment And Their Fate And Removal During Wastewater Treatment. *Sci. Total Environ.* 473-474, 619-641.

Maeng, S.K., Choi, B.G., Lee, K.T., Song, K.G., 2013. Influences Of Solid Retention Time, Nitrification And Microbial Activity On The Attenuation Of Pharmaceuticals And Estrogens In Membrane Bioreactors. *Water Res.* 47, 3151-3162.

Mason, C., 2002. *Biology Of Freshwater Pollution*. Pearson Education, Harlow, UK.

Maurer, M., Escher, B.I., Richle, P., Schaffner, C., Alder, A.C., 2007. Elimination Of Beta-Blockers In Sewage Treatment Plants. *Water Res.* 41, 1614-1622.

Mcmullan, G., Meehan, C., Conneely, A., Kirby, N., Robinson, T., Nigam, P., Banat, I., Marchant, R., Smyth, W., 2001. Microbial Decolourisation And Degradation Of Textile Dyes. *Appl Microbiol Biotechnol* 56, 81-87.

Menzies, R., Quinete, N.S., Gardinali, P., Seba, D., 2013. Baseline Occurrence Of Organochlorine Pesticides And Other Xenobiotics In The Marine Environment: Caribbean And Pacific Collections. *Mar. Pollut. Bull.* 70, 289-295.

Mestre, A.S., Pires, J., Nogueira, J.M.F., Carvalho, A.P., 2007. Activated Carbons For The Adsorption Of Ibuprofen. *Carbon* 45, 1979-1988.

Michael, I., Rizzo, L., Mcardell, C.S., Manaia, C.M., Merlin, C., Schwartz, T., Dagot, C., Fatta-Kassinos, D., 2013. Urban Wastewater Treatment Plants As Hotspots For The Release Of Antibiotics In The Environment: A Review. *Water Res.* 47, 957-995.

Miège, C., Choubert, J.M., Ribeiro, L., Eusèbe, M., Coquery, M., 2009. Fate Of Pharmaceuticals And Personal Care Products In Wastewater Treatment Plants - Conception Of A Database And First Results. *Environ. Pollut.* 157, 1721-1726.

Modin, O., Fukushi, K., Yamamoto, K., 2008. Simultaneous Removal Of Nitrate And Pesticides From Groundwater Using A Methane-Fed Membrane Biofilm Reactor. *Water Sci. Technol.* 58, 1273-1279.

Moliner-Martínez, Y., Herraez-Hernandez, R., Verdú-Andres, J., Campíns-Falcó, P., Garrido-Palanca, C., Molins-Legua, C., Seco, A., 2013. Study Of The Influence Of Temperature And Precipitations On The Levels Of BTEX In Natural Waters. *J. Hazard. Mater.* 263, Part 1, 131-138.

Nabais, J.M.V., Gomes, J.A., Suhas, Carrott, P.J.M., Laginhas, C., Roman, S., 2009. Phenol Removal Onto Novel Activated Carbons Made From Lignocellulosic Precursors: Influence Of Surface Properties. *J. Hazard. Mater.* 167, 904-910.

Naddeo, V., Belgiorno, V., Ricco, D., Kassinos, D., 2009a. Degradation Of Diclofenac During Sonolysis, Ozonation And Their Simultaneous Application. *Ultrason. Sonochem*. 16, 790-794.

Naddeo, V., Meric, S., Kassinos, D., Belgiorno, V., Guida, M., 2009b. Fate Of Pharmaceuticals In Contaminated Urban Wastewater Effluent Under Ultrasonic Irradiation. *Water Res.* 43, 4019-4027.

Nam, S.W., Jo, B.I., Yoon, Y., Zoh, K.D., 2014. Occurrence And Removal Of Selected Micropollutants In A Water Treatment Plant. *Chemosphere* 95, 156-165.

Neumann, M., Schulz, R., Schafer, K., Muller, W., Mannheller, W., Liess, M., 2002. The Significance Of Entry Routes As Point And Non-Point Sources Of Pesticides In Small Streams. *Water Res. 3*6, 835-842.

Nidheesh, P.V., Gandhimathi, R., 2012. Trends In Electro-Fenton Process For Water And Wastewater Treatment: An Overview. *Desalination* 299, 1-15.

Nidheesh, P., Gandhimathi, R., Ramesh, S., 2013. Degradation Of Dyes From Aqueous Solution By Fenton Processes: A Review. *Environ Sci Pollut Res* 20, 2099-2132.

Nourmoradi, H., Nikaeen, M., Khiadani, H., 2012. Removal Of Benzene, Toluene, Ethylbenzene And Xylene (BTEX) From Aqueous Solutions By Montmorillonite Modified With Nonionic Surfactant: Equilibrium, Kinetic And Thermodynamic Study. *Chem. Eng. J.* 191, 341-348.

Novotny, C., Trost, N., Susla, M., Svobodova, K., Mikeskova, H., Valkova, H., Malachova, K., Pavko, A., 2012. The Use Of The Fungus Dichomitus Squalens For Degradation In Rotating Biological Contactor Conditions. *Bioresour. Technol.* 114, 241-246.

Pakshirajan, K., Kheria, S., 2012. Continuous Treatment Of Coloured Industry Wastewater Using Immobilized Phanerochaete Chrysosporium In A Rotating Biological Contactor Reactor. *J. Environ. Manage.* 101, 118-123.

Pakshirajan, K., Singh, S., 2010. Decolorization Of Synthetic Wastewater Containing Azo Dyes In A Batch-Operated Rotating Biological Contactor Reactor With The Immobilized Fungus Phanerochaete Chrysosporium. Ind. *Eng. Chem. Res.* 49, 7484-7487.

Pal, A., Gin, K.Y.-H., Lin, A.Y.-C., Reinhard, M., 2010. Impacts Of Emerging Organic Contaminants On Freshwater Resources: Review Of Recent Occurrences, Sources, Fate And Effects. *Sci. Total Environ.* 408, 6062-6069.

Park, Y., Ayoko, G.A., Frost, R.L., 2011. Application Of Organoclays For The Adsorption Of Recalcitrant Organic Molecules From Aqueous Media. *J. Colloid Interface Sci.* 354, 292-305.

Park, Y., Ayoko, G.A., Kurdi, R., Horváth, E., Kristóf, J., Frost, R.L., 2013. Adsorption Of Phenolic Compounds By Organoclays: Implications For The Removal Of Organic Pollutants From Aqueous Media. *J. Colloid Interface Sci.* 406, 196-208.

Park, Y., Sun, Z., Ayoko, G.A., Frost, R.L., 2014. Removal Of Herbicides From Aqueous Solutions By Modified Forms Of Montmorillonite. *J. Colloid Interface Sci*. 415, 127-132.

Parrish, Z.D., Banks, M.K., Schwab, A.P., 2004. Effectiveness Of Phytoremediation As A Secondary Treatment For Polycyclic Aromatic Hydrocarbons (Pahs) In Composted Soil. *Int. J. Phytoremediat.* 6, 119-137.

Pearce, C.I., Lloyd, J.R., Guthrie, J.T., 2003. The Removal Of Colour From Textile Wastewater Using Whole Bacterial Cells: A Review. *Dyes Pigment.* 58, 179-196.

Pei, Z.G., Kong, J.J., Shan, X.Q., Wen, B., 2012. Sorption Of Aromatic Hydrocarbons Onto Montmorillonite As Affected By Norfloxacin. *J. Hazard. Mater.* 203, 137-144.

Peng, K., Luo, C., Lou, L., Li, X., Shen, Z., 2008. Bioaccumulation Of Heavy Metals By The Aquatic Plants *Potamogeton Pectinatus* L. And *Potamogeton Malaianus* Miq. And Their Potential Use For Contamination Indicators And In Wastewater Treatment. *Sci. Total Environ.* 392, 22-29.

Peng, X.J., Wang, J., Fan, B., Luan, Z.K., 2009. Sorption Of Endrin To Montmorillonite And Kaolinite Clays. *J. Hazard. Mater.* 168, 210-214.

Pereira, T.R., Laird, D.A., Johnston, C.T., Teppen, B.J., Li, H., Boyd, S.A., 2007. Mechanism Of Dinitrophenol Herbicide Sorption By Smectites In Aqueous Suspensions At Varying Ph. *Soil Sci. Soc. Am. J.* 71, 1476-1481.

Perelo, L.W., 2010. Review: In Situ And Bioremediation Of Organic Pollutants In Aquatic Sediments. *J. Hazard. Mater.* 177, 81-89.

Polati, S., Angioi, S., Gianotti, V., Gosetti, F., Gennaro, M.C., 2006a. Sorption Of Pesticides On Kaolinite And Montmorillonite As A Function Of Hydrophilicity. *J. Environ. Sci. Health Part B-Pestic. Contam. Agric. Wastes* 41, 333-344.

Polati, S., Gosetti, F., Gianotti, V., Gennaro, M.C., 2006b. Sorption And Desorption Behavior Of Chloroanilines And Chlorophenols On Montmorillonite And Kaolinite. *J. Environ. Sci. Health Part B-Pestic. Contam. Agric. Wastes* 41, 765-779.

Potvin, C.M., Long, Z.B., Zhou, H.D., 2012. Removal Of Tetrabromobisphenol A By Conventional Activated Sludge, Submerged Membrane And Membrane Aerated Biofilm Reactors. *Chemosphere* 89, 1183-1188.

Prieto-Rodriguez, L., Oller, I., Klamerth, N., Aguera, A., Rodriguez, E.M., Malato, S., 2013. Application Of Solar Aops And Ozonation For Elimination Of Micropollutants In Municipal Wastewater Treatment Plant Effluents. *Water Res*. 47, 1521-1528.

Putra, E.K., Pranowo, R., Sunarso, J., Indraswati, N., Ismadji, S., 2009. Performance Of Activated Carbon And Bentonite For Adsorption Of Amoxicillin From Wastewater: Mechanisms, Isotherms And Kinetics. *Water Res.* 43, 2419-2430.

Qiao, T.J., Yu, Z.R., Zhang, X.H., Au, D.W.T., 2011. Occurrence And Fate Of Pharmaceuticals And Personal Care Products In Drinking Water In Southern China. *J. Environ. Monit.* 13, 3097-3103.

Radjenovic, J., Petrovic, M., Barceló, D., 2007. Advanced Mass Spectrometric Methods Applied To The Study Of Fate And Removal Of Pharmaceuticals In Wastewater Treatment. *Trac-Trends Anal. Chem*. 26, 1132-1144.

Rafatullah, M., Sulaiman, O., Hashim, R., Ahmad, A., 2010. Adsorption Of Methylene Blue On Low-Cost Adsorbents: A Review. *J. Hazard. Mater.* 177, 70-80.

Ramakrishna, K.R., Viraraghavan, T., 1997. Dye Removal Using Low Cost Adsorbents. *Water Sci. Technol.* 36, 189-196.

Ratola, N., Cincinelli, A., Alves, A., Katsoyiannis, A., 2012. Occurrence Of Organic Microcontaminants In The Wastewater Treatment Process. A Mini Review. *J. Hazard. Mater.* 239-240, 1-18.

Rawajfih, Z., Nsour, N., 2006. Characteristics Of Phenol And Chlorinated Phenols Sorption Onto Surfactant-Modified Bentonite. *J. Colloid Interface Sci.* 298, 39-49.

Reichenberger, S., Bach, M., Skitschak, A., Frede, H.G., 2007. Mitigation Strategies To Reduce Pesticide Inputs Into Ground- And Surface Water And Their Effectiveness; A Review. *Sci. Total Environ.* 384, 1-35.

Rivera-Jimenez, S.M., Lehner, M.M., Cabrera-Lafaurie, W.A., Hernandez-Maldonado, A.J., 2011. Removal Of Naproxen, Salicylic Acid, Clofibric Acid, And Carbamazepine By

Water Phase Adsorption Onto Inorganic-Organic-Intercalated Bentonites Modified With Transition Metal Cations. *Environ. Eng. Sci.* 28, 171-182.

Rivera-Utrilla, J., Sánchez-Polo, M., Ferro-García, M.Á., Prados-Joya, G., Ocampo-Pérez, R., 2013. Pharmaceuticals As Emerging Contaminants And Their Removal From Water. A Review. *Chemosphere* 93, 1268-1287.

Rodriguez, A., Ovejero, G., Mestanza, M., Garcia, J., 2010. Removal Of Dyes From Wastewaters By Adsorption On Sepiolite And Pansil. *Ind. Eng. Chem. Res.* 49, 3207-3216.

Rytwo, G., Kohavi, Y., Botnick, I., Gonen, Y., 2007. Use Of CV- And TPP-Montmorillonite For The Removal Of Priority Pollutants From Water. *Appl. Clay Sci*. 36, 182-190.

Sadaf, S., Bhatti, H.N., Bibi, I., 2013. Efficient Removal Of Disperse Dye By Mixed Culture Of Ganoderma Lucidum And Coriolus Versicolor. *Pak. J. Agric. Sci.* 50, 261-266.

Safe, S.H., 1994. Polychlorinated-Biphenyls (Pcbs) - Environmental-Impact, Biochemical And Toxic Responses, And Implications For Risk Assessment. *Crit. Rev. Toxicol*. 24, 87-149.

Saien, J., Ojaghloo, Z., Soleymani, A.R., Rasoulifard, M.H., 2011. Homogeneous And Heterogeneous Aops For Rapid Degradation Of Triton X-100 In Aqueous Media Via UV Light, Nano Titania Hydrogen Peroxide And Potassium Persulfate. *Chem. Eng. J*. 167, 172-182.

Salman, J.M., Hameed, B.H., 2010. Adsorption Of 2,4-Dichlorophenoxyacetic Acid And Carbofuran Pesticides Onto Granular Activated Carbon. *Desalination* 256, 129-135.

Sanchez, R.M.T., Genet, M.J., Gaigneaux, E.M., Afonso, M.D., Yunes, S., 2011. Benzimidazole Adsorption On The External And Interlayer Surfaces Of Raw And Treated Montmorillonite. *Appl. Clay Sci.* 53, 366-373.

Santos, L.H.M.L., Araújo, A.N., Fachini, A., Pena, A., Delerue-Matos, C., Montenegro, M.C.B.S., 2010. Ecotoxicological Aspects Related To The Presence Of Pharmaceuticals In The Aquatic Environment. *J. Hazard. Mater*. 175, 45-95.

Senturk, H.B., Ozdes, D., Gundogdu, A., Duran, C., Soylak, M., 2009. Removal Of Phenol From Aqueous Solutions By Adsorption Onto Organomodified Tirebolu Bentonite: Equilibrium, Kinetic And Thermodynamic Study. *J. Hazard. Mater*. 172, 353-362.

Serrano, D., Suarez, S., Lema, J.M., Omil, F., 2013. Use Of Activated Carbon For The Removal Of Pharmaceutical And Personal Care Micropollutants In Biological Reactors. *Afinidad* 70, 175-182.

Shen, X.Y., Lu, Y.Y., Zhu, L.Z., Lu, S.Y., 2004. Sorption Of BTEX Mixtures To Organobenonites. *J. Environ. Sci.* 16, 222-225.

Sheng, G.Y., Johnston, C.T., Teppen, B.J., Boyd, S.A., 2002. Adsorption Of Dinitrophenol Herbicides From Water By Montmorillonites. *Clay Clay Min.* 50, 25-34.

Si, J., Cui, B.K., Dai, Y.C., 2013. Decolorization Of Chemically Different Dyes By White-Rot Fungi In Submerged Cultures. *Ann. Microbiol.* 63, 1099-1108.

Sipma, J., Osuna, B., Collado, N., Monclus, H., Ferrero, G., Comas, J., Rodriguez-Roda, I., 2010. Comparison Of Removal Of Pharmaceuticals In MBR And Activated Sludge Systems. *Desalination* 250, 653-659.

Skakkebaeck, N.E., Leffers, H., Rajpert-De Meyts, E., Carlsen, E., Grigor, K.M., 2000. Should We Watch What We Eat And Drink? Report On The International Workshop On Hormones And Endocrine Disrupters In Food And Water: Possible Impact On Human

Health, Copenhagen, Denmark, 27-30 May 2000. *Trends Endocrinol. Metab.* 11, 291-293.

Snyder, S.A., Adham, S., Redding, A.M., Cannon, F.S., Decarolis, J., Oppenheimer, J., Wert, E.C., Yoon, Y., 2007. Role Of Membranes And Activated Carbon In The Removal Of Endocrine Disruptors And Pharmaceuticals. *Desalination* 202, 156-181.

Srivastava, H.P., Arthanareeswaran, G., Anantharaman, N., Starov, V.M., 2011. Performance Of Modified Poly(Vinylidene Fluoride) Membrane For Textile Wastewater Ultrafiltration. *Desalination* 282, 87-94.

Streat, M., Patrick, J.W., Perez, M.J.C., 1995. Sorption Of Phenol And Para-Chlorophenol From Water Using Conventional And Novel Activated Carbons. *Water Res.* 29, 467-472.

Susarla, S., Medina, V.F., Mccutcheon, S.C., 2002. Phytoremediation: An Ecological Solution To Organic Chemical Contamination. *Ecol. Eng*. 18, 647-658.

Tahar, A., Choubert, J.M., Coquery, M., 2013. Xenobiotics Removal By Adsorption In The Context Of Tertiary Treatment: A Mini Review. *Environ Sci Pollut Res* 20, 5085-5095.

Tauxe-Wuersch, A., De Alencastro, L.F., Grandjean, D., Tarradellas, J., 2005. Occurrence Of Several Acidic Drugs In Sewage Treatment Plants In Switzerland And Risk Assessment. *Water Res.* 39, 1761-1772.

Tijani, J.O., Fatoba, O.O., Petrik, L., 2013. A Review Of Pharmaceuticals And Endocrine-Disrupting Compounds: Sources, Effects, Removal, And Detections. *Water Air Soil Pollut* 224, 1-29.

Tizaoui, C., Grima, N., 2011. Kinetics Of The Ozone Oxidation Of Reactive Orange 16 Azo-Dye In Aqueous Solution. *Chem. Eng. J.* 173, 463-473.

Tolls, J., 2001. Sorption Of Veterinary Pharmaceuticals In Soils: A Review. Environ. *Sci. Technol.* 35, 3397-3406.

Tyler, C.R., Jobling, S., Sumpter, J.P., 1998. Endocrine Disruption In Wildlife: A Critical Review Of The Evidence. *Crit. Rev. Toxicol.* 28, 319-361.

Ugurlu, M., 2009. Adsorption Of A Textile Dye Onto Activated Sepiolite. *Microporous Mesoporous Mat.* 119, 276-283.

UNEP, 1998. Status Report On UNEP's And Other Related Activities On Persistent Organic Pollutants (Pops). *United Nations Environment Programme*, Nairobi, Kenya.30-1-2014).

UNEP, 2013. Persistent Organic Pollutants. United Nations Environment Programme. *Http://Www.Chem.Unep.Ch/Pops/*, Last Accessed: 30-1-2014).

Upson, R.T., Burns, S.E., 2006. Sorption Of Nitroaromatic Compounds To Synthesized Organoclays. *J. Colloid Interface Sci.* 297, 70-76.

USEPA, 2004. *Phytoremediation Field Studies Database For Chlorinated Solvents, Pesticides, Explosives, And Metals. Office Of Superfund Remediation And Technology Innovation*, Washington, DC, USA.30-1-2014).

Usharani, K., Muthukumar, M., 2013. Optimization Of Aqueous Methylparathion Biodegradation By Fusarium Sp In Batch Scale Process Using Response Surface Methodology. *Int. J. Environ. Sci. Technol.* 10, 591-606.

Verlicchi, P., Al Aukidy, M., Zambello, E., 2012. Occurrence Of Pharmaceutical Compounds In Urban Wastewater: Removal, Mass Load And Environmental Risk After A Secondary Treatment-A Review. *Sci. Total Environ.* 429, 123-155.

Wang, C.P., Ding, Y.J., Teppen, B.J., Boyd, S.A., Song, C.Y., Li, H., 2009. Role Of Interlayer Hydration In Lincomycin Sorption By Smectite Clays. *Environ. Sci. Technol.* 43, 6171-6176.

Wang, J.L., Xu, L.J., 2011. Advanced Oxidation Processes For Wastewater Treatment: Formation Of Hydroxyl Radical And Application. *Crit. Rev. Environ. Sci. Technol.* 42, 251-325.

Wu, R.S.S., 1999. Eutrophication, Water Borne Pathogens And Xenobiotic Compounds: Environmental Risks And Challenges. *Mar. Pollut. Bull.* 39, 11-22.

Yoon, Y., Westerhoff, P., Snyder, S.A., Wert, E.C., 2006. Nanofiltration And Ultrafiltration Of Endocrine Disrupting Compounds, Pharmaceuticals And Personal Care Products. *J. Membr. Sci.* 270, 88-100.

Zadaka, D., Nir, S., Radian, A., Mishael, Y.G., 2009. Atrazine Removal From Water By Polycation-Clay Composites: Effect Of Dissolved Organic Matter And Comparison To Activated Carbon. *Water Res*. 43, 677-683.

Zaroual, Z., Azzi, M., Saib, N., Chainet, E., 2006. Contribution To The Study Of Electrocoagulation Mechanism In Basic Textile Effluent. *J. Hazard. Mater.* 131, 73-78.

Zhang, S.Y., Zhang, Q.A., Darisaw, S., Ehie, O., Wang, G.D., 2007. Simultaneous Quantification Of Polycyclic Aromatic Hydrocarbons (Pahs), Polychlorinated Biphenyls (Pcbs), And Pharmaceuticals And Personal Care Products (Ppcps) In Mississippi River Water, In New Orleans, Louisiana, USA. *Chemosphere* 66, 1057-1069.

Zhang, W.H., Ding, Y.J., Boyd, S.A., Teppen, B.J., Li, H., 2010. Sorption And Desorption Of Carbamazepine From Water By Smectite Clays. *Chemosphere* 81, 954-960.

Zhou, Q., Frost, R.L., He, H., Xi, Y., Zbik, M., 2007. TEM, XRD, And Thermal Stability Of Adsorbed Paranitrophenol On DDOAB Organoclay. *J. Colloid Interface Sci.* 311, 24-37.

Zhu, H.T., Li, W.N., 2013. Bisphenol A Removal From Synthetic Municipal Wastewater By A Bioreactor Coupled With Either A Forward Osmotic Membrane Or A Microfiltration Membrane Unit. *Front. Env. Sci. Eng.* 7, 294-300.

Zhu, L.F., Zhu, R.L., 2011. Simultaneous Adsorption Of Malachite Green And Hydrophobic Organic Compounds Onto Bentonite. Fresenius Environ. *Bull.* 20, 521-527.

Zhu, L., Ma, J., 2008. Simultaneous Removal Of Acid Dye And Cationic Surfactant From Water By Bentonite In One-Step Process. *Chem. Eng. J*. 139, 503-509.

Zodrow, J.J., 1999. Recent Applications Of Phytoremediation Technologies. *Remediat. J*. 9, 29-36.

Zollinger, H., 2003. *Chemistry. Synthesis, Properties And Applications Of Organic Dyes And Pigments.* Wiley-VCH, Weinheim, Germany.

In: Clays and Clay Minerals
Editor: Liam R. Wesley
ISBN: 978-1-63117-779-8

Chapter 5

USING SOLID WASTES AS RAW MATERIALS IN CLAY BRICKS

***Lázaro V. Cremades*[*,1], *Joan A. Cusidó*[2], *Cecilia Soriano*[3] *and Martí Devant*[2]**

[1] Departament de Projectes d'Enginyeria, Universitat Politècnica de Catalunya, Barcelona, Spain

[2] Departament de Física i Enginyeria Nuclear, Universitat Politècnica de Catalunya, Barcelona, Spain

[3] International Center for Numerical Methods in Engineering (CIMNE), Barcelona, Spain

ABSTRACT

The large quantities of sewage sludge that are currently generated require new alternatives for its recycling and final destination, beyond already known methods in the agriculture and cement industry. The use of this sludge as raw material for the production of structural ceramics, such as clay bricks, may become an interesting alternative, both from an industrial and environmental point of view.

This chapter is focused on the use of solid wastes, such as for example sewage sludge or forest residues, to serve as additive raw materials for the production of clay bricks. It is based on our experience with the Ecobrick® material and our subsequent research on producing some raw materials from WWTP sludge suitable for the ceramic industry. The chapter shows some formulations of raw materials in ceramic mixtures, their physical properties and to analyze their environmental characteristics. The final purpose is to illustrate the possibility of designing tailor-made ceramics that fulfill custom-physical properties, which are appropriate for particular construction use.

* corresponding author: Departament de Projectes d'Enginyeria, Universitat Politècnica de Catalunya, Avda. Diagonal, 647, 08028 Barcelona (Spain)

1. INTRODUCTION

During the past 20 years, the production of sludge from WWTPs has grown exponentially, creating the necessity of finding environmentally acceptable destinations for this type of waste. It can be used in agriculture as a fertilizer or for soil remediation (Kruse and Barrett, 1985), used in the cement industry (Tay et al., 2000), used as a comburent material (Lee and Bae, 2009) and, to a lesser extent, used as a raw material for manufacturing clay bricks (Alleman and Berman, 1984; Weng et al., 2003; Liew et al., 2004a; Kaosol, 2010; Montero et al., 2009). These alternatives are at the higher level of the pollution-prevention hierarchy, from prevention and reduction (the most preferable option), to recycling and reuse, treatment, and disposal (the least preferable option). In this sense, the transformation of these wastes into usable materials is a societal challenge to which significant scientific and technological efforts should be devoted.

The incorporation of waste into ceramic matrices has been studied extensively over the past twenty years (Berman, 1982; Anderson, 2002). The large amount of sludge produced in waste water treatment plants (WWTPs) and the high demand of structural ceramics for construction suggest that the confluence of both productions may be a good solution for the final waste destination. This new use can be a successful alternative, or at least a complement, to other more common destinations for sludge, such as the agriculture and cement industry. Underlying this issue is the fact that sewage sludge cannot be disposed of in a controlled landfill due to the high organic matter content (Council Directive, 1999).

Since the early work of Alleman and Berman (1984) and Tay (1987), there has been a considerable amount of literature on the production of clay bricks using binary mixtures (Wiesbusch et al., 1999; Weng et al. 2003; Jordan et.al., 2005, Liew et al., 2004a; Liew et al., 2004b; Monteiro et al., 2008) and ternary mixtures (Montero et al., 2009; Chiang et al., 2009).

In most of these studies, the sludge used for the production of clay bricks was originated in WWTPs. In some cases, however, dehydrated sewage sludge or incinerated sewage sludge ash were used (Lin and Weng, 2001). Other studies used industrial wastewater sludge from the paper industry (Demir et al., 2005), the galvanic industry (Magalhaes et al., 2004) or the olive oil industry (Monteiro and Vieira, 2005). More recently, pelletized dehydrated WWTP sludge were used to produce bricks (Qi et al., 2010).

Finally, as an alternative to the production of structural ceramics from sludge waste, some efforts were directed toward its use in the manufacturing of concrete blocks (Kaosol, 2010).

As for ternary mixtures, several possibilities that may be added to the clay and WWTP sludge include the following: rice husks, agricultural wastes, forest weeding wastes, chips and sawdust from old furniture, by-products of the marble and stone industry and grogs (chamottes) from the ceramic industry.

Considering all of the above facts, the main advantages of ternary mixtures of clay, sewage sludge and forest waste can be summarized in the following points:

i Adding forest waste to sludge provides higher granulometry to the mixture. Crushed forest residues are impregnated with the sludge, which alone is a flocculated paste, and the mixture adopts the grain size of the forest waste.

ii The extrusion limit of the ceramic green body is highly dependent on the composition of the mixture. The use of ternary mixtures allows a high content of sewage sludge of the extrudable mix. For example, a formulation with 0% forest waste allowed the addition of a maximum of 6% sludge; a ternary mixture with 10% forest allowed the addition of 10% sludge.

iii If the mixture of sewage sludge with forest waste is carried out in WWTP facilities, which is strongly encouraged, it becomes easy to handle and helps to reduce and almost eliminate leaching during storage and transport. The emission of odors is also minimized.

iv Sewage sludge and forest wastes from old furniture or vegetable waste with harmful compounds are simultaneously leading to valorized products.

v The higher heating value (HHV) of the ternary mixture implies an important energy saving, improving the ceramic process from an energetic point of view.

In view of the facts and the advantages described above, the objective of this chapter is to show some formulations of raw materials in ceramic mixtures, their physical properties and to analyze their environmental characteristics. The final purpose is to illustrate the possibility of designing tailor-made ceramics that fulfill custom-physical properties, which are appropriate for particular construction use.

This chapter is based on our experience with the Ecobrick® material dated since 1995, and our subsequent research on producing raw materials from WWTP sludge suitable for the ceramic industry (Cusidó et al., 2003; Cusidó and Soriano, 2011; Devant et al., 2011; Cusidó and Cremades, 2012a,b). First, the Ecobrick® material is presented: composition, technical properties, and environmental issues, i.e., leachability of the product and gaseous emissions associated. Second, an alternative to produce raw material from WWTP sludge is proposed, which process is based on spray drying. The resulting product is a fine powder with interesting properties for some ceramic applications. Finally, the production of pellets from WWTP sludge is presented to be used in lightweight clay ceramics.

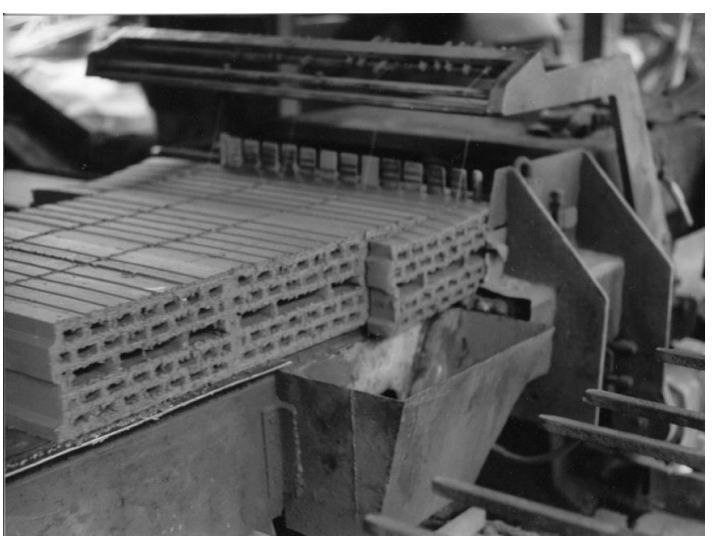

Figure 1. Picture of some bricks made of Ecobrick® material.

1. BUILDING CERAMICS FROM WWTP SLUDGE

The Ecobrick® is a trademark for a ceramic material (Figure 1) consisting of a ternary mixture: clay, WWTP sludge and forest waste. This material is interesting from the technical, economical and environmental points of view, whose characteristics are described below.

2.1. Selection of Raw Materials

Three sludges were obtained from the biological treatment of three WWTPs: Gavà (SG), Martorell (SM) and Tarragona (ST). All of them are medium-size cities with a strong industrial base, located at a short distance from Barcelona, Spain. The forest wastes were sawdust for domestic uses (FW1) and sawdust from shredding of old furniture (FW2). Clay was supplied from two quarries at El Papiol (CP1, CP2) and one at Alcoletge (CA), both in Catalonia.

The moisture content of the clays varied between 3% and 9%. The moisture of the forest wastes varied between 7% and 10%. The water content of the sewage sludge varied between 72% and 85%. Due to the large variation of the water contents, the formulations were retained to the dried mater (d.m.).

The granulometry analysis of the clays revealed a Gaussian distribution, which made them suitable for the ceramization process. The approximate composition was 33% sand, 41% silt and 26% clay minerals. The mineralogical analysis (Philips X-ray diffractometer PW 1710) is shown in Table 1.

Table 1. Qualitative mineral analysis of clays used in this work obtained by X-ray diffractometry (* indicates minor presence of the compound and ** indicates major presence)**

Mineral group	Mineral	Clay		
		CP1	CP2	CA1
Quartz	Quartz	****	****	****
Carbonates	Calcite	**	**	**
	Dolomite	*	*	*
Feldspars	Feldspars	*	*	*
Mineral group	Mineral	Clay		
		CP1	CP2	CA1
Clays	Muscovite	**	**	**
	Chlorite	**	**	**
	Montmorillonite	**	**	-
Hematite	Hematite	*	*	-
Goethite	Goethite	-	-	*

The selection of the sludge for the tests was based on their capacity for the retention of heavy metals during incineration. Heavy metal content and arsenic and selenium concentration were analyzed after calcination at 450 °C (Table 2). The experimental analysis was done by total extraction of the samples with acid, as described in EN 12457-1 (2002). The three types of sludge used in this work arrived to the laboratory with high water content. The standard analytical method to measure the concentration of heavy metals and other

elements required both the elimination of water and organic matter from the samples. For this reason they had to be calcinated at 450 °C. This fact explains the low concentrations of volatile metals (Hg, As, Cd) found in the calcinated samples, in comparison with the concentration of the rest of the elements in Table 2.

Mineral content of the sludge calcinated at 450 °C (Table 3, Figure 2) was similar to that of the clays CP1, CP2 and CA (Table 1). Pure illite minerals start melting at 1050 °C, but the presence of chlorite decreases the melting point to 900 °C, whereas the presence of carbonates (calcite) increases it (Brownell, 1976). These values are important to consider when choosing the appropriate sintering temperature.

Table 2. Concentration of heavy metals (plus As and Se) in the sludge. (d.m) dried material; (c.m) material calcined

Element	Sludge		
	SG	SM	ST
Hg (ppm)	2.3±0.1	3±2	3.0±0.3
As (ppm)	11±2	6.9±0.2	7±1
Se(ppm)	<3.2	<4.2	<3.2
Zn (ppm)	1200±10	975±5	1100±100
Pb (ppm)	290±25	62.5±0.6	103±6
Ni (ppm)	260±20	30.0±0.2	30±1
Cu (ppm)	8005±40	1084±4	285±25
Cr (ppm)	420±10	46.9±0.1	87±6
Mn (ppm)	130±10	145±2	199±3
Cad (ppm)	2.5±0.2	4.7±0.1	2.8±0.1
Total (% d.m.)	0.31	0.24	0.18
Total (% c.m.)	0.74	0.56	0.55

Table 3. Qualitative mineral analysis obtained by X-ray diffractometry of the sludge after calcination at 450 °C

Mineral	Sludge		
	SG	SM	ST
Quartz	***	***	***
Calcite	****	****	****
Dolomite	***	*	***
Albite	*	**	-
Microcline	*	*	***
Muscovite	*	*	*
Chlorite	*	*	-
Montmorillonite	-	*	*
Sepiolite	-	-	*
Baryte	*	-	-
Anhydrite	-	*	-

The sludge finally chosen to prepare the samples was that of Tarragona (ST). Because this particular sludge did not contain chlorite, its capability for adsorption of heavy metal ions was low, especially for Pb and Cr ions. Among the clays, CP1, with the lowest concentration of chlorite, was chosen because chlorite increases the amount of the vitreous phase at low temperatures. Regarding the forest waste, the choice was the sawdust produced from

shredding of old furniture (FW2) due to its higher pollution as compared to wood sawdust (FW1). Therefore, all the selections were in agreement with the worst case scenario hypothesis.

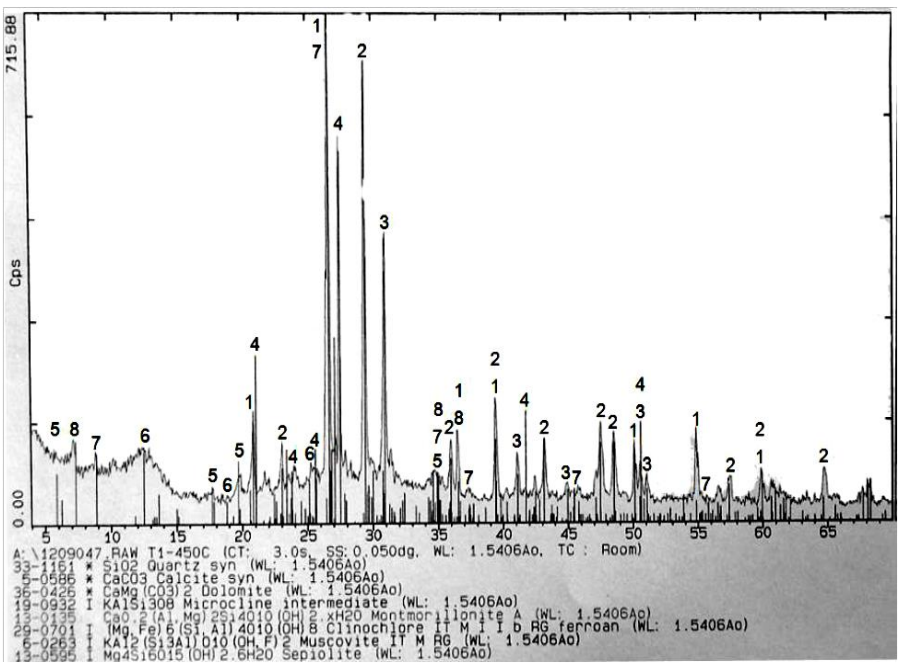

Figure 2. X-ray diffractogram of sludge ST incinerated at 450 °C. Numbers identify main compounds found: 1-Quartz, 2-Calcite, 3-Dolomite, 4-Microcline, 5-Montmorillonite, 6-Clinochlore, 7-Muscovite and 8-Sepiolite.

2.2. Sample Preparation and Sintering

A number of 30 ceramic pieces were made from a mixture of 10 kg. By comparison, industrial tests would require the use of a minimum of 10,000 kg of material to prepare 30 samples.

A set of 31 mixtures were prepared according to Table 4. The clay content in the mixtures was between 79% and 83%. Clay contents below 79% were not considered because the resulting material had insufficient mechanical strength.

The mixtures were extruded and cut into test pieces 5 to 12 cm long for the compression tests. Cylindrical pieces of 5 cm diameter and 1.5 cm height were used for thermal conductivity tests. Other ceramic properties, such as retraction, water absorption, density, and porosity were studied with rectangular pieces of 12 cm.

The pieces were fired in a propane oven (Formagas, model HG-150) at a heating rate of 160 °C h^{-1}, from room temperature to 980 °C. They were maintained at this maximum temperature for 3 h, after which they were removed from the oven and cooled down during 12 h to reach room temperature. The temperature curve was chosen similar to that for industrial structural ceramic materials, such as clay bricks.

Table 4. Ternary mixtures samples prepared (under the worst case scenario) to produce the ternary pseudo diagram, and their corresponding values of green body moisture (h, %), extrusion pressure (p, expressed in bars), porosity (por, %), mechanical strength (σ, kp cm^{-2}) and thermal conductivity (λ, W m^{-1} °C^{-1})

Sample	Composition (fraction of unity)			h	p	por	σ	λ
	c (clay)	x (sludge)	fw (forest waste)	(moisture,%)	(ext. pres., bar	(porosity, %)	(kp cm^{-2})	(W m^{-1} °C^{-1})
1	1	0	0	14.0±0.1	16±0.5			
2	1	0	0	14.8±0.2	8.5±0.5		419±45	
3	1	0	0	15.0±0.5	20.5±0.5		391±85	
4	1	0	0	16.4±0.2	10±0.5	32±3	420±45	0.69±0.01
5	1	0	0	18.0±0.4	6.5±0.5			
6	0.79	0.08	0.13	29.3±0.1	9.5±0.5	64±1	77±14	0.29
7	0.79	0.09	0.12	29.5±0.1	9±0.5	61±2	81±11	0.26
8	0.79	0.10	0.11	24±2	13.5±0.5	59±1	64±8	
9	0.79	0.10	0.11	28.4±0.1	11.5±0.5	62±1	76±9	0.30
10	0.79	0.10	0.11	29.6±0.1	9.5±0.5	62±1	90±10	
11	0.79	0.11	0.10	29.9±0.1	9±0.5	59±1	88±16	0.30
12	0.79	0.12	0.09	30±0.3	7±0.5		80±22	
13	0.79	0.14	0.07	33.2±0.1	5±0.5		99±5	
14	0.79	0.21	0	28.1±0.2	11±0.5	56±1	88±8	0.19
15	0.833	0	0.167	25.3±0.3	9±0.5	58±2	122±12	0.36±0.01
16	0.833	0	0.167	23.9±0.2	11±0.5			
17	0.831	0.033	0.136	30.8±0.1	3.5±0.5	61±2	90±7	0.26±0.03
18	0.83	0.043	0.127	21.6±0.1	11±0.5			
19	0.83	0.043	0.127	28.4±0.1	6±0.5	58±2	118±19	0.30±0.01
20	0.829	0.054	0.117	24.2±0.2	10±0.5			
21	0.829	0.054	0.117	28.9±0.1	4.5±0.5	58±1	131±24	0.30±0.01
22	0.828	0.065	0.107	25.8±0.2	7.5±0.5			
23	0.828	0.065	0.107	26.1±0.5	12±0.5	58±2	146±21	032±0.02
24	0.827	0.076	0.097	26.2±0.2	9.5±0.5			
25	0.827	0.076	0.097	26.3±0.3	8.5±0.5	56±2	122±12	0.28±0.02
26	0.818	0.182	0	27±5	0±0.5			
27	0.818	0.182	0	29.6±0.2	5±0.5		105±32	0.36±0.01
28	0.80	0.15	0.05	28.5±0.1	7.5±0.5			
29	0.75	0.126	0.124	34.4±0.1	4.5±0.5		64±12	
30	0.718	0.18	0.102	39.9±0.2	0±0.5		51±9	
31	0.677	0.238	0.085	46±0.1	0±0.5		50±3	

After sintering, and in agreement with Jordán et al. (2005), the mineral phases were gehlenite, anorthite, wollastonite, diopside and spinel. The composition was very similar to that identified in a standard clay brick (Brownell, 1976).

The thermal decomposition of sewage sludge and solid wastes, in general, is the main problem regarding its use as a raw material in the production of bricks (Lee and Bae, 2009). The presence of sewage sludge and forest waste leads to emission gases during firing (Cusidó et al., 2003). These gaseous emissions cause the high porosity of the ceramics (Figure 3). Increasing sintering temperatures increased the pore diameter of the material (Chiang et al., 2009).

The microscopic porosity in the final product was similar to that of 100% clay bricks. The porosity due to the decomposition of the organic material and volatile compound was about 3% of the total porosity of the product.

The inorganic compounds of the sludge were incorporated in the amorphous or vitreous phase of the product.

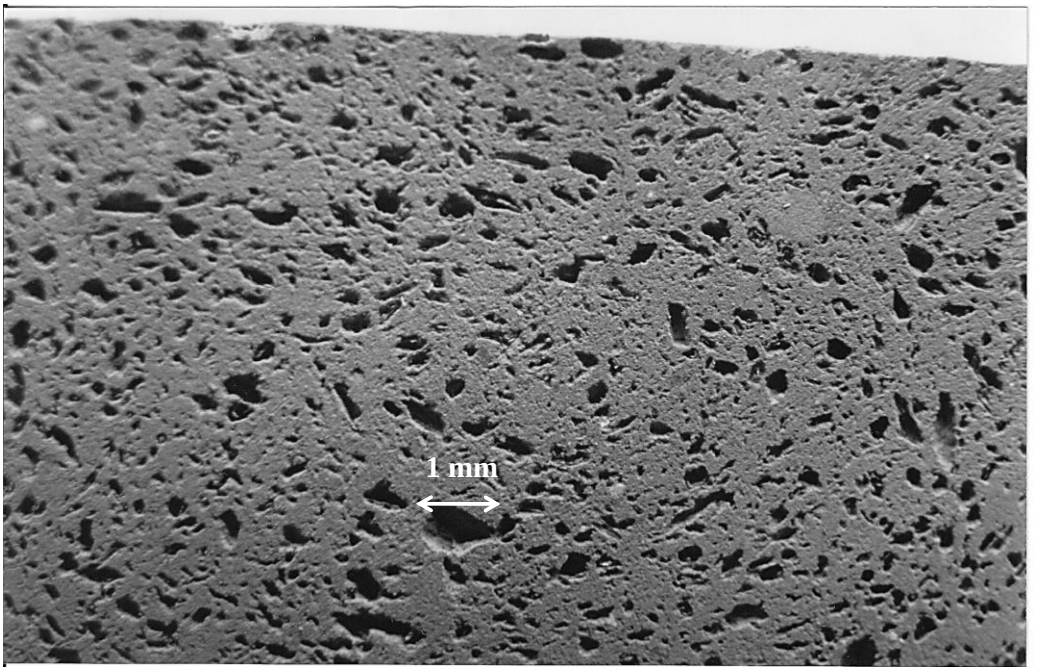

Figure 3. Optical microscopy photograph at 10× showing the microstructure of a ceramic piece of ternary mixture (sample #25, 83% clay, 7% sludge, 10% forest waste). Sintering temperature was 980 °C. The open porosity can reach diameters on the order of 1 mm. The presence of the pores provided lightness and improved the thermal and acoustic insulation properties of the material.

2.3. Characterization and Environmental Analysis of the Ceramic Pieces

2.3.1. Physical Properties

The moisture content of the ceramic pieces was measured using the method of constant mass at 105 °C (APHA, 1992). The extrusion pressure was measured with an analogical manometer. The mechanical resistance was measured with an Instron LC8800 system according to norm UNE-67-026-94. The porosity was calculated using the expression (Harlbut and Klein, 1992):

$$por = 100\ (1- \rho_r /\rho_a) \quad (1)$$

where ρ_r is the density measured by pycnometry and ρ_a is the bulk density, measured as the mass-to-volume ratio of the parallelepiped pieces where the total volume includes particle volume, interparticle void volume and internal pore volume.

The thermal conductivity of the pieces was measured using a Holometrix ED 200 LT-A guarded heat-flow meter. A thermal flow was applied at a constant rate through a cylindrical sample, and thermocouples were placed at both sides of the sample for measurements.

Table 5. Extraction scheme according to NEN 7345

Extraction	Extraction time (days ± 10%)
1st	0.25
2nd	1
3rd	2.25
4th	4
5th	9
6th	16
7th	36
8th	64

Table 6. Leaching tests NEN 7345 of sample #28 (80% clay, 15% sludge and 5% forest waste). Concentrations and standard deviation of 3 parallel samples expressed in mg m^{-2} except for (1) (in µg m^{-2}) or (2) (in g m^{-2}). (n.d.) under the detection limit of the instrument

Elem.	Leaching extraction (leaching concentration expressed in mg m^{-2}, except in (1) and (2))								Cumula-tive leaching	Limit (NEN-7345)
	1st	2nd	3rd	4th	5th	6th	7th	8th		
As	n.d.	n.d.	n.d.	n.d.	n.d.	n.d.	n.d.	n.d.	n.d.	40
Ba	n.d.	n.d.	n.d.	n.d.	0.74±0.1	0.54±0.5	n.d.	1.2±0.1	2.5±0.6	600
Cd	n.d.	n.d.	n.d.	n.d.	n.d.	n.d.	n.d.	n.d.	n.d.	1
Co	n.d.	n.d.	n.d.	n.d.	n.d.	n.d.	n.d.	n.d.	n.d.	25
Cr	1.6±0.3	2.5±0.4	4.2±0.4	n.d.	n.d.	n.d.	n.d.	1.8±0.6	10±1	150
Mo	n.d.	n.d.	n.d.	n.d.	n.d.	n.d.	n.d.	n.d.	n.d.	15
Ni	n.d.	n.d.	n.d.	n.d.	n.d.	n.d.	n.d.	n.d.	n.d.	50
Pb	n.d.	n.d.	n.d.	n.d.	n.d.	n.d.	n.d.	n.d.	n.d.	100
Sb(1)	30±1(1)	23±0.1(1)	10±10(1)	21±2(1)	50±10(1)	46±5(1)	100±30(1)	320+90(1)	3500(1)	3500(1)
Se	n.d.	n.d.	n.d.	n.d.	n.d.	n.d.	n.d.	n.d.	n.d.	1.5
Sn	n.d.	n.d.	n.d.	n.d.	n.d.	n.d.	n.d.	n.d.	n.d.	25
V	15±3	11±1	5±1	12±1	9±5	8±5	7±1	11±3	79±3	250
Zn	n.d.	n.d.	n.d.	n.d.	n.d.	n.d.	n.d.	n.d.	n.d.	200
Br^-	n.d.	n.d.	n.d.	n.d.	n.d.	n.d.	n.d.	n.d.	n.d.	25
Cr	n.d.	n.d.	n.d.	n.d.	n.d.	n.d.	n.d.	n.d.	n.d.	20000
F	n.d.	n.d.	n.d.	n.d.	n.d.	n.d.	30±30	65±60	95±92	1500
SO_4^{2-} (2)	3.8±0.l(2)	2.9±0.1(2)	3.4±0.2(2)	3.4±0.4(2)	3.1±0.7(2)	1.3±0.8(2)	1.7±0.1(2)	0.02±0.01(2)	20±l(2)	25(2)

2.3.2. Leaching Tests

The leaching tests were performed according to norm NEN 7345 of the Netherlands Tank Leaching Test (NEN 7345, 1993), a regulation specifically dedicated to building materials and widely used in the EU. The EU standard EN 12457-2 – Characterization of Waste Leaching Compliance Test for Leaching of Granular Waste Materials and Sludges – (EN 12457-1, 2002) was not applicable in this case because it is designated to characterize sludge per-se.

Leaching tests were performed with 8 cm long samples and consisted of the introduction of a sample into acidic water, followed by a measure of concentration of inorganic components during different time intervals.

For each sample, eight extractions were performed. The sample was left in the solution for a certain number of days, depending on the number of extraction (Table 5). Extractions were done without stirring the solution, and the extractant agent was replaced after every extraction.

Leaching tests were conducted on samples corresponding to different compositions of the ternary mixtures, including sample blanks (Table 6, for sample #28). Refractory metals (such as Va, Cr) do not react with aluminum-silicates and therefore were not incorporated into their vitreous matrix (Kingery et al., 1976). Instead, they remain encapsulated (Eddings et al., 1994), and its weak fixation on the material makes them easy to leach. Other heavy metals are first volatilized from the surface during cooking, and later they start to react with aluminum silicates, becoming incorporated into the vitreous matrix making leaching more difficult.

The tests revealed leaching concentration far below the limit defined in NEN 7345 for a material to be classified for building uses. In most of the cases, the concentrations were below the detection level of the technique used. Detectable concentration levels were only found for V, Cr, Sb, Ba and F. The presence of these elements in the leachate was directly related to the properties of CP2, the main component of the ternary mixture. Adding sludge into the mixture did not vary the concentration of these elements in the leachate.

2.3.3. Leaching/Extraction Test Related to Building Materials

Development of leaching studies have issued a high scientific controversy about which should be the right methodology, specially as far as methods of chemical extraction of leachates are concerned. In this sense, there is a wide international literature and research (Wiebusch et al., 1998).

In the present study, we have followed the norm NEN 7345 from the Netherlands Tank Leaching Test (NEN 7345, 1993). This norm is expressely dedicated to building materials and largely applied in Netherlands and EU, in general.

To carry out the tests, three samples of 8 cm long were prepared to which volume, surface area and mass were measured, in each case. The samples were put into distilled water and the concentration of inorganic compounds was measured at several time intervals. Procedure was as follows.

Preparation of samples

Each piece was introduced into a polyethylene container and covered with distilled water at pH fitted to 4 by adding nitric acid which was used as extractant agent, according to NEN 7345. In total, there were 12 sample recipients, three of them containing a blank (100% clay

ceramic piece). Volume of extractant agent in each recipient should had to be 5 times the volume of the sample, and the sample had to be covered by a layer of not less than 5 cm high.

For each sample, 8 extractions were done. The sample was left a given number of days, such as indicated in Table 7, without agitation. The extractant agent was changed every further sampling.

Table 7. Time of eight extractions in the leaching test following the norm NEN 7345

Extraction no.	Cumulative time (days)
1	0.25
2	1
3	2.25
4	4
5	9
6	16
7	36
8	64

Leachate obtained from each extraction was filtered through a 0.45 mm filter, its pH was corrected with nitric acid, and chemical elements were analyzed following their appropriate technique:

- Heavy metals at pH = 2.
- Fluor at pH = 5-6.
- Cianures and ions: without pH correction.

Measurement and calculation

Elements measured and techniques used were those described in Table 8.

Equation (2) was used to compute leachability of each pollutant at the i-th extraction:

$$E_i = \frac{(C_i - C_o)\,V}{1000\,A} \tag{2}$$

where:

E_i: Leachability of a pollutant at the i-th extraction (mg m^{-2})

C_i: Pollutant concentration at the i-th extraction (mg L^{-1})

C_o: Pollutant concentration in the blank (mg L^{-1})

V: Volume of extractant agent (L)

A: Surface area of the sample (m^2)

After 8 extractions, Equation (3) was used to compute the leachability, E, for each pollutant in the sample:

$$E = \sum_{i=1}^{8} E_i \tag{3}$$

Table 8. Experimental techniques used in the leaching test (NEN 7345)

Compounds	Technique used
Cyanides	Absorption spectrophotometry, after distillation to calculate total cyanides
Heavy metals	Atomic emission spectrometry by inductively coupled plasma
Fluor	Selective electrode
Ions	Ion chromatography

Evaluation

According to the norm NEN 7345, building materials are classified in relation with the leachability test in two categories: a) materials without any environmental restriction (<U1), and b) materials having a restricted use (<U2). Materials whose total leachability is comprised between U1 and U2 values do not have any environmental restriction as far as their use in building, but the pollutant that exceeds the U1 threshold should be removed at the end of the product life (dismantling). Finally, materials whose leachability thresholds are above U2 should have a restricted use in building and dismantling.

2.3.4. Outgassing and Offgassing Tests for Toxicity Evaluation

Outgassing and offgassing tests aim to determine the gases and particles emitted by the material tested in general (ESA PSS-01-729, 1991; ESA PSS-01-702, 1994). They are accelerated tests to cover a simulated time equivalent of 10 years to prove the absence of potential health risks, in our case applied to users of houses built with materials made from sewage sludge and/or other wastes. These tests are used to allow the presence of such materials in manned spacecrafts. We have chosen them as the most rigorous testing for our samples.

The following tests were performed:

- Outgassing test ESA PSS-01-702 (1994). It allows to ascertain the outgassing properties of materials obtaining data about percentage of weight loss of material (WLM) as well as volatile condensed matter (VCM). It is performed by creating an overpressure in the interior of a camera specially equipped for this purpose.
- Offgassing test ESA PSS-01-729 (1991). It determines the amount of carbon monoxide (CO) and total organic compounds (TOC) emitted by the material, if their presence is detectable (concentrations above 10 mg g^{-1} of material tested).

Both tests have been approved by the European Space Agency (ESA) and are equivalent to those used by NASA.

To carry out these tests we used samples of 5 cm in length for different percentages of sludge in the ceramic matrix (in triplicate). The experimental methodology according to the norms was as follows:

a) ESA PSS-01-702.

Samples were cut using a minimum size of 2x2 cm^2, according to the capacity of sample holders. Their geometry was approximately cubic. The minimum weight of each sample had to be 5 g. Samples were inserted within a special chamber with two collector plates. The extraction was done by subjecting the sample to a vacuum of 10^{-3} Pa, and keeping a temperature of 125 ºC for 24 hours. Gases that emerge from the sample were deposited by condensing them on a chrome-plated aluminum collector plate constantly maintained at 25 °C.

After 24 hours, the system was vented with dry nitrogen or inert gas to a pressure between 104 and 208 Pa. As the system cooled to 50 ºC, pressure continued to decrease to reach the ambient air pressure.

Once removed the specimens, they were allowed to dry for 30 minutes and collector plates for 1 hour. After this process, both were kept in a closet or temperature-and- humidity-controlled room (20 ºC and 65%) for 24 hours.

The plates, after this process, were analyzed by infrared spectroscopy to get the concentrations of contaminants condensed.

b) ESA PSS-01-729.

Samples were prepared by cutting them into pieces of 1.25 ± 0.2 cm thick and an apparent total area of 50 ± 5 cm^2 per liter of the working chamber.

First, the chamber was purged with dry hydrogen or helium, at 80 ºC and vacuum of less than 1.3 Pa for 24 hours. Then, the samples were introduced into that sealed chamber by keeping the following working conditions: 50 ºC, 1 atm and air with 25% oxygen. These conditions were maintained for 72 hours. Finally, the chamber was connected to the sampling equipment.

After, the chamber was allowed to cool to room temperature and samples were taken from air to be subsequently analyzed.

2.3.5. Gas Sampling and Firing Conditions

Gases produced during the firing step were sampled and analyzed following the U.S. EPA Reference Methods (EPA, 1994). Gas samples were taken from the oven stack. Stack diameter is 300 mm. Sampling hole was located at 6.9 diameters from the lower disturbance and 3.1 diameters from the upper disturbance. Draught is natural with manual control at the oven exit to allow additional inlet of air.

Sampling instruments used were the following ones:

- Isokinetic probe of 1.5 m long (Lear-Siegler pm-100).
- Gas sampling train with liquid absorbents and pumps of adjustable flow (MCV).
- Continuous monitor of CO (Neotronic CO-101, 0-4000 ppm).
- Continuous monitor of O_2 (Unigas, 0-21%).
- Continuous monitor of CO_2 (Unigas, 0-21%).
- Opacimeter (Brigon).

- Datalogger (Digitron, model LZ) equipped with temperature interface TKSFH and K-type temperature probe.
- Digital manometer (Digitron, model P-100, 0-1000 bar).
- Analytical balance (Mettler AE166).
- pH meter (Crison Microph 2002).
- Chloride ion selective electrode.
- Reference electrode (Orion 92-02).
- Spectrophotometer (UV/vis Beckman, model DBG).
- Plasma induction spectrophotometer (Jobin-Yvon, model JY38-VHR).

VOCs were retained in tubes packed with suitable adsorbents. Sample flow was fixed to 40 ml min^{-1}. Each sample was formed by a sequence of 3 steel tubes (6.1 mm OD, 90 mm length, Perkin-Elmer) connected by Teflon tubing and packed with Carbotrap C, Carbotrap B and Carbosieve III, respectively. These tubes were preconditioned following the manufacturer's specifications: 250 ºC (30 min), 300 ºC (30 min), 325 ºC (30 min) and 350 ºC (30 min) and then stored in 40-ml glass vials with Teflon-lined screw-top caps. After sampling, sorbent tubes were kept at 4 ºC in the same containers and processed within 48 h.

Temperature ranges, sampling times and sample volumes are shown in Table 9. Three samples were obtained during the production of Ecobrick® (15% dry sludge, 80% clay and 5% forest wastes) one for each temperature range, and three more for a conventional ceramics (100% clay) that will be called "clay-brick". Emission conditions are summarized in Tables 2a and 2b for the Ecobrick® and clay-brick firing, respectively.

Table 9. Sampling scheme

Ceramics	Sample code	Sample tube codes	Temperature (°C)	Time (min)	Volume (L)
Ecobrick®	A	A1, A2, A3	80-250	83	3.3
	B	B1, B2, B3	250-600	141	5.6
	C	C1, C2, C3	600-940	118	4.7
Clay-brick	D	D1, D2, D3	80-250	90	3.6
	E	E1, E2, E3	250-600	180	7.2
	F	F1, F2, F3	600-940	155	6.2

2.3.6. Analytical Method

All samples were analyzed using automated thermal desorption coupled to gas chromatography with mass selective detection.

Desorption and analysis of sample tubes were carried out using a thermal desorber (Perkin-Elmer ATD 400) connected via a transfer line (200 ºC) to a gas chromatograph (Hewlett-Packard 5890) equipped with a mass selective detector (Hewlett-Packard 5970). Trapped compounds were desorbed at 290 ºC for 10 minutes at a carrier gas (He) pressure of 11.5 psi approximately, with inlet and outlet splits of the thermal desorber set at 0 and 5 ml min^{-1}, respectively. The cold trap (glass tube loaded with 20 mg Carbotrap C) was initially held at –30 ºC and heated afterwards to 290 ºC for 3 min. Separation of compounds was achieved using a capilar column (J&W Scientific, DB-624) and He as the carrier gas at approximately 0.5 ml min-1 .

The initial oven temperature of 40 ºC was maintained for 1 minute, then increased to 65ºC at 20 ºC min^{-1} and maintained for 5 minutes, increased again to 115 ºC at 4 ºC min^{-1} and finally raised to 250 ºC at 30ºC min^{-1} (for 12 additional minutes). Detector temperature was set at 290 ºC.

For the quantitative analysis, the method of external standard was adopted. The standard solution was injected in a tube that was analyzed by following identical conditions to those for the sample tubes. The standard solution was prepared with organochlorine compounds (dichloromethane, trichloromethane and trichloroethane), aromatic compounds (benzene, toluene, ethylbenzene, and m-xylene), a sulphur compound (dimethylsulfide) and a nitrogen compound (pyridine). Each compound in the samples was quantified as a function of the response factor of the most similar compound present in the standard solution.

Condensate compounds were analysed by purging with He from 5 ml of the absorbent solution and trapping VOC in a set of 3 tubes packed with the same adsorbent material as above. Then, these compounds were thermally desorbed and introduced into a gas chromatograph/mass spectrometer (Fisons MD-800, EI 250), following the same procedure as above.

2.3.7. Results and Discussion About Gaseous Emissions

There is no Spanish regulation concerning individual VOCs. Therefore the internationally accepted TLV-TWA (Threshold Limit Values - Time Weighted Average) (ACGIH, 1995) emission values will be adopted for comparison purposes. This value for a VOC corresponds to its time average concentration to which a person can be repeteadly exposed (8 h per day) during 5 days without noticing adverse effects. Other relevant values are the Odour Detection (OD) and the Odour Recognition (OR) thresholds which represents the VOC concentration above which odour is detected and recognized, respectively, by half of population (Verschueren, 1977).

There are no specific regulations for ceramic emissions, so all the Spanish regulations that could be applied to Ecobrick® production are presented in Table 10. In a laboratory bench furnace the emission values for the substances referred in Table 10 have been measured and compared with those corresponding to the strictest regulations.

Table 10. Spanish regulations for VOC emissions

Activity	Regulation	VOC (mg Nm^{-3}) [a]
Ceramic	Royal Decree 833/1975	---
Wastewater sludge incineration	Royal Decree 833/1975	---
Diverse activities	Royal Decree 833/1975	---
Incineration of urban solid wastes [b,c]	Royal Decree 1088/1992	20
Incineration of special wastes [c]	Order 323/1994	20

[a] Normal cubic meter (Nm^3) refers to normal conditions: T = 0 ºC and p = 760 torr.
[b] Values refer to 3 t h^{-1} of incineration (a medium ceramic factory produces about 5 t h^{-1}).
[c] Values refer to normal conditions, 11% of O_2 and dry gas.

Table 11. VOCs emitted during the firing process[a]

Family	VOC	Formula	Ecobrick® firing emissions ($\mu g\ m^{-3}$)	Clay-brick firing emissions ($\mu g\ m^{-3}$)	TLV-TWA ($\mu g\ m^{-3}$)	OD [b] ($\mu g\ m^{-3}$)	OR [c] ($\mu g\ m^{-3}$)
	trichlorofluorome-thane	CCl_3F	0.0	571.9	5620		
Chlorinated	chloromethane	CH_3Cl	536.5	0.0		20462	20462
hydrocarbons	dichloromethane	CH_2Cl_2	1846.7	0.0	174000	550008	790637
	trichloromethane	$CHCl_3$	179.5	940.5			
Mercaptans	methylmercaptan	CH_3SH	16.0	0.0	980	1.1	2.0
	carbon disulfide	CS_2	728.8	142.7	31000	1306.3	1306.3
Sulfides	dimethyl disulfide	$S_2(CH_3)_2$	68.4	0.0		7.7	
	dimethyl trisulfide	$S_3(CH_3)_2$	0.0	0.0		5.2	
Thiocianates	methyl thiocyanate	CH_3SCN	169.9	0.0			
Aliphatic	propanone	C_3H_6O	1142.4	0.0		147160	308561
ketones	3-methyl-3-buten-2-one	C_5H_8O	151.8	0.0			
	2-methyl propanal	C_4H_8O	233.0	0.0			
Aliphatic	2-methyl propenal	C_4H_6O	303.5	0.0			
aldehydes	3-methyl butanal	$C_5H_{10}O$	305.6	0.0			
	hexanal	$C_6H_{12}O$	104.7	0.0			
	heptanal	$C_7H_{14}O$	183.8	0.0			
Aromatic	furfural	$C_5H_4O_2$	255.4	0.0	7900	2498.6	2498.6
aldehydes	benzoaldehyde	C_7H_6O	594.2	0.0			
	hydroxybenzal-dehyde	$C_7H_6O_2$	5.3	0.0			
Aliphatic nitriles	acetonitrile	C_2H_3N	1688.5	0.0	67000		
	benzonitrile	C_7H_5N	318.5	0.0			
Aliphatic	acetic	$C_2H_4O_2$	2533.8	0.0	25000	181.7	
acids	2-methylpropanoic	$C_4H_8O_2$	32.1	0.0			
Aliphatic esters	methyl acetate	C_3H_6O	238.3	0.0	606000	427238	
	pyrazine	$C_4H_4N_2$	160.3	0.0			
Aromatic	pyridine	C_5H_5N	454.2	0.0	16000	2133.7	2392.4
amines	4-methylpyrazine	$C_5H_6N_2$	226.6	0.0			
	4-methylpiridine	C_6H_7N	56.6	0.0			
Alifatic	acetamide	C_2H_5NO	237.2	0.0			
amides	3-methylbutanamide	$C_5H_{11}NO$	0.0	0.0			
Monoterpenes	α-pinene	$C_{10}H_{16}$	11.8	24.5		64	
	n-nonane	C_9H_{20}	160.3	0.0	1050000		
	n-decane	$C_{10}H_{22}$	536.5	37.3			
Linear	n-undecane	$C_{11}H_{24}$	0.0	37.3			
aliphatic	n-dodecane	$C_{12}H_{26}$	89.8	0.0			
hydrocarbons	n-tridecane	$C_{13}H_{28}$	361.2	0.0			
	n-tetradecane	$C_{14}H_{30}$	0.0	0.0			
	n-pentadecane	$C_{15}H_{32}$	0.0	0.0			
	n-hexadecane	$C_{16}H_{34}$	245.8	0.0			
	2,2-dimethylpentane	C_7H_{16}	5686.4	10693.3			
Branched	nonanes	C_9H_{20}	0.0	0.0			
aliphatic	decanes	$C_{10}H_{22}$	0.0	0.0			
hydrocarbons	undecanes	$C_{11}H_{24}$	0.0	0.0			
Polycyclic hydrocarbons	decahydronaphthalene	$C_{12}H_{18}$	0.0	0.0			
	methyl-decahydronaphthalene	$C_{13}H_{20}$	0.0	0.0			
	benzene	C_6H_6	961.8	92.7	32000	194712	
Monocyclic	toluene	C_7H_8	582.4	182.1	188000	6023.9	41414
aromatic	ethylbenzene	C_8H_{10}	56.6	0.0	434000	2602.7	2602.7
hydrocarbons	m+p –xylene	C_8H_{10}	190.2	22.4	434000	86757.2	
	styrene	C_8H_{10}	166.7	0.0	434000	85120.3	

[a] Units are referred to standard conditions: T = 25 ºC and p = 760 torr.

[b] Odour Detection Threshold.

[c] Odour Recognition Threshold.

Table 11 shows the VOC emissions measured during the firing of test Ecobrick® and clay-brick pieces. Concentrations shown are normalized to standard conditions. As expected, VOC emissions from the Ecobrick® material are in general higher than those from conventional ceramics. However, no VOC exceeds the threshold limit values with time weighted average (TLV-TWA). Only a few compounds (methyl mercaptane, dimethyl disulfide, acetic acid) have concentrations that exceed their OD. In the case of the clay-brick firing, no VOC concentration higher than its OD or OR has been detected, and obviously the values obtained are due to the propane gas used during furnace process. Some differences can be observed related to those obtained by direct sewage sludge burned at one fluidized-bed incinerator, especially in more complex compounds as benzene, toluene, ethylbenzene, acrylonitrile and acetonitrile (Tirey et al., 1991).

As to the inorganic compound emissions, Table 12 shows the mean values of emission concentration obtained for the major compounds during the firing of both ceramics. For comparison purposes, their maximum limit values allowed by the most severe present legislation in Catalonia (solid waste incineration) are also indicated (DOGC, 1994).

Table 12. Mean emission levels of selected major inorganic compounds during the firing process and maximum limits allowed in special wastes incinerators in Catalonia[a]

Pollutant	Units	Ecobrick®	Clay brick	Limit allowed [b]
Particles	mg Nm^{-3}	48.3	11.4	20
SO_2	mg Nm^{-3}	43	8.4	200
CO	mg Nm^{-3}	83	26	125
NO_x	mg Nm^{-3} NO_2	811	805	616
HCl	mg Nm^{-3}	112	0.7	60
HF	mg Nm^{-3}	1.2	1.6	4
Cd+Tl	mg Nm^{-3}	0.007	n.d.[c]	0.1
Sb+As+Pb+Cr+Co+ +Cu+Mn+Ni+V+Sn	mg Nm^{-3}	0.44	0.02	1

[a] Units are referred to normal conditions: T = 0 ºC, p = 760 torr, 11% O_2 and dry gas.

[b] Decree 323/1994 of the Generalitat de Catalunya that regulates the facilities for waste incineration and determines their atmospheric emission limits. Values correspond to the strictest limits, i.e., those applicable to special waste incinerators (DOGC, 1994).

[c] "not detected".

Inorganic emissions from the Ecobrick® material are again higher than those from the clay-brick firing, except for the hydrogen fluoride (HF), which is therefore more due to the clay than to the wastes introduced in the Ecobrick®.

Only three pollutants exceed the maximum levels (Table 12):

- NO_x: similar and close to the maximum level values were found for both ceramics. It is well known that NO_x emissions are extremely sensible to the flame temperature and to the atmosphere in the oven (Patrick, 1994; Niessen, 1995). These variables were controlled by hand in the laboratory. However, since NO_x emissions can be better controlled in an industrial oven, it is expected to find their values lower than the maximum limit allowed.

- Suspended particles: their concentration depends on the oven type (recirculations, internal streams, etc.), in such a way that it is difficult to extrapolate it for testing on a different scale. In any case, the concentration of suspended particles during the Ecobrick® firing is four times higher than that for conventional ceramics and exceeds more than 50% the legal limit.
- HCl: its concentration in the emissions of the Ecobrick® material is twice the maximum limit. Its value is directly proportional to the percentage of sludge in Ecobrick®. This problem also arises in the direct incineration of sludges (Wherther and Ogada, 1999). This is mainly due to the use of chlorinated products as a correcting factor in the waste water treatment plants, but this practice is expected to be gradually reduced in the future.

Although the emission of heavy metals is below the maximum limit allowed of 1 mg Nm^{-3}, its value is 20 times greater than the one for firing conventional clay ceramics. In the firing of pure ceramics, the most worrying pollutants are lead and fluorine, whereas Hg is negligible (Timellini et al., 1993). So, if Hg was appearing in gaseous emissions from the Ecobrick® process, it should be as a direct relation to its presence in the sludges. In the chemical analyses carried out to the sludges as raw material, Hg was not detected (Cusidó et al., 1996), therefore it should not be found in the exhaust gases.

The analysis of the particulate material in exhaust gases, especially dioxines and furanes, is left for future works. The possible effects of chemical recombination between the propane gas of the oven and the gases emitted during the firing process have not either been studied. However, results between the combustion with and without sludges using the same firing conditions have been compared, so that the possible role of propane gas to produce (or remove) VOCs is counterbalanced.

In conclusion, some environmental problems appear in relation to the gaseous emissions, although they can be corrected by means of technologies of gas purification, post-combustion and/or by improving the treatment of urban waste water which would allow the obtaining of sludge with a lower chlorinated compounds content. Finally, this research is to be continued with measurements at industrial scale, as some differences may arise on scale-up the emission values obtained in this work.

3. ATOMIZED SLUDGES VIA SPRAY-DRYING

The idea of applying the technology of spray-drying to sludges is not unknown. Sludge drying in general (flocculation, electro-osmotic dewatering and then thermal drying, etc.), and spray-drying of sludges in particular, are issues still under investigation, as evidenced by several works (Amos, 1998; Novak, 2006; Arlabosse and Chitu, 2007; Woo et al., 2007).

We propose a new process based on spray drying raw sludges (90-95% water) coming from the classical primary treatment in WWTP. As previous preliminary step, these raw sludges have to be filtered through wire mesh to separate particles that could obstruct the inlet hole of the spray-dryer wheel. In contrast with the classical treatment of raw sludge, there is no need for sludge floculation. But, gases exiting the spray dryer —basically steam, with

traces of volatile organic compounds (VOC) and some particles of sludges (see afterwards)—have to be cleaned before they are released.

The main equipment of this process is the spray dryer. Some experiments have been carried out at laboratory scale by using the spray dryer NIRO Mobile Minor. Relevant data about the raw sludges tested in this work are listed in Table 13. The laboratory-scale procedure followed is described next.

Table 13. Main characteristics of raw sludges from WWTP (physico-chemical treatments) used in this study

Origin	WWTP from Sabadell (Spain)
Color	Black
Odor	Yes
Lower heating value	14,080 kJ kg^{-1}
COD (dry basis)	219,866 mg O_2 kg^{-1}
BOD5 (dry basis)	38,104 mg O_2 kg^{-1}
pH	8.3
Moisture	94%
Clay content (dry basis)	6.5%
Inorganic matter (dry basis)	25.3%

3.1. Preparation of Slurry

WWTP raw sludge tested contained 94% water. The solid part consisted of inorganic and organic particles, and molecules in colloidal suspension. For the formation of raw sludge, coagulants such as trivalent iron salts and polyelectrolytes flocculants were added. First, the slurry must have a basic pH (≈ 8) and, if necessary, its rheology must be corrected by adding some deflocculants (sodium polyphosphate), which had not been necessary in this work, in order to reach a viscosity of around 300-400 cP. Finally, the slurry was sieved through a 1.25 mm mesh. Heating the slurry slightly improves the performance of the operation.

3.2. Spray Drying

The spray-drying process involves the removal of the liquid phase of a slurry on one continuous operation to get the solid phase as dry as possible. The slurry tested contained 94% of liquid phase. The spray drier worked under the following conditions: hot air inlet temperature: 350 ºC; centrifugation speed: 30,000 rpm; inlet flow of slurry: 68 cm^3 min^{-1}; inlet temperature of slurry: 90 ºC; outlet temperature of dry sludge: 120 ºC.

Inlet and outlet temperatures were chosen especially low given the high content of organic matter that could be decomposed and produce dangerous atmospheres inside the spray drier. A scheme of the estimated spray-drying process is shown in Figure 4, related to the formation of atomized particles.

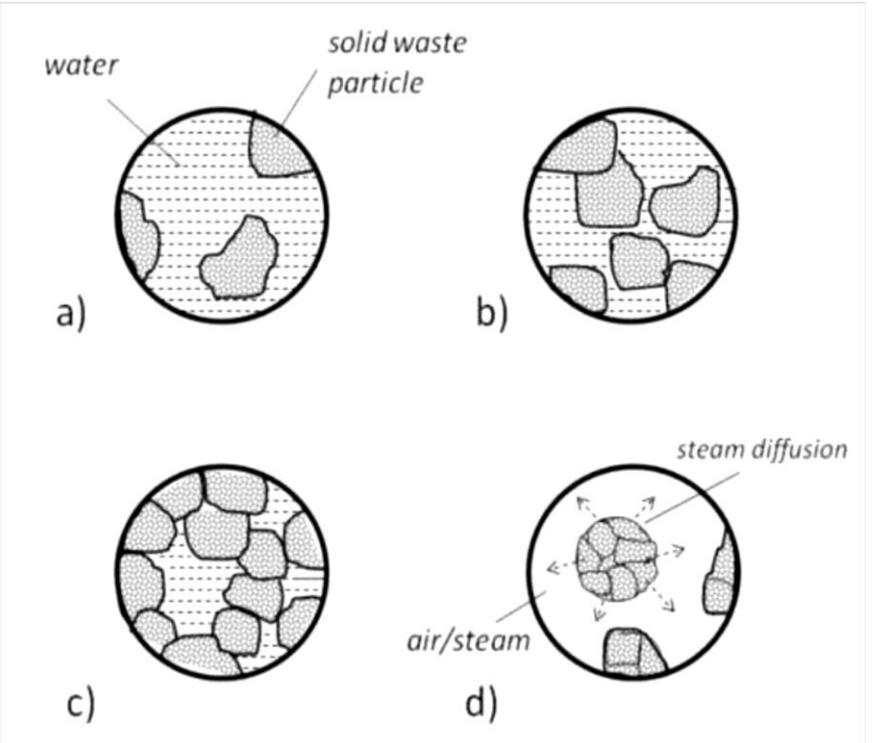

Figure 4. Schematic view of different drying stages of raw sludge for the proposed treatment: a) raw sludge with 80% water content; b) raw sludge after centrifugation, >50% water; c) aggregates of particles with interstitial water after spray-drying; d) final dried spherical atomized sludge, <5% water.

3.3. Resulting Product

The product has low density (270 kg m^{-3}). Size analysis was done by using a conventional mechanical sizer Filtra 76-13. Sizes of detected particles ranged from 100 to 400 μm (Figure 5). A summary of the main characteristics of the product is presented in Table 14. Volatile suspended solids (VSS) emitted during the spray-drying process are estimated as 11.6%, which is equal to the difference between organic matter content in raw sludge (74.7%) and in atomized sludge (62.9%).

Although it is noted that the sprayed sludge does not smell, it should be mentioned that, because of its granulometry, atmospheres formed from the product in contact with moisture from the pituitary can result in a pungent odor of hydrogen sulfide. The final product is stabilized and seems to be pathogen-free because no change in color, texture, moisture, and/or leachates with time has been observed in 6-year-old samples.

Finally, its chemical composition corresponds to the presence of aluminium, calcium, and phosphorus, as well as non-halogenated solvents. X-ray diffraction (Figure 6) indicates the presence of mineral species such as α-quartz, calcite and dolomite mostly, although more than 60% is organic matter (amorphous phase), is similar in composition to the conventional secondary wet sludge.

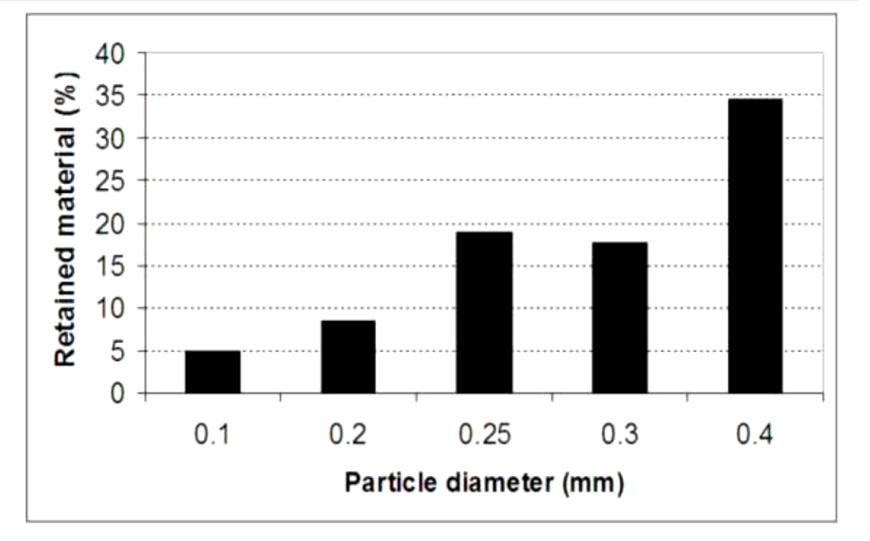

Figure 5. Size analysis of the atomized sludges obtained. In case of full scale, the diameter of particles is slightly larger.

Table 14. Main characteristics of spray-dried sludge from WWTP (physico-chemical treatments) obtained

Origin	WWTP from Sabadell (Spain)
Color	Dark grey (concrete)
Odor	No
Density	270 kg m^{-3}
Weight loss at 500 ºC	62.9 %
Moisture	5.0 %

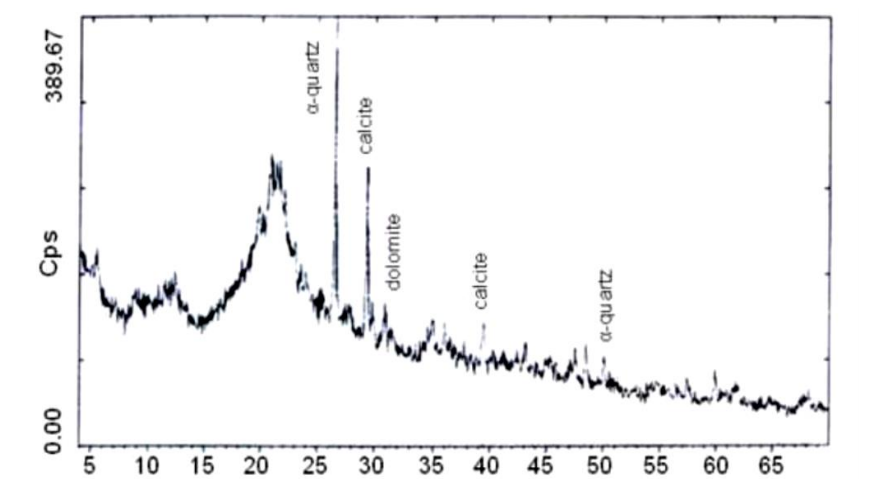

Figure 6. X-ray diffractometry of the atomized sludges. An organic amorphous phase and inorganic α-quartz, calcite and dolomite are detected as majority components.

3.4. An Alternative Plant Proposed

Once the feasibility of spraying WWTP raw sludge has been verified experimentally, the possibility of building a plant capable of full-scale operation is proposed. This plant would operate as follows:

- Step 1: Primary treatment based on conventional screening, sand removal, and degreasing. Its aim is to equalize the sludge prior to a phase of sedimentation.
- Step 2: High-speed centrifugation of raw sludges. Clarified water is sent to a tertiary treatment for reuse. The resulting sludge would be sieved and prepared as sprayable slurry.
- Step 3: Spray-drying of sludges. Vapors would be biofiltered to eliminate odors and to condense them for further tertiary treatment and reuse. The solid fraction from the atomizer and cyclone would be collected into appropriate hoppers to prevent dust from escaping into the atmosphere. Finest particles would be removed by an electrostatic filter at exhaust gases.
- Step 4: Adequate packaging of the solid fraction as a product for shipment or destination. It should take care of minimizing air handling in order to prevent fire/explosion hazard. The resulting water would be discharged into the river basin or reused once the residual pollutants are removed (if any, in a tertiary treatment plant).

A plant of this kind would not need any secondary treatment and would reduce by over 50% the area of land occupied. A scheme of the proposed sludge treatment plant is shown in Figure 7.

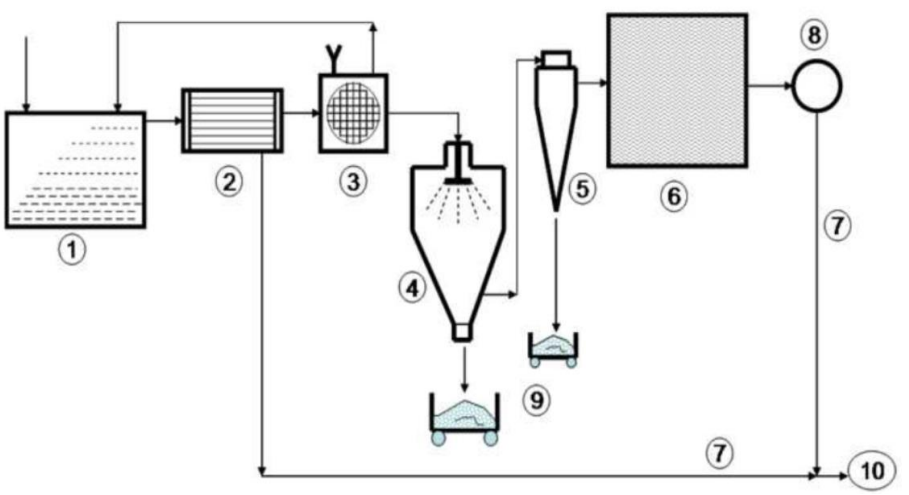

Figure 7. Schematic view of different steps for the proposed plant treatment based on spray drying sewage primary or colloidal sludges: 1) settler, 2) high velocity centrifugation, 3) sieve and additives, if any, 4) spray drier, 5) cyclone, 6) gas cleaning (biofilter), 7) clear water, 8) condenser, 9) dried sludge, and 10) tertiary treatment, if necessary.

3.5. Environmental Considerations

The procedure proposed for the spray-drying process would require an environmental analysis of both the spray drying operation, and the product obtained. In this section we analyze only the first one of these stages.

First, in relation to the reception of WWTP primary or colloidal sludges and their storage, environmental impact is negligible, since they consist of a liquid waste that can be easily transported through ducts and stored in ponds like those that are used in the treatment lines of conventional sludges. Also, the processes of sieving sludges do not require preventive measures beyond those in a conventional WWTP, being an automated process that does not require manipulation. Removal of such wastes gives off intense smells that are easily treatable through suitable ventilation systems and recommended use of masks and hermetic glasses.

The outlet stream from the spray drier goes into a cyclone system to recover the fraction of settled particles which otherwise could leave to the atmosphere with acceptable efficiency. Outlet gases include CO_2 and NH_3, mostly, but also some n-heptane, CH_4, and volatile fatty acids, as well as other trace gases.

Spray drying is done at low temperature (<120 ºC). Because of the relatively low temperature, organic compound gases that are evacuated along with hot air and water vapor through the chimney come off on a low odor level in the surroundings of the WWTP. Probably, a post-combustion of gases or a biofilter would totally remove the remains of VOC. In any case, although this stage is not considered as essential in the proposed process, it could be easily adopted given its low cost of implementation.

Concerning the storage and transportation of the final product, it is important to remark that this product is dry and dusty, with small granulometry (0.1 to 0.4 mm). Left to stand, it does not release any odor, but when breeze stirs up dust and it enters the nostrils, in contact with the pituitary (which is moist), an extremely unpleasant odor results. Therefore, hermetic systems of packing or closed tanks for its storage are required.

Concentrations of methane, hydrocarbons and other volatile organic compounds must be monitored and controlled through safety detectors throughout the entire treatment plant because a localized deflagration can spread to the rest of the plant. The internal atmosphere of the spray chamber should receive a special attention. In this work, in order to prevent this problem, tests were carried out, starting with a very dilute slurry and then increasing the concentration of the slurry up to the working concentration (82% moisture).

Other considerations relevant to human manipulation call for the use of masks as well as natural and/or forced controlled ventilation of storage hoppers. Oxygen concentration in the entire building should be controlled as proposed in the operational circular applied in the UK (HSEOC, 2005).

There are no specific regulations for emissions from spray-drying processes; however, gaseous and particulate matter emissions in general should not exceed their legal limit values, being below 50-75 mg Nm^{-3}, depending on the pollutant (Enrique et al., 2000). Otherwise, these levels are easy to achieve by cleaning organic vapors emitted from the cyclone outlet.

It should be noted that spray-drying allows the use of cogeneration systems which would reduce energy costs considerably. Besides, there is a saving in the cost of implementation of secondary treatment and its corresponding line for sludge treatment in a WWTP. Then, economical differences in the global cycle of each of the systems are reduced drastically, making the alternative system feasible. This alternative provides, moreover, the following

advantages: a) reduction of area occupied by the plant; b) integrated and simplified system; c) line of purified, sterile and better quality water; d) reduction of 60% or more of the final solid waste; e) more opportunities for adding value from solid waste, and f) reduced sanitary risks.

The resulting product can be a raw material for the manufacture of clay bricks in a percentage of 10-20%.

4. VALORISATION OF PELLETS FROM WWTP

The thermokinetic drying technique for dehydration (reducing water content from 60% to 5% moisture) was developed as a way to reduce the volume of the generated sewage sludge. The introduction of this sludge into rotary dryers results in the production of granulated agglomerates, called pellets, with a diameter of a few millimeters, for which specific methods of valorization should be found.

Because there have been few reports in the literature to date on the use and valorization of this material, the transformation of this sludge into a ceramic pelletized product similar to expanded clays, called Pellexpended®, was proposed in this study. The scheme of the production sequence for this new material is shown in Figure 8.

In brief, the WWTP sludge was thermokinetically dried in a rotary drying kiln at a low temperature to obtain pelletized dehydrated sludge during the valorization process.

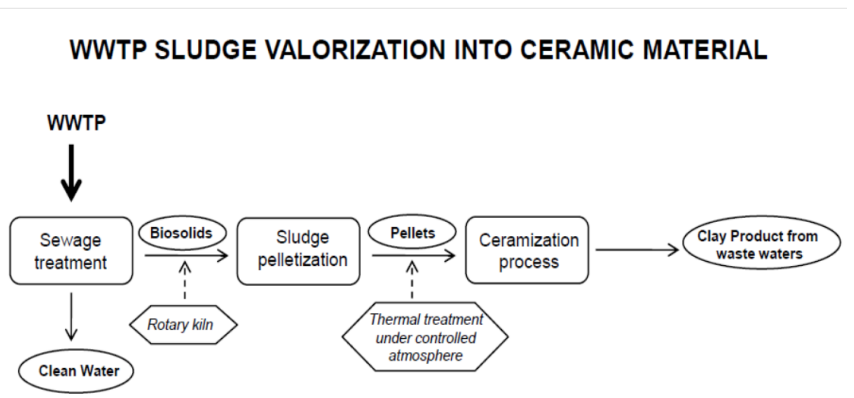

Figure 8. Valorization process of WWTP sewage sludge to obtain lightweight clay ceramics.

Next, it was introduced into a furnace for ceramization at controlled conditions up to 1050 °C, resulting in a perfectly ceramized granulate suitable for uses similar to those of expanded clays.

To validate this valorization process, the physical and environmental properties of the production process and the final product form of the proposed material were studied.

From the economic viewpoint, it should be noted that the current commercial price of expanded clays (around 60 € m^{-3}) makes the Pellexpended® a valuable market product that supports the economic viability of this proposal. Some ceramic applications of this material could be: expanded clays for lightweight frameworks, gardening, and technical fillers.

4.1. Literature Review

Qi et al. (2010) reported the production of a material similar to Pellexpended® that was obtained from a mixture of pelletized sludge and clay by a two-step process (drying followed by firing). Sintering took place in an electric oven, which suggests that important differences can be expected from the Pellexpended® in gaseous emissions and in the final product. Nevertheless, the existing differences between the product of the two methods (namely the Pellexpended® obtained from the pelletized sludge in this work and that obtained by Qi et al. where clay was added to the process) did not affect the organic burn-out temperature, which took place in our case around 550 °C, and was in agreement with the value of 564 °C reported by Qi et al. (2010).

Xu et al. (2008) described structural improvements (in terms of compressing strength) in the ceramic product obtained with Al_2O_3-enriched sludge before pelletization, and how the compressing strength decreased with increasing SiO_2 percentage. This is a logical result and could be applied to refine the final product in our case, if necessary.

In Chiou et al. (2006), sewage sludge was mixed with pelletized sludge to produce a ceramic product comparable to expanded clays. In their work, a more complex process, but unnecessary from our point of view, was used to obtain results similar to those described here.

Others have reported investigations on the development of lightweight ceramic aggregates from incinerated sludge ash (Tay et al., 2000; Cheeseman and Virdi, 2005; Bhatly, 1989). Although materials similar to this work were obtained, the energy costs in those cases were much higher because of the double thermal process (first to obtain the ash and later to put the ash through the ceramization process) and made the process less economically favorable than the Pellexpended® process.

In summary, comparable literature references listed above sufficiently demonstrate the interest and viability of the Pellexpended® process and product proposed in this chapter, suggesting that the construction of a pilot plant on a larger scale would be advisable to confirm the results found in the laboratory.

4.2. Raw Material and Experimental Methods

4.2.1. Sludge Pellets Analysis

Raw material (pelletized sludge) was supplied by the Barcelona-Besós WWTP. As received, it retained a low residual moisture (5-7 %) and was dark gray in color. It arrived in the form of spheres 1 to 4 mm in diameter with a fibrous texture and little compactivity. It emitted a strong unpleasant odor but much lower than that of the conventional sewage sludge. For conservation, it was kept permanently refrigerated at 4°C. Over time, it became slightly white on the surface due to the growth of fungi (as with conventional sludge).

The inorganic chemical composition of the pelletized sludge was studied with an inductively coupled plasma atomic emission spectrometer (Jobin-Yvon JY-38-VHR) and an atomic absorption spectrometer (Philips PU9200).

The mineral species present in the pelletized sludge were determined by X-ray diffractometry (X-ray diffractometer Philips PW 1710).

Results of these measurements and the remaining tests described in this section are shown and discussed afterwards.

4.2.2. Ceramization Process of the Sludge Pellets

For the production of the proposed ceramic material, 5 kg of pellets were placed inside a propane gas furnace (Formagas®, model HG). The maximum temperature was set to 1050 °C, the typical temperature employed in the manufacture of clay bricks. It was reached by following a heating curve with a controlled and constant slope over eight hours (Figure 9).

It should be noted that self-incineration of waste occurred starting at 450 °C, a process that must be carefully controlled for the transformation of the pellets into ceramic material. Between 450 °C and 550 °C, the interior of the furnace was maintained as a reducing atmosphere, which was accomplished by closing the exit vent of the oven almost completely and closing all air inlets aside from the inputs to the furnace flame.

Any internal flame from the combustion of the pellets must be extinguished as quickly as possible to maintain the reducing atmosphere; otherwise, the process will lead to the formation of a black core in the final ceramic product. The manual regulation of the input airflow during this part of the process was critical for a successful final product with optimum ceramization. The quality of the product thus depended on this procedure and could easily be evaluated by the color of the final pellets, which was red for the optimum final product or gray otherwise (Figure 10).

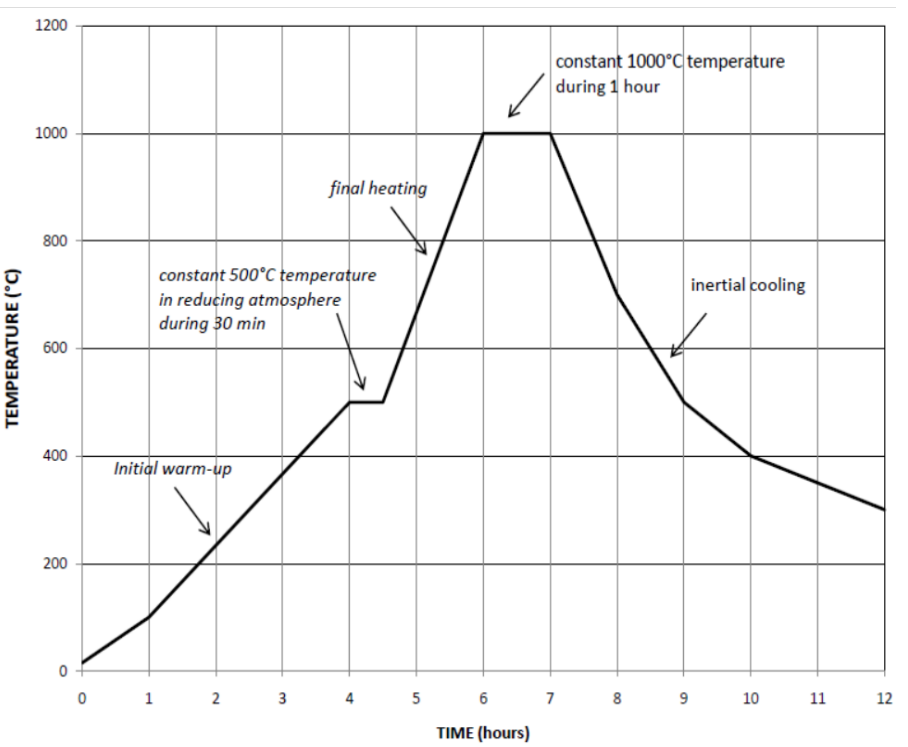

Figure 9. Thermal-treatment curve applied to the pelletized sludge for its ceramization.

Figure 10. Picture of the ceramized product Pellexpended®. At the top of the picture, there is a piece of light concrete produced with this material.

During the thermal process, the residual water content of the pellets (5%) was removed along with the residual organic matter content (65%). The lower heating value (LHV) was evaluated from Equation (4), where A is the concentration of inert matter in the dry residue (varying between 23% and 29%), C is the content of carbon (C = 55-62%), H is the contents of hydrogen (H = 7.9-8.7%), O is the content of oxygen (O = 26.5-29%) and N is the content of nitrogen (N = 3.5-6.8%):

$$LHV = [339.6\ C + 1193.9\ H - 177.4\ O + 94.2\ N]\ (100 - A)\ (kJ\ kg^{-1}) \quad (4)$$

Neglecting the residual moisture of the pellets and considering the variability in sludge composition, the LHV values obtained were in the range of 18,000 to 19,600 kJ kg^{-1} (Velo, 1998). This suggested that the pellets contributed significantly to the energy input necessary for the ceramization process, which significantly reduced the energy cost of sintering and therefore the total cost of the process. Regulating the atmosphere and the temperature curve inside the furnace were required to achieve this cost reduction.

The combustion process of the pelletized sludge was quite complex and took place in several stages. First, dehydration and devolatilization took place at the same time and occurred from the surface to the interior of the pellet. Next, steam and volatiles produced in the process flowed from the interior to the surface, passing through the hot surface layers and reacting with the char produced from devolatilization. Finally, volatiles and syngas burned around the pellet surface, increasing its surface temperature and improving ceramization. Examination of the inner furnace conditions revealed that the pellet surface could be affected by heat transfer from the burning of the volatiles released from the interior of the pellet (Cui et al., 2006).

The main differences between using pellets as a combustible material and the ceramization process can be summarized in the following two points:

- The temperature regime of the furnace was located near 1050 °C in the ceramization process (higher than the temperature of incineration, around 800 °C).
- The duration of the entire ceramization process and its associated thermal curve were always longer than 12 hours and continued long after the incinerable or volatile compounds of the pellets were consumed. In the case of simple incineration, the residence time of the pelletized sludge was on the order of minutes.

The advantage in this case was that the proposed process produced no incineration ash as a final waste but rather a valorized product having a composition similar to other ceramic materials (such as quartz, calcite, albite, phyllosilicates or feldspars). Therefore, no residual fluxes resulted from the production process (with the exception of gaseous emissions, as will be discussed afterwards).

It should be mentioned that a rotary kiln was not necessary in this study at the laboratory scale. However, it would be advisable to use one for industrial and largescale productions to achieve uniform ceramization and to avoid black-core ceramics or the agglomeration of pellets.

4.2.3. Ceramic Product Testing Methods

Physical characterization of the resulting product began with measuring the bulk density of the material as the mass-to-volume ratio (where the total volume included particle volume, interparticle void volume and internal pore volume). Next, the actual density of the product, excluding the gaps between the granules, was determined by immersing a certain mass of the product in water and measuring the volume of the displaced liquid.

Water absorption (over 24 h) was calculated from Equation (5):

$$\text{Water absorption} = \frac{\text{Mass of 1 h saturated wet pellets} - \text{mass of dry pellets}}{\text{Mass of dry pellets}} \quad (5)$$

Mechanical resistance was measured with an Instron LC8800 system when Pellexpended® was added to concrete. Granulometry measurements were performed using Filtra brand vibrating screens.

Finally, the thermal conductivity of the product was measured using a Holometrix ED 200 LT-A guarded heat-flow meter. In this method, a thermal flow was applied at a constant rate through a cylindrical sample approximately 5 cm in diameter and 1.5 cm thick, and thermocouples were placed at both sides of the sample for measurements.

4.2.4. Environmental Analysis

Leaching and toxicity tests

When a new material or product is obtained from hazardous wastes, it must undergo strict testing to ensure its safety for end users and to assess any possible health risks.

The first test performed in this study was a leaching test. The extraction method chosen was DIN 30 414 S4 according to the material type (DIN 38 414-S4, 1984). The liquid phase of the material was separated using a centrifuge (Heraeus Labofuge 200), the pH adjustment

was done with a pH meter (Crison Micro pH 2001) and agitation was conducted with a paddle agitator (Raypa AG-2).

For comparison purposes, leaching tests were conducted both for the pelletized sludge and for the ceramized product Pellexpended®. The concentrations of metals (copper, chromium, nickel, lead, selenium, thallium, tellurium, vanadium and zinc) and the pH of the leachate were determined for both materials.

After studying the leaching behavior of the material, its toxic potential during use was assessed. The aim was to determine the possibility that this material could release gases or particulate phases during its use that could present a health risk to end users. Two tests were carried out to reproduce, in an accelerated manner, what would happen to the material over a ten-year span. The standard norms used were ESA PSS-01-702 (1994) and ESA PSS-01-729 (1991) of the European Space Agency (in accordance with equivalent NASA regulations).

For the first test, the piece was introduced into a vacuum chamber at 10^{-3} Pa and a temperature of 125 °C, where it remained for 24 hours. After that time, weight loss mass (WLM) during degassing and volatile condensed matter (VCM) condensed on a chrome plate were measured. In the second test, carbon monoxide (CO) and total organic carbon (TOC) emissions were measured for a sample kept for three days in a chamber held at 1 atm and 50 °C.

Gaseous emissions tests

Of particular importance in the environmental analysis of a product is the study of gaseous emissions during the ceramization process, when most of the emissions are expected. The study of inorganic emissions was conducted following a sequence of measurements during the firing of ceramic pieces made with clays from El Papiol

(Barcelona). The emissions study of inorganic ceramic samples of pure clay allowed us to determine any increase in measurable emissions during the ceramization of the pelletized sludge.

The complete experimental procedure applied has been described in detail in Cusidó et al. (2003). For the determination of pollutants, it was necessary to determine the so-called emission parameters along the firing curve. Similarly, emission parameters were determined for the firing of the pellets to produce Pellexpended®.

Finally, the concentrations of volatile organic compounds (VOCs) in the samples were obtained by thermal desorption and were found by identifying the peaks in the chromatogram and the peak intensities while accounting for the contributions of each sampling tube.

4.3. Results and Discussion

4.3.1. Sludge Pellets Characterization

The inorganic chemical composition of the pelletized sludge is shown in Table 15. The high contents found for iron (10,200 mg kg^{-1}) and aluminum (34,800 mg kg^{-1}), both hydrophilic components, were due in part to the reagents added during wastewater processing. The presence of potassium, magnesium and calcium was likely caused by sediments and material dredged from the urban sewage system as the water circulated through. The pellets were characterized by a lipid-rich composition and were thus classified

as hydrophilic organics. Because organic substances were thermally destroyed during the treatment and did not participate in the ceramic process, they were of no interest in this study.

Table 15. Chemical composition of the pelletized sludge

Chemical species	Concentration (mg kg^{-1})
Fe	10200
Al	34800
Na	1690
Mg	4130
Ca	37900
K	1220
N (total organic)	14000
P (total)	25500
Halogenated solvents	0.5
Non-halogenated solvents	12.6
TOC (leached)	20600
Heavy metals	Concentration (ppm)
Hg	2.3
As	11.0
Se	<3.2
Zn	1210
Pb	292
Ni	261
Cu	811
Cr	413
Va	66.1
Mn	122
Cd	2.5

The mineral species present in the pelletized sludge consisted mainly of α-quartz (SiO_2), calcite ($CaCO_3$) and others (see detailed constituents in Table 16) with 25.3% dry matter.

Table 16. Qualitative mineral analysis of the pelletized sludge

Mineral group	Mineral	Chemical formula	Abundance (qualitative)
Quartz	Quartz	SiO_2	***
Carbonates	Calcite	$CaCO_3$	****
	Dolomite	$CaMg(CO_3)_2$	**
Feldspars	Albite	$NaAlSi_3O_8$	*
	Microcline	$KAlSi_3O_8$	*
Clays	Muscovite	$K(AlSi_3)O_{10}Al_2(OH,F)_2$	*
	Chlorite	$(Si,Al)_4O_{10}Al_2(Mg,Fe)_6(OH)_8$	**
	Sepiolite	$Mg_4Si_6O_{15}(OH)_2$-$6H_2O$	-
Salt	Halite	NaCl	*
Gypsum	Anhydrite	$CaSO_4$	-

* indicates minor presence of the compound and **** indicates major presence. Note the absence of sepiolite and anhydrite, compounds usually present in common clay ceramics.

The rest of the material consisted of organic compounds and residual or interstitial moisture. The inorganic fraction of the pellets consisted of materials similar to those found in the silty fractions of clays, and they were therefore deemed suitable for direct ceramization.

4.3.2. Ceramic Product Characterization

The resulting ceramic product was very similar to that obtained with expanded clays (i.e., Montmorillonite type), as can be seen in Figure 11. Table 17 presents a summary of the properties of the Pellexpended® material obtained from the different tests.

The bulk density of the material was found to be 583.2 kg m^{-3}, a value corresponding to a semi-light expanded aggregate material. Alternative technologies and operating parameters in the thermokinetic drying process should easily allow the producer to vary the density of the final pelletized product to density values typical of lightweight expanded aggregates (300 kg m^{-3}). The actual density of the product was 2050 kg m^{-3}, a typical value for structural ceramic materials.

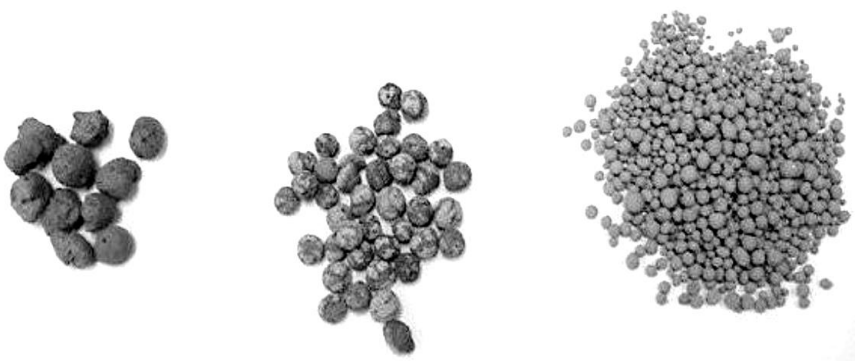

Figure 11. Comparison between two types of commercial expanded clays and the product obtained with Pellexpended® pelletized sludge.

Table 17. Main macroscopic properties of the Pellexpended® ceramized sludge pellets

Color	Red ceramic
Odor	No
Bulk density	583.2 kg m^{-3}
Actual density	2000 kg m^{-3}
Water absorption	62 % (d.m.)
Thermal conductivity	0.09 W m^{-1} K^{-1}
Resistance of the concrete-added material	40 kg dm^{-2}

The water absorption value was approximately 62%, much higher than that of structural ceramics, which are generally around 13%. A high water-absorption capacity is desirable in expanded clays.

As mentioned in the experimental methods section, mechanical resistance was measured when Pellexpended® was added to concrete because of the granulated nature of the material. Therefore, the final value of this property was highly dependent on the percentage of pellets added to concrete. For pellet fractions above 20%, mechanical resistance values were higher than 40 kp dm^{-2}.

The Pellexpended® granulometry results remained virtually identical to those of the pellets before heat treatment. It is believed that the spherical shape of the product was maintained due to the expansive force generated by gas emission during the combustion of organic matter. Most of the agglomerates found in the samples had diameters in the range of 1.25 to 3.15 mm, as seen in Figure 12.

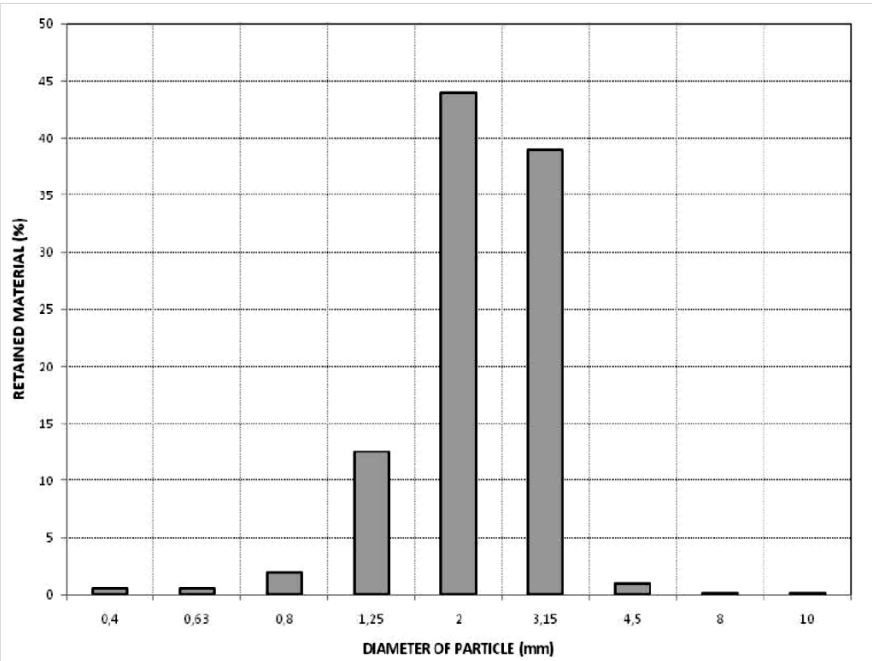

Figure 12. Granulometry of the ceramized sludge pellets.

The dimensions of the granulated material obtained depended on the original size of the precursor pellets. Grain size could be altered by modifying the operating parameters of the thermokinetic drying process (pelletization). Grain decomposition was avoided in this study because a larger grain size or higher moisture content would affect the ceramization process and in some cases result in grain decomposition (Lee and Bae, 2009).

The average conductivity value for the ceramized product was 0.09 W m^{-1} K^{-1}. This conductivity value classifies the material as a thermal insulator. The thermal conductivity value for Pellexpended® was one order of magnitude lower than that of conventional red ceramics (in the range of 0.9 to 1.2 W m^{-1} K^{-1}). The high porosity of the material is believed to be the reason for the low thermal conductivity. One of the reasons for the extended use of expanded clays, in addition to their lightness, is their suitability as thermal and acoustic insulators.

The high value of water absorption (62%) correlated with the open porosity of this granulated material, as can be observed in Figure 13. The material was characterized by a homogeneous bulk open porosity distribution, with an average pore diameter of 50 μm that resulted in the high water absorption value. In addition to its higher porosity, the microstructure of the material was similar to that of clay bricks, with the typical red color of structural ceramics due to the significant presence of iron salts in the vitreous phase of the product.

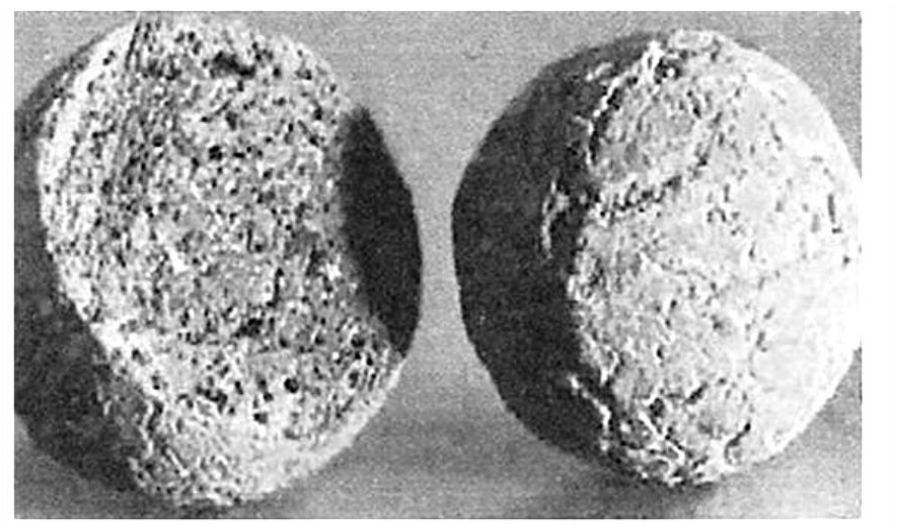

Figure 13. Internal microstructure of a ceramized pellet, where the important porosity of the product (62%) can be observed.

In the sintering of sewage-sludge ashes, it has been observed that the pores in the resulting material decreased with increasing firing temperature (Lin et al., 2006). This suggests that higher vitrification, where virtually all the porosity of the final material is eliminated, could be achieved by increasing the maximum firing temperature to 1200 °C. This is because at high temperatures, the liquid phase of glass would contribute to closing the pores in the resulting material. However, more experiments should be conducted to confirm this fact.

The diffractometric analysis did not reveal significant differences between Pellexpended® and red clays; α-quartz, albite and phyllosilicates were the major components in both cases. It should be noted that during the thermal-destruction stage (350-550 °C), the expansion of the pyrolytic combustion gases helped to maintain the spherical shape of the original pellets. The formation of a dusty or agglomerated material with a gray color was thereby avoided due to the black core phenomenon.

In the case of the leachate from the sludge pellets, the only element detected was nickel (Ni). The concentration of Ni in the first leaching test was 539 mg Ni kg^{-1} d.m. This corresponded to 0.14 mg Ni L^{-1} of leachate and was far below the 1 mg Ni L^{-1} limit set in the Decree 34/1996 (Decret 34, 1996) of the Catalan Catalogue of Wastes. This result means that the sludge pellets can be considered an inert waste with respect to their leaching behavior. In this case, however, the high concentration of lipid material classifies the pelletized sludge as a special waste (toxic and dangerous).

As expected, metal levels in the leachate from Pellexpended® were also found to be below the detection levels of the instrumentation except vanadium. The vanadium concentration was 635 mg V kg^{-1} d.m., which corresponded to 0.16 mg V L^{-1} of leachate. The concentration might be the result of some mineralogical transformation occurring during the process. However, this element is not included in the list of metals described in the legislation regulating lixiviates from wastes (Decret 34, 1996). These results would classify Pellexpended® as an inert waste in the absence of organic matter according to the Decree 34/1996.

CONCLUSION

In this chapter we have shown some alternatives of using sewage sludge from urban wastewater for inclusion in ceramic matrices devoted to building. Their main advantages are the savings in raw material (clays) and water constituting a direct saving in energy costs. But, their main concern lies in the disposal of such wastes considered toxic and hazardous to the environment.

It should be mentioned that there are also many other possibilities of using solid wastes equally valid to be incorporated as raw materials into ceramic materials for construction. Some examples are: ashes from incineration, sludge from paper industry, wastes from galvanizing processes, wastes from dyeing processes in textile industry, and in general many industrial processes whose treatment and final disposal is also problematic. The percentage to be incorporated in the composition of the mixture of these residues usually can not exceed 10 % to obtain a marketable final product (i.e. to meet the technical requirements for use as building material). In general, the use of such a product would be as ceramic pieces for indoor as masonry, boards, etc. It would not be recommended for external use in construction (outdoor or front view bricks) nor to develop load-bearing walls.

Finally, while the number of products of this kind is still in an early stage of production an important increase in production is expected in the near future. To this, it is essential to have the support of public administration and the development of specific environmental regulations to differentiate these processes of waste recycling from those that are mere waste incineration treatments.

REFERENCES

ACGIH, 1995. 1995-1996 Threshold Limit Values for Chemical Substances and Physical Agents and Biological Exposure Indices. *American Conference of Governmental Industrial Hygienists*, Cincinatti OH.

Alleman, J.E., Berman, N.A., 1984. Constructive sludge management: Biobrick, *J. Environ. Eng*. 110 (2), 301-311.

Amos, W.A., 1998. Report on Biomass Drying Technology. *National Renewable Energy Laboratory*, NREL/TP-570-25885, Golden, Colorado.

Anderson, M., 2002. Encouraging prospects for recycling incinerated sewage sludge ash (ISSA) into clay-based building products. *J. Chem. Technol. Biotechnol.* 77, 352–360.

APHA, 1992. *Métodos normalizados para el análisis de aguas potables y residuales.* APHA-AWWA-WPCF (American Public Health Association-American Water Works Association-Water Pollution Control Federation*), Ediciones Díaz de Santos*, S.A., Madrid. [in Spanish].

Arlabosse, P., Chitu, T., 2007. Identification of the limiting mechanism in contact drying of agitated sewage drying. *Drying Technology*, 25 (4), 557-567.

Bhatly, J.I., 1989. Lightweight aggregates from incinerated sludge ash, *Waste Manage. Res.* 1 (7), 363-376.

Berman, N.A., 1982. Brick: an innovative sludge solidification process. *Master on Science Project*, Mary land University (USA).

Brownell, W.E., 1976. *Structural Clay Product*. Springer-Verlag, Wien-New York.

Cheeseman, C.R., Virdi, G.S., 2005. Properties and microstructure of lightweight aggregate produce from sintered sewage sludge ash, Resour. *Conserva. Recycling* 45, 18-30.

Chiang, K.-Y., Chou, P.-H., Hua, C.-R., Chien, K.-L., Cheeseman, C., 2009. Lightweight bricks manufactured from water treatment sludge and rice husks. *J. Hazard. Mater*. 171, 76–82.

Chiou, I.-J., Wang, K.-S., Chen, C.-H., Lin, Y.-T., 2006. Lightweight aggregate made from sewage sludge and incinerated ash, *Waste Manage*. 26, 1453-1461.

Council Directive, 1999. 99/31/EC of 26 April 1999.

Cui, H., Ninomiya, Y., Masui, M., Mizokoshi, H., Sakano, T., Kanaoka, C., 2006. Fundamental Behaviors in Combustion of Raw Sewage Sludge, *Energy Fuels* 20 (1), 77-83.

Cusidó, J.A., Cremades, L.V., 2012a. Atomized sludges via spray-drying at low temperatures: An alternative to conventional wastewater treatment plants. *J. of Env. Manag.* 105, 61-65.

Cusidó, J.A., Cremades, L.V., 2012b. Environmental effects of using clay bricks produced with sewage sludge: leachability and toxicity studies. *Waste Manag*. 32, 1202-1208.

Cusidó, J.A., Cremades, L.V., González, M., 2003. Gaseous emissions from ceramics manufactured with urban sewage sludge during firing processes. *Waste Manag*. 23, 273–280.

Cusidó, J.A., Devant, M., Celebrovsky, M., Riba, J., Arteaga, F., 1996. A new ceramic material for solar buildings. *Ren. Energy* 8 (1-4), 327-332.

Cusidó, J.A., Soriano, C., 2011. Valorization of pellets from municipal WWTP sludge into lightweight clay ceramics. *Waste Manag*. 31, 1372–1380.

Demir, I., Serhat Baspinar, M., Orhan, M., 2005. Utilization of kraft pulp production residues in clay brick production. *Build. Environ*. 40, 1533–1537.

Decret 34, 1996. Published on 9/1/1996, *Generalitat de Catalunya, Diari Oficial de la Generalitat de Catalunya*, 2166, 1186-1203 [in Catalan].

Devant, M., Cusidó, J.A., Soriano, C., 2011. Custom formulation of red ceramics with clay, sewage sludge and forest waste. *Applied Clay Sci.* 53 (4), 669-675.

DIN 38 414-S4, 1984. German standard methods of the examination of water, waste water and sludge. Sludge and sediments (group S). *Determination of leachability by water* (S4). Deutches Institut für Normung. Berlin. Germany.

DOGC, 1994. Decret 323/1994 del Departament de Medi Ambient (Generalitat de Catalunya) del 4 de novembre per el cual es regulan les instal.laccions d'incineració de residus i els seus límits d'emissió a l'atmosfèra. *Diari Oficial de la Generalitat de Catalunya no. 1986* (16.12.1994), 8200-8205 [in Catalan].

Eddings, E.G., Lighty, J.S., Kozinski, J., 1994. Determination of metal behavior during the incineration of a contaminated montmorillonite clay. *Environ. Sci. Technol.* 28, 1791–1800.

EN 12457-1. *Characterization of waste. Leaching: Compliance test for leaching of granular waste materials and sludges*. UE. Publication date 15.10.2002.

Enrique, J.E., Monfort, E., Busani, G., Mallol, G., 2000. Reciclado de aguas residuales en la fabricación de baldosas cerámicas. *Boletin Soc. Esp. Ceram.* Vidrio, 39 (1), 149-154 [in Spanish].

EPA, 1994. *New Source Performance Standards* (NSPS). Code of Federal Regulations, 40 CRF 60, Environmental Protection Agency, Washington.

ESA PSS-01-702, 1994. Issue 2, *A Thermal Vacuum Test for the Screening of Space Materials*. European Space Agency. October.

ESA PSS-01-729, 1991. Issue 1, *The determination of Offgassing Products from Materials and Assembled Articles to be used in a Manned Space Vehicle Crew Compartment*. European Space Agency. March.

Harlbut Jr., Klein C., 1992. *Manual de mineralogia de Dana*, Ed. Reverté, Barcelona [in Spanish].

HSEOC, 2005. Sewage Sludge Drying Plant. Health and Safety Executive *Operational Circular* 847/9, UK.

Jordán, M.M., Almendro-Candel, M.B., Romero, M., Rincón, J.M., 2005. Application of sewage sludge in the manufacturing of ceramic tile bodies. *Appl. Clay Sci*. 30, 219–224.

Kaosol, T., 2010. Reuse water treatment sludge for hollow concrete block manufacture. *Energy Res. J.* 1 (2), 131–134.

Kingery, W.D., Bowen, H.K., Uhlmann, D.R., 1976. *Introduction to ceramics*, Ed. Wiley, New York.

Kruse, E.A., Barrett, G.W., 1985. Effects of municipal sludge and fertilizer on heavy metal accumulation in earthworms, *Environ. Pollut. Ser. A. Ecological and Biological*, 3 (38), 235-244.

Lee, H.-S., Bae, K., 2009. Combustion kinetics of sewage sludge and combustible wastes. *J. Mater. Cycles Waste* 11, 203–209.

Liew, A.G., Idris, A., Samad, A.A., Wong, C.H.K., Jafafar, M.S., Baki, A.M., 2004a. Reusability of sewage sludge in clay bricks. *J. Mater. Cycles Waste* 6, 41–47.

Liew, A.G., Idris, A., Wong, C.H., Samad, A.A., Noor, M.J., Baki, A.M., 2004b. Incorporation of sewage sludge in clay brick and its characterization. *Waste Manag. Res*. 22 (4), 226–233.

Lin, K.-L., Chiang, K.-Y., Lin, D.-F., 2006. Effect of heating temperature on the sintering characteristics of sewage sludge ash, *J. Hazard. Mater*. B128, 175-181.

Lin, D.-F., Weng, C.-H., 2001. Use of sewage sludge ash as brick material. *J. Environ. Eng.* 10 (127), 922–927.

Magalhaes, J.M., Silva, J.E., Castro, F.P., Labrincha, J.A., 2004. Effect of experimental variables on the inertization of galvanic sludges in clay-based ceramics. *J. Hazard. Mater*. 106B, 139–147.

Monteiro, S.N., Vieira, C.M.F., 2005. Effect of oily waste addition to clay ceramics. *Ceram. Int.* 31, 353–358.

Monteiro, S.N., Alexandre, J., Margem, J.I., Sánchez, R., Vieira, C.M.F., 2008. Incorporation of sludge waste from water treatment plant into red ceramic. *Constr. Build. Mater*. 22, 1281–1287.

Montero, M.A., Jordán, M.M., Hernández-Crespo, M.S., Danfeliu, T., 2009. The use of sewage sludge and marble residues in the manufacture of ceramic the tile bodies. *Appl. Clay Sci*. 46, 404–408.

NEN 7345, 1993. *Determination of the release of inorganic characteristics of inorganic constituents from construction materials and stabilized waste products*, NNI Delft (Netherlands), Formerly Draft NEN 5432.

Niessen W.R., 1995. *Combustion and incineration processes: applications in environmental engineering*. Marcel Dekker Inc., New York.

Novak, J.T., 2006. Dewatering of sewage sludge. *Drying Technology*, 24 (10), 1257-1262.

Patrick D.R., 1994. *Toxic Air Pollution Handbook, 1st ed*., Van Nostrand Reinhold, New York.

Qi, Y., Yue, Q., Han, S., Yue, M., Gao, B., Yu, H., Shao, T., 2010. Preparation and mechanism of ultra-lightweight ceramics produced from sewage sludge. *J. Hazard. Mater*. 176, 76–84.

Tay, J.-H., 1987. Bricks manufactured from sludge. *J. Environ. Eng*. 113 (2), 278–283.

Tay, J.-H., Hong, S.-Y., Show, K.-Y., 2000, Reuse of industrial sludge as palletized aggregate for concrete, *J. Environ. Eng.* 3 (126), 834-844.

Tirey D.A., Striebich R.C., Dellinger B., Bostian H.E., 1991. Comparison of organic emissions from laboratory and full-scale thermal degradation of sewage sludge. *Hazard. Waste & Hazard. Mat*. 8 (3), 201-218.

Timellini G., Cremonini F. and Palmonari C., 1993. Air pollution from ceramic tile processes. *Ceram. Eng. Sci. Proc*. 14 (1-2), 445-456.

UNE-67-026-94, 1994. Ladrillos y bloques cerámicos de arcilla cocida. *Determinación de resistencia a compresión* [in Spanish].

Velo, E., 1998. Potencial energético y sistemas de secado. *Proceedings Explore-recycling'98, II Fórum Ambienta*l, pp.53-68, Barcelona [in Spanish].

Verschueren K., 1977. *Handbook of environmental data on organic chemicals.* Van Nostrand Reinhold Co., New York.

Weng, C.-H., Lin, D.-F., Chiang, P.-C., 2003. Utilization of sludge as brick materials. *Adv. Environ. Res*. 7, 679–685 Waste Manag.

Wherther J. and Ogada T., 1999. Sewage sludge combustion. *Prog. in Energy and Comb. Sci.* 25 (1), 55-116.

Wiebusch, B., Ozaki, M., Watanabe, H., Seyfried, C.F., 1998. Assessment of leaching tests on construction material made of incinerator ash (sewage sludge). Investigations in Japan and Germany, *Water Sci. Technol*. 38 (7), 195–205.

Woo, M.W., Daud, W.R.W., Tasirin, S.M., Talib, M.Z.M., 2007. Optimization of the spray drying operating parameters – A quick trial-and-error method. *Drying Technology*, 25 (10), 1741-1747.

Xu, G., Zou, J., Li, G., 2008. Ceramsite made with water and wastewater sludge and its characteristics affected by SiO2 and Al2O3, *Environ. Sci. Technol*. 42, 7417-7423.

In: Clays and Clay Minerals
Editor: Liam R. Wesley
ISBN: 978-1-63117-779-8

Chapter 6

THE WORKABILITY OF NATURAL CLAYS AND CLAYS IN THE CERAMICS INDUSTRY

Graham Barnes
Graham Barnes Consultancy, UK

ABSTRACT

The property of workability is important in the ceramics industry, particularly in association with extrusion processes, in the construction industry where natural and stabilised clay soils are required to be worked, moulded and compacted and in the agricultural industry where the conditions for good tillage and ploughing are related to a friable or brittle condition close to the plastic limit. The work required to carry out the processes of extrusion and compaction of clays in the plastic state can be related to their toughness which in turn depends on the clay mineralogy, water content, particle size distribution and soil fabric. Toughness has previously only been studied in an indirect and qualitative manner. The results of tests conducted with an apparatus developed by the author to produce rolling of a soil thread comparable to the procedure in the Atterberg plastic limit test are discussed. A well-defined ductile-brittle transition in relation to water content is achieved resulting in a much more accurate determination of the plastic limit compared to the poor reproducibility of the standard test. The toughness of a ductile clay can be determined as a measure of work/unit volume from a stress-strain curve over a range of water contents. Unique toughness-water content relationships are obtained for a wide variety of natural clays, ball clays and brick clays. The range of water contents between the liquid and plastic limit, conventionally referred to as the plasticity index, can be distinguished into three regions, described as adhesive-plastic, soft-plastic and stiff-plastic regions and these are defined by the water content at zero toughness, the toughness limit, the water content at the stiffness transition between the soft-plastic and stiff-plastic regions and the plastic limit. The effects of coarse-grained particles, silts and sands, on toughness is small at low contents but at high contents is affected by the requirements not only to mould the clay component but to displace the coarse particles. Mixing different clays together is found to produce non-linear variations in their properties, depending on the total clay content and the content of a dominant clay mineral.

THE DUCTILE-BRITTLE TRANSITION

The ductile-brittle transition has been recognised as a fundamental phenomenon in respect of changing temperature on stress-strain behaviour for a range of materials, such as metals, rocks, glass and wax. However, for soils with respect to water content this transition has not received the attention it deserves. The term ductility is used to denote the ability of a cohesive soil to hold together when rolled out into thin sheets or threads. On the ductile side of the transition a cohesive soil contains sufficient water to allow it to display plasticity, in that it can be deformed considerably and can retain a deformed shape. In rolling out a thread of soil the term toughness is introduced to define the amount of work per unit volume required to remould and deform the soil.

On the brittle side of the transition a soil thread can no longer be rolled out, as demonstrated in a standard plastic limit test (BS1377:1990; ISO/TS 17892-12:2004; ASTM D4318-10). The plastic limit is then the water content at the ductile-brittle transition. The behaviour of a brittle soil can be explained by the generation of internal tensile stresses during rolling of the thread. These stresses seek out and develop defects in the soil structure such as microcracks, air voids or fractures producing crack propagation until the soil collapses.

PLASTICITY, WORKABILITY AND TOUGHNESS

Many researchers have had difficulty in defining plasticity, never mind finding a method to measure it, for example, Worrall (1982), Dinsdale (1986) and Ryan and Radford (1987). Most recently this difficulty has been summarized by Reeves et al. (2006) as "The definition of a parameter which provides a useful indication of the plasticity of clays used in the production of pottery has presented a challenge yet to be satisfactorily resolved." In relation to a stress-strain curve plasticity can be seen as the ability of a substance to be deformed (stressed beyond its yield point) considerably without rupture (with large, mostly plastic strains) and on ceasing the deformation (removal of stresses) the (plastic) strains are not recovered and the substance retains its deformed shape.

In the ceramics industries the term workability is more commonly used, applied to clays with water contents mainly above their plastic limits and below the sticky limit giving a workable range of water contents. In the agricultural industries a soil is generally deemed workable for tillage when its water content lies below the plastic limit and for deeper working such as ploughing in the stiff-plastic region, see later.

Several novel, empirical tests have been applied over the years in the ceramics industry to assess workability for brick making, pressing, extrusion etc. based on either a deformability or extrusion property but none of these could give a measure of the work required to deform the material when in its plastic state, instead they provide parameters with tenuous associations with workability.

In rolling out a thread of soil the term toughness is introduced to define the amount of work per unit volume required to remould and deform the soil. Casagrande (1932) recognised the importance of the toughness property of a soil at water contents near to the plastic limit and even suggested that clays could be classified according to their toughness. Later, Casagrande (1947) stated that the toughness near the plastic limit increases as the plastic limit

decreases. He gave a classification of toughness by referring to the 'cohesiveness at the plastic limit' with terms in the order: very weak, weak, firm, medium tough, tough, very tough. However, few researchers have since pursued the study of this property.

CLASSIFICATIONS OF PLASTICITY AND TOUGHNESS

Atterberg (1911) considered that the degree of plasticity of a soil could be represented by his plasticity number, now called the plasticity index, I_p, the liquid limit minus the plastic limit. Classifications for the degree of plasticity based on the ease of rolling and the smallest diameter to which a thread of soil can be rolled have been suggested by Burmister (1970) and Karlsson and Hansbo (1981) with very thin threads denoting high plasticity. Soils that can not be rolled out are described as non-plastic.

To assess the viability of using various clays in extrusion processes the diagram produced by Bain and Highley (1979) is often referred to. In relation to the Casagrande plasticity chart this diagram shows that clays mainly in the intermediate plasticity region (w_L = 35 – 50% according to BS5930:1999) and above the A-line give optimal extrusion qualities. Clays with plasticity index I_p < 10% are not appropriate for building related products and clays with I_p > 34 % would be tougher and difficult to extrude. This diagram, however, does not recognise that extrudability would also be a function of the water content of the clay.

Based on the Casagrande plasticity chart, zones of toughness at the plastic limit are given for the USCS system in a NAVFAC (1986) document, using the terms slight, medium and high although these are not defined. This classification recognises the difference in toughness for soils above and below the A-line.

BS5930:1999 gives a classification for plasticity based on the liquid limit alone, from low to extremely high. This classification is independent of the plastic limit with no acknowledgement that M soils which lie below the A-line on the Casagrande plasticity chart and C soils that lie above have different toughnesses. This Standard describes toughness of a fine soil as the 'character' of a moist thread when rolled out and moulded together, with inorganic clays of high plasticity being fairly stiff and tough and those of low plasticity are softer and more crumbly.

Plasticity is defined in BS EN ISO 14688-1:2002 as the property of a cohesive soil that permits its consistency limits (liquid and plastic limits) to be determined and to change its mechanical behaviour with change of moisture content. Two classes are described, high and low plasticity. Soils of high plasticity can be rolled into thin threads, they are ductile and would have water contents above the plastic limit; soils of low plasticity have cohesion but cannot be rolled to thin threads (about 3mm diameter) so they would have water contents below the plastic limit. BS EN ISO 14688-2:2004 states that the degree of plasticity should be based on the results of laboratory tests, the liquid and plastic limits, with a classification using the terms non-plastic, low, intermediate and high plasticity but this standard gives no guidance on the liquid limit or plastic limit values to assign to each term.

FIELD TESTS FOR CLASSIFICATION OF TOUGHNESS

In the US Department of Agriculture Soil Survey Manual (Anon, 1993) toughness classes of low, medium or high are given based on the force in Newtons required to form with the fingers a soil thread 3 mm diameter at a water content near the plastic limit. These criteria are more related to work/unit volume, which provides a better definition of toughness.

In the New South Wales USCS field method (Anon, no date) toughness is described as the consistency at the plastic limit and this document explains that the tougher the soil thread the more potent is the colloidal clay fraction. This property is distinguished by means of the ribbon strength, dry strength, toughness and stickiness of the soil.

ASTM D 2488-09A describes toughness on the basis of a subjective assessment of the pressure (low, medium or high) required to roll a soil thread at a water content just above the plastic limit and the stiffness of a lump of the soil formed from the crumbled threads when the water content is just below the plastic limit. According to this Standard a soil with medium toughness and low plasticity (CL) is identified as a lean clay and one with high toughness and high plasticity (CH) is described as a fat clay.

PREVIOUS TESTS TO MEASURE WORKABILITY

Many tests have been devised to provide a measure of workability, both simple and intricate and some now disused, with different ways of representing this property.

To distinguish workable plasticity and to eliminate the 'potter's feel' for the condition of clay McDowell (1928) devised a simple compression device comprising a 8kg mass placed on top of a 2 inch cube of the clay for 30 seconds and measuring the resultant height of the specimen. Compared with the performance of the clay in the works, limits for the height reduction could be set within which a clay was deemed workable and this approach was found to be more reproducible than the potters' judgements.

Heindl and Pendergast (1947) investigated a test originally designed to apply a set number of twenty impacts from a fixed weight and height of drop onto loose soil clods inside a steel cylinder. They found that twenty impacts was insufficient to fully compact some soils, those of high toughness, and considered that it would be preferable to base the workability of a soil on the number of blows required to remould the clods and reach full compaction or the maximum bulk density. They had identified that the purpose of the test was to determine the amount of work required for remoulding. A similar test to determine the 'workability index' of fireclays and refractory clays is covered in ASTM C181-11.

The above test is very similar in function and outcome to the moisture condition apparatus (MCA) and test (Parsons and Boden, 1979) which was devised to determine the suitability of mainly cohesive soils for use in the construction of embankments and other earthworks. 1.5kg of moist soil reduced to 20 mm maximum size clods is placed in a steel cylinder and compacted by the impacts of a 7 kg rammer falling 250 mm onto the soil. The moisture condition value (MCV) is measured as the log number of blows to fully compact the soil. The MCV is a measure of toughness with tougher soils, and with lower water contents, giving higher MCVs because more compaction energy is required to remould the lumps of clay. The trafficability of heavy earthmoving machinery has been assessed in relation to the

MCV of the soils traversed (Parsons and Darley, 1082). A discussion on the efficiency of earthmoving is given in Barnes (2010a).

The Pfefferkorn method (Andrade et al., 2011) comprises an impact device that deforms a cylindrical specimen of clay from the impact of a free falling mass. Tests are conducted on clays with varying water contents with the ratio of the initial height to the deformed height increasing as the water content increases. To compare different clays the Pfefferkorn value is taken as the water content at 30% contraction of the specimen.

An indentation method proposed by De Oliveira Modesto and Bernardin (2007) comprises a determination of plasticity by means of the measurement of force applied to a spherical indenter. Assorted penetrometer devices are described by Göhlert and Uebel (2009) comprising small diameter plungers pressed into the clay with resistance measured as a force or pressure.

The Brabender plastograph described by Marshall (1955) and West and Lawrence (1959) is a torque rheometer comprising an electrically driven mixing chamber with measurement of torque on the mixing blades as water is added to the air-dried, ground clay. This is a rather crude device but a useful result was that montmorillonite was found to require higher torques and over a wider range of water contents than kaolinite.

Carty and Lee (1996) recognised that in the ceramics industry the property of plasticity lies between suspension rheology for which viable tests were available and soil mechanics for which remoulding tests were not available. Using a high pressure shear rheometer and from a plot of torsional shear stress vs. applied pressure they determined the cohesion, or yield shear stress as the intercept of the plot, and the pressure dependence, the gradient of the plot. A kaolinite clay was found to have the highest pressure dependence.

Extrusion tests conducted by Fitzjohn and Worral (1980) on several brick clays, measuring extrusion rates vs. applied pressure showed that their ‘index of plasticity’ was reasonably well correlated with the clay content. The ‘index of plasticity’ was defined as the ratio of the yield stress (the applied pressure required to commence extrusion) and the ‘bottom bend’ (the additional amount of pressure required to promote steady extrusion). A high clay content would be expected to provide the greatest resistance to extrusion.

The Martin Flow Instrument was designed by CERAM Research (Kessel, 1998) to extrude a sample of clay through a die, measuring the flow rate and the applied pressure. As the rate of extrusion is determined by the toughness of the clay the most significant controlling factor was found to be the water content.

Astbury et al. (1966) carried out cyclic torsion tests on clays used in the ceramics industry and defined the area of the hysteresis loop of stress vs. strain as the amount of energy absorbed by the specimen during one cycle. They found that this amount of energy was significantly dependent on the water content. Their plot of energy per hysteresis cycle vs. water content is very similar to the relationships obtained for work/unit volume vs. water content using the Barnes plastometer, see below.

Compression, impact, extrusion, indentation and penetrometer devices test the clay by mobilising its shear strength or yield strength. In relation to a stress-strain curve a clay only behaves plastically when it is stressed beyond its yield strength when the clay deforms extensively with large plastic strains. Only tests that take measurements of stress and strain in the plastic region can be said to provide true plasticity determinations.

The workability of clays can be obtained from a measure of the yield stress multiplied by the maximum deformation from a shearing test, e.g., Norton (1938); Schwartz (1952). Norton

(1938) carried out tests on clays using a torque machine and from plots of torque versus angle of rotation found an increasing measure of toughness (product of the yield point of torque and the maximum deformation) as the water content decreased. He stated that a plastic body for ceramics purposes would need a high value of the yield point and a high extensibility. If it has a low yield point, or low strength, it would slump after working and if it has a low extensibility it will be 'short'[1] and difficult to form, by developing brittleness.

Two plastometers, a compression device and a torsion device, were described by Moore (1963). With the former device, the specimen was compressed by more than 60% and the stress at 50% compression was used as a plasticity parameter. From the torsion test a hysteresis loop was obtained by cycling the stress and measuring the angular rotation with the area of this loop used as a measure of the energy required to deform a specimen, as suggested by Astbury et al. (1966). The compression test did not allow for the significant change in shape of the specimen and in the torsion test the separation of elastic from plastic strains would be difficult.

Baran et al. (2001) defined a workability parameter for clays as $\sigma_{0.2}\varepsilon_0$* which, at first sight, would appear to be the area beneath part of a stress(σ)-strain(ε) curve to give a measure of work/unit volume. However, the $\sigma_{0.2}$ value was obtained from compression tests on cylinders of clay as the stress at a fixed strain of 0.2 and ε_0* was determined as the plastic tensile strain obtained from a set of 'upset tests' measured at zero compression strain. With the stress and strain values derived from two very different tests on different specimens with different water contents, there would be difficulties in obtaining a compatible value of work/unit volume.

MICROSTRUCTURAL VIEW OF TOUGHNESS AND PLASTIC LIMIT OF CLAY

The early concepts of microstructure of clay held that the single clay platelet dominated the framework with a double layer theory controlling the attractive and repulsive forces between the particles (Mitchell, 1956). From scanning electron microscope studies of natural clays and silts Collins and McGown (1974) found that the single clay platelet arrangements were rare and that face to face groups of clay platelets were dominant. They identified a number of particle assemblages including discrete aggregations of clay particles, clay-coated silt and sand grains, clay connectors or bridges between silt/sand particles, semi-continuous, interweaving bunches or strands of clay particles connected together and in soils with high clay contents general particle matrix assemblages. Cetin et al. (2007) also described the clay structure at water contents above the compaction optimum water content to be characterised by long strings of differently oriented particle groups in the form of curved trajectories. The toughness of a clay soil can be seen as resistance to deformation from these clay particle structures, particularly the interweaving strands.

Within the clay strands a simple representation of toughness has been developed (Barnes, 2013a) for the interaction between individual clay particles assuming an adsorbed water layer

[1] A term also used in pastry making.

on the surfaces that determines the forces acting between them. The work required to produce displacement of the particles, referred to as the toughness *T*, is shown to increase with

1) increasing surface area of the clay particles,
2) increasing attraction between the clay particles assuming the attraction to be inversely proportional to the separating distance,
3) increasing friction between the clay particles which would be related to the angle of friction and
4) decreasing water content.

Delage et al. (1996) postulated that the plastic limit could be the limit between a uniform matrix structure and a structure of aggregated clay particles. As the water content approaches the plastic limit it is feasible that the clay/water matrix not only forms into aggregates but these aggregates coalesce between silt and sand grains to form clay bridges. Associated with changes in the soil structure there will be changes in the pore size distribution.

Bimodal pore size distributions have been found in samples of compacted kaolin/silt mixtures (Garcia-Bengochea et al., 1979 and Sivakumar et al., 2006) at water contents above and below the compaction optimum water content with groups of small and large pore sizes. The smaller pore sizes probably exist within the aggregates (intra-aggregate) while the larger ones are inter-aggregate or inter-silt pores.

Diamond (1970) showed that the clay mineral type had a marked effect on the pore size distribution with the smallest pore sizes obtained in a montmorillonite sample (typically 0.01 – 0.05 μm), larger pore sizes in kaolinite (0.1 – 0.2 μm) and much larger pore sizes in natural soils (1 – 5 μm). According to Tanaka et al. (2003) the mean pore size also increases with increasing silt and sand content probably due to the presence of clay connectors or bridges between the coarser grains.

The effect of reducing water content towards the plastic limit can be seen to be one of changing from a structure that holds together, can be rolled out and displays cohesiveness and ductility to one that breaks into distinct units and crumbles under deformation.

As the water content reduces towards the plastic limit larger void sizes develop probably as a result of coalescence of finer voids. Some of the larger voids would also be likely to contain air. Cafaro (2002) showed that the suction at the plastic limit was close to the air entry value, i.e. the onset of desaturation. The air-filled pore spaces will provide defects in the soil structure that will be preferentially exercised by the cyclic stressing in the rolling plastic limit test promoting crack propagation and leading to the brittle failure of the soil thread.

THE BARNES PLASTOMETER

Casagrande (1932) devised a mechanical means of conducting the liquid limit test as first proposed by Atterberg, the cup method, but did not attempt to mechanize the plastic limit test. The apparatus of Bobrowski and Griekspoor (1992) provides a rolling device to make a soil thread reduce to the diameter of 3.2 mm as required in the ASTM D4318-10 method but no measurements of the behaviour of the soil during the rolling process are recorded.

The author has devised and developed an apparatus (Barnes, 2009, 2010b, 2013a, 2013b) for measuring the stress-strain behaviour of a thread of cohesive soil as it is rolled in a manner that replicates Atterberg's rolling technique for the determination of the plastic limit. Since the apparatus enables measurement of the plasticity properties of a cohesive soil it is referred to herein as the Barnes plastometer.

The apparatus comprises a top glass plate and a bottom steel plate with the outer faces of the plates inclined outwards at a shallow angle of 1 in 40 so that when a thread of soil is rolled between the plates the thread extrudes longitudinally as it reduces in diameter. The top plate is kept stationary and the bottom plate is moved forward and back above a sliding mechanism to mimic the hand rolling method so that the soil thread rolls forward 50 mm and then back 50 mm, referred to as one traverse. The outer strips of the plates are lightly smeared with petroleum jelly to provide a form of lubricated platens to ensure a consistent smooth surface in these areas and to permit freer extrusion of the thread during rolling.

The top plate is attached to a loading bar with a force applied to the soil thread during each traverse and adjusted by means of a moveable mass on top of the loading bar. The force is varied according to the strength of the soil and to produce adequate deformation on each traverse. The operation is force-controlled with the force increments chosen to maintain suitable changes in diameter. The diameter of the thread is measured for each traverse by means of a dial gauge positioned on the loading bar. From the applied force F and the measured mean diameter $\overline{D}$, values of the nominal stress on the thread are determined for each traverse from the split cylinder formula as

$$\sigma_{\text{nom}} = \frac{F}{L\overline{D}} \tag{1}$$

where L is the length of the soil thread between the plates, 50 mm. The diametral strain for each traverse of the soil thread is determined from

$$\delta\varepsilon = \frac{\delta D_{\text{i}}}{D_{\text{i}}} \tag{2}$$

where δD_{i} is the change in diameter and D_{i} is the diameter at the start of the i^{th} traverse. The cumulative strain is determined by summation for the traverses.

The formula for stress given in the split cylinder or Brazilian test described in ASTM D3967-08 is considered to be appropriate to the application of force in the plastic limit test (Wood, 1990). The nominal stress derived from equation 1 is considered to act as a 'quasi-all-round pressure' that causes the ductile thread to undergo longitudinal extrusion and reduction of the diameter in a triaxial extension mode of shearing.

The effect of a high proportion of large particles in a small diameter thread is found to be significant so it is necessary to remove all particles greater than 425 μm from the soil, preferably by wet sieving, before preparing a soil thread. This is the maximum particle size permitted for the determination of the liquid and plastic limits in the Standards. The soil thread is prepared by static compaction in a specially made thread maker at a diameter of about 8 mm and with a precise circular cross section to ensure that the thread rolls smoothly between the plates.

Tests are conducted over a range of water contents starting from a high water content where the soil is very soft but not sticky, otherwise the surface of the thread sticks to the plates. The ductile threads are rolled until the diameter reduces to 3 mm or less. With decreasing water content the soil becomes stiffer or tougher and higher forces are required to produce the required changes in diameter.

With a thread diameter starting at about 8 mm increasing loads and continual traverses take the soil thread to a yield condition beyond which the thread undergoes fairly steady plastic straining as the thread is continually rolled, Figure 1. The product of nominal stress and diametral strain for each traverse provides a measure of the work per unit volume for that traverse. The number of stress reversals applied to the soil thread increases for each traverse as the thread reduces in diameter. The work/unit volume per traverse is normalised to a constant number of 100 reversals.

From a nominal stress-diametral strain plot the work per unit volume *W*, as the area beneath the curve, is calculated for each traverse

$$W = \sigma_{\text{nom}} \times \delta\varepsilon_{\text{D}} \tag{3}$$

The cumulative work/unit volume for all of the traverses required to reduce the thread from a diameter of 6 mm to a diameter of 4 mm, within the range of plastic straining, is determined as the toughness *T* with units of kJ/m^3.

Tests are conducted until the soil is at a water content when it becomes brittle and a thread will no longer reduce in diameter and extrude but fails in a brittle manner. The effect of the stress cycling within the soil thread from compression to tension and vice versa probably increases, with the tensile stresses in the thread, in particular, impacting on the more aggregated soil structure and promoting opening of microcracks and small air voids that are developing with reduced water content. The plastic limit is the water content at the ductile-brittle transition.

A typical plot of nominal stress vs. diameter is presented in Figure 1, for a sample of Lias clay from Charmouth, Dorset, UK. The plots show the ductile behaviour of the soil threads over a range of water contents with yielding observed followed by continuous diametral plastic deformation, also involving longitudinal extrusion. For each of these tests the toughness *T* is determined from the area beneath each curve between the diameters of 6 and 4 mm and plotted against the water content in Figure 2.

The initial state of a clay affects the toughness-water content plot, with air-dried samples giving a stiffer initial response, yielding at higher stresses and higher toughnesses at the same water content compared to oven-dried samples. It is considered that oven-drying of a clay soil causes some aggregation of the clay particles and leaves the soil with a smaller proportion of continuous matrix. For natural clay soils it is preferable to conduct the test on samples commencing from their natural water content providing the requirement to remove all particles larger than 425 μm is achieved.

The relationships between toughness and water content have been found to be typical of all of the soils tested with the following properties identified.

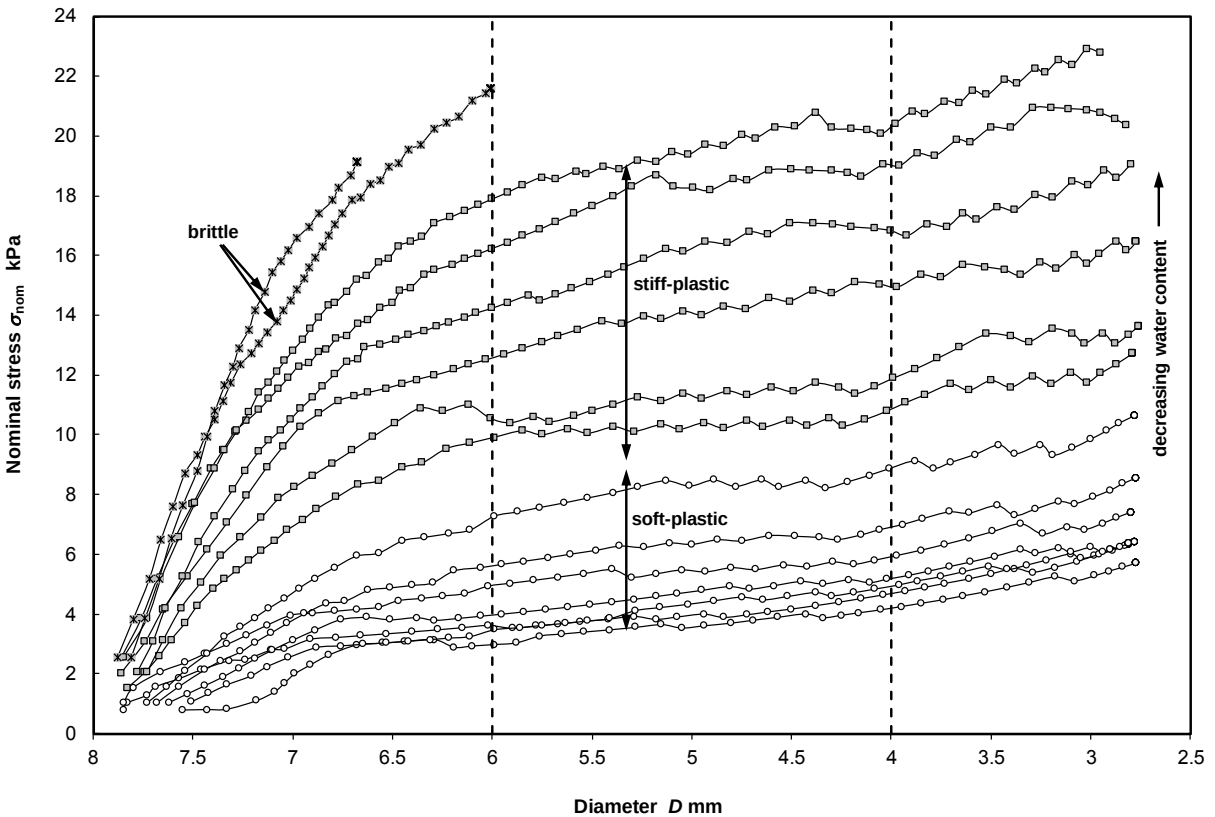

Figure 1.

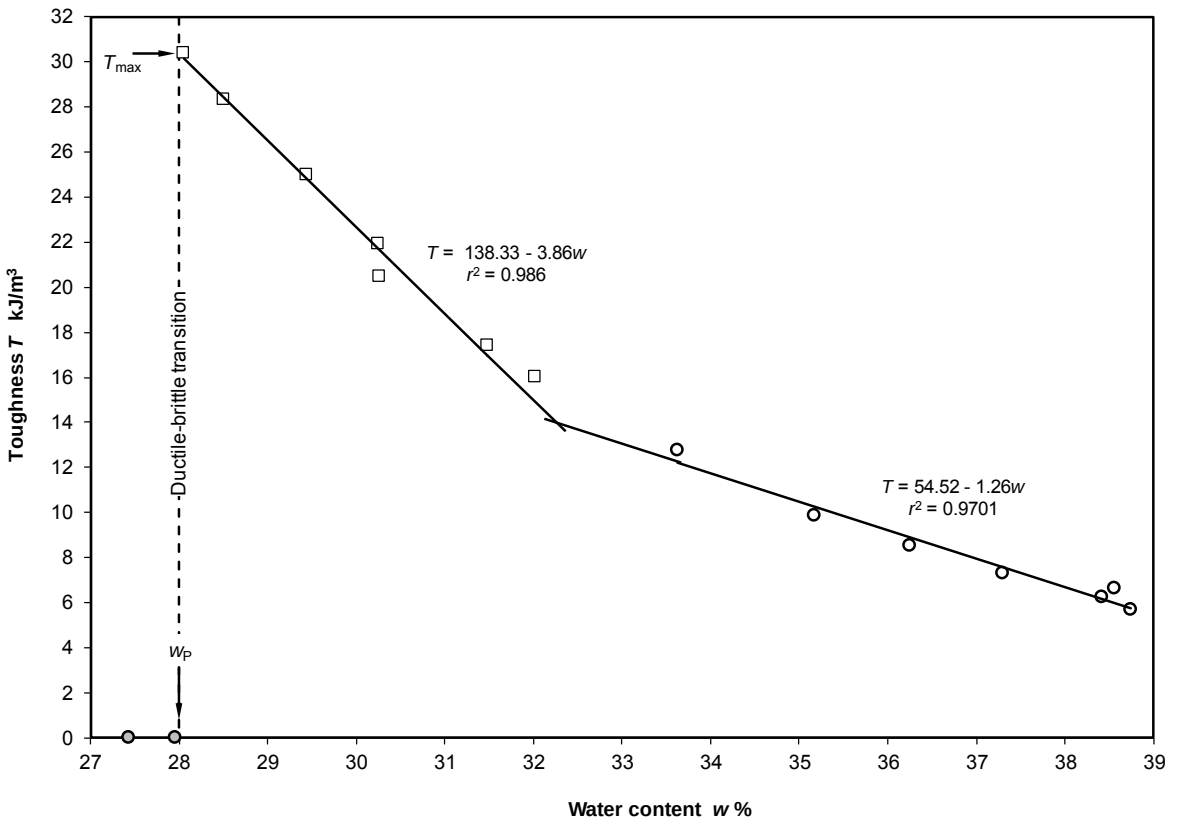

Figure 2.

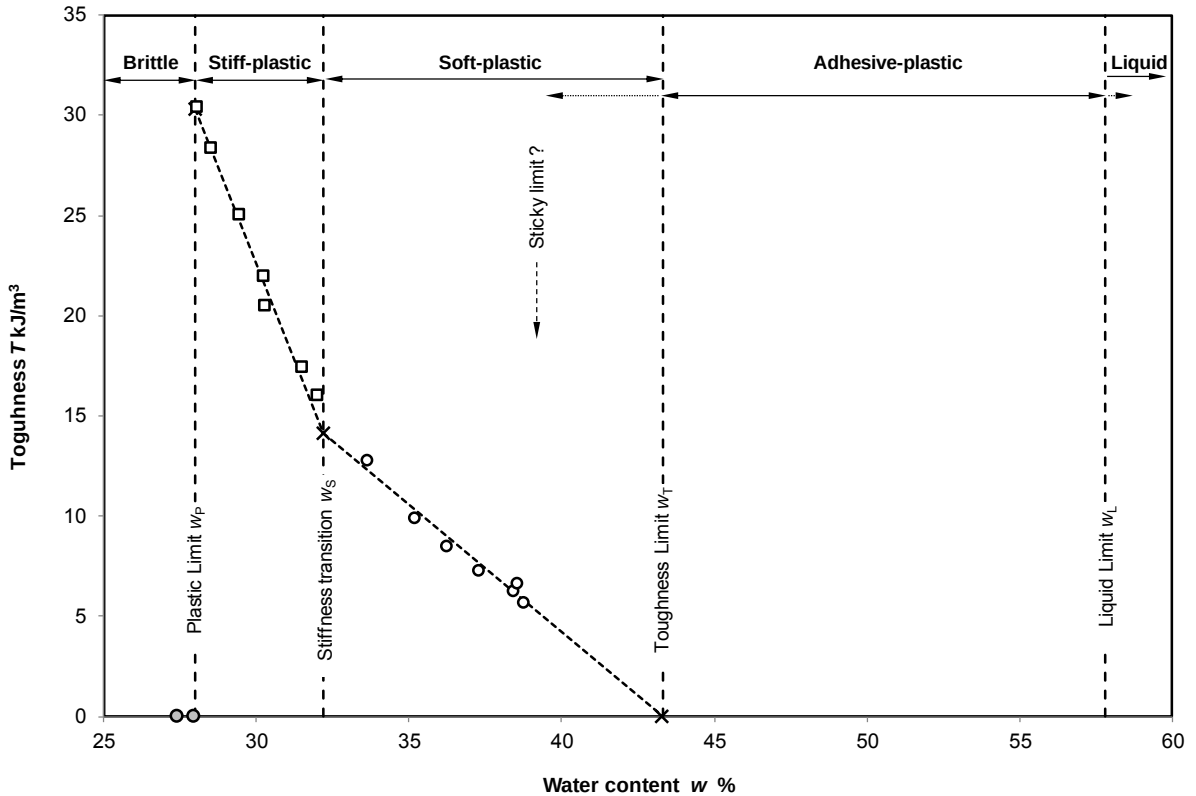

Figure 3.

PROPERTIES DETERMINED FROM THE TOUGHNESS VS. WATER CONTENT RELATIONSHIP

The plot of toughness vs. water content in Figure 2 has been re-plotted in Figure 3 to include the water contents up to the liquid limit to illustrate several properties associated with this relationship.

1) Plasticity Regions

The range between the liquid limit and the plastic limit, referred to as the plasticity index, can now be subdivided into three regions, an adhesive-plastic (or sticky-plastic) region, a soft-plastic and a stiff-plastic region defined between the liquid limit, the toughness limit, the stiffness transition and the plastic limit. The zone below the plastic limit is referred to as brittle. Above the liquid limit soils can still be described as adhesive because they would stick to a steel spatula and below the toughness limit soils are found to retain some stickiness so the toughness limit does not correspond with the sticky limit as proposed by Atterberg (1911).

The plasticity regions and the toughness property can be used to distinguish clays that will provide greater resistance to deformation while still remaining plastic. In the ceramics industry control of toughness and water content would be important to the forming processes of manufactured clay products. In the construction industry toughness would be relevant for the assessment of the flexible behaviour of clay components in earthworks such as where clay membranes are required in landfill and canal construction and in the cores of earth dams. Conversely tougher soils require more effort in placing and compaction affecting the choice of machinery and the efficiency and costs of earthworks construction.

2) Toughness Limit, w_T

The toughness limit is the water content at zero toughness obtained by extrapolation from the reasonably correlated straight line above the stiffness transition to zero toughness. Due to the stickiness of soil at the higher water contents in the soft-plastic region it is not possible to extend the tests to zero toughness values. From experience, the sticky limit as suggested by Atterberg (1911) lies at a water content below the toughness limit. This limit defines an adhesive (or sticky)-plastic region which has no toughness and is virtually non-workable and a workable or tough-plastic region.

Although in the same range of water contents the toughness limit is considered to be unrelated to the sticky limit as the latter applies to a different phenomenon, associated with surface tension of a soil in contact with a metal or other hard surface. Nevertheless the toughness limit could be used to denote the upper limit of the toughness or workability of a soil.

3) Maximum Toughness, T_{max}

In the stiff-plastic region the toughness and water content values plot on a reasonably correlated line that can be extrapolated to give the maximum toughness at the plastic limit, T_{max}, with units of kJ/m^3. This property can be used to compare the toughnesses of different clays.

4) Stiffness Transition, w_S and T_s

It has been found that many clays display an additional but more subtle transition on the toughness vs. water content plot in the tough-plastic region, referred to as the stiffness transition. This is often observed to correspond to a noticeable change in the nominal stress-strain behaviour of the clay. The water content at this transition is referred to as w_S and T_s is the toughness. For some soils such as clayey silts and some ball clays it is difficult to distinguish a stiffness transition. For these soils strain-hardening occurs at all water contents so there is little distinction between the shapes of the stress-strain curves.

In the ceramics industry water content adjustment and control are essential to regulate the plasticity properties of the clay bodies. Allowing the water content to reduce below the stiffness transition would increase the toughness disproportionately and could significantly reduce the efficiency of the operating machinery.

5) Toughness Coefficients, T_C

The gradients of the straight lines each side of the stiffness transition are assigned the term, toughness coefficient, T_C. These values represent the sensitivity of toughness of a clay to changes in water content and demonstrate the significance of the stiffness transition.

6) Toughness Index, I_T

This is defined as the difference between the toughness limit and the plastic limit and gives the full range of water contents over which the soil would be plastic and workable.

$$I_T = w_T - w_P. \tag{4}$$

7) Workability Index, I_W

In a similar form to the liquidity index, the workability index identifies the water content, w, of a soil in relation to the toughness index.

$$I_W = \frac{w - w_P}{w_T - w_P} \tag{5}$$

The workability index could be used, in preference to the liquidity index, in the specification of processed clays and earthworks control to denote the degree of workability since with water contents above the toughness limit a clay would be deemed non-workable.

EFFECTS OF SILT AND SAND PARTICLES

The results of tests on mixtures of clay and silt and clay and sand are discussed in Barnes (2013a). It has been found that the plastic limit and the maximum toughness decrease with decreasing clay content and that for clay contents above about 15% the maximum toughness increases almost linearly with clay content. However, the relationship between plastic limit and clay content follows the linear law of mixtures only for clay contents above about 50%. Neither of the relationships between water content and plastic limit and maximum toughness passes through the origin because it would be expected that a soil with zero clay content could not display toughness nor be rolled out to give a plastic limit. With a clay content of about 10% or less the toughness was found to be negligible and the soil would be described as non-plastic.

For mixtures containing the same granular content (silt or sand) there will be more particles present in the mixtures with the smaller particle sizes. It has been found that for mixtures of clay and silt and clay and sand those containing finer granular particles (silt) require more water to produce the same toughness.

With a larger number of, albeit smaller, granular particles the spacing between them decreases and the clay matrix surrounding them becomes less continuous. Also the larger number of particles provides a greater surface area and a larger number of grain:matrix interfaces. There are more opportunities for dislocation of the clay matrix and between the clay matrix and the surface of the granular particles. Cycling compressive and tensile stresses in the rolling plastic limit test will seek out these weaknesses preferentially in the soils with the smaller granular particles, causing the soil to become brittle at higher water contents and lower maximum toughnesses.

TESTS ON CERAMIC CLAYS

In the ceramics industry the manufacturers of products ranging from tiles to tableware refer to the use of clay 'bodies'. Mixing two or more different clays together is a common practice with other ingredients such as quartz, grog[2] and other fluxing agents added to provide adequate green strength[3], low shrinkage and good firing properties. The clay types and proportions are usually chosen for their firing properties, finished colour and texture. However when these bodies are in the plastic form for moulding and shaping their toughness properties related to the water content will be important and will be determined by the clay types and proportions. To optimise energy efficiency in the manufacturing processes improved control of the mixing water contents that could be obtained from the toughness vs. water content relationships would be beneficial.

[2] Grog is ground up previously fired clay.
[3] Strength of the unfired, formed product.

The effects on toughness and the plastic limit of mixing two different clay types used in the ceramics industry are described in Barnes (2013a). For mixtures of known proportions by mass of two processed clays, a fireclay and a ball clay the toughness vs. water content relationships do not coincide with a linear interpolation between the relationships for the two clays on their own. Both clays have distinct soft-plastic and stiff-plastic regions with well-defined stiffness transitions. The toughness of the ball clay in the soft-plastic region (10 – 17 kJ/m^3) was much greater than for the fireclay (6 – 10 kJ/m^3) but when mixed together ball clay contents up to about 10% appear to have little effect on the toughness properties of the fireclay.

The proportion of the clay minerals from the ball clay in the total clay content of a mixture was found to be a useful property in assessing the test results.

The plastic limits of the mixtures also did not coincide with a linear interpolation between the two clays on their own. The presence of the ball clay in a mixture results in the toughness vs. water content relationship extending above the location where the maximum toughness would be expected to occur, giving lower plastic limits. With ball clay in the mixtures it is envisaged that interactions between the clay minerals can maintain a continuous strand arrangement and will subdue dislocations that would otherwise occur in the coarser fireclay to provide a higher maximum toughness at a lower plastic limit.

WORKABILITY IN THE CONSTRUCTION INDUSTRY

Prior to the introduction of the moisture condition apparatus (MCA) in the UK (Parsons and Boden, 1978) the main criterion used for the suitability of a clay fill material for use in earthworks construction was that the water content of the clay w must be less than the plastic limit multiplied by a factor (Barnes, 2010a)

$$w \leq w_P \times \text{factor} \tag{6}$$

With water contents greater than this value the clay fill would be deemed to be unacceptable for use. A factor of 1.2 in equation 6 was commonly adopted for most clay types to provide a clay fill with sufficient strength to maintain the trafficability of earthmoving scrapers (Arrowsmith, 1978). For the tests described in Barnes (2013a) adopting this factor would ensure toughnesses and strengths mostly in the stiff-plastic region. A factor of 1.3, considered to give a feasible maximum water content, has been adopted as the limit for ‘wet’ clay fill (Barnes, 2010a). It was found that the toughnesses and strengths then extend further into the soft-plastic region and this would require the use of lighter earthmoving plant.

For wide tracked, low pressure vehicles to move satisfactorily over a clay fill a limiting factor of 1.4 has been suggested (Farrar and Darley, 1975), although this factor would take the clay fill to the limits of acceptable workability. The ‘factor’ approach to the suitability of clay fills is seen to be feasible but was discontinued in the 1970s because of the poor accuracy of the plastic limit determination from the standard test.

WORKABILITY IN THE AGRICULTURAL CONTEXT

In the agricultural industry the water content of the surface soil in relation to its plastic limit, whether ductile or brittle and the toughness at water contents in the ductile state are paramount factors in determining the ability of agricultural equipment to carry out efficient operations. Unlike in the ceramics industry, where the ductile condition is required and water contents above the plastic limit are relevant, for agricultural purposes the soils are required to display friability and brittleness with water contents on the 'dry' side of the plastic limit.

Mueller et al. (2003) found that the optimum water content for tillage purposes was at 0.9 x w_p. Above this water content the soil would be too 'wet' because the soil is in a cohesive or mouldable state, air can easily be excluded and the soil would compact under the equipment, damaging the soil structure and texture. Other values such as the standard Proctor compaction test optimum water content w_{opt} and a consistency index I_c of 1.15 were also found to be appropriate values for optimum tillage, particularly for shallow tillage.

For deeper working, such as ploughing Müeller et al. (2003) also found the workability limit coincided with an arbitrary 'stickiness' limit at a consistency index of 0.75, or a liquidity index of 1.25 when operation of equipment was significantly affected by smearing and adhesion from the soil.

Utomo and Dexter (1981) found that for two sandy loams the friability of the soils was greatest at water contents approximately equal to their plastic limits. Hoogmoed et al. (2003) described a 'wet workability limit' to identify suitable working conditions. Although they used sophisticated tests to determine properties such as the air permeability and the suction-water content relationship they found that the wet workability limit for a loam and a clay soil lay very close to the plastic limits of these soils. Thus, in agriculture if the water content lies above the plastic limit damaging compaction is likely.

Concerning the behaviour of soils under the action of a plough Campbell et al. (1980) measured the draft force on a tine pushed through a clay soil to represent the ploughing mechanism and found that the draft force was highest at the plastic limit when the clay was at its toughest, with a plastic failure mechanism. The draft force was lower at water contents above the plastic limit when the clay would have lower toughness and at water contents below the plastic limit when brittle failure occurred.

REFERENCES

Ahmed, S., Lovell, C. W. & Diamond, S. (1974). Pore sizes and strength of compacted clay. *ASCE, Journal of the Geotechnical Engineering Division*, 100(GT4), April, 407-425.

Andrade, F. A., Al-Qureshi, H. A. & Hotza, D. (2011). Measuring the plasticity of clays: A review. *Applied Clay Science, 51*, 1 -7.

Anon. (n.d.). *Unified Soil Classification System: field method*. Department of Sustainable Natural Resources, New South Wales, Australia.

Anon. (1993). *Soil Survey Manual Chapter 3 Examination and description of soils*. Soil Conservation Service, US Dept. of Agriculture. Natural Resources Conservation Service, Handbook 18, Soil Survey Division Staff.

Arrowsmith, E. J. (1978). Roadwork fills – a material engineer's viewpoint. *Proceedings Clay Fills Conference*, ICE, London, 25-36.

Astbury, N. F., Moore, F. & Lockett, J. A. (1966). A cyclic torsion test for study of plasticity. *Transactions British Ceramic Society, 65*, 435-461.

ASTM C181-11 *Standard test method for workability index of fireclay and high-alumina refractory plastics*. ASTM International, West Conshohocken, PA, USA DOI: 10.1520/C0181-11.

ASTM D2488 - 09a. (2009). *Standard Practice for Description and Identification of Soils (Visual-Manual Procedure)*. ASTM International, West Conshohocken, PA, USA DOI 10.1520/D2488-09A.

ASTM Standard *ASTM D3967-08 Standard Test Method for Splitting Tensile Strength of Intact Rock Core Specimens*. ASTM International, West Conshohocken, PA, USA DOI:10.1520/D3967-08.

ASTM (2010) D4318-10: *Standard Test Methods for Liquid Limit, Plastic Limit, and Plasticity Index of Soils*. ASTM International, West Conshohocken, PA, USA. doi:10.1520/D4318-10.

Atterberg, A. (1911). Uber die physikalische Bodenuntersuchung und uber die Plastizitat der tone. (On the physical testing of soil and the plasticity of clays). *Internationale Mitteilungen fur Bodenkunde*, *1*(1), 10-43.

Bain, J. A. & Highley, D. E. (1979). regional appraisal of clay resources – A challenge to the clay mineralogist. *International Clay Conference, Developments in Sedimentology*, *27*, 437 – 448.

Baran, B., Erturk, T., Sarikaya, Y. & Alemdaroglu, T. (2001). Workability test method for metals applied to examine a workability measure (plastic limit) for clays. *Applied Clay Science*, *20*(1-2), Sept, 53-63.

Barnes, G. E. (2009). An apparatus for the plastic limit and workability of soils. *Proc. Institution of Civil Engineers*, *162*(3), 175–185.

Barnes, G. E. (2010a). *Soil Mechanics, Principles and Practice*, Palgrave Macmillan, Basingstoke, UK.

Barnes, G. E. (2010b). *Apparatus and method for measuring plastic properties*. Patent No GB2443537.

Barnes G.E. (2013a). *The plastic limit and workability of soils*. PhD thesis, University of Manchester.

Barnes G. E. (2013b). An apparatus for the determination of the workability and plastic limit of clays. *Applied Clay Science*, 80-81, 281-290. doi.org/ 10.1016/j.clay.2013.04.014.

Bobrowski, L. J. Jr. & Griekspoor, D. M. (1992). Determination of the plastic limit of a soil by means of a rolling device. *Geotechnical Testing Journal*, *15*(3), Sept., 284-287.

BS1377:1990 *Methods of test for soils for civil engineering purposes, Part 2: Classification tests*. BSI, London, UK.

BS 5930:1999 *Code of practice for site investigations*, BSI, London, UK.

BS EN 14688-1:2002 *Geotechnical investigation and testing. Identification and classification of soil. Identification and description*. BSI, London, UK.

BS EN 14688-2:2004 *Geotechnical investigation and testing. Identification and classification of soil. Principles for a classification*. BSI, London, UK.

Burmister, D. M. (1970). Suggested methods of test for identification of soils. *ASTM, STP479*, ASTM International, West Conshohocken, PA, USA.

Cafaro, F. (2002). Metastable states of silty clays during drying. *Canadian Geotechnical Journal*, *39*, 992-999.

Carty, W. M. & Lee, C. (1996). *The characterization of plasticity*. Science of Whitewares. The American Ceramic Society, Columbus, OH, 89-101.

Casagrande, A. (1932). Research on the Atterberg limits of soils. *Public Roads 13*(8), 121-130, 136.

Casagrande, A. (1947). Classification and identification of soils. *Proceedings American Society Civil Engineers*, *73*(6), 783-810.

Cetin, H., Fener, M., Sollemez, M. & Gunaydin, O. (2007) Soil structure changes during compaction of a cohesive soil. *Engineering Geology*, *92*, 38 – 48.

Collins, K. & McGown, A. (1974). The form and function of microfabric features in a variety of natural soils. *Geotechnique*, *24*(2), 223-254.

De Oliveira Modesto, C. & Bernardin, A. M. (2007). Determination of clay plasticity: Indentation method versus Pfefferkorn method. *Applied Clay Science*, doi:2007.06.007.

Delage, P., Audiguier, M., Cui, Y-J. & Howat, M. D. (1996). Microstructure of a compacted silt. *Canadian Geotechnical Journal*, *33*, 150-158.

Diamond, S. (1970). Pore size distribution in clays. *Clays and Clay Minerals*, *18*, 7-23.

Dinsdale, A. (1986). *Pottery Science Materials, Process, and Products*. Ellis Horwood Limited Chichester.

Farrar, D. M. & Darley, P. (1975). *The operation of earthmoving plant on wet fill*. RRL Report LR688, Crowthorne, Berkshire.

Fitzjohn, W. H. & Worrall. W. E. (1980). Physical properties of raw brick clays. *Transactions and Journal of the British Ceramic Society*, *79*(3), 74-81.

Garcia-Bengochea, I., Lovell, C. W. & Altschaeffl, G. (1979). Pore distribution and permeability of silty clays. *ASCE, Journal of Geotechnical Engineering*, *105*(GT7), 839-856.

Göhlert, K. & Uebel, M. (2009). *Test methods for plasticity and extrusion behaviour*. Chapter 21, in Händle, ed., Extrusion in Ceramics. Springer-Verlag Berlin Heidelberg.

Heindl, R. A. & Pendergast, W. L. (1947). Reliability of "workability index" of fire-clay plastic refractories. *Journal of the American Ceramic Society*, *30*(11), 329-334.

ISO. (2004). CEN ISO/TS 17892-12:2004 *Geotechnical investigation and testing - Laboratory testing of soil - Part 12: Determination of Atterberg limits*. International Organization for Standardization**,** Geneva, Switzerland.

Karlsson, R. & Hansbo, S. (1981). Soil classification and identification. *Swedish Geotechnical Society*, Stockholm, Sweden.

Kessel, S. (1998). Ceramic rheology tester gets the thumbs up. *Material World*, *16*(8), 474-475.

Marshall, C. L. (1955). A new concept of clay plasticity. *Ceramics Bulletin*, *34*, 54-56.

McDowell, S. J. (1928). Notes on a method for determination of workability of plastic clays. *Journal of the American Ceramic Society*, *1*(2), 99-102.

Mitchell, J. K. (1956). The fabric of natural clays and its relation to engineering properties. *Proc. Highways Research Board*, *35*, 693-713.

Moore, F. (1963). Two instruments for studying the plasticity of clays. *Journal of Scientific Instruments*, *40*, 228-231.

Müeller, L. Schindler, U. Fausey, N. R. & Lal, R. (2003). Comparison of methods for estimating maximum soil water content for optimum workability. *Soil and Tillage Research, 72*(1), July, 9-20.

NAVFAC. (1986). *Soil Mechanics Design Manual 7.01*. Naval Facilities Engineering Command, Alexandria, Virginia, USA.

Norton, F. H. (1938). An instrument for measuring the workability of clays. *Journal American Ceramic Society, 21*, 33-36.

Parsons, A. W. & Boden, J. B. (1979). *The moisture condition test and its potential applications in earthworks*. TRRL Supplementary Report 522. TRRL, Crowthorne, Berkshire.

Parsons, A. W. & Darley, P. (1982). *The effect of soil conditions on the operation of earthmoving plant*. TRRL Report LR 1034, Department of Transport, Crowthorne, Berks.

Reeves, G. M., Sims, I. & Cripps, J. C. (eds). (2006). *Clay Materials Used in Construction*. Geological Society, London, *Engineering Geology Special Publication, 21*.

Ryan, W. & Radford, C. (1987). *Whitewares Production, Testing and Quality Control*. The Institute of Ceramics. Pergamon Press, Oxford.

Schwartz, B. (1952). Fundamental study of clay: XII, A note on the effect of the surface tension of water on the plasticity of clay. *Journal American Ceramic Society, 35*(2), 41-43.

Sivakumar, V., Tan, W. C., Murray, E. J. & McKinley, J. D. (2006). Wetting, drying and compression characteristics of compacted clay. *Geotechnique, 56*(1), 57-62.

Tanaka, H., Shiwakoti, D. R., Omukai, N., Rito, F., Locat, J. & Tanaka, M. (2003). Pore size distribution of clayey soils measured by mercury intrusion porosimetry and its relation to hydraulic conductivity. *Soils and Foundations, 43*(6), 63-73.

West, R. R. & Lawrence, W. G. (1959). The plastic behavior of some ceramic clays. *Ceramics Bulletin, 38*(4), 135-138.

Wood, D. M. (1990). *Soil behaviour and critical state soil mechanics*. Cambridge University Press, Cambridge. England.

Worrall, W. E. (1982). *Ceramics Raw Materials*. Second Revised Edition. Institute of Ceramics Textbook Series, Pergamon Press, Oxford.

In: Clays and Clay Minerals
Editor: Liam R. Wesley
ISBN: 978-1-63117-779-8

Chapter 7

INFLUENCE OF TEMPERATURE, pH AND IONIC STRENGTH IN THE ABILITY TO REMOVE THE DYE REACTIVE NAVY BLUE USING BENTONITE CLAY/CHARCOAL COMPOSITE BY FACTORIAL DESIGN

Neucineia Vieira Chagas*[*], *Jeferson Meira Santos, Maria Lurdes Felsner, Marcos Roberto da Rosa and Karin Cristiane Justi
Department of Chemistry, Campus Cedeteg,
Universidade Estadual do Centro-Oeste, Guarapuava, Brazil

ABSTRACT

In the last decades, our planet has been systematically harmed by contamination processes, mainly by the industrial activity. Within such context, the textile industry is responsible by the generation of great amount of highly colored effluents, composed of dyes which are harmful both for men and the environment. Amongst the several methods of dyes removal, adsorption has been increasingly applied, due to low cost and simplicity of this this technique. Therefore, the development and study of low cost adsorbent materials with good adsorption capability have been carried out. Nowadays, hybrid materials present great appeal, as they have unique features, which are not seen in the precursors when isolated. Clays are amongst the most used materials, as they are low cost material and have lamellar structure which might serve as a support to other substances interlayer in the preparation of mixed materials. In this study, a composite material obtained from the mixture of bentonite clay and *pinus* activated charcoal, which presented very interesting properties regarding reactive dye adsorption, was used. In order to evaluate the composite adsorption potential to remove dyes in aqueous solution, a reactive navy blue dye was used and some parameters which influence the process, such as pH, ionic strength and temperature were evaluated by factorial design. Results

[*] Corresponding author, e-mail: neucineia@uol.com.br.

revealed that all variables under study influenced the reactive navy blue dye adsorption process, as well as the interaction between pH and temperature, ionic strength and temperature and also amongst the three variables. Thus, the results of experimental design showed that the variables pH, ionic strength and temperature cannot be studied separately. Besides this, it enabled reduction in the number of experiments carried out.

INTRODUTION

Due to the textile industry widespread, a significant increase in the production of effluents containing dyes has been noticed. Such dyes employed in the textile industry represent the main source of pollution through coloring compounds, once about 15 % of this element is released into the effluent during the dying process [1]. Textile industries consume high amounts of water and chemical products, mainly in the coloring and finishing processes. The chemical reagents used by the textile industry vary in their chemical composition, ranging from inorganic to polymeric compounds. The contamination through these compounds is harmful to the aquatic life, causing serious environmental problems [2]. Besides that, studies have shown that some dye classes, mainly azocolorants, and their byproducts, might be carcinogenic and/or mutagenic [3].

It is estimated that 10.000 dyes are produced annually such as reactive, acid, basic and disperse dyes, and all them present as a common property the light absorption in the visible region, due to the chromophore groups such as nitro, nitrous, azo and carbonyl. The reactive dyes present an electrophilic group able to form covalent bonds with the hydroxyl groups in cellulosic fibers, with amino, hydroxyl and thiol groups of the protein fibers, as well as with the polyamide amino groups [1,4,5].

The azo reactive dyes are characterized by the presence of one or more groups –N=N- bonded to aromatic groupings; these are largely used, representing around 30% of the dye market. The Remazol line is composed of reactive dyes that have in their structure a sulphate-ethylsulfonic group ($SO_2CH_2CH_2$-OSO_3H), which forms a strong covalent bond with the substituent groups present in the textile fiber [6,7,8].

Due to the solubility of most dyes in water, the stability to photo-degradation, biodegradation and the action of oxidant agents, increasing investigation has been carried out on physical or chemical methods to remove the color or colored effluents. Among these methods, the adsorption has outstood for its action to decolorize textile effluents, and also for being a low cost and easy technique [2].

The adsorption is a physico-chemical process in which certain components of a fluid phase (gas or liquid) are transferred (adsorbed) to the surface of a solid (adsorbent). The concept of adsorbent is usually applied to a solid that keeps the solute on the surface through the action of physical forces, and the substance absorbed is called adsorbate. Several factors affect the adsorption process such as temperature, pH and ionic strength [9].

In the last 50 years the interest in clays as well as their composites and carbon materials to be used in the treatment of industrial effluents has increased [10]. Composites are materials formed from the combination of two or more constituents, present synergic properties, which differ from those of the individual components. According to this principle of combined action, these materials present unique properties, which are difficult to be obtained from the individual components when isolated [11].

Studies using factorial design has been useful to reducing the number of experiments. The reported study in the literature was conducted the assessment of the best conditions for adsorption of contaminants on activated charcoal powder obtained from a palm typical Malaysian using 2^3 factorial design. This study was evaluated the response of activated charcoal on adsorption of phenol by varying of the temperature, contact time and activation gas flow [12].

The objective of this study was to prepare a composite from clay and activated charcoal and apply it to the adsorption of the navy blue reactive dye. A 2^3 factorial design was employed to evaluate the variables which are relevant to the adsorption process.

MATERIALS AND REAGENTS

The sodic bentonite Clay used in the study was the Argel T ($Argel_{100}$), commercialized by the Buntech Tecnologia de Insumos Ltda (Brazil). According to the supplier, this clay presents thixotropic and anti-settling properties. Its composition is 63 % (m/m) SiO_2, 18 % (m/m) Al_2O_3, 4 % (m/m) Fe_2O_3, 3 % (m/m) MgO, 2 % (m/m) CaO, 2,5 % (m/m) Na_2O, < 1 % (m/m) TiO_2. The pulverized Pinus activated charcoal ($Charcoal_{100}$) was obtained from the supplier Alphacarbo Industrial Ltda (Guarapuava, Brazil). In the adsorption study, the navy blue Remazol reactive dye was employed supplied by Dystar Indústria e Comércio de Produtos Químicos Ltda.

The textural properties of the precursors $Charcoal_{100}$ and $Argel_{100}$ obtained by the BET tecnique indicate specific area (S_{BET}), external surface area (S_{ext}), micropore surface area (S_{mic}), micropore volume (V_{mic}), pore diameter (D_p) which are shown in Table 1.

All chemical reagents used were of analytical grade and the solutions were prepared with ultra-pure water, resistivity equal 18,2 MOhm (HUMAN90®).

Table 1. Textural properties of precursors $Charcoal_{100}$ and clay $Argel_{100}$

Properties	$Charcoal_{100}$	$Argel_{100}$
S_{BET} ($m^2\ g^{-1}$)	632.24	51.53
S_{ext} ($m^2\ g^{-1}$)	227.5	36.53
S_{mic} ($m^2\ g^{-1}$)	404.66	14.99
V_{mic} ($cm^3\ g^{-1}$)	0.188	0.0067
D_p (Å)	41.36	92.31

COMPOSITE PREPARATION

The composite were prepared from samples of activated charcoal and clay Argel T, without prior chemical treatment. They were initially dried at 110 °C for 24 hours. Then mixtures of clay and charcoal were prepared, resulting in composition of 50 mass % of charcoal and 50 mass % of dry clay. Next, an aqueous dispersion of the mixtures was prepared under constant agitation for 15 minutes at ambient temperature. Subsequently, the dispersion was allowed to stand for 24 hours and then dried in an oven at 110 °C for 24 hours.

The sample was then calcined for 30 minutes, in a muffle furnace at 500 °C, being temperatures at which the clay does not lose its thixotropic properties. The composite samples obtained were pulverized and standardized using a sieve number 70–400 mesh (ABNT – Brazilian Association for Standards and Techniques).

ADSORPTION TESTS

The adsorption tests were performed using a stock solution of dye with 200 mg L^{-1} concentration, pH 5, with controlled temperature at 25 °C and constant agitation of 150 rpm for 3 hours and mass of adsorvent of 300 mg. Measurements used a UV/Vis spectrophotometer SP 2000 UV – Spectrum, with 616 nm wavelength which corresponds to the maximum of the dye adsorption.

Then samples were filtered at once for simple quantitative filter paper with black belt filter, and in the supernatant were determined and the absorbance signals and final pH of the solution. The adsorbed amount (q, mg g^{-1}) dye was obtained from the difference between the initial concentration (C_i) (mg L^{-1}) and the end concentration (C_f) of the dye solution, the mass of adsorbent (g) used and by the volume (L) of the solution according to the equation [13,14]:

$$q = (C_i - C_f)\ (V / m)$$

FACTORIAL DESIGN STUDY

The influence of variables such as pH, temperature and ionic strength in the adsorption of navy blue reactive dye by composite was investigated by the 2^3 factorial design, each factor being assessed at two levels. The dye absorbance readings adsorbed by the composite were carried out randomly for all combinations of the levels of factors presented in Table 2.

Table 2. Factors and levels of the 2^3 factorial design study

Factor	Level (-)	Level (+)
pH (1)	2.0	uncontrolled
Temperature (°C) (2)	30	50
Ionic Strength (3)	0	0.10

The effects of factorial design were calculated through: $E_f = (\bar{R}_+) - (\bar{R}_-)$ where ($\bar{R}_+$) and ($\bar{R}_-$) are the averages at the (+) and (-) levels of the factors involved.

The factor effects on adsorption of the dye by the composite were tested for the statistical significance by Pareto plot 95 % confidence level. All the statistical analyses were carried out using the software “Minitab for Windows 16”.

RESULTS AND DISCUSSION

Several studies have been carried out on the adsorption of dyes by clay and activated charcoal [12;15]. Hence, the current work includes investigations to evaluate the potential of the composite prepared from these materials for adsorption of a reactive dye. In preliminary study, the composite presented better performance than charcoal and clay in the removal of the navy blue reactive dye, with 70 % of removal. The charcoal showed removal efficiency of 56 % while the bentonite clay Argel T did not presente adsorption for this reactive dye.

In any adsorption processes, the main parameters to be considered are the dye concentration, pH, particle size, contact time, temperature, agitation speed and salt addition. For the navy blue reactive dye, the relations between adsorption efficiency and the variables temperature, pH, and ionic strength (through the addition of a 0.10 mol L^{-1} potassium chloride solution) were investigated.

Table 3 shows the results obtained from the replicate of the 2^3 factorial design to remove the navy blue reactive dye by the adsorbent.

The analysis of data presented in Table 3 revealed that except for the tests two and four, all the others presented removal efficiency higher than 90 %. The composite is shown to be promising once its performance in removing the navy blue reactive dye in most tests was satisfactory. Therefore, the material becomes interesting once it aggregates value to the clay which is an abounding natural resource. In a previous work, the adsorption efficiency for methylene blue dye (not reactive) for the composite material using bentonite clay Volclay trated at 500 °C exhibited an efficiency of 84 % [14]

Table 3. Result obtained from the 2^3 factorial design matrix to remove the navy blue reactive dye by composite. Conditions: dye concentration 200 mg L^{-1}, 300 mg adsorbent, 150 rpm, 25±1 ºC, 50.00 mL, 3 hours

Tests	pH*	Temperature (° C)	Ionic Strength	q ± SD** (mg g^{-1})
1	(-) 2.0	(-) 30	(-) 0.0	30.32 ±0.13
2	(+)uncontrolled	(-) 30	(-) 0.0	11.07 ±0.07
3	(-) 2.0	(+) 50	(-) 0.0	31.19 ±0.07
4	(+)uncontrolled	(+) 50	(-) 0.0	19.80 ±0.02
5	(-) 2.0	(-) 30	(+) 0.10	32.08 ±0.35
6	(+)uncontrolled	(-) 30	(+) 0.10	31.01 ±0.04
7	(-) 2.0	(+) 50	(+) 0.10	32.69 ±0.16
8	(+)uncontrolled	(+) 50	(+) 0.10	32.31 ±0.03

*(+)uncontrolled pH = 5.0.

**SD: standard deviation.

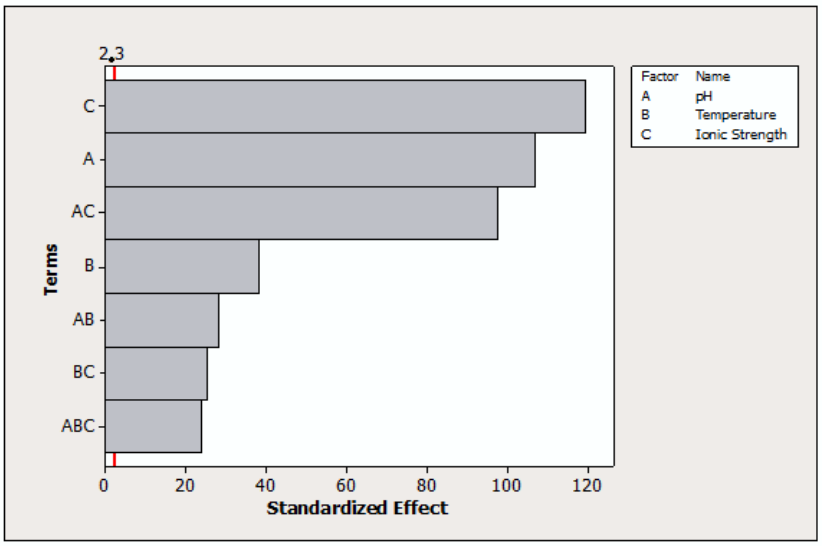

Figure 1. Pareto plot at 95 % confidence level of the effects of 2^3 factorial design.

In the study carried out to evaluate the adsorption process using the green coconut mesocarp to remove reactive gray dye presented in the literature [15], the 2^3 factorial design was used to assess the influence of the variables adsorbent mass, agitation ratio and adsorbent granulometry and thus obtain the best working conditions. As a result of the factorial design, it was observed that the highest *q* value was 18.7 mg g^{-1} when the adsorbent mass used was 100 mg, granulometry <0.419 mm and 30 rmp agitation. These conditions were employed in the kinetic and chemical equilibrium study. In this study, a 2^3 factorial design was used to evaluate the influence of factors temperature, pH, ionic strength, temperature and the interaction between them in the removal of navy blue reactive dye by composite prepared. The results are shown in the Pareto plot (Figure 1).

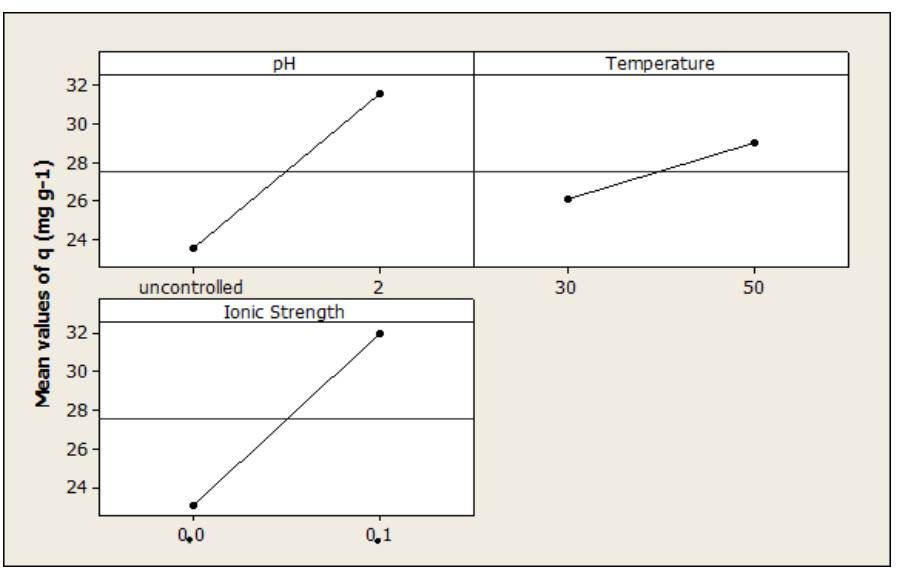

Figure 2. Main effects plot of 2^3 factorial design.

The Pareto plot shows that all variables under study are significant in the navy blue reactive dye adsorption as well as the interactions: pH and temperature, temperature and ionic strength and that there is interaction among the three variables. Thus, it was seen that the variables cannot be analyzed separately. Figure 2 shows that there is increase in the adsorption capability when the pH is equal 2.0, which is an interesting result regarding its application to the removal of dyes from residual water. This can be justified, because at acid pH the material surface is positively charged, thereby attracting $-SO_3$ groups present in the dye structure (Figure 3) promoting higher adsorption capability, Al-Degs et. al. (2000.2008) observed in their studies using activated charcoal as adsorbent of Yellow remazol, Black reamzol and Red remazol reactive dyes that at pH below 7.5 the surface of the adsorbent material would be positively charged, favoring in this case the adsorption of anionic dyes. It is also observed that adding salt concentration of 0.10 mol L^{-1}, and increasing the temperature from 30 °C to 50 °C the q values become higher, indicating an improvement in adsorption capability of the material adsorbent.

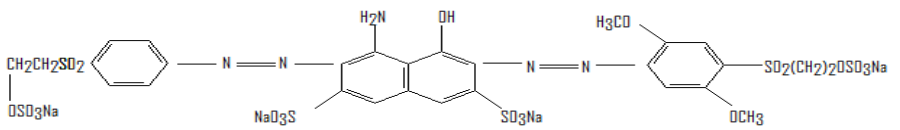

Figure 3. Molecular structure of reactive dye Navy [Tetrasodium-4-amino-6-[2,5-dimethoxy-4-(2-sulfoxyethylsulfonyl)phenylazol]-5-hidroxy-3-(4-(2-(sulfoxye thylsulfonyl)phenylazo)naphtalelene-2,7-disulfonate] ($C_{28}H_{29}N_5O_{21}S_6.4Na$)[16].

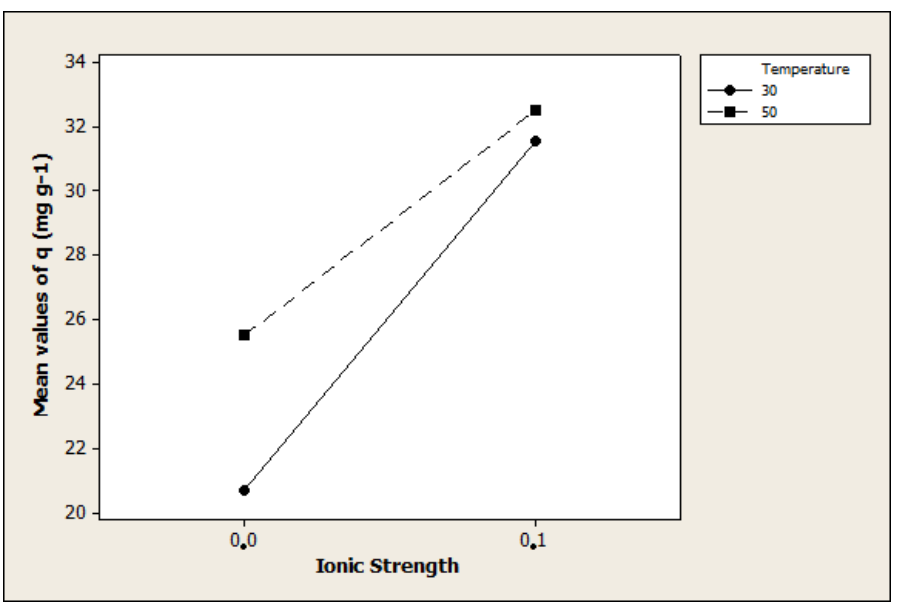

Figure 4. Interation effect plot between temperature and ionic strength of 2^3 factorial design.

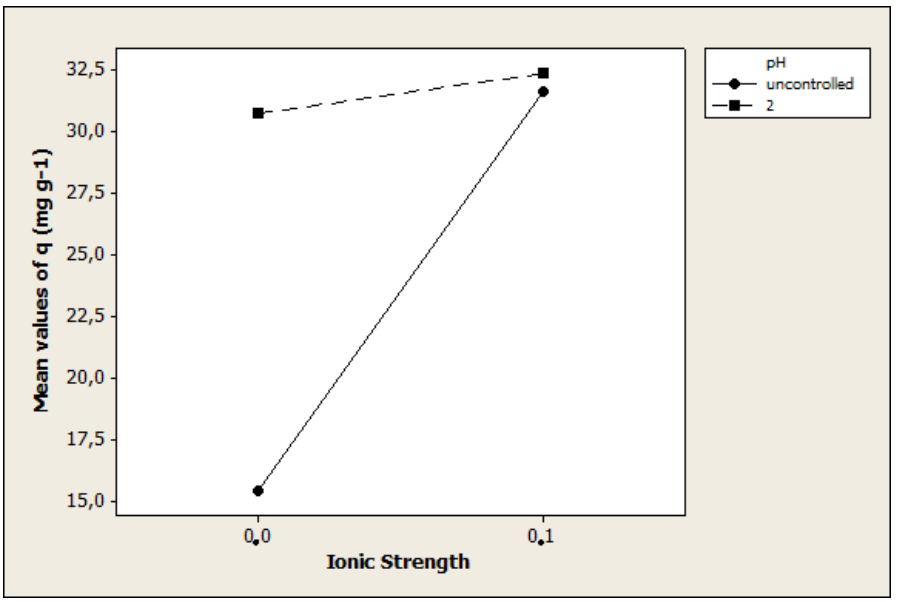

Figure 5. Interation effect plot between pH and ionic strength of 2^3 factorial design.

Results in Figure 4 presented the effect interaction between the variables temperature and ionic strength, where it is seen that with and without salt addition, there is an increase in the adsorption capability of the navy reactive dye with increased temperatures of 30 °C for 50 °C. However, without the addition of KCl and in the temperature of 50 °C there seems to be higher dye adsorption by the adsorbent compared to studies with salt added.

It was also observed that the ionic strength promoted by the addition of potassium chloride led to a significant contribution to the dye adsorption by the composite. This effect suggests that the presence of salt, in the form of KCl, favors the electrostatic interaction of the anionic dye by the adsorbent surface positively charged, thus increasing the capability of adsorbent for adsorption by the navy blue reactive dye.

In this study, the significant effect of the interaction between the variables pH and ionic strength was observed, that is, these variables cannot be assessed separately. The effect of interaction between pH and ionic strength (Figure 4), revealed that, without the pH control, there was increase in the adsorption capability for the ionic strength of 0.10 mol L^{-1}. This result can be interesting for industrial application, where the pH is close to 5, because there is no need to change the pH of the solution for effective adsorption of navy blue dye. Again, these results indicate that the addition of salt, or by changing the ionic strength of the solution to 0.1 mol L^{-1} is improved electrostatic interaction between the dye and the surface of the composite, increasing the adsorption capability in nearly 2 times. Regarding pH 2.0, there was no significant increase in the *q* value with the addition of salt and may be seen that occurs a slight improvement in the adsorption capability. In this case, since the adsorbent surface is positively charged, due to the acidic pH of the solution, therefore the effect of the salt addition was not as significant.

It can be seen in Figure 6 the results for the interaction between the three variables: pH, temperature and ionic strength. It is observed that the adsorption of the navy blue reactive dye by the composite presented better results without control of the pH, ionic strength of 0.1 mol L^{-1} and temperature of 50 °C. However, it can be seen that the experiments that presented

better q values (32.310 and 31.010 mg g^{-1}) are observed for both temperatures studied, which suggests that the temperature in these test conditions did not influence significantly the present process of adsorption and could be 30 °C or 50 °C.

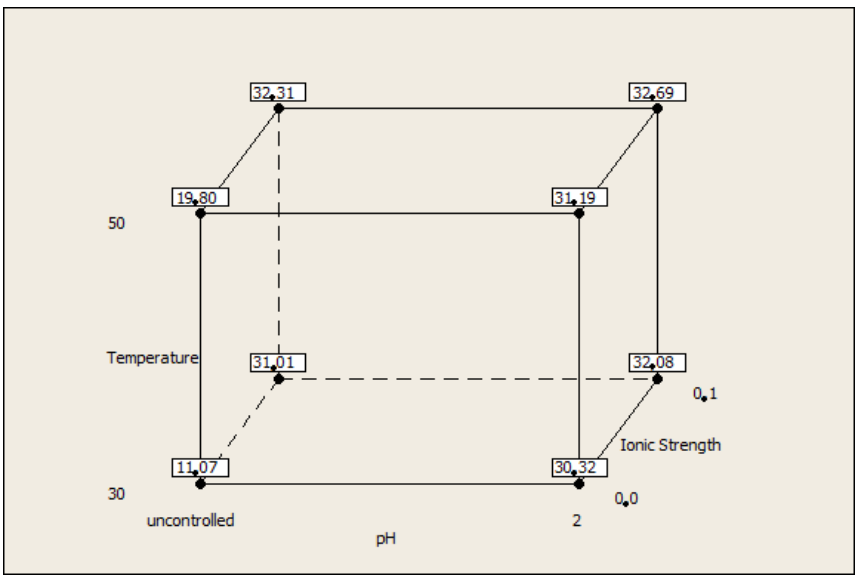

Figure 6. Interaction effect plot between pH, temperature and ionic strength of 2^3 factorial design.

CONCLUSION

The factorial design results revealed that the temperature, pH and ionic strength variables influenced the dye adsorption process by the composite under study, and that a significant interaction effect was observed between the three variables studied, suggesting that these cannot be optimised independently. These results might be advantageous for specific industrial use.

REFERENCES

[1] Guaratini, C. C. I. ; Zanoni, M. V. B.; (2000) Corante Têxteis. *Química Nova*, 23(1).

[2] Khaled, A.; EL Nemr, A.; El-Sikaily, A.; Abdelwahab, O.; (2009) Removal of direct N Blue-106 from artificial textile dye effluent using activated carbon from orange peel: Adsorption isotherm and kinetic studies. *Journal of Hazardous Materials*, 165, p. 100-110.

[3] Kunz, A.; Zamora, P. P.; Moraes, S. G.; Durán, N.; (2002) Novas tendências no tratamento de efluentes têxteis. *Química Nova*, 25, p. 78-82.

[4] Bulut, E.; Özacar, M.; Sengil, I. A.; (2008) Adsorption of malachite green onto bentonite: equilibrium and kinetic studies and process design. *Microporous and Mesoporous Materials*, 115, p. 234-246.

[5] Nandi, B. K.; Goswami, A.; Purkait, M. K.; (2009) Removal of cationic dyes from aqueous solutions by kaolin: kinetic and equilibrium studies. *Applied Clay Science*, 42, p. 583-590.

[6] Catanho, M.; Malpass, P. G. R.; Motheo, A. J.; (2006) Avaliação dos tratamentos eletroquímicos e fotoeletroquímico na degradação de corantes têxteis. *Química Nova*, 29, p. 983-989.

[7] Pearce, C. I.; Lloyd, J. R.; Guthrie, J. T.; (2003) The removal of colour from textile wastewater using whole bacterial cells: a review. *Dyes and Pigments*, 58, p. 179-183.

[8] Kimura, I. Y. ; Fávere, V. T.; Laranjeira M. C. M.; Josué, A.; Nascimento A.; (2000) Avaliação da capacidade de adsorção do corante reativo laranja 16 pela quitosana *Acta Scientiarum* 22(5): 1161-1166.

[9] Eastoe, J.; Dalton, J. S.; (2000) Dynamic surface tension and adsorption mechanism of surfactants at the air – water interface; *Adv. Colloid Interf. Sci*. 85, 103.

[10] Bangash, F. K.; Alam, S.; (2009) Adsorption of acid blue 1 on activated carbon produced from the wood of Ailanthus altissima. *Brazilian Journal of Chemical Engineering*, 36, 275–285.

[11] Anaissi, F. J.; Demets, G. J. F.; Toma, H. E.; Dovidauskas, S.; Coelho, A. C. V.; (2001) Characterization and properties of mixed bentonite–vanadium(V) oxide xerogels. *Materials Research Bulletin*, 36, 289–306.

[12] Alam, Md.Z.; Ameem, E.S.; Muyibi, S.A.; Kabbashi, N.A.; (2009) The factors affecting the performance of activated carbon prepared from oil palm empty fruit bunches for adsorption of phenol. *Chem. Eng. J.*, 155, 191–198.

[13] Coelho, A.C.V.S.; Santos, P. S.; Santos, H.S.S.; (2007) Argilas especiais: o que são, caracterização e propriedades. *Quim Nova*, v. 30, n.1, 146-152.

[14] Chagas, N.V.; Quinaia, S.P.; Anaissi, F.J.; Santos, J.M.; Felsner, M.L.; Justi, K.C.; (2014) Clay and charcoal composite: characterisation and application of factorial design analysis for dye adsorption. *Chem. Pap.*, 68 (4), 553-563.

[15] Brindley, G.W.; (1955) Structural Mineralogy of Clays, *Clays and Clays Technology Bulletin*, v.53, 169.

[16] Erden,E.; Ucar, M.C.; Gezer, T.; Pazarlioglu, N.K.; (2009) Screening for ligninolytic enzymes from autochthonous fungi and applications for descolorization of remazole marine blue. *Braz J Microbiol*, v.40, n.2, 346-353.

[17] Al-Degs, Y.S., Khraisheh, M. A. M., Allen, S. J., & Ahmad, M. N.; (2000) Effect of carbon surface chemistry on the removal of reactive dyes from textile effluent. *Water Research*, 34, 927–935. DOI: 10.1016/s0043-1354(99)00200-6.

[18] Al-Degs, Y.S., El-Barghouthi, M. I., El-Sheikh, A. H., & Walker, G. M.; (2008) Effect of solution pH, ionic strength, and temperature on adsorption behavior of reactive dyes on activated carbon. *Dyes and Pigments*, 77, 16–23. DOI: 10.1016/j.dyepig.2007.03.001.

In: Clays and Clay Minerals
Editor: Liam R. Wesley
ISBN: 978-1-63117-779-8

Chapter 8

USING SIMPLEX LATTICE EXPERIMENTAL DESIGN TO OPTIMIZE CLAY BRICK FORMULATION

A. Z. Destefani[1] and J. N. F. Holanda[2]
[1]Fluminense Federal Institute, Campos dos Goytacazes-RJ, Brazil
[2]Northern Fluminense State University, Laboratory of Advanced Materials/
Group of Ceramic Materials, Campos dos Goytacazes-RJ, Brazil

ABSTRACT

Since ancient times that the fired clay bricks have been used as building materials. In general, the common clays are the most widely used raw materials for clay bricks. It is known fact that the clay brick bodies are empirically formulated with clays of different technical characteristics. This empirical approach makes the economically unviable industrial experiments, since the costs and execution time are high. On the other hand, the technological properties of clay bricks are influenced primarily by the combination of the raw materials and processing conditions. When the processing conditions are kept constant, the experimental design technique with mixture could be used to optimize the clay body formulation. In this context, the present chapter focuses on the use of experimental design in simplex lattice to optimize a clay brick formulation using two distinct sedimentary clays from south-eastern Brazil. Emphasis special is given on the effect of the clayey formulation on the technical properties of clay bricks.

Keywords: Clay bricks, formulation, experimental design, simplex-lattice

1. INTRODUCTION

It is well-known that since ancient times the clay bricks are used as ceramic building materials. The majority of the nations already have used the clay bricks for buildings [1, 2]. The main reasons for the large use of clay bricks as ceramic building materials are: 1) technical properties; ii) beauty; iii) little maintenance; and low cost. In particular, the technical properties more important of the clay bricks are [1, 3-5]: mechanical strength, water

absorption (open porosity), density, fire resistance, durability, good thermal insulation, non-combustible, and poor conductor.

The industrial processing of clay bricks is basically compound by three main steps [1, 3, 6]: preparation of the clayey bodies, conformation (extrusion, pressing or manual), and thermal treatment (drying and firing). The clay bricks are produced in a wide firing temperature range (~ 600 – 1100 ºC) using a slow-firing cycle (~ 1 ºC/min).

The raw materials for clay bricks are mainly common clays with varied colors after firing, which are very abundant worldwide [1, 3]. Clayey soils, soft slate, and shale can also be used. The common clays used in clay bricks are complex mixtures of clay minerals (kaolinite, illite/mica, montmorilonite, chlorite, etc) and nonclay minerals (quartz, gibbsite, goethite, calcite, dolomite, feldspar, phosphates, etc). In addition, organic matter and other crude impurities (stone, gravel, wood, etc) can also to be present. The common clays show a very broad range of chemical and mineralogical compositions (Table 1). One of the most important properties of the common clays is the development of plasticity when mixed with water, which gives favorable conditions for ceramic processing [3].

A key issue in the production of clay bricks is the clayey body formulation, which is included in the step of preparation of the clayey bodies. In general, the clay brick industry uses two or more common clays with different characteristics in the clay body formulation [11, 12]. These clays present different compositions of the clay fraction (clay minerals) and non clay fraction (non clay minerals), which influence strongly the technological properties and sintered microstructure of the clay bricks. However, the clay brick industry uses in the most of the countries an empirical approach in the clayey body formulation. This empirical approach makes the economically unviable industrial experiments, since the costs and execution time are high.

Table 1. Chemical composition of several common clays used by the clay brick industry (wt-%) [12-15]

Oxide	Common Clays			
	Brazil	Spanish	Italy	Morocco
SiO_2	40.31	66.68	45.20	50.80
Al_2O_3	32.15	19.28	11.90	19.20
Fe_2O_3	10.83	3.81	5.71	9.4
TiO_2	1.49	1.03	0.70	0.80
MnO	…	0.01	0.10	0.05
MgO	0.78	0.37	2.90	4.30
CaO	0.32	0.34	14.90	0.30
K_2O	2.37	1.93	2.30	4.30
Na_2O	0.62	0.34	0.80	1.60
P_2O_5	…	0.09	0.10	…
LOI *	11.03	5.94	16.30	8.30

* LOI: Loss on ignition.

On the other hand, the technological properties of clay bricks are influenced primarily by the clayey body formulation and processing conditions. This chapter focuses on the use of experimental design in Simplex lattice to optimize a clay brick formulation using two distinct sedimentary clays from south-eastern Brazil. The experimental design approach has been

used successfully in distinct fields [13, 14]. This approach is highly useful for measuring the effects (or influence) of one or more variables on the response of a process.

2. EXPERIMENTAL DETAILS

2.1. Common Clays

Two sedimentary clays used by a clay brick maker from south-eastern Brazil (Campos dos Goytacazes-RJ) were selected to clay brick body formulation. These common clays with distinct technical characteristics are named as: i) "weak clay"; and ii) "strong clay". The chemical composition of the clay samples was determined using X-ray fluorescence. The particle size distribution was determined by a combination of sieving and sedimentation procedures according to NBR 7181. The plasticity of the sedimentary clays was determined by the Atterberg method according to the NBR 6459 and NBR 7180 standardized procedures. The real density was determined by the picnometry method according to the NBR 6508 standard.

2.2. Clay Brick Processing

Clay brick compositions were prepared (Table 2) using mixtures with the "weak" clay and "strong" clay. The "weak" clay was partially replaced with 0, 10, 20, 30, 40, and 50 wt.% "strong" clay. The clayey bodies were dry mixed, homogenized using a cylindrical mixer during 30 min, and then sieved until the fraction passing in a 60 mesh (250 μm ASTM). The moisture content of the clayey formulations was adjusted to 7 % (moisture mass/dry mass).

The clay bricks were prepared by uniaxial pressing in a rectangular die (11.50 x 2.54 cm^2) under a load of 25 MPa. The resulting bricks were dried at 110 ºC for 24 h, fired at 800 ºC for 3 h, and then cooled to room temperature (24 h cold to cold). Heating and cooling rates have been controlled to simulate the actual firing process used in the clay brick industry.

2.3. Technological Properties

The following technological properties of the clay bricks were determined:

Linear Shrinkage (LS)

$$LS = l_d - l_f / l_f \times 100 \quad (1)$$

in which l_d is the length of the clay brick dried at 110 ºC and l_f is the length of the clay brick fired at 800 ºC.

Table 2. Compositions of the clay brick formulations (wt.%)

Samples	"Weak" Clay	"Strong" Clay
WC	100	0
WC10SC	90	10
WC20SC	80	20
WC30SC	70	30
WC40SC	60	40
WC50SC	50	50
SC	0	100

Water Absorption (WA)

$$WA = Wu - Wd / Wd \times 100 \quad (2)$$

in which Wu is the weight of the water saturated brick (immersed in boiling water for 2h) and Wd is the weight of the clay brick dried at 110 ºC.

Flexural Strength (FS)

$$FS = 3PL / 2bd^2 \quad (3)$$

in which P is the rupture load, L is the length between the supports, b is the wide of the fired brick, and d is the thickness of the fired brick.

2.4. Experimental Design

In this chapter the methodology of Simplex –lattice design [13, 15, 16] was used for clay brick body formulation using two distinct sedimentary clays. The proportions of the sedimentary clays for the tests were calculated mathematically. After the numerical model has been found for the response of interest, the experimental confirmation of the efficiency of the model generated by analysis of variance (ANOVA) has been obtained [17].

In the experiments of mixtures any variation that occurs in the components, it is expected a proportional variation in the response. That is, if the amounts of all components of the mixture are duplicated, the mixture will also be duplicated. The proportions of the various components of a mixture are not independent and obey the expression:

$$\sum_{i=1}^{q} x_i = 1{,}0 \quad (4)$$

in which the letter q represents the number of mixture components (or factors). The graphical representation of the expression (4) for two components (q = 2) is shown in Figure 1.

To evaluate the influence of the processing variables ("weak" clay content and "strong" clay content) on the technological properties (linear shrinkage, water absorption, flexural strength) of the clay bricks a two component Simplex-lattice design was proposed.

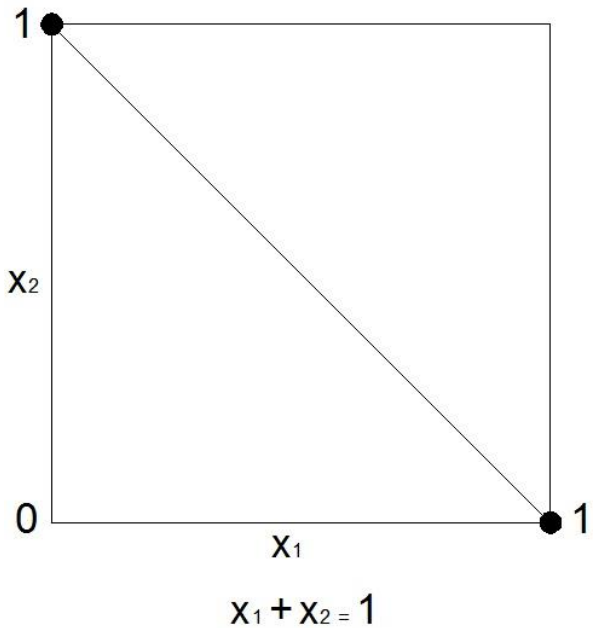

Figure 1. Representation of the Simplex-lattice to two components (response surface).

The response surfaces for each technological property were carried out with the software Statistica.

3. CLAY BRICK BODY FORMULATION

3.1. Characteristics of the Sedimentary Clays

The X-ray diffraction analysis of the "weak" clay sample is shown in Figure 2. The sample exhibited peaks that are characteristics of quartz (SiO_2), kaolinite ($Al_2O_3.2SiO_2.2H_2O$), gibbsite ($Al_2O_3.3H_2O$), goethite ($Fe_2O_3.H_2O$), and illite/mica. It can be observed that the "weak" clay is rich in quartz. In contrast, the "strong" clay from Campos dos Goytacazes-RJ are rich in kaolinite [18].

The chemical composition and loss on ignition of the clay samples are given in Table 3. SiO_2, Al_2O_3, and Fe_2O_3 are the major components, which correspond to about 82.73 % ("weak" clay) and 82.40 % ("strong" clay). However, the "weak" clay presented higher silica (SiO_2) content and lower loss on ignition.

Particle size distribution and real density of the clay samples are given in Table 4. As expected, the "strong" clay presented higher content of the clay fraction (< 2 μm). This indicates that the "strong" clay is rich in clay minerals, particularly of kaolinite particles. The "strong" clay also has higher real density.

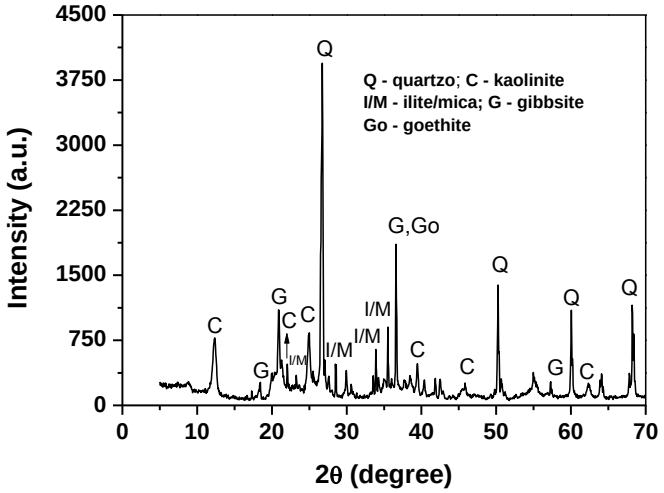

Figure 2. X-ray diffraction pattern of the "weak" clay.

Table 3. Chemical compositions of the sedimentary clays (wt.%)

Compounds	"Weak" Clay	"Strong" Clay
SiO_2	46.70	40.24
Al_2O_3	28.63	34.29
Fe_2O_3	7.40	8.21
TiO_2	2.21	1.34
MgO	-	0.62
CaO	0.98	0.12
K_2O	3.80	0.97
Na_2O	-	0.35
MnO	0.07	0.02
LOI	7.80	13.83

LOI = loss on ignition.

Table 4. Particle size distribution and real density of the clay samples

Samples	< 2 μm	2 ≤ x < 63 μm	63 ≤ x < 600 μm	Real density (g/cm^3)
"Weak" Clay	21	49	30	2.61
"Strong" Clay	40	42	18	2.65

Table 5. Atterberg consistency limits of the clay samples

Samples	UPL (%)	LPL (%)	PI (%)
"Weak" Clay	46	27	19
"Strong" Clay	59	31	28

The Atterberg consistency limits of the clay samples are given in Table 5. UPL and LPL are respectively the upper and lower plastic limits and PI is the plastic index, given by the difference between UPL and LPL. It can be seen that the "strong" clay presented higher

plastic index, proving to be more plastic than the "weak" clay. This is directly related to the higher content of the clay fraction. In fact, the greater the clay mineral content, the greater the plasticity of the clays [3].

3.2. Technological Properties of the Fired Bricks

The measured values of the technological properties (linear shrinkage, water absorption, and flexural strength) of the fired test specimens as a function of the clay body formulation are given in Table 6. It can be observed that the linear shrinkage for "strong" clay is higher than that of "weak" clay. This is related to a higher content of clay minerals, mainly kaolinite particles. Between 0 and 10 % "strong" clay a small reduction in linear shrinkage occurred. For additions above 10 wt.% "strong" clay, as a ruler, the values of linear shrinkage tends to increase. It should be emphasized that all the linear shrinkage values (0.39 – 0.70 %) are within the suitable range for clay bricks industrial production.

Table 6. Technological properties of the test specimens fired at 800 ºC

Property	Clay Body Formulation						
	WC	WC10SC	WC20SC	WC30SC	WC40SC	WC50Sc	SC
Linear shrinkage, %	0.52	0.39	0.49	0.54	0.51	0.53	0.70
Water absorption, %	24.19	23.84	23.53	23.66	23.73	23.50	23.35
Flexural strength, MPa	2.23	2.49	2.92	4.31	4.11	3.26	2.69

WC – weak clay; SC – strong clay.

It is found in Table 6 that the "strong" clay has lower water absorption. For additions up to 30 wt.% "strong" clay, a reduction in water absorption of the clay bricks occurred. Above 30 wt.% "strong" clay, however, the addition of "strong" clay tends to promote higher water absorption of the fired pieces. The WC30SC sample presented the lowest water absorption (21.06 %).

The results of the Table 6 also showed that the "strong" clay has higher flexural strength than "weak" clay. The WC30SC sample presented the highest value of mechanical strength 4.31 MPa). This is in accordance with the water absorption (open porosity).

3.3. Clay Brick Body Formulation Using Simplex Lattice Design

Tables 7 – 9 present the comparisons between the observed and predict values by the Simplex-lattice model for each technological property.

Table 7. Comparisons between the observed and predict values by the Simplex-lattice model for linear shrinkage

Experimental points		Responses		Error
Weak Clay	Strong Clay	Observed	Model	
1.0	0.0	0.52	0.51	0.01
0.9	0.1	0.39	0.50	0.11
0.8	0.2	0.49	0.50	0.01
0.7	0.3	0.54	0.51	0.03
0.6	0.4	0.51	0.51	0.00
0.5	0.5	0.53	0.53	0.00
0.0	0.0	0.70	0.70	0.00
Coefficient of determination (R^2) = 0.9149				

Table 8. Comparisons between the observed and predict values by the Simplex-lattice model for water absorption

Experimental points		Responses		Error
Weak Clay	Strong Clay	Observed	Model	
1.0	0.0	24.19	24.19	0.00
0.9	0.1	23.84	24.01	0.17
0.8	0.2	23.53	23.85	0.32
0.7	0.3	23.66	23.71	0.05
0.6	0.4	23.73	23.60	0.13
0.5	0.5	23.50	23.50	0.00
0.0	0.0	23.35	23.35	0.00
Coefficient of determination (R^2) = 0.9601				

Table 9. Comparisons between the observed and predict values by the Simplex-lattice model for flexural strength

Experimental points		Responses		Error
Weak Clay	Strong Clay	Observed	Model	
1.0	0.0	2.23	2.23	0.00
0.9	0.1	2.49	2.56	0.07
0.8	0.2	2.92	2.83	0.09
0.7	0.3	4.31	3.04	1.27
0.6	0.4	4.11	3.18	0.93
0.5	0.5	3.26	3.26	0.00
0.0	0.0	2.69	2.69	0.00
Coefficient of determination (R^2) = 0.8064				

These Tables also give the results of the analysis of variance (ANOVA) of the obtained regression equations. It can be observed that the coefficient of determination (R^2) are within the 0.8064 – 0.9601 range. The closer the unit is the value of R^2, the better the model fit to the observed data.

Pareto diagrams for the regression model of each technological property are presented in Figures 3-5. This diagram shows in a fast and efficient way the effects that are statically significant. Thus, the effects that are on the right of the dividing line (p = 0.5) should be considered in the mathematical model. Thus, the evolution of the technological properties (linear shrinkage – LS, water absorption – WA, and flexural strength – FS) against the

processing parameters ("weak" clay content and "strong" clay content) according with the methodology of Simplex-lattice design, obeys the following expressions:

$$LS = 0.213 – 0.052*x + 1.139*y + 0.352*x*x – 0.603*x*y – 0.655*y*y \quad (5)$$

$$WA = 24.747 + 1.05*x - 2.814*y – 1.603*x*x – 1.273*x*y + 1.417*y*y \quad (6)$$

$$FS = 1.974 – 1.448*x + 3.862*y + 2.167*x*x + 1.771*x*y – 3.609*y*y \quad (7)$$

The calculated response surfaces for each technological property (LS, WA, and FS) of the test specimens of the clay bricks fired at 800 ºC are presented in Figures 6 – 8. The response surfaces allowed the simultaneous assessment of both processing variables ("weak" clay content and "strong" clay content), and also the determination of the regions with best performance of the technological properties.

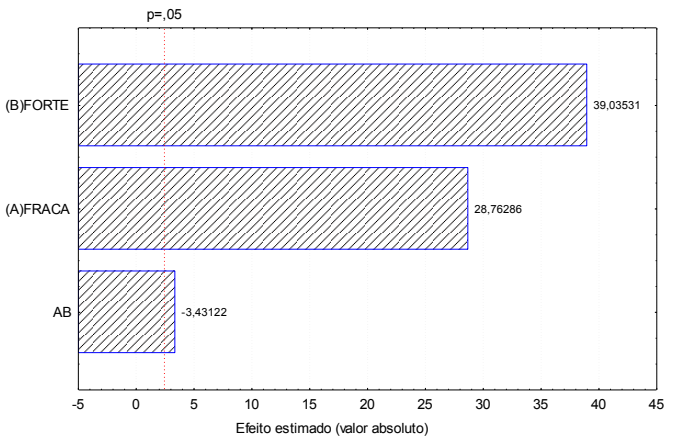

Figure 3. Pareto diagram for the linear shrinkage.

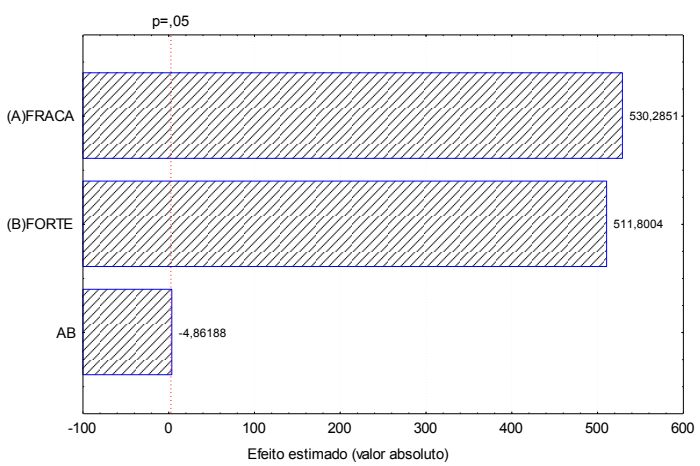

Figure 4. Pareto diagram for the water absorption.

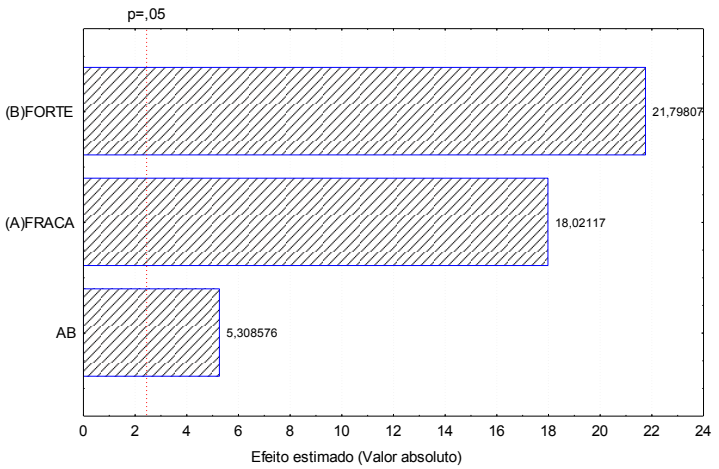

Figure 5. Pareto diagram for the flexural strength.

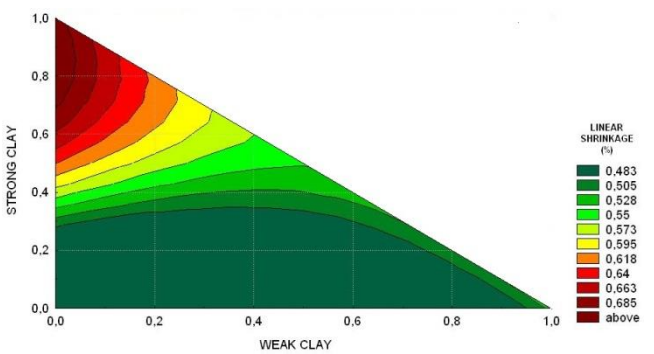

Figure 6. Response surface for the linear shrinkage.

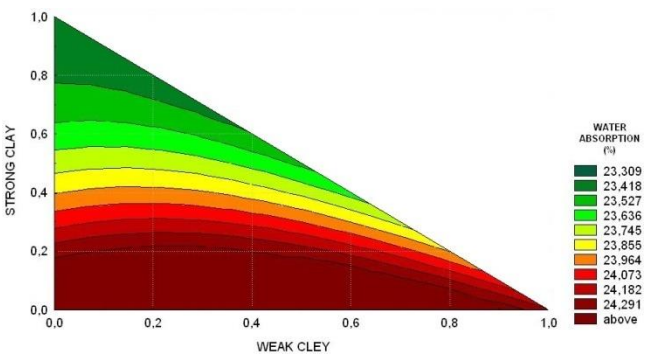

Figure 7. Response surface for the water absorption.

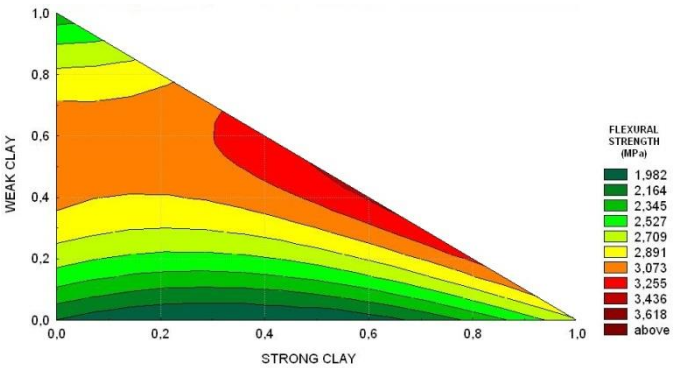

Figure 8. Response surface for the flexural strength.

It can be seen in Figs 6-8 that the partial substitution of "weak" clay with "strong" clay tends to influence the technological properties of the clay bricks. Thus, the results generated by the response surfaces for each technological property indicated that the most appropriate region for the clay brick body formulation using both sedimentary clays corresponds to "weak" clay with 30 – 50 wt.% of "strong" clay.

CONCLUSION

In this chapter the Simplex-lattice experimental design was used to optimize clay brick body formulation with two sedimentary clays from south-eastern Brazil. It has established that the "weak" clay is rich in quartz (lower plasticity), while the "strong" clay is rich in kaolinite (higher plasticity). In addition, the "strong" clay has higher linear shrinkage, higher mechanical strength, and lower water absorption. The use of Simplex-lattice experimental design proved to be a viable tool for clay brick body formulation using distinct sedimentary clays. According to the response surfaces, the "strong" clay influences the behavior of the "weak" clay and the technological properties of the clay bricks. The results also indicated that the most appropriate clay brick formulation with the sedimentary clays used is one compound of "weak" clay with 30 – 50 wt.% "strong" clay.

REFERENCES

[1] Santos, P.S. *Ciência e tecnologia de argilas*, 2nd ed. Edgard Blücher: São Paulo, SP, 1989, Vol. 1.

[2] Christine, B. *Masonry design and detailing*: *for architects and contractors*, 5th ed. Mc-Graw Hill: New York, 2004.

[3] Gomes, C.F. *Argilas - o que são e para que servem*, Fundação Calouste Gulbenkian: Lisboa, 1988.

[4] Lynch, G.C.J. Bricks: properties and classifications, *Structural Survey*, 1994, 13, 15-20.

[5] Mamlouk, J.P.; Zaniewski, M.S. *Materials for civil and construction engineers*, 2nd ed. Pearson Prentice Hall: New Jersey, 2006.

[6] Dondi, M. *Int. Ceram. J*. 2003, 55-59.
[7] Carretero, M.I.; Dondi, M.; Fabbri, B.; Raimondo, M. *Appl. Clay Sci*. 2002, 20, 301-306.
[8] Bauluz, B.; Mayayo, M.J.; Fernandez-Nieto, C.; Cultrone, G.; López, J.M.G. *Appl. Clay Sci*. 2003, 24, 121-126.
[9] Khalfaoui, A.; Hajjaji, M. *Appl. Clay Sci*. 2009, 45, 83-89.
[10] Saleiro, G.T.; Holanda, J.N.F. *Cerâmica*. 2012, 58, 393-399.
[11] Pracidelli, S.; Melchiades, F.G. *Cerâmica Industrial*, 1997, 2, 31-35.
[12] Motta, J.F.M.; Zanardo, A.; Cabral Jr, M.; Tanno, L.C.E.; Cichierato, G. *Cerâmica Industrial*, 2004, 9, 33-46.
[13] Cornell, J.A. *Experiments with mixtures: designs, models, and the analysis of mixture data.* 2nd ed., John Wiley & Sons: New York, 1990.
[14] Montgomery, D.C. *Design and analysis of experiments*. 4th ed., John Wiley & Sons: New York, 1997.
[15] Barros Neto, B.; Spacino, I.S.; Bruns, R.E. *Como fazer experimentos: pesquisa e desenvolvimento na indústria*, 2nd ed. Editora da UNICAMP: Campinas, 2003.
[16] Bahiense, A.V.; Manhães, R.T.; Alexandre, J.; Xavier, G.C.; Neves, S.N.; Vieira, C.M.F. Cerâmica, 2008, 54, 395-403.
[17] Calado, V.; Montgomery, D. *Planejamento de experimentos usando o Statistica*, E-papers Serviços Editoriais: Rio de Janeiro, 2003.
[18] Souza, G.P.; Sánchez, R.; Holanda, J.N.F. *Cerâmica*. 2002, 42, 102-107.

In: Clays and Clay Minerals
Editor: Liam R. Wesley
ISBN: 978-1-63117-779-8

Chapter 9

RECENT ADVANCES IN HYDRAULIC PERFORMANCE OF CLAY LINERS

M. T. Rayhani[1,•] and A. A. Aldaeef[1]
[1]Dept. of Civil and Environmental Engineering,
Carleton University, Ottawa, Canada

ABSTRACT

This chapter presents recent advances on the hydraulic performance of clay liners. Due to their low hydraulic conductivity, clay liners are used as hydraulic barriers in many engineering and environmental applications including earth dams, embankments, levees, landfills, and pond liners, to prevent leakage of water or leachate from reservoirs and/or landfills. The hydraulic performance of clay liners is related to the mineralogy, the manner of deposition and the exposure conditions, which could involve chemical exposure, potentially large physical stresses, thermal and freeze-thaw cycles, and elevated operating temperatures due to waste biodegradation in landfills. Changes in the clay hydraulic conductivity by several orders of magnitude have been reported in the literature upon exposure to thermal cycles or permeation with high-concentration leachate solutions. The latest findings on the hydraulic performance of clay liners under various field conditions such as daily thermal and wet-dry cycles, elevated temperatures, leachate exposure, and the combined effect of temperature and chemical exposure conditions are described. The hydraulic performance of composite liners (i.e., clay liner along with a layer of geomembrane) under simulated field conditions is also discussed.

Keywords: Clay liners, hydraulic conductivity, shrinkage, temperature, leachate

INTRODUCTION

Clay liners have long been used as hydraulic barriers in many engineering and environmental applications including earth dams, embankments, levees, landfills, and pond

• E-mail: mohammad.rayhani@carleton.ca.

liners to prevent leakage of water or leachate from reservoirs and/or landfills. The hydraulic performance of clay liners is related to the mineralogy, the manner of deposition and the stress history of the liner (Benson et al., 1999; Rowe et al., 2004). The field performance of a clay liner also depends on the exposure conditions, which could involve thermal and/or freeze-thaw cycles, chemical exposure, potentially large physical stresses, and elevated operating temperatures due to waste biodegradation in landfills. Exposure to solar radiation can result in moisture loss from the soil that could cause shrinkage and potential desiccation cracking. Clay liners might also be exposed to wet-dry cycles due to rainfall, and following dry spells. These weather circumstances can cause severe changes in the hydraulic performance of the liner. In landfill applications, clay liners would be exposed to the simultaneous effects of elevated temperature and leachate chemicals. The temperature is generated by organic waste biodegradation, which also is responsible for generating a considerable volume of landfill leachate. Temperatures of 60°C and 70°C were recorded in landfills in Germany (Collins, 1993) and Japan (Yoshida et al., 1996) 10 years and 6 years post-closure, respectively. Previous case studies in North America have also shown temperatures higher than 55°C at the bottom of the landfill close to the liner (Hanson et al., 2010; Rowe et al., 2010; Yeşiller et al., 2011).

Changes in the clay hydraulic conductivity by several orders of magnitude have been reported in the literature upon exposure to thermal cycles (e.g., Ayad et al., 1997; Yuen et al., 1998; Brian and Benson, 2001; Eigenbrod, 2003; Rayhani et al., 2007) or permeation with high-concentration leachate solutions (e.g., Quigley et al., 1988; Narasimha and Mathew 1995; Petrov et al., 1997; Shackelford et al., 2000; Elhajji et al., 2001; Allen, 2005; Frempong, 2006). Many researchers have also investigated the effects of elevated temperature on the hydraulic aspects of clay liners (e.g., Doll, 1997; Heibrock, 1997; Rowe, 1998; Yesiller and Yoshida, 2011; Hanson et al., 2010). The combined effect of temperature and chemical exposures on the hydraulic performance of clay liners has recently been investigated by Aldaeef and Rayhani (2014).

This chapter presents a review of recent research on the hydraulic performance of clay liners. More specifically, recent advances in understanding of the mechanisms affecting the hydraulic performance of clay liners under various field conditions such as daily thermal and wet-dry cycles, and the combined effect of temperature and chemical exposure conditions are presented. The hydraulic performance of composite liners (i.e., clay liner along with a layer of geomembrane) under simulated field conditions is also discussed.

HYDRAULIC PERFORMANCE OF CLAY LINERS WHEN EXPOSED TO WEATHER

For optimal performance, clay liners are usually hydrated and compacted at 2-3% wet of their optimum moisture contents. This procedure is believed to enable the breakdown of clay clods and the reduction of void volume which would eventually result in lower hydraulic conductivity. However, liners compacted at wet of optimum moisture contents would encounter larger mobilized pore water which might be lost upon desiccation when left exposed to the atmosphere, especially in dry regions. This would enhance the liner's desiccation and lead to larger volumetric shrinkage.

Shrinkage

Upon desiccation and evaporation, soils tend to lose a considerable amount of their moisture content. Reduction in water content of the soil leads to a decrease in pore-water pressure and a gradual increase in metric suction (Konrad and Ayad 1997; Nahlawi and Kodikara 2006; Tang et al., 2011). Outgoing water flow, which is caused by a gradient of pore water pressure, occurs through the surface as well as at certain depths within the soil. This upward water movement generates voids between soil particles. Following void generation, the soil particles are reorganized under an internal compression effect, which increases with an increase in soil suction. As a result, vertical and horizontal subsidence occurs causing a reduction in the soil matrix volume known as shrinkage (Albrecht and Benson 2001; Peron et al., 2009; Tang et al., 2011).

Early studies on soil shrinkage behaviour have identified three stages of soil shrinkage due to water evaporation; normal shrinkage, residual shrinkage, and zero-shrinkage (Haines, 1923). In the normal shrinkage stage, the total volumetric shrinkage is equal to the volume of water evaporated and the orientation of the soil particles remains the same as in the saturated condition. As evaporation proceeds, the tendency of the shrinkage curve changes and the soil particles are rearranged to occupy a smaller space. The residual shrinkage stage is reached when the soil particles come in contact with each other, and air enters the pores.

Eventually, due to the particle contact, no more volumetric reduction occurs and water loss at this time is equal to the volume of air flow. This stage is defined as the zero-shrinkage stage, or rigid stage (Haines, 1923). Clay content plays an important role in determining the shrinkage severity (Albrecht and Benson, 2001). Soils show residual shrinkage when they contain low clay contents, while normal shrinkage occurs over a broad range of water contents in soils with high clay contents (Fox, 1964; DeJong and Warkentin 1965; Bronswijk, 1988). Liquid limits and plasticity limits are the most used Atterberg limits, which can provide an indication of the percentage of clay fraction in the soil, as well as the mineral compositions. Higher clay contents lead to higher liquid limits and plasticity indices. Figure 1 shows the variation of volume shrinkage with plasticity indices for compacted clay specimens subjected to daily thermal cycles.

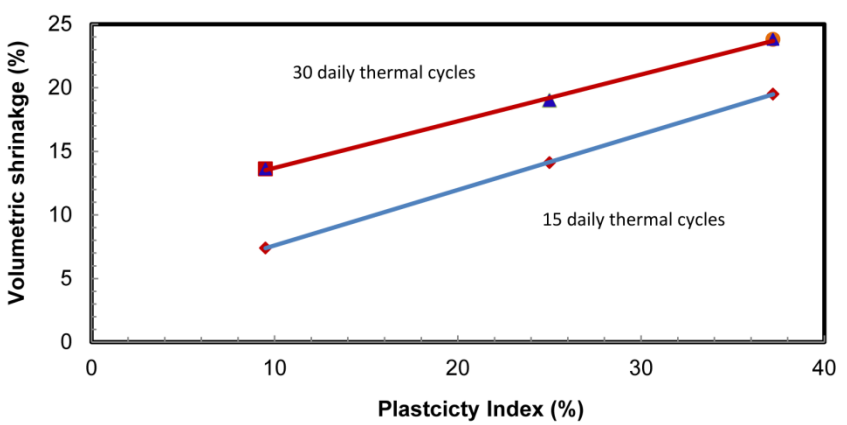

Figure 1. Soil volume shrinkage under daily thermal cycles.

As the plasticity index, and hence the clay content, increases, the soil specimens demonstrate higher volumetric shrinkage.

Several investigators have reported a considerable effect of initial water content on volumetric shrinkage of clayey soil. An increase in volumetric shrinkage was reported whether the soil is compacted wet or dry of optimum (Albrecht and Benson 2001). This was attributed to the decrease in the dry unit weight that would happen when the soil is compacted wet or dry of optimum. The decrease in the dry unit weight results in more water molecules and fewer solid particles in the soil matrix upon saturation. Therefore, as water evaporates, more space is generated between soil particles resulting in a larger volumetric shrinkage (Albrecht and Benson 2001; Tay et al., 2001).

Several studies reported the important role of clay mineralogy as an indicator of total volumetric shrinkage. Smectite soils showed higher amounts of volumetric shrinkage (16.4%) compared to illite soils, which shrank up to 11.7% of their initial volume (Omidi et al., 1996). Albrecht and Benson (2001) stated that when smectite was dominant, soils exhibited very high volumetric shrinkage, while illite, kaolinite, and quartz soils experienced less shrinkage. This was linked to the capability of smectite minerals to contain more water and consequently undergoing higher shrinkage upon desiccation. The same finding was reported by Tay et al. (2001) when sand soil was amended with different percentages of bentonite.

Desiccation Cracking

If the volumetric shrinkage of clayey soils is restricted, cracks occur when the soil's tensile strength fails to resist the growing tensile stresses (Nahlawi and Kodikara, 2006; Tang et al., 2011). The restriction of soil shrinkage could generate increasing horizontal stresses, which eventually would be relieved by cracking (Groisman and Kaplan, 1993). The generation of these tension stresses is mainly related to the boundary conditions (George, 1968). When the soil is free to uniformly shrink and insignificant friction is provided by the subgrade, then stresses will not have a chance to generate. Significant volumetric shrinkage was reported for different clay specimens, without forming any significant crack areas, when a smooth boundary condition was provided by the test container (Aldaeef and Rayhani, 2014a). In field conditions, only the upper part of the soil is exposed to the atmosphere. Therefore, desiccation leads to non-uniform shrinkage and the development of friction between the upper soils and underlying layers, which eventually results in cracking.

Once cracks initiate, they spread throughout the soil matrix following the same path of desiccation. Cracks tend to propagate in both vertical and horizontal directions. Vertical propagation is mostly restricted by the increase in confining stresses due to self-weighting of the soil, while horizontal propagation is limited by crack intersections (Morris et al., 1991). As desiccation proceeds, cracks in both directions (i.e., depth and length) become larger and the crack network becomes more explicit. Even though cracks tend to propagate randomly on the surface, they intersect each other at approximate right angles (90°) (Morris et al., 1991). Subsequent secondary cracks appear, and tend to break the blocks between existing cracks into smaller polygons. Secondary cracks initiate at the most restrained points within the existing blocks, which is at the middle of the longest side of each block.

Layer thickness, ambient temperature, humidity, and wet-dry cycles are some factors that were found to influence the final crack patterns and dimensions (Groisman and Kaplan 1993;

Nahlawi and Kodikara 2006; Tang et al., 2008; Peron et al., 2009). Tang et al. (2008) defined the crack intensive factor (CIF) as the ratio between the areas of formed cracks to the total surface area. Significant increases in crack width and the crack intensive factor (CIF) were reported as the layer thickness increased. This was attributed to the increase in normal and effective stresses as the layers become thicker (Tang et al., 2008). Evaporation rates can vary based on the ambient temperature and humidity. Low evaporation rates cause cracks to be wider, longer, and deeper. The CIF value also becomes higher as the evaporation rate drops. Crack length, width, and average area of segmentations were found to be sensitive to the temperature as well as to the number of wet-dry cycles. Increases in the ambient temperature lead to increases in crack length, crack width, and average area of segmentations (Tang et al., 2008).

Self-Healing

Fractured clayey soils tend to change their behavior as their water content increases again. In rainfall seasons, water fills cracks and fissures and soaks the soil particles leading to a decrease in soil strength and an increase in unit weight. Therefore, soil particles tend to collapse and slide on each other due to the decrease in the soil shear strength. Sliding leads soil particles to fall into the cracks and fissures, resulting in partial crack closures known as self-healing. This could induce re-establishment of the soil permeability approaching its original intact permeability (Rayhani et al., 2007; Eigenbrod, 2003).

In the field, clay liners may be exposed to several wet-dry and/or freeze-thaw cycles during the year. These cycles result in crack formation as the soil desiccates or freezes. However, the subsequent wetting or thawing can lead to partial crack closure, which results in what is known as the self-healing phenomenon. Even though self-healing contributes widely to the curing of previously formed cracks, these cracks continue to act as macropores that promote easier water movement within the soil matrix. As a result, desiccation cracking degrades the hydraulic performance of the soils in barrier systems (Gray, 1989; Omidi, 1993; Rayhani et al., 2008). Given the same water content, cracks promote a higher hydraulic conductivity in fractured soils compared to the intact soils (Morris et al., 1991).

Hydraulic Conductivity

Hydraulic conductivity is the main assessment tool utilized to choose the most appropriate materials for clay barrier construction. Enormous variations in hydraulic conductivity of clayey soils were recorded due to changes in one or more factors such as the method of testing, sample size, particle arrangement, degree of saturation, mineral composition, and/or compaction efforts (Lambe, 1985; Boynton and Daniel, 1985; Omidi et al., 1996; Rayhani et al., 2008). Hydraulic conductivity was also found to be sensitive to moulding water content. A water content 1-2% wet of the optimum water content was found to yield the lowest hydraulic conductivity given the same compacting conditions (Benson and Daniel, 1990).

Since Terzaghi (1925) expected a positive correlation between Atterberg limits and hydraulic conductivity, several studies have been carried out in this field. A study was

conducted on 67 landfill sites, which represented several types of clayey soils, to evaluate the effect of soil composition on the hydraulic performance of CCLs (Benson et al., 1994). The investigation indicated that an increase of the liquid limit and plasticity limit leads to a decrease in hydraulic conductivity. A rapid decrease in hydraulic conductivity coincided with an increase in the plasticity index from 10% to 30%. Similar results were reported by Benson and Trast (1995) who observed a decrease in hydraulic conductivity as the plasticity index increased from 10 to 30% and the liquid limit increased from 20 to 40%. This was attributed to the decrease in the size of microscale pores as a result of the increase in the clay content (Benson and Trast 1995). More recently Aldaeef and Rayhani (2014a) reported an eight times reduction in the hydraulic conductivity of compacted clay liners (CCLs) as the plasticity index increased from 9.5% to 37% (Figure 2).

In composite landfill liner systems, a layer of geomembrane overlies the clay liner to provide more isolation and protection. When geomembrane exists and overlies the clay liner, daily thermal cycles were found not to have any significant impact on the hydraulic performance of the clay liner (Aldaeef and Rayhani, 2014a). These results underscore the importance of a geomembrane in providing protection and sealing from weathering effects for clay liners. This can be explained by the lower moisture loss of the liner when covered by a geomembrane. Suction force is applied by the atmosphere in order to reach humidity equilibrium with the soil matrix. However, when a geomembrane overlies the liner, there would not be an immediate exposure to the atmosphere, thereby diminishing the role of suction, preventing water movement out of the soil, and minimizing the risk of volume shrinkage and crack generation.

HYDRAULIC PERFORMANCE OF CLAY LINERS IN LANDFILLS

Clay liners in landfills may undergo different exposure circumstances and chemical interactions during their lifespan. After waste placement, clay liners might be isolated from the effects of the atmosphere. However, the impact of elevated temperature and chemical leachate exposure would exist and might affect the hydraulic performance of the liner. As municipal waste is being deposited in the landfill, vertical stresses would be generated and applied to the barrier system underneath. Moreover, this barrier system may be exposed to combined thermo-chemical effects. These factors would facilitate the depletion of the geomembrane in a composite liner system (Rowe et al., 2010), thus, clay liners might be immediately confronted with the combined influences of vertical stresses, landfill leachate, and elevated temperatures. The increase in vertical stresses due to waste placement was reported to be beneficial when simultaneous decreases in clay void space and hydraulic conductivity were also recorded (e.g., Quigley et al., 1988; Quigley et al., 1989; Frempong, 2006).

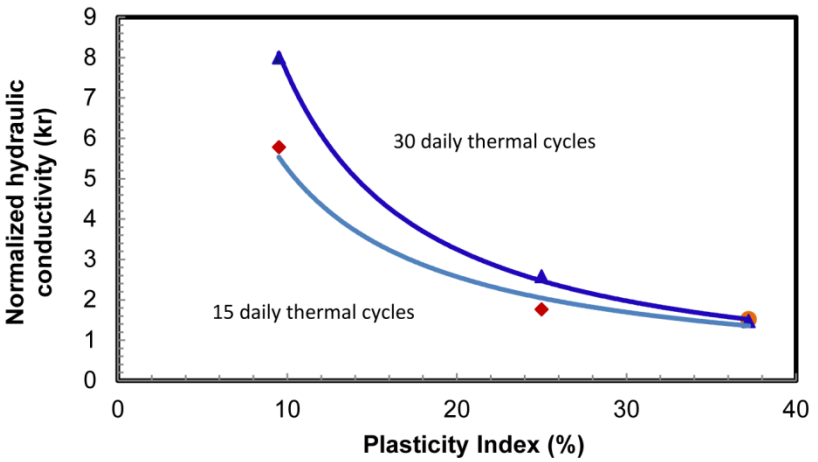

Figure 2. Correlation between soil plasticity and normalized hydraulic conductivity.

While general agreement was reached about the negative effect of elevated temperature on the hydraulic performance of the liner, the effect of landfill leachate on the hydraulic performance of the clay liners was less conclusive. The following is a brief summary of some field and laboratory investigations that have been conducted in an attempt to address the issue of hydraulic performance of clay liners after waste placement in landfills.

Influence of Elevated Temperature on the Hydraulic Performance of Clay Liners

Although municipal solid waste landfills provide reliable protection for the surrounding environment, the level of heat that is produced within the landfills might influence the integrity of their barrier systems. The elevated temperature at the bottom of landfills significantly affects their mechanical functions and hydraulic aspects (Rowe, 1998). Hydraulic performance of the liner can be assessed by potential fluid movement throughout the soil matrix. This fluid movement is widely affected by landfill temperature, which can also change the water content of the soil. Moreover, landfill temperature may impact the mechanism of contaminant transport since it affects the diffusion rate across barriers of low permeability such as clay liners, and geomembrane (Rowe, 1998).

Clay liners in conventional landfills, where the heat release is expected, might undergo severe volume shrinkage and desiccation cracking. Even with low levels of temperature, i.e., as low as 25°C on top of the liner, critical levels of desiccation may be encountered (Doll, 1997). Moreover, physical properties and mechanical behaviours were reported to be sensitive to the thermal effects (Jefferson and Rogers, 1998; Romero et al., 2001; Villar and Lloret, 2004; Romero et al., 2005; Villar et al., 2005). Some researchers have reported a decrease in liquid limits as temperatures increased, whereas they witnessed less significant correlation to plasticity limits (e.g., Youssef et al., 1961; Ctori, 1989). Jefferson and Rogers (1998) reported a slight decrease in the liquid limit of kaolinite clay when the temperature was increased. This behaviour was attributed to the decrease in the inter-particle bond strength as the temperature increased. For smectite clays, the opposite was reported as the

elevated temperature caused an increase in the soil liquid limit. This was attributed to a rearrangement of the soil particles that resulted in a heavier texture, or what was called coagulation.

Villar and Lloret (2004) suggested that the change in hydraulic performance of clayey barriers subjected to thermal exposure could be linked to potential changes in water retention characteristics. Furthermore, physical properties such as the hydration rate and saturation time, and mechanical behaviours such as swelling pressure, contraction and dilatation are expected to undergo significant changes upon temperature exposure (Romero et al., 2001; Villar and Lloret 2004; Romero et al., 2005; Villar et al., 2005). To estimate the effect of temperature on the water retention capacity of clay soils, Villar and Lloret (2004) established Soil-Water Characteristic Curves (SWCCs) at different levels of temperature. Results showed a decrease in the water retention capacity as the temperature increased. This behaviour was attributed to the change in water properties such as water viscosity and density. Moreover, water micropores within the micro-fabric were also thought to contribute to the dependency of the water retention capacity on the temperature. A similar finding was suggested by Romero et al. (2001) when the water retention curve was determined at low and high water contents under the effects of different levels of temperature. For low water content and at a given suction value, the increase in temperature resulted in a decrease in water content. However, at a given water content, the total suction was found to decrease when the temperature increased. This was attributed to the temperature dependence of surface tension as well as changeable clay fabric and pore water chemistry (Romero et al., 2001; Romero et al., 2005). Aldaeef and Rayhani (2014b) reported increases in the hydraulic conductivity of clay liners by two to three times their initial hydraulic conductivity when exposed to 55℃ for 75 days. This increase was attributed to the decrease in permeant viscosity due to elevated temperature as well as micro-crack generation within the soil (Figure 3).

Influence of Landfill Leachate on the Hydraulic Performance of Clay Liners

Landfill leachate results from waste leaching and organic waste degradation. When a clay liner is exposed to landfill leachate, different chemical interactions and mineral transformations are expected. These interactions most likely would cause changes in the soils' chemical compositions (Quigley et al., 1988; Narasimha and Mathew, 1995; Allen, 2005; Frempong, 2006), mineral compositions (Quigley et al., 1988; Joseph at al., 2001; Frempong, 2006;), and physical properties (e.g., Atterberg limits) (Allen, 2005; Frempong, 2006). Following these changes, the hydraulic performance of the treated clay might change. Liner/leachate incompatibility may allow leachate to escape and reach groundwater, contaminating local water sources (Quigley et al., 1989). Aldaeef and Rayhani (2014b) reported that landfill leachate exposure alone initially increased the hydraulic conductivities for all compacted clay specimens due to the difference in the viscosity of the permeant compared to water.

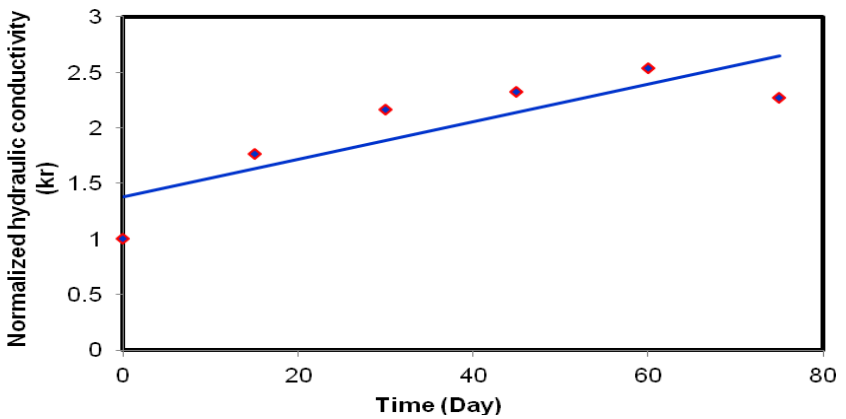

Figure 3. Hydraulic performance of CCL specimens when exposed to 55°C for 75 days.

However, as the leachate exposure time increased, the hydraulic conductivity readings showed significant reductions that sometimes reached an order of magnitude after 75 days of leachate permeation at room temperature (22°C). The gradual decrease in the CCLs hydraulic conductivities was most likely due to chemical precipitation and clogging of pore voids within the soils (Figure 4). Similarly, Griffin et al. (1976) proposed a decrease in the hydraulic conductivity of clayey soils upon exposure to domestic waste leachate due to bacterial clogging, double layer expansion, and Na^+ adsorption. Petrov and Rowe (1997) stated that the hydraulic conductivity of Geosynthetic Clay Liners (GCLs) could be an order of magnitude larger when the GCL was permeated with landfill leachate instead of distilled or tap water, providing the same level of applied stresses.

Cation Exchange Capacity (CEC), thickness of the double layer, and mineral composition are parameters that were used to assess the effect of landfill leachate on the hydraulic performance of clay barriers. Jo et al. (2005) attributed the increase in hydraulic conductivity of sodium bentonite to the replacement of sodium ions by other cations available in the solution where this replacement most likely would be followed by changes in water adsorption capacity.

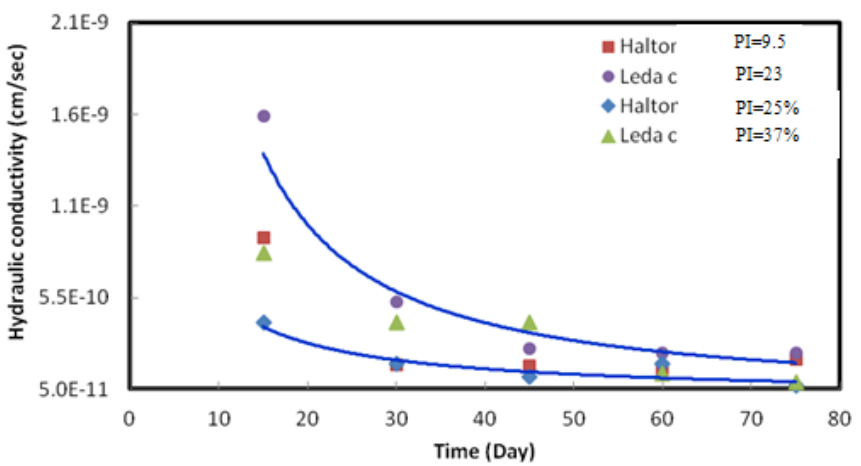

Figure 4. Hydraulic performance for CCLs when exposed to leachate permeation at room temperature.

Landfill leachate typically has high concentrations of sodium, calcium, magnesium and potassium ions. These ions most likely would interact with a clay soil's ions and impose chemical changes.

Thereby, changes in the hydraulic performance of the clay barrier might result. Shackelford et al. (2000) believes that divalent calcium ions can easily replace the sodium ions in sodium bentonite. However, the higher valence of calcium ions would reduce the ion concentration between the clay sheets. Lower ion concentration results in lower repulsive force, which in turn would cause double layer contraction (Shackelford et al., 2000; Van Olphen, 1964). In contrast, Quigley et al. (1988), Frempong (2006), and Quigley et al. (1989) indicated absorption of sodium and potassium ions and desorption of calcium and magnesium ions out of the soil matrices. However, the length of time and the number of pore volumes that were required to reach chemical equilibrium varied from soil to soil. Quigley et al. (1989) referred to soil salinity as a controlling factor in ion exchange. Highly saline soils showed a drop in their salt concentrations because of exposure to leachate with lower ion concentration. However, low salinity soils had a tendency to adsorb sodium and potassium ions and desorb calcium and magnesium when the leachate ion concentration was higher. Furthermore, Quigley et al. (1988) observed that the compacted clay samples with lower void ratios (e= 0.54) exhibited lower sodium and potassium adsorption and that they achieved chemical equilibrium faster than the soils with higher void ratios (e= 0.74). This behaviour was linked to the flow channels that developed due to compaction-induced fractures in the denser soil structure.

Marine clays commonly show lower potassium content than sodium (Quigley et al., 1988; Quigley et al., 1989). On the other hand, a significant concentration of potassium ions in landfill leachate has been reported (e.g., Joseph et al., 2001; and Quigley et al., 1989). For instance, the potassium concentration in the Westminster landfill leachate (London, Ontario) was 372 mg/l, while the highest potassium concentration among the liner soils (marine clay) was 57 mg/l (Quigley et al. 1989). This considerable difference in concentration would induce soil particles to absorb potassium and desorb other ions such as sodium in order to reach chemical equilibrium. In addition, the lower sodium concentration in the landfill leachate compared to marine clays might lead to leaching of the sodium ions from the soil matrix. Chloride and sodium ion concentrations in the soil sample were reduced upon leachate permeation after 2 and 4 pore volumes respectively. On the other hand, potassium ion concentration achieved equilibrium after 7 pore volumes, and demonstrated a substantial increase from an initial value of 57 mg/l to a final concentration of 275 mg/l. Decreasing sodium concentration and trapping of potassium ions, which is known as the potassium fixation phenomenon, would decrease both the repulsive force and the swelling capacity. Although sodium and potassium ions have the same valence, sodium ions can yield a higher hydrated radius and double layer thickness compared to potassium ions. Therefore, potassium fixation would decrease the hydrated radius and cause a reduction of the double layer thickness. Moreover, reduction in the cation exchange capacity would occur in parallel with potassium fixation. This would increase the potential contraction in the crystal volume. Thus, an increase in effective pore space would result, and consequently lead to an increase in hydraulic conductivity (Quigley et al., 1988; Shackelford et al., 2000).

Clay particle arrangement can also be affected by ion charges. Clay particles commonly have positive charges at their edges and negative charges on the surface. Flocculation in particle arrangement results due to the attraction between the different charges of the edges

and surfaces of the clay particles. When clay soil is exposed to a concentrated chemical solution, ion concentrations within the soil would increase. This increase might cause the clay layers to be rearranged in a parallel manner (dispersion) under the effect of these ion charges, resulting in lower hydraulic conductivity (Das, 2002). However, an increase in the ion valence and hence a decrease in ion concentration, would decrease the repulsive forces as well as the double layer thickness (Van Olphen, 1964). This decrease in the repulsive force might lead to a flocculated arrangement of the clay particles and an increase in hydraulic conductivity would most likely result. Narasimha and Mathew (1995) observed a dispersed arrangement for low valence clay fabric (Na^+ clay) and a flocculated arrangement for high valence clay fabric (Al^{3+} clay). In terms of hydraulic performance, the hydraulic conductivity of Al^{3+} clay was 13 times higher than the Na^+ clay because of soil particle flocculation in the Al^{3+} clay.

Potential mineral transformation due to chemical interaction between clay soils and landfill leachate was intensively studied. Quigley et al. (1988) compared the mineral compositions of two soils before and after being treated with 0.5N KCl for air-dried soil and water-wet soil samples. Results showed a significant collapse of smectite clays to form illite when the air-dried soil samples were treated with 0.5N KCl. However, for the case of water-wet samples, less smectite collapse was observed. Therefore, the mineral analysis for water-wet samples would be more relevant to actual field conditions, with less potential for mineral transformation (Quigley et al., 1988; Joseph et al. 2001). In contrast, Frempong, (2006) reported significant mineral transformation upon leachate permeation. Mixed layer minerals of illite/vermiculate were collapsed to form single illite and vermiculate minerals. Moreover, smectite and Fe-chlorite minerals were transformed to smectite-organic minerals and chlorite-organic minerals.

Waste management practices and landfill type would both control the properties of landfill leachate. For example, landfill leachate generated from bioreactor landfills would be different in composition and concentration compared to leachate produced in regular landfills. Therefore, the level of clay/leachate compatibility would be site-dependent. The hydraulic performance of the clay liner can vary widely based on the leachate component with which the liner is permeated (Quigley et al. 1988). For example, a hydraulic conductivity of $7x10^{-12}$ m/s was recorded when a sample of GCL was permeated with tap water, while permeation with real and synthetic leachate yielded hydraulic conductivities of $1x10^{-12}$m/s and $2x10^{-8}$ m/s respectively (Ruhl and Daniel 1997). The real leachate yielded lower permeability, even though it had lower salt concentration. This was attributed to the presence of bacteria that might cause pH increase and pore medium clogging due to bacterial precipitation (Rowe, 1998). Therefore, Rowe (1998) suggested using a simulated chemical leachate (synthetic leachate) for laboratory investigations as a conservative procedure since it may be difficult to predict whether or not the bacterial behavior would be beneficial. Aldaeef and Rayhani (2014b) recorded the production of a black film on the top surfaces as well as within clay specimens even when the permeant was a synthetic leachate. This film was reported to encourage pore volume clogging and a subsequent decrease in the hydraulic conductivity of clay liners.

The presence of landfill leachate in the form of water- soluble organic liquids could result in raising of the hydraulic conductivity of water-compacted clay. Many factors are involved in this phenomenon such as the viscosity and dielectric constant of the permeant, which all influence the ease of permeant flow and the thickness of the double layer (Fernandez and

Quigley, 1988; Aldaeef and Rayhani, 2014b). Attempts were made to quantify the concentration of organic liquids in a leachate solution at which the hydraulic conductivity of water-compacted clay would significantly increase. Permeant viscosity was shown to increase as the organic content increased, reaching a maximum viscosity value at 60% dioxane concentration and 40% ethanol concentration (Fernandez and Quigley, 1988). Further increases in the organic contents beyond these values resulted in decreases in the permeant viscosities. On the other hand, the dielectric constant for different solutions significantly decreased as the organic content increased.

In terms of hydraulic performance, the hydraulic conductivity slightly decreased when methanol and dioxane concentrations were increased in the permeants up to 60% and 70% respectively. Soil samples experienced an increase in hydraulic conductivity by half an order of magnitude and two orders of magnitude when permeated with 80% and 85% ethanol and dioxane respectively. Maximum increases in hydraulic conductivities by two and three orders of magnitude were recorded for the soil samples permeated with concentrated methanol and concentrated dioxane respectively. The decrease in hydraulic conductivity at the beginning was referred to the increase of viscosities as the ethanol and dioxane concentrations increased. The maximum permeant viscosities were achieved when the ethanol and dioxane contents in the permeants reached 40% and 60% respectively. When the concentrations of the organic contents (ethanol and dioxane) go beyond these points, the viscosities start to decrease and, in turn, increase the hydraulic conductivity. However, this increase was attributed mainly to the collapse of the double layer, which became dominant over the viscosity effect at high organic contents. Double layer contraction would cause reduction of the water film around the particles. This reduction would increase the effective pore space at constant void ratio, and eventually might lead to an increase in hydraulic conductivity of the soil (Fernandez and Quigley 1988).

Combined Thermo-Chemical Exposure Effects on Hydraulic Performance of Clay Liners

After waste placement in landfills, clay liners might be exposed to the combined effects of landfill leachate and elevated temperatures, both of which could impact the hydraulic performance of the liners. Figure 5 shows the variation of hydraulic conductivity with temperature for compacted clay specimens when permeated with synthetic leachate (Aldaeef and Rayhani, 2014b). The curves demonstrate the inverse correlation between temperature and the hydraulic conductivity reduction of CCLs when subjected to combined thermo-chemical exposure. The highest reductions in hydraulic conductivity occurred at lower exposure temperature (room temperature, 22°C), while the lower hydraulic conductivity reductions corresponded to the higher exposure temperature (55°C). In other words, as the temperature increased, the final hydraulic conductivity of the soil specimens increased. This behaviour can be attributed to the decrease in permeant viscosity as the temperature increases, which leads to higher hydraulic conductivity at higher temperatures. In addition, a visual inspection after test termination showed a decrease in biofilm generation as the exposure temperature increased (Figure 6). Intense biofilm generation due to bacterial growth was observed on the surface and within the soil specimens exposed to leachate permeation at room

temperature. However, the tendency for biofilm formation decreased as the temperature increased toward 55°C. Thus, lower biological clogging may occur at higher temperatures, which, along with decreased viscosity, could lead to higher hydraulic conductivity at higher temperatures when combined thermo-chemical conditions are applied.

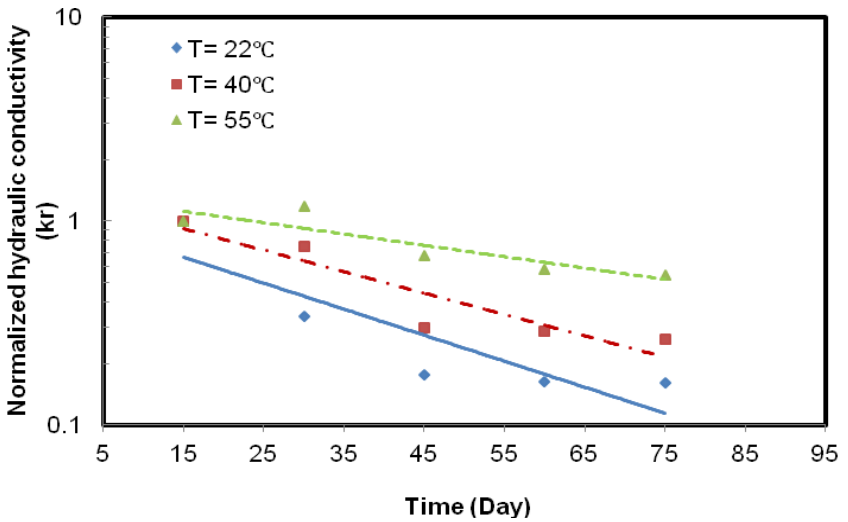

Figure 5. Effect of temperature on hydraulic performance of CCLs when exposed to leachate.

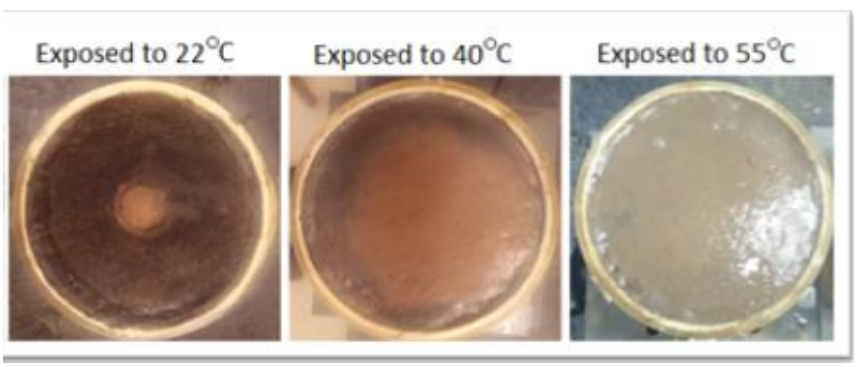

Figure 6. Effect of temperature on biofilm formation during leachate permeation.

REFERENCES

Albrecht, B. A., and Benson, C. H. 2001. Effect of desiccation on compacted natural clays. Journal of Geotechnical and Geoenvironmental Engineering, 127(1), pp. 67-75.

Aldaeef, A. A., and Rayhani, M. T. 2014a. Hydraulic performance of compacted clay liners under simulated daily thermal cycles. *Journal of Engineering Geology*, (under review).

Aldaeef, A. A., and Rayhani, M. T. 2014b. Hydraulic performance of compacted clay liners under combined temperature and leachate exposure conditions. *Journal of Waste Managenent*, (under review).

Allen, W. M. 2005. The relationship between plasticity ratio and hydraulic conductivity bentonite clay during exposure to synthetic landfill leachate. M.Sc. thesis, University of south Florida.

Benson, C., and Daniel, D. 1990. Influence of clods on hydraulic conductivity of compacted clay. Journal of Geotechnical Engineering, 116(8), pp. 1231-1248.

Benson, C. H., Daniel, D. E., and Boutwell, G. P. 1999. Field performance of compacted clay liners. *Journal of Geotechnical and Geoenvironmental Engineering*, 125(5), pp. 390-403.

Benson, H. C. and Trast, J. M. 1995. Hydraulic conductivity of thirteen compacted clays. *Clays and Clay Minerals*, 43(6), pp. 669-681.

Boynton, S. S. and Daniel, D. E. 1985. Hydraulic conductivity tests on compacted clay. *Journal of Geotechnical Engineering*, 111(4), pp. 465-478.

Bronswijk, J., 1988. Modeling of water balance, cracking and subsidence of clay soils. *Journal of Hydrology*, Volume 97, pp. 199-212.

Collins, H. 1993. Impact of the temperature inside the landfill on the behaviour of barrier systems. *Proceedings of the 4th International Landfill Symposium*, Sardinia '93, Volume 1, pp. 417–432.

Ctori, P. 1989. The effects of temperature on the physical properties of cohesive soils. *Ground Engineering*, 22(5), pp. 26-27.

Das, B. 2002. Principles of geotechnical engineering. 5th ed, Thomas Learning, Inc. ISBN: 0-534-55144-0.

DeJong, E., and Warkentin, B. P. 1965. Shrinkage of soil samples with varying clay content. *Canadian Geotechnical Journal*, 2(1), pp. 16-22.

Doll, P. 1997. Desiccation of mineral liners below landfills with heat generation. *Journal of Geotechnical and Geoenvironmental engineering*, 123(11), pp. 1001-1009.

Fernandez, F., and Quigley, R. M, 1988. Viscosity and dielectric constant controls on the hydraulic conductivity of clayey soils permeated with water-soluble organics. *Canadian Geotechnical Journal*, Volume 25, pp. 582-589.

Fox, W. 1964. A study of bulk density and water in a swelling soil. *Soil Science*, 98(5), pp. 307-316.

Frempong, E. 2006. Compatibility of tropical clayey soil liners with industrial and domestic leachates, PhD, thesis, University of Western Ontario, ON, Canada.

George, K. P. 1968. Craking in cement-treated bases and to minimizing it. Highway Research Record, Volume 225, pp. 59-71.

Gray, C. W., Allbrook, R. 2002. Relationships between shrinkage indices and soil properties in some New Zealand soils. *Geoderma*, 108(3-4), pp. 287-299.

Gray, D. H. 1989. Geotechnical engineering of land disposal systems. The Landfill: reactor and final storage. *Lecture Notes in Earth Sciences*, Volume 20, pp 145-173.

Griffin, R. A., Cartwright, K., Shimp, N. F., Steel, J. D., Ruch, R. R., White, W. A., Hughes, G. M., Gilkeson, R. H, 1976. Attenuation of pollutants in municipal landfill leachate by clay minerals: Part I-Column leaching and field verification, Environmental Protection Agency, Washington, D.C., EPA/600/2-78/157.

Groisman, A., and Kaplan E. 1993. An experimental study of cracking induced by desiccation. *Europhysics Letters*, 25(6), pp. 415-420.

Haines, W. 1923. The volume change associated with variations of water content in soil. *The Journal of agricultural science*, 13(3), pp. 296-310.

Hanson, J. L., Yeşiller,N., and Oettle, N. K. 2010. Spatial and temporal temperature distributions in municipal solid waste landfills. *Journal of Environmental Engineering*, 136(8), pp. 1095-1102.

Heibrock, G. 1997. Desiccation cracking of mineral sealing liners. Proceedings of 6th International Landfill symposium, S. Margherita di Pula, Cagliari, Italy, October, Vol. 3, pp. 101-113.

Jefferson, I., and Rogers, C. D. F. 1998. Liquid limit and the temperature sensitivity of clays. *Engineering Geology*, Volume 49, pp. 95-109.

Jo, H. Y., Benson, C. H., Shackelford, C. D., Lee, J., and Edil, T. B. 2005. Long-term hydraulic conductivity of a geosynthetic clay liner permeated with inorganic salt solutions. *Journal of Geotechnical and Geoenvironmental Engineering*, 131(4), pp. 405-417.

Joseph, J. B., Styles, J. R., Yuen, S. T. S., and Cressey, G. 2001. Variations in clay mineral performance in the presence of leachates. Proceeding of the Eighth International Landfill Symposium, Sardinia, Italy, 10p.

Konrad, J. M., and Ayad, R. 1997. Desiccation of sensitive clay: Field experimental observations. *Canadian Geotechnical Journal*, 34(6), pp. 929-942.

Morris, P. H., Graham, J., and Williams, D. J. 1991. Cracking in drying soils. *Canadian Geotechnical Journal*, Volume 29, pp. 263-277.

Nahlawi, H., and Kodikara, J. H. 2006. Laboratory experimental on desiccation cracking of thin soil layers. *Geotechnical and Geological Engineering*, Volume 24, pp. 1641-1664.

Narasimha, R. S., and Mathew, P. 1995. Effect of exchangeable cations on hydraulic conductivity of a marine clay. *Clays and Clay Minerals*, 43(4), pp. 433-437.

Omidi, G. H., Thomas, J. C., and Brown, K. W, 1996. Effect of desiccation cracking on the hydraulic conductivity of compacted clay liner. *Water Air and Soil Pollution*, Volume 89, pp. 91-103.

Peron H., Hueckel, T., Laloui L., and Hu, L. 2009. Fundamentals of desiccation cracking of fine grained soils: Experimental characterisation and mechanisms identification. *Canadian Geotechnical Journal*, Volume 46, pp. 1177-1201.

Petrov, R. J., and Rowe, R. K. 1997. Geosynthetic clay Liner compatibility by hydraulic conductivity testing factors impacting performance. *Canadian Geotechnical Journal*, 34(6), pp. 863-885.

Quigley, R. M., Fernandez, F., Rowe, R. K. 1988. Clayey barrier assessment for impoundment of domestic waste leachate (southern Ontario) including clay - leachate compatibility by hydraulic conductivity testing. *Canadian Geotechnical Journal*, Volume 25, pp. 574-581.

Quigley, R. M., Frenandez, F., and Ohikere, C. 1989. Clay/leachate compatibility study: Hydraulic conductivity of Ottawa/Carleton "Leda" clay barrier soils permeated with domestic waste leachate, Geotechnical Research Centre, Faculty of Engineering Science, University of Western Ontario, ON, Canada.

Rayhani, M. T., Yanful, E. K., and Fakher, A. 2007. Desiccation-induced cracking and its effect on the hydraulic conductivity of clayey soils from Iran. *Canadian Geotechnical Journal*, 44 (3): 276-283.

Rayhani, M. T., Yanful, E. K., and Fakher, A. 2008. Physical modeling of desiccation cracking in plastic soils. *Journal of Engineering Geology*, 97: 25-31.

Romero, E., Gens, A., and Lloret, A. 2001. Temperature effects on the hydraulic behaviour of an unsaturated clay. *Geotechnical and Geological Engineering,* Volume 19, pp. 311-332.

Romero, E., Villar, M. V., and Lloret, A. 2005. Thermo-hydro-mechanical behaviour of two heavily overconsolidated clays. *Engineering Geology,* Volume 81, pp. 255-268.

Rowe, R. K. 1998. Geosynthetics and the minimization of contaminant migration through barrier systems beneath solid waste. In: Rowe, R.K. (Ed.), 1998. Proceedings of 6th International Conference on Geosynthetics, Atlanta, 1. Industrial Fabrics Association International, St. Paul, MN, pp. 27e103.

Rowe, R. K., Quigley, R. M., Brachman, R. W. I., Booker, J. R., 2004. Barrier systems for waste disposal facilities. Taylor and Francis Books Ltd (E and FN Spon), London, UK.

Rowe, R. K., Islam, M. Z., Brachman, R. W. I., Arnepalli, D. N., and Ewais, A. 2010. Antioxidant depletion from a high densitypolyethylene geomembrane under simulated landfill conditions. *Journal of Geotechnical and Geoenvironmental Engineering,* 136(7), pp. 930-939.

Ruhl, J. L. and Daniel, D. E. 1997. Geosynthetic clay liners permeated with chemical solutions and leachates. *Journal of Geotechnical and Geoenvironmental Engineering,* 123(4), pp. 369-380.

Shackelford, C. D., Benson, C. H., Katsumi, T., Edil, T. B., and Lin, L. 2000. Evaluating the hydraulic conductivity of GCLs permeated with non-standard liquids. *Geotextiles and Geomembranes*, 18(2-4), pp. 133-161.

Tang, C. S., Shi, B., Liu, C., Gao, L., and Inyang, H. I. 2011. Experimental investigation of the desiccation cracking behaviour of soil layers during drying. *Journal of Materials in Civil Engineering*, 23(6), pp. 873-878.

Tang, C. S., Shi, B., Liu, C., Zhao, L. Z., and Wang, B. J. 2008. Influencing factors of geometrical structure of surface shrinkage cracks in clayey soils. *Engineering Geology,* Volume 101, pp. 204-217.

Terzaghi, K. 1925. Structure and volume of voids of soils. Pages 10, 11, 12, and part of 13. Erdbaumechanik auf Bodenphysikalisher Grundlage, translated by Casagrande, A. in: From Theory to Practice in Soil Mechanics, John Wiley and Sons, New York, 1960, pp. 146–148.

Tay. Y. Y., Stewart. D. I., and Cousens. T. W. 2001. Shrinkage and desiccation cracking in bentonite-sand landfill liners. Engineering Geology, Volume 60, pp. 263-274.

Van Olphen, H. 1964. An introduction to clay colloid chemistry. Interscience Publishers, Div. of John Wiley and Sons, New York.

Villar, M. V., and Lloret, A. 2004. Influence of temperature on the hydro-mechanical behaviour of a compacted bentonite. *Applied Clay Science*, 26(1-4), pp. 337-350.

Villar, M. V., Martin, P. L., and Barcala, J. M. 2005. Modification of physical, mechanical and hydraulic properties of bentonite by thermo-hydraulic gradients. *Engineering Geology*, Volume 81, pp. 284-297.

Yeşiller. N., Hanson. J. L., Yoshida. H.. 2011. Landfill temperatures under variable decomposition conditions. In: Proceedings of the Geo-Frontiers 2011 Conference, Dallas, TX, USA, 13 March 2011, pp. 1055–1065. Reston, VA: ASCE, American Society for Civil Engineers, Dallas, TX.

Yoshida, H., Hozumi, H., and Tanaka, N. 1996. Theoretical study on temperature distribution in a sanitary landfill. Proc. 2nd Int. Congress on Environ. Geotech., Osaka volume 1, pp. 323–328.

Youssef, M. S., Sabry, A., and Ramli, A. H. E. I. 1961. Temperature changes and their effects on some physical properties of soils. Proceedings of the 5th International Conference on Soil Mechanics and Foundation Engineering, Paris, Volume 1, pp. 419–421.

Yuen, K. K., Graham, J., and Janzen, P. 1998. Weathering-induced fissuring and hydraulic conductivity in a natural plastic clay. *Canadian Geotechnical Journal*, 35(6), pp. 1101-1108.

In: Clays and Clay Minerals
Editor: Liam R. Wesley
ISBN: 978-1-63117-779-8

Chapter 10

PRODUCTION OF SPECIALIZED MINERAL PRODUCTS FROM MODIFIED KAOLINS

Bernard A. Goodman[1] and Niramon Worasith[2*]
[1]State Key Laboratory for Conservation and Utilization of Subtropical Agro-Bioresources, Guangxi University, Nanning, Guangxi, China
[2]Department of Chemistry, Rajamangala University of Technology Krungthep, Sathorn, Bangkok, Thailand

ABSTRACT

The kaolins are a group of dioctahedral 1:1 layer silicates, in which each layer consists of a combination of one sheet of tetrahedral and one sheet of octahedral cations linked by bridging oxygen atoms. The surface of the tetrahedral sheet consists of oxygen atoms, whereas that of the octahedral sheet contains hydroxyl groups, and neighbouring layers are held together by hydrogen bonds. Kaolin deposits are widely distributed throughout the World, but they also exhibit considerable variations in both their chemical and structural compositions; the latter are exhibited both in the nature of the stacking of adjacent layers, but also in the inclusion of water molecules in the interlayer region. The kaolin minerals are used extensively in the ceramics, paint and paper industries, and can also be used as source materials for the production of higher-value products for a wide range of industrial uses. In addition, kaolins can be modified to produce new materials with a wide range of physical and chemical properties that have the potential for the development of additional uses for the mineral.

This chapter reviews recent publications on the generation, characterization, and properties of modified kaolins, and these results are supplemented by the inclusion of some previously unpublished results obtained using materials from two of the main kaolin deposits in Thailand. A final section discusses potential uses for some of these products and possible further developments in the production of novel kaolin-derived materials.

Keywords: Physical damage, chemical alteration, sintering, metakaolin, adsorbents, zeolites

* E-mail address: niramon.w@rmutk.ac.th.

KAOLIN MINERALS AND THEIR CHARACTERIZATION

Introduction

The name kaolin is derived from Kauling in Kiangsi Province, China, where the mineral also known as China clay was first recorded (Chen et al., 1997). Kaolin is actually a family of aluminosilicate minerals with 1:1 layer structures in which individual layers in the minerals consist of a single silicate sheet with tetrahedrally-coordinated Si bound to a single aluminum hydroxide sheet in which the Al has octahedral coordination (Murray, 2007). These minerals are all dioctahedral, since they nominally have only 2/3 of their octahedral cation sites occupied. In the minerals kaolinite, dickite and nacrite, individual layers are bound to one another through hydrogen bonds to form platy structures. These minerals differ only in the stacking arrangements of the layers, whilst the layers in the closely related mineral halloysite have a curved morphology with water between them (and thus is often found as needle-like structures), but otherwise it has a similar composition to the other kaolin group minerals. The number of water molecules in the interlayer region of halloysite samples is variable; the *d*(001) XRD peak of fully hydrated halloysite is at lower angle (8.75 °2θ) than in the other kaolin minerals (12.37 °2θ), but it collapses to about 12.28 °2θ when the humidity is below 30%.

The serpentine minerals are the trioctahedral analogues of the kaolins with the octahedral sites completely filled by Mg, and hisingerite is a relatively rare Fe-rich 1:1 layer silicate that has as a curved ferric 7-Å structure analogous to dehydrated halloysite (Eggleton and Tilley, 1998). In principle these could form interstratified phases in the kaolin minerals.

Kaolin deposits are widespread throughout the World, and kaolin is the dominant clay in many tropical and subtropical soils, where it exerts a strong influence on surface chemical reactions. However, in contrast to standard reference minerals from major kaolin deposits, soil kaolins commonly have high concentrations of defects in their structures, very small particle size with complex morphologies and often contain appreciable amounts of structural iron, so caution should be exercised in extrapolating the results of experiments performed with well-defined kaolin specimens to reactions expected with soils and other environmental situations.

Diversity of Natural Kaolins

As with many aluminosilicates, the kaolin group minerals can have both structural and chemical disorder, and isomorphous substitutions of various metal ions are found for both Si and Al. Substitution of Al^{3+} or Fe^{3+} for Si in the tetrahedral sheet generates an electron surplus, which may be compensated by either the generation of a layer charge, or protonation of oxygen atoms to generate hydroxyl groups on the edge surfaces of the tetrahedral sheet (e.g., Huertas et al., 1998). There is evidence that much of the observed cation exchange capacity (CEC) in kaolinites is derived from hydroxyl groups on edges and basal surfaces of the mineral (Ma and Eggleton, 1999), but the CEC can vary appreciably between different samples, and recently Castellano et al., (2010) described the kaolinite surface as almost neutral in some commercial kaolins.

Various metal ions, such as V^{4+}, Mn^{4+}, Fe^{3+}, Fe^{2+}, Mg^{2+}, Mn^{2+}, etc. are frequently found in kaolin mineral structures in addition to some Al-for-Si substitution. Individual specimens may also contain regions of serpentine structure, in which three Mg^{2+} ions substitute for two Al^{3+} ions, although in a study of a synthetic Mg-rich kaolinite Bentabol et al. (2006) found Mg-for-Al replacement in the octahedral sheet rather than serpentine-like layers interstratified in the kaolinite structure. The trace element compositions of kaolin minerals reflect those of the parent minerals from which they were derived and the fluids with which they had contact during their formation. Also, since clay mineral formation can be a slow process, there can be appreciable changes in the compositions of such fluids during the formation of a mineral deposit, which may thus possess a considerable degree of heterogeneity. Furthermore, kaolins can be formed from many different minerals, and the stability field for kaolinite is bounded by those of gibbsite, K-mica, K-feldspar, and amorphous silica (Garrels and Christ, 1965). Although the formation of kaolinite is slow under ambient conditions, it can be obtained from gels in days or weeks at elevated temperatures (Dixon, 1989). Also, it may be assisted by organic substances which complex Al, and certain plant species are able to convert biotite to kaolinite (e.g., Spyridakis et al., 1967).

Unsurprisingly, the source material and mechanism of formation can have an appreciable influence on the physical and chemical properties of kaolin minerals. For example, the kaolin in deposits in the Kauling and neighbouring Dazhou mining areas were formed from granite (Chen et al., 1997), probably as a result of alteration of feldspar by hydrothermal fluids, followed by weathering to produce a mixture of kaolinite and halloysite. Halloysite admixed kaolinite was also reported to be the major mineral in kaolins formed by weathering of gneissic rocks under temperate (Tsolis-Katagas and Papoulis, 2004) and tropical (De Oliveira et al., 2007) climates whereas, kaolin formed from hydrothermally altered rhyolitic rocks contained a misture of dickite and kaolinite (Tsolis-Katagas and Papoulis, 2004). Evidence for the transformation of halloysite to kaolinite was provided by De Oliveira et al. (2007) who observed halloysite tubes in polygonal forms that were thought to be transitional between kaolinite and halloysite. Also, temporal evolution of pedogenic Fe-smectite to Fe-kaolin via an interstratified kaolin–smectite was described by Ryan and Huertas (2009) for a moist tropical soil chronosequence derived from basaltic–andesitic parent material. These kaolins had a relatively high CEC, which was considered to be the result of the presence of small amounts of octahedral Mg and/or tetrahedral Al; such substitutons are thus of potential importance for clay mineral reactions and elemental cycling in moist tropical soils.

Synthetic clay minerals can be tailored to promote specific properties, and also help with understanding the mechanisms involved in the formation of natural mineral counterparts. Zhang et al. (2010) summarized recent advances in the synthesis of various clay minerals including kaolinite, and showed how their crystallization, properties and morphology were influenced by the chemical composition and structure of starting materials as well as hydrothermal conditions and isomorphous substitution.

Characterization of Individual Kaolin Specimens

X-ray diffraction (XRD) has long been the fundamental method for identifying kaolin mineral phases (e.g., Ross and Kerr, 1930); an example for a Thai kaolin is presented in Figure 1. Most of the peaks can be accounted for by kaolin minerals; the strong peaks at 7.14,

3.57 and 1.49Å correspond to the kaolinite *d*(001), *d*(002) and *d*(060) reflections and the peaks at 4.45, 2.56, 2.49, 2.34, 1.99, 1.66, and 1.49 are all consistent with kaolinite. Positive identification of halloysite from these data is difficult, because the main peaks from halloysite-10 Å at 10Å and halloysite-7 Å at 4.42 Å both overlap with peaks from illite, and the peak at 4.34 Å can correspond to either halloysite or kaolinite (Brindley and Brown 1980).

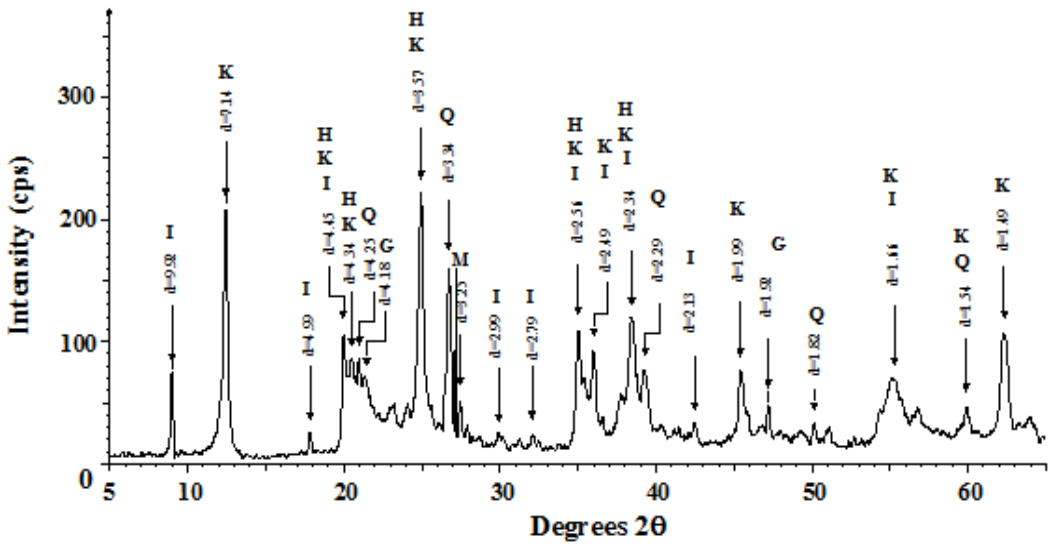

Figure 1. Powder X-ray diffraction pattern of a kaolin from Thailand (from Worasith et al., 2012). K = kaolinite, H = halloysite, Q = quartz, I = illite, G = goethite and M = microcline.

XRD is also very useful for detecting the presence of crystalline impurity phases. Illite, which is a common impurity in kaolin-minerals, is seen by the presence of major peaks at 9.92 and 2.56 Å and others at 4.99 and 2.99 Å. The principal reflection of quartz is at 3.34 Å, and associated minor peaks are at 4.25, 2.29, 1.82, and 1.54 Å. In addition, weak peaks at 4.18 and 3.25 Å could correspond to the main reflections from goethite and microcline, respectively, so these minerals may also be present as minor impurities.

Careful work is needed to distinguish individual kaolin minerals from some impurity phases, such as illites or smectites, although this is possible in combination with various chemical and heat treatments (e.g., Hughes et al., 2009) as illustrated in Figure 2.

The insensitivity of the peaks at ~10.0 Å to ethylene glycol, and heating to 550 ^{o}C means that they correspond at least mainly to the *d*(001) reflections from illite, and that halloysite-10 Å makes only a minor contribution (if any) to their intensity. Halloysite-7 Å and kaolinite are unaffected by glycolation, but become amorphous to x-rays after heating to 550 ^{o}C, and Figure 2 shows the conversion of peaks at *d* ~ 7 Å and ~3.5 Å to an amorphous phase at ~12.38°2θ at this temperature. Finally, since intercalation with formamide results in a increase in the *d*(001) reflection of halloysite-7 Å to ~ 10.0 Å, the peak at 7.17 Å in the original kaolin corresponds primarily to halloysite. XRD can also be used to discriminate various silica forms after orthophosphoric acid digestion and thermal treatment (Kahraman et al., 2005). This can have important safety implications, since α-cristobalite is a potential

carcinogen and pneumoconiosis associated with kaolin mining may be caused at least partially by the presence of silica polymorphs in the kaolins (Altekruse et al., 1984). However, the sensitivity of XRD is such that it often cannot detect small variations in lattice parameters that arise from isomorphous substitutions, especially when they occur at relatively low levels, and the presence of such substitutions is generally inferred from a combination of chemical analyses and measurement of ion exchange capacities. Also, poorly crystalline phases, such as aluminium and/or iron oxides/oxyhydroxides, may be difficult to detect when present in small amounts, since their diffraction patterns are broad and weak, although such phases may have major roles in determining surface properties, because of their large surface areas. Thus, the presence of even small quantities of unrecognized impurity phases can result in misleading conclusions concerning the compositions of minerals, and this approach is of little value in determining the chemical compositions of individual components in mixed mineral specimens.

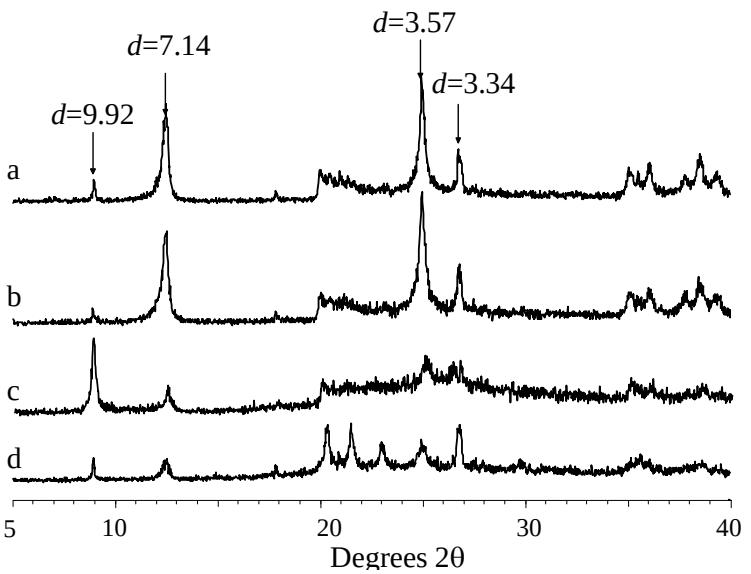

Figure 2. Powder X-ray diffraction patterns of oriented kaolin after (a) air drying, (b) glycolation, (c) intercalation with formamide, and (d) heating to 550 °C.

A variety of chemical and spectroscopic methods have been developed for additional characterization of clay minerals (e.g., Hawthorne, 1988; Coyne et al., 1998). These include electron microscopic techniques (transmission electron microscopy (TEM) and scanning electron microscopy (SEM)) and various spectroscopic methods, such as nuclear magnetic resonance (NMR), infra-red (IR), Mössbauer spectroscopy, etc., which have general applications to mineral characterization. In addition, with mineral samples such as kaolins that have relatively low levels of paramagnetic ions, electron paramagnetic resonance (EPR) spectroscopy can provide valuable information on the nature and distribution of paramagnetic transition metal ions and on free radical defects (e.g., Calas, 1988).

IMPROVEMENTS IN KAOLIN PROPERTIES BY PHYSICAL AND/OR CHEMICAL TREATMENT

Removal of Impurity Phases

For many uses, kaolin quality is based on its brightness and whiteness, and this is a function of the iron content, since iron in the aluminosilicate structure, and especially as an associated oxide phase, produces undesirable colour (e.g., Jepson, 1988; Bertolino et al., 2010). However, improvements in the quality of natural kaolins can be achieved by beneficiation to remove coloured impurity phases. Flocculation and flotation can separate kaolinite from iron and titanium contaminants. Kaolins are hydrophilic and are easily dispersed in water, and this may be aided by the addition of anions, such as phosphate or citrate, which reduce interparticle attraction (Leong et al., 2012), although cations, such as polyethylenimine are more effective.

Paramagnetic impurities, such as iron and titanium oxides, can be removed from kaolins by high gradient magnetic separation and such beneficiation can improve the quality of low grade kaolins (e.g., Chandrasekhar and Ramaswamy, 2002). Iron impurities can also be removed by the action of Fe-reducing bacteria, and the effectiveness of this approach is influenced by nutrients and other chemical species in the leaching solutions (He et al., 2011). Chlorination is another approach that can be used to remove Fe and Ti from kaolins, as illustrated by the work of González and Ruiz (2006), who reported major improvements in the colour of clay pellets after calcining in Cl_2 at 700-950 °C.

Alteration of Kaolin Minerals by Physical and/or Chemical Treatments

Dry grinding results in two concurrent processes, fragmentation of the original structure with exposure of new, amphoteric surfaces, and recombination into large spheroidal aggregates of fine particles; at the same time there is a gradual transformation of hydroxyl groups in the kaolinite structure and an increase in the cation exchange capacity (e.g., Gonzalez Garcia et al., 1991; Vdović et al., 2010). Figure 3 shows SEM micrographs for kaolins containing halloysite (a) and kaolinite (c), which are identified by their characteristic needle and platy morphologies, respectively. After grinding, the original mineral structures are lost (Figure 3b,d).

X-ray diffractograms (Figure 4) show that the kaolin mineral crystallinity is degraded by grinding and little evidence for the presence of the kaolinite/halloysite remains after extracting the ground mineral with sulfuric acid, even though sulfuric acid had little effect on the original structure. In general, grinding followed by acid treatment results in major increases in surface areas with both micro- and mesopores being increased substantially, whereas only micropores are increased in samples produced by thermal alteration (San Cristóbal et al., 2009; Worasith et al., 2011b; Tang et al., 2012). In addition, increased grinding time increases the degree of amorphization and enhances the leaching behavior, with the result that both SiO_2 content and porosity are increased by subsequent acid treatment. Furthermore, prior grinding also inhibits the formation of mullite on heating acid treated samples to 990 °C (San Cristóbal et al., 2009).

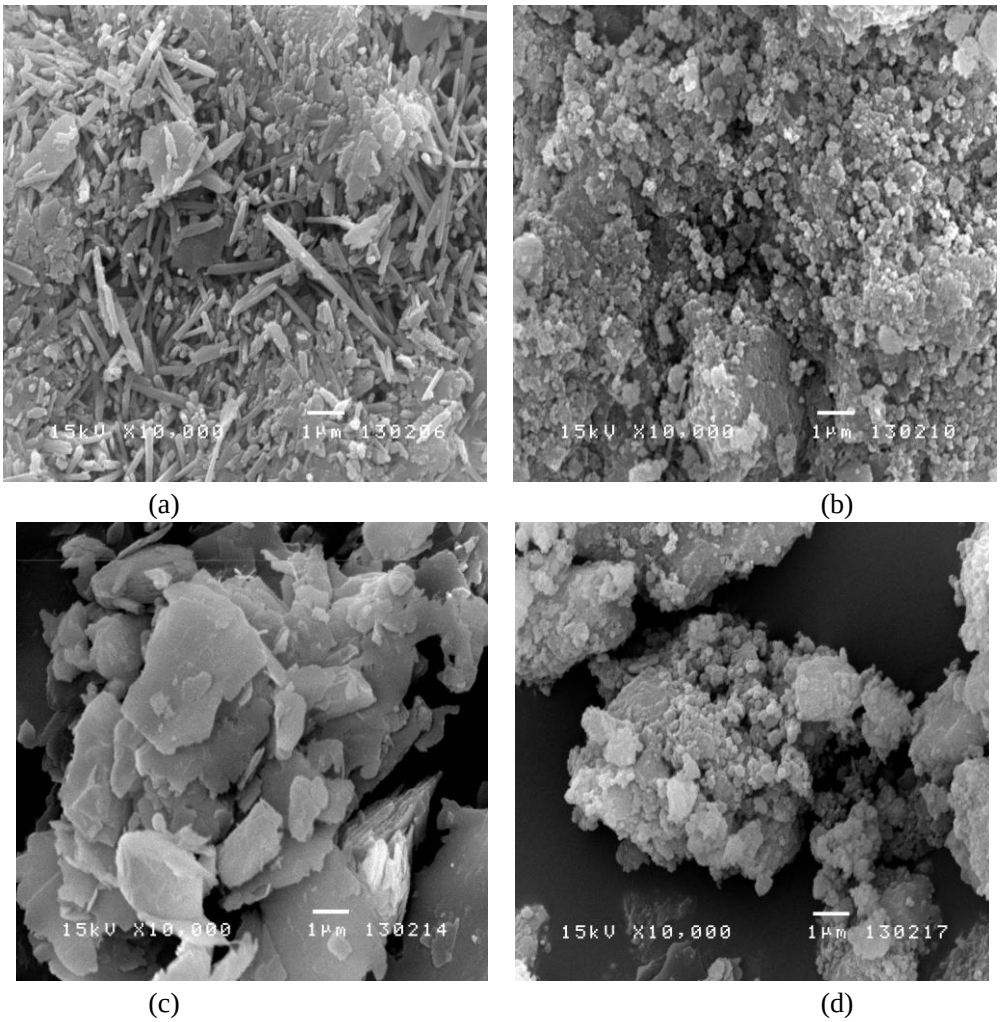

Figure 3. Scanning electron micrographs of kaolins from (a,b) Ranong and (c,d) Lampang after deferration with oxalic acid (a,c) and subsequent grinding for 60 min at 300 rpm in a ball mill with a weight ratio ball : clay of 30:1(b,d).

Changes Induced by Heat Treatment of Kaolin Minerals

Calcining kaolins produces materials with some improved properties compared to the parent mineral, and calcined kaolins also represent sources of Si and/or Al for the preparation of other products. A series of phase transformations take place as kaolins are heated with metakaolins being formed at ~650 °C, mullite at 1050-1100 °C, and refractory grog at ~1300 °C (Murray, 2000; Ghorbel et al., 2008). In a MAS NMR study of the surface properties of calcined kaolins, Liu et al. (2001) showed that the chemical environments of surface Al but not Si were affected by modification with a silane coupling agent.

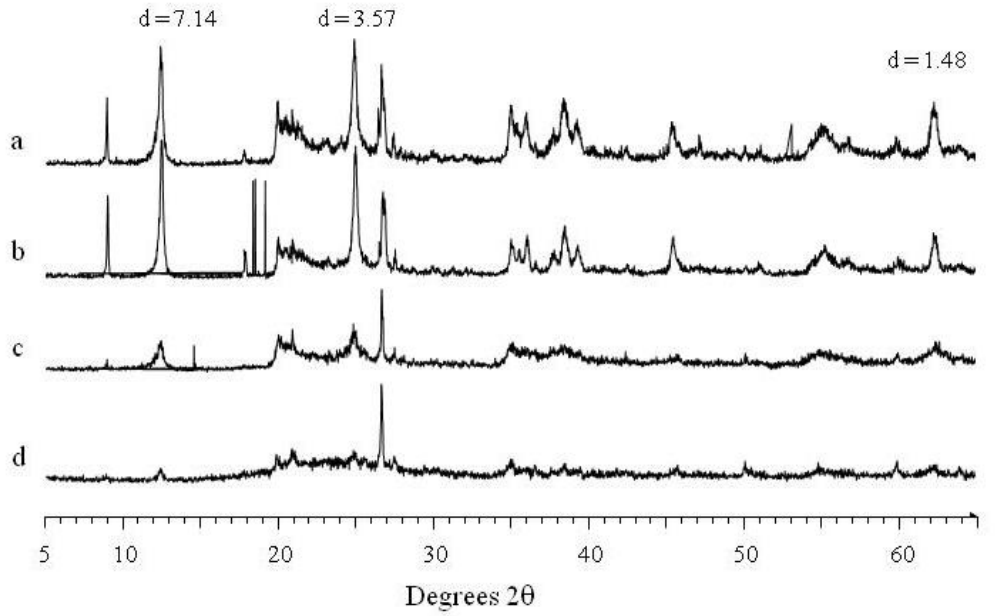

Figure 4. Powder X-ray diffraction patterns for kaolin from Ranong, Thailand (a) untreated, (b) extracted with 18% H_2SO_4, (c) ground for 60 min at 300 rpm in a ball mill, and (d) ground and then extracted with 18% H_2SO_4.

The solubility of calcined kaolin is strongly influenced by pH and the type and level of dispersant/flocculant used (Yuan et al., 1998). In addition, surface properties can be altered by the application of ionic and/or polar non-ionic surfactants to improve dispersion and to generate more functional fillers for the plastics and rubber industries. The dissolution kinetics of calcined kaolin in HCl solution follows the unreacted core model for spherical particles of constant size (Altiokka and Hoşgün, 2003). When used in paper-making, for example, calcined kaolin is required to have good flow characteristics and viscosity stability, both of which are largely controlled by the type and level of soluble salts in kaolin suspensions. Kaolinites and metakaolinites both react with NaOH, but their products are different (Heller-Kallai and Lapides, 2007); kaolinites react with aqueous NaOH under hydrothermal conditions to produce basic hydrosodalite, whereas the metakaolinites derived from them produce mainly zeolite A.

Prolonged grinding of kaolinite–gibbsite mixtures leads to the formation of an X-ray amorphous product (Temuujin et al., 2000), which results from mechanochemical reaction between the kaolinite and α-alumina. Grinding kaolinite-boehmite mixtures produced mullite precursors which were more homogeneous than those in which the kaolinite had been dehydroxylated, suggesting the participation of structural water from the kaolinite. Secondary mullite was formed during thermal reaction of these mixtures by a solution-precipitation mechanism. The mullite initially formed was alumina-rich, but approached the stoichiometric composition with increasing firing temperature.

SYNTHESIS OF NEW MINERALS FROM KAOLINS

Introduction

There are many reports of kaolin minerals being modified by physical or chemical treatments and then characterized to provide an understanding of their potential use as starting materials in the production of materials with novel physical and chemical properties (e.g., Frost et al., 2001a,b, 2004; Temuujin et al., 2001a,b; Belver et al., 2002; Meenakshi et al., 2008; Vágvölgyi et al., 2008; Steudel et al., 2009). This section will provide some selected examples of products prepared from kaolins.

Preparation of Mullite

As mentioned in the previous section, mullite is formed by sintering kaolin minerals; it has the composition $3Al_2O_3.2SiO_2$ or $2Al_2O_3.SiO_2$, and is best known for its ceramic properties. A method for preparing mullite ceramics from kaolinite was described by Pascual et al. (2000). Firstly, a precursor was co-precipitated in the mixture using hexamethylenediamine (HMDA) and a solution of aluminum chloride from acid dissolution of aluminum metal wastes. The use of HMDA instead of ammonium hydroxide, and ground kaolinite produced single-phase mullite and enhanced the flexural strength ($\leq$ 49 MPa) of the resultant ceramic porous bodies after firing at 1550-1600 °C.

The preparation of mullite and mullite/alumina composites by sintering kaolinite and alumina at temperatures >1000 °C was described by Chen et al. (2000). Primary mullite appeared at ~1200 °C, and was unaffected by the presence of alumina, which started to react with the silica in the glassy phase to form secondary mullite at >1300 °C. The formation of secondary mullite decreased the amount of glassy phase, and addition of alumina reduced the size of mullite grains and their aspect ratio. The strength and toughness of the resulting mullite increased with increasing alumina content, but the mechanical properties of the mullite and mullite/alumina composites were lower than those of alumina. In a microstructural study of mullite obtained by sintering kaolinite and α-alumina mixtures in the temperature range 1150-1700°C, Sainz et al. (2000) reported two kinds of morphology corresponding to primary (elongated grains) and secondary (equiaxed grains) in SEM/TEM micrographs, whilst a bimodal crystallite size distribution was detected by XRD microstructural analysis of samples prepared at >1300°C.

As mentioned in the previous section, prolonged grinding of kaolinite–gibbsite and kaolinite-boehmite mixtures produces mullite precursors, which are more homogeneous than those in which the kaolinite has been dehydroxylated (Temuujin et al., 2000). Secondary mullite is formed by a solution-precipitation mechanism when these mixtures are heated.

Sources of Alumina (and Silica)

Kaolins can be used as cheap source materials for the preparation of various forms of alumina of high purity required for use in advanced ceramics and catalysts. The preparation

of iron-free $Al_2(SO_4)_3.18H_2O$ was described by Kang et al., (1995) as being precipitated with ethanol from H_2SO_4 extracts of kaolin powder that had been heated to 800 °C for 3 h. This can then be used as a pure form of Al for transformation to various alumina products. The preparation of *γ*-alumina by selective leaching of silica from calcined kaolin minerals was described by Okada et al., (1995). Initially, very fine spinel-phase grains, consisting of *γ*-alumina with several wt.% of silica, precipitating within an amorphous silica matrix, were obtained by calcining kaolin minerals at around 950 °C. Then porous *γ*-alumina was obtained by selectively dissolving the amorphous silica in KOH solution at 25-90 °C. This *γ*-alumina had a very narrow unimodal pore size range with 2-3 nm radius, specific surface area of ~270 $m^2\ g^{-1}$, and total pore volume of 0.84 ml g^{-1}. In contrast, *γ*-alumina obtained from tubular halloysite had a bimodal pore size distribution with radii of ~2-3 nm and ~10-20 nm, specific surface area of ~320 $m^2\ g^{-1}$, and 0.69 ml g^{-1} total pore volume. The efficiency of the extraction process for alumina from kaolin can be improved appreciably by using microwaves instead of a conventional heating source (Park et al., 2000).

A simple synthesis and characterization of large surface area Al_2O_3 from kaolins were described by Liu and Yang (2010a,b) and Yang et al. (2010). High contents of 5-coordinated Al induced by the coexistence of a macro-mesoporous network indicated a potential application as heterogeneous catalyst. In addition, nanosized γ-Al_2O_3 was synthesized from acid-leachates of calcined kaolin by Yang et al. (2010). Aluminium (hydr)oxide was precipitated with ammonia from the leachate in the presence of polyethylene glycol, and on calcination this was converted to nanosized γ-Al_2O_3 particles with rod-like morphology of about 7 nm width and 20 nm length.

C-shaped time-temperature-transformation curves (T-T-T curves) for cristobalite formation and L-shaped T-T-T curves for α-alumina reaction were established by Liu et al. (1994) for a high-purity kaolinite-α-alumina mixture during heating. Cristobalite formation was retarded by the presence of α-alumina at 1250-1350 °C and prevented at >1380°C due to the formation of secondary mullite. Reaction of α-alumina with kaolinite was initiated at ~1250 °C, was extensive at >1380°C and extremely fast at ≥1600°C as a result of the strong effect of eutectic liquid formation.

Preparation of Cordierite

Cordierite is a ceramic material with composition $Mg_2Al_3Si_5AlO_{18}$ with wide uses as a result of its low thermal expansion and dielectric constant coupled with high chemical and thermal stability. Thermal reactions of magnesium compounds with kaolinite were investigated by Kobayashi et al. (2000) as a potential route to the production of dense cordierite ceramics without the use of additives. Magnesium hydroxide was precipitated from aqueous solution in the form of ultrafine hexagonal tabular particles of about 0.1 μm, and heating this mixture with submicron particles of kaolinite to give $MgO:Al_2O_3:SiO_2$ in a 1:1:2 molar ratio resulted in the formation of an amorphous state at about 900°C. μ-Cordierite then crystallized from the amorphous phase at ~950°C, and gradually transformed into *α*-cordierite at 950-1200°C. Firing the pressed specimens at 1350°C produced *α*-cordierite ceramics with a relative density > 95%, negligible open porosity, and a linear thermal expansion coefficient of 2.2×10^{-6}/K. Kurama et al. (2004) described the preparation of cordietite from kaolin and

ultrafine $Mg(OH)_2$ by heating in the temperature range 900-1200°C with B_2O_3 being added to the mixtures before sintering to address the problem of the short vitrification range. In addition, Chandrasekhar and Pramada (2004) have described the synthesis of zeolite Y from kaolin, and its conversion to MgY by ion exchange and subsequent sintering at 1250 °C to produce cordierite.

The synthesis of cordierite monolithic honeycombs by solid state reaction at high temperature of alumina, kaolin, talc and silica was studied by González-Velasco et al. (1999). The crystal composition was strongly dependent on the temperature and time of reaction, but thermal treatment of the monolithic precursors at 1400°C for 30 minutes allowed formation of high purity cordierite with high crystallinity, whilst maintaining the desired monolithic structure of the honeycombs.

Production of Zeolites from Kaolins

Zeolites are an important family of aluminosilicate materials with unique porous chemical structures. There are many different types of zeolite with various pore sizes and compositions, and they are used extensively as catalysts or adsorbents for gases and low molecular mass molecules. Although naturally occurring, zeolites can also be synthesized by hydrothermal reaction of sodium aluminosilicate gels prepared from pure chemicals in alkaline medium. However, the kaolin minerals are also a convenient source of Si and Al, and can be used in the synthesis of various zeolites especially the low silica types A, X and Y. Zeolites derived from kaolin minerals are generally considered to be inferior to those produced from pure chemicals because of lower brightness as a result of their association with coloured impurities such as micaceous, titanoferrous and ferruginous compounds. Nevertheless, beneficiation processes (as discussed above) can improve the brightness of the original kaolin, and Chandrasekhar et al. (1997) have discussed various stages at which iron-containing minerals can be removed during the preparation of zeolite 4A, a substitute for sodium tri-polyphosphate as a water softening agent in detergents. Recent reports of the synthesis and characterization of Zeolite 4A from kaolins have also been presented by Ugal et al. (2010) and Loiola et al. (2012). Zeolite A along with another zeolite in the form of 0.8-2.3 μm microspheres, can be prepared by alkali activation of mechanically modified kaoliniferous sand and thermally and mechanically modified washed kaolin. This reaction results in a huge increase in the CEC (San Cristóbal et al., 2010), whilst structural disorder in the mechanically modified washed kaolin favours the formation of a single type of zeolite. The hydrothermal synthesis from kaolin or mordenite of zeolites with high Cr(III) exchange capacity was described by Covarrubias et al. (2006). These zeolites had higher Cr(III)-exchange capacity than commercial zeolites, suggesting a potential use in the removal of Cr(III) from industrial wastewaters.

A process for the synthesis of a kaolin-derived zeolite A membrane by electrophoresis was described by Mohammadi and Pak (2002). A tubular module of kaolin was prepared initially by electrophoretic deposition on a cylindrical electrode, then removed, dried, and calcined. Autoclaving with NaOH solution produced a thin membrane of zeolite A on the kaolin tube, which was useful for ethanol/water separation. As was the case for alumina formation in the previous section, an appreciable improvement in the rate of synthesis of

zeolite A from metakaolin can be obtained if microwaves are used as the heat source (Chandrasekhar and Pramada, 2008; Youssef et al., 2008). Furthermore, these products have higher crystallinity than those prepared by conventional hydrothermal synthesis.

In the formation of zeolites from kaolin extrudates, Akolekar et al. (1997) described the transformation to metakaolin followed by conversion to low-silica zeolite X plus a small amount of zeolite A in alkaline solution. The amount of zeolite A decreased with increasing synthesis time, which also resulted in an overall increase in product crystallinity and surface area. A similar approach was used by Alkan et al. (2005) to produce Na zeolite A and hydroxy sodalite from kaolinite, which was first converted to metakaolin by calcining at 600 °C for 2 h, then to zeolite using 4 M NaOH at 105 °C for 2 h in an autoclave. The relative amounts of the products were dependent on the solid/liquid ratios with zeolite A being the main product for lower and hydroxy sodalite for higher ratios. This work also showed that metakaolinisation could be achieved at 600 °C which is much lower than the temperatures (700-900 °C) normally used, and the time necessary for formation of zeolite NaA was less than that reported in the previous literature. With conventional hydrothermal alkaline activation of kaolinite, Ríos et al. (2009b) reported co-crystallization of sodalite and cancrinite, probably via an unstable zeolite intermediate, whilst addition of a SiO_2 source promoted the co-precipitation of several zeolite phases with traces of sodalite and cancrinite. However, if the hydrothermal reaction was preceded by alkaline fusion, kaolinite was converted into zeolite Linde Type A, and the synthesized materials appeared stable thermodynamically.

The conversion of kaolin minerals was taken a step further by Chandrasekhar and Pramada (2001) by sintering Ca-exchanged zeolites A and X formed from a natural kaolinite. The zeolite structure was retained during ion exchange and on sintering up to 750 °C, but further heating resulted in crystallisation of anorthite and the production of an anorthite-glass composite. A firing rate of 3 °C/min resulted in a material with large volume expansion, high porosity and water absorption and low density, but a lower rate of heating (1°C/min) resulted in a normal sintering behaviour and products with high shrinkage and density and good hermeticity. However, the strength of the products was low, and the sintering behaviour seemed to be influenced by the zeolite composition. The hydrothermal transformation of metakaolin in alkaline medium at 473 K to low silica zeolites is influenced by inorganic additives (Lin et al., 2004). Zeolite A was formed in a short period of the initial reaction of metakaolin in the NaOH solution, but this could then be transformed to JBW zeolite with high crystallinity. CAN and SOD zeolites crystallized from reactant mixtures containing K^+ and Na^+ in the presence of additional nitrate and halide, respectively, whereas Li-ABW formed in a LiOH medium.

Zeolite N, an edingtonite-type framework structure, with $1.0 < Si/Al < 2.2$ was produced in < 20 h from a variety of kaolinites and montmorillonites at low temperature (<100 °C) using KOH in the presence of KCl, NaCl, KCl+NaCl and KCl+NaOH, and also under high potassium molarities in the absence of KCl (Mackinnon et al., 2010). Subsequently, Mackinnon et al., (2012) described the production of zeolite N from kaolin between 100 °C and 200 °C in a continuously stirred reactor using KOH and (K,Na)OH and a range of anions, such as F^-, Cl^-, Br^-, I^-, NO_3^-, NO_2^- and CO_3^{2-}. The extent of zeolite N formation was influenced by temperature and KOH molarity, and the introduction of Na to the starting mixture or use of

a single K reagent reduced its stability field. At higher temperatures or higher KOH molarity, other phases such as kalsilite or kaliophyllite were formed.

Zeolite synthesis using kaolin as the Si and Al source is influenced by crystallization time and seed addition (Mignoni et al., 2008). For example, kaolin yielded mordenite, whereas ZSM-5 was obtained from calcined kaolin. Longer synthesis times and seed addition favored mordenite formation, and seed addition led to more highly crystalline phases. Also, zeolite X is obtained if the Si:Al molar ratio is increased by dealumination of kaolin samples before the gel formation step (Colina and Llorens, 2007).

Monolith granular extrudates of 5A zeolite were synthesized from kaolin by Shams and Mirmohammadi (2007), who also investigated the effect of binders on its sieving/adsorption properties. Firstly, the kaolin was calcining at 600 °C, then converted to type A zeolite by immersion in NaOH solution. Monolith extrudates of 4A zeolite powder were prepared using different percentages of kaolin and carboxymethylcellulose as binding agent, and finally converted to 5A type by ion exchange in $CaCl_2$ solution. The highest purity of 5A zeolite, highest rate of Ca^{2+} exchange, and best sieving results were obtained when 30 wt % of kaolin were used. The use of a small amount of carboxymethylcellulose as organic binder had a profound effect on the adsorption properties of the synthesized 5A zeolite, probably as a result of de-clogging cylindrical pores due to carboxymethylcellulose gasification in the final calcination stage.

Hydrothermal synthesis of ZSM-5 using expanded perlite or kaolin as the source of Al was reported by P. Wang et al. (2007). These zeolites had distinctive pore systems, which were a combination of a medium pore ZSM-5 zeolite and a large pore matrix perlite or kaolin, and showed a better fluid catalytic cracking activity in the naphtha aromatization reaction than conventional ZSM-5. Also, a new type of zeolite beta with a multi-pore system was synthesized recently from kaolin by Wan et al. (2010), and shown to have potential value in the formation of composite catalysts for hydrodesulfurization of diesel feed.

Preparation of Composites

Kaolins are also important components of several types of composite materials of varying degrees of complexity. For example Liu et al. (2003) report the synthesis of a series of composites consisting of kaolin, Na zeolite Y, and the aluminosilicate molecular sieve MCM-41 through a two-step crystallization process with kaolin as the starting material. Initially NaY was crystallized on kaolin *in situ*, then MCM-41 was formed on the surface of these kaolin/NaY composites. These triple composites have characteristics of well-ordered mesoporous MCM-41 and NaY zeolite, and a stepwise-distributed pore structure with much higher hydrothermal stability and more Brønsted and Lewis acid sites than a mechanical mixture of the components. Furthermore, cetyltrimethylammonium bromide attached on the NaY phase produced major interactions between the silanol groups in the mesopores.

Another example of kaolin-based composites was reported recently by Lungu et al. (2012) who described the synthesis of kaolin-polymer hydrogel composites via redox-initiated polymerization of acrylic acid in a concentrated aqueous dispersion of kaolin using N,N′-methylene bisacrylamide as a crosslinker. Kaolin had a negative effect on the polymerization rate, which decreased the stiffness of the green bodies prepared at room temperature. However, crosslinking continued to a higher degree on drying at 105 °C, and

larger kaolin contents yielded stiffer composites. The compressive strength increased with acrylic acid concentration up to >25 mass % (relative to kaolin). The equilibrium swelling ratio of the fully-cured kaolin/poly(acrylic acid) composites in water increased with increasing acrylic acid content, and formed porous kaolin ceramics with porosity > 60% after burning off the organic materials.

La^{3+}- and Ce^{3+}- containing micro/mesoporous composite molecular sieves were prepared by Li et al. (2010) under hydrothermal conditions using kaolin as the source of Si and Al. XRD and N_2 adsorption data confirmed the presence of mesoporous MCM-41 and microporous ZSM-5 in the composite, and high resolution TEM and SEM studies showed that the micro- and meso-porosity of the composite were different from that of a mechanical mixture of ZSM-5 and MCM-41. The samples contained large amounts of Brønsted and Lewis acidic sites, and the amount of Brønsted acidic sites was increased significantly by La^{3+} or Ce^{3+} incorporation.

The mechanical properties of organomodified kaolin/natural rubber vulcanizates were described by Yahaya et al. (2009). Kaolin modified with the sodium salt of rubber seed oil (RSO-Na) was compounded with natural rubber by melt intercalation. The tensile and tear properties increased with increasing filler loading. The swelling index was reduced by filling with modified kaolin, and the storage modulus value for the modified samples was higher than for natural rubber vulcanizates with unmodified kaolin. Furthermore, the chemical crosslink density of modified kaolin samples indicated better reinforcement of the rubber-filler matrix, and morphological studies by SEM revealed that incorporation of modified kaolin resulted in an improvement of failure properties of the resulting vulcanizates.

Catalysts consisting of composites with hierarchical pore structures can be prepared via *in situ* assembly of zeolite nanoclusters on kaolin as described by Tan et al. (2007) who synthesized materials with a macro–meso–micro-porous structure from zeolite Y nanoclusters on kaolin using cetyltrimethylammonium bromide as a template under alkaline conditions. The mesophase in the composite contained primary and secondary structural building units of zeolite Y, which contributed micropores in the composite, whereas the kaolin substrate contributed macropores.

Synthesis of Geopolymers

Water plays an important role in geopolymer synthesis from kaolin minerals, and residual water has been shown to depress the activity development of calcined kaolin before stable crystalline phases form (Zuhua et al., 2009). High liquid/solid ratios accelerated dissolution and hydrolysis of Si^{4+} and Al^{3+} compounds, but hindered the polycondensation reaction at high OH^- concentrations, although the presence of some nonevaporable water was necessary for the development of stable geopolymer strength.

The halloysite content of kaolins also influences the dissolution behavior of precursors and the formation of geopolymers (Zhang et al. 2012). The rates of dissolution of Si and Al from kaolin containing halloysite and its metakaolin were higher than from kaolinite and its metakaolin. When mixed with sodium silicate activator, metakaolin derived from kaolin containing halloysite had greater heat evolution at 20 °C and hence a higher geopolymerization rate. The presence of halloysite in the initial kaolin also improved the reactivity of metakaolin under air (20 °C) and steam (80 °C) curing. However, there were

only minor differences in the pore distribution and porosity between products from kaolins with and without halloysite, and both were amorphous to X-rays.

The presence of organic material can also have an important influence on the properties of heated products because of its pore forming effect. For example, organic material can be used to decrease the thermal conductivity of fired clay bricks prepared by extrusion or uniaxial pressing (Gualtieri et al. 2010).

USES OF MODERN KAOLIN-DERIVED PRODUCTS

Traditional Uses of Kaolins

Kaolin minerals play important roles in many areas of life, including agriculture, construction, engineering, and environmental control, because of their desirable physical properties, natural abundance, and low cost; particle sizes are generally very small, yet the minerals are also chemically inert. There have been many reviews of the industrial uses of kaolins (e.g., Keller, 1982; Jepson, 1984; Prasad et al., 1991; Murray, 2000, 2006). Kaolins have traditional applications in the ceramics, paper, paint, and plastics industries, and for use as drilling fluids; samples with low Fe and Ti are also used in the production of fiberglass. Calcined kaolins have extensive uses such as extenders for TiO_2, and as described above may be used as starting materials for to the preparation of various compounds, including zeolites. In addition, their surface properties can be modified so that they will disperse in organophilic and hydrophobic systems. However, new applications of kaolin-derived materials are constantly being generated as result of improved mining and processing technologies, and the development of new procedures to produce products with modified physical and chemical properties. Some recent examples of such applications are briefly reviewed in the following sections.

Ceramics

As mentioned in the previous paragraph, one of the major traditional uses for kaolins is in the production of ceramics. In addition, novel ceramic materials derived from the kaolin minerals are constantly are constantly being developed. Some examples of such products are presented in this sub-section.

Ceramic membranes based on kaolin supported zeolites are useful agents for the removal of water from organic molecules. However, the calcination temperature is critical for separation of water and organic molecules (Morigami et al., 2001) and for the strength of the membrane, which is enhanced as a result of the formation of mullite and spinel phases at high calcination temperatures (Mohammadi and Pak, 2003). Kaolin may also be used as the starting material in the preparation of low cost ceramic membranes for micro- and ultra-filtration. The pore size of such membranes is influenced by the sintering temperature and Nandi et al. (2008) found an increase from 550 to 810 nm when the temperature was increased from 850 to 1000 °C, although the porosity was reduced and flexural strength increased. Such membranes are hydrophobic in nature and potentially useful for the

separation of oil and bacteria from oil-water emulsions and solutions containing bacteria (Vasanth et al., 2011).

Jana et al. (2010) have described the preparation from kaolin of low-cost ceramic microfiltration membranes for the removal of chromate from aqueous solutions by micellar enhanced microfiltration using cetylpyridinium chloride. Improved performance was obtained by incorporating small amounts of sodium carbonate, sodium metasilicate and boric acid into the sintered kaolin. Kaolin-derived ceramic microfiltration membranes incorporating Brewers' yeast as biomass can also be used for removal of Cr(VI) from waters (Vasanth et al., 2012). The efficiency is strongly pH dependent, with high Cr removal at low pH, because of stronger binding with the biomass. Removal efficiency also increased with increasing biomass concentration and decreased with increasing metal ion concentration.

Macroporous mullite ceramic membrane supports have been prepared by *in situ* sintering from natural kaolin combined with $Al(OH)_3$ and AlF_3 as additional Al sources (Chen et al., 2008). Excess SiO_2 from the kaolin was consumed rapidly by addition of the alumina precursors and secondary mullite was formed in the temperature range 1300-1500 °C. During the sintering process, pore structure and stiff skeleton needle-like structure mullite formed in the support, which resulted in good pore structure and high mechanical strength making it suitable for preparing asymmetric ceramic membranes. Furthermore, the pore structure and the micromorphology of the support could be controlled by the amount of Al and the sintering temperature.

Kaolin-Derived Adsorbents

A major use for modified kaolins is in the production of specialized adsorbents, although there have also been several reports of the use of natural kaolins as low cost adsorbents for the removal of toxic cationic (Nandi et al., 2009a,b) and anionic dyes (Vimonses et al., 2009) from wastewaters. However, activation of kaolin minerals to modify their surface properties improves their adsorption capacities for anions (Gogoi and Baruah, 2008), cations (Bhattacharyya and Sen Gupta, 2007) and dyes (Karaoğlu et al., 2010).

Although acid treatment of kaolins is an effective way to remove poorly crystalline impurities, Panda et al. (2010) showed that hydrothermal treatment with strong acid also selectively removes Al from the aluminosilicate structure, thereby increasing the Si/Al ratio, surface area, and pore volume, and hence their function as adsorbents and catalyst supports. Furthermore, kaolin modified with Co or Cu can act as a catalyst for electrochemical oxidation of wastewater, and B. Wang et al. (2007) have described an electrolytic batch reactor with graphite plates as electrodes for treating wastewater from the pulp and paper making industry. H_2O_2 produced on the cathode surface reacts with the catalysts to form hydroxyl radicals, which then destroy pollutants at the kaolin surface. Reactions of copper with kaolin are also important in determining the transport of copper in the environment, and Cu adsorption by kaolin is well described by the Langmuir and Freundlich adsorption equations (Wang et al., 2009); adsorption is largely non-specific and increases with increasing pH.

Natural organic materials such as humic acids enhance the metal adsorption capacity of kaolin surfaces (Arias et al., 2002). Cationic surfactants alter the adsorption properties of clays by changing the hydrophobic character of their surfaces, and Klumpp et al. (1992) have

shown that the amount and rate of adsorption on clays, such as kaolin, illite, and bentonite of aromatic compounds is increased greatly by the presence of cationic C16-surfactants. Also, Li et al. (2011) reported recently that a novel environmental friendly adsorbent, based on calcium alginate immobilized kaolin, has spontaneous and endothermic Cu(II) adsorption at levels much greater than untreated kaolin. In addition, exchange of kaolin with the cetyltrimethylammonium ion greatly increases the adsorption capacities for toxic pollutants, such as o-xylene, phenol and Cu(II) (Sayed Ahmed, 2009), although these are still much lower than with activated carbons.

Kaolins modified by a combination of grinding and acid extraction are able to remove effectively undesirable colored material from rice bran oil (Worasith et al., 2011a), and Worasith and Goodman (2013) showed subsequently that the α-tocopheroxyl radical had exceptional stability in this oil. Adsorption of polymers, such as polyvinyl alcohol or partly hydrolysed polyvinyl acetate on kaolins is strongly influenced by the mineral surface chemical properties (Backfolk et al., 2006), and adsorption is increased by pre-adsorption of anionic dispersants. However, the highest adsorption levels were observed with kaolins containing >1 % montmorillonite, and there was only low affinity of the polymers for montmorillonite-free kaolins, a result which strongly suggests that silanol groups on the basal plane of kaolin particles do not act as anchor sites for the polymer. Lim et al. (1980) also reported that expandable 2:1 mineral impurities were responsible for most of the observed variations in Ca CEC in kaolins, and also found a positive correlation between the Ca CEC and the K-mica content, a result which suggested that the Ca CEC may be related to the degree of mica weathering through an expandable mineral stage. Furthermore, the Cs-retention capacity of the same kaolin was closely related to the vermiculite content and appeared to be related primarily to the presence of interlayer wedges at mica/vermiculite XY interfaces.

Kaolin can function as a support for biofilms, and biosorption of metals on kaolin supported *E. coli* was found by Quintelas et al. (2009) to be in the order Fe(III) > Cd(II) > Ni(II) > Cr(VI) with the adsorption presumably controlled by functional groups on the cell wall surface of the biomass. The optimum conditions for removal of heavy metals from synthetic solutions by zeolites A and X prepared from a local kaolin were described by Jamil et al. (2010), and the adsorption behavior was found to be dependent on the diameter of the hydrated divalent cations in the order Pb > Cd > Cu > Zn >Ni (Ibrahim et al., 2010). These locally prepared zeolites were highly efficient in heavy metal removal at optimum conditions, and were effective as molecular sieves in the separation of some small molecules. Hydrothermal synthesis from kaolin or mordenite of zeolites with high Cr(III) exchange capacity was described by Covarrubias et al. (2006). These zeolites had higher Cr(III)-exchange capacity than commercial zeolites, suggesting a potential use in the removal of Cr(III) from industrial wastewaters.

Microfiltration membranes prepared by *in situ* hydrothermal synthesis from NaA zeolite (which can be prepared from kaolin) on α-Al_2O_3 tubes have been used for treating oil contaminated water (Cui et al. 2008). Oil rejection of >99% was obtained with membranes having pore sizes of 1.2 μm, and water containing less than 1 mg/L oil was produced at 85 L m^{-2} h^{-1} at a membrane pressure of 50 kPa. Consistent membrane performance was maintained by a regeneration regimen involving frequent backwashing with hot water and alkali solution.

Kaolin-Derived Catalysts

The kaolin minerals are an inexpensive source of Al and Si that can be used in the synthesis of micro/mesoporous molecular sieves and catalysts. Some recent examples of such applications are presented in this section.

Thermally treated flint kaolin activated with H_2SO_4 solutions has potential use as an eco-friendly catalyst (do Nascimento et al. 2011), and its performance in the esterification of oleic acid with methanol suggested that could function as a raw material for the production of new solid acid catalysts for biodiesel production. A heterogeneous catalyst prepared from natural kaolin that was dehydroxylated at 800 °C for 10 h, then NaOH-activated at 90 °C for 24 h, and finally calcined again at 500 °C for 6 h was described by Dang et al. (2013) as useful for biodiesel production from trans-esterification of vegetable oils in excess methanol. This catalyst has the advantages of easy preparation, low cost and superior catalytic ability. Efficiencies for the conversion of soybean and palm oils to biodiesel were >95 % under optimal conditions. In addition, a Ni-exchanged Zeolite A prepared from Egyptian kaolin by hydrothermal treatment with alkali solution was reported by Selim et al. (2004) to be 1.36 times more active than the commercial Ni/SiO_2 catalyst for the hydrogenation of sunflower oil.

Herarchical macro–meso–micro-porous structures in composite materials, as discussed in Section 3.6 for the *in situ* assembly of zeolitic nanoclusters on substrates such as kaolin, have superior catalytic performance in cracking heavy crude oil (Tan et al., 2007). Also, composite catalysts based on multi-pore β-zeolite (synthesized from kaolin) with NiW/Al_2O_3 and NiW/TiO_2-Al_2O_3 had much higher hydrodesulfurization (HDS) activity with FCC diesel feed than NiW/γ-Al_2O_3 (Wan et al., 2010). In addition, incorporation of TiO_2 into the composite further increased the HDS conversion activity, which was mainly associated with the appropriate ratio of Brönsted and Lewis acids, and enhanced hydrogenation activity. Duan et al. (2011) have described the optimum acid pretreatments of kaolin for the synthesis of β-zeolite, and the preparation of a series of supported NiMo/β- zeolite/Al_2O_3 catalysts. These catalysts exhibited higher HDS activities than conventional $NiMo/Al_2O_3$ catalysts, and incorporation of acidic zeolite in the support could favor the deep removal of sulfur compounds and meet the S regulation of ultra clean diesel in the Euro-V specification.

Nanoporous aluminosilicates with narrow pore size distributions and large surface areas synthesised using an evaporation-induced self-assembly approach under acidic conditions were shown by Robinson et al. (2009) to function as Lewis acid catalysts for the addition of alcohols to styrene oxide and cyclohexene oxide; samples with high Al contents had optimum activity. Dispersion of kaolin powder in a solid styrene-butadiene solid rubber matrix acts as an additive which decreases the random movement of the polybutadiene chains. The stiffness was shown by Lagazzo et al. (2010) to be related to the yield stress of kaolin dispersion in liquid polybutadiene rubber up to the percolation threshold. Also, a novel fluid catalytic cracking catalyst prepared by mixing microspheres containing ZSM-5 with modified NaY/kaolin composite microspheres synthesized from calcined kaolin showed high performance for the production of propylene (Liu et al., 2007).

Clays such as kaolins and iron-oxide minerals also have potential use as catalysts of Fenton-like reactions for decontamination of soils, groundwaters, sediments, and industrial effluents (Garrido-Ramírez et al., 2010). Oxidation processes involving the generation of

highly oxidizing free radicals have considerable potential for eliminating recalcitrant organic pollutants from various environmental matrices. Additionally, the introduction of nanoparticles in heterogeneous catalytic processes has led to appreciable improvements in catalytic efficiency.

Geopolymers and Cement

Metakaolin is an effective pozzolan which gives major improvements in pore structure, durability, and resistance of concrete to the action of harmful solutions; its utilization in mortar and concrete was reviewed by Sabir et al. (2001). More recently, Liew et al. (2012) demonstrated that geopolymerization of calcined kaolin could produce an alternative to Portland cement, the manufacture of which is environmentally damaging. In an evaluation of the pozzolanic activity of metakaolins formed by heating kaolins to various temperatures, Fabbri et al. (2013) found that it is related to particle size, but independent of kaolinite content, specific surface area or Al coordination number.

The dehydroxylation/amorphization process during the heating of natural and artificial kaolin clays with different amounts of metakaolin has been investigated by Shvarzman et al. (2003), and a procedure for quantitative estimation of the amorphous phase developed. However, Bich et al. (2009) found no direct relationship between the pozzolanic activity of metakaolin and the degree of dehydroxylation, although the highest activity in that work was obtained when the degree of dehydroxylation was >95%. The pozzolanic activity of kaolins after calcination at 650°C for 3 h, was found by Kakali et al. (2001) to be strongly related to the crystallinity of the original kaolinite with well-ordered kaolinite being transformed into less reactive metakaolinite.

The pozzolanic activities of metakaolins obtained by thermal treatment at 700 °C for 1 h, and amorphous kaolin obtained by mechanochemical treatment in a Herzog oscillating mill for 15-120 min were compared by Vizcayno et al. (2010). Both treatments produced reactive pozzolans, but that obtained by mechanochemical treatment of raw kaolin with high quartz content performed especially well. The pozzolanic index and the mechanical resistances obtained by grinding were similar to those by thermal treatment, but were influenced by both the mineralogical composition of the kaolin and the grinding time. The ideal calcination temperature for producing geopolymer cements by dissolving the amorphous products in strong alkali was found to be ~700 °C (Elimbi et al. 2011); products formed under these conditions had the lowest linear shrinkage after aging hardened pastes for 21-28 days, and the highest compressive strengths.

The synthesis of inorganic polymers with Mohs hardness >7, Vickers hardness ~54, and compressive strength of 48.1 MPa was described by Barbosa et al. (2000) for products formed from metakaolinite condensed with sodium silicate in strong alkali. These products contained polymeric Si-O-Al three-dimensional structures with charge-balancing cations in the framework cavities. High-strength geopolymers with Vickers hardness values of ~200 MPa were synthesized by Lecomte et al. (2003) by mixing dehydroxylated kaolin with solutions of sodium metasilicate and KOH followed by the addition of 45 wt.% of ground-granulated blast furnace slag. In both cases the products were completely amorphous, whilst ^{27}Al NMR showed that Al was in tetrahedral coordination, and ^{29}Si NMR spectra indicated a range of Si-O-Al environments.

The hydrothermal synthesis of hydrogarnet and tobermorite from kaolinite and metakaolinite was examined by Rios et al. (2009a) at 175 °C for 24 h in the CaO-Al_2O_3-SiO_2-H_2O system, which is important in cement chemistry. It is closely related to the pozzolanic reaction, the CaO-aggregate reaction, and glass fibre reinforcement of hardened cement. Several poorly crystalline materials were formed, and unreacted $Ca(OH)_2$ was observed at shorter reaction times. Hydrogarnet formed more rapidly than tobermorite, but was transformed into Al-substituted tobermorite with curing. CaO was involved in further reaction with SiO_2; calcium silicate hydrates were formed, and the released Al^{3+} ions were incorporated into tobermorite.

In quicklime-lateritic gravel mixes with ≤ 8 wt.% quicklime, the presence of quicklime reduced the clayey fraction, plasticity index, methylene blue value and maximum dry density, increased optimum moisture content, and resulted in the formation of calcium silicate hydrate type I, portlandite and calcite (Millago et al., 2012). The calcium silicate hydrate was formed by pozzolanic reaction between some kaolinite and hydrated lime in the basic medium; crystallization increased with curing time and the amount of quicklime. This helped improve the mechanical properties and make these lime modified lateritic gravels suitable for use as a base course in road construction.

Other Properties and Uses of Kaolins

Intercalation compounds of kaolinites with urea can be prepared by direct reaction with urea aqueous solution or by dry grinding without water (Fukamachi et al., 2007; Vágvölgyi et al., 2008), although the latter procedure is more effective and produces smaller particle sizes. Grinding kaolins with KH_2PO_4 or $NH_4H_2PO_4$ produces amorphous materials in which K^+, NH_4^+ and PO_4^{3-} are incorporated into the modified kaolin structure (Solihin et al., 2011). The nutrients are only released slowly when the product is dispersed in water, thus demonstrating its potential value as a slow release fertilizer.

Polymers with specific physical characteristics can be utilized to manipulate the properties of clay fabrics. For example, in kaolin-polyacrylamide systems Kim and Palomino (2009) showed that there was a relationship between polymer characteristics, solids contents, and micro-scale particle arrangement. The polymer charge type affected fabric formation only at polymer concentrations above a threshold, whereas the floc/aggregate size and density increased with increasing polyacrylamide concentration, and high molecular-mass polyacrylamides tended to induce the formation of open flocculated structures.

Kaolins can also be modified to act as carriers for organic molecules. By modifying kaolin with the cationic surfactant cetyltrimethylammonium bromide, Sunardi et al. (2011) showed that it could function as a carrier material for gibberellic acid, which was partitioned into the organic phase created by the surfactant tails. Optimum adsorption capacity occurred with a surfactant/kaolin CEC ratio of 2.0. Modified zeolites can be used for drug delivery, so this is a logical development for appropriately modified kaolins. For example, Tomečkova et al. (2012) described modification of clinoptilolite with the flavonoids, quercetin and quercetin dihydrate as anticancer products. The cytotoxicity of zeolite was influenced by the water content of the channel system, and activation at 110°C was more effective than at 400 °C. Also, zeolite modified with quercetin dihydrate had higher cytotoxicity on carcinoma cell lines than that modified with quercetin.

Consumption of kaolin can also aid the recovery from illness, and several types of animal naturally eat clays when sick. In a recent paper, De Jonghe et al. (2009) investigated the effects of kaolin consumption on the recovery from an injection of cisplatin, a toxic chemotherapy agent. Relative to saline-injected controls, cisplatin-injected rats reduced food and water intake and lost weight, but this occurred to a lesser extent with animals with access to kaolin, a result which suggests that kaolin consumption might be useful as an adjunct therapy for other animals, including humans, experiencing visceral malaise.

CONCLUSION AND PROSPECTS FOR THE FUTURE

Kaolins are highly abundant minerals, with commercial quantity deposits present in many regions of the World. However, they are very diverse in terms of both structure and composition, and the presence of impurity phases can have a strong influence on some of their properties. Several traditional uses for kaolins are strongly influenced by their whiteness and brightness as well as their stabilities, but every year sees reports of new potential uses for kaolin-derived materials, in addition to further developments in their traditional uses. Many of these take advantage of the low cost of the minerals to use them as starting materials for the synthesis of a wide range of value-added products. The kaolin industry can, therefore look forward increasing demands for the foreseeable future.

Because of the wide diversity in the composition and properties of different kaolin deposits, the majority of applications of the minerals have focused on a relatively small number of major deposits in different regions of the World. There is, therefore, still need for research to refine the determination of specific characteristics of kaolin minerals that identify their suitability for various novel products. Although technology has been developed to improve the quality of kaolins for traditional uses, it is by no means certain if this is adequate or even desirable for some novel applications of the minerals. As increasing numbers of kaolin deposits become characterized and investigated for potential uses, it is to be expected that yet more uses for this group of minerals will be developed in the future.

ACKNOWLEDGMENTS

NW acknowledges the Rajamangala University of Technology Krungthep for funding to investigate the modification of natural kaolin minerals

REFERENCES

Akolekar, D.; Chaffee, A.; Howe, R.F. The transformation of kaolin to low-silica X zeolite. *Zeolites*, 1997, *19*, 359-365.

Alkan, M.; Hopa, C.; Yilmaz, Z.; Güler, H. The effect of alkali concentration and solid/liquid ratio on the hydrothermal synthesis of zeolite NaA from natural kaolinite. *Microporous and Mesoporous Materials*, 2005, *86*, 176-184.

Altekruse, E.B.; Chaudhary, B.A.; Pearson, M.G.; Morgan, W.K.C. (1984). Kaolin dust concentrations and pneumoconiosis at a kaolin mine. *Thorax*, 1984, *39*, 436-441.

Altiokka, M.R.; Hoşgün, H.L. Investigation of the dissolution kinetics of kaolin in HCl solution. *Hydrometallurgy*, 2003, *68*, 77-81.

Arias, M.; Barral, M.T.; Mejuto, J.C. Enhancement of copper and cadmium adsorption on kaolin by the presence of humic acids. *Chemosphere*, 2002, *48*, 1081-1088.

Backfolk, K.; Rosenholm, J.B.; Husband, J.; Eklund, D. The influence of surface chemical properties of kaolin surfaces on the adsorption of poly(vinyl alcohol). *Colloids and Surfaces A: Physicochemical and Engineering Aspects*, 2006, *275*, 133-141.

Barbosa, V.F.F; MacKenzie, K.J.D; Thaumaturgo, C. Synthesis and characterisation of materials based on inorganic polymers of alumina and silica: sodium polysialate polymers. *International Journal of Inorganic Materials*, 2000, *2*, 309–317.

Belver, C.; Muñoz, M.A.B.; Vicente, M.A. Chemical activation of kaolinite under acid and alkaline conditions. *Chemistry of Material*s, 2002, *14*, 2033-2043.

Bentabol, M.; Cruz, M.D.R.; Huertas, F.J.; Linares, J. Hydrothermal synthesis of Mg-rich and Mg-Ni-rich kaolinite. *Clays and Clay Minerals*, 2006. *54*, 667-677.

Bertolino, L.C.; Rossi, A.M.; Scorzelli, R.B.; Torem, M.L. Influence of iron on kaolin whiteness: An electron paramagnetic resonance study. *Applied Clay Science*, 2010, *49*, 170-175.

Bhattacharyya, K.G.; Sen Gupta, S. Influence of activation of kaolinite and montmorillonite on adsorptive removal of Cd(II) from water. *Industrial & Engineering Chemistry Research*, 2007, *46*, 3734-3742.

Bich, Ch.; Ambroise, J.; Péra, J. Influence of degree of dehydroxylation on the pozzolanic activity of metakaolin. *Applied Clay Science*, 2009, *44*, 194-200.

Brindley, G.W.; Brown G. (1980) *Crystal Structures of Clay Minerals and Their Identification*. Mineralogical Society Monograph No. 5. Mineralogical Society, London.

Calas. G. Electron paramagnetic resonance. In: *Spectroscopic Methods in Mineralogy and Geology*, *Reviews in Mineralogy*, *Vol. 18*, F.C. Hawthorne (Ed.). Washington, DC, Mineralogical Society of America, pp. 573-563, 1988.

Castellano, M.; Turturro, A.; Riani, P.; Montanari, T.; Finocchio, E.; Ramis, G.; Busca, G. Bulk and surface properties of commercial kaolins. *Applied Clay Science*, 2010, *48*, 446-454.

Chandrasekhar, S.; Pramada, P.N. Sintering behaviour of calcium exchanged low silica zeolites synthesized from kaolin. *Ceramics International*, 2001, *27*, 105-114.

Chandrasekhar, S.; Pramada, P.N. Kaolin-based zeolite Y, a precursor for cordierite ceramics. *Applied Clay Science*, 2004, *27*, 187-198.

Chandrasekhar, S.; Pramada, P.N. Microwave assisted synthesis of zeolite A from metakaolin. *Microporous and Mesoporous Materials*, 2008, *108*, 152-161.

Chandrasekhar, S.; Raghavan, P.; Sebastian, G.; Damodaran, A.D. Brightness improvement studies on 'kaolin based' zeolite 4A. *Applied Clay Science*, 1997, *12*, 221-231.

Chandrasekhar, S.; Ramaswamy, S. Influence of mineral impurities on the properties of kaolin and its thermally treated products. *Applied Clay Science*, 2002, *21*, 133-142.

Chen, C.Y.; Lan, G.S.; Tuan, W.H. Preparation of mullite by the reaction sintering of kaolinite and alumina. *Journal of the European Ceramic Society*, 2000, *20*, 2519-2525.

Chen, G.; Qi, H.; Xing, W.; Xu, N. Direct preparation of macroporous mullite supports for membranes by *in situ* reaction sintering. *Journal of Membrane Science*, 2008, *318*, 38-44.

Chen, P.-Y.; Lin, M.-L.; Zheng, Z. On the origin of the name kaolin and the kaolin deposits of the Kauling and Dazhou areas, Kiangsi, China. *Applied Clay Science*, 1997, *12*, 1-25.

Colina, F.G.; Llorens, J. Study of the dissolution of dealuminated kaolin in sodium–potassium hydroxide during the gel formation step in zeolite X synthesis. *Microporous and Mesoporous Materials*, 2007, *100*, 302-311.

Covarrubias, C.; García, R.; Arriagada, R.; Yánez, J.; Garland, M.T. Cr(III) exchange on zeolites obtained from kaolin and natural mordenite. *Microporous and Mesoporous Materials*, 2006, *88*, 220-231.

Coyne, L.M.; Blake, D.F.; Mckeever, S.W.; Mckeever, S.W.S. (Eds.). *Spectroscopic Characterization of Minerals and their Surfaces*, ACS Symposium Series, No. 415, Washington, D.C, American Chemical Society, *1998.*

Cui, J.; Zhang, X.; Liu, H.; Liu, S.; Yeung, K.L. Preparation and application of zeolite/ceramic microfiltration membranes for treatment of oil contaminated water. *Journal of Membrane Science* 2008, *325*, 420-426.

Dang, T.H.; Chen, B.-H.; Lee, D.-J. Application of kaolin-based catalysts in biodiesel production via transesterification of vegetable oils in excess methanol. *Bioresource Technology*, 2013, *145*, 175-181.

De Jonghe, B.C.; Lawler, M.P.; Horn, C.C.; Tordoff, M.G. Pica as an adaptive response: kaolin consumption helps rats recover from chemotherapy-induced illness. *Physiology & Behavior*, 2009, *97*, 87-90.

De Oliveira, M.T.G.; Furtado, S.M.A.; Formoso, M.L.L.; Eggleton, R.A.; Dani, N. Coexistence of halloysite and kaolinite – a study on the genesis of kaolin clays of Campo Alegre Basin, Santa Catarina State, Brazil. *Annals of the Brazilian Academy of Sciences*, 2007, *79*, 665-681.

Dixon, J.B. Kaolin and serpentine group minerals. Chapter 10 In: *Minerals in Soil Environments* (Eds. J.B. Dixon & S.B. Weed) (2nd Edition) - Soil Science Society of America, Book Series, no. 1, pp. 467-525, 1989.

do Nascimento, L.A.S.; Tito, L.M.Z.; Angélica, R.S.; da Costa, C.E.F.; Zamian, J.R.; da Rocha Filho, G.N. Esterification of oleic acid over solid acid catalysts prepared from Amazon flint kaolin. *Applied Catalysis B: Environmental*, 2011, *101*, 495-503.

Duan, A.; Wan, G.; Zhang, Y.; Zhao, Z.; Jiang, G.; Liu, J. Optimal synthesis of micro/mesoporous beta zeolite from kaolin clay and catalytic performance for hydrodesulfurization of diesel. *Catalysis Today*, 2011, *175*, 485-493.

Eggleton, R.A.; Tilley, D.B. Hisingerite: a ferric kaolin mineral with curved morphology. *Clays and Clay Minerals*, 1998, *46*, 400-413.

Elimbi, A.; Tchakoute, H.K.; Njopwouo, D. Effects of calcination temperature of kaolinite clays on the properties of geopolymer cements. *Construction and Building Materials*, 2011, *25*, 2805-2812.

Fabbri, B.; Gualtieri, S.; Leonardi, C. Modifications induced by the thermal treatment of kaolin and determination of reactivity of metakaolin. *Applied Clay Science*, 2013, *73*, 2-10.

Frost, R.L.; Makó, É.; Kristóf, J.; Horváth, E.; & Kloprogge, J.T. Mechanochemical treatment of kaolinite. *Journal of Colloid and Interface Science*, 2001a, *239*, 458-466.

Frost, R.L.; Makó, É.; Kristóf, J.; Horváth, E.; & Kloprogge, J.T. Modification of kaolinite surfaces by mechanochemical treatment. *Langmuir*, 2001b, *17*, 4731-4738.

Frost, R.L.; Horvath, E.; Mako, E.; Kristof, J. Modification of low- and high-defect

kaolinite surfaces: implications for kaolinite mineral processing. *Journal of Colloid and Interface Science*, 2004. *270*, 37-46.

Fukamachi, C.R.B.; Wypych, F.; Mangrich, A.S. Use of Fe^{3+} ion probe to study the stability of urea-intercalated kaolinite by electron paramagnetic resonance. *Journal of Colloid and Interface Science*, 2007, *313*, 537-541.

Garrels, R.M.; Christ, C.L. *Solutions, Minerals and Equilibria.*Harper and Row, New York, 1965.

Garrido-Ramírez, E.G.; Theng, B.K.G.; Mora, M.L. Clays and oxide minerals as catalysts and nanocatalysts in Fenton-like reactions - A review. *Applied Clay Science*, 2010, *47*, 182-192.

Ghorbel, A.; Fourati, M.; Bouaziz, J. Microstructural evolution and phase transformation of different sintered kaolins powder compacts. *Materials Chemistry and Physics*, 2008, *112*, 876-885.

Gogoi, P.K.; Baruah, R. Fluoride removal from water by adsorption on acid activated kaolinite clay. *Indian Journal of Chemical Technology*, 2008, *15*, 500-503.

González, J.A.; Ruiz, M. del C. Bleaching of kaolins and clays by chlorination of iron and titanium. *Applied Clay Science*, 2006, *33*, 219-229.

Gonzalez Garcia, F.; Ruiz Abrio, M.T.; Gonzalez Rodriguez, M. Effects of dry grinding on two kaolins of different degrees of crystallinity. *Clay Minerals*, 1991, *26*, 549-565.

González-Velasco, J.R.; Gutiérrez-Ortiz, M.A.; Ferret, R.; Aranzabal, A.; Botas, J.A. Synthesis of cordierite monolithic honeycomb by solid state reaction of precursor oxides. *Journal of Materials Science*, 1999, *34*, 1999-2002.

Gualtieri, M.L.; Gualtieri, A.F.; Gagliardi, S.; Ruffini, P.; Ferrari, R.; Hanuskova, M. Thermal conductivity of fired clays: Effects of mineralogical and physical properties of the raw materials. *Applied Clay Science*, 2010, *49*, 269-275.

Hawthorne, F.C. (Ed.) *Spectroscopic Methods in Mineralogy and Geology*, Reviews in Mineralogy, Vol. 18, Washington, DC, Mineralogical Society of America, 1988.

He, Q.-X.; Huang, X.-C.; Chen, Z.-L. Influence of organic acids, complexing agents and heavy metals on the bioleaching of iron from kaolin using Fe(III)-reducing bacteria. *Applied Clay Science*, 2011, *51*, 478-483.

Heller-Kallai, L.; Lapides, I. Reactions of kaolinites and metakaolinites with NaOH - comparison of different samples (Part 1). *Applied Clay Science*, 2007, *35*, 99-107.

Huertas, F.J.; Chou, L.; Wollast, R. Mechanism of kaolinite dissolution at room temperature and pressure: Part 1. Surface speciation. *Geochimica et Cosmochimica Acta*, 1998, *62*, 417-431.

Hughes, J.C.; Gilkes, R.J.; Hart, R.D. Intercalation of reference and soil kaolins in relation to physico-chemical and structural properties. *Applied Clay Science*, 2009, *45*, 24-35.

Ibrahim, H.S.; Jamil, T.S.; Hegazy, E.Z. Application of zeolite prepared from Egyptian kaolin for the removal of heavy metals: II. Isotherm models. *Journal of Hazardous Materials*, 2010, *182*, 842-847.

Jamil, T.S.; Ibrahim, H.S.; El-Maksoud, I.H.A.; El-Wakeel, S.T. Application of zeolite prepared from Egyptian kaolin for removal of heavy metals: I. Optimum conditions. *Desalination*, 2010, *258*, 34-40.

Jana, S.; Purkait, M.K.; Mohanty, K. Preparation and characterization of low-cost ceramic microfiltration membranes for the removal of chromate from aqueous solutions. *Applied Clay Science*, 2010, *47*, 317-324.

Jepson, W.B. Kaolins: Their properties and uses. *Philosophical Transactions of the Royal Society London A*, 1984, *311*, 411-432.

Jepson, W.B. Structural iron in kaolinites and in associated ancillary minerals. In: *Iron in Soils and Clay Minerals* Stucki, J.W.; Goodman, B.A.; Schwertmann, U. (Eds.), Dordrecht, Holland, D. Reidel Publishing Company, pp. 467-536, 1988

Kahraman, S.; Önal, M.; Sarıkaya, Y.; Bozdoğan, İ. Characterization of silica polymorphs in kaolins by X-ray diffraction before and after phosphoric acid digestion and thermal treatment. *Analytica Chimica Acta*, 2005, *552*, 201-206.

Kakali, G.; Perraki, T.; Tsivilis, S.; Badogiannis, E. Thermal treatment of kaolin: the effect of mineralogy on the pozzolanic activity. *Applied Clay Science*, 2001, *20*, 73-80.

Kang, H. K.; Kim, K.H.; Park, H.C. Preparation of Fe-free alumina powder from kaolin. *Journal of Materials Science Letters*, 1995, *14*, 425-427.

Karaoğlu, M.H.; Doğan, M.;Alkan, M. Removal of reactive blue 221 by kaolinite from aqueous solutions. *Industrial & Engineering Chemistry Research*, 2010, *49*, 1534-1540.

Keller, W.D. Kaolin - a most diverse rock in genesis, texture, physical properties, and uses. *Geological Society of America Bulletin*, 1982, *93*, 29-36.

Kim, S.; Palomino, A.M. Polyacrylamide-treated kaolin: a fabric study. *Applied Clay Science*, 2009, *45*, 270-279.

Klumpp, E.; Heitmann, H.; Lewandowski, H.; Schwuger, M. J. Enhancing effects during the interaction of cationic surfactants and organic pollutants with clay minerals. *Progress in Colloid and Polymer Science*, 1992, *89*, 181-185.

Kobayashi, Y.; Sumi, K.; Kato, E. Preparation of dense cordierite ceramics from magnesium compounds and kaolinite without additives. *Ceramics International*, 2000, *26*, 739-743.

Kurama, S.; Ozel, E.; Ay, N. Synthesis and sintering of cordierite at low temperature from kaolin and magnesium hydroxide. *Key Engineering Materials*, 2004, *264-268*, 925-928.

Lagazzo, A.; Lenzi, S.; Botter, R.; Cirillo, P.; Demicheli, F.; Beruto, D.T. A rheological method for selecting nano-kaolin powder as filler in SBR rubber. *Particuology*, 2010, *8*, 245-250.

Lecomte, I.; Liégeois, M.; Rulmont, A.; Cloots, R.; Maseri, F. Synthesis and characterization of new inorganic polymeric composites based on kaolin or white clay and on ground-granulated blast furnace slag. *Journal of Materials Research*, 2003, *18*, 2571-2579.

Leong, Y.-K. Teo, J.; Teh, E.; Smith, J.: Widjaja, J.; Lee, J.-X.; Fourie, A.; Fahey, M.; Chen, R. Controlling attractive interparticle forces via small anionic and cationic additives in kaolin clay slurries. *Chemical Engineering Research and Design*, 2012, *90*, 658-666.

Li, X.; Li, B.; Xu, J.; Wang, Q.; Pang, X.; Gao, X.; Zhou, Z.; Piao, J. Synthesis and characterization of Ln-ZSM-5/MCM-41 (Ln=La, Ce) by using kaolin as raw material. *Applied Clay Science*, 2010, *50*, 81-86.

Li, Y.; Xia, B.; Zhao, Q.; Liu, F.; Zhang, P.; Du, Q.; Wang, D.; Li, D.; Wang, Z.; Xia. Y. Removal of copper ions from aqueous solution by calcium alginate immobilized kaolin. *Journal of Environmental Sciences*, 2011, *23*, 404-411.

Liew, Y.M.; Kamarudin, H.; Mustafa Al Bakri, A.M.; Luqman, M.; Khairul Nizar, I.; Ruzaidi, C.M.; Heah, C.Y. Processing and characterization of calcined kaolin cement powder. *Construction and Building Materials*, 2012, *30*, 794-802.

Lim, C. H.; Jackson, M.L.; Koons, R.D.; Helmke, P.A. Kaolins: sources of differences in cation-exchange capacities and cesium retention. *Clays and Clay Minerals*, 1980, *28*, 223-229.

Lin, D.-C.; Xu, X.-W.; Zuo, F.; Long, Y.-C. Crystallization of JBW, CAN, SOD and ABW type zeolite from transformation of meta-kaolin. *Microporous and Mesoporous Materials*, 2004, *70*, 63-70.

Liu, H.; Bao, X.; Wei, W.; Shi, G. Synthesis and characterization of kaolin/NaY/MCM-41 composites. *Microporous and Mesoporous Materials*, 2003, *66*, 117-125.

Liu, H.; Zhao, H.; Gao, X.; Ma, J. A novel FCC catalyst synthesized via *in situ* overgrowth of NaY zeolite on kaolin microspheres for maximizing propylene yield. *Catalysis Today*, 2007, *125*,163-168.

Liu, K.-C.; Thomas, G.; Caballero, A.; Moya, J.S.; de Aza, S. Time-temperature-transformation curves for kaolinite-α-alumina. *Journal of the American Ceramic Society*, 1994, *77*, 1545-1552.

Liu, M.; Yang, H. Facile synthesis and characterization of macro-mesoporous γ-Al_2O_3. *Colloids and Surfaces A: Physicochemical and Engineering Aspects*, 2010a, *371*, 126-130.

Liu, M.; Yang, H. Large surface area mesoporous Al_2O_3 from kaolin: Methodology and characterization. *Applied Clay Science*, 2010b, *50*, 554-559.

Liu, Qinfu; Spears, D.A.; Liu, Qinpu. MAS NMR study of surface-modified calcined kaolin. *Applied Clay Science*, 2001, *19*, 89-94.

Loiola, A.R.; Andrade, J.C.R.A.; Sasaki, J.M.; da Silva, L.R.D. Structural analysis of zeolite NaA synthesized by a cost-effective hydrothermal method using kaolin and its use as water softener. *Journal of Colloid and Interface Science*, 2012, *367*, 34-39.

Lungu, A.; Perrin, F.X.; Belec, L.; Sarbu, A.; Teodorescu, M. Kaolin/poly(acrylic acid) composites as precursors for porous kaolin ceramics. *Applied Clay Science*, 2012, *62-63*, 63-69.

Ma, C.; Eggleton, R.A. Cation exchange capacity of kaolinite. *Clays Clay Minerals*, 1999, *47*, 174-180.

Mackinnon, I.D.R.; Millar, G.J.; Stolz, W. Low temperature synthesis of zeolite N from kaolinites and montmorillonites. *Applied Clay Science*, 2010, *48*, 622-630.

Mackinnon, I.D.R.; Millar, G.J.; Stolz, W. Hydrothermal syntheses of zeolite N from kaolin. *Applied Clay Science*, 2012, *58*, 1-7.

Meenakshi, S.; Sairam Sundaram, C.; Sukumar, R. Enhanced fluoride sorption by mechanochemically-activated kaolinites. *Journal of Hazardous Materials*, 2008, *153*, 164-172.

Mignoni, M.L.; Petkowicz, D.I.; Fernandes Machado, N.R.C.; Pergher, S.B.C. Synthesis of mordenite using kaolin as Si and Al source. *Applied Clay Science*, 2008, *41*, 99-104.

Millogo, Y.; Morel, J.-C.; Traoré, K.; Ouedraogo, R. Microstructure, geotechnical and mechanical characteristics of quicklime-lateritic gravels mixtures used in road construction. *Construction and Building Materials*, 2012, *26*, 663-669.

Mohammadi, T.; Pak, A. Making zeolite A membrane from kaolin by electrophoresis. *Microporous and Mesoporous Materials*, 2002, *56*, 81-88.

Mohammadi, T.; Pak, A. Effect of calcination temperature of kaolin as a support for zeolite membranes. *Separation and Purification Technology*, 2003, *30*, 241-249.

Morigami, Y.; Kondo, M.; Abe, J.; Kita, H.; Okamoto, K. The first large-scale pervaporation plant using tubular-type module with zeolite NaA membrane. *Separation and Purification Technology*, 2001, *25*, 251-260.

Murray, H.H. Traditional and new applications for kaolin, smectite, and palygorskite: a general overview. *Applied Clay Science*, 2000, *17*, 207-221.

Murray H.H. Chapter 5 Kaolin Applications. *Developments in Clay Science*, *2006*, *2*, *85-109.*

Murray H.H. *Applied Clay Mineralogy: occurences, processing, and application of kaolins, bentonites, palygorskite-sepiolite, and common clays*. Amsterdam, Elsevier, 2007.

Nandi, B.K.; Uppaluri, R.; Purkait, M.K. Preparation and characterization of low cost ceramic membranes for micro-filtration applications. *Applied Clay Science*, 2008, *42*, 102-110.

Nandi, B.K.; Goswami, A.; Purkait, M.K. Adsorption characteristics of brilliant green dye on kaolin. *Journal of Hazardous Materials*, 2009a, *161*, 387-395.

Nandi, B.K.; Goswami, A.; Purkait, M.K. Removal of cationic dyes from aqueous solutions by kaolin: Kinetic and equilibrium studies. *Applied Clay Science*, 2009b, *42*, 583-590.

Okada, K.; Kawashima, H.; Saito, Y.; Hayashi, S.; Yasumori, A. New preparation method for mesoporous γ-alumina by selective leaching of calcined kaolin minerals. *Journal of Materials Chemistry*, 1995, *5*, 1241-1244

Panda, A.K.; Mishra, B.G.; Mishra, D.K.; Singh, R.K. Effect of sulphuric acid treatment on physico-chemical characteristics of kaolin clay. *Colloids Surfaces A*, 2010, *363*, 98-104.

Park, S.S.; Hwang, E.H.; Kim, B.C.; Park, H.C. Synthesis of hydrated aluminum sulfate from kaolin by microwave extraction. *Journal of the American Ceramic Society*, 2000, *83*, 1341-1345.

Pascual, J.; Zapatero, J.; Jiménez de Haro, M.C.; Ramírez del Valle, A.J.; Pérez-Rodríguez, J.L.; Sánchez-Soto, P.J. Preparation of mullite ceramics from coprecipitated aluminum hydroxide and kaolinite using hexamethylenediamine. *Journal of the American Ceramic Society*, 2000, *83*, 2677-2680.

Prasad, M.S.; Reid, K.J.; Murray, H.H. Kaolin: processing, properties and applications. *Applied Clay Science*, 1991, *6*, 87-119.

Quintelas, C.; Rocha, Z.; Silva, B.; Fonseca, B.; Figueiredo, H.; Tavares, T. Removal of Cd(II), Cr(VI), Fe(III) and Ni(II) from aqueous solutions by an *E. coli* biofilm supported on kaolin. *Chemical Engineering Journal*, 2009, *149*, 319-324.

Rios, C.A.; Williams, C.D.; Fullen, M.A. Hydrothermal synthesis of hydrogarnet and tobermorite at 175 °C from kaolinite and metakaolinite in the CaO-Al_2O_3-SiO_2-H_2O system : A comparative study. *Applied Clay Science* 2009a, *43*, 228-237

Ríos, C.A.; Williams, C.D.; Fullen, M.A. Nucleation and growth history of zeolite LTA synthesized from kaolinite by two different methods. *Applied Clay Science*, 2009b, *42*, 446-454.

Robinson, M.W.C.; Davies, A.M.; Mabbett, I.; Apperley, D.C.; Taylor, S.H.; Graham, A.E. Synthesis and catalytic activity of nanoporous aluminosilicate materials. *Journal of Molecular Catalysis A: Chemical*, 2009, *314*, 10-14.

Ross, C.S.; Kerr, P.F. The kaolin minerals. *Journal of the American Ceramic Society*, 1930, *13*, 151-160.

Ryan, P.C.; Huertas, F.J. The temporal evolution of pedogenic Fe–smectite to Fe–kaolin via interstratified kaolin–smectite in a moist tropical soil chronosequence. *Geoderma*, 2009, *151*, 1-15.

Sabir, B.B.; Wild, S.; Bai, J. Metakaolin and calcined clays as pozzolans for concrete: a review. *Cement & Concrete Composites*, 2001, *23*, 441-454.

Sainz, M.A.; Serrano, F.J.; Amigo, J.M.; Bastida, J.; Caballero, A. XRD microstructural analysis of mullites obtained from kaolinite–alumina mixtures. *Journal of the European Ceramic Society*, 2000, *20*, 403-412.

San Cristóbal, A.G.; Castelló, R.; Martín Luengo, M.A.; Vizcayno, C. Acid activation of mechanically and thermally modified kaolins. *Materials Research Bulletin*, 2009, *44*, 2103-2111.

San Cristóbal, A.G.; Castelló, R.; Martín Luengo, M.A.; Vizcayno, C. Zeolites prepared from calcined and mechanically modified kaolins. A comparative study. *Applied Clay Science*, 2010, *49*, 239-246.

Sayed Ahmed, S.A. Removal of toxic pollutants from aqueous solutions by adsorption onto organo-kaolin. *Carbon Letters*, 2009, *10*, 305-313.

Selim, M.M.; Hamdy, I.; El-Maksoud, A. Hydrogenation of edible oil over zeolite prepared from local kaolin. *Microporous and Mesoporous Materials*, 2004, *74*, 79-85.

Shams, K.; Mirmohammadi, S.J. Preparation of 5A zeolite monolith granular extrudates using kaolin: Investigation of the effect of binder on sieving/adsorption properties using a mixture of linear and branched paraffin hydrocarbons. *Microporous and Mesoporous Materials*, 2007, *106*, 268-277.

Shvarzman, A.; Kovler, K.; Grader, G.S.; Shter, G.E. The effect of dehydroxylation/amorphization degree on pozzolanic activity of kaolinite. *Cement and Concrete Research*, 2003, *33*, 405-416.

Solihin; Zhang, Q.; Tongamp, W.; Saito, F. Mechanochemical synthesis of kaolin–KH_2PO_4 and kaolin–$NH_4H_2PO_4$ complexes for application as slow release fertilizer. *Powder Technology*, 2011, *212*, 354–358.

Spyridakis, D. E.; Chesters, G.; Wilde, S.A. Kaolinization of biotite as a result of coniferous and deciduous seedling growth. *Soil Science Society of America Journal*, 1967, *31*, 203-210.

Steudel, A.; Batenburg, L.F.; Fischer, H.R.; Weidler, P.G.; Emmerich K. Alteration of non-swelling clay minerals and magadiite by acid activation. *Applied Clay Science*, 2009, *44*, 95-104.

Sunardi, Irawati, U.; Arryanto, Y.; Sutarno. Modified kaolin with cationic surfactant for gibberellic acid carrier materials. *Indonesian Journal of Chemistry*, 2011, *11*, 96-102.

Tan, Q.; Bao, X.; Song, T.; Fan, Y.; Shi, G.; Shen, B.; Liu, C.; Gao, X. Synthesis, characterization, and catalytic properties of hydrothermally stable macro–meso–micro-porous composite materials synthesized via *in situ* assembly of preformed zeolite Y nanoclusters on kaolin. *Journal of Catalysis*, 2007, *251*, 69-79.

Tang, A.; Su, L.; Li, C. Effect of dry grinding on the physicochemical properties of silica materials prepared from kaolin residue. *Powder Technology*, 2012, *218*, 86-89.

Temuujin, J.; MacKenzie, K.J.D.; Schmücker, M.; Schneider, H.; McManus, J.; Wimperis, S. Phase evolution in mechanically treated mixtures of kaolinite and alumina hydrates (gibbsite and boehmite). *Journal of the European Ceramic Society*, 2000, *20*, 413-421.

Temuujin, J.; Burmaa, G.; Amgalan, J.; Okada, K.; Jadambaa, Ts.; MacKenzie, K.J.D. Preparation of porous silica from mechanically activated kaolinite. *Journal of Porous Materials* 2001a, 8, 233-238

Temuujin, J.; Okada, K.; MacKenzie, K.J.D.; Jadambaa, Ts. Characterization of porous silica prepared from mechanically amorphized kaolinite by selective leaching. *Powder Technology*, 2001b, *121*, 259-262.

Tomečkova, V.; Rehakova, M.; Mojžišová, G.; Magura, J.; Wadsten, T.; Zelenakova, K. Modified natural clinoptilolite with quercetin and quercetin dehydrate and the study of their anticancer activity. *Microporous and Mesoporous Materials*, 2012, *147*, 59-67.

Tsolis-Katagas P. and Papoulis D. Physical and chemical properties of some Greek kaolins of different environments of origin. *Bulletin of the Geological Society of Greece*, 2004, *36*, 130-138.

Ugal, J.R.; Hassan, K.H.; Ali, I.H. Preparation of type 4A zeolite from Iraqi kaolin: characterization and properties measurements. *Journal of the Association of Arab Universities for Basic and Applied Sciences*, 2010, *9*, 2-5.

Vágvölgyi, V.; Kovács, J.; Horváth, E.; Kristóf, J.; Makó, É. Investigation of mechanochemically modified kaolinite surfaces by thermoanalytical and spectroscopic methods. *Journal of Colloid and Interface Science*, 2008, *317*, 523-529.

Vasanth, D.; Pugazhenthi, G.; Uppaluri, R. Fabrication and properties of low cost ceramic microfiltration membranes for separation of oil and bacteria from its solution. *Journal of Membrane Science*, 2011, *379*, 154-163.

Vasanth, D.; Pugazhenthi, G.; Uppaluri, R. Biomass assisted microfiltration of chromium(VI) using Baker's yeast by ceramic membrane prepared from low cost raw materials. *Desalination*, 2012, *285*, 239-244.

Vdović, N.; Jurina, I.; Škapin, S.D.; Sondi, L. The surface properties of clay minerals modified by intensive dry milling - revisited. *Applied Clay Science*, 2010, *48*, 575-580.

Vimonses, V.; Lei, S,; Jin, B.; Chow, C.W.K.; Saint C. Adsorption of Congo red by three Australian kaolins. Applied Clay Science, 2009, *43*, 465-472.

Vizcayno, C.; de Gutiérrez, R.M.; Castello, R.; Rodriguez, E.; Guerrero, C.E. Pozzolan obtained by mechanochemical and thermal treatments of kaolin. *Applied Clay Science*, 2010, *49*, 405-413.

Wan, G.; Duan, A.; Zhang, Y.; Zhao, Z.; Jiang, G.; Zhang, D.; Gao, Z. Zeolite beta synthesized with acid-treated metakaolin and its application in diesel hydrodesulfurization. *Catalysis Today*, 2010, *149*, 69-75.

Wang, B.; Gu, L.; Ma, H. Electrochemical oxidation of pulp and paper making wastewater assisted by transition metal modified kaolin. *Journal of Hazardous Materials*, 2007, *143*, 198-205.

Wang, P.; Shen, B.; Shen, D.; Peng, T.; Gao, J. Synthesis of ZSM-5 zeolite from expanded perlite/kaolin and its catalytic performance for FCC naphtha aromatization. *Catalysis Communications*, 2007, *8*, 1452-1456.

Wang, S.; Nan, Z.; Li, Y.: Zhao, Z. The chemical bonding of copper ions on kaolin from Suzhou, China. *Desalination*, 2009, *249*, 991-995.

Worasith, N.; Goodman, B.A. Vitamin E oxidation and tocopheroxyl radical stabilization in bleached rice bran oil identified by EPR spectroscopy. *Food Bioscience*,2013, *4*, 46-49.

Worasith, N.; Goodman, B.A.; Jeyachoke, N.; Thiravetyan, P. Decolorization of rice bran oil using modified kaolin. *Journal of the American Oil Chemists' Society*, 2011a, *88*, 2005-2014.

Worasith, N.; Goodman, B.A.; Neampan, J.; Jeyachoke, N'; Thiravetyan, P. Characterisation of modified kaolin from the Ranong deposit Thailand by XRD, XRF, SEM, FTIR, and EPR techniques. *Clay Minerals*, 2011b, *46*, 525-545.

Yahaya, L.E.; Adebowale, K.O.; Menon, A.R.R. Mechanical properties of organomodified kaolin/natural rubber vulcanizates. *Applied Clay Science*, 2009, *46*, 283-288.

Yang, H.; Liu, M.; Ouyang, J. Novel synthesis and characterization of nanosized γ-Al_2O_3 from kaolin. *Applied Clay Science*, 2010, *47*, 438-443.

Youssef, H.; Ibrahim, D.; Komarneni, S. Microwave-assisted versus conventional synthesis of zeolite A from metakaolinite. *Microporous and Mesoporous Materials*, 2008, *115*, 527-534.

Yuan, J.; Garforth, W.L.; Pruett, R.J. Influence of dispersants on the solubility of calcined kaolin. *Applied Clay Science*, 1998, *13*,137–147.

Zhang, D.; Zhou, C.-H. ; Lin, C.-X.; Tong, D.-S.; Yu W.-H. Synthesis of clay minerals. *Applied Clay Science*, 2010, 50, 1–11.

Zhang, Z.; Wang, H.; Yao, X.; Zhu, Y. Effects of halloysite in kaolin on the formation and properties of geopolymers. *Cement & Concrete Composites*, 2012, *34*, 709-715.

Zuhua, Z.; Xiao, Y.; Huajun, Z.; Yue, C. Role of water in the synthesis of calcined kaolin-based geopolymer. *Applied Clay Science* 2009, *43*, 218-223.

In: Clays and Clay Minerals
Editor: Liam R. Wesley
ISBN: 978-1-63117-779-8

Chapter 11

DNA ADSORPTION CHARACTERISTICS OF CLAY AND COMPOSITE HYDROGEL FORMATION

Yoko Matsuura[1], Shuichi Arakawa[1] and Masami Okamoto[1,•]
1Advanced Polymeric Nanostructured Materials Engineering, Graduate School of Engineering, Toyota Technological Institute,
Hisakata, Tempaku, Nagoya, Japan

ABSTRACT

Clay mineral surfaces have been important for the prebiotic organization and protection of nucleic acids. The adsorption of DNA to mineral surfaces is of great interest because of gene transfer, drug release, bio-adhesion (cell capture) and origins of life studies. Here, we present the morphology observation to provide insight into the adsorption structure and characteristics of DNA by natural allophane particles. The molecular orbital computer simulation has been used to probe the interaction of DNA and/or adenosine 5'-monophosphate and allophane with active sites. Our simulations predicted the strand undergoes some extent of the elongation, which induces the alteration of the conformation of the phosphate backbone, base-base distance and excluded volume correlation among bases. We discuss the general adsorption mechanism for the DNA/allophane complexation and hydrogel formation.

1. INTRODUCTION

1.1. Clay on the Ancient Earth

Clay minerals, comprising a family of layer silicate, are the most ubiquitous nanoscale materials in soil. Nanoscale smectites (e.g., montmorillonite (MMT), hectorite and saponite) are for the most part inherited from the parent rock, i.e., weathering processes [1]. Bacteria also play a vital role in the formation of mineral nanoparticles. Bacteria are well investigated

• Tel: +81-528091861, fax: +81-528091864, E-mail: okamoto@toyota-ti.ac.jp.

for mediating mineral formation in that they have a large surface area to volume ratio, while their cell walls are negatively charged. Accordingly, the bacterial cells are efficient accumulators of charge-balancing cations. This formation of various clay minerals by bacteria in microbial communities, associated with hot spring and deep ocean hydrothermal vents are well known [2].

Besides such environments have generated particular interest as a possible source of the first life forms [3]. One of the leading theories regarding the origins of life is the RNA world hypothesis [4], in which ribozyme plays important roles both information molecules and enzymes and has been made at the very beginning of the origins of life [5]. According to the seminal hypothesis of Bernal in 1949 [6], many prebiotic scenarios including clay minerals were described and many prebiotic experiments were conducted using clays [7]. MMT has been found to catalyze a number of organic reactions on the primitive Earth [7]. The formation of oligomer of RNA that contains monomer units from 2 to 50 is catalyzed by MMT. The oligomer of this length is formed because this catalyst controls the structure of the oligomers synthesized and does not generate all possible isomers. Evidence of sequence-, regio- and homochiral selectivity in these oligomers has been obtained [8]. For many years MMT has been associated in part with the RNA world hypothesis.

The ribozyme, which plays important roles both information molecules and enzymes, has been made at the very beginning of the origin of life in the RNA world hypothesis [4]. However, ultraviolet degrades extracellular RNA and DNA molecules produced through this hypothesis. For the protection of DNA, the adsorption of DNA molecules on clay particles may be significant, as it shall give insights into the origin of life and subsequent survival of the same on this planet.

Moreover, the persistent ability of the DNA molecules could transform competent cells when the DNA molecules bound to clay minerals and humic acids [9].

1.2. Clay Structure

The clays belong to the family of phyllosilicates. Their crystal structure consists of layers made up of two silica tetrahedral fused to an edge-shared octahedral sheet of either aluminium or magnesium hydroxide. The layer thickness is around 1nm and the lateral dimensions of these layers may vary from 30 nm to several microns and even larger depending on the particular layered silicate. Stacking of the layers leads to a regular van der Waals gap between the layers called the *interlayer* or *gallery*. Isomorphic substitution within the layers (for example, Al^{+3} replaced by Mg^{+2} or by Fe^{+2}, or Mg^{+2} replaced by Li^{+1}) generates negative charges that are counterbalanced by alkali and alkaline earth cations situated inside the galleries, as shown in Figure 1 and Table 1.

Allophane is a short-range-order clay mineral and occurs in some soils derived from volcanic ejecta and is able to protect the extracellular DNA and RNA molecules from ultraviolet light. The primary particle of the allophane is a hollow spherule with an outer diameter of 3.5–5.0 nm and a wall of about 0.6–1.0 nm thick, which has perforations as shown in Figures 1 and 2 [10, 11]. The surface area of allophane is as high as ~1000 m^2/g, which is often larger than activated carbon. In addition to this large surface area, the $(OH)Al(OH_2)$ groups exposed on the wall perforations are the source of the pH-dependent charge characteristics of allophane.

2. SURFACE CHARGE CHARACTERISTICS

The surface charge characteristics of MMT and hectorite possess a negative charge.

The surface charge density is particularly important because it determines the interlayer structure of intercalants as well as cation exchange capacity (CEC). Lagaly proposed the method consisting of total elemental analysis and the dimension of the unit cell [12]:

$$\text{Surface charge: } e^-/nm^2 = \xi/ab \quad (1)$$

where ξ is the layer charge (0.33 for montmorillonite (MMT). a and b are cell parameters of MMT (a=5.18 Å, b=9.00Å [13]).

The zeta potential values for the surface of the MMT are negative over the entire pH range from 3 to 11 and even more smaller negative (~ -30 mV) at a higher pH value (Figure 3).

The surface charge characteristics of allophane are very different from that of MMT. Allophane has a variable or pH-dependent surface charge, because the (HO)Al(OH_2) groups, exposed at surface defect sites, can either acquire or lose protons depending on the pH of the ambient solution. They become $^+$(OH_2)Al(OH_2) by acquiring protons on the acidic side of the point of zero charge (PZC), and become (OH)Al(OH)$^-$ by losing protons on the alkaline side (Figure 3) [14].

The PZC of natural allophane (provided by Shinagawa Chemicals Ltd.) was (pH) ~ 6. In the pH range of 5-7, both positively and negatively charged species are present on the surface of allophane particle. They are able to adsorb cations and anions at the same time [14].

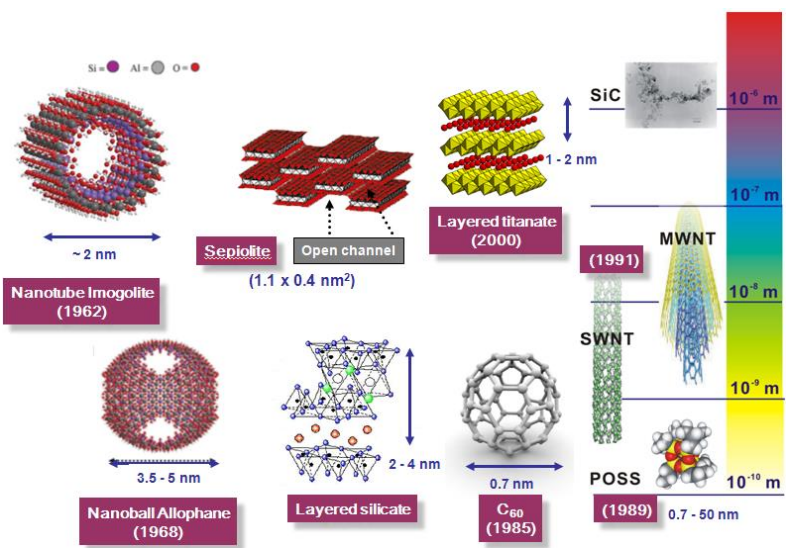

Figure 1. Schematic representation nanostructured materials with dimension. The number in the parenthesis indicates the year of discovery.

Table 1. Clay mineral (phyllosilicates) classification

Type	Group	Groupoid	Species	Tetrahedron	Octahedron	Interlayer cation
2:1 $Si_4O_{10}(OH)_2$	Pyrophyllite Talc (x ～0)	di.	Pyrophyllite	Si_4	Al_2	—
		tri.	Talc	Si_4	Mg_3	—
	Sumectite (0.25< x <0.6)	di.	Montmorillo-nite	Si_4	$(Al_2, Mg)_2$	Na, Ca, H_2O
		di.	Hectorite	Si_4	$(Mg_2, Li)_2$	Na, Ca, H_2O
		di.	Beidellite	$(Si, Al)_4$	Al_2	Na, Ca, H_2O
		tri.	Saponite	$(Si, Al)_4$	Mg_3	Na, Ca, H_2O
	Vermiculite (0.25< x <0.9)	di.	Vermiculite	$(Si, Al)_4$	$(Al, Mg)_2$	K, Al, H_2O
		tri.	Vermiculite	$(Si, Al)_4$	$(Mg, Al)_3$	K, Mg, H_2O
	Mica (x ~1)	di.	Muscovite	$Si_3 \cdot Al$	Al_2	K
			Paragonite	$Si_3 \cdot Al$	Al_2	Na
	Brittle mica (x ~2)	tri.	Phlogopite	$Si_3 \cdot Al$	$(Mg, Fe^{2+})_3$	K
			Biotite	$Si_3 \cdot Al$	$(Fe^{2+}, Mg)_3$	K
2:1:1 $Si_4O_{10}(OH)_8$	Chlorite (large variation of x)	di.	Donbassite	$(Si, Al)_4$	Al_2	$Al_2(OH)_6$
		di.-tri.	Sudoite	$(Si, Al)_4$	$(Al, Mg)_2$	$(Mg, Al)_3(OH)_6$
		tri.	Clinochlore	$(Si, Al)_4$	$(Mg, Al)_3$	$(Mg, Al)_3(OH)_6$
			Chamosite	$(Si, Al)_4$	$(Fe, Al)_3$	$(Fe, Al)_3(OH)_6$

Type	Group	Groupoid	Species	Tetrahedron	Octahedron	Interlayer cation
1:1 Si_2O_5 $(OH)_4$	Kaolin- mineral Serpentinite (x ~ 0)	di.	Kaolinite	Si_2	Al_2	—
			Halloysite	Si_2	Al_2	H_2O
		tri.	Chrysotile	Si_2	Mg_3	—
Needle	Sepiolite Palygorskite (x ~ 0)	tri.	Sepiolite Palygorskite	Si_{12} Si_8	Mg_8 Mg_8	$(OH_2)_4 \cdot H_2O$ $(OH_2)_4 \cdot H_2O$
Amorphous -low crystalline			Imogolite	SiO_3OH	$Al(OH)_3$	—
			Allophane Hisingerite	(1-2) SiO_2 $Al_2O_3 \cdot$ (5-6) H_2O SiO_2—Fe_2O_3—H_2O		

x indicates degree of isomorphaus substitution.

di: indicates dioctahedral, and tri: indicates trioctahedral.

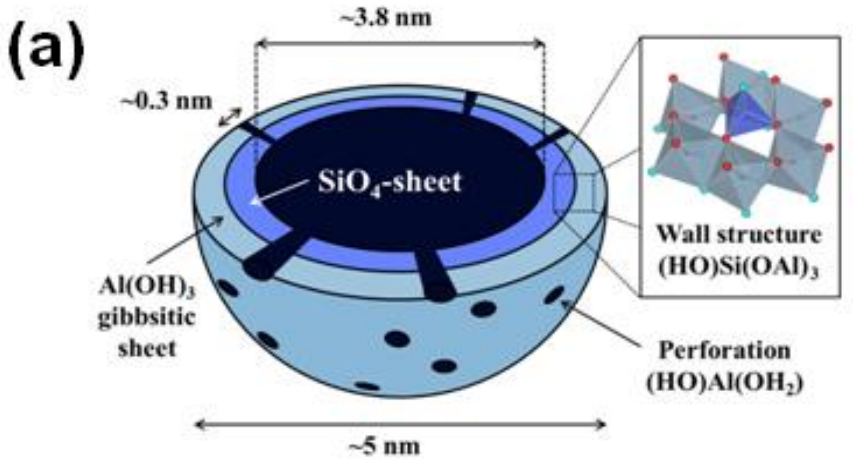

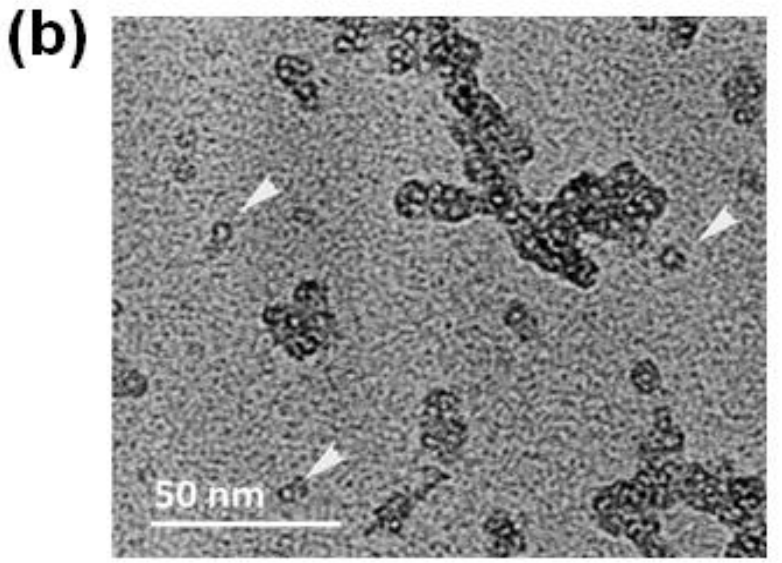

Reproduced with permission from [10]. © 2012, Elsevier Ltd.

Figure 2. (a) Schematic representation of allophane structure. The overall size of a single allophane particle is ~ 5 nm. The pore-size distribution of allophane shows a peak at ~ 1.9 nm. (b) High resolution TEM image of clustered particles of allophane, rather than singular particles. Arrows indicate single unit particles of allophane [10]. The surface area of allophane is as high as ~1000 m2/g, which is often larger than activated carbon.

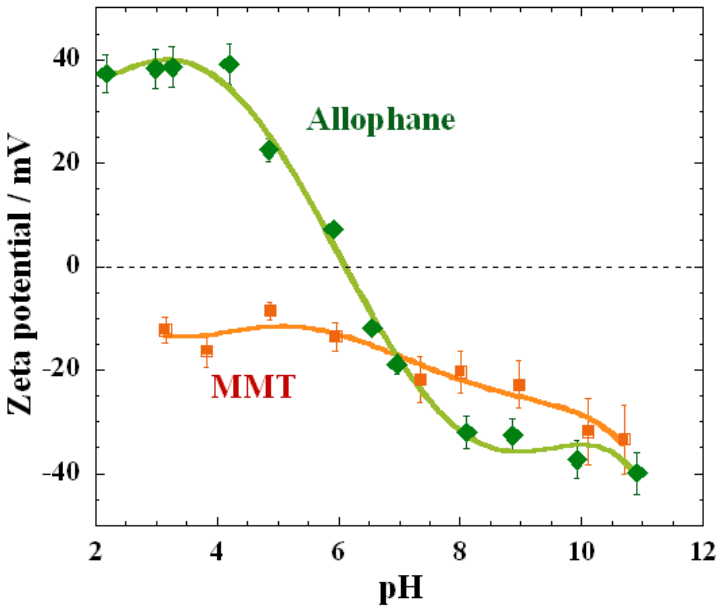

Reproduced with permission from [25]. © 2013, Elsevier Ltd.

Figure 3. Zeta potential versus pH of allophane (provided by Shinagawa Chemicals Ltd.) and MMT [13]. Point of zero charge of allophane is (pH) ~ 6. Results are expressed as mean ± S.D. (n=4).

The phosphate groups of DNA molecules possess a negative charge(PO_2^-). The zeta potential values for the surface of both ss-DNA (Sigma-Aldrich D8899; M_w = 1.64 x 10^7 Da, 5 x 10^4 base) and double-stranded DNA (ds-DNA) (Sigma-Aldrich D1626; M_w = 1300 x 10^3 Da, ca. 2000 base pairs (bps)) are negative over the entire pH range from 2 to 11 and even more smaller negative (~ -40 mV) at a lower pH value, which may be attributed by the acquiring protons to the phosphate groups on the acidic side (Figure 4). Furthermore, the values decrease with increasing continuously to attain -90 mV at pH 7.0. Beyond pH 7.0 for ss-DNA and 10.0 for ds-DNA, the zeta potential values increase again, presumably due to the two differently charged substituted purine groups [15].

3. Adsorption of DNA to Mineral Surfaces

It is possible to investigate the origin of the living organisms and environments of the ancient earth by researching DNA in allophane clusters of the soil.

The adsorption behavior of DNA or RNA molecules on allophane particles has been investigated. Many researchers have discussed the adsorption by using the Langmuir adsorption equation without deep insights into the morphological feature [16-18]. For this reason, the mechanism of DNA molecule adsorption and its sustenance (morphology) in clustered allophane particles was not fully revealed yet.

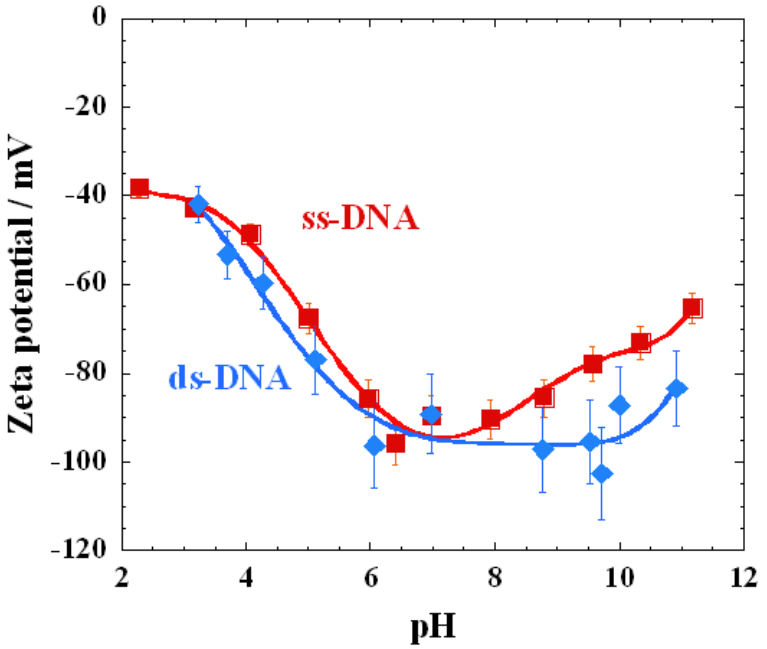

Reproduced with permission from [25]. © 2013, Elsevier Ltd.

Figure 4. Zeta potential versus pH of ss-DNA (Sigma-Aldrich D8899) and ds-DNA (Sigma-Aldrich D1626). Results are expressed as mean ± S.D. (n=4).

3.1. Adsorption of Adenosine 5'-Monophosphate (5'-AMP) and ss-DNA

Hashizume and Theng have reported in 2007 that the large propensity of allophane to retain 5'-AMP is ascribed to ligand exchange between the phosphate of 5'-AMP and the hydroxyl of (HO)Al(OH_2) groups, exposed at perforations on the wall of allophane spherules, giving rise to a surface complex [19]. However, their research have not demonstrated the real complexation and detailed molecular level information.

Matsuura and Okamoto [20] examined the adsorption experiments of 5'-AMP and ss-DNA at 25 °C in the pH 6.5. The isotherms were fitted the by the Freundlich equation with r^2 values ≥ 0.95, and the values are listed in Table. 2. K_f is the relative adsorption capacity of the adsorbent and N is the adsorption intensity, which describes the shape of the isotherm. The adsorption isotherms exhibited a marked curvature, with slopes ($1/N$) significantly < 1.0, indicating a convex up curvature, or *L*-type isotherm. The slope of the isotherms steadily decreased with increasing adsorptive concentration because the vacant sites became less accessible with the progressive covering of the adsorbent surface [21].

The adsorption of 5'-AMP by AK70 shows five order of magnitude higher value of K_f (= 0.157 mol/g mol/$l^{-1/N}$) than that of the ss-DNA (K_f = 2.83 x 10^{-6} mol/g mol/$l^{-1/N}$). The adsorption capacities in mass of adsorbates per unit mass of AK70 are 0.46 and 0.045 g/g g/$l^{-1/N}$ for 5'-AMP and for ss-DNA, respectively. That is, the adsorption capacity of ss-DNA on AK70 exhibits one order of magnitude lower value as compared with that of 5'-AMP. The adsorptions of both 5'-AMP and ss-DNA are facilitated by the interaction between the phosphate groups and the (HO)Al(OH_2) groups on the wall perforations and the interstitial

spaces of the cluster of allophanes. The ss-DNA chains are macromolecules, which hindered the adsorption of the same on the allophanes as compared to the small and compact 5'-AMP molecules.

Table 2. Adsorption parameters of 5'-AMP and ss-DNA and zeta potential of AK70

Adsorbents	Adsorbates	pH	K_f /	N	$r^{2\ a)}$	E_a /
		-	mol/g mol/l$^{-1/N}$	-	-	kJ/mol
AK70	5'-AMP	6.5	0.157	1.23	0.95*	-
	ss-DNA	6.5	2.83×10^{-6}	2.39	0.96	-
		3.0	4.53×10^{-3}	1.38	0.99	24.3
		7.0	1.59×10^{-5}	2.04	0.98	32.0
		9.0	3.08×10^{-7}	2.97	0.97	59.1

[a)] The values are calculated by a log-log linear regression.

* significant at p=0.05 level.

Source: Reproduced with permission from [20]. © 2013, Elsevier Ltd.

The adsorption capacity of ss-DNA decreases with increasing pH (Table 2). The functional groups exposed on the wall perforations of allophane shall be protonated with a lower pH value of the ss-DNA medium. The phosphate groups of ss-DNA possess a negative charge (PO_2^-) that bind directly to the protonated $^+(OH_2)Al(OH_2)$ groups through an electrostatic interaction leading to an increased adsorption. On the contrary, the $(OH)Al(OH_2)$ groups possess a negative charge through deprotonation with an increase in pH of the medium. Thus the adsorption ability of allophanes is highly depended on the interactions of phosphate and $(OH)Al(OH_2)$ groups through protonation and deprotonation with a varying pH.

The activation energy was also assessed by the temperature dependence of the adsorption behavior of ss-DNA at different pHs. A significant decrease in K_f is correlated with E_a associated with higher energy barrier for the adsorption of ss-DNA, which leads to an inverse in adsorption.

In addition, Matsuura and Okamoto [20] examined the morphology observation to provide insight into the adsorption structure and characteristics of ss-DNA by the allophane particles, which was the first time of the real images obtained from microscopic experiment.

Transmission electron microscopy (TEM) offers a qualitative understanding of the adsorption structure through direct visualization. Figure 5 shows the results of TEM bright field images. Before adsorption on allophane, the ss-DNA exhibits a helical configuration with a width of ~ 10 nm (Figure 5a). A single ss-DNA molecule isolated from entangled molecules is highly flexible and continuous over lengths of several micrometers. After the adsorption of ss-DNA molecules on allophane at pH 7.0, typically discrete ss-DNA, ~ 300 nm in length, accompanied with clustered allophane particle with a width of ~ 20 nm on the surface of ss-DNA molecule is observed (Figure 5b), which possibly represented individual ss-DNA molecule adsorbed on allophane surface. Interconnected discrete chains associated with condensation of the allophane clusters could also be observed (Figure 5c). The interstitial spaces of the cluster may play an important role in the adsorption of ss-DNA

molecules. The clustered allophane particles may lead to the formation of network structure as well as bundled thicker strand. Significantly, the allophane cluster is covered over single ss-DNA molecule associated with surface binding. This could be routinely imaged (Figure 5d). The ss-DNA is imaged as a hairpin tube like double-stranded DNA [22].

For aforementioned discussion, the mumerical value of 1/*N* indicates that adsorption capacity is only slightly suppressed at lower equilibrium concentrations.

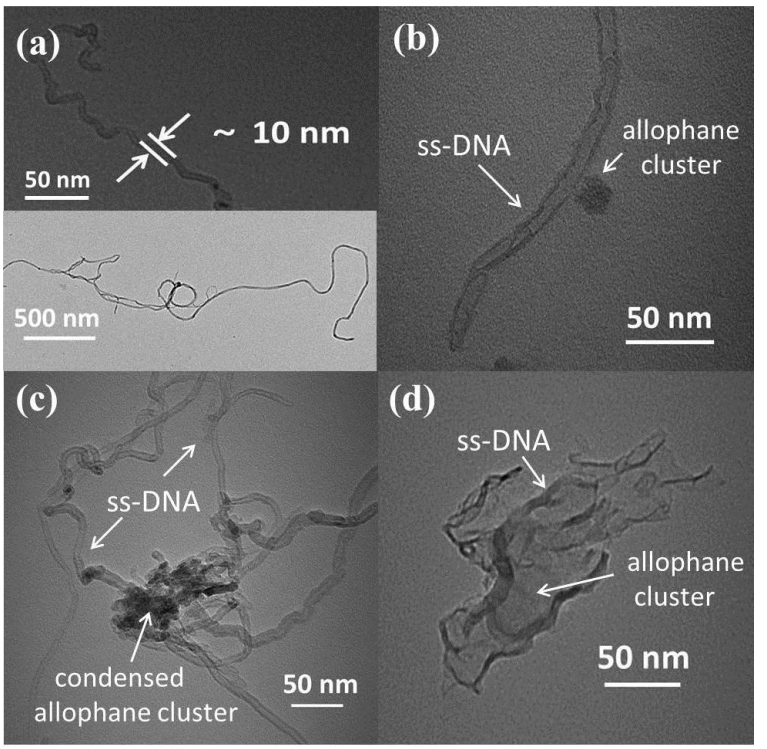

Reproduced with permission from [20]. © 2013, Elsevier Ltd.

Figure 5. TEM images showing (a) single ss-DNA molecule (inset shows lower magnification image), (b) discrete ss-DNA accompanied with the allophane cluster, (c) interconnected discrete chains associated with condensation of the allophane clusters, and (d) individual ss-DNA with mono-layer coverage of the cluster [20].

This isotherm does not predict any saturation of the ss-DNA by the clustered allophane particles: thus infinite surface coverage is predicted [23]. This reasoning is consistent with the adsorption morphologies as expected. The formation of the interaction between PO_2^- groups of ss-DNA and allophane surfaces has been revealed by Fourier transform infrared (FTIR) analysis [20].

3.2. Adsorption Enthalpies of 5'-AMP on Allophane

To understand the generic adsorption in terms of the electrostatic attraction between allophane and negatively charged phosphate (PO_2^-) groups along the backbone of the DNA

single strand and/or 5'-AMP, Matsuura and Okamoto [20] proposed the molecular structures of 5'-AMP and ss-DNA (Figure 6a).

For the generation of accurate model amorphous structure allophane single particle (m-All) (Figure 6b and inset), the constitutive repeating unit (CRU: $(OH)_3Al_2O_3SiOH$) was built and its geometry optimized by energy minimization. Here they compared the results obtained from the simulation of the systems having positively charged ($^{+}(OH_2)Al(OH_2)$), negatively charged ($(OH)Al(OH)^{-}$) sites and $(OH)Al(OH_2)$ as a neutral site on the PZC (Figure 6c). The inset in Figure 6a shows the conformation of 5'-AMP before adsorption by m-All. Taking the corresponding configuration between 5'-AMP and the active sites of m-All the stable configuration based on the minimization of the total energy was extracted from the final simulation snapshot (Figure 7a-c). Clearly, the active site of $(OH)Al(OH_2)$ groups significantly alter the conformation of 5'-AMP with a varying pH as compared to the corresponding structure in the initial state. The conformation is conserved over the duration of MO simulation, indicating the minimization of the total energy regarding heat of formation is arisen from adopting this new configuration consisted of the base (adenine), 2-deoxyribose (sugar) and the phosphate group.

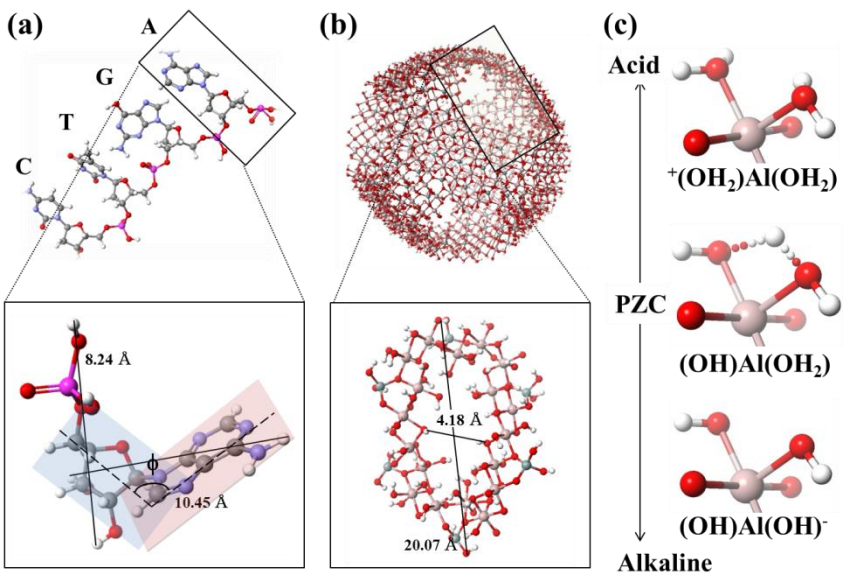

Figure 6. (a) Configuration of ss-DNA with four DNA nts (5'-AGTC-3') and 5'-AMP before adsorption (initial state). (b) Allophane single particle with amorphous structure and modeled allophane (m-All) fragment having a perforation with six (OH)Al(OH2) groups. The incompatible dimensions of the wall perforation (length of 20.07 and width of 4.18 Å) of m-All and the size of 5'-AMP (lengths of 8.24 and 10.45 Å) are constructed. (c) pH variation of active sites from acid to alkaline through PZC. For visualization of the dihedral angle (ϕ), the deoxyribose and adenine have been shaded light blue and pink, respectively, in the inset of (a). Atom colors: O (red), H (white), C (gray), N (blue), P (pink) Si (light gray) and Al (light pink).

The calculated results show that the adsorption enthalpy (ΔH_{ads}) value of the complexation on the acidic site is strongly attractive as compared with that of the complexation on the PZC (Table 3). The ΔH_{ads} values are calculated by using the following equation.

$$\Delta H_{ads} = \Delta H_{complex} - (\Delta H_{ss\text{-}DNA/5'\text{-}AMP} + \Delta H_{m\text{-}All}) \quad (2)$$

where the $\Delta H_{complex}$ value is the heat of formation (in kcal mol^{-1}) of the complexes (such as ss-DNA-m-All or 5'-AMP-m-All) after adsorption, $\Delta H_{ss\text{-}DNA/5'\text{-}AMP}$ is the corresponding ss-DMA or 5'-AMP, and $\Delta H_{m\text{-}All}$, which are the isolated components, respectively.

However, both complexations are more stable than the isolated m-All itself. Naturally those values exhibit much greater than that of the cohesive energy (~ 5 kcal/mol) in case of the physical adsorption [24].

On the other hand, the ΔH_{ads} value on the alkaline side shows positive value, indicating the strong repulsive force is generated between phosphate group in 5'-AMP and $(OH)Al(OH)^-$ active site. On the acidic side, PM6 predicts the bond distances to be 2.10 and 3.04 Å for two P-O·H-O bonds (Figure 7d).

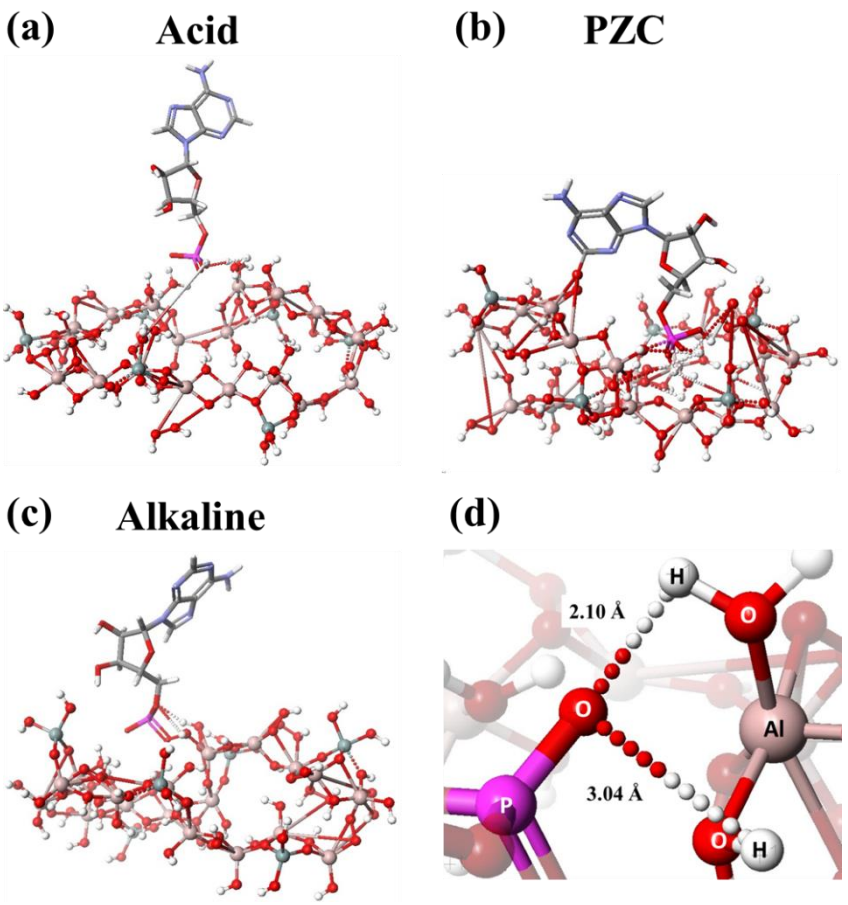

Figure 7. Extracted configuration from the final simulation snapshot of adsorbed 5'-AMP (cylinder model) by m-All (stick and ball model) on acid side (a), on PZC (b), and on alkaline side (c). (d) Two bond distances for P-O···H-O bonds (2.10 and 3.04 Å) on acid side. Color-coding is the same as in Figure 6.

This does not involve the formation of inner-sphere complex through a ligand-exchange reaction between (OH)Al(OH_2) and phosphate groups ($(HO)_2OP=O$ for 5'-AMP), which was proposed by Hashizume et al. [19].

For visualization of the dihedral angle (ϕ) between 2-deoxyribose and adenine, the deoxyribose and base have been shaded light blue and light pink, respectively, in inset (Figure 6a). The estimated angle ϕ of the base against the plane of the 2-deoxyribose exhibits a certain inclination of 113.3 ° in the initial state (Table 3). On the acidic side (at a lower pH), the inclination of the dihedral angle shows large value (154.1 °), then the angle decreases up to 90.9 ° (much smaller than that of the initial state) on the alkaline side (at a higher pH). These values display the extent of the differences caused by the stabilized structure after adsorption on m-All. Those structures can be discerned from the heat of formation that may be calculated in terms of the difference between $\Delta H_{\text{complex}}$ and $\Delta H_{\text{m-All}}$ values (eq. (2)), displaying in Table 3.

The strong complexation might affect the conformation of the phosphate group and hence the base-sugar distance and the excluded volume correlation.

Another interesting feature is that the defect site on the PZC exhibits another complexation between purine and O-Al group of m-All (Figure 7b). For the case of adenine without phosphate group, this implies that the evidence for some possibility of the interaction between adenine ring and allophane particles via combination of electrostatic forces. The results have been demonstrated in the recent paper [10], in which the adenine without phosphate group has some possibility of the interaction between allophane particles.

Table 3. Heat of formation, adsorption enthalpy of complexes, and dihedral angles of adenine against the plane of 2-deoxyriboses after complexation of 5'-AMP-m-All

pH	active sites	Heat of Formation / kcal/mol			$\Delta H_{complex}$-$\Delta H_{m\text{-}All}$	ΔH_{ads}	Dihedral angle[a]
		m-All	5'-AMP	Complexes	kcal/mol	kcal/mol	ϕ / °
acidic	+(OH2) Al(OH2)	-1394.4	-248.3	-1755.0	-360.6	-112.3	154.1
PZC	(OH)Al (OH2)	-3531.1		-3820.8	-289.7	-41.3	132.9
alkaline	(OH)Al (OH)-	-4984.1		-5096.7	-112.6	135.7	90.9

[a] The angle ϕ of 5'-AMP is 113.3 ° in the initial state.

3.3. Adsorption Enthalpies of ss-DNA on Allophane

Figure 8b (upper) shows the proposed conformation of the ss-DNA with four DNA nucleotides (nts) containing individual nucleotide bases (adenine (A), guanine (G), thymine (T), and cytosine (C)) and comprising the following sequences: 5'-AGTC-3', before adsorption. After complexation with m-All, the strand undergoes some extent of the elongation and then the configurations of the bases, 2-deoxyribose and the phosphate

backbone are altered (Figure 8a, b (lower) and angles ϕ in Table 4). As expected, the DNA strand interacts strongly with the active site on the acidic side. As seen in greater enthalpy (-3390.9 kcal/mol) calculated from ($\Delta H_{complex} - \Delta H_{m\text{-}All}$), the positively charged $^{+}(OH_2)Al(OH_2)$ having large ion size might alter the structure of the DNA strand because of the more stable complexation (Table 4). These results confirm the importance of the complexation in changing the DNA structure. For this reason, the repositioning of the individual nucleotide before and after adsorptions by the active site on the acidic side was observed (Figure 8b). The addition of the positively charged $^{+}(OH_2)Al(OH_2)$ to the ss-DNA leads to a significant increase in ΔH_{ads} (-2729.0 kcal/mol) as well as $\Delta H_{complex}$ (-4785.3 kcal/mol) (Table 4) on the acidic side. The enhanced interaction gained through complexation adds considerably to the adsorption of ss-DNA to the allopane particle.

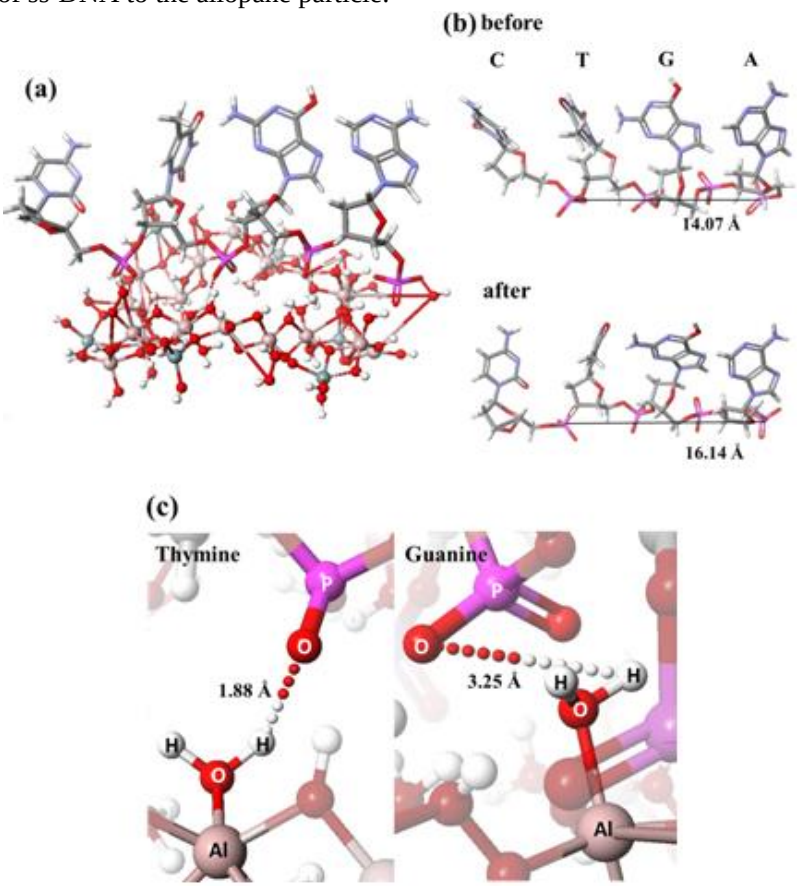

Figure 8. (a) Extracted configuration from the final simulation snapshot of ss-DNA (5'-AGTC-3') (cylinder model) adsorbed by m-All (stick and ball model) on the acidic side. (b) Close up of the configuration of ss-DNA before (upper) and after (lower) adsorptions. m-All has been hidden to increase clarity. (c) Two P-O···H-O distances (1.88 for (T)-nt and 3.25 Å for (G)-nt). Color-coding is the same as in Figure 6.

PM6 predicts the distance between two phosphate groups through 5'- and 3'-terminal sequences to be 16.14 Å as compared to that of the initial state (14.07 Å, displaying in Figure 8b (upper)). The simulation also predicts the two bond distances for P-O·H-O to be 1.88 for (T)-nt and 3.25 Å for (G)-nt, respectively (Figure 8c). The former distance seems to be

stabilized and exhibit much shorter than those of 5'-AMP adsorption due to the orientation of approach of ss-DNA to the active site and the ss-DNA effectively pinned to the site by the two phosphate groups.

Table 4. Heat of formation and dihedral angles of bases against the plane of 2-deoxyriboses of ss-DNA before and after adsorptions

Molecules	Heat of formation / kcal mol^{-1}	Bases	ϕ / °
ss-DNA (initial state)	-662.0	A: adenine G: guanine T: thymine C: cytosine	123.6 144.3 84.5 125.7
ss-DNA-m-All (pH acidic)	-4785.3 (-3390.9)[a] [-2729.0][b] [-1364.5][c]	A G T C	132.1 99.6 85.7 131.1
ss-DNA-m-All (PZC)	-6485.3 (-1993.2)[a] [-1178.5][b] [-589.3][c]	A G T C	90.1 94.8 65.2 104.4
ss-DNA-$(H_2O)_4$ (pH 7)	-1289.1 (-1053.0)[a] [-389.9][b] [-97.5][d]	A G T C	124.9 98.9 72.6 114.1

[a] The value (in kcal mol^{-1}) in the parenthesis is calculated from ($\Delta H_{complex} - \Delta H_{m\text{-}All}$).
[b] The value (in kcal mol^{-1}) in the bracket is an adsorption enthalpy (ΔH_{ads}) calculated by eq. (2).
[c] The value (in kcal mol^{-1}) in the bracket is an adsorption enthalpy (ΔH_{ads}) per one bonding.
[d] The value (in kcal mol^{-1}) in the bracket is an adsorption enthalpy (ΔH_{ads}) per one water molecule.

The angle ϕ for (G)-nt also is discerned from the strong adsorption by m-All. The elongation of the phosphate backbone induces the alteration of the base-base distance and excluded volume correlation among bases.

The strong adsorption enthalpy is a main factor in determining the effectiveness of the interface in the complexation, accompanied by the large exothermic per one bonding (-1364.5 kcal/mol). This value is one order of magnitude greater than that of 5'-AMP adsorption by m-All (-112.3.0 kcal/mol, displaying in Table 4). Owing to the significant difference between ss-DNA molecular and the allophane cluster size (Figure 5b, c), and the incompatible dimensions of the wall perforation and one nt, most of the nts on the phosphate backbone could not act as the active sites.

As described earlier, on the acidic side (pH < PZC), one can postulate that the negatively charged PO_2^- groups along the backbone of the ss-DNA interact with the positively charged ($^+(OH_2)Al(OH_2)$) sites of allophane and subsequently the larger adsorption capacity of ss-DNA is led associated with lower energy barrier as well when we compared with those on the PZC (Table 4). On the PZC, the same features are seen in the corresponding case of 5'-AMP-m-All complexation after adsorption. That is, the ΔH_{ads} value of the complexation on PZC becomes half as compared with that of the MO simulation on the acidic site.

The main difference is the phosphate backbone adopts a more compact conformation as compared with the extended structure of the 5'-AGTC-3' on the acidic side. The distance

between two phosphate groups through 5'- and 3'-terminal sequences is 12.47 Å presumably due to the weak adsorption enthalpy. The visualizations in Figure 8b show the lying more flat on the positively charged ($^{+}(OH_2)Al(OH_2)$) sites.

The result obtained from the complexation with water molecules was also compared. The calculated result shows that the ΔH_{ads} (-97.5 kcal/mol per one water molecule) in ss-DNA-$(H_2O)_4$ is less attractive as compared with that of ss-DNA-m-All (Table 4).

4. DNA/CLAY COMPOSITE HYDROGELS

After adsorption of DNA molecules on the allophane surface, the hydrogel was formed in the clustered allophane particles [25]. The hydrogels based on DNA molecules and natural allophane clusters should also be useful in the conception of new forms of drugs release with highly-specific dosage and an improvement of the technological and biopharmaceutical properties in polymer/clay nanocomposite hydrogels [26-35]. The adsorption of DNA to mineral surfaces is of great interest because of gene transfer, drug release and bio-adhesion (cell capture).

4.1. Morphological Feature of Freeze-Dried Hydrogels [25]

The field emission scanning electron microscope (FE-SEM) images of freeze-dried hydrogels clearly reveal the clustered or agglomerated particles range of 10-20 μm, which are rather than singular particles (a diameter of ~ 5 nm) (Figure 9). The clustered allophane particles are connected each other to form the network structure in water. The FE-SEM image of ds-DNA (Sigma-Aldrich D1626; M_w = 1300 x 10^3 Da, ca. 2000 bps)/allophane (2/8) hydrogel at the same area shows that the C (green), N (purple) and P (light blue) atoms derived from ds-DNA molecules and Al (red), Si (blue) and Fe (brown) corresponding to allophane are distributed on the agglomerated particles as revealed by energy dispersive X-ray spectrometry (EDX) mapping (Figure 9a). The EDX spectrum of allophane confirms the presence of impurities such as Fe-containing minerals. The ds-DNA molecules are probably more readily covered by the agglomerated particles of allophane because the negative charges of ds-DNA molecules are neutralized by the immobilized positive charges of the allophane surfaces.

For the image of ds-DNA/allophane (5/5) hydrogel (Figure 9b), the DNA bundle structure with a width of ~ 2 μm and a length of ~ 15-20 μm rather than single DNA tubes (a diameter and length of 2 [36] and 680 nm [37], respectively) is generated beside the clustered allophane particles. The C, N and Si atoms are also distributed on the structure, suggesting that the DNA molecules are wrapped around the allophane clusters. The ds-DNA bundle structure may play an important role of the interwined network formation in hydrogels.

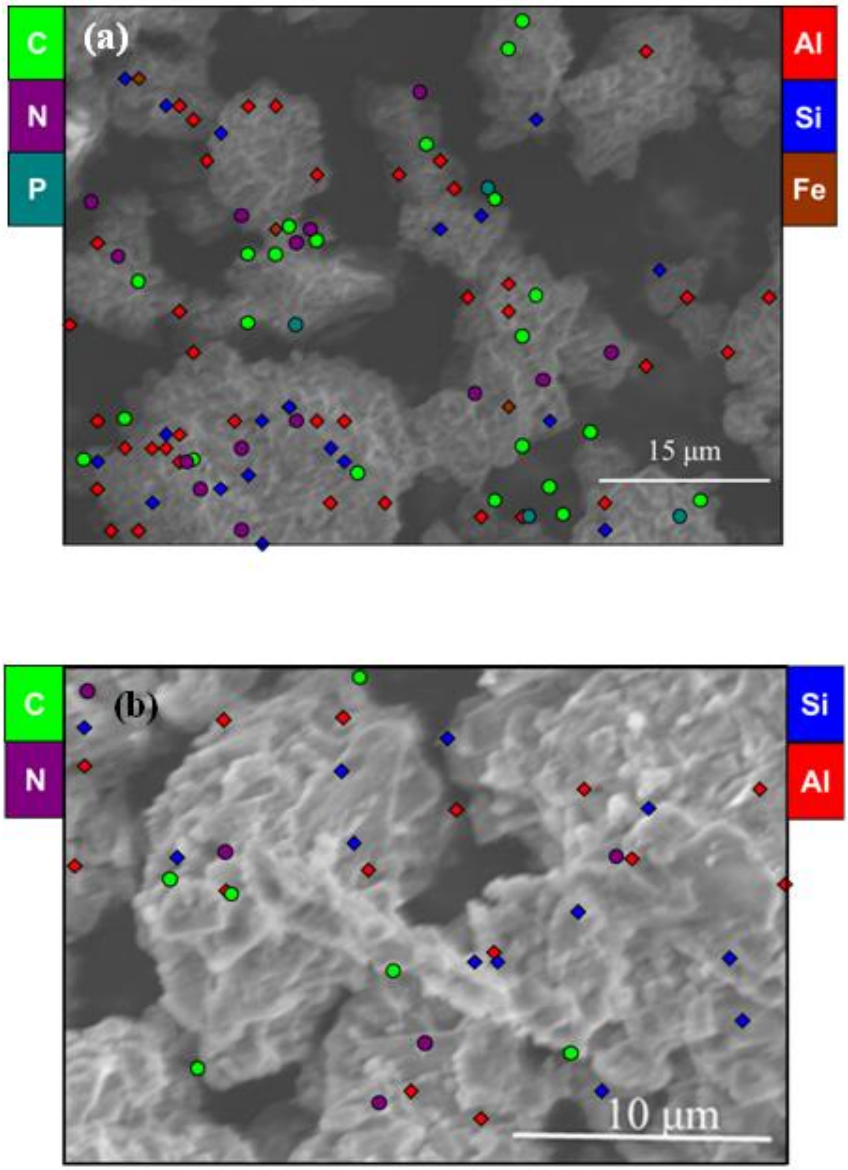

Reproduced with permission from [25]. © 2013, Elsevier Ltd.

Figure 9. FE-SEM images showing freeze-dried (a) ds-DNA/ allophane (2/8) and (b) ds-DNA/allophane (5/5) hydrogels. EDX mapping at the same areas for C (green), N (purple) and P (light blue) atoms derived from DNA, and Al (red), Si (blue) and Fe (brown) corresponding to allophane [25].

4.2. Electrophoresis Analysis of Freeze-Dried Hydrogels [25]

Using electrophoresis analysis we observed that the structure of ds-DNA is changed upon adsorption on the allophane surfaces. Before adsorption of the pristine ds-DNA, the appearance of main peak is observed at 1500 bp having size range from 700-10k bps, whereas the remnant shoulder is located around 100-700 bps size (Figure 10a). As conjectured, the distribution is broad owing to the heterogeneous base composition of the salmon testes DNA.

For the supernatant solution of 90 % adsorption of ds-DNA, the elution profile in the electropherogram remains the short bps around the ds-DNA ladder indicators for a standard range from 100-900 bps (Figure 10b). The electropherogram for 70 % adsorption exhibits the profile similar to that of 90 % adsorption (Figure 10c). The peak mainly consists of short molecule for a standard range from 200-400 bps where it appears. The reason is not obvious at present. However, what is striking in our observation is the magnitude of the mobility of ds-DNA molecules on the surfaces of allophane for the desorption process.

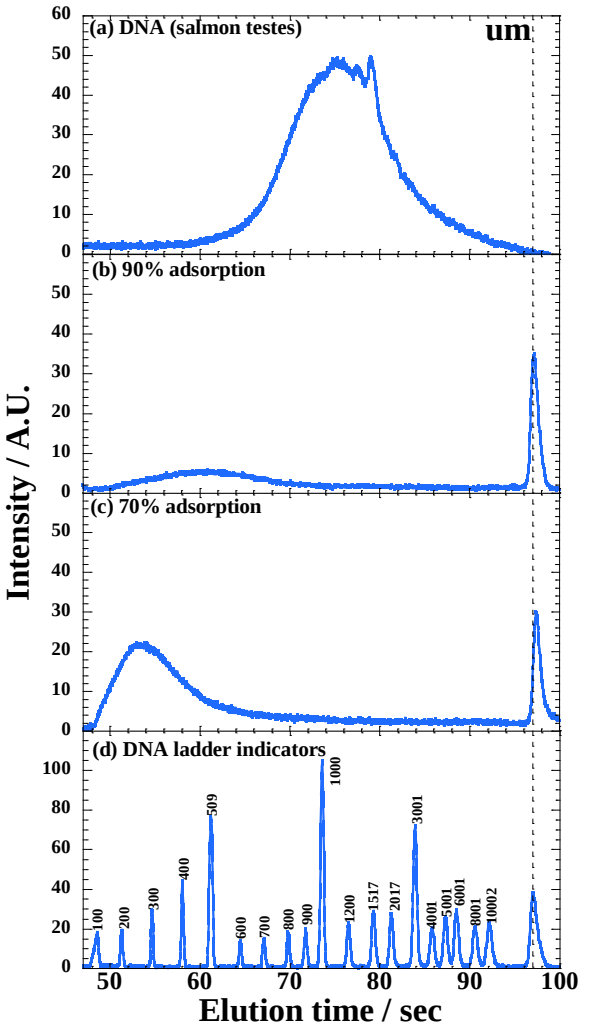

Reproduced with permission from [25]. © 2013, Elsevier Ltd.

Figure 10. Electropherogram of (a) pristine ds-DNA (salmon testes), supernatant solution of (b) 90 % adsorption of ds-DNA and (c) 70 % adsorption of ds-DNA, and (d) ds-DNA ladder indicators range from 100-10002 bps. The dashed line represents the upper marker (um). The lower marker (lm) appears precisely at the elution time of 44.5 s (data not shown) [25].

Thus, we need to consider the possibility that the short bps in ds-DNA cause desorption of the ds-DNA molecules from the allophane surfaces.

4.3. Thermal Denaturation of DNA Molecules in Freeze-Dried Hydrogels [25]

The effect of temperature upon the ds-DNA duplex was investigated by temperature-modulated differential scanning calorimetry (TMDSC), which measures the heat absorbed during thermal denaturation and melting transition [38]. By monitoring the progress of the transition, the TMDSC measurement provides the T_m and associated changes in the calorimetric heat capacity.

Figure 11 shows the temperature-induced unfolding (helix-coil transition) of the DNA duplex in the hydrogels after freeze-drying. As expected, the melting transition of freeze-dried ds-DNA (red) is broad owing to the heterogeneous base composition of the salmon testes DNA, as mentioned above. The excess heat capacity curve of three examined DNA duplexs melting develops from rather high temperature and is somewhat asymmetric as compared to that of the helix-coil transition of DNA duplex (160 ±5 bp) in an aqueous solution of 5 mM sodium cacodylate at pH 6.5 [39]. The values of T_m and calorimetric enthalpy (ΔH) per bp of three examined DNA duplexes, i.e., pristine and ds-DNA/allophane hydrogels are summarized in Table 5. In case of the freeze-dried DNA duplex, the calculated value of ΔH is one order of magnitude greater than that of DNA duplex in an aqueous solution [39], probably due to the transition in solid-state. Obviously, the thermal denaturation is strongly affected by the restricted solid-state. The suppression of the melting (increase of ΔH) may be ascribed to the restricted molecular motions of the DNA duplex in bulk. This feature is much enhanced in ds-DNA/allophane hydrogels.

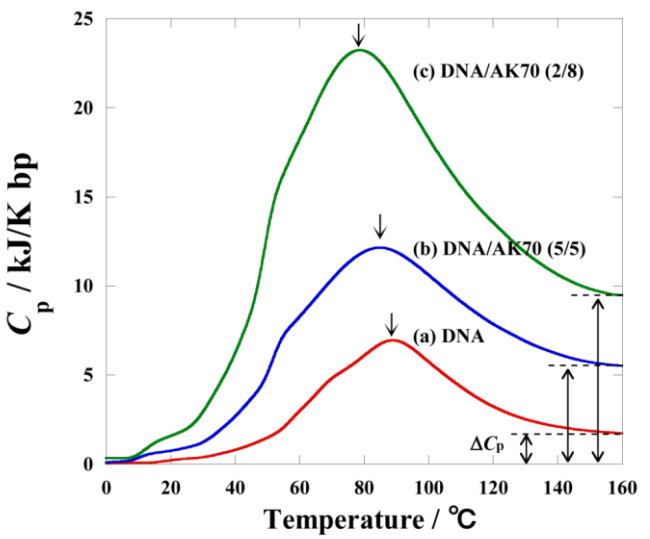

Reproduced with permission from [25]. © 2013, Elsevier Ltd.

Figure 11. TMDSC thermograms for freeze-dried (a) pristine ds-DNA, (b) ds-DNA/allophane (5/5) and (c) ds-DNA/allophane (2/8) hydrogels. Arrows on the excess heat capacity curves indicate melting temperatures. ΔCp is obtained as a baseline-derived gap [25].

The value of ΔH reflects the importance of the interaction generated between phosphate groups of ds-DNA molecules and functional (OH)Al(OH_2) groups on the allophane wall perforations. For the DNA duplexs in DNA/allophane hydrogels, the strand dissociation

occurs in the further region of the endotherm, judging by its sharpness (blue for ds-DNA/allophane (5/5) and green for ds-DNA/allophane (2/8), respectively). The melting temperature (T_m) values as a heat absorption peak slightly decreases with increasing allophane content in hydrogel. Other interesting feature is the non-zero (positive) heat capacity change (ΔC_p) accompanying the helix-coil transition observed in the TMDSC thermograms.

Table 5. Thermodynamic parameters of freeze-dried DNA/AK70 hydrogels and pristine DNA (salmon testes). Results are expressed as mean ±s.d. (*n*=4)

Samples	ΔH / kJ bp^{-1} [a)]	T_m / ℃
DNA/AK70 (2/8)	1024±25	77.8±0.4
DNA/AK70 (5/5)	585±18	83.8±0.3
DNA	321±16	88.5±0.5
DNA (in aq. solution) [b)]	28	75.5

[a)] The values are calculated per base pair (bp).

[b)] The value is measured in an aqueous solution (containing 5 mM sodium cacodylate) of DNA having 160 ±5 bp (5 % w/w) at pH 6.5 and reported by Duguid et al. [39].

Source: Reproduced with permission from [25]. © 2013, Elsevier Ltd.

The ΔC_p for the melting is significant to discuss the changes in enthalpy and entropy for the helix-coil transition [40].

FUTURE OUTLOOKS

Clays are commonly used in the pharmaceutical industry as excipients or active substances. Several studies are related with the decrease in the oral absorption of numerous medicines by the coadministration with clays, but such interactions may also be used to reach technological and biopharmaceutical advantages. This was the starting point in the use of clays in systems of modified drug release [41]. Based upon properties such as swelling, bioadhesion and cell capture, biological polymer/clay composite hydrogels are being targeted to the conception of new forms of drugs release with highly-specific dosage and gene transfer.

The introduction of DNA, RNA, or oligonucleotides into eukaryotic cells is called transfection. This process involves the uptake of extracellular molecules trough the cell membrane into the cytoplasm and also into the nucleus. When DNA is brought into the nucleus, it can be incorporated into a cell's genetic material and induce the production of specific proteins [42]. The transient transfection (DNA does not integrate into the host chromosome) and stable transfection (the foreign DNA is integrated into the chromosome and passed over to the next generation) are distinguished. In contrast, the introduction of small-interfering RNA (siRNA) can selectively turn off the production of specific proteins (gene silencing or antisense technology) [43, 44]. Naked DNA itself cannot successfully enter cells; it requires the assistance of a suitable vector. A tail-vein injection of naked DNA into mice

did not result in gene expression in major organs [45] because of its rapid degradation by nucleases in the blood [46].

Conventional lipoplexes and polyplexes consist of cationic lipids, liposomes, or polymers (poyethyleneimine, poly(L-lysine), poly(D-lysine)) that electrostatically condense nucleic acids into nanoparticles. However, these charged complexes maintain several disadvantages during in vivo delivery including rapid aggregation, high clearance from the bloodstream, and inflammatory toxicity [47]. It has become clear that polyplexes alone are insufficient to meet the transfection requirements of modern medicine, however the studies demonstrate how research is going to meet the demands of non-viral gene delivery.

The clustered allophane particles mediated gene delivery may lead to an advantageous strategy for gene transfer. The inclusion of the complexes in the DNA/clay composite hydrogels may be a step in the right direction for delivery. For this reason, the inflammatory toxicity of allophane particles with bioactive inorganic phases will be in the center of attention in combination with stem cell seeding. The combinational approach of scaffold and the complexes has increased alongside the growth in the knowledge base on the mechanism of gene delivery [48].

REFERENCES

[1] Wilson, M. J. The origin and formation of clay minerals in soils: past, present and future perspectives. *Clay Minerals*, 1999, 34, 7-25.

[2] Tazaki, K. Clays, microorganisms, and biomineralization. In Handbook of Clay Science; Bergaya, F. Theng, B. K. G., Lagaly. G. Eds.; Elsevier: Amsterdam, 2006, pp 477-497.

[3] Wächtershäuser, G. From volcanic origins of chemoautotrophic life to Bacteria, Archaea and Eukarya. *Philos. Trans. R. Soc. London, Ser. B,* 2006, 361, 1787-1808.

[4] Gilbert, W. The RNA world. *Nature,* 1986, 319, 618.

[5] Dworkin, J. P.; Lazcano, A.; Miller, S. L. The roads to and from the RNA world. *J. Theor. Biol.,* 2003, 222, 127-134.

[6] Bernal, J. D. The physical basis of life. *The proceedings of the Physical Society Selection A,* 1949, 62, 537-558.

[7] Nikalje, M. D.; Puhukan, P.; Sudalai, A. Recent advances in clay-catalyzed transformations. *Org. Prep. Proced. Int.,* 2000, 32, 1-40.

[8] Ferris, J. P. Montmorillonite-catalysed formation of RNA oligomers: the possible role of catalysis in the origins of life. *Phil. Trans. R. Soc. B,* 2006, 361, 1777-1786.

[9] Stotzky, G. Persistence and biological activity in soil of insecticidal proteins from Bacillus thuringiens and of bacterial DNA bound on clays and humic acids. *J. Environ. Qual.,* 2000, 29, 691-705.

[10] Iyoda, F.; Hayashi, S.; Arakawa, S.; Okamoto, M. Synthesis and adsorption characteristics of hollow spherical allophane nano-particles. *Appl. Clay Sci.,* 2012, 56, 77-83.

[11] Brigatti, M. F.; Galan, E.; Theng, B. K. G. Structures and mineralogy of clay minerals. In Handbook of Clay Science; Bergaya, F., Theng, B. K. G., Lagaly, G. Eds.; Elsevier: Amsterdam, 2006, pp 19-86.

[12] Lagaly, G. Layer charge determination by alkylammonium ions. In Layer Charge Characteristics of Clays. Mermut, A. R. Ed.; CMS Workshop Lectures, 6, The Clay Minerals Society, Boulder, Colorado 1994, pp 1-16.
[13] Yoshida, O.; Okamoto, M. Diret Melt Intercalation of Polylactide Chains into Nano-Galleries: Interlayer Expansion and Nano-Composite Structure. *Macromol. Rapid Commun.,* 2006, 27, 751-757.
[14] Yuan, G.; Wada, S. I. Allophane and imogolite nanoparticles in soil and their environmental applications. In Nature's Nanostructures; Barnard, A.S., Guo, H.B. Eds.; Pan Stanford Publishing Pte. Ltd.: Shingapore, 2012, pp 485-508.
[15] Schellman, J. A.; Stigter, D. Electrical double layer, zeta potential and electrophoretic charge of double-stranded DNA. *Biopolymers,* 1977, 16, 1415-1434.
[16] Saeki, K.; Sakai, M.; Wada, S. I. DNA adsorption on synthetic and natural allophanes. *Appl. Clay Sci.,* 2010, 50, 493-497.
[17] Taylor, D. H.; Wilson, A. T. The adsorption of yeast RNA by allophane. *Clays Clay Miner,* 1979, 27, 261-268.
[18] Cleaves II, H. J.; Crapster-Pregont, E.; Jonsson, C. M.; Jonsson, C. L.; Sverjensky, D. A.; Hazen, R. A. The adsorption of short single-stranded DNA oligomers to mineral surfaces. *Chemosphere,* 2011, 83, 1560-1567.
[19] Hashizume, H.; Theng, B. K. G. Adenine, adenosine, ribose and 5'-AMP adsorption to allophane. *Clays Clay Miner,* 2007, 55, 599-605.
[20] Matsuura Y.; Iyoda F.; Arakawa S.; John B.; Okamoto M.; Hayashi H. DNA adsorption characteristics of hollow spherule allophane nano-particles. *Mater. Sci. Eng., C* 2013, 33, 5079-5083.
[21] Giles, C. H.; MacEwan, T. H.; Nakhwa, S. N.; Smith, D. Studies in adsorption. Part XI. A system of classification of solution adsorption isotherms, and its use in diagnosis of adsorption mechanisms and in measurement of specific surface areas of solids. *J. Chem. Soc.,* 1960, 148, 3973-3993.
[22] O'Neill, P. R.; Young, K.; Schiffels, D.; Fygenson, D. K. Few-Atom Fluorescent Silver Clusters Assemble at Programmed Sites on DNA Nanotubes. *Nano lett.,* 2012, 12, 5464-5469.
[23] Hasany, S. M.; Saeed, M. M.; Ahmed, M. Sorption and thermodynamic behavior of zinc(II)-thiocyanate complexes onto polyurethane foam from acidic solutions. *J. Radioanal. Nucl. Chem.,* 2002, 252, 477-484.
[24] Okada, K.; Nishimuta, K.; Kameshima, Y.; Nakajima, A. Effect on uptake of heavy metal ions by phosphate grafting of allophane. *J. Colloid Interface Sci.,* 2005, 286, 447-454.
[25] Kawachi, T.; Matsuura, Y.; Iyoda, F.; Arakawa, S.; Okamoto, Preparation and characterization of DNA/allophane composite hydrogels. *Colloids Surf., B* 2013, 112, 429-434.
[26] Campbell, K.; Craig, D. Q. M.; McNally, T. Poly(ethylene glycol) layered silicate nanocomposites for retarded drug release prepared by hot-melt extrusion. *Int. J. Pharmaceut,* 2008, 363, 126-131.
[27] Wang, X.; Du, Y.; Luo, J. Biopolymer/montmorillonite nanocomposite: preparation, drug-controlled release property and cytotoxicity. *Nanotechnology,* 2008, 19, 1-7.

[28] Silva, G. R.; Ayres E.; Orefice R. L.; Moura S. A.; Cara D. C.; Cunha Ada Jr. S. Controlled release of dexamethasone acetate from biodegradable and biocompatible polyurethane and polyurethane nanocomposite. *J. Drug Target,* 2009, 17, 374-383.

[29] Ribeiro, C.; Arizaga, G. G. C.; Wypych, F.; Sierakowski, M. R. Nanocomposites coated with xyloglucan for drug delicary: in vitro studies. *Int. J. Pharmaceut,* 2009, 367, 204-210.

[30] Thatiparti, T. R.; Tammishetti, S.; Nivasu, M. V. UV curable polyester polyol acrylate/bentonite nanocomposites: synthesis, characterization, and drug release. *J Biomed. Mater. Res. B,* 2010, 92, 111-119.

[31] Yuan, Q.; Shah, J.; Hein, S.; Misra, R. D. K. Controlled and extended drug release behavior of chitosan-based nanoparticle carrier. *Acta Biomater.,* 2010, 6, 1140-1148.

[32] Kevadiya, B. D.; Joshi, G. V.; Bajaj, H. C. Layered bionanocomposites as carrier for procainnamide. *Int. J. Pharmaceut,* 2010, 388, 280-286.

[33] Perioli, L.; Ambrogi, V.; di Nauta, L.; Nocchetti, M.; Rossi, C. Effects of hydrotalcite-like nanostructured compounds on biopharmaceutical properties and release of BCS class II drugs: the case of flurbiprofen. *Appl. Clay Sci.,* 2011, 51, 407-413.

[34] Salcedo, I.; Aguzzi, C.; Sandri, G.; Bonferoni, M. C.; Mori, M.; Cerezo, P.; Sanchez, R.; Viseras, C.; Caramella, C. In vitro biocompatibility and mucoadhesion of montmorillonite chitosan nanocomposite: a new drug delivery. *Appl. Clay Sci.,* 2012, 55, 131-137.

[35] Kevadiya, B. D.; Patel T. A.; Jhala D. D.; Thumbar R. P.; Brambhatt H.; Pandya M. P.; Rajkumar S.; Jena P. K.; Joshi G. V.; Gadhia P. K.; Tripathi C. B.; Bajaj H. C. Layered inorganic nanocomposites: a promising carrier for 5-fluorouracil(5-FU). *Eur. J. Pharm. Biopharm.,* 2012, 81, 91-101.

[36] Rosa, M.; Dias, R.; Miguel, M. G.; Lindman, B. DNA-Cationic Surfactant Interactions Are Different for Double- and Single-Stranded DNA. *Biomacromolecules,* 2005, 6, 2164-2171.

[37] Patil, A. J.; Li, M.; Dujardin, E.; Mann, S. Novel Bioinorganic Nanostructures Based on Mesolamellar Intercalation or Single-Molecule Wrapping of DNA Using Organoclay Building Blocks. *Nano Lett.,* 2007, 7, 2660-2665.

[38] Breslauer, K. J.; Freire, E. Straume M. Calorimetry: a tool for DNA and ligand-DNA studies. *Methods Enzymol.,* 1992, 211, 533-567.

[39] Duguid, J. G.; Bloomfield, V. A.; Benevides, J. M.; Thomas, G. J. Jr. DNA melting investigated by differential scanning calorimetry and raman spectroscopy. *Biophysical Journal,* 1996, 71, 3350-3360.

[40] Tikhomirova, A.; Taulier, N.; Chalikian, T. V. Energetics of nucleic acid stability: The effect of ΔC_p. *J. Am. Chem. Soc.,* 2004, 126, 16387-16394.

[41] Aguzzi, C.; Cerezo, P.; Viseras, C.; Caramella, C. Use of clays as drug delivery systems: possibilities and limitations. *Appl. Clay Sci.,* 2007, 36, 22–36.

[42] McNeil, S. E.; Perrie, Y. Gene delivery using cationic liposomesa. *Expert Opin. Ther. Pat.,* 2006, 16, 1371-1382.

[43] Mello, C. C.; Conte, D. Jr. Revealing the world of RNA interference. *Nature,* 2004, 431, 338-342.

[44] Mitterauer, B. Gene silencing: a possible molecular mechanism in remission of affective disorder. *Med. Hypotheses,* 2004, 62(6), 907-910.

[45] Mahato, R. I.; Kawabata, K.; Takakura, Y.; Hashida, M. In vivo disposition characteristics of plasmid DNA complexed with cationic liposomes. *J. Drug Target,* 1995, 3, 149-157.

[46] Sakurai, F.; Terada, T.; Yasuda, K.; Yamashita, F.; Takakura, Y.; Hashida, M. The role of tissue macrophages in the induction of proinflammatory cytokine production following intravenous injection of lipoplexes. *Gene Ther.*, 2002, 9, 1120-1126.

[47] Balazs, D.; Godbey, W. Liposomes for Use in Gene Delivery. *J. Drug Delivery,* 2011, 326497.

[48] Wong, S. Y.; Pelet, J. M.; Putnam, D. Polymer systems for gene delivery—past, present, and future. *Prog. Polym. Sci.*, 2007, 32, 799-837.

In: Clays and Clay Minerals
Editor: Liam R. Wesley
ISBN: 978-1-63117-779-8

Chapter 12

CHARACTERISTICS OF CLAY MINERALS IN THE PRINCIPAL SLIP ZONE OF AN ACTIVE FAULT: A CASE STUDY FROM THE TAIWAN CHELUNGPU FAULT DRILLING PROJECT

Li-Wei Kuo [*] ***and Sheng-Rong Song***
National Taiwan University, Taipei, Taiwan

ABSTRACT

Direct observations of physical structures and chemical composition of the seismogenic zones of active faults are rare, due to the difficulty in reaching the fault zone at depth. Thus, the physico-chemical processes, triggered by energies released from coseismic faulting, remain largely unknown. The Chelungpu thrust fault was northward ruptured as a result of the Mw 7.6 Chi-Chi earthquake which struck central Taiwan on 21st September 1999. To fill the knowledge gaps raised by the 1999 Chi-Chi earthquake, such as what the absolute stress levels was on the fault during the earthquake, how the stresses recover afterward to prepare for the next event, and how the material properties of the Chelungpu fault affect its propensity to catastrophically slide rather than creep, the Taiwan Chelungpu fault Drilling Project (TCDP) was conducted in 2005 and drilled to a depth of 2,003 m. On the basis of continuous coring, a suite of geophysical measurements, and microstructural observation, three fault zones of the Chelungpu fault were identified at the depth of 1,111 m, 1,153 m, and 1,222 m (described as FZ1111, FZ1153, and FZ1222 hereafter). The active fault zone of the Chelungpu fault corresponding to the 1999 Chi-Chi earthquake was recognized at the depth of 1,111 m (FZ1111). By characterizing clay mineral assemblages with continuous sampling from fresh materials of the Chelungpu fault, we aim at achieving the objectives of (1) characterization of clay mineralogy of the Chelungpu fault zones, (2) recognition of the PSZ within the active fault zone(s) corresponding to the 1999 Chi-Chi earthquake, (3) determination of the physico-chemical processes occurred during seismic slip and plausible slip weakening mechanism operated at seismic rates, and (4) estimation of earthquake source parameters (e.g., estimate of temperature for calculating associated

[*] Corresponding author: liweikuo@ntu.edu.tw, liweikuo@gmail.com

frictional energy and thickness of the PSZ for calculating associated surface fracture energy). Distinct clay mineral assemblage within the principal slip zone (PSZ) of FZ1111 show that (1) a decrease in clay content; and (2) significant decline of illite, disappearance of chlorite and kaolinite, and a spike in smectite. Meanwhile, the microstructural observation provides the evidence of melting, and the temperature within the fresh black gouge is estimated to be from 900°C to 1100°C by comparing the SEM images of in-situ natural samples with those of heated materials. The interval of clay anomaly within the PSZ resulted from frictional melting was determined by state-of-art in-situ synchrotron X-ray diffraction analysis and was estimated to be 1 mm. Thus, the characteristics of clay within the PSZ suggest that pseudotachylyte were possibly produced during the 1999 Chi-Chi earthquake and promptly altered to smectite. In addition, based on the estimation of the thickness of the PSZ, the contribution of surface fracture energy to earthquake breakdown work is quantified to be 1.9%. The huge remaining part of the breakdown work would be turned into chemical work (mineral transformation) and mechanic work associated with several processes to lubricate the Chelungpu fault such as thermal pressurization, elastohydrodynamic lubrication, and melting lubrication.

INTRODUCTION

Rupture propagation and slip on the fault during a large earthquake releases energies such as radiated energy, fracture energy, and frictional energy (Beeler et al., 2003; Kanamori and Heaton, 2000; Venkataraman and Kanamori, 2004) and triggers associated physico-chemical processes to lubricate faults (e.g., Brantut et al., 2010; Di Toro et al., 2006; Goldsby and Tullis, 2011; Han et al., 2007, 2010; Rice, 2006; Reches and Lockner, 2010; Smith et al., 2012). However, large earthquakes critical for human activities usually nucleate at about 7 to 15 km depth (Scholz, 2002). Traditionally earthquakes are studied using seismological (seismic wave inversion), geophysical or remote-sensed methods (e.g., GPS, InSAR). These techniques allow to retrieve key parameters related to earthquake sources (e.g., seismic moment, static stress drop, radiated energy), but could not provide fundamental information both on earthquake mechanics such as the dynamic fault strength (fault friction) and the energy budget (frictional energy and fracture energy) of an earthquake during seismic slip, and on the associated physico-chemical processes triggered by faulting.

To fill the gaps of knowledge on seismogenic sources, several continental fault-zone drilling projects have been conducted in active faults after catastrophic earthquakes. These include the Nojima fault project following the 1995 Mw 7.2 Kobe earthquake in Japan (Boullier et al., 2001); the Taiwan Chelungpu fault Drilling Project (TCDP) following the 1999 Mw 7.6 Chi-Chi earthquake in Taiwan (Ma et al., 2006); Wenchuan earthquake Fault Scientific Drilling (WFSD) following the 2008 Mw7.9 Wenchuan earthquake in China, (Li et al., 2013). The main goals of these drilling projects are to measure in-situ stress, strain, pore pressure, and other physical properties within active fault zones (e.g., porosity and permeability) (e.g., Zoback et al., 2010; Kuo et al., 2014). Besides, weathering (and exhumation) might erase and/or transform the signature, recorded in the fault rocks, of the physico-chemical process (e.g., melting, dehydration, etc.) occurring at depth during seismic slips (e.g., Kuo et al., 2012). To diminish the effects resulted from postseismic alteration on fault rocks, these continental fault-zone drilling projects were conducted rapidly after the

main shocks and were expected to provide fresh fault rocks to be directly investigated the physico-chemical processes within active fault zones during coseismic events.

Fault zones are composed of rocks in variable degrees of deformation states, often with a lower strain fracture-dominated "damage zone" surrounding a more highly strained heterogeneous "core zone". A damage zone was resulted from the initiation, propagation, interaction and built-up of slip along faults (e.g., Cowie and Scholz, 1992; McGrath and Davison, 1995). The development of different structures within damage zones gives valuable information about fault propagation and growth (Kim et al., 2001a, b; McGrath and Davison, 1995; Vermilye and Scholz, 1998, 1999), fluid flow (Martel and Boger, 1998; Sibson, 1996), and about earthquake initiation and termination (Aki, 1989; King, 1986; Sibson, 1985; Thatcher and Bonilla, 1989).

Current description of fault cores show a number of recurring elements such as one or several slip surfaces, fracture/deformation band sets, fault rocks (gouge, breccias and cataclasites), shale smears, oblique Riedel shears, and lenses of protolith of fault rock (e.g., Bastesen et al., 2009; Bonson et al., 2007; Braathen et al., 2009; Caine et al., 1996; Childs et al., 1996; Lindanger et al., 2007; Wibberley et al., 2008). On the basis of geological and geophysical observations from both active and exhumed fault zones, it suggests that the bulk of coseismic displacement during individual earthquake ruptures is accommodated within highly localized slip zones less than a few centimetres thick, with some evidence of extreme localization within zones millimetres or less in thickness in fault cores (Chester and Chester, 1998; Chester et al., 1993; Kuo et al., 2014; Power and Tullis, 1989; Sibson, 2003; Smith et al., 2011; Wibberley and Shimamoto, 2003). These localized slip zones named principal slip zones (PSZ; Sibson, 2003) within an enclosing fault core were normally the place where physico-chemical processes were driven by the most shear displacement and/or high strain during an individual coseismic event.

Therefore, one of the use of active faults to retrieve information on earthquakes relies on the recognition of PSZ produced during faulting. Characteristics of microstructures and mineralogy of the PSZ within fault cores have the potential to furnish significant insight into deformation processes active during slip. In addition, the study of PSZ in active faults may not only provide information about earthquake physics (e.g., earthquake energy budgets such as energy dissipation and fault behavior such as dynamic fault weakening and involved mechanisms that allow rupture nucleation and propagation, Kanamori and Heaton, 2000), but it may also enable recognition of diagnostic microstructures formed at different strain rates during various stages of the seismic cycle.

This chapter presents detailed clay mineralogical and microstructural observation of the Chelungpu thrust fault which slipped on 21st September 1999 with Mw7.6 earthquake near Chi-Chi town in central Taiwan. All of the samples analyzed were collected from the Taiwan Chelungpu fault Drilling Project (TCDP) which was conducted in 2005 and the details will be described later. By means of these results, we aim at achieving the objectives of (1) characterization of clay mineralogy of the Chelungpu fault zone, (2) recognition of the PSZ within the active fault zone(s) corresponding to the 1999 Chi-Chi earthquake, (3) determination of the physico-chemical processes occurred during seismic slip, and (4) estimation of earthquake source parameters (e.g., temperature for calculating associated frictional energy and thickness of the PSZ for calculating associated fracture energy).

GEOLOGICAL SETTING

The Taiwan mountain belt illustrates an oblique convergent boundary between the Eurasian and Philippine Sea Plates (Figure 1a; insert; e.g., Barrier and Angelier, 1986; Biq, 1972; Bowin et al., 1978; Ho, 1986; Liu et al., 1997; Lu and Hsu, 1992; Teng, 1990; Wu et al., 1997). The South China Sea of the Eurasian Plate is subducting eastward beneath the southern Philippine Sea Plate and producing the Luzon Arc. The Luzon Arc seated on the Philippine Sea Plate moving toward 306° at a speed of 81 mm yr -1 (Yu et al. 1997) is colliding with the Eurasian continental margin and resulting in Taiwan island. At the same time, the northern Philippine Sea Plate is subducting beneath the Eurasian continental margin in the northeast of Taiwan creating the Ryukyu Trench and the Okinawa Trough. This ongoing oblique collision and intersection between two subduction systems results in active faulting, numerous earthquakes and crustal deformation within the Taiwan mountain belt.

The Taiwan mountain belt, from west to east, can be physiographically divided into the Coastal Plain, the Western Foothills, the Hsuehshan Range, the Central Range, the Longitudinal Valley, and the Coastal Range (Ho, 1988). Among these physiographic domains, one of the most active regions within the Taiwan island is along the boundary between the Coastal Plain and the Western Foothills. The active region includes more than ten active faults and several disastrous earthquakes have been observed along this boundary, including the 1999 Chi-Chi earthquake (Wang et al., 2000). The related stratigraphic formation around this active region are Pleistocene Toukashan Formation (1 - 2 km thick conglomerate and alternations of fluvial-shallow marine sandstone and siltstone), early Pleistocene-Pliocene Cholan Formation (1.5 - 2.5 km thick monotonous alternating sandstone and siltstone), early Pliocene Chinshui Shale (~300 m thick shale and siltstone), late Miocene-early Pliocene Kueichulin Formation (0.8 - 2 km thick shallow marine sandstone and shale) and middle Miocene Nanchuang Formation (800 - 900 m thick core-bearing sandstone, siltstone and shale) (Figure 1a; Ho, 1988). In addition, the formation was crosscut and over stacked by three major faults around this active seismic belt. From west to east, these faults are the Changhua, Chelungpu, and Shuangtung faults (Figure 1a). They are forming the west-verging imbrication structure of a fold-and-thrust belt (Davis et al., 1983; Suppe, 1981). Among these faults, the Chelungpu fault zone plays the major role in the 1999 Mw7.6 Chi-Chi earthquake.

The Chelungpu fault zone is a west-verging thrust fault of over 90 km in length and separates the low level plain and basin regions from the high altitude areas of hills and mountains. Because of its distinct geomorphic feature, this fault is considered as an active fault (Bonilla, 1977). The Chelungpu fault zone originally was described as the Chinshui Shale overthrusting the Toukashan Formation in the southern Taichung Basin (Chang, 1971). During the Chi-Chi earthquake, the surface rupture closely followed the Chelungpu fault zone. In contrast, two other major fault zones next to the Chelungpu fault zone (i.e., Changhua fault zone in the west and Shuangtung fault zone in the east) did not slip significantly (Yu et al., 2001; Hung et al., 2002; Pahier et al., 2003). Because of no distinctive slip in the deformation front (i.e., the Changhua fault zone) during the Chi-Chi earthquake, it is reasonable to say that the Chi-Chi earthquake faulting is an out-of-sequence event. Result of focal mechanism and focal depth determined by seismologic inversion and relocation also indicates the characteristics of an out-of-sequence event (Kao and Chen, 2000). Regionally,

the surface displacement during the Chi-Chi earthquake is approximately parallel to the direction of tectonic convergence (Yang et al., 2000). On the surface survey, the hanging wall of the Chi-Chi earthquake rupture is composed of alternating beds of sandstone and siltstone of Pliocene Cholan Formation and the early Pliocene Chinshui Shale. The footwall is composed of Pleistocene Toukashan Formation and recent alluvial deposits.

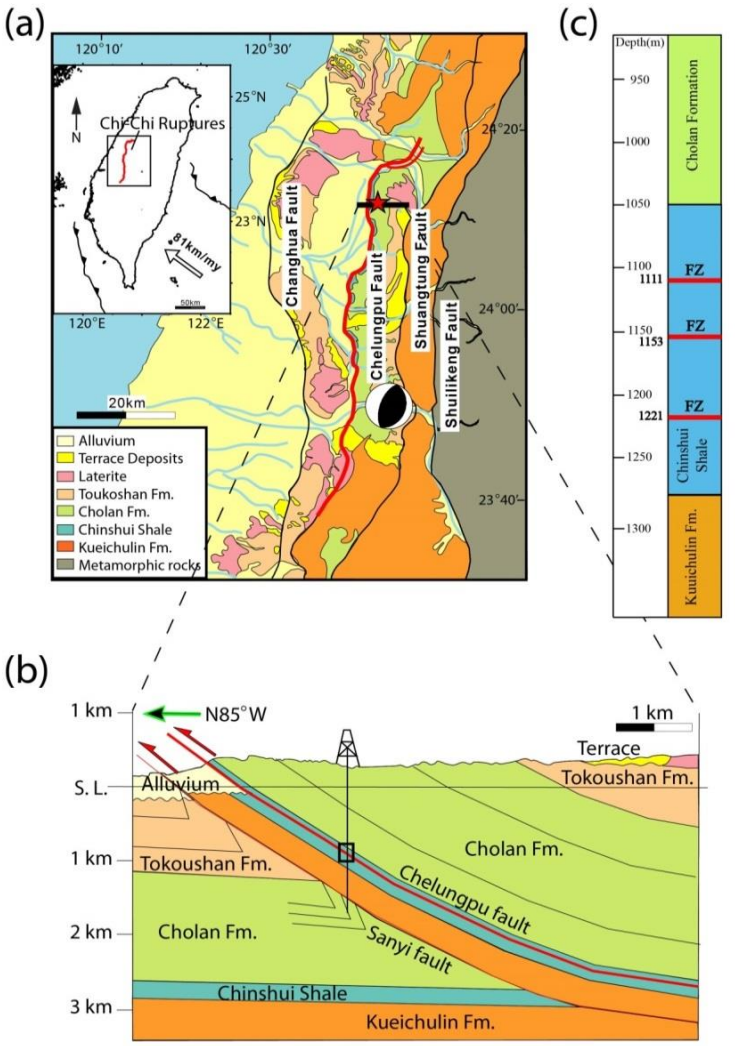

Figure 1. Geological setting of the 1999 Mw7.6 Chi-Chi earthquake and location of the TCDP-A drilling site. (a) Location of the TCDP-A drilling site and the 90-km-long surface ruptures associated with the Mw7.6 earthquake at the central part of western Taiwan. The TCDP site is indicated by a red star. The focal mechanism of the Chi-Chi main shock is located at the hypocenter of the Chi-Chi earthquake. The insert box is the tectonic setting of Taiwan. (b) An E-W cross section of the TCDP-A showing the Chelungpu fault zone and surrounding formations encountered in the borehole (after Hung et al., 2007). The rectangle displaying the active slip zone during the 1999 mainshock identified in the borehole and enlarged in the right panel as (c). (c) The image exhibiting major portions of the Chelungpu-fault along the borehole of the TCDP Hole-A.

Thus, the relationship of hanging wall and footwall between the Chi-Chi earthquake and the Chelungpu fault zone is consistent. Also, the earthquake surface rupture dips 30° toward the east, similar to the dip of the Chelungpu fault zone. Most slip of the Chi-Chi earthquake is found within and nearly parallel to the bedding plane of Chinshui Shale (Lee et al., 2001).

CHI-CHI EARTHQUAKE AND TAIWAN CHELUNGPU FAULT DRILLING PROJECT

The Chelungpu thrust fault is an active fault which slipped on 21st September 1999 with Mw7.6 near Chi-Chi in central Taiwan (Figure 1a). The Chi-Chi earthquake produced a northward propagating rupture with a ~90 km long north-south trending rupture surface (Chen et al., 2001; Lee et al., 2001; Ma et al., 2000). The coseismic slip and rupture velocity increased northward along the fault trace with a slip of 5-9 m horizontal displacement on the northern segment, compared to the average slip of 2 m on the southern part (Chen et al., 2001; Lee et al., 2001; Ma et al., 2000; Yue et al., 2005). In addition, strong ground motion of high-frequency acceleration decreased from south to north (Lin et al., 2001). This N-S trending thrust dips eastward at about 30°, and displacement was nearly pure thrust slip near the epicenter and changed to oblique northward thrust with a strong left-lateral component during the Chi-Chi event (Chen et al., 2001; Dalguer et al., 2001).

In order to obtain more advanced and comprehensive physical and chemical details of the Chelungpu-fault zone, the Taiwan Chelungpu-fault Drilling Project (TCDP) was conducted in 2005. The drill site of the TCDP is located on Dakeng, Taichung County, 2 km east of the surface rupture of the Chi-Chi faulting (Figure 1a). The elevation of the drill site (120.73916°E, 24.20083°N) is about 247 m. Subsurface structures around the drill site were constructed by high-resolution shallow reflection seismic profiles (Wang et al., 2002, 2004). The mapping suggested that the Chi-Chi rupture is at a depth of 1,100 m beneath the drill site (Figure1b). In addition, the constraint of spatial slip distribution from strong motion stations (Ma et al., 2001) and geodetic data (Lee et al., 2003; Yang et al., 2000; Yu et al., 2001) show a coseismic slip of 12 m around the drill site.

TCDP drilled two holes named Hole-A and Hole-B, and the distance between the two holes is 40 m. TCDP carried out continuous coring from 500 to 2,003 m depth for Hole-A and from 948 m to 1,353 m depth for Hole-B, respectively. Well logs for Hole-A were carried out for 500 - 1,870 m with 3 sections in order to evaluate the physical properties of fault rock and wall rock. The azimuth of the borehole was around N275 - 290° above 1,110 m, which was consistent with the prediction, provided the dip direction N105° of regional bedding. A general description and fault structures of core samples for Hole-A have been reported by Song et al. (2007), Yeh et al. (2007), and Sone et al. (2007) (Figure 1c), and those for Hole-B were described by Hirono et al. (2008a). On the basis of the current core observation, three major fault zones composed of “damage zone” surrounding a “core zone” were identified at 1,111 m, 1,153 m, and 1,222 m depth for Hole-A , which correspond to 1,136 m, 1,194 m, and 1,243 m depth for Hole-B (Figure 1c for Hole-A). Three fault zones of the TCDP Hole-A were named FZ1111, FZ1153, and FZ1222 and were characterized in this chapter.

DISCUSSION

1. Characterization of Clay Mineralogy of the Chelungpu Fault

1.1. Variability of Mineralogy of the Sedimentary Formations

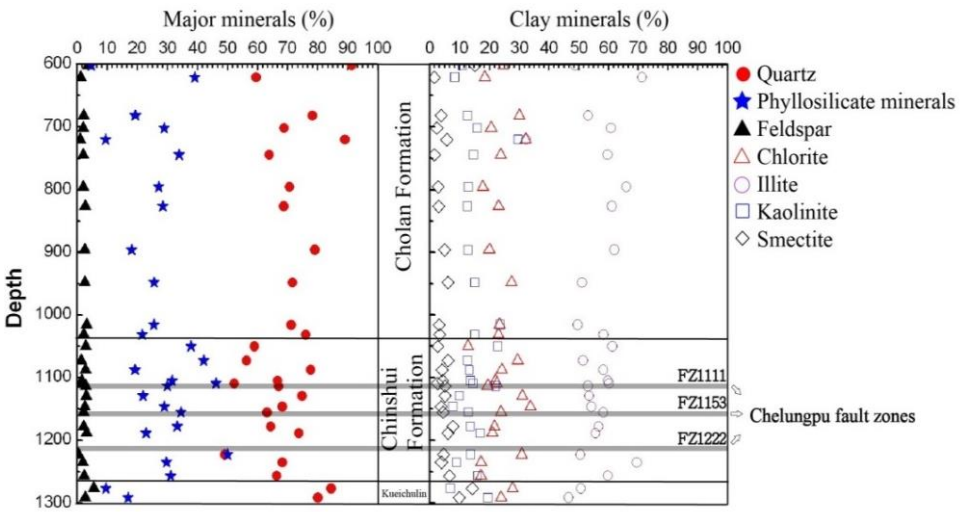

Figure 2. Results of relative percentage of major minerals and clay minerals from the TCDP cores from 600 to 1,300 m in depth (after Kuo et al., 2009). Left panel is the plot of major minerals from bulk XRD analysis. Right panel is the result of clay mineral percentages by clay mineral XRD analysis. The three Chelungpu-fault zones are noted as gray areas.

In order to obtain the variability of mineralogy of the sedimentary formations, a sequential and continuous collection of fresh samples was made and 28 samples from the host rocks were collected for depths of 600 m to 1,300 m. The major mineral assemblages via bulk XRD experiments were identified as quartz, feldspar, and phyllosilicate minerals such as muscovite/illite, smectite, kaolinite and chlorite (Figure 2). On the basis of the semi-quantitative XRD method (Biscaye, 1965), the relative clay percentage of the sedimentary formations was found in the constant range of 20-40%. Clay minerals of <2 μm from our samples were recognized as illite, smecctite, chlorite, and kaolinite, and were estimated by semi-quantitative XRD method. The relative percentage of illite varies between 50% and 80% for all samples. The relative percentage of chlorite and kaolinite for all interval are around 10~20% and 15~35% respectively (Figure 2). In addition, smectite is rare or absent in the Cholan Formation, the Chinshui Shale, and the Kueichulin Formation. It seems that the variability of major minerals and clay minerals in Cholan Formation is larger than the ones of Chinshui Shale and upper part of Kueichulin Formation (Figure 2).

1.2. Characteristics of the Fault Core in FZ1111

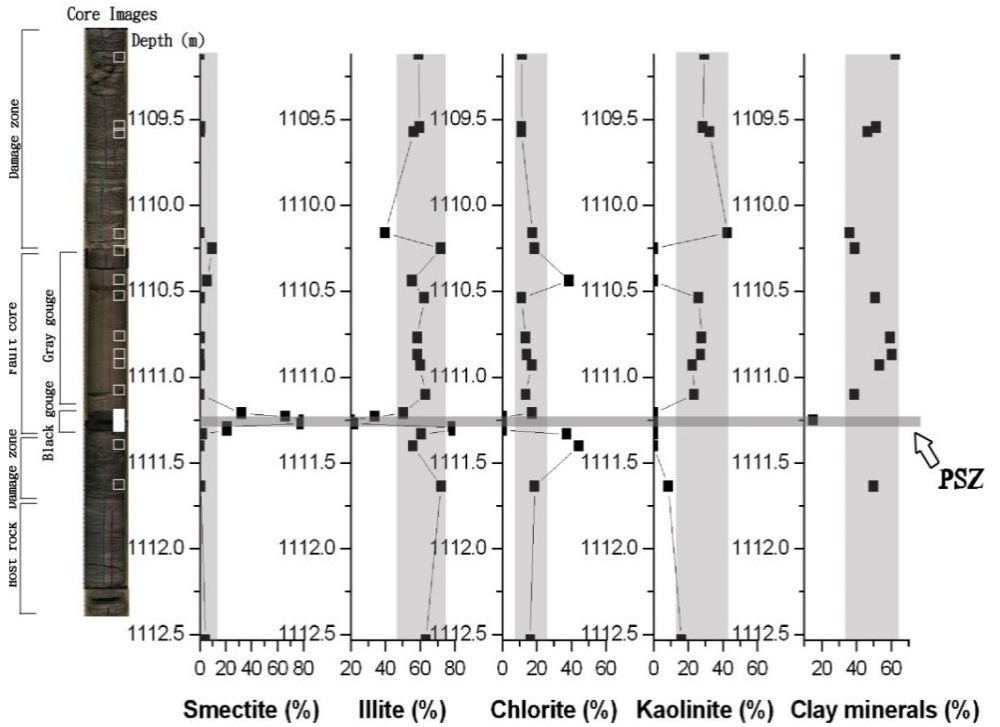

Figure 3. Clay mineral percentage and interpreted fault components in FZ1111. White rectangles are the sample locations. The results of relative clay mineral percentage by clay mineral XRD analysis are shown in the right side, where illite, smectite, chlorite, and kaolinite are shown by the side. Gray area is the PSZ of the Chi-Chi earthquake.

The Core image in figure 3 covers a depth range of between 1,109.20 m and 1,112.35 m. The fault is nearly bedding parallel and the fault zone consists of a damage zone of 1 m in width and a fault core including light gray clayey gouge zone of 1.1 m and black gouge zone of 12 cm in width, respectively. The damage zone (1,109.20 m to 1,110.40 m depth) appeared to be resulted from a continuous increase in fracture frequency toward the fault zone from the hanging-wall side. From 1109.20 m down, a wide zone of soft, light gray clayey gouge appears. The grain size of the gouge content is silt and clay. In addition, black gouge zone was found close to the bottom of the fault core region. A 2-cm thick hard layer of "black material" was found at the bottom of the black gouge and the black material appeared to be massive and uniform in texture. Below the hard black material is a sharp contact with another light gray clayey gouge layer. At the bottom end of the core in Figure 3, the fracture frequency has dropped rapidly to the point where only several fractures are found.

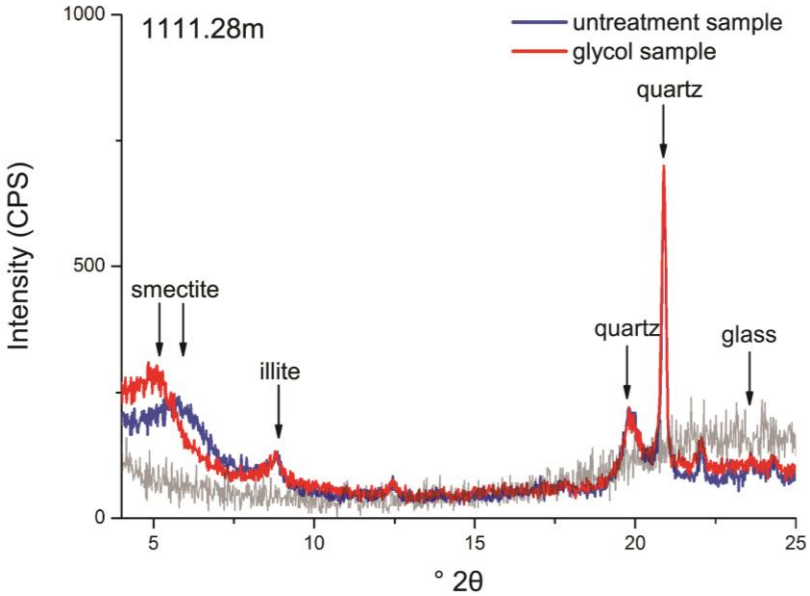

Figure 4.X-ray diffraction patterns of the PSZ for identifing the I/S mix-layer. Blue and red lines are the results from untreated and glycolated samples, respectively. Light gray lines are shown as glass peaks (the glass is the melt of Chinshui Shale) if pseudotachylyte existed in the sample.

Twenty six powdered samples extracted from each part of fault components were examined by XRD analysis. Clay minerals of <2 μm from our samples are recognized as illite, smecctite, chlorite, and kaolinite (Figure 3). The variation of illite and chlorite in light gray clayey gouge zone (1,109.20 m to 1,110.40 m depth) represents the normal variability of mineral proportion without anomalies of clay minerals proportion. The relative percentage and presence of clay minerals vary drastically in 1,111.28m depth. The relative percentage of illite varies between 50% and 80% for all samples except in the bottom of the black gouge zone where dramatically decreases to 20% (Figure 3). The relative percentage of chlorite and kaolinite for all interval are around 10~20% and 15~35% respectively, but they diminish to zero in the bottom of the black gouge zone. On the other hand, smectite is rare or absent in all portions of the fault zone and the Chinshui Shale but becomes abundant (up to ~80%) in the bottom of the black gouge zone (Figure 3). In summary, smectite is present, and its relative percentage increases to 80%; chlorite and kaolinite are absent, and the relative percentage of illite decreases to 20%. The XRD patterns of ethylene-glycol samples indicate only smectite but no Illite/Smectite mineral in the bottom of the black gouge zone (Figure 4). The 2-cm thick hard layer of black material found at the bottom of the black gouge was recognized as the presumable PSZ and other evidence will be shown in later section.

1.3. Characteristics of the Fault Core in FZ1153

The Core image in figure 5 covers a depth from 1,151.40 m to 1,155.50 m. FZ1153 is nearly bedding parallel and consists of a 0.70-m wide fault gouge zone sandwiched with two 1.3 m-wide damage zones. The texture of the gouge-zone is random at the top, but some foliation appears from 1,153.20 m down and increases towards the bottom. Some features contrasting with FZ1111 were that two possible regions of black materials were found and were situated at the top and the bottom of the fault gouge zone (Figure 5).

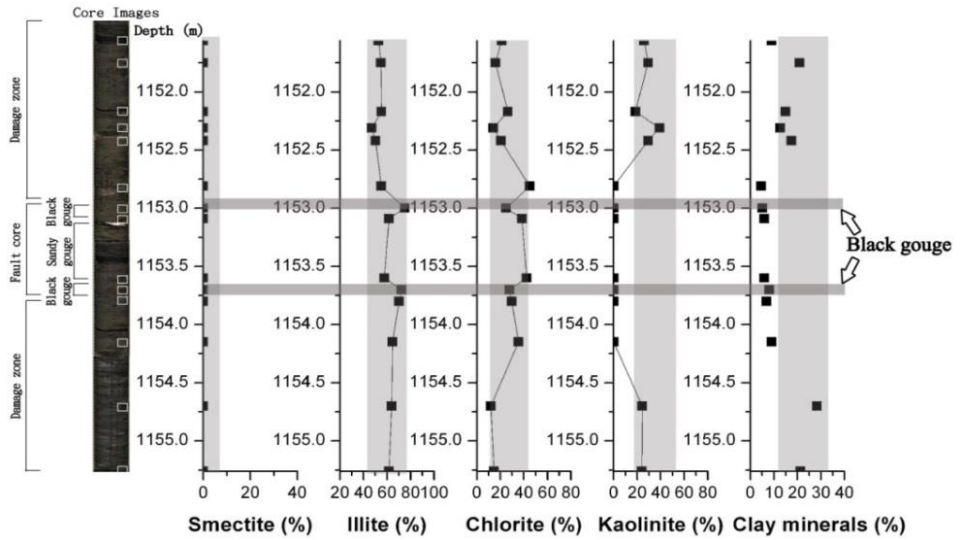

Figure 5. Clay mineral percentage and interpreted fault components in FZ1153. White rectangles are the sample locations. The results of relative clay mineral percentage by clay mineral XRD analysis are shown in the right side, where illite, smectite, chlorite, and kaolinite are shown by the side. Gray areas are shown as the possible slip zones of Chelungpu fault.

Fourteen powdered samples extracted from each part of fault components were examined by XRD analysis (Figure 5). The relative clay percentage of host rocks was found in a constant range of 20-40%, but drastically decreases to <20% in the fault core (Figure 5). Clay minerals of <2 μm from our samples are recognized as illite, chlorite, and kaolinite. The relative percentage of illite varies between 50% and 80% for all samples, and there is no smectite in FZ1153 (Figure 5). The relative percentage of chlorite and kaolinite for all intervals is around 10-20% and 20-40%, respectively, but the content of kaolinite drops to zero in a wide span of ~1.3 meter, which includes the entire fault core, regardless of the constituents (black gouge or sandy gouge), and some parts of damage zone (Figure 5). The small peak of kaolinite from 1152.2 m to 1152.3 m depth represents the normal variability of mineral proportion instead of the anomaly by faulting.

1.4. Characteristics of the Fault Core in FZ1222

The Core image in figure 6 covers a depth from 1,219.40 m to 1,222.80 m. FZ1222 is characterized by a 1.25 m width fault core sandwiched by two layers of black material close to the damage zone. The damage zone with gouge layers appears at 1,219.64 m to 1,220.65 m (Figure 6). From 1,220.65 m to 1,221.90 m, fault rocks are distributed. In the top 0.25 m of the fault rock region (1,220.65 m to 1,220.90 m) is a gouge zone, in which a 3-cm thick black material layer is found. In addition, the amount of rock fragments increases and the damage zone starts from 1220.90 m. The damage zone contains larger size rock fragment clasts compared to the previous damage zones encountered in FZ1111 and FZ1153. Also a thin layer of black material (<5 mm) was found at around 1221.80 m, also parallel to the general orientation of the fractures. The bottom of the damage zone is cut by a sharp high angle fault plane. After this sharp structure follows a small fracture zone of 5 cm to 10 cm in width, and finally the fractured foot-wall rock appears.

Fourteen powdered samples extracted from FZ1222 and were examined by XRD analysis (Figure 6). The relative clay percentage of sedimentary formations is found in the constant range of 10-40%. Such a variation in relative clay percentage in FZ1222 is larger than that in FZ1222 and FZ1153, and could have been caused by sandstone-shale interbedding (Figure 6). Given this lithological variation in FZ1222, it is required to collect samples along the drilled core to minimize the effect of lithological change when identifying the clay anomaly. Clay minerals (<2 μm) from our FZ1222 samples are recognized as illite, smectite, chlorite, and kaolinite. The relative percentage of illite varies from 60% to 80% for all samples, but abruptly increases to ~90% in the upper black gouge of FZ1222. The relative percentage of chlorite and kaolinite for all intervals is ~ 8-20% and 9-25%, respectively, but drops to less than 5% in the upper black gouge of FZ1222. Smectite is very uncommon or absent in the Chinshui Shale, but slightly increases in the fault core of FZ1222.

In comparison with the relative clay content of the Chinshui shale, the characteristics of clay minerals in three fault zones are briefly summarized as follows: the 2cm-thick FZ1111 PSZ has a high content in smectite (80%), kaolinite is absent within 1.3m around FZ1153 and the relative percentage of clays slightly varies in the FZ1222 black gouge.

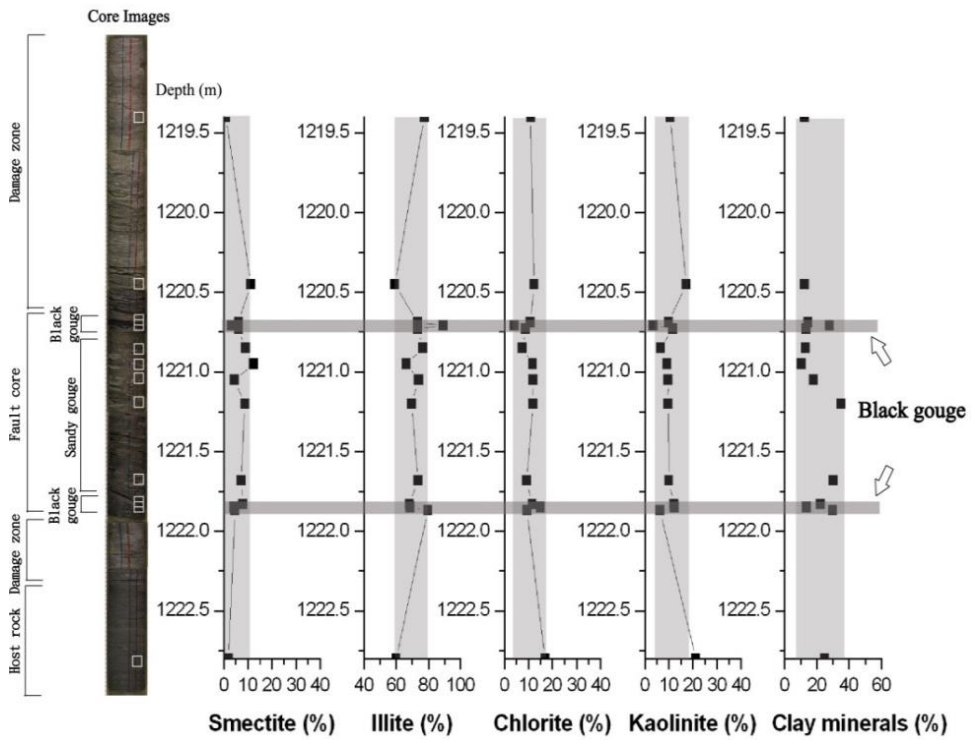

Figure 6. Clay mineral percentage and interpreted fault components in FZ1222. White rectangles are the sample locations. The results of relative clay mineral percentage by clay mineral XRD analysis are shown in the right side, where illite, smectite, chlorite, and kaolinite are shown by the side. Gray areas are shown as the possible slip zone of Chelungpu fault.

2. Recognition of the PSZ Corresponding to the 1999 Chi-Chi Earthquake

Semi-quantitative results of bulk and clay minerals from X-ray diffraction analysis show the extreme clay anomalies of the FZ1111 among the Chelungpu fault zones. Thus we put emphasis on the discussion of the FZ1111 of the TCDP. A drastic decrease in clay percentage for the black-gouge zone of the PSZ could possibly be explained by two different processes: 1) sedimentation; and 2) tectonic deformation. The first possibility can be presumably ruled out for the following two reasons. First, the Chinshui Shale is almost homogeneous and its clay percentage is relatively high according to our data (Figure 2) and the literature (Liao, 2003; Issacs et al., 2007). So, the probability of a lower clay content caused by any special sedimentation event within the several-centimeter horizon of the short sampling interval would be very low. Second, the clay assemblage in the PSZ is completely different from other portions of the fault zone and wall rocks. If this difference between clay assemblages resulted from sedimentation processes, it should show a transition zone with gradual changes in clay minerals. However, no such transition zone has been observed but only a clear-cut boundary has been revealed under a dense sampling. Thus, the most obvious possibility is that tectonic processes have to be responsible for the decrease in clay percentage in the PSZ. Furthermore, the high clay content of surrounding gray gouge is consistent with the prediction of fault core characteristics (Caine et al., 1996).

Microstructural observation of the PSZ was made to complement the plausible possibility we mentioned above. The SEM images from the PSZ show the melting-origin textures (Figure 7a, 7b). Many vesicles of about 1- to 40-μm diameter within the PSZ are found, indicating that this material was exposed heat and indeed melted. Also, thin strings connecting grains are expected to be stretched during its melted or amorphous (Figure 7b). In addition, TEM images of the PSZ show that no crystal lattice spots and suggest that the phenomena of melting certainly occurred (Figure 7c, 7d). The finding of no clear bump in the XRD patterns of PSZ (Figure 4) indicates that glass content is less than 25% (Lin, 1994).

Amorphous materials can be produced by melting during frictional seismic sliding (0.1-3 m/s) (e.g., Di Toro et al., 2006), and also at subseismic slip rates (<< 0.1 m/s) (Yund et al., 1990; Pec et al., 2012). In the TCDP case, the stresses, ambient temperature and displacement at the TCDP borehole depth are of the order of tens of MPa, less than 50 degree Celsius, and 6-9 m, respectively (Tanaka et al., 2007; Ji et al., 2003). It seems that amorphous materials within the PSZ were neither at high stresses (up to 1.5 GPa) and large ambient temperature (300 to 500 degree Celsius) suggested by Pec et al. (2012), nor with the short displacement (less than 40 cm) conducted by Yund et al. (1990). Consequently, we conclude that the amorphous materials in the PSZ were presumably the product of solidification of melts (pseudotachylyte) resulted from frictional seismic slips, but may have been at a level where it was too little or not preserved sufficiently to be observed by eye or with microscopes.

The abundance of smectite in the TCDP Hole-A is rare to nonexistent in all parts of the FZ1111 but significantly increases in the PSZ. Since sedimentary origin is not favored as previously discussed and no Illite/Smectite mineral is observed, the alteration of smectite in

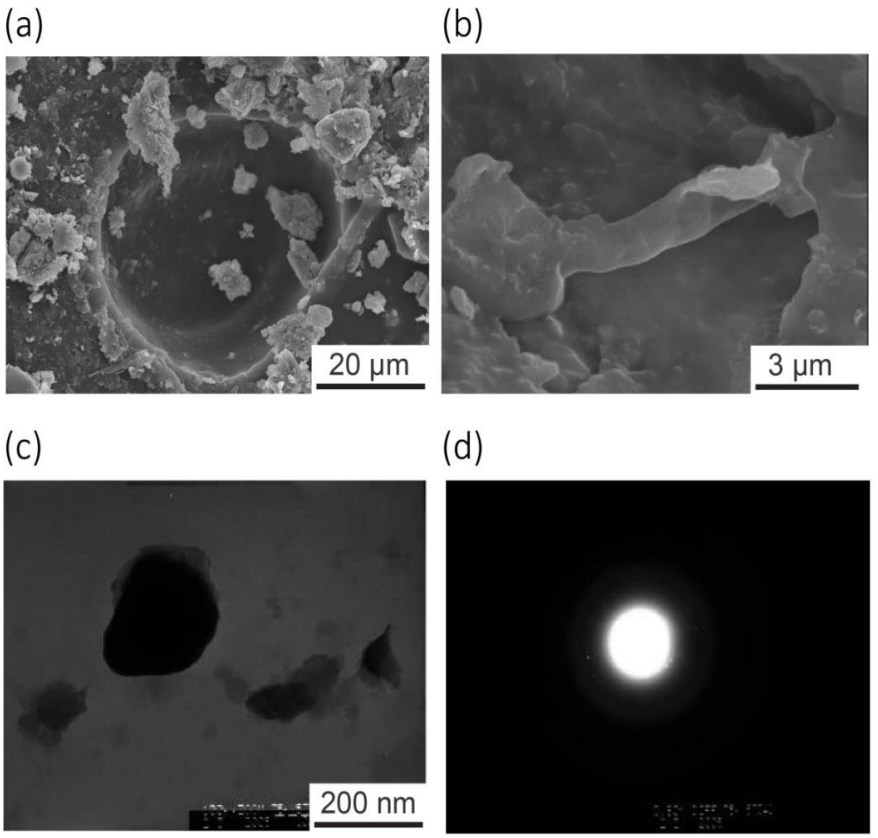

Figure 7. (a) SEM image of the typical surface texture of the pseudotachylyte sample in the PSZ. The image shows several vesicles or bubbles on the surface in the PSZ. (b) SEM image of pseudotachylyte displays string that is melted material drawn out when cracks opened. (c) TEM image of the grains collected from the PSZ, and (d) No crystal lattice spots are evident indicating no crystal lattice in this grain. These images indeed provide evidence of melting and suggest pseudotachylyte indeed existed.

the PSZ from glass (pseudotachylyte) may be the most possible scenario. Although we do not directly observe the occurrence of glass-smectite reaction under the microscope, such a reaction is well documented in many natural environments and experimental tests (Bauluz et al., 2004). Generally, the advance of glass-smectite reaction only takes 3 days at 90°C with 1-10M NaOH solution (Tomita et al., 1993). Provided that the achieved temperature of the Chi-Chi slip zone was at least over 400°C (Ishikawa et al., 2008; Mishima et al, 2006, 2009) and fluid was sealed in the fault, it is a very reasonable conclusion that the transformation of smectite from glass occurred in less than a few days to years after the Chi-Chi earthquake, even though the kinetics of this reaction is not probed because of a lack of chemical composition of glass, and fluid in this stage.

Average-clay-content anomalies and relative individual clay percentages across the FZ1111 can be explained by tectonic process involving melting caused by friction. Due to comminution and chemical alteration between fluid and rocks, clay mineral content within the fault core has increased, compared with wall rocks. However, within the PSZ, frictional heat may have caused mineral melting or thermal decomposition depending on temperatures achieved and reaction temperatures for clay mineral formation. The occurrence of

pseudotachylyte is imaged as extremely fine droplets widely spread throughout the matrix of the PSZ instead of from old clasts, as described by Boullier et al. (2009) via counting the relative percentage of smectite and old clasts. The frictional temperature of the Chi-Chi earthquake must have been at least 800°C because of the melting or thermal decomposition of chlorite (Brindley et al., 1950). It is expected that heat and fluid exist for glass-smectite reaction which are necessary factors for the model of thermal pressurization as well. Thus, we are providing the possible scenario for the PSZ of Chi-Chi earthquake that frictional heat melted most of the clay except for illite, then thermal pressurization proceeded and altered tiny glass to smectite. This particular description of a transfer process for pseudotachylyte could explain why it is rarely identified in exhumed clay-rich hydrated fault zones, certainly not in proportion to the expected dominance of seismic slip.

So far, there have been many studies focusing on the shallowest fault zone (FZ1111) of the Chelungpu-fault, for example, residual temperature anomaly (Kano et al., 2006), grain size distribution (Ma et al., 2006), geophysical logs (Wu et al., 2007), microstructures (Boullier et al., 2009), and characteristics of clay minerals (Kuo et al., 2009) for Hole-A, and magnetic susceptibility (Hirono et al., 2006a), inorganic carbon content (Hirono et al., 2006b), clay mineral reaction (Hirono et al., 2008b), and microstructures (Boullier et al., 2009) for Hole-B. These different kinds of characteristics indicate that the PSZ within the FZ1111 was active during the 1999 Chi-Chi earthquake. The presence of smectite thus mark the plausible PSZ of the 1999 Chi-Chi earthquake located in the black gouge, and this is consistent with previous suggestions.

3. Determination of the Processes Occurred during Coseismic Slip

Fault rock assemblages reflect the physico-chemical processes by which faults accommodate deformation. Since the bulk of coseismic displacement is suggested to be accommodated within the PSZ, the mineral assemblage and associated textures of the Chi-Chi PSZ was supposed to reflect the physico-chemical processes triggered during coseismic slip. The distinguishing characteristics were discovered within the PSZ: grain size distribution (Ma et al., 2006), microstructures (Boullier et al., 2009), clay-clast aggregates (CCAs) (Boutareaud et al., 2008, 2010), magnetic anomaly (Hirono et al., 2006a, Mishima et al., 2006, 2009; Chou et al., 2012a, b), inorganic carbon content (Hirono et al., 2006b), major and trace elements (Ishikawa et al., 2008), and clay anomaly (Hirono et al., 2008b; Kuo et al., 2009, 2011). Several associated physico-chemical processes were then suggested based on those characteristics. For instance, in the case of magnetic minerals, the PSZ is dominantly composed of magnetite in the principal slip zone, and neoformed goethite elsewhere in the gouge (Chou et al., 2012a). A model of the physico-chemical processes during coseismic slip was proposed that the magnetic record (1) is preserved during interseismic time, (2) is erased during coseismic time, and (3) is imprinted during postseismic time when fluids cooled down. Chou et al. (2012a) thus concluded that the identification of a stable magnetic record carried by neoformed goethite may be a signature of a frictional heating process in a seismic slip zone.

In this chapter, the PSZ is enriched in smectite and depleted in illite, chlorite, and kaolinite (Figure 3). In addition, microstructural observations of the PSZ show the melting-origin textures (Figure 7a, 7b) and the phenomena of melting (Figure 7c, 7d). Integration of

our microstructural observation (Figure 7) and clayey characteristics (Figure 3) within the PSZ, a plausible model of the physico-chemical processes during coseismic slip was suggested that (1) clay minerals were thermal decomposed by frictional heat generated by coseismic slip within the PSZ and produced amorphous materials and/or pseudotachylyte, and (2) amorphous materials and/or pseudotachylyte promptly transferred to smectite with hot fluid during postseismic period.

Current research of TCDP suggests that several physico-chemical processes were triggered during past coseismic events, but how the physico-chemical processes controlling dynamic fault weakening during the 1999 Chi-Chi earthquakes are largely unknown. On the basis of experimental data and theoretical considerations, several processes have been suggested to result in coseismic fault lubrication (Brantut et al., 2010; Di Toro et al., 2006; Goldsby and Tullis, 2011; Han et al., 2007, 2010; Rice, 2006; Reches and Lockner, 2010; Smith et al., 2012), but with the exception of frictional melting evidence for these processes in natural fault zones is lacking (Di Toro et al., 2006). On the basis of the evidence of microstructural observation (Boullier et al., 2009; Boutareaud et al., 2010), thermal perturbations (Hirono et al., 2006b, 2008; Ishikawa et al., 2008; Kuo et al., 2009, 2011; Mishima et al., 2006, 2009; Chou et al., 2012a, b) and fluid infiltrations (Ishikawa et al., 2008; Chou et al., 2012a, b) within the PSZ, the dominant slip weakening process was suggested as thermal pressurization responsible for a slip of 8.3 m on the fault near the drill site constrained from close strong motion and GPS data (Ma et al., 2001; Ji et al., 2003)

4. Estimation of Earthquake Source Parameters

4.1. Temperature Estimates of the Chelungpu Fault Zones

Temperature plays an essential role in manipulating earthquake faulting. With frictional heating, the fault strength could be dramatically reduced because of various proposed slip weakening mechanisms, such as frictional melting (Di Toro et al., 2006; Mackenzie and Brune, 1972), and thermal pressurization (Boullier et al., 2009; Wibberley and Shimamoto, 2005). Also, frictional energy comprises a fair amount of total released earthquake energy (Chester et al., 2005; Sibson, 1973; Scholz, 2002). Therefore, the information regarding a temperature rise by frictional heating in earthquake faults is important for investigating the fault strength and earthquake energy budgets (Di Toro et al., 2005; 2006; Hirose and Shimamoto, 2005).

The temperatures of PSZ of the Chelungpu-fault zones for Hole-A and Hole-B during coseismic events were estimated by using magnetic susceptibility (Mishima et al., 2006; 2009), inorganic carbon content (Hirono et al., 2006a), compositions of major and trace elements (Ishikawa et al., 2008), and the occurrence of pseudotachylyte (Otsuki et al., 2009). However, these estimates were either a lower limit (350°C by Ishikawa et al., 2008; 450°C by Mishima et al., 2006, 2009; 550°C by Hirono et al., 2006a), or a wide range (750°C-1700°C by Otsuki et al., 2009) for the frictional heat generated by coseismic slips. Those results are too rough to provide more insights into the true faulting mechanisms.

Here we performed isothermal heating experiments and examined some specific characteristics of clay minerals to place a better constraint on the temperature range of the Chelungpu fault zones. We also integrate the TGA results of chlorite and kaolinite in current research, and discuss the reactions such as thermal decomposition/dehydroxylation and spinel

recrystallization to define the possible temperature range during coseismic slips. The temperature estimates of the Chelungpu fault zones are intended to offer important information to investigate the faulting mechanism and to calculate the energy budget.

4.1.1. Estimate of the Maximum Temperature Achieved in FZ1111

The SEM and TEM images described in the previous section suggest that clay minerals within ~2 cm of PSZ were melted (Figure 7). Therefore, we carried out the isothermal heating experiments and XRD analysis of heated material (Figure 8), observed the surface melting with SEM (Figure 9), and identified the major type of chlorite semi-quantitatively with SEM/EDX (Figure 10) to investigate the maximum temperature achieved in the fault zones (see the details in Kuo et al., 2011). The change of mineral assemblages by different heating temperatures can be clearly observed in Figure 8. The PSZ mineral assemblages of FZ1111 include quartz, feldspar, rare illite, abundant smectite (Figure 8a), and the presence of clay minerals is similar to that of the heated materials at T= 900°C (Figure 8f) despite the fact that much of smectite formed from alteration of glasses (Kuo et al., 2009). The similar mineral assemblage between PSZ and the materials heated at 900°C may suggest that 900°C might be achieved by faulting in coseismic events in the PSZ of FZ1111. Besides, it should be noted that the presence of spinel is observed in the heated materials at 1,100°C (Figure 8h), and the presence of spinel is the result of recrystallization of kaolinite achieved at 1,100°C (Traoré et al., 2006). After thermal decomposition/dehydroxylation of kaolinite, the

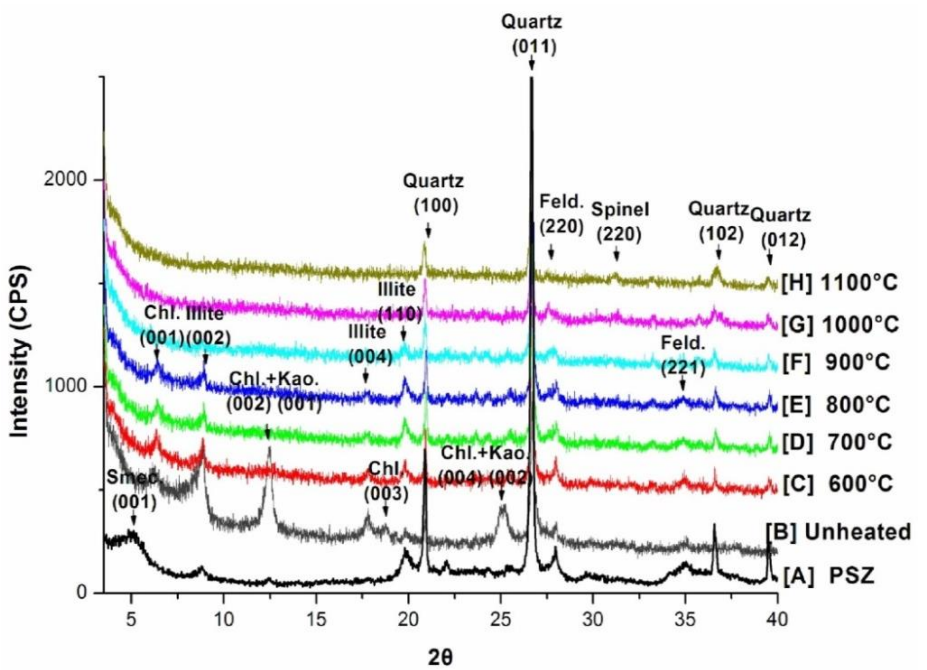

Figure 8. Comparison of XRD analyses between the PSZ sample and isothermal heating materials. The all apparent peaks are identified with CuKα radiation (the wavelength is 1.5406 Å) and signed with mineral names. (Chl.: chlorite, Kao.: Kaolinite, Smec.: Smectite, and Feld.: feldspar)

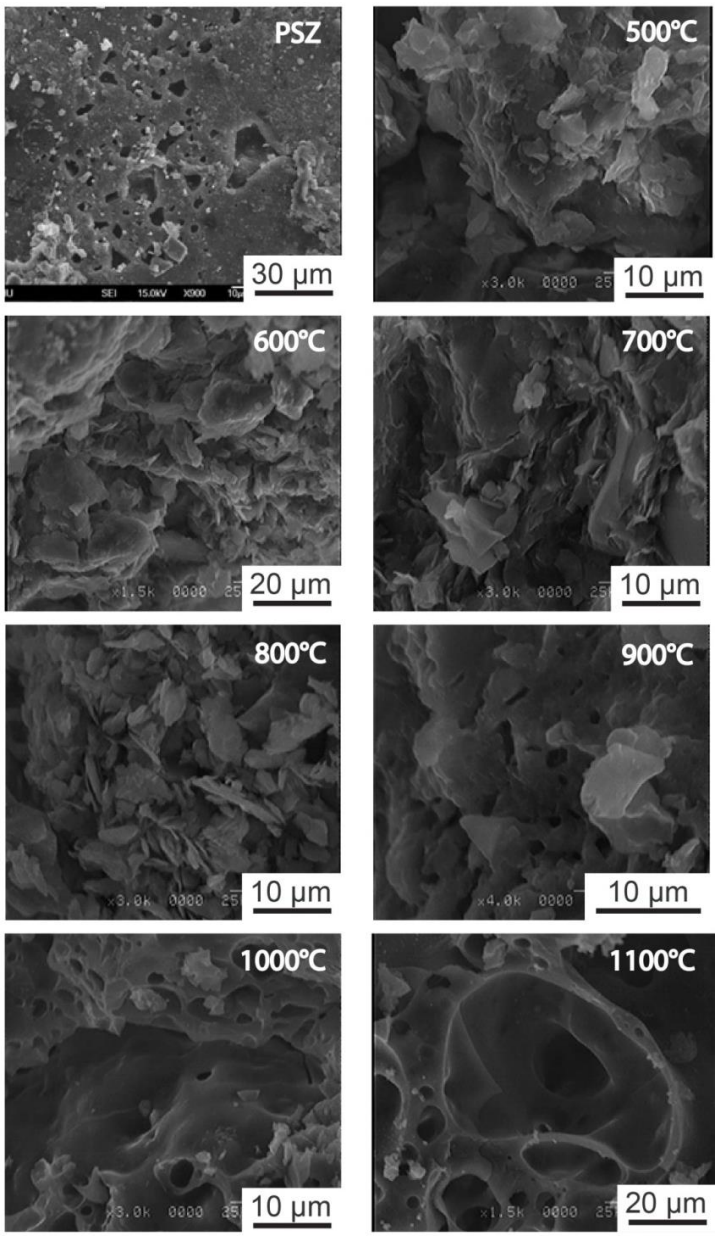

Figure 9. SEM images of the PSZ and isothermal heating materials. It is noted that vesicles appear at 900°C, and the vesicles become larger within increasing temperatures.

decomposed kaolinite remains as a secondary mineral, such as amorphous aluminosilicates, and these amorphous aluminosilicates could recrystallize into spinel when temperature increases to 1,100°C (Traoré et al., 2006). The lack of spinel peak in the XRD pattern of the PSZ of FZ1111 (Figure 8a) indicates that such recrystallization of kaolinite did not happen in the PSZ of FZ1111, and therefore suggests that the temperature did not achieve 1,100°C during faulting. Thus, 1,100°C could be considered as the upper bound of temperature during coseismic slip.

The various surface textures of heated material at different experimental temperatures can be used as a reference to which in situ materials of fault zones can be compared (Figure 9). The appearance of vesicles on the surface of heated samples is important for identifying melting occurrence via increasing temperatures. The original host rocks contain flake-shaped minerals, such as phyllosilicates, and granular-shaped minerals, such as quartz (Figure 9b). The vesicles on the surface were not formed in heated materials until 900°C (Figure 9f). These vesicles on the surface grew larger after 900°C (Figure 9g-h). By comparing the size of vesicles on the surface of the PSZ of FZ1111 with the experimental results, we infer that the temperature in the PSZ of FZ1111 might have been above 900°C. This is indeed consistent with what is inferred from the correlation of isothermal heating materials XRD patterns, and suggests that 900°C is the lower temperature limit of FZ1111. It should be noted that the pressure was not probed in this work, and should be considered to be another important factor to affect the size of vesicles in the future studies.

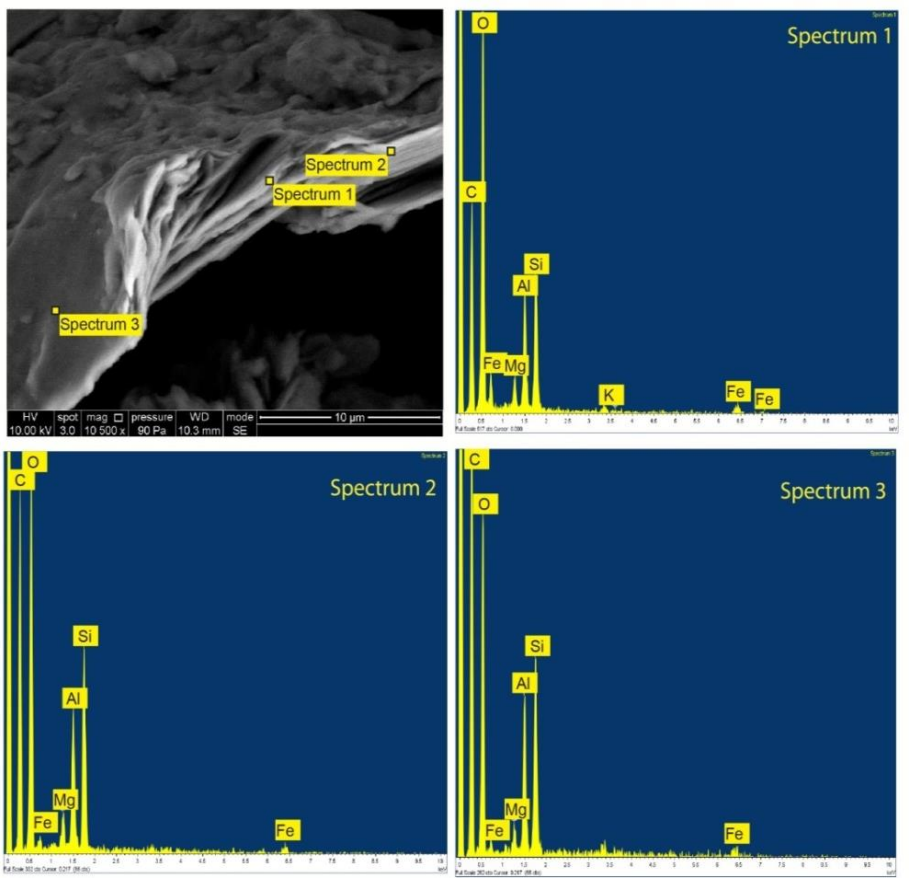

Figure 10. SEM image and EDS analyses of a section of the aggregates of clay minerals extracted from Chuishui shale. Note that the oxides of Mg appear adjacent to the center part of the aggregates of clay minerals. The oxides of K and Fe are negligible amount in spectrum 2 and 3.

It is interesting to compare our results with previous studies. The results of clay mineral of Hole-B were interpreted in terms of dehydroxylation of kaolinite and dehydration of interlayer water, dehydroxylation, and illitization of smectite occurred during coseismic

frictional heating (Hirono et al., 2008b). It implies that the temperature of faulting was not high enough to cause melting that we mentioned here. The different characteristics of clay minerals in the fault zone between Hole-A and Hole-B can be interpreted as a result of heterogeneous frictional heating on the fault surface caused by different asperities (Childs et al., 2008), even though they are only 40 m away.

On the other hand, it seems that the illitization of smectite did not occur in the FZ1111 of TCDP Hole-A. The reaction of smectite to illite in sedimentary basins is well documented and considered a classic reaction of clastic diagenesis (Abercrombie et al., 1994). The reaction seems to rely on five variables: 1) time, 2) heat, 3) the availability of K+, 4) fluids, and 5) confining pressures and water pressures (Velde et al., 1986; Moore and Reynolds, 1997; Whitney, 1990). Several studies have presented that seismic energy (shear stress and coseismic heat flow) overcomes the kinetic barrier and drives smectite to illite reactions (Evans and Chester, 1995; Wintsch et al., 1995; Vrolijk and van der Pluijm, 1999). Thermodynamic modeling of smectite to illite with consideration of temperature, pressure, and water activity, was also considered (Vidal and Dubacq, 2009; Dubacq et al., 2010). However, given the very short time of heating by faulting and lab friction experiments with high velocity and high heating rates that failed to trigger clay reactions (Boutareaud et al., 2010), the reaction of smectite-illite mentioned above seems to be caused mostly by low heating rate processes (diagenesis). It strongly suggests that normal thermal decomposition/dehydroxylation, instead of high heating rate caused by faulting, might have been the driving force for the reaction of smectite to illite. This mechanism might explain why the illitization of smectite is not observed (Hole-A) or not complete (Hole-B) after careful examinations of the characteristics of clay minerals from the TCDP (Hirono et al., 2008b; Kuo et al., 2009).

4.1.2. Estimate of Tthe Maximum Temperature Achieved in FZ1153

The clay results of XRD show that the disappearance of kaolinite was located in a relatively wider interval ~1.3 m of FZ1153 (compared to the clay anomaly of FZ1111) (Figure 5), and the relative percentage of clay minerals is lower than the average one of chinshui formation at the same interval. The occurrence of kaolinite might have been caused by thermal decomposition/dehydroxylation because of frictional heating during earthquakes, and this absence of kaolinite is also observed in the materials that experienced high velocity rotary shear experiments (Brantut et al., 2008). In addition, the temperature of thermal decomposition/dehydroxylation is controlled by heating rates (Sembira and Dunn, 1996). The variation in heating rates on the endothermic reaction for kaolinite indicates that in general, the slower the heating rate, the broader the peak and the lower the temperature of the peak (e.g., 5°C/min to 20°C/min) (Spiel et al., 1945). The thermal decomposition/dehydroxylation of kaolinite with a normal heating rate is proposed at T = 500°C to 550°C (Killingly & Day, 1990; Temuujin et al., 1998). Therefore, we set 500°C as a lower bound of temperature on FZ1153 during coseismic slip if we are estimating a truthful temperature range of faulting.

Additionally, we discuss more details about chlorite with our results of SEM/EDX, and several previous studies to estimate the temperature range of thermal dehydroxylation of chlorite in the fault zone. Nutting (1943) reported several dehydroxylation curves for different chlorites, and some of them showed a gradual continuous loss of weight from about 600°C to 850°C, where dehydroxylation is essentially complete. Meanwhile, other chlorites studied in Nutting (1943) show a relatively slight loss between 600°C and about 750°C to 800°C, and

then a relatively abrupt loss from 800°C to essentially complete dehydroxylation at 850°C to 900°C. The experiments show that the dehydroxylation characteristics of chlorite vary with composition. The data of dehydroxylation temperature for chlorite with various cations in the octahedral layers were also provided by Caillère and Hénin (1960). Their data indicate that the dehydroxylation temperature of Mg-chlorite (820°C) is higher than that of Fe-chlorite (530°C). Therefore, identification of chemical composition of chlorite is critical to estimating the thermal records during faulting.

The results of SEM/EDX show that the mixtures of clay extracted from Chinshui shale are composed of illite (spectrum 1) and Mg-chlorite (spectrum 2, 3) (Figure 10). Analysis of individual and collective reflections of chlorite XRD pattern as shown by Grim (1968) and Carroll (1969) indicates that the chlorite in this chapter is a trioctahedral Mg-rich chlorite, and contains essentially no iron. These observations and results show that Mg-rich chlorite, instead of Fe-rich chlorite, is dominant in our samples, and imply that the estimated complete dehydroxylation temperature of chlorite should be 900°C. Hashimoto et al. (2008) have documented that Mg-chlorite is abundant in the samples of Hole-B, and interpreted the negligible amount of Fe-chlorite in the black gouge as the clay anomaly due to fluid-rock interaction and thermal decomposition. Comparing with the clay results of Hole-A and Hole-B, the presence of Mg-chlorite presumably indicates different thermal effects during coseismic events in the TCDP case.

Thermal decomposition/dehydroxylation of kaolinite and chlorite mentioned above were all conducted at 1 atm. Yeskis et al. (1985) showed that the dehydroxylation of kaolinte varies with different pressures in high pressure DTA experiments (20°C/min). The dehydroxylation temperature of kaolinite is 525°C (1 bar), 627°C (30.5 bars), and 670°C (5,270 bars) under an inert pressurizing medium with argon, whereas the temperature is 650°C (46.5 bars), 520°C (1,088 bars), and 571°C (5,716 bars) under an inert pressurizing medium with water. Bai et al. (1993) reported that the dehydroxylation temperature of chlorite varied from 738°C to 869°C (1 bar to 770 bars) in closed capsules. These studies indicate that the pressure and water partial pressure are important factors of thermal decomposition/dehydroxylation, and that the difference in thermal decomposition/dehydroxylation between kaolinite and chlorite is small at high pressures as discussed above. In the TCDP case, the pores are located at 1 km depth, which translates to an equivalent surrounding pressure of 100 bars. Based on the interpolation of high pressure DTA experiments in previous studies (Yeskis et al., 1985; Bai et al., 1993), the temperature of thermal decomposition/dehydroxylation is 620°C (kaolinite), 770°C (Fe-chlorite), and 855°C (Mg-chlorite), respectively. The temperature range between kaolinite and chlorite under 100 bars is smaller than what we offer under the normal pressure. Therefore, our inferred temperature range could be considered a conservative estimate, and thus should be applicable to high pressure conditions (5.7 kbars for kaolinite and 0.7 kbars for chlorite).

Furthermore, the XRD results of isothermal heating experiments are showing that total thermal dehydroxylation of chlorite occurs at T= 900°C (Figure 8). It indicates that the temperature of thermal dehydroxylation of chlorite in the Chinshui shale is lower than 900°C. Hence, from the characteristics of clay minerals, thermal decomposition/dehydroxylation between kaolinite and chlorite, and the comparison between XRD results of FZ1153 and of isothermal heating experiments, it is a conclusive result that the temperature of FZ1153 achieved 500°C to 900°C during coseismic events.

4.1.3. Estimate of the Maximum Temperature Achieved in FZ1222

In contrast to FZ1111 and FZ1153, FZ1222 seems to have no obvious clay anomalies of lower clay mineral percentage and clay dehydroxylation driven by large frictional heat (Figure 6). However, a notable phenomenon in FZ1222 is that the relative percentage of illite increases to almost 90%, but that of smectite, chlorite, and kaolinite slightly decreases in the upper black gouge zone of ~2 cm interval. We propose that frictional heating and acid fluids may play a role in initiating the smectite to illite reaction and chlorite vanishing reaction in the black gouge zone to increase relative percentage of illite, but decrease that of smectite and chlorite (Huang et al., 1993; Moore and Reynolds, 1997; Senkayi et al., 1981; Vrolijk and van der Pluijm, 1999). Here we focus on the discussion of heat source and its temperature range for this hypothesis. First, the temperature record of the TCDP Hole-A was 46.5°C at 1200m depth along the bore hole (Kano et al., 2006). It is much lower than the temperature (100°C - 150°C) of smectite to illite transformation (Freed and Peacor, 1989; Hyndman, 2004). Second, if considering the smectite to illite reaction at T = 100°C to 150°C (the maximun burial temperature, Freed and Peacor, 1989; Hyndman, 2004; Yue et al., 2005), the clay mineral assemblages in our samples should show a similar trend within the diagenesis process. The clay mineral anomaly in FZ1222 was localized in ~2 cm interval instead of being widely distributed. It suggests that diagenesis is not the main process to drive the transformation of smectite to illite. Last, relative clay percentages in FZ1222 are not lower than the ones of Chinshui, which means that no thermal decomposistion/ dehtdroxylation occurred. Therefore, frictional energy produced by coseismic events is the most possible heat source to drive smectite to transfer to illite, instead of thermal decomposistion/dehtdroxylation during diagenesis. Furthermore, the temperature constraint provided from the TCDP Hole-B suggests that high temperature fluid (>350°C) has interacted with fault core material (Ishikawa et al., 2008). However, chlorite is in a stable phase and should not be depleted in this temperature range. Therefore, the consumption of chlorite in this chapter may be related to acid fluid (Senkayi et al., 1981). We propose that chlorite in fault gouge might have been altered by acid fluid and have further transferred to trioctahedral smectite or dissolved (Senkayi et al., 1981). Thus, the reaction of smectite-illite and the consumption of chlorite with assisting high temperature acid fluid caused by frictional heat were probably proceeded to produce the occurrence of rich illite and less smectite and chlorite in FZ1222. The hot acid fluids interacted in FZ1222 may be due to the thermal heat pulse during coseismic slip.

4.1.4. Limitation of Temperature Estimate and its Significance

We simply utilize the breakdown temperature of clay minerals to estimate the peak temperature in coseismic events. However, the fault surfaces were not only heated, but they are also rubbed and grinded during frictional sliding in the same time. Rubbing induces tribochemical reactions which include mechanically- and thermally-activated reactions. Tribochemical reactions result in the formation of new compounds and trigger dehydroxylation and dehydration reactions in the case of clays, and they also induce different reaction mechanisms. It suggests that tribochemical reactions may occur at lower activation energies (and thus their kinetics is more efficient at a given temperature) than thermo-chemical reactions (Steinike and Tkácová, 2000). Thus, considering the effects of tribochemical reaction, the determined temperature range for three fault zones, or the highest temperature achieved in the slipping zone, might be overestimated. Here we present the

approaching temperature estimates instead of lower bounds provided in the past, and these estimates may provide constraints on the studies of (i) the physico-chemical processes activated during seismic slip (e.g., melting in FZ1111), (ii) the activation of coseismic dynamic weakening mechanism and, more in general (thermal pressurization), (iii) earthquake energy budget for the Chelungpu fault.

4.2. Thickness of Chi-Chi PSZ

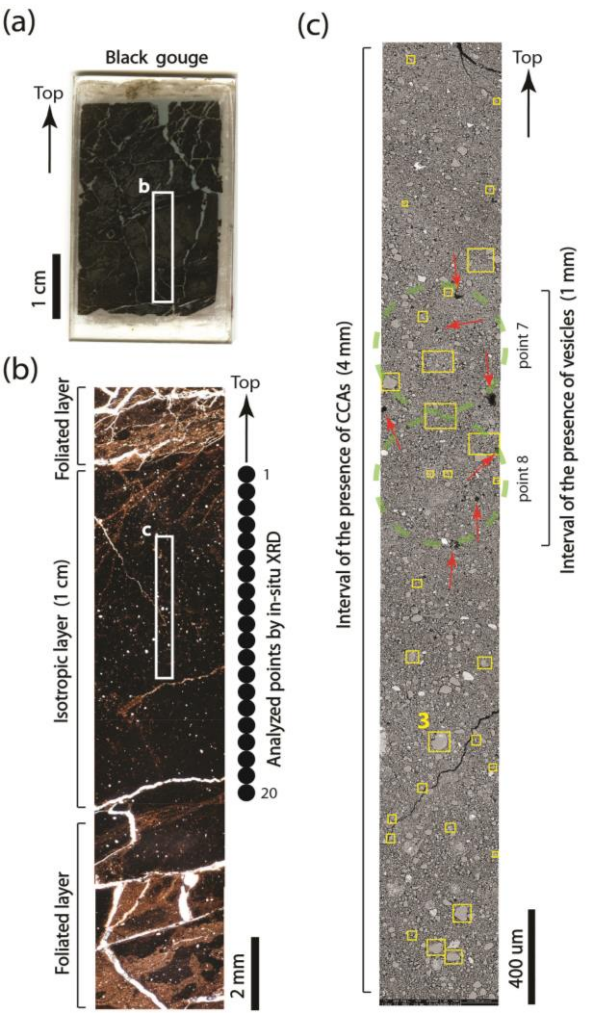

Figure 11. Microstructural observation of black gouge hosting the Chi-Chi PSZ. (a) The scan of the thin section of black gouge indicating the fracturing zone and the isotropic layer. (b) Microstructures in the isotropic layer showing the matrix-support clasts which are quartz fragments and ultrafine grained clays defined as the isotropic layer by Boullier et al. (2009). Twenty analyzed points by in-situ synchrotron XRD were shown in the right side of the image. (c) Backscattered electron SEM images of the isotropic layer contains large quartz clasts, very fine grains of clays, vesicles indicated by red arrows, and CCAs marked with yellow rectangular boxes. One representative CCA was shown in Figure 12.

On the basis of current research of TCDP, the Chi-Chi PSZ was presumably set at the depth of 1,111 m. Since the thickness of the PSZ is a key parameter to obtain the surface fracture energy and associated seismic efficiency (Ma et al., 2006), we might estimate the thickness of the PSZ from the PSZ thin section by utilizing microstructural observation and in-situ analysis. A distinguishing gouge layer within the black gouge (Figure 11a and b) characterizing by an ultracataclastic texture with matrix-support clasts was found in the black gouge (Figure 3 left panel). The 1-cm thick gouge layer does not contain any fracture, cleavage, vein, banding, or shearing structure and is defined as the isotropic layer (followed by Boullier et al. 2009) (Figure 11b). The isotropic layer was surrounding by foliated layers which contain deformed veins, oriented clay-rich layers, fragments of old gouges and quartz, shear deformation and apparent cracks.

Thin section observation by SEM shows that a clastic core mantled by concentric fine-grained aggregated materials called clay-clast aggregates (CCAs) (Boullier et al., 2009) were found in 4-mm thick within the isotropic layer (Figure 11c). The inner cores (central clasts hereafter) of the CCAs are fragments of quartz and feldspar, and the diameter of the central clasts varies from 1 μm to 130 μm (Figure 12). The CCAs were marked with yellow rectangular boxes in Figure 11c and was not identified in the surrounding black gouges or elsewhere in the fault zone. FESEM/EDX element mapping conducted on a typical monomineralic CCAs displays a higher relative atomic density of Al, Na, K, Fe and Mg in the cortex which highlights clays concentrically coating the central clast which the atomic density is dominant in Si (Figure 12). In addition, the vesicles presumably resulted from thermal decomposition/dehydroxylation processes (Kuo et al., 2009, 2011) (Figure 7 and 9) were indicated by red arrows (Figure 11c). The presence of vesicles was estimated as 1-mm thick within the isotropic layer.

The presence of smectite within PSZ was presumably derived from the alteration of pseudotachylye and/or amorphous materials resulted from frictional heating during the 1999 Chi-Chi earthquake (Kuo et al., 2009). The interval of smectite-rich layer was estimated as 2-cm thick due to the restriction on sampling. On the basis of the characteristics of clays within PSZ (Figure 3), high spatial resolution synchrotron XRD analysis was conducted on the black gouge thin section to directly determine the interval of smectite-rich layer (Figure 13; see the details in Kuo et al., in press). Although the traditional identification of swelling clays following the process of air-drying and ethylene-glycol solvation was not performed in this chapter, the distinct wide peaks from 4 to 6 of two theta were presumably resulted from new formed smectite suggested by Kuo et al. (2009). The relatively high abundance of smectite within the isotropic layer was detected in point 7 and point 8, and moderate abundance of smectite was detected in point 9 and point 10 (Figure 11b). Combined with the occurrence of vesicles likely resulted from frictional heat (Figure 11c) (Kuo et al., 2011), the interval of the heated zone where the process of thermal decomposition/dehydroxylation occurred was estimated as 1 mm.

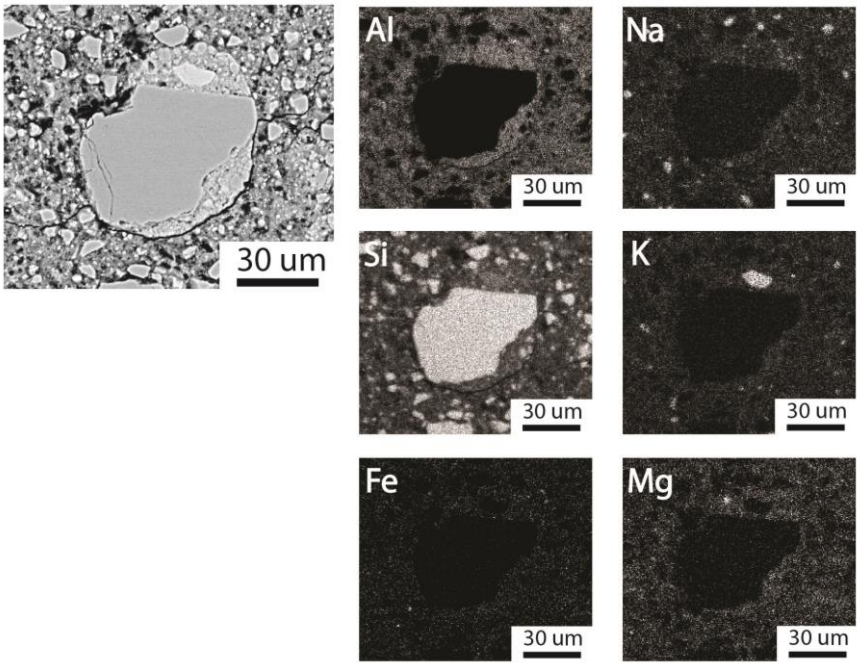

Figure 12. EDX-SEM element composition mapping of a typical CCA in the isotropic layer. Only Al, Na, K, Fe and Mg elements show a strong signal for the cortex of CCAs.

The formation of CCAs in fault gouges caused by seismic faulting is still a debate (Han and Hirose, 2012). Han and Hirose (2012) systematically conducted rock deformation experiments at a wide range of slip rates and demonstrated that the presence of CCAs is not necessarily produced at seismic rates. However, the findings of TCDP were showing that frictional heat were generated during coseismic faulting (Hirono et al., 2006a, 2008; Ishikawa et al., 2008; Kuo et al., 2009, 2011; Mishima et al., 2006, 2009), and it suggests that the CCA within the isotropic layer were likely produced at seismic rates, at least in this locality. In addition, considering the presence of coseismic fluid mentioned above, the occurrence of CCAs appears to be a possible indicator for thermal pressurization and/or gouge fluidization in the TCDP case suggested by Boutareaud et al. (2010). The interval of the presence of CCAs was estimated as 4 mm (Figure 2c) which illustrates the affected area of the mechanism of thermal pressurization.

So far, the thickness of PSZ from the aspect of microstructural observation was obtained as (1) 2 cm identified from the fault core of TCDP (Ma et al., 2006; Boullier et al., 2009), (2) 50-300 μm of fault cores from surface outcrops (Heermance et al., 2003), and (3) 7 mm of fault gouge at 330m depth from shallow hole (Tanaka et al., 2002). The variation of the thickness of PSZ might be due to the heterogeneity of the fault at different depths (Gratier, 2003) and this issue is not probed in this chapter. Thus, 1-mm thick was estimated from the interval of thermal decomposition/dehydroxylation of clay minerals and 4-mm thick was measured from the interval of the presence of CCAs within the isotropic layer. Here we utilize 1-mm as the thickness of Chi-Chi PSZ followed by the definition of PSZ which was accommodated most shear displacement and/or high strain followed with high frictional heat generated.

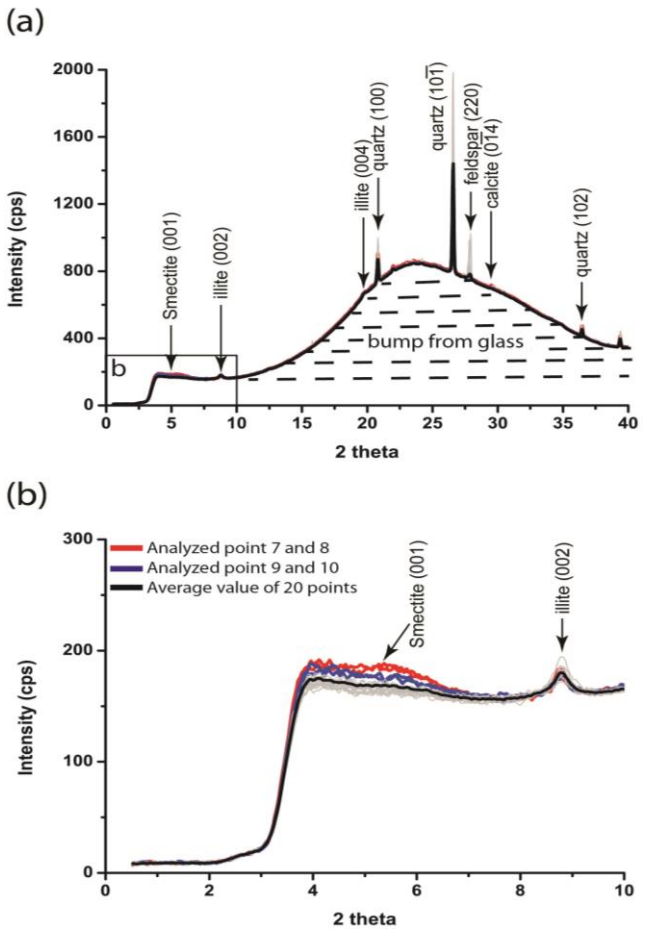

Figure 13. (a) All apparent peaks are identified by the in-situ synchrotron XRD analyses and signed with mineral names. The bump caused by the peak of glass was drawn with dashed lines. The insert box is the signal of smectite and was enlarged in (b). (b) All results were drawn in light gray lines, and the average value of all experiments was drawn in black lines except relatively high abundance of smectite. The highest abundance of smectite was drawn in red lines and the moderate one was drawn in blue lines.

4.3. Surface Fracture Energy of the PSZ and Contribution of the Breakdown Work

The breakdown work, considered as an equivalent to seismic fracture energy, is the energy spent for rupture to advance during earthquakes (Tinti et al., 2005). The breakdown work is composed of surface fracture energy and plastic deformation of grains associated with the creation of small grains within the slipping zones, and frictional heat driving physico-chemical processes along the fault slip surface. The breakdown work could be obtained by calculating the integral of the shear traction versus slip, from zero slip to the point that the traction drops to a minimum (Tinti et al. 2005):

$$W_b = \int_0^{tb} (\tau(t) - \tau_{min}) \cdot v(t) dt \quad (1)$$

where v(t) is the slip velocity, τ(t) is the shear traction, and t_b is the time at which minimum traction τ_{min} is reached. In the TCDP case, a grid size (fault block) of 0.95 km and a time interval of 0.054s, based on the kinematic results of the temporal-spatial slip distribution (Ji et al., 2003), were used to calculate the breakdown work. The shear traction (stress-slip curve) was obtained by combining the stress-time history and slip-time history from kinematic inversion. The integral of the equation (1) gives a value of the breakdown work of 11.6 MJm^{-2} for a small patch of the subfault 1 km beneath the drill site (Ma et al., 2006). Several assumptions were made for the calculation as following: 1) the breakdown work was homogeneously distributed beneath the drill site over the subfault, 2) fault core thickness, fault geometry, and grain size distribution did not vary in the subfault. Ben-Zion and Sammis (2003) determined how different aspects of a fault zone may be alternatively described in different frameworks, and the clarification of the assumption, either from field geology side or from the laboratory side, still remains challenging (Niemeijer et al., 2012). The value of breakdown work obtained in this chapter might be risky to stand for the 1999 Chi-Chi earthquake, but at least it is convincible at this locality.

The particle surface area (S_{msz}) of the major slip zone (MSZ) of the TCDP Hole-A was obtained from the microstructural observation and the value of S_{msz} was estimated of 6.46 x 105 m^2 per metre squared area (Ma et al., 2006). The mineral composition of MSZ which was composed of 70% of quartz, 5% feldspar, and 25% clays gives a specific fracture energy G_c of about 1 Jm^{-2} (McGarr et al., 1979; Scholz, 2002). A corrected parameter for grain roughness λ of 0.66 was utilized (Wilson et al., 2005). Thus, the total surface fracture energy of the 2-cm MSZ of the TCDP Hole-A was obtained by:

$$G_{msz} = S_{msz}\lambda G_c \quad (2)$$

Ma et al. (2006) provided a value of 4.3 MJ per metre squared area for the total surface fracture energy from equation (1). Since the fault materials of the 2-cm MSZ defined by Ma et al. (2006) is consistent with the one of the isotropic layer in this chapter, the total surface fracture energy can be proportionally utilized for the 1-cm isotropic layer and the value of total surface fracture energy would be 2.15 MJ per metre squared area.

Ma et al. (2006) estimated the thickness of MSZ as 3.3 mm from which the ratio (T/D) of the slip thickness (T = 12 cm) to the total displacement (D = 300 m) multiples 8.3 m slip of the Chi-Chi earthquake (Heermance et al., 2003; Yue et al., 2005). In addition, the chapter assumed that similar displacement of repeating earthquakes took place in the MSZ and the number of coseismic events in the 2-cm MSZ is between 6 and 7. Thus, the surface fracture energy associated to a single earthquake on average was 0.65 MJ per metre squared area. Given the breakdown work (Wb) of 11.6 MJm^{-2} , the value of the process of pulverizing grain is about 6%.

Following the plausible assumption based on the microstructural observation suggested by Ma et al. (2006), the thickness of PSZ determined as 1 mm suggests that the number of repeated earthquakes in the 1-cm isotropic layer is 10. The surface fracture energy associated to a single large earthquake on average (e.g., 1999 Chi-Chi earthquake) was 0.22 MJ per metre squared area. Thus, the correlated contribution of the surface fracture energy to the breakdown work corresponding to 1999 Chi-Chi earthquake is estimated to be 1.9%. We consider the estimate to be the minimum for the assumption that there is no fracture energy generated during the earthquake. Since the surface fracture energy is much less, it suggests

that the huge remaining part of the breakdown work would be turned into heat which was associated with several processes suggested to result in coseismic fault lubrication such as thermal pressurization (Boullier et al., 2009; Hirono and Tanikawa, 2011), elastohydrodynamic lubrication (Brodsky and Kanamori, 2001), and frictional melting lubrication (Di Toro et al., 2006).

CONCLUSION

The fault zones of the Chelungpu fault and the plausible PSZ corresponding to the 1999 Chi-Chi earthquake are characterized with clay mineral assemblages from the TCDP. Distinct clay mineral anomaly and microstructural observation within the PSZ of FZ1111 suggests that frictional heat generated by faulting melted most of the clay except for illite, then promptly altered tiny glass to smectite. In addition, the temperatures among three fault zones of the Chelungpu fault estimated from the characteristics of clay minerals are summarized as follow: (1) temperature range of FZ1111 was from 900°C to 1,100°C and the clay anomaly was localized with the PSZ, (2) temperature range of FZ1153 was from 500°C to 900°C and the clay anomaly was widely distributed in a wide interval (~1.3m), and (3) temperature range in FZ1222 was between 350°C and 500°C and clay change via high temperature fluid-rock interaction occurred in the upper black gouge zone (~2cm). Meanwhile, the interval of the clay anomaly within the PSZ determined by state-of-art in-situ synchrotron X-ray diffraction analysis was estimated to be 1 mm and the contribution of surface fracture energy to earthquake breakdown work is quantified to be 1.9%. On the basis of the estimates of earthquake source parameters (temperature and thickness of the PSZ), it suggests that the huge part of the breakdown work released by the 1999 Chi-Chi earthquake was turned into chemical work (mineral transformation) and mechanic work, and several processes such as thermal pressurization, elastohydrodynamic lubrication, and melting lubrication may operate during this coseismic slip.

ACKNOWLEDGMENT

The authors would like to thank the TCDP team for their assistance with the on-site work. This research was funded by the National Science Council of Taiwan under grant NSC 102-2116-M-002-015.

REFERENCES

Abercrombie, H. J., Hutcheon, I. E., Bloch, J. D., de Caritat, P., 1994. Silica activity and the smectite-illite reaction. *Geology* 22(6), p.539-542.

Aki, K., 1989. Geometric features of a fault zone related to the nucleation and termination of an earthquake rupture. *United States Geological Survey Open-File Report* 89-315, p. 1-9.

Bai, T. B., Guggenheim, S., Wang, S. J., 1993. Metastable phase relations in the chlorite-H2O system. *American Mineralogist* 78, p. 1208-1216.

Barrier, E., Angelier, J., 1986. Active collision in eastern Taiwan: The Coastal Range. *Tectonophysics* 125, p. 39-72.

Bastesen, E., Braathen, A., Nøttveit, H., Gabrielsen, R. H., Skar, T., 2009. Extensional fault cores in micritic carbonates, a case study from Gulf of Corinth, Greece. *Journal of Structural Geology* 31, p. 403-420.

Bauluz, B., Peacor, D. R., Hollis, C. J., 2004. TEM study of meteorite impact glass at New Zealand Cretaceous-Tertiary sites: evidence for multiple impacts or differentiation during global circulation? *Earth and Planetary Science Letters* 219, p. 209-219.

Beeler, N. M., Wong, T. F., Hickman, S. H., 2003. On the expected relationships among apparent stress, static stress drop, effective shear fracture energy, and efficiency. *Bulletin of the Seismological Society of America* 93, p. 1381-1389.

Ben-Zion, Y., Sammis, C. G., 2003. Characterization of fault zones. *Pure and Applied Geophysics* 160, p. 677-715

Biq, C., 1972. Dual trench structure in the Taiwan-Luson region. *Proceedings of the Geological Society of China* 15, p. 65-75.

Biscaye, P. E., 1965. Mineralogy and sedimentation of recent deep-sea clays in the Atlantic Ocean and adjacent seas and oceans. *Geological Society of America Bulletin* 76, p. 803-832.

Bonilla, M. G., 1977. Summary of Quaternary faulting and elevation changes in Taiwan. *Memoir of Geological Society of China* 2, p. 43-55.

Bonson, C. G., Childs, C., Walsh, J. J., Schopfer, M. P. J., Carboni, V., 2007. Geometric and kinematic controls on the internal structure of a large normal fault in massive limestones: the Maghlaq Fault, Malta. *Journal of Structural Geology* 29 (2), p. 336-354.

Boullier, A.-M., Ohtani, T., Fujimoto, K., Ito, H., Dubois, M., 2001. Fluid inclusions in pseudotachylytes from the Nojima Fault, Japan. *Journal of Geophysical Research* 106 (B10), p. 21965-21977.

Boullier, A.-M., Yeh, E. C., Boutareaud, S., Song, S. R., Tsai, C. H., 2009. Micro-scale anatomy of the 1999 Chi-Chi earthquake fault zone. *Geochemistry Geophysics Geosystems* 10 (3), Q03016.

Boullier, A.-M., 2011. *Fault-zone geology: lessons from drilling through the Nojima and Chelungpu fault. Geological Society*, London, Special Publications 359, p. 17-37.

Boutareaud, S., Calugaru, D.- G., Han, R., Fabbri, O., Mizoguchi, K., Tsutsumi, A., Shimamoto, T., 2008. Clay-clast aggregates: a new textural evidence for seismic fault sliding? *Geophysical Research Letters* 35 (5), L05302.

Boutareaud, S, Boullier, A.-M., Andréani, M., Calugaru, D. G., Beck, P., Song, S.-R., Shimamoto, T., 2010. Clay clast aggregates in gouges: New textural evidence for seismic faulting. *Journal of Geophysical Research* 115, B02408, doi:10.1029/2008jb006254.

Bowin, C., Lu, R. S., Lee, C. S., 1978. Plate convergence and accretion in Taiwan-Luzon region. *American Association of Petroleum Geologists Bulletin* 62, p. 1645-1672.

Braathen, A., Tveranger, J., Fossen, H., Skar, T., Cardozo, N., Semshaug, S. L., Bastesen, E., Sverdrup, E., 2009. Fault facies and its applications to sandstone reservoirs. *American Association of Petroleum Geologists Bulletin* 93, p. 891-917.

Brantut, N., Schubnel, A., Rouzaud, J. N., Brunet, F., Shimamoto, T., 2008. High-velocity frictional properties of a clay-bearing fault gouge and implications for earthquake mechanics. *Journal of Geophysical Research* 113, B10401, doi:10.1029/2007JB005551.

Brantut, N., Schubnel, A., Corvisier, J., Sarout, J., 2010. Thermochemical pressurization of faults during coseismic slip. *Journal of Geophysical Research* 115, B05314, doi:05310.01029/02009JB006533.

Brindley, G.W., Ali, S.Z., 1950. Thermal Transformations in Magnesium *Chlorites, Acta Crystallographica* 3, p.25-30.

Brodsky, E. E., Kanamori, H., 2001. Elastohydrodynamic lubrication of faults. *Journal of Geophysical Research* 106, p. 16357-16374.

Caillère, S., Hénin, S., 1960. Relationship between the crystallochemical constitution of phyllites and their dehydration temperature, Application in the case of chlorites. *Bulletin of Society France Ceramic* 48, p. 63-67.

Caine, J. S., Evans, J. P., Forster, C. B., 1996. Fault zone architecture and permeability structure. *Geology* 24, p. 1025-1028.

Carroll, D., 1970. *Clay Minerals: A guide to their X-Ray Identification.*

Chang, S. L., 1971. Subsurface geologic study of the Taichung basin. *Petroleum Geology of Taiwan* 8, p. 21-45.

Chen, Y. G., Chen, W. S., Lee, J. C., Lee, Y. H., Lee, C. T., Chang, H. C., Lo, H. C., 2001. Surface rupture of 1999 Chi-Chi earthquake yields insights on active tectonics of central Taiwan. *Bulletin of the Seismological Society of America* 91, p. 977-985.

Chester, F. M., Evans, J. P., Biegel, R. L., 1993. Internal structure and weakening mechanisms of the San Andreas fault. *Journal of Geophysical Research* 98(B1), p. 771-786.

Chester, F. M., Chester, J. S., 1998. Ultracataclasite structure and friction processes of the Punchbowl fault, San Andreas system, *California. Tectonophysics* 295(1-2), p. 199-221.

Chester, J. S., Chester, F. M., Kronenberg, A. K., 2005. Fracture surface energy of the Punchbowl fault, San Andreas system. *Nature* 437, p. 133-136.

Childs, C., Watterson, J., Walsh, J. J., 1996. A model for the structure and development of fault zones. *Journal of the Geological Society of London* 153, p. 337-340.

Childs, C., Manzocchi, T., Walsh, J. J., Bonson, C. G., Nicol, A., Schöpfer, M. P. J., 2008. A geometric model of fault zone and fault rock thickness variations. *Journal of Structural Geology* 31 (2), p. 117-127.

Chou, Y. M, Song, S. R., Aubourg, C., Lee, T. Q., Boullier, A.-M., Song, Y. F., Yeh, E. C., Kuo L. W., Wang, C. Y., 2012a. An earthquake slip zone is a magnetic recorder. *Geology*, doi:10.1130/G32864.1.

Chou, Y. M, Song, S. R., Aubourg, C., Song, Y. F., Boullier, A.-M., Lee, T. Q., Evans, M., 2012b. Pyrite alteration and neoformed magnetic minerals in the fault zone of the Chi-Chi earthquake (Mx 7.6, 1999): Evidence for frictional heating and co-seismic fluids. *Geochemistry Geophysics Geosystems* 13 (8), Q08002, doi: 10.1029/2012GC004120.

Cowie, P. A., Scholz, C. H., 1992. Physical explanation for the displacement-length relationship of faults, using a post-yield fracture mechanics model. *Journal of Structural Geology* 14, p. 1133-1148.

Dalguer, L. A., Irikura, J. D., Riera, J. D., Chiu, H. C., 2001. The importance of the dynamic source effects on strong ground motion during the 1999 Chi-Chi, Taiwan, earthquake: brief interpretation of the damage distribution on building. *Bulletin of the Seismological Society of America* 91, p. 1112-1127.

Davis, D., Suppe, J., Dahlen, F. A., 1983. Mechanics of fold-and-thrust belts and accretionary wedges. *Journal of Geophysical Research* 88, p. 1153-1172.

Di Toro, G., Goldsby, D., Tullis, T., 2004. Friction falls towards zero in quartz rock as slip velocity approaches seismic rates. *Nature* 427, p. 436-439.

Di Toro, G., Pennacchioni, G., Teza, G., 2005. Can pseudotachylytes be used to infer earthquake source parameters? An example of limitations in the study of exhumed faults. *Tectonophysics* 402, p. 3-20.

Di Toro, G., Hirose, T., Nielsen, S., Pennacchioni G., Shimamoto T., 2006. Natural and experimental evidence of melt lubrication of faults during earthquakes. *Science* 311, p. 647-649.

Dubacq, B., Vidal, O., Andrade, V. D., 2010. Dehydration of dioctahedral aluminous phyllosilicates: thermodynamic modelling and implications for thermobarometric estimates. *Contributions to Mineralogy and Petrology* 159, p.159-174; DOI 10.1007/s00410-009-0421-6.

Gratier, J.-P., Favreau, P., Renard, F., 2003. Modeling fluid transfer along California faults when integrating pressure solution crack sealing and compaction process. *Journal of Geophysical Research* 108, doi:10.1029/2001JB000380.

Goldsby, D. L., Tullis, T. E., 2011. Flash Heating Leads to Low Frictional Strength of Crustal Rocks at Earthquake Slip Rates. *Science* 334, p. 216-218, doi:10.1126/science.1207902.

Grim, R. E., 1968. *Clay Mineralogy*, 2nd ed. McGraw-Hill, New York.

Evans, J. P., Chester, F. M., 1995. Fluid-rock interaction in faults of the San Andreas system: Inferences from San Gabriel fault rock geochemistry and microstructures. *Journal of Geophysical Research* 100, p. 13,007-13,020.

Freed, R. L., Peacor, D. R., 1989. Variability in temperature of the smectite/ illite reaction in Gulf Coast sediments. *Clay Minerals* 24(2), p. 171-180.

Han, R., Shimamoto, T., Hirose, T., Ree, J.-H., Ando, J., 2007. Ultralow friction of carbonate faults caused by thermal decomposition. *Science* 316, p. 878-881.

Han, R., Hirose, T., Shimamoto, T., 2010. Strong velocity weakening and powder lubrication of simulated carbonate faults at seismic slip rates. *Journal of Geophysical Research* 115, B03412, doi:03410.01029/02008JB006136.

Han, R., Hirose, T., 2012. Clay-clast aggregates in fault gouge: An unequivocal indicator of seismic faulting at shallow depths? *Journal of Structural Geology* 43, p. 92-99.

Hashimoto, Y., Tadai, O., Tanimizu, M., Tanikawa, W., Hirono, T., Lin, W., Mishima, T., Sakaguchi, M., Soh, W., Song, S. R., Aoike, K., Ishikawa, T., Murayama, M., Fujimoto, K., Fukuchi, T., Ikehara, M., Ito, H., Kikuta, H., Kinoshita, M., Masuda, K., Matsubara, T., Matsubayashi, O., Mizoguchi, M., Nakamura, N., Otsuki, K., Shimamoto, T., Sone, H., Takahashi, M., 2008. Characteristics of chlorites in seismogenic fault zones: the Taiwan Chelungpu Fault Drilling Project (TCDP) core sample, e-Earth 3 (*http://www.electronic-earth. net/3/issue1.html*), p. 1-6.

Heermance, R.V., Shipton, Z. K., Evans, J. P., 2003. Fault structure control on fault slip and ground motion during the 1999 rupture of the Chelungpu fault, Taiwan. *Bulletin of the Seismological Society of America* 93, 1034-1050.

Ho, C. S., 1986. A synthesis of the geologic evolution of Taiwan. *Tectonophysics* 125, p. 1-16.

Ho, C. S., 1988: An Introduction to the Geology of Taiwan-Explanatory Text of the Geologic Map of Taiwan, 2nd Ed., *Central Geological Survey*, MOEA, Taipei, Taiwan, ROC, 163 pp.

Hirono, T., Lin, W., Yeh, E. C., Soh, W., Hashimoto, Y., Sone, H., Matsubayashi, O., Aoike, K., Ito, H., Kinoshita, M., Murayama, M., Song, S. R., Ma, K. F., Hung, J. H., Wang, C. Y., Tsai, Y. B., 2006a. High magnetic susceptibility of fault gouge within Taiwan Chelungpu fault: Nondestructive continuous measurements of physical and chemical properties in fault rocks recovered from Hole B, TCDP. *Geophysical Research Letters* 33, L15303, doi:10.1029/2006GL026133.

Hirono, T., Ikehara, M., Otsuki, K., Mishima, T., Sakaguchi, M., Soh, W., Omori, M., Lin, W., Yeh, E. C., Tanikawa, W., Wang, C. Y., 2006b. Evidence of frictional melting within disk-shaped black materials discovered from the Taiwan Chelungpu fault system. *Geophysical Research Letters* 33, L19311, doi:10.1029/2006GL027329.

Hirono, T., Sakaguchi, M., Otsuki, K., Sone, H., Fujimoto, K., Mishima, T., Lin, W., Tanikawa, W., Tanimizu, M., Soh, W., Yeh, E. C., Song, S. R., 2008a. Characterization of slip zone associated with the 1999 Taiwan Chi-Chi earthquake: X-ray CT image analyses and microstructural observations of the Taiwan Chelungpu fault. *Tectonophysics* 449, p. 63-84.

Hirono, T., Fujimoto, K., Yokoyama, T., Hamada, Y., Tanikawa, W., Tadai, O., Mishima, T., Tanimizu, M., Lin, W., Soh, W., Song, S. R., 2008b. Clay mineral reactions caused by frictional heating during an earthquake: An example from the Taiwan Chelungpu fault. *Geophysical Research Letters* 35, L16303, doi:10.1029/2008GL034476.

Hirono, T., Tanikawa, W., 2011. Implications of the thermal properties and kinetic parameters of dehydroxylation of mica minerals for fault weakening, frictional heating, and earthquake energetics. *Earth, Planets, and Space Letters* 307, p. 161-172.

Hirose, T., Shimamoto, T., 2005. Slip-weakening distance of faults during frictional melting as inferred from experimental and natural pseudotachylytes. *Bulletin of the Seismological Society of America* 95, p. 1666-1673.

Huang, W. H., Longo, J. M., Pevear, D. R., 1993. An experimental derived kinetic model for the smectite-to-illite conversion and its use as a geothermometer. *Clays and Clay Minerals* 41, p. 162-177.

Hung, J. H., Zhan, H. P., Wiltschko, D. V., Feng, P., 2002. Geodetically observation surface displacements of the 1999 Chi-Chi earthquake near southern termination of the Chelungpu fault. *Terrestrial, Atmospheric and Oceanic Sciences* 13, p. 355-366.

Hung, J. H., Wu, Y. H., Yeh, E. C., Wu, J. C., TCDP Scientific Party, 2007. Subsurface structure, physical properties, and fault zone characteristics in the scientific drill holes of Taiwan Chelungpu-fault Drilling Project. Terrestrial, *Atmospheric and Oceanic Sciences* 18, p. 271-293, doi: 10.3319/TAO.2007.18.2.271(TCDP).

Hyndman, R. D., 2004. Controls on subduction thrust earthquakes: downdip changes in composition and state, in *Rheology and Deformation of the Lithosphere at Continental Margins.* In: Karner, G. D., B. Taylor, N. W. Driscoll, and D. L. Kohlstedt (Eds.), Columbia University Press, New York, p. 166-178.

Ishikawa, T., Tanimizu, M., Nagaishi, K., Matsuoka, J., Tadai, O., Sakaguchi, M., Hirono, T., Mishima, T., Tanikawa, W., Lin, W., Kikuta, H., Soh, W., Song, S. R., 2008. Coseismic fluid-rock interactions at high temperatures in the Chelungpu fault. *Nature Geosciences* 1, doi:10.1038/ngeo308.

Issacs A. J., Evans, J. P., Song, S. R., Kolesar, P. T., 2007. Characterizing brittle deformation, damage parameters, and clay composition in fault zones: variations along strike and with

depth in the Chelungpu Fault zone. *Terrestrial, Atmospheric and Oceanic Science* 18, p. 183-221.

Ji, C., Helmberger, D. V., Wald, D. J., Ma, K. F., 2003. Slip history and dynamic implication of the 1999 Chi-Chi, Taiwan, earthquake. *Journal of Geophysical Research* 108(B9), 2412. doi:10.1029/2002JB001764.

Kanamori, H., Heaton, T. H., 2000. In *Geocomplexity and the physics of earthquakes* (eds Rundle, J. B., Turcotte, D. L. & Klein, W.) (American Geophysical Union, Washington DC).

Kano, Y., Mori, J., Fujio, R., Ito, H., Yanagidani, T., Nakao, S., Ma, K. F., 2006. Heat signature on the Chelungpu fault associated with the 1999 Chi-Chi, Taiwan earthquake. *Geophysical Research Letters* 33, L14306. doi:10.1029/ 2006GL026733.

Kao, H., Chen, W. P., 2000. The Chi-Chi earthquake sequence: Active out-of-sequence thrust faulting in Taiwan. *Science* 288, p. 2346-2349.

Killingley, J. S., Day, S. J., 1990. Dehydroxylation kinetics of kaolinite and montmorillonite. *Fuel* 69 (10), p. 1145-1149.

Kim, Y.-S., Andrews, J. R., Sanderson, D. J., 2001a. Reactivated strike-slip faults: examples from north Cornwall, UK. *Tectonophysics* 340, p. 173-194.

Kim, Y.-S., Andrews, J. R., Sanderson, D. J., 2001b. Secondary faults and segment linkage in strike-slip fault systems at Rame Head, southern Cornwall. *Geoscience in South-West England* 10, p. 123-133.

King, G. C. P., 1986. Speculations on the geometry of the initiation and termination processes of earthquake rupture and its relation to morphology and geological structure. *Pure and Applied Geophysics* 124, p. 567-585.

Kuo, L.W., Song, S. R., Yeh, E. C., Chen, H. F., 2009. Clay mineral anomalies in the fault zone of Chelungpu Fault, Taiwan, and its implication. *Geophysical Research Letters* 36, L18306. doi:10.1029/2009GL039269.

Kuo, L.W., Song, S. R., Huang, L., Yeh, E. C., Chen, H. F., 2011. Temperature estimates of coseismic heating in clay-rich fault gouges, the Chelungpu fault zone, Taiwan. *Tectonophysics* 502, p. 315-327.

Kuo, L.W., Song, S. R., Yeh, E. C., Chen, H. F., Si, J., 2012. Clay mineralogy and geochemistry investigations in the host rock of the Chelungpu fault, Taiwan: Implication for faulting mechanism. *Journal of Asian Earth Sciences* 59, p. 208-218.

Kuo, L. W., Li, H., Smith, S., Di Toro, G., Suppe, J., Song, S. R., Nielsen, S., Sheu, H. S., Si., J., 2014. Gouge graphitization and dynamic fault weakening during the 2008 Mw 7.9 Wenchuan earthquake. *Geology* 42, p.47-50, doi: 10.1130/G34862.1.

Kuo, L. W., Hsiao, H. S., Song, S. R., Sheu, H. S., Suppe, J. Coseismic thickness of principal slip zone from the Taiwan Chelungpu fault Drilling Project-A (TCDP-A) and correlated fracture energy. *Tectonophysics*, in press.

Lee, J. C., Chen, Y. G., Sieh, K., Mueller, K., Chen, W. S., Chu, H. T., Chan, Y. C., Rubin, C., Yates, R., 2001. A vertical exposure of the 1999 surface rupture of the Chelungpu fault at Wufeng, western Taiwan: structural and paleoseismic implications for an active thrust fault. *Bulletin of the Seismological Society of America* 91, p. 914-929.

Lee, Y. H., Hsieh, M. L., Lu, S. D., Shi, T. S., Wu, W. Y., Sugiyama, Y., Azuma, T., Kariya, Y., 2003. Slip vectors of the surface rupture of the 1999 Chi-Chi earthquake, western Taiwan. *Journal of Structural Geology* 25, p. 1917-1931.

Li H.B., Wang, H., Xu, Z. Q., Si, J. L., Pei, J. L., Li, T. F., Yao, H., Song, S. R., Kuo, L. W., Sun, Z. M., Chevalier, M.-L., Liu, D. L., 2013. Characteristics of the fault-related rocks, fault zones and the principal slip zone in the Wenchuan earthquake Fault Scientific Drilling project Hole-1 (WFSD-1). *Tectonophysics* 584, p. 23-42.

Liao, C. F., 2003. Analysis of fault rock deformation and clay minerals from fault cores of Chelungpu fault zone. *Master's thesis of National Central University, in Chinese, summary in English*, p. 132.

Lin, A., 1994. Microlite morphology and chemistry in pseudotachylyte from the Fuyun fault zone, China. *Journal of Geology* 102, p. 317-329.

Lindanger, M., Gabrielsen, R. H., Braathen, A., 2007. Analysis of rock lenses in extensional faults. *Norwegian Journal of Geology* 87, p. 361-372.

Liu, C. S., Huang, I. L., Teng, L. S., 1997. Structural features off southwestern Taiwan. *Marine Geology* 137, p. 305-319.

Lu, C. Y., Hsu, K. J., 1992. Tectonic evolution of the Taiwan mountain belt. *Petroleum Geology of Taiwan* 27, p. 21-46.

Ma, K. F., Song, T. R. A., Lee, S. J., Wu, H. I., 2000. Spatial slip distribution of the Septmber 20, 1999, Chi-Chi, Taiwan, earthquake, Mw 7.6 - Inverted from teleseismic data. *Geophysical Research Letters* 27, p. 3417-3420.

Ma, K. F., Mori, J., Lee, S. J., Yu, S. B., 2001. Spatial and temporal distribution of slip for the 1999 Chi-Chi, Taiwan, earthquake. *Bulletin of the Seismological Society of America* 91, p. 1069-1087.

Ma, K. F., Tanaka, H., Song, S. R., Wang, C. Y., Hung, J. H., Tsai, Y. B., Mori, J., Song, Y. F., Yeh, E. C., Soh, W., Sone, H., Kuo, L. W., Wu, H. Y., 2006. Slip zone and energetics of a large earthquake from the Taiwan Chelungpu-fault Drilling Project. *Nature* 444, p. 473-476.

Mackenzie, D., Brune, J. N., 1972. Melting on fault planes during large earthquakes, *Geophysical Journal Royal Astronomical Society* 29, p. 65-78.

Martel, S. J., Boger, W. A., 1998. Geometry and mechanics of secondary fracturing around small three-dimensional faults in granitic rock. *Journal of Geophysical Research* 103, p. 21299-21314.

McGarr, A., Spottiswoode, S. M., Gay, N., 1979. Observations relevant to seismic driving stress, stress drop, and efficiency. *Journal of Geophysical Research* 84, p. 2251-2261.

McGrath, A.G., Davison, I., 1995. Damage zone geometry around fault tips. *Journal of Structural Geology* 17, p. 1011-1024.

Mishima, T., Hirono, T., Soh, W., Song, S. R., 2006. Thermal history estimation of the Taiwan Chelungpu fault using rock-magnetic methods. *Geophysical Research Letters* 33, L23311.

Mishima, T., Hirono, T., Nakamura, N., Tanikawa, W., Soh, W., Song, S. R., 2009. Changes to magnetic minerals caused by frictional heating during the 1999 Taiwan Chi-Chi earthquake. *Earth, Planets and Space Letter* 61, p. 797- 801.

Moore, D. M., Reynolds, Jr., R. C., 1997. Chapter 5: Individual Clay Minerals, *X-ray Diffraction and the Identification and Analysis of Clay Minerals,* Oxford University Press, New York.

Niemeijer, A., Di Toro, G., Griffith, W. A., Bistacchi, A., Smith, S. A.F., Nielsen, S., 2012. Inferring earthquake physics and chemistry using an integrated field and laboratory approach. *Journal of Structural Geology* 39, p. 2-36, doi:10.1016/j.jsg.2012.02.018.

Nutting, P. G., 1943. Some standard thermal dehydration curves of minerals, U. S. *Geological Survey*, Profess paper 197E, p. 197-216.

Otsuki, K., Hirono, T., Omori, M., Sagaguchi, M., Tanigawa, W., Lin, W., Soh, W., Song, S. R., 2009. Analyses of pseudotachylyte from Hole-B of Taiwan Chelungpu Fault Drilling Project (TCDP); their implications for seismic slip behaviors during the 1999 Chi-Chi earthquake. *Tectonophysics*, doi:10.1016/j.tecto.2009.01.008.

Pathier, E., Fruneau, B., Deffontaines, B., Angelier, J., Chang, C. P., Yu, S. B., Lee, C. T., 2003. Coseismic displacements of the footwall of the Chelungpu fault caused by the 1999, Taiwan, Chi-Chi earthquake from In SAR and GPS data. *Earth and Planetary Science Letters* 212, p. 73-88.

Pec, M., Stünitz, H., Heilbronner, R., 2012. Semi-brittle deformation of granitoid gouges in shear experiments at elevated pressures and temperatures. *Journal of Structural Geology* 38, p. 200-221.

Power, W., Tullis, T., 1989. The Relationship between slickenside surfaces in fine-grained quartz and the seismic cycle. *Journal of Structural Geology* 11(7), p. 879-893.

Reches, Z., Lockner, D. A., 2010. Fault weakening and earthquake instability by powder lubrication. *Nature* 467, p. 452-455, doi:10.1038/Nature09348.

Rice, J. R., 2006. Heating and weakening of faults during earthquake slip. *Journal of Geophysical Research* 111, B05311, doi:05310.01029/02005JB004006.

Scholz, C. H., 2002. *The Mechanics of Earthquakes and Faulting*. Cambridge University Press, Cambridge.

Sembira, A. N., Dunn, J. G., 1996. High temperature calibration of DTA and DSC apparatus using encapsulated samples. *Thermochimica* 274, p. 113-124.

Senkayi, A. L., Dixon, J. B., Hossner, L. R., 1981. Transformation of chlorite to smectite through regularly interstratified intermediates. *Soil Science Society of America Journal* 45, p. 650-656.

Sibson, R. H., 1973. Interaction between temperature and pore-fluid pressure during earthquake faulting-a mechanism for partial or total stress relief. *Nature Physical Sicence* 243, p. 66-68.

Sibson, R. H., 1985. Stopping of earthquake ruptures at dilational fault jogs. *Nature* 316, p. 248-251.

Sibson, R. H., 1996. Structural permeability of fluid-driven fault-fracture meshes. *Journal of Structural Geology* 18, p. 1031-1042.

Sibson, R. H., 2003. Thickness of the seismic slip zone. *Bulletin of the Seismological Society of America* 93(3), p. 1169-1178.

Smith, S.A.F., Billi, A., Di Toro, G., Spiess, R., 2011. Principal slip zones in limestone: microstructural characterization and implications for the Seismic Cycle (Tre Monti Fault, Central Apennines, Italy*). Pure and Applied Geophysics* 168, p. 2365-2393.

Smith, S. A. F., Di Toro, G., Kim, S., Ree, J.-H., Nielsen, S., Billi, A., Spiess, R., 2013, Coseismic recrystallization during shallow earthquake slip. *Geology* 41, p. 63-66, doi:10.1130/G33588.1.

Sone, H., Yeh, E. C., Nakaya, T., Hung, J. H., Ma, K. F., Wang, C. Y., Song, S. R., Shimamoto, T., 2007. Mesoscopic structural observations of cores from the Chelungpu fault system, Taiwan Chelungpu-fault Drilling Project Hole-A, Taiwan. *Terrestrial, Atmospheric and Oceanic Science* 18, p. 359-377.

Song, S. R., Kuo, L. W., Yeh, E. C., Wang, C. Y., Hung, J. H., Ma, K. F., 2007. Characteristics of the Lithology, Fault-related Rocks and Fault Zone Structures in the TCDP Hole-A. *Terrestrial, Atmospheric and Oceanic Science* 18, p. 243-269.

Spiel S., Berkelheimer, L. H., Pask, J. A., Davies, B., 1945. Differential thermal analysis-Its application to clays and other aluminous minerals. *Bulletin and Technical Papers of the United States Bureau of Mines*, p. 664.

Steinike, U., Tkácová, K., 2000. Mechanochemistry of solids-real structure and reactivity. *Journal of Materials Synthesis and Processing* 8 (3-4), p. 197-203.

Suppe, J., 1981. Mechanics of mountain building and metamorphism in Taiwan. *Memoir of Geological Society of China* 4, p. 67-89.

Tanaka, H., Wang, C. Y., Chen, W. M., Sakaguchi, A., Ujie, K., Ito, H., Ando, M., 2002. Initial science report of shallow drilling penetrating into the Chelungpu fault zone, Taiwan. *Terrestrial, Atmospheric and Oceanic Science* 13, p. 227-251.

Tanaka, H., Chen, W. M., Kawabata, K., Urata, N., 2007. Thermal properties across the Chelungpu fault zone and evaluations of positive thermal anomaly on the slip zones: Are these residuals of heat from faulting? *Geophysical Research Letters* 34, L01309, doi:10.1029/2006GL028153.

Temuujin, J., Okada, K., Mackenzie, K. J. D., Jadambaa, T., 1998. The effect of water vapor atmospheres on the thermal transformation of kaolinite investigated by XRD, FTIR and solid state MAS NMR. *Journal of the European Ceramic Society* 19, p. 105-112.

Teng, L. S., 1990. Geotectonic evolution of late Cenozoic arc-continent collision in Taiwan. *Tectonophysics* 183, p. 57-76.

Thatcher, W., Bonilla, M. G., 1989. Earthquake fault slip estimation from geologic, geodetic and seismologic observations: implications for earthquake mechanics and fault segmentation. *United States Geological Survey Open-File Report* 89-315, p. 386-399.

Tinti, E., Spudich, P., Cocco, M., 2005. Earthquake fracture energy inferred from kinematic rupture models on extended faults. *Journal of Geophysical Research* 110 (B12), B12303.

Tomita, K., Yamane, H., Kawano, M., 1993. Synthesis of smectite from volcanic glass at low temperature. *Clay and Clay Minerals* 41 (6), p. 655-661.

Traoré, K., Gridi-Bennadji, F., Blanchart, P., 2006. Significance of kinetic theories on the recrystallization of kaolinite. *Thermochimica Acta* 451, p. 99-104.

Venkataraman, A., Kanamori, H., 2004. Observational constraints on the fracture energy of subduction zone earthquakes. *Journal of Geophysical Research* 109, B05302.

Vermilye, J. M., Scholz, C. H., 1998. The process zone: a microstructural view of fault growth. *Journal of Geophysical Research* 103, p. 12223-12237.

Vermilye, J. M., Scholz, C. H., 1999. Fault propagation and segmentation: insight from the microstructural examination of a small fault. *Journal of Structural Geology* 21, p. 1623-1636.

Velde, B., Suzuki, T., Nicot, E., 1986. Pressure-temperature-composition of illite/smectite mixed-layer minerals: niger delta mudstones and other examples. *Clay and Clay Minerals* 34 (4), p. 435-441.

Vidal, O., Dubacq, B., 2009. Thermodynamic modelling of clay dehydration, stability and compositional evolution with temperature, pressure and H2O activity. *Geochimica et Cosmochimica Acta* 73, P. 6544-6564.

Vrolijk, P., and van der Pluijm, B. A., 1999. Clay Gouge. *Journal of Structural Geology* 21, p. 1039-1048.

Wang, C. Y., Chang, C. H., Yen, H. Y., 2000. An interpretation of the 1999 Chi-Chi earthquake in Taiwan based on the thin-skinned thrust model. *Terrestrial, Atmospheric and Oceanic Sciences* 11, p. 609-630.

Wang, C. Y., Li, C. L., Su, F. C., Leu, M. T., Wu, M. S., Lai, S. H., Chern, C. C., 2002. Structural mapping of the 1999 Chi-Chi earthquake fault, Taiwan by seismic reflection methods. *Terrestrial, Atmospheric and Oceanic Sciences* 13, p.211-226.

Wang, C. Y., Li, C. L., Lee, H. C., 2004. Constructing subsurface structures of the Chelungpu fault to investigate mechanisms leading to abnormally large ruptures during the 1999 Chi-Chi earthquake, Taiwan. *Geophysical Research Letters* 31, L02608.

Wilson, B., Dewers, T., Reches, Z., Brune, J., 2005. Particle size and energetics of gouge from earthquake rupture zone. *Nature* 434, p. 749-752.

Whitney, G., 1990. Role of water in the smectite-to-illite reaction. *Clays and Clay Minerals* 38:4, p. 343-350.

Wibberley, C. A. J., Shimamoto, T., 2003. Internal structure and permeability of major strike-slip fault zones: the Median Tectonic Line in Mie Prefecture, Southwest Japan. *Journal of Structural Geology* 25(1), p. 59-78.

Wibberley, C. A. J., T. Shimamoto, 2005. Earthquake slip weakening and asperities explained by thermal pressurization. *Nature* 436, p. 689-692.

Wibberley, C. A. J., Yielding, G., Di Toro, G., 2008. Recent advances in the understanding of fault zone internal structure: a review. In: Wibberley, C.A.J., Kurz, W., Imber, J., Holdsworth, R.E., Collettini, C. (Eds.), The Internal Structure of Fault Zones: Implications for Mechanical and Fluid-Flow Properties. *Geological Society of London*, Special Publication 299, p. 5-33.

Wintsch, R. P., Christofferson, R., Kronenberg, A. K., 1995. Fluid-rock reaction weakening of fault zones. *Journary of Geophysical Research* 100(B7), p. 13021-13032.

Wu, F. T., Rau, R. J., Salzerg, D., 1997. Taiwan orogeny: thin-skinned or lithospheric collision? *Tectonophysics* 247, p. 191-220.

Wu, H., Ma, K. F., Zoback, M., Boness, N., Ito, H., Hung, J., Hickman, S., 2007. Stress orientations of Taiwan Chelungpu-fault Drilling Project (TCDP) hole-A as observed from geophysical logs. *Geophysical Research Letters* 34, L01303. doi:10.1029/2006GL028050.

Yang, M., Rau, R. J., Yu, J. Y., Yu, T. T., 2000. Geodetically observed surface displacements of the 1999 Chi-Chi, Taiwan, earthquake. *Earth, Planets and Space* 52, p. 403-413.

Yeh, E. C., Sone, H., Nakaya, T., Ian, K. H., Song, S. R., Hung, J. H., Lin, W., Hirono, T., Wang, C. Y., Ma, K. F., Soh, W., Kinoshita, M., 2007. Core Description and Characteristics of Fault Zones from the Hole-A of the Taiwan Chelungpu-Fault Drilling Project. Terrestrial, *Atmospheric and Oceanic Science* 18, p. 327-357.

Yeskis, D., Koster van Groos, A. F., Guggenheim, S., 1985. The dehydroxylation of kaolinite. *American Mineralogist* 70, p. 159-164

Yu, S. B., Chen, H. Y., Kuo, L. C., 1997. Velocity field of GPS stations in the Taiwan area. *Tectonophysics* 274, p. 41-59.

Yu, S. B., Kuo, L. C., Hsu, Y. J., Su, H. H., Lui, C. C., Hou, C. S., Lee, J. F., Lai, T. C., Liu, C. C., Tseng, T. F., Tsai, C. S., Shin, T. C., 2001. Preseismic deformation and coseismic displacement associated with the 1999 Chi-Chi, Taiwan, earthquake. *Bulletin of the Seismological Society of America* 91, p. 995-1012.

Yue, L. F., Suppe, J., Hung, J. H., 2005. Structural geology of a classic thrust belt earthquake: the 1999 Chi-Chi earthquake Taiwan (Mw=7.6). *Journal of Structural Geology* 27, p. 2058-2083.

Yund, R. A., Blanpied, M. L., Tullis, T. E., Weeks, J. D., 1990. Amorphous material in high strain experimental fault gouges. *Journal of Geophysical Research* 95 (B10), p. 15589-15602.

Zoback, M., Hickman, S., Ellsworth, W., 2010. *Scientific drilling into the San Andreas fault zone: Eos* (Transactions, American Geophysical Union) 91, p. 197-199, doi:10.1029/2010EO220001.

In: Clays and Clay Minerals
Editor: Liam R. Wesley
ISBN: 978-1-63117-779-8

Chapter 13

CHARACTERIZATION OF PARAMAGNETIC CENTRES IN CLAY MINERALS AND FREE RADICAL SURFACE REACTIONS BY EPR SPECTROSCOPY

Niramon Worasith[1], Sumalee Ninlaphurk[2], Harinate Mungpayaban[2], Deng Wen[3] and Bernard A. Goodman[4*]

[1] Department of Chemistry, Rajamangala University of Technology Krungthep, Soi Suan Plu, Sathorn, Bangkok, Thailand
[2]Office of Atoms for Peace, Bangkok, Thailand
[3]Department of Physics, Guangxi University, Nanning, Guangxi, China
[4]State Key Laboratory for Conservation and Utilization of Subtropical Agro-Bioresources, Guangxi University, Nanning, Guangxi, China

ABSTRACT

Free radicals and other paramagnetic centres are a common occurrence in mineral species. Paramagnetic metal ions may be incorporated into mineral structures during or after formation, whereas free radical centres are mainly generated by natural radiation, although they can also be the consequence of chemical and physical processes during and after mineral formation. This chapter reviews the types of paramagnetic centre that have been observed in clay minerals and their characterization by electron paramagnetic resonance (EPR) spectroscopy, with special attention being given to natural kaolin samples, which illustrate the diversity of these minerals from different parts of the World. In addition, clay minerals contain reactive surfaces, and have important function in controlling the mobility and stability of ions and molecules in environmental situations, as well as having potential uses as catalysts. Examples are also presented of potentially useful free radical reactions that are catalyzed by clay mineral surfaces.

Keywords: Radiation damage, kaolin, smectite, iron, manganese, vanadium

* E-mail address: bernard_a_goodman@yahoo.com.

INTRODUCTION

Silicate minerals represent ~90% of the Earth's crust, and can be divided into four main groups based on the structures of the silicate building blocks (e.g., Deer et al., 1992). Briefly, the orthosilicates are made up of $[SiO_4]^{4-}$ tetrahedra connected by interstitial cations (e.g., olivines and garnets), $(Si_2O_7)^{6-}$ double tetrahedral (e.g., epidote), or rings of $(Si_3O_9)^{6-}$ or $(Si_6O_{18})^{12-}$. Chain silicates consist of interlocking chains of either SiO_3 for single chains (e.g., pyroxenes), or Si_4O_{11}, for double chains (e.g., amphiboles). The phyllosilicates, or sheet silicates, contain sheets of silicate tetrahedra with a Si_2O_5 composition. Finally, the framework silicates are made up of 3-dimensional frameworks with a composition of SiO_2, the most important examples being quartz, feldspar and zeolites.

Clays may be simply defined as fine-grained mineral particles with sizes in the micrometre range that are formed by the weathering of primary minerals and low temperature hydrothermal alteration. Six main groups of aluminosilicate clay minerals were described by Newman and Brown (1987), namely (i) kaolinite-serpentine group, (ii) pyrophyllite-talc group, (iii) micas, (iv) chlorites, (5) smectites and vermiculites, (vi) fibrous palygorskite and sepiolite. In addition, although both Fe and Al readily form clay-sized oxide or oxyhydroxide particles in soils, and can have an appreciable influence on soil chemistry, this chapter will focus exclusively on free radicals that are observed in aluminosilicate minerals or are formed during clay mineral reactions. The compositions of clay minerals reflect those of their parent materials and the geological fluids with which they have had contact. Natural samples commonly experience extensive isomorphous substitutions with variable amounts of cations, such as Fe^{3+}, Fe^{2+}, Mg^{2+}, Ca^{2+}, Na^{+}, and K^{+}, and there is considerable diversity in the compositions of many clay minerals that nominally bear the same name. Furthermore crystal defects resulting from isomorphous substitutions can function as sites for the formation and stabilization of free radical centres that are the subject of this review. Also, because of the influence of interactions between neighbouring paramagnetic centres on the resolution of the EPR technique, examples presented in this chapter are largely concerned with samples containing relatively low concentrations of iron and other transition metals.

ELECTRON PARAMAGNETIC RESONANCE (EPR) SPECTROSCOPY

EPR spectroscopy and associated double resonance techniques represent the principal methods for characterizing free radicals and other paramagnetic components in solid matrices, such as clay minerals. It is a versatile and sensitive technique based on the observation of transitions between the spin states of unpaired electrons, whose energies are different in the presence of a magnetic field. These energies are typically in the microwave region of the electromagnetic spectrum, and an EPR spectrum is usually obtained by measuring the absorption of microwaves of a fixed energy whilst the magnetic field is varied. The equation for the EPR transition is

$$h\nu = g\beta_e B_0$$

where ν is the electromagnetic radiation frequency, B_0 is the magnetic field, h is Planck's constant (6.626×10^{-34} J.s), β_e is the Bohr magneton (9.274×10^{-24} $J.T^{-1}$), and *g* is a constant characteristic of the paramagnetic species and equal to 2.0023 for an isolated electron. The magnitude of *g* can vary with the orientation of the molecular orbital containing the unpaired electron relative to the direction of the applied magnetic field, and the results from a single crystal are characterized by three values g_x, g_y and g_z, which correspond to the orientation of the principal axes of the paramagnetic species in the direction of the magnetic field. In fluid solutions, where molecules are tumbling rapidly, an average g-value ($g_{iso} = (g_x + g_y + g_z)/3$) is observed. However, in powder or polycrystalline samples (which are typical of the specimens that are relevant for many environmental problems) an EPR spectrum consists of the sum of all orientations weighted according to their probabilities. Representative spectra are illustrated in Figure 1. When the paramagnetic species has axial symmetry, $g_z = g_{//}$ and g_x, $g_y = g_{\perp}$.

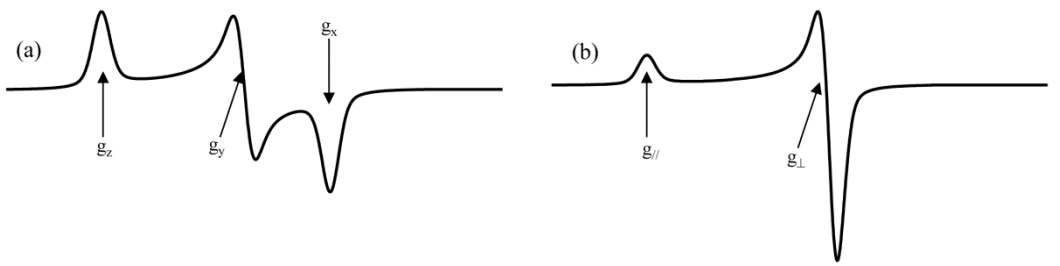

Figure 1. Representative EPR spectra for powder samples (a) general case, and (b) for axial symmetry.

If the unpaired electron is able to interact with a nucleus with spin, $I \neq 0$, the energy levels are split into 2I + 1 components, and the selection rules for the allowed transitions are $\Delta m_S = 1$, $\Delta m_I = 0$. The resulting structure in a spectrum is known as hyperfine structure (hfs), and its magnitude is related to the unpaired electron density at that nucleus; hence it provides information on the delocalisation of the orbital containing the unpaired electron. Furthermore, hfs patterns when they are resolved can provide evidence for the identification of specific free radical species. A typical spectrum for a $^{51}V^{4+}$ ion (I = 7/2) with axial symmetry is illustrated in Figure 2. It should be noted that with the separations between hf peaks are not identical.

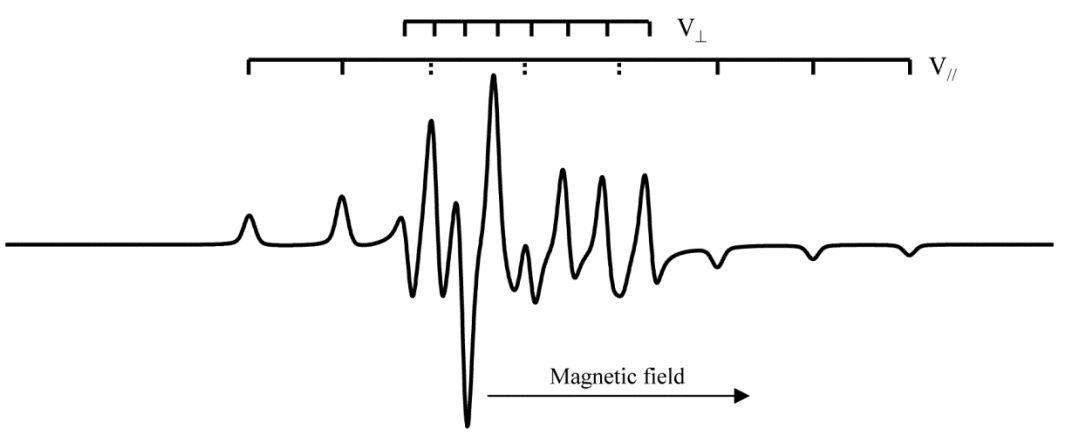

Figure 2. Typical EPR spectrum for a V^{4+} ion in which $g_{//} < g_{\perp}$.

The g-value and hfs patterns provide useful "fingerprints" for the presence of certain nuclei, especially ^{51}V, ^{55}Mn and $^{63,65}Cu$, which have values for I of 7/2, 5/2 and 3/2, respectively. In general, EPR spectroscopy is amenable to the study of paramagnetic chemical species, containing an odd number of unpaired electrons, but those with an even number of unpaired electrons may be more difficult to observe. Electron spin – electron spin interactions produce a splitting of the electron energy levels in the absence of a magnetic field, as illustrated in Figure 3 for the principal component for the triplet state lower (Figure 3a,c) or higher (Figure 3b,d) than the singlet state, where D is the zero field splitting. If D is large, the only transition that may be observable in an EPR spectrum is the "forbidden" one with $\Delta M_S = 2$ (Figure 3c,d).

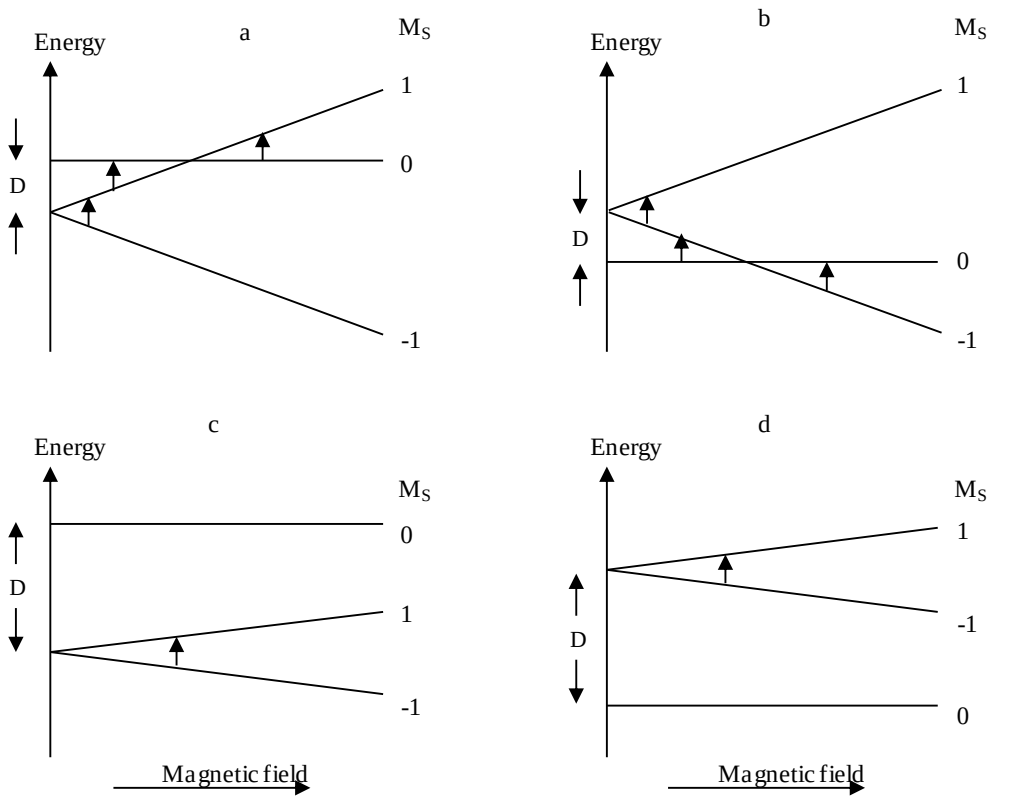

Figure 3. Location of the EPR transitions indicated by arrows for an S = 1 ion with the principal axis aligned parallel to the magnetic field.

MECHANISMS FOR THE FORMATION OF FREE RADICALS AND THEIR STABILIZATION IN MINERALS

(a) Ionizing Radiation

Ionizing radiation is able to eject an electron from an atom in a crystal lattice leaving a positively charged entity (also known as an electron hole). As illustrated in Figure 4, the

ejected electron can either recombine with the electron hole centre, or travel through the structure until it is trapped at another position, such as the site of an impurity, or it migrates to the surface where it can react with external species.

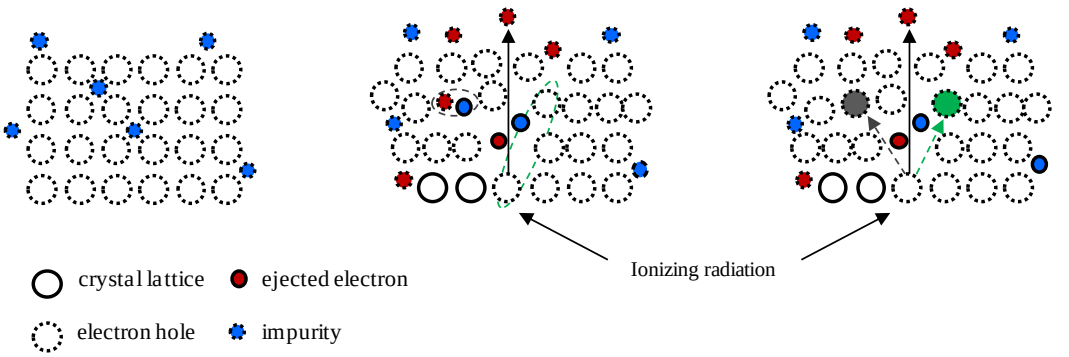

Figure 4. Illustration of the effects of radiation damage in a mineral structure.

(b) Physical Damage

Physical damage through the application of pressure and/or heat results in the breaking of chemical bonds, and depending on the fragmentation mechanism this can result in the formation of free radicals. Physical damage which leads to increased electron mobility can also lead to the destruction of free radical centres in mineral structures.

(c) Stabilization of Free Radicals at Chemical Defects

There are various mechanisms through which paramagnetic centres may be stabilized in minerals. For example, an electron hole can be stabilized by the loss of a proton from an adjacent oxygen atom, whilst the ejected electron can be captured by a transition metal impurity, such as Fe, with a reduction in the oxidation state from Fe^{3+} to Fe^{2+}, or accompanied by protonation when trapped at a surface oxygen atom.

FREE RADICAL CENTRES IN ROCK-FORMING MINERALS

Although the various rock-forming minerals do not form part of this book, physical breakdown may lead to their structures being present as “impurities” in natural clay samples. Therefore, in any consideration of free radical centres in natural clay mineral samples, it is important to be able to identify any that might be derived from small quantities of the major rock-forming minerals, especially since EPR is a sensitive technique for the detection of paramagnetic species with narrow linewidths and little anisotropy.

(a) Quartz

EPR spectra of free radical centres in quartz are well known and were first described in the 1950s by Griffiths et al. (1954) and Weeks (1956), who reported their generation as a result of neutron irradiation. Now > 50 different paramagnetic centres have been observed in quartz samples from various origins with the spectral properties determined by the chemical nature of impurity ions that are present in the quartz structure. There have been hundreds of publications on their characterization by EPR spectroscopy; the comprehensive reviews by Weil (1984, 1993) provide an excellent source of information on the early work on paramagnetic defects in crystalline quartz, and these should be consulted for more information. Many different electron hole centres on oxygen atoms associated with various impurity ions (A1, H, Cu, Ag, Ge, P, Ti, Fe) were described in addition to defects associated with oxygen vacancies in the quartz structure. More recently, Götze et al. (2004, 2005) reported that the defect structure and trace-element composition of pegmatite quartz samples are different from those of quartz samples of hydrothermal, igneous and metamorphic origins, and their EPR measurements showed an almost complete absence of lattice defects associated with O or Si vacancies. Some trace elements (Al, Ti, Ge,) can occupy substitutional sites in the quartz lattice, whilst others (Li, Na, K) occupy interstitial positions, and EPR results suggest that electron irradiation possibly results in a redistribution of alkali ions, with diamagnetic $[AlO_4/M^+]^0$ centres being converted into paramagnetic $[AlO_4]^0$ centres, whilst the M^+ may be captured by $[TiO_4]^0$ or $[GeO_4]^0$ to form paramagnetic centers ($[TiO_4/Li^+]^0$ or $[GeO_4/Li^+]^0$).

(b) Feldspars

Feldspars are very common primary minerals and natural samples invariably contain stable free radical centres formed as a result of exposure to natural radiation. These have been the subjects of several EPR investigations. The most common radical seen in feldspars is an electron hole center on an oxygen atom adjacent to two aluminum atoms (Speit & Lehmann, 1982). The principal values for the *g*-tensor are not identical for different specimens and are thus influenced by subtle details of the mineral composition and/or structure. However, the principal values are approximately 2.004, 2.008, and 2.03, and Speit & Lehmann (1982) reported that the ^{27}Al hfs was largely isotropic with a value of ~25MHz (~0.9 mT). Irradiation of feldspars at 77K, and recording their EPR spectra without warming, showed electron hole centres on oxygen atoms adjacent to only one Al, which transformed to the more common electron hole centre with two Al atoms in adjacent sites on annealing at room temperature. A similar conversion of an electron hole centre adjacent to a single Al to one adjacent to two Al on warming from 77K to room temperature was reported by Hashimoto et al. (2004) who also observed near linear responses for doses up to several hundred Gy, although saturation behavior was observed for doses >1 kGy. Other radiation defects associated with Ti^{3+} and electron holes on oxygen ions adjacent to a small divalent ion on a tetrahedral site with Si and in some cases also Pb as further neighbors were reported by Speit & Lehmann (1982).

The work of Petrov (1994) on single crystals of feldspars with varying degrees of Al-Si order and from different petrogenetic areas represents an excellent summary of the

complexity of the free radical chemistry of these minerals. Five separate electron hole centres on oxygen atoms associated with two neighbouring Al atoms were identified, and in albite one additional centre was observed with two adjacent quasi-equidistant Na atoms. The presence of large cations such as K or Ba, was found to influence the relative amounts of the different electron hole centres, independent of the degree of long range Al-Si order in the structure.

In addition to paramagnetic centres associated with electron holes on oxygen, EPR spectra of lattice-stabilized CH_3, C_2H_5, and NO_2 free radicals were also observed by Petrov (1994) in pegmatitic microcline and hyalophane. These spectra are similar to those reported by Matyash et al. (1982) for microcline from pegmatites and granites, although in that work the hydrocarbon radicals were interpreted as HN_3^+, and the NO_2 radical as N^{2-}.

The EPR spectrum of irradiated microcline (potassium feldspar, $KA1Si_3O_8$), consists of an asymmetric six-line pattern centred on g = 2.024 from $[SiO_4/K^+]^{2+}$ and a peak at g_{eff} = 2.009, which corresponds to an electron hole shared between two nonbonding oxygens on Si (Hofmeister & Rossman, 1985). Samples with structurally bound water produced signals with lower intensity, a result which Hofmeister & Rossman (1985) explained in terms of hydrogen atom formation as a result of water fragmentation, and its subsequent destruction of the normal radiation-induced centres. When samples were irradiated and maintained at low temperature, EPR spectra showed the presence of $H^{\cdot}$ atoms (Hashimoto et al., 2004), thus providing support for the mechanism proposed by Hofmeister and Rossman.

(c) Chain Silicates

In single chain silicates each SiO_4 shares two oxygens with two adjacent tetrahedrons, and result in the formation of long chains. In double chain silicates adjacent tetrahedrons share either two oxygens to continue the chain, or three oxygen atoms to connect also to a second chain, giving rise to parallel double chains. Metal ions link the chains to each other, and the linking of chains with one another results in the formation of fibrous crystals.

There are relatively few reports of EPR spectra of chain silicates, although single-crystal investigations of prehnite revealed at least six paramagnetic defects, three involving Fe^{3+} one V^{4+}, one Mn^{2+}, and an electron hole centre on an oxygen atom associated with an aluminum ($Al\text{-}O^-$) (Pan et al., 2009; Mao et al., 2010b). Spectral parameters indicated that the Fe and V atoms were all located in octahedral sites, whereas the $Al\text{-}O^-$ centre was interpreted as corresponding to the loss of a hydrogen atom from an apical hydroxyl oxygen coordinated to an octahedral Al^{3+} ion.

(d) Other Minerals

EPR spectra of limestone and dolomite minerals at room temperature exhibit a sextet hyperfine pattern characteristic of Mn^{2+} (Gunasekaran & Anbalagan, 2008). In limestone, the spectral parameters were characteristic of Mn^{2+} in calcite which was present as an impurity phase, whereas in dolomite separate components were observed corresponding to Mn^{2+} substituted in the Ca and Mg lattice sites.

Irradiated zircon ($ZrSiO_4$) has an anisotropic EPR spectrum with g_{xx}= 2.0168, g_{yy} = 2.0076 and g_{zz} = 2.0033 and corresponds to a electron hole-centre associated with Y^{3+} substituted at Zr^{4+} sites (Abdel-Monem et al., 2010). The intensity of the peak with g = 2.0033 is proportional to the radiation dose, and is suitable for use in dosimetry and dating of natural zircons.

PARAMAGNETIC CENTRES IN LAYER SILICATES

The layer silicates are classed according to the arrangements of the tetrahedral silicate and octahedral hydroxide sheets from which they are built. Thus a 1:1 mineral consists of layers containing one tetrahedral and one octahedral sheet, whereas a layer of a 2:1 mineral contains an octahedral sheet sandwiched between two tetrahedral sheets. In addition, the cation sites in the octahedral sheet may be filled with divalent ions, or 2/3 filled with trivalent ions, and the resulting minerals are known as trioctahedral or dioctahedral, respectively. The principal dioctahedral 1:1 minerals are those of the kaolin group kaolinite, dickite, halloysite, and nacrite (polymorphs of $Al_2Si_2O_5(OH)_4$), whereas the trioctahedral analogues belong to the serpentine group ($Mg_3Si_2O_5(OH)_4$) (Bailey, 1980). The layers are held together primarily by hydrogen bonding and the minerals have little cation exchange capacity (CEC). The smectite group consists of 2:1 aluminosilicates that are readily able to expand by incorporation of water and cations between layers; examples of dioctahedral minerals include montmorillonite and nontronite, whereas saponite and hectorite are examples of a trioctahedral smectites. In these minerals adjacent layers are held together by cations in the interlayer regions, and they can have appreciable CEC. Other 2:1 layer silicates include illite, sepiolite, attapulgite and micas. whereas chlorite is best described as a 2:1:1 layer silicate in which brucite-like sheets are formed between layers of a smectite; these all have considerable variability in their chemical compositions. Furthermore, mixed layer clay variations are quite common, and the ordering of layers may be regular or random.

Early research on the applications of EPR spectroscopy to the characterization of paramagnetic species in clay minerals was reviewed by Hall (1980a,b) and Goodman & Hall (1994). These papers described both transition metal and free radical species. More recently Allard et al. (2012) presented an up-to-date summary of radiation-induced defects in kaolinite, dickite, montmorillonite, illite and sudoite, which included their characterization, stability and consequences for subsequent reaction of the clay minerals. As with the rock-forming minerals described above, many radiation-induced defects in clay minerals are electron holes located on oxygen atoms. However, because of the small particle sizes of clay minerals, detailed characterization is more difficult, and only a few publications have been able to describe the orientation of radical defect centres within the aluminosilicate structures. Furthermore, natural clay specimens often contain additional mineral phases or occlusions, which complicate the interpretation of EPR spectroscopic results.

(a) Kaolin Group Minerals

The kaolin group minerals consist of kaolinite, dickite, and nacrite, which are distinguished by the ordering of the component layers, along with halloysite, which in addition has varying amounts of H_2O between layers. Although diverse EPR spectra have been reported for kaolin samples of different origins, they can all be subdivided into three regions: low field signals, transition metal signals centred on g ~ 2.0, and free radical signals. Spectra usually contain a single weak feature with g ~ 9 and a triplet centred on g = 4.27, although there are considerable differences in the resolution and relative intensities of the individual peaks. These signals all arise from isolated Fe^{3+} ions, and were described originally for kaolinites by Jones et al. (1974) and Meads & Malden (1975). The separate features are related to structural order within the specimen (Mestagh et al., 1980; Brindley et al., 1986; Delineau et al., 1994; Gaite et al., 1997), and do not correspond to Fe^{3+} in inequivalent octahedral sites in the kaolin mineral structures, which can be distinguished by a splitting of the peaks around g = 5.0 and 3.5 in well-crystalline kaolinites (Gaite et al., 1993; Balan et al., 1999; Lombardi et al., 2002). Kaolin samples usually contain a broad signal with g ~ 2.0 from paramagnetic ions that are sufficiently close to one another to experience dipolar interactions with unpaired electrons on their neighbours. If there is a range of distances separating such ions, broad featureless EPR spectra are produced, and the most common origin for such a signal is poorly crystalline iron oxides (e.g., Herbillon et al., 1976; Goodman & Hall, 1994), small amounts of which are commonly associated with clay minerals (e.g., Angel & Vincent, 1978; Fysh et al., 1983; Malengreau et al., 1994). Other transition metal signals that have been reported for natural kaolin samples arise from V^{4+}, Cu^{2+}, and Mn^{2+} or Mn^{4+} ions, which have one, nine, five, and three 3*d* electrons, respectively. These ions also normally produce hyperfine structure (hfs) resulting from interaction of the unpaired electron(s) with the ^{51}V (I = 7/2), $^{63,65}Cu$ (I=3/2), and ^{55}Mn (I = 5/2) nuclei, and such hfs patterns consist of eight, four and six peaks, respectively. In addition, the signals from V^{4+} and Cu^{2+} are anisotropic as a result of these ions containing a single unpaired 3*d* electron, whereas Mn^{2+} and Mn^{4+} signals are frequently isotropic.

There are several reports of kaolin samples with a strong anisotropic signal from V^{4+}, although there are differences in the magnitudes of the spectral parameters (McBride, 1990; Gehring et al., 1993; Mosser et al., 1996; Worasith & Goodman, 2012). These differences are too large to be the result of interpretational or measurement errors, and indicate some variability in the V environment in different samples. Indeed, Worasith & Goodman (2012) actually observed appreciable differences in the ^{51}V hyperfine coupling constants in different size fractions from a sample of a Georgia kaolin. Sextet isotropic signals from ^{55}Mn have also been reported for some kaolin specimens, and have been interpreted as arising from Mn^{2+} either adsorbed on the mineral surface (e.g., McBride et al., 1975; Muller & Calas, 1993) or in impurity phases (e.g., Sengupta et al., 2006), or Mn^{4+} substituting isomorphously for Si in tetrahedral sites (Worasith et al., 2011, Worasith & Goodman, 2012). In addition, Worasith & Goodman (2012) reported the presence in several samples of a peak with g ~ 2.07, which is consistent with the $g_\perp$ region of a Cu^{2+} resonance (e.g., Goodman & Raynor, 1970).

A total of eight different free radical signals have been reported in kaolin samples, and these vary with their sources. The most common signal, which is anisotropic with $g_{//}$ = 2.050 and $g_\perp$ = 2.008, is generally referred to as the A-centre (Figure 5a), and a similar signal with

lower anisotropy ($g_{//} = 2.040$) referred to as the A' centre is also sometimes observed; both the A and A' centres correspond to electron holes.

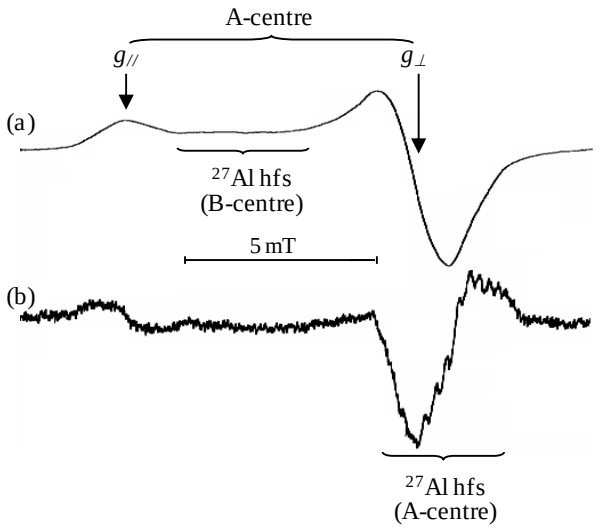

Figure 5. EPR spectra of the A-centre in kaolinite (a) 1st derivative, and (b) 2nd derivative recordings (from Worasith & Goodman 2012).

In work with oriented kaolinite samples, Lombardi et al. (2002) showed that the principal axis of the A-centre is perpendicular to the sheet, whereas the A' centre has its principal axis in the plane of the sheet. This latter centre was, therefore, considered to be associated with surface oxygen atoms on the tetrahedral sheet, whereas the A-centre was assigned to defects on the oxygen atoms linking the octahedral and tetrahedral sheets.

Under 2nd harmonic recording weak ^{27}Al hfs was observed on the $g_{\perp}$ feature of the A-centre by Worasith & Goodman (2012); up to 11 peaks were resolved with a separation of ~0.23 mT which is much smaller than the ^{27}Al hyperfine coupling constants for the B- or C-centres (see below), or that observed in feldspars (see above). The observation of this ^{27}Al hfs supports the assignment of the A-centre to oxygen atoms linking the octahedral and tetrahedral sheets. Furthermore, Cuttler (1980, 1981) provided strong evidence for the association of this free radical signal with defects at the boundaries of clusters of trioctahedral cells in the normal dioctahedral structure, so it is possible that the ^{27}Al hfs could arise as a result of some Al-for-Si substitution in the tetrahedral sheet.

The B-centre radical (Figure 6a) contains ^{27}Al hfs arising from two aluminium atoms with separations in the range 0.71-0.84 mT (Meads & Malden, 1975; Clozel et al., 1994, 1995; Worasith et al., 2011). This is similar to the ^{27}Al hfs observed in feldspars (see above) and is assigned to an electron hole on an oxygen atom coordinated to two Al atoms. It should be noted that although the magnitude of the ^{27}Al hyperfine coupling is > 3 times that observed with the A-centre, it still corresponds to only a small fraction of the unpaired electron density, which is located largely on the oxygen (Worasith & Goodman, 2012). Although the presence of ^{27}Al hfs demonstrates that the B-centre is associated with two aluminium atoms, there is no firm evidence to distinguish between a location on the surface of the octahedral sheet or the oxygen atoms which bridge the octahedral and tetrahedral sheets.

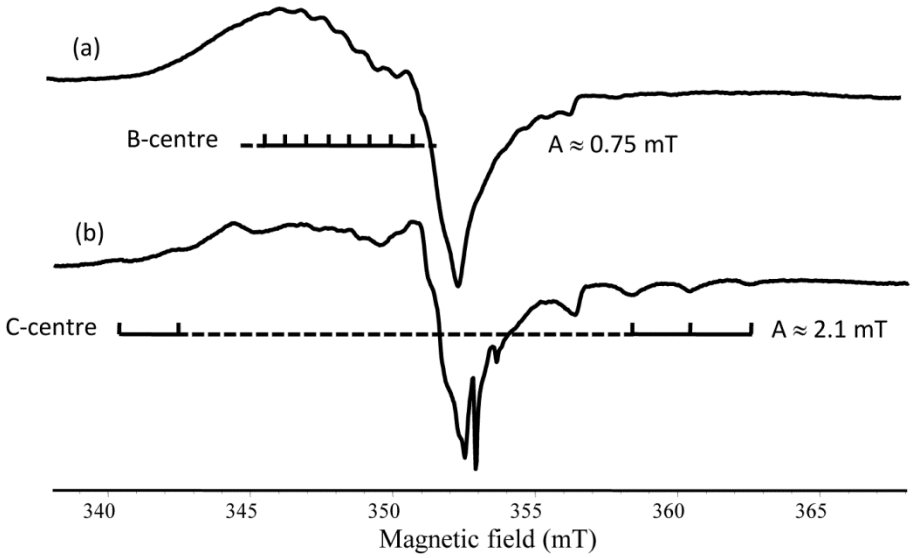

Figure 6. EPR spectra of irradiated kaolins showing the signals from (a) the B-centre and (b) the C-centre (adapted from Worasith et al., 2013).

Worasith et al. (2011) found an improvement in the resolution of the ^{27}Al hfs after extraction with sulphuric acid, and suggested that this radical centre might be associated (at least partially) with a surface O atom on the octahedral sheet, since the most likely effect of the acid treatments is removal of surface-adsorbed species. However, the absence of any ^{1}H hyperfine structure indicates that this oxygen is not protonated, and hence favors a location on bridging oxygen atoms, since defect centres associated with hydrogen atoms produce large ^{1}H hfs (see below). It may be significant that the B-centre is most clearly observed with specimens in which the low field Fe^{3+} signal indicates a high degree of structural order. The B-centre appears to be less stable than the A-centre; Worasith & Goodman (2012) reported it is more sensitive than the A-centre to physical treatment, although both were destroyed by prolonged grinding, and Worasith et al. (2013) observed that the B-centre was the major paramagnetic species formed by γ-irradiation of an halloysite-rich kaolin, even though the A-centre was the major free radical in the unirradiated specimen.

An additional radical centre, referred to as the C-centre (Figure 6b), with several peaks having separations of ~2.1 mT to the low and high field sides of the A- and B-centres has been reported recently by Worasith et al. (2013) for γ-irradiated kaolin samples. These probably correspond to extensive hfs from ^{27}Al with the central region being obscured by resonances from the A- and B-centres. Although the observed peaks of the C-centre are consistent with an 11-peak hyperfine structure corresponding to two equivalent ^{27}Al atoms, this assignment cannot be made with any certainty. However, the much larger hfs than observed with the B-centre indicates that the C-centre has a correspondingly greater unpaired electron density on its Al atoms, and its absence from natural samples indicates that it is less stable than either the A- or B-centres.

Because of the presence of ^{27}Al hfs, both the B- and C-centre radicals are likely to be located on O atoms that are coordinated to Al atoms in the octahedral sheet, and it is plausible that they correspond to defect centres located on bridging and surface oxygen atoms, respectively. Surface radicals might be expected to be less stable than those associated with O

atoms bridging the octahedral and tetrahedral sheets, because of the possibility of direct interaction with O_2 and other paramagnetic species in the environment. It is also unclear why the relative levels of production of these two centres by γ-irradiation should be different for different kaolin mineral samples, although it seems likely that external components, such as H_2O in halloysite are responsible.

Finally, Worasith & Goodman (2012) reported four additional free radical centres for a kaolin of hydrothermal origin. Each of these centres (designated I-IV) contained substantial ^{1}H hfs (Fig 7), and in Centre IV the large hfc constant of 2.45 mT from four equivalent ^{1}H atoms accounts for almost 20% of the unpaired electron density (Note the ^{1}H hfc constant for a hydrogen atom, H^-, is ~50.7 mT (Jen et al., 1958; Bader & Gesser, 1972). The line widths were also quite small, indicating an absence of unresolved hfs from ^{27}Al, and Worasith & Goodman (2012) suggested that all four radical signals probably correspond to radical centres associated with protonated oxygen atoms associated with surface or edge sites of the tetrahedral sheet. They suggested that in centres I and II the unpaired electron is associated with two Si-OH groups with additional interactions with one and two remote ^{1}H atoms, respectively. In Centre III, the single ^{1}H hfc constant suggested that the unpaired electron interacts with a single Si-OH group, whilst the four equivalent ^{1}H hfc constants in Centre IV suggested a Si hole around which the O atoms are protonated to maintain charge balance. However, there is little collaborative evidence to support these assignments. It is also interesting that peaks corresponding to the A-centre were not observed in these spectra, which could, therefore, originate from unidentified impurities in the kaolin deposits.

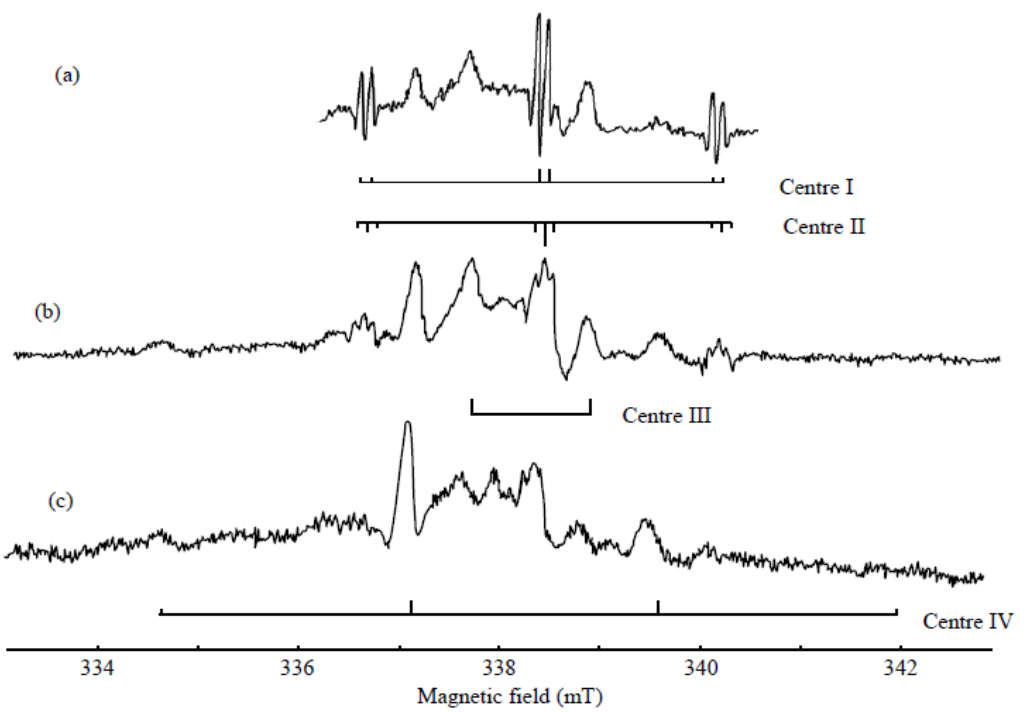

Figure 7. EPR spectra from various size fractions from a kaolin of hydrothermal origin showing the signals from Centres I – IV (from Worasith & Goodman, 2012).

(b) Serpentines

The EPR spectra of the serpentine mineral chrysotile show signals from Fe^{3+} and Mn^{2+} (Anbalagan et al., 2008; Sengupta et al., 2010). These results were interpreted in terms of Fe^{3+} in both tetrahedral and octahedral sites and Mn^{2+} solely in octahedral sites. To the best of our knowledge, there are no reports of natural free radicals in serpentine minerals, although there have been several investigations of the generation of free radical species on their surfaces (see Worasith et al., 2014a).

(c) Illites

Unambiguous identification of natural radiation-induced defects in illites was made by Morichon et al. (2008), as a result of the saturation behaviour of their EPR spectra being different from similar centres in other clays, such as kaolinite, dickite or smectite. However, saturation properties are strongly influenced by the concentrations and distributions of paramagnetic ions in mineral structures, so caution should be exercised in their general use to distinguish different types of structure. At least two, and possibly more, different electron hole defects were revealed in Q-band spectra by Morichon et al. (2008). The major centre, had an anisotropic signal with $g_{//}$ = 2.032 and $g_{\perp}$= 1.993, and by using an oriented specimen the $g_{//}$ component was shown to be perpendicular to the (ab) plane of the illite. This centre has similar EPR parameters to the A-centre in kaolinite and dickite (see below), and the absence of hyperfine structure indicates that it likely associated with Si. Furthermore, the formation of stable free radical centres suggests that illites could have a role as geological dosimeters.

(d) Smectites

Generally, smectites do not contain stable free radical defect centres, possibly because the presence of interlayer water produces H atoms which react with and destroy radiation-induced centres in the aluminosilicate structure by a mechanism similar to that described by Hofmeister & Rossman (1985) for feldspars with bound water. However, there are reports of defect centres being formed as a result of exposure to γ-irradiation (e.g., Gournis et al., 2001), and these were accompanied by migration of small interlayer cations (such as Li^{+}) into structural sites. More detailed information on free radical centres in montmorillonites has been presented by Sorieul et al. (2005), who observed two natural centres both of which are consistent with electron holes on oxygen atoms. The major centre with an orthorhombic spectrum with g_x = 2.004 ± 0.005 g_y = 2.010 ± 0.003, g_z = 2.065 ± 0.002 resembled that of the A-centre in kaolinite, but with a higher degree of anisotropy, whilst a minor centre was isotropic with g = 2.019 ± 0.005. Both defect centres were annealed at 500 °C, and the half-life of the major centre was estimated to be approximately 3,000 years. In addition, β-irradiation produced two additional radical centers of lower stability and distinct EPR parameters which could potentially be used for dosimetry for large dose ranges.

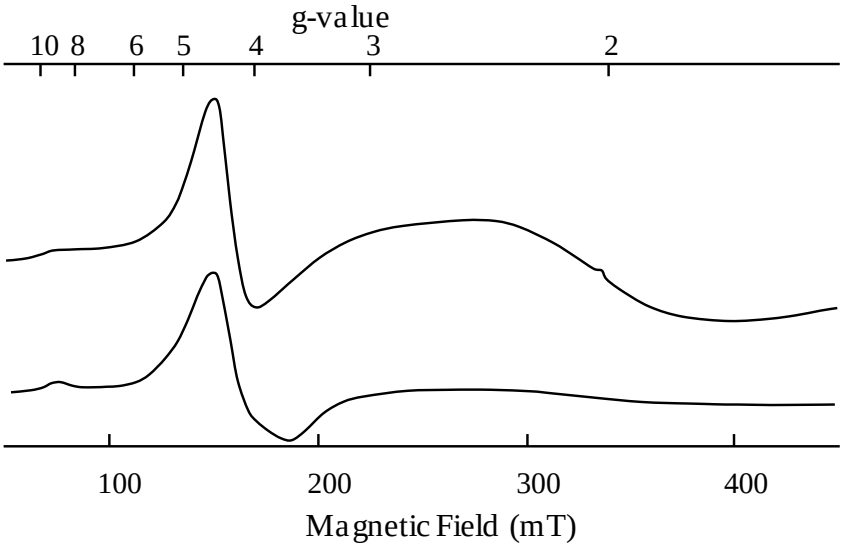

Figure 8. EPR spectra of two bentonite samples illustrated the different relative amounts of the signals from magnetically dilute Fe3+ (around g = 4.3) and Fe-rich phases which produce a broad signal centred on g = 2.0.

Smectites normally contain some structural iron and often other paramagnetic metal ions are present in minor amounts. Their characterization is important because the redox properties of such ions can have appreciable effects on both physical and chemical properties of these minerals. EPR spectroscopy can usually only make valuable contributions to the characterization of such samples if their Fe content is low; at higher Fe concentrations, exchange or dipolar interactions between neighbouring Fe^{3+} or Fe^{2+} ions results in broad lines which dominate the spectral intensity. It is, therefore, a useful method for determining compositional heterogeneity in mineral specimens with low iron content, as illustrated in Figure 8, which shows the EPR signals from bentonite samples containing magnetically dilute paramagnetic ions centred around g = 4.3 and low concentrations of iron-rich components as a broad peak centred on g = 2.0 (Goodman et al., 1988).

Ions other than Fe^{3+} can also be identified when the major isotope has non-zero spin. The presence of Mn^{2+} (I=5/2) has been seen in the EPR spectra of many clay mineral samples, and the spectral parameters are able to discriminate between the presence of the ion in structural sites, as seen in for example in montmorillonite (McBride, 1995) and talc (Schlossleder et al., 1998), or adsorbed on mineral surfaces (McBride et al., 1975; Flogeac et al., 2005). Furthermore, Worasith et al. (2011) have suggested that Mn^{4+} might substitute isomorphously for Si in some kaolin samples. The presence of V^{4+} (I=7/2) is also readily identified by EPR and the spectra allow discrimination between occupancy of structural sites, as seen for example with some kaolinites (Gehring et al., (1993); Mosser et al., (1996); Worasith & Goodman, 2012) or rectorite **(**Goodman & Nadeau, 1990), and surface adsorbed species (e.g., Pinnavaia et al., 1974; McBride, 1979). Similarly, Cu^{2+} can be identified in structural sites (in for example synthetic kaolinite, Petit et al., 1995), adsorbed Cu^{2+} ions on (e.g., montmorillonite, Clementz et al., 1974, He et al., 2001; kaolinite, Hyun et al., 2005; pillared clay, Braddell, 1987), or Cu^{2+} complexes on clay surfaces (e.g., Fu et al., 1996; Mortland &

Pinnavaia, 1971; Pinnavaia & Mortland, 1971; Rupert, 1973). Identification of the location of paramagnetic centres in smectite structures and determination of the nature of their coordination to mineral surfaces can be facilitated by the preparation of oriented samples which have some of the properties of single crystals (e.g., Clementz et al., 1974; Lombardi et al., 2002).

The cation exchange capacity, and hence the physical and chemical properties, of smectites can be changed by altering the oxidation state of structural iron. EPR spectroscopy was used by Gan et al. (1992) to investigate the relationship between the Fe reduction mechanism in a Na-saturated ferruginous smectite and free radical activity in the reducing agent. Of several reducing agents investigated, only $Na_2S_2O_4$ exhibited paramagnetic free-radical behavior, producing a signal at about g = 2.011, which was attributed to the sulphoxylate (SO_2^-) radical. Although the radical was labile in aqueous solution, it was stabilized and enhanced by adding $Na_2S_2O_4$ to aqueous suspensions of the clay. Thus either the clay surface stabilizes the SO_2^- radical or the additional unpaired electrons are produced from the clay structure. Various redox mechanisms in iron-containing smectites were reviewed by Stucki et al. (1996), who reported reductive strength decreasing in the order $S_2O_4^{2-} > S^{2-} > C_6H_8O_6 > S_2O_3^{2-} > C_6H_6O_2 \approx C_2H_2O_4$. The heat of reaction decreased in the order $S_2O_4^{2-} > S_2O_3^{2-} > S^{2-}$, a result which suggests that entropy changes are greater in the S^{2-} treatment. EPR results suggested that free radical formation was associated with the highest reductive potential, and measurements of rheological properties showed that reduced clay suspensions had higher viscosity than their oxidized counterparts as a result of greater attractive forces between particles.

(e) Pyrophyllite – Talc Minerals

The EPR spectrum of talc ($Mg_3Si_4O_{10}(OH)_2$) is characterized by an Fe^{3+} signal at g = 4.28 and a sextet structure from Mn^{2+} (Abdel-Monem et al., 2010) corresponding to substitution for Mg^{2+} in octahedral sites. The enhancement of the Mn^{2+} sextet by γ-irradiation increased the area occupied by the signals and made it difficult for use with dosimetric applications.

(f) Apophyllites

An O^- centre was reported by Mao et al. (2010a) at the hydroxyl oxygen site in natural hydroxylapophyllite. In addition, weak satellite peaks from four geometrically distinct pairs of neighbouring O^- centres (*i.e.*, biradicals) were observed in single-crystal EPR spectra. This O^- centre in hydroxylapophyllite, which most likely formed from natural radiation, could be enhanced by γ-radiation, but was annealed out at 300°C. At least four paramagnetic centres, including two from V^{4+}, the NH_2 free radical and an O-associated center were reported by Mao & Pan, (2009) in the EPR spectra of a fluorapophyllite. The spin-Hamiltonian parameters of the NH_2 free radical in a single-crystal showed that it was oriented parallel to (and rapidly rotated about) the crystallographic **c** axis. This radical was stable on annealing at 300 °C, but was bleached at 340 °C.

FREE RADICAL REACTIONS ASSOCIATED WITH CLAY MINERALS

The generation of free radicals on the surfaces of clay minerals and the consequent health effects of dust inhalation are considered in more detail by Worasith et al. (2014a). They will, therefore, be mentioned only briefly here, and emphasis in the current section will be on the chemistry of free radical reactions involving clay minerals. However, it should be pointed out that the formation of reactive oxygen species, such as the superoxide and hydroxyl radicals can be catalyzed by the surfaces of various types of clay mineral, and that the effectiveness of this catalytic reaction is related to both the particle size and the structural iron (and presumably also other transition metal) content (Gournis et al., 2002b).

It has long been known that clay surfaces are able to catalyze various polymerization reactions via free radical mechanisms, and EPR spectroscopy has played a major role in developing our understanding of such reactions. However, as described by Solomon (1968), clay minerals contain both electron accepting and electron donating sites, and thus can catalyze or inhibit the polymerization of unsaturated organic compounds. The electron acceptor sites are associated with crystal edges and high oxidation state transition metal ions in the aluminosilicate structures, whereas electron donor sites are associated with low oxidation state transition metal ions. In the catalyzed polymerization of unsaturated organic molecules, radical cations or radical anions are formed depending on whether the mineral accepts an electron from or donates an electron to the organic molecule. Inhibition of polymerization occurs when subsequent reactions with mineral surfaces convert these reactive intermediates to non-reactive entities.

The relative contributions of edge and structural sites to electron accepting or donating behaviour can be distinguished by observing the effects of masking the edge sites. This was demonstrated by Solomon (1968) for the benzidine blue reaction by using polyphosphate to destroy the electron accepting properties of the crystal edge. For the same reaction, McBride (1979) was able to distinguish between the effects of adsorbed and structural iron using hectorite as the clay mineral. Results indicated that the benzidine blue reaction not only requires an oxidizing agent to form the radical, but also a clay surface to adsorb and stabilize it against further oxidation. Furthermore, in an investigation of the adsorption and oxidation of 3,3',5,5'-tetramethyl benzidine (TMB) on hectorite, McBride (1985) observed oxidation to the monomeric radical cation for low adsorption levels, whereas at higher adsorption level, intercalation of TMB exceeded the CEC of the hectorite, and a π-π charge-transfer complex was formed. The TMB monomers appeared to lie flat in the layer silicate interlayers, whereas the molecules in the charge-transfer complexes assumed a near-vertical orientation relative to the surface.

Although the work of McBride (1979) showed that surface adsorbed Fe^{3+} had no detectable activity on the benzidine blue reaction, Mortland and Halloran (1976) observed the polymerization of both benzene and phenol after adsorption on Fe^{3+}- or Cu^{2+}- exchanged smectites. EPR showed that the reactions proceeded via radical cation formation as a result of electron transfer from the aromatic species to the Cu. In the case of benzene most of the reaction products could not be attributed to coupled benzene rings, whereas extensive coupling occurred with phenol. Boyd and Mortland (1988) observed similar radical formation mechanisms for the polymerization of chlorophenols and anisoles on Cu^{2+}-exchanged smectite, and EPR spectra were obtained for radical cations for pentachlorophenol, 4-

chlorophenol, and 3-chloroanisole. The electron withdrawing properties of the Cl substituents did not prevent oxidation of the aromatic species, and dimers from the pentachlorophenol and 3-chloroanisole radicals were formed along with partial dechlorination of pentachlorophenol to 2,3,5,6-tetrachlorophenol.

Na^{+}-, Ca^{2+}-, Al^{3+}-, or Fe^{3+}-exchanged smectites were shown by Sawhney et al. (1984) to be able to adsorb and transform 2,6-dimethylphenol with the reaction being influenced by the exchange cation in the order Fe >> Al > Ca > Na. Yong et al. (1997) also found that a significant proportion of the capacity of montmorillonite to oxidize phenols such as 2,6-dimethylphenol and *o*-methylphenol was associated with exchangeable Fe^{3+}. In addition, Polubesova et al. (2010) observed the oxidative transformation of phenolic acids on Fe^{3+}-exchanged montmorillonite, a result which was interpreted as demonstrating the importance of Fe^{3+}-clay surfaces in the abiotic formation of humic materials in soils and for the transformation of phenolic pollutants.

In addition to their role in the transformation of phenolic pollutants, clay minerals may also have applications in the detoxication of recalcitrant halogenated aromatic molecules by conversion to less toxic products through polymerization and/or dechlorination reactions. Thus, Mortland and Boyd (1989) reported that polymerization of chloroethenes occurred via a radical-cation mechanism on refluxing with Cu^{2+}-exchanged smectite in carbon tetrachloride. EPR measurements showed that radical-cation formation was accompanied by a loss of the Cu^{2+} signal as the copper was reduced to the Cu^{+} state. The radical cations appeared to react with water associated with smectite leading to the replacement of Cl- by O-containing functional groups to generate products with potentially decreased toxicity.

Other types of organic molecule may also be transformed by clay minerals, although the mechanisms may be complex. Thus for example, Cloos et al. (1979) described the adsorption of aniline and p-chloroaniline as involving a simultaneous combination of direct or indirect coordination to the clay and protonation of the adsorbate, with the extent of each process being governed mainly by the exchange cation. Radical cations were observed in the EPR spectra recorded after reaction with Fe^{3+}-, $A1^{3+}$- and H^{+}- exchanged montmorillonite, whilst infrared spectroscopy showed loss of aromatic character of the organic molecule with these clays, but not with Cu^{2+}-montmorillonite. Oxidation of the organic molecules occurred on heating with the ion-exchanged clays in air, but with Fe^{3+}- and Cu^{2+}- exchanged montmorillonite the reaction also occurred *in vacuo* and at ambient temperature in methanol solution. Furthermore, Eastman et al. (1996) subsequently showed interlayer aniline polymerization in Cu^{2+}-exchanged hectorite.

The value of clay minerals for adsorbing and catalyzing the alteration of organic molecules is not limited to the environmental sciences, and synthetic mineral catalysts play huge roles in the chemical industry. The chapter by Worasith et al. (2014a) considers possible health implications of reactions that occur on the surface of clay minerals. Furthermore, clays an have important catalytic functions, some of which are described in the chapter by Worasith & Goodman (2014b) on the modification of kaolin minerals to produce novel value-added materials including zeolites. Pillared clays possess catalytic and molecular sieving properties that are related to those of zeolites, except that there is a greater potential for the creation of a wide range of pore sizes in the pillared clays. Strategies for testing new materials, such as modified clays, for catalytic activities involving free radical polymerization have been reviewed by Gridnev & Ittel (2001), and pillared clays are good catalysts for the wet oxidation of phenols by H_2O_2 (Barrault et al., 2000; Guo & Al-Dahhan, 2003).

The smectite structure is also able to protect unstable species from reaction, as illustrated by Gournis et al. (2002a) for the tyrosinate radical, which was able to be stabilized within the layers of a synthetic laponite containing intercalated tyrosinate ester molecules. The radical was stable for more than two months as a result of a combination of electrostatic interactions with the negative surface of the clay and protection from polymerization.

In addition to the characterization of paramagnetic centres in aluminosilicate structures, and the production of organic radicals as a result of redox reactions, EPR results have also shown that aluminosilicate structures are also able to stabilize organic free radicals produced as a result of exposure to γ-irradiation (Gournis et al., 2001). Such organic radicals can be derived from organic compounds present as impurities in the minerals.

DISCUSSION AND CONCLUSION

Questions are often asked about the value of having a detailed knowledge of trace paramagnetic ions, free radical defect centres, and radical reactions associated with clay mineral structures as produced by EPR spectra. However, as described briefly in this chapter, these can have an appreciable influence on both the chemical and physical properties of the mineral species. Understanding catalytic properties of various clay minerals, for example, would not be possible without knowledge of the roles played by surface components and trace paramagnetic species that are present in their structures. Since there are generally considerable variations in the trace components that substitute isomorphously within the aluminosilicate structures of different clay specimens, a knowledge of these and the defect sites associated with them or produced by irradiation can help to understand their various properties. In addition, many reactions catalyzed by clay minerals proceed via free radicals, and thus knowledge of such intermediates can provide an understanding of the relevant reaction mechanisms and sometimes also help to evaluate the effectiveness of different clay mineral specimens for particular functions.

The importance of radiation-induced defects in clay minerals has been summarized by Allard et al. (2012), who described two main uses for that information in the context of storage of radioactive waste materials and as tracers of historical radioactivity. Leakage of transuranic elements from radioactive waste can result in amorphization of smectites, which can lead to enhancement of the kinetics of their dissolution. Although Allard et al. (2012) estimated that this is likely to occur on a timescale of millennia, it is a factor that must be taken into account in the prediction of the long term behavior of engineered barriers. Also, if there is independent knowledge of the age of the clays in geological systems, it is possible to use free radical signal intensities to determine ancient migrations of radioactive elements, which can represent natural analogues of high level nuclear waste repositories. Alternatively, if a constant (or known) radiation dose rate can be justified, then free radical signal intensities can be used to date clay populations. The basic concepts, methods and models for EPR dating are described by Jonas (1997), who also presented reviews of some studies using the method.

The formation of defect centres in crystalline mineral components of soils can be used to investigate shorter term problems. A good example was the use of the intensity of radiation-induced defect centres in quartz samples by Brik et al. (1996) to determine the radiation doses

that were received in various locations in the Ukraine after the Chernobyl nuclear power station accident.

Because of its inertness, plasticity and ability to inhibit the transport of radionuclides, bentonite is a favored material for use as an engineered barrier for repositories for high level nuclear waste. γ-irradiation has little effect on the physicochemical properties of various clay minerals, such as montmorillonite, illite and samples of the serpentine–kaolin group, even at high doses. However, Plötze et al. (2003) observed a reduction in the oxidation state of structural iron and a corresponding decrease in CEC in smectites, whilst kaolinite experienced a weak loss of "crystallinity" as a result of receiving high doses of radiation. Moreover, Holmboe et al. (2009) reported increased colloid stability as a result of exposure of Na^+-montmorillonite to γ-radiation. However, amorphization of the structure of clay minerals was shown by Allard and Calas (2009) to occur on irradiation of smectite with an ion beam or on doping with alpha emitters, although its consequences for physico-chemical properties such as swelling, CEC, and solubility are still not fully understood.

In conclusion, several important uses of clay minerals are strongly influenced by the presence or formation of paramagnetic components either within their structures or as a result of surface reactions. EPR spectroscopy is an important technique for their characterization and it is likely to continue to play a useful role in the refinement and development of novel uses for various types of clay mineral.

REFERENCES

Abdel-Monem, A. A., Abdel-Razek, Y. A., Hassan, G. M., Eissa, H. M., Rasheed, N. M. & Morsy, M. (2010). ESR Dosimetric Properties of Talc and Zircon. *Radiation Measurements*, *45*, 71-77.

Allard, Th., Balan, E., Calas, G., Fourdrin, C., Morichon, E. & Sorieul, S. (2012). Radiation-Induced Defects in Clay Minerals: A Review. *Nuclear Instruments and Methods in Physics Research B*, *277*, 112-120.

Allard, Th. & Calas, G. (2009). Radiation Effects on Clay Mineral Properties. *Applied Clay Science*, *43*, 143-149.

Anbalagan, G., Sakthi Murugesan, K., Balakrishnan, M. & Gunasekaran, S. (2008). Structural analysis, optical absorption and EPR spectroscopic studies on chrysotile. *Applied Clay Science*, *42*, 175-179.

Angel, B. R. & Vincent, W. E. J. (1978). Electron Spin Resonance Studies of Iron Oxides Associated with the Surface of Kaolins. *Clays and Clay Minerals*, *26*, 263-272.

Bader, L. W. & Gesser, H. D. (1972). Hydrogen Atom Recombination on Glass Surfaces. *Canadian Journal of Chem*istry, *50*, 2305-2312.

Bailey, S. W. (1980). Structures of Layer Silicates. In: *Crystal Structures of Clay Minerals and their X-ray Identification*, Brindley, G. W. & Brown, G, editors, London, Mineralogical Society, pp. 1-124.

Balan, E., Allard, T., Boizot, B., Morin, G. & Muller, J.-P. (1999). Structural Fe^{3+} in Natural Kaolinites: New Insights from Electron Paramagnetic Resonance Spectra Fitting at X and Q-Band Frequencies. *Clays and Clay Miner*als, *47*, 605-616.

Barrault, J., Bouchoule, C., Tatibouët, J.-M. Abdellaoui, M., Majesté, A., Louloudi, I.,Papayannakos, N. & Gangas, N. H. (2000). Catalytic Wet Peroxide Oxidation Over Mixed (Al-Fe) Pillared Clays. *Studies in Surface Science and Catalysis*, *130*, 749-754.

Boyd, S. A. & Mortland, M. M. (1988). Radical Formation and Copper(II)-Smectite Polymerization of Chlorophenols. *Environmental Science and Technology, 20*, 1056-1058.

Braddell, O., Barklie, R. C., Doff, D. H., Gangas, N. H. J. & McKimm, A. (1987). EPR of Cu^{2+} Ions in Pillared Clay. *Zeitschrift für Physikalische Chemie, 151*, 157-164.

Brik, A. B., Degoda, V. Ya., Marazuev, Yu. A. & Radchuk, V. V. (1996). Reconstruction of the Doses of Radioactive Irradiation of α-Quartz Crystals from the Chernobyl Zone. *Journal of Applied Spectroscopy, 63*, 128-130.

Brindley, G. W., Chih-Chun Kao, T., Harrison, J. L., Lipsicas, M. & Raythatha, R. (1986). Relation between Structural Disorder and other Characteristics of Kaolinites and Dickites. *Clays and Clay Minerals, 34*, 239-249.

Clementz, D. M., Mortland, M. M. & Pinnavaia, T. J. (1974). Properties of Reduced Charge Montmorillonites: Hydrated Cu(II) Ions as a Spectroscopic Probe. *Clays and Clay Minerals, 22*, 49-57.

Cloos, P., Moreale, A., Broers, C. & Badot, C. (1979). Adsorption and Oxidation of Aniline and p-Chloroaniline by Montmorillonite. *Clay Minerals, 14*, 307-321.

Clozel, B., Allard, T. & Muller, J.-P. (1994). Nature and Stability of Radiation-Induced Defects in Natural Kaolinites: New Results and a Reappraisal of Published Works. *Clays and Clay Minerals, 42*, 657-666.

Clozel, B., Gaite, J.-M. & Muller, J.-P. (1995).Al-O-Al Paramagnetic Defects in Kaolinite. *Physics and Chemistry of Minera*ls, *22*, 351-356.

Cuttler, A. H. (1980). The Behaviour of a Synthetic ^{57}Fe-Doped Kaolin: Mössbauer and Electron Paramagnetic Resonance Studies. *Clay Minerals, 15*, 429-444.

Cuttler, A. H. (1981). Further Studies of a Ferrous Iron Doped Synthetic Kaolin: Dosimetry of X-Ray Induced Defects. *Clay Minerals, 16*, 69-80.

Deer, W. A., Howie, R. A. & Zussman, J. (1992). *An Introduction to the Rock-Forming Minerals, 2nd edition*, Essex, UK, ELBS.

Delineau, T., Allard, T., Muller, J.-P., Barges, O., Yvon, J. & Cases, J.-M. (1994). FTIR Reflectance *vs.* EPR studies of Structural Iron in Kaolinites. *Clays and Clay Minerals, 42*, 308-320.

Eastman, M. P., Hagerman, M. E., Atruso, J. L., Bain, E. D. & Porter, T. L. (1996). Polymerization of Benzene and Aniline on Cu(II)-Exchanged Hectorite Clay Films: A Scanning Force Microscope Study. *Clays and Clay Minerals, 44*, 769-773.

Flogeac, K., Guillon, E. & Aplincourt, M. (2005). Adsorption of Several Metal Ions onto a Model Soil Sample: Equilibrium and EPR studies. *Journal of Colloid and Interface Science*, *286*, 596-601.

Fu, L., Weckhuysen, B. M., Verberckmoes, A. A. & Schoonheydt, R. A. (1996). Clay Intercalated Cu(II) Amino Acid Complexes: Synthesis, Spectroscopy and Catalysis. *Clay Minerals*, *31*, 491-500.

Fysh, S. A., Cashion, J. D. & Clark, P. E. (1983). Mössbauer Effect Studies of Iron in Kaolin. I. Structural Iron. *Clays and Clay Minerals, 31*, 285-292.

Gaite, J.-M., Ermakoff, P. & Muller, J.-P. (1993). Characterization and Origin of Two Fe^{3+} EPR Spectra in Kaolinite. *Physics and Chemistry of Minerals, 20*, 242-247.

Gaite, J.-M., Ermakoff, P., Allard, T. & Muller, J.-P. (1997). Paramagnetic Fe^{3+}: a Sensitive Probe for Disorder in Kaolinite. *Clays and Clay Minerals, 45*, 496-505.

Gan, H., Stucki, J. W. & Bailey, G. W. (1992). Reduction of Structural Iron in Ferruginous Smectite by Free Radicals. *Clays and Clay Minerals, 40*, 659-665.

Gehring, A. U., Fry, I. V., Luster, J. & Sposito, G. (1993). The Chemical Form of Vanadium (IV) in Kaolinite. *Clays and Clay Minerals, 41*, 662-667.

Götze, J., Plötze, M., Graupner, T., Hallbauer, D. K. & Bray, C. J. (2004). Trace Element Incorporation into Quartz: a Combined Study by ICP-MS, Electron Spin Resonance, Cathodoluminescence, Capillary Ion Analysis, and Gas Chromatography. *Geochimica et Cosmochimica Acta, 68*, 3741-3759.

Götze, J., Plötze, M. & Trautmann, T. (2005). Structure and Luminescence Characteristics of Quartz from Pegmatites. *Americal Mineralogist 90*, 13-21.

Goodman, B. A. & Hall, P. L. (1994). Electron Paramagnetic Resonance Spectroscopy. In: *Clay Mineralogy: Physical Determinative Methods*, Wilson M.J., editor, London, Chapman & Hall, pp. 173-225.

Goodman, B. A. & Raynor, J. B. (1970). Electron Spin Resonance of Transition Metal Complexes. *Advances in Inorganic Chemistry and Radiochemistry, 13*, 135-362.

Goodman, B. A. & Nadeau, P. H. (1990). Electron Paramagnetic Resonance Study of Non-Exchangeable Vanadium(IV) in Rectorites. *Clay Minerals, 25*, 283-287.

Goodman, B. A., Nadeau, P. H. & J. Chadwick, J. (1988). Evidence for the Multiphase Nature of Bentonites from Mössbauer and EPR spectroscopy. *Clay Minerals, 23*, 147-159.

Gournis, D., Mantaka-Marketou, A. E., Karakassides, M. A. & Petridis, D. (2001). Ionizing Radiation-Induced Defects in Smectite Clays. *Physics and Chemistry of Minerals, 28*, 285-290.

Gournis, D., Deligiannakis, Y., Karakassides, M. A. Boussac, A., Ioannidis, N. & Petridis, D. (2002a). Stability Study of Tyrosinate Radical in a Restricted Phyllomorphous Medium. *Langmuir, 18*, 10024-10029.

Gournis, D., Karakassides, M. A. & Petridis, D. (2002b). Formation of Hydroxyl Radicals Catalyzed by Clay Surfaces. *Physics and Chemistry of Minerals, 29*, 155-158.

Griffiths, J. H. E., Owen, J., & Ward, I. M. (1954). Paramagnetic Resonance in Neutron-Irradiated Diamond and Smoky Quartz. *Nature, 173*, 439-442**.**

Gridnev, A. A. & Ittel, S. D. (2001). Catalytic Chain Transfer in Free-Radical Polymerizations. *Chemical Reviews, 101*, 3611–3660.

Gunasekaran, S. & Anbalagan, G. (2008). Optical Absorption and EPR Studies on Some Natural Carbonate Minerals. *Spectrochimica Acta Part A, 69*, 383-390.

Guo, J. & Al-Dahhan, M. (2003). Catalytic Wet Oxidation of Phenol by Hydrogen Peroxide over Pillared Clay Catalyst. *Industrial & Engineering Chemistry Research*, **2003**, *42* (12), pp 2450–2460

Hall, P. L. (1980a). The Application of Electron Spin Resonance Spectroscopy to Studies of Clay Minerals: I. Isomorphous Substitutions and External Surface Properties. *Clay Minerals, 15*, 321-335.

Hall, P. L. (1980b). The Application Of Electron Spin Resonance Spectroscopy To Studies Of Clay Minerals: II. Interlamellar Complexes - Structure, Dynamics and Reactions. *Clay Minerals, 15*, 337-349.

Hashimoto, T., Nishiyama, E. & Yanagawa, Y. (2004). Radiation-Induced Luminescence and Hydrogen Radical Formation Associated with Thermal Annealing Treatments on Feldspars. *Journal of Radioanalytical and Nuclear Chemistry, 255*, 81-85.

He, H., Guo, J., Xie, X. & Peng, J. (2001) Location and migration of cations in Cu^{2+}-adsorbed montmorillonite. *Environment International, 26*, 347-352.

Herbillon, A. J., Mestdagh, M. M., Vielvoye, L. & Derouane, E. (1976). Iron in Kaolinite with Special Reference to Kaolinite from Tropical Soils. *Clay Minerals, 11*, 201-220.

Hofmeister, A. M. & Rossman, G. R. (1985). A Model for the Irradiative Coloration of Smoky Feldspar and the Inhibiting Influence of Water. *Physics and Chemistry of Minerals, 12*, 324-332.

Holmboe, M., Wold, S., Jonsson, M. & García-García, S. (2009). Effects of γ-irradiation on the stability of colloidal Na+-Montmorillonite dispersions. *Applied Clay Science, 43*, 86-90.

Hyun S.P., Cho Y.H. & Hahn P.S. (2005) An Electron Paramagnetic Resonance Study of Cu(II) Sorbed on Kaolinite. *Applied Clay Science, 30*, 69-78.

Jen, C. K., Foner, S. N., Cochran, E. L. & Bowers, V. A. (1958). Electron Spin Resonance of Atomic and Molecular Free Radicals Trapped at Liquid Helium Temperature. *Physical Review, 112*, 1169-1182.

Jonas, M. (1997). Concepts and Methods of ESR Dating. *Radiation Measurements, 27*, 943-973.

Jones, J. P. E., Angel, B. R. & Hall, P. L. (1974). Electron Spin Resonance Studies of Doped Synthetic Kaolinite II. *Clay Minerals, 10*, 257-269.

Lombardi, K., Guimarães, J. L., Mangrich, A. S., Mattoso, N., Abbate, M., Schreiner, W. H. & Wypych, F. (2002). Structural and Morphological Characterization of the PP-0559 Kaolinite from the Brazilian Amazon Region. *Journal of the Brazilian Chemical Society, 13*, 270-275.

McBride, M. B. (1979). Reactivity of Adsorbed and Structural Iron in Hectorite as Indicated by Oxidation of Benzidine. *Clays and Clay Minerals, 27*, 224-230.

McBride, M.B. (1985). Surface Reactions of 3,3',5,5'-Tetramethyl Benzidine on Hectorite. *Clays and Clay Minerals, 33*, 510-516.

McBride, M. B. (1990). Electron Spin Resonance Spectroscopy: In *Instrumental Surface Analysis of Geological Materials*, Perry D. L., editor, New York, VCH Publishers, pp. 233-281.

McBride, M. B. (1995). On the Natural Mn(II) EPR Signal of Swy-1 Montmorillonite. *Clays and Clay Minerals, 43*, 383-384.

McBride M. B. (1979) Mobility and reactions of VO^{2+} on hydrated smectite surfaces. *Clays and Clay Minerals, 27*, 91-96.

McBride M. B., Pinnavaia T. J. & Mortland M. M. (1975) Electron Spin Relaxation and the Mobility Of Manganese (II) Exchange Ions in Smectites. *American Mineralogist, 60*, 66-72.

Malengreau, N., Muller, J.-P. & Calas, G. (1994). Fe-Speciation in Kaolins: a Diffuse Reflectance Study. *Clays and Clay Minerals, 42*, 137-147.

Mao, M. & Pan, Y. (2009). Radiation-Induced Defects in Apophyllites. I. The NH_2 Free Radical in Fluorapophyllite. *European Journal of Mineralogy, 21*, 317-324.

Mao, M., Nilges, M.J. & Pan, Y. (2010a). Radiation-Induced Defects in Apophyllites. II. An O^- Centre and Related O^-–O^- Pairs in Hydroxylapophyllite. *European Journal of Mineralogy*, *22*, 89-102.

Mao, M., Nilges, M. J. & Pan, Y. (2010b). Single-Crystal EPR and ENDOR Study of an Al-O^- Center in Prehnite: Implications for Aluminum-Associated Oxyradicals in Layer Silicates. *European Journal of Mineralogy*, *22*, 381-392.

Matyash, I. V., Bagmut, N. N., Litovchenko, A. S. & Proshko, V. Ya. (1982). Electron Paramagnetic Resonance Study of new Paramagnetic Centers in Microcline-Perthites from Pegmatites. *Physics and Chemistry of Minerals*, *8*, 149-152.

Meads, R. E. & Malden, P. J. (1975). Electron Spin Resonance in Natural Kaolinites Containing Fe^{3+} and other Transition Metal Ions. *Clay Minerals*, *10*, 313-345.

Mestagh, M. M., Vielvoye, L. & Herbillon, A. J. (1980). Iron in Kaolinite: II. The Relationship between Kaolinite Crystallinity and Iron Content. *Clay Minerals*, *15*, 1-13.

Morichon, E., Allard, T., Beaufort, D. & Patrier, P. (2008). Evidence of Native Radiation-Induced Paramagnetic Defects in Natural Illites from Unconformity-Type Uranium Deposits. *Physics and Chemistry of Minerals*, *35*, 339-346.

Mortland, M. M. & Boyd, S.A. (1989). Polymerization and Dechlorination of Chloroethenes on Cu(II)-Smectite via Radical-Cation Intermediates. *Environmental Science and Technology*, *23*, 223-227.

Mortland, M. M. & Halloran, L. J. (1976). Polymerization of Aromatic Molecules on Smectite. *Soil Science Society of America Journal*, *40*, 367-370.

Mortland, M. M. & Pinnavaia, T. J. (1971). Formation of Copper (II) Arene Complexes on the Interlamellar Surfaces of Montmorillonite. *Nature Phys. Sci.* 229, 75-77.

Mosser, C., Boudeulle, M., Weber, F. & Pacquet, A. (1996). Ferriferous and Vanadiferous Kaolinites from the Hydrothermal Alteration Halo of The Cigar Lake Uranium Deposit (Canada). *Clay Minerals*, *31*, 291-299.

Muller, J.-P. & Calas, G. (1993). Mn^{2+}-Bearing Kaolinites from Lateritic Weathering Profiles: Geochemical Significance. *Geochimica et Cosmochimica Acta*, *57*, 1029–1037.

Newman, A. C. D. & Brown, G. (1987). *The Chemical Constitution of Clays*. Mineralogical Society, London, pp. 1-128.

Pan, Y., Mao, M. & Lin, J. (2009). Single-Crystal EPR Study of Fe^{3+} and VO^{2+} in Prehnite from the Jeffrey Mine, Asbestos, Quebec, *Canadian Mineralogist*, *47*, 933-945.

Petit S., Decarreau A., Mosser S. M., Ehret G. & Grauby O. (1995) Hydrothermal Synthesis (250°C) of Copper-Substituted Kaolinites. *Clays and Clay Minerals*, *43*, 482-494.

Petrov, I. (1994). Lattice-Stabilized CH_3, C_2H_5, NO_2, and O^{1-} Radicals in Feldspar with Different Al-Si Order. *American Mineralogist*, *79*, 221-239.

Pinnavaia, T. J., Hall, P. L., Cady, S. S. & Mortland, M. M. (1974) Aromatic Radical Cation Formation on the Intracrystal Surface of Transition Metal Layer Lattice Silicate. *Journal of Physical Chemistry*, *78*, 994-999.

Pinnavaia, T. J. & Mortland, M. M. (1971). Interlamellar Metal Complexes on Layer Silicates. I. Copper (II) Complexes on Montmorillonite. *Journal of Physical Chemistry*, *75*, 3957-3962.

Plötze, M., Kahr, G. & Hermanns Stengele, R. (2003). Alteration Of Clay Minerals - Gamma-Irradiation Effects on Physicochemical Properties. *Applied Clay Science*, *23*, 195-202.

Polubesova, T., Eldad, S. & Chefetz, B. (2010). Adsorption and Oxidative Transformation of Phenolic Acids by Fe(III)-Montmorillonite. *Environmental Science and Technology*, *44*, 4203-4209.

Rupert, J. P. (1973). ESR Spectra of Interlamellar Cu (II)-Arene Complexes on Montmorillonite. *Journal of Physical Chemistry*, *77*, 784~790.

Sawhney, B. L., Kozloski, R. K., Isaacson, P. J. & Gent, M. P. N. (1984). Polymerization of 2,6-Dimethylphenol on Smectite Surfaces. *Clays and Clay Minerals, 32*, 108-114.

Schossleler P. M., Weidler P. G. & Gehring A. U. (1998) Octahedral Sites in Talc Revisited; an EPR Study. *Clay Minerals*, **33**, 661-664.

Sengupta, P., Saikia, N. J., Bharali, D. J., Saikia, P. C. & Borthakur, P. C. (2006). ESR Investigation of Deferration Treatment of Iron-Rich Kaolinite Clay from Deopani, Assam, India. *Current Science*, *91*, 86-90.

Sengupta, A., Kadam, R. M., Rajeswari, B., Dhobale, A. R., Babu, Y. & Godbole, S. V. (2010). Characterization of Indian Serpentine by X-Ray Diffraction, Photoacoustic Spectroscopy and Electron Paramagnetic Resonance Spectroscopy. *Applied Clay Science*, *50*, 305-310.

Solomon, D. H. (1968). Clay Minerals as Electron Acceptors and/or Electron Donors in Organic Reactions. *Clays and Clay Minerals, 16*, 31-39

Sorieul, S., Allard, T., Morin, G., Boizot, B. & Calas, G. (2005). Native and Artificial Radiation-Induced Defects in Montmorillonite. An EPR Study. *Physics and Chemistry of Minerals*, *32*, 1-7.

Speit, B. & Lehmann, G. (1982). Radiation Defects in Feldspars. *Physics and Chemistry of Minerals*, *8*, 77-82.

Stucki, J. W., Bailey, G. W. & Gan, H. (1996). Oxidation-Reduction Mechanisms in Iron-Bearing Phyllosilicates. *Applied Clay Science*, *10*, 417–430.

Weeks, R. A. (1956). Paramagnetic Resonance of Lattice Defects in Irradiated Quartz. *Journal of Applied Physics*, *27*, 1376-1381.

Weil, J. A. (1984). A Review of Electron Spin Spectroscopy and its Application to the Study of Paramagnetic Defects in Crystalline Quartz. *Physics and Chemistry of Minerals*, *10*, 149-165.

Weil, J. A. (1993). A Review of the EPR Spectroscopy of the Point Defects in α-Quartz: The Decade 1982–1992. In: *The Physics and Chemistry Of SiO_2 and the Si-SiO_2 Interface 2* (Eds. C.R. Helms and B.E. Deal), Springer-Verlag, pp 131-144.

Worasith, N., Goodman, B. A., Jeyachoke, N. & Thiravetyan, P. (2011). Characterisation of Modified Kaolin from the Ranong Deposit Thailand Studied by XRD XRF SEM FTIR and EPR. *Clay Minerals*, *46*, 539-559.

Worasith, N. & Goodman, B.A. (2012). Influence of Particle Size on the Paramagnetic Components of Kaolins from Different Origins. *Clay Minerals*, *47*, 539-557.

Worasith, N., Ninlaphruk, S., Mungpayaban, H. & Goodman, B. A. (2013). Irradiation-Induced Free Radicals in Thai Kaolins. *Proceedings of the Pure and Applied Chemistry International Conference 2013 (PACCON 2013)*, pp. 294-297.

Worasith, N., Deng, W. & Goodman, B. A. (2014a). Free Radical Reactions Associated with Aluminosilicate Clay Minerals and Nanoparticles: Implications for the Health Effects of Dust Inhalation. *Clays and Clay Minerals: Geological Origin, Mechanical Properties and Industrial Applications*, 14, pp. 361-378.

Worasith, N. & Goodman, B. A. (2014b). Production of Specialized Mineral Products from Modified Kaolins. *Clays and Clay Minerals: Geological Origin, Mechanical Properties and Industrial Application, 10,* pp. 243-272.

Yong, R. N., Desjardins, S., Farant, J. P. & Simon, P. (1997). Influence of pH and Exchangeable Cation on Oxidation of Methylphenols by a Montmorillonite Clay. *Applied Clay Science, 12,* 93-110.

In: Clays and Clay Minerals
Editor: Liam R. Wesley
ISBN: 978-1-63117-779-8

Chapter 14

FREE RADICAL REACTIONS ASSOCIATED WITH ALUMINOSILICATE CLAY MINERALS AND NANOPARTICLES: IMPLICATIONS FOR THE HEALTH EFFECTS OF DUST INHALATION

Niramon Worasith[1], Deng Wen[2] and Bernard A. Goodman[3*]
[1]Department of Chemistry, Rajamangala University of Technology Krungthep, Soi Suan Plu, Sathorn, Bangkok, Thailand
[2]Department of Physics, Guangxi University, Nanning, Guangxi, China
[3]State Key Laboratory for Conservation and Utilization of Subtropical Agro-Bioresources, Guangxi University, Nanning, Guangxi, China

ABSTRACT

Inhalation of dust is an important cause of lung disease, and it has long been associated with premature deaths in the mining industry. However, it is now also becoming recognized as an important problem associated with air pollution. Reactions associated with the surfaces of clay mineral particles can generate highly toxic reactive oxygen species (ROS) such as the hydroxyl radical and the superoxide radical anion, and also lead to lipid peroxidation in the lungs after inhalation. The production of free radicals can be identified by a combination of electron paramagnetic resonance (EPR) spectroscopy and spin trapping technology, which converts highly reactive radicals into long(er) lived species that can be studied and identified. In this chapter we review the evidence for the generation of these free radical species by the surfaces of silicate mineral particles, and discuss their implications for health problems associated with mineral dust inhalation.

Keywords: Pneumoconiosis, free radical, EPR spectroscopy, lipid peroxidation, silica, asbestos

* E-mail address: Bernard_a_goodman@yahoo.com

INTRODUCTION - DISEASES ASSOCIATED WITH DUST INHALATION

Mineral dust is responsible for a range of diseases, known collectively as pneumoconioses; these may be characterized by diffuse collagenous reactions to relatively small lung exposure to bioactive dusts (e.g., silicosis, asbestosis) or largely non-collagenous reactions caused by larger dust exposure, normally in an industrial setting, where retention of a particular component is a key causative factor (Becklake 1992; Fishwick & Barber 2012). The damage to lungs caused by mineral dusts is a function of both the particle sizes of the minerals and their toxicity. If particles have diameters < 10 μm, they can penetrate the alveoli, and toxic particles then can cause permanent damage. However, reactions to mineral dust exposure are generally particle specific, and the release of pro-inflammatory cytokines results in fibroblast formation, and leads eventually to fibrosis. The asbestos minerals and silica dust are highly fibrogenic, but there is a large variability in the ability of a particular type of particle to cause fibrosis. Thus a cytotoxicity assay to predict the potential of minerals to cause lung disease would be of great value as a prevention strategy in industrial settings, and for evaluation of the risks associated with exposure to different types of dust generally. However, the development of such an assay requires a detailed knowledge of the nature of the interactions that occur between mineral particle surfaces and lung tissue.

(a) Asbestosis

Asbestosis results from inhalation of dusts containing asbestos minerals (Wagner et al., 1960; Newhouse and Thompson, 1965). The two main asbestos minerals are white asbestos or chrysotile (a serpentine) and blue asbestos or crocidolite (an amphibole), but they may also include other amphiboles, such as actinolite, amosite, anthophyllite and tremolite. Asbestosis is incurable and may be progressive even after dust exposure has ceased (Wagner 1997). The health risks associated with exposure to blue asbestos are well-known, and its use is strictly controlled in many countries, but there is still some controversy concerning the toxicity of white asbestos, and there has been a belief that it is relatively safe. However, in a review of the risks associated with white asbestos, Kanarek (2011) documented many cases of mesothelioma caused by chrysotile exposure. In addition, the health risks associated with asbestos exposure are exacerbated by cigarette smoking (Wagner 1997), and it would seem prudent for anyone with a history of asbestos exposure to refrain from smoking. A characteristic of mesothelioma is that there is a long latency period (20-30 years) before symptoms of the disease are apparent (Niklinski et al. 2004), and early diagnosis is difficult. Thus even though the use of asbestos has declined considerably since the 1970s, there is still an appreciable risk associated with the demolition of old buildings containing asbestos insulation. Furthermore, there has been growing evidence during the past 30 years of small airway lesions resulting from exposure to non-aspestos minerals (e.g., Churg & Wright 1983); these are addressed in the following sections

(b) Silicosis

Silicosis is the pneumoconiosis caused by inhalation of crystalline silica dust; it occurs widely and is a cause of morbidity and mortality throughout the world. Like asbestosis, silicosis is incurable and may progress long after exposure (Wagner 1977). Silica-derived hazards currently represent an important health problem, and as pointed out by Leung et al. (2012), increased efforts are needed for their recognition and control, especially in developing countries. However, the risks associated with quartz exposure vary dramatically depending on its origin, the presence of various trace elements in its structure, the presence of associated minerals, or modification of its surface through contact with other chemicals (Fubini 1998). Differences in the biological activity of different quartz samples was clearly demonstrated by Clouter et al. (2001), who found that a standard experimental quartz caused inflammation of rat lungs following intratracheal instillation, whereas samples of workplace quartz did not. These differences could not be completely explained by surface area, particle diameter, or extractable iron, and surface reactivity was deemed to be a major factor in the production of inflammation by quartz particles. Thus unlike most chemicals, silica cannot be regarded as a single hazard entity, and there are difficulties in reliably assessing the risks associated with different types of silica-containing dusts, although crystalline silica (quartz) is classified as a carcinogen by the International Agency for Research on Cancer (IARC 1997).

By considering several large long-term studies of silica dust inhalation in workers at varying levels of exposure, Collins et al., (2005) produced an inhalation chronic reference exposure level for silica below which no adverse effects due to prolonged exposure would be expected in the general public. However, it should also be recognized that there is a general underestimation of silicosis when it is simply assessed by radiography, and there are often considerable uncertainties in the estimation of individual exposure levels. Furthermore, Martínez et al. (2010) recently described cases of silicosis in young construction workers handling artificial silica conglomerates, thus highlighting the need to use protective measures for a wide range of silica related materials. Since the problem of toxicity seems to be related to both the structural and surface compositions of individual particles, greater knowledge is needed in order to understand fully the risks associated with different quartz samples.

(c) Pneumococioses from Other Aluminosilicate Minerals

Pneumoconiosis arising from talc inhalation was described by Gibbs et al. (1992), on the basis of both pathological and mineralogical analyses and a comparison of results from primary, secondary, and tertiary exposures. The expression “talcosis” was proposed for a disease associated with a variety of mineral samples containing talc; in this work, the presence of asbestos mineral impurities was eliminated as the origin of the pneumococioses in the majority of the cases. Gibbs et al. (1992) also described mixed dust fibrotic lesions for mineral samples containing substantial quantities of quartz, mica or kaolin in addition to talc, and pointed out the importance of lung dust mineral analysis, for evaluating causes of pathologic reactions for complex exposures.

In an examination of the genotoxic effects induced by bentonite particles, Zhang et al. (2011), showed that *in vitro* DNA damage induced by native and activated bentonites was significantly higher than that induced by gypsum, and increased with both exposure

concentration and duration. Although the native and active bentonites contained appreciable quantities of quartz, both induced significantly higher DNA damage than a standard DQ-12 quartz, which was used for comparison. In addition, DNA damage induced by activated bentonite was found to be significantly higher than with the native sample. However, the water soluble fractions from both bentonites did not induce significant DNA damage and micronuclei, indicating that it is the insoluble mineral fractions (i.e. the mineral dust and not soluble adsorbed species) that are largely responsible for the genotoxic effects of bentonites. More recently, Huang et al. (2013) found that occupational exposure to organic bentonite particles produced genetic damage and lipid peroxidation, both of which increased with increasing level of exposure. This result is in contrast to the report of Geh et al. (2006), who observed only a weak genotoxic effect for untreated and organic activated bentonite particles containing up to 6 % quartz. Furthermore, this was influenced by the quartz content of the bentonite samples, and ROS generation was dependent on their transition metal content. Clearly the health risks associated with exposure to bentonites are complex and there are factors that are still not understood.

(d) Lung Diseases of Farm Workers

Early studies of respiratory diseases in agricultural workers focused on allergic disorders caused by exposure to organic dusts. However, farm workers are often exposed to substantial concentrations of inorganic dusts from soils, especially in dry climates. Although there have been limited studies of farmworkers exposed to inorganic dusts, the evidence for respiratory symptoms and restrictive pulmonary function supports a causal association of mineral dust exposure and pneumoconiosis. Furthermore, a recent study of human lung samples from deceased Latino males demonstrated that farm work was significantly associated with pneumoconiosis and small airways disease caused by inhalation of mineral dust (Schenker et al. 2009). Cigarette smoking was independently associated with these diseases, although there was not a significant interaction between mineral dust and smoking.

On the basis of *in vitro* toxicity studies, Schenker (2010) reported that the cytotoxicity of agricultural dusts is intermediate between those of controls and crystalline silica, but in some assays of ROS generation, such as H_2O_2, hydroxyl radical, and nuclear factor κB generation, the agricultural dusts were actually more potent than silica. Thus Schenker (2010) concluded that inorganic mineral dusts should not simply be considered to be just a nuisance, but a cause of mixed-dust pneumoconiosis, the prevalence and natural history of which are still unknown.

POTENTIAL RISKS ASSOCIATED WITH AMBIENT DUSTS

In addition to the specific health problems associated with dust inhalation by farm workers discussed in the previous section, there is currently concern about potential health problems for the general public imposed by ambient dusts. However, the risks are difficult to predict, because of the various types of dust particles, which include mineral, industrial and automobile sources, and the large variation in toxicity between different mineral and organic components. Nevertheless, the potential health problem of ambient urban dust inhalation is

illustrated by a recent analysis of hospital admission records for the Taipei metropolitan area in which it was revealed that dust storm events were followed 1-4 days later by appreciable increases in the number of pneumonia cases requiring hospitalization (Kang et al. 2012).

Distinguishing between different sources of dust represents an additional problem when attempting to estimate risks from air-borne particulate matter. In a novel approach, Branquinho et al. (2008) used accumulation in lichen to assess the contributions of different pollution sources to the composition of atmospheric dust. Different types of dust were found to have different time-patterns for Ca accumulation, which was also related to differences in the influences of wet and dry periods on the lichen accumulation process.

Differences in chemical compositions of size-resolved particulate matter from urban sites in the greater Beirut area were investigated recently by Daher et al. (2013). They showed that background ambient particles were mainly of secondary origin and present at significantly lower levels than close to a freeway, where elemental carbon and polyaromatic hydrocarbons were much higher than at roads in similar areas in the U.S. with comparable meteorology and geomorphology. The oxidative potential and chemical speciation of size-resolved particulate matter showed the presence of many metals and trace elements of vehicular origin with moderate-to-high water-solubility (> 30%) in the small size fractions (Daher et al. 2014), and thus constituted an added health risk. ROS-activity was also dependent on size, composition and origin of the particulate matter, and 1.5–2.8 times greater near the freeway than at the background location. A detailed analysis by Fujiwara et al. (2011) of the compositions of urban dusts for 15 sites in Buenos Aires over a 2-month period produced 2 major groups, one with elements of both geological and anthropogenic origin (Cu, Fe, Ni and Sn) and the other typical traffic related elements (Cd, Mn, Pb, S, Sb and Zn).

Rock quarrying and processing represents a source of coarse and fine particulate matter, which may have an environmental impact on the surrounding area. In an investigation of the possible environmental impact of dust from a limestone quarry in north Israel during the dry summer season, Bluvshtein et al. (2011) reported that the major component of the quarried rock (calcite) was enriched downwind from the quarry relative to an upwind site, whereas major components of background dust were enriched both upwind and downwind. Pollution derived from cement manufacture and concrete usage is another cause for environmental concern, especially in regions with dry climates, since in recent years there have been large increases in the use of concrete in infrastructure construction associated with the rapid increase in urbanization in developing regions of the world.

MECHANISMS FOR THE INITIATION OF LUNG DISEASE BY CLAY MINERALS

Current ideas on the mechanisms through which clay minerals initiate pneumoconioses stem from the work of Donaldson and Borm (1998), who demonstrated that the apparently conflicting findings of cancer incidence in quartz-exposed industries could be understood in terms of surface reactivity. The ability to generate free radicals and cause oxidative stress was considered to be especially important, and it was demonstrated that free radical generation could be modified by substances that affect the quartz surface. This concept was extended by Fubini (1998) in a more general discussion of the toxicity characteristics of different

particulates to explain the observation that different biological responses can be elicited from particles with the same chemical composition, but with different structural forms and surface compositions.

As discussed by Shi et al. (1998), there are four main factors in the development of carcinogenesis, namely direct DNA damage, excessive cell proliferation, loss of growth regulation, and division of damaged cells. Since reactive oxygen species (ROS) can contribute to each of these processes, they could represent a critical factor in the development of lung cancer, as illustrated in Figure 1. The presence of free radical centres on mineral surfaces and the production of reactive oxygen species (ROS) by reactions involving structural Fe were implicated in oxidative stress. These were considered to represent key components in the development of fibrosis and lung cancer, although other chemical functionalities related to cytotoxicity were able to modulate the overall pathogenicity by regulating transport and clearance. The role of ROS, which are formed directly by the interaction of silica with aqueous media and silica-stimulated cells, in the fibrogenic and carcinogenic activity of silica particles was supported by Ding et al. (2002), who also described the molecular mechanisms of silica-induced NF-κB activation, and its relationship to cyclooxygenase II and TNF-α generation.

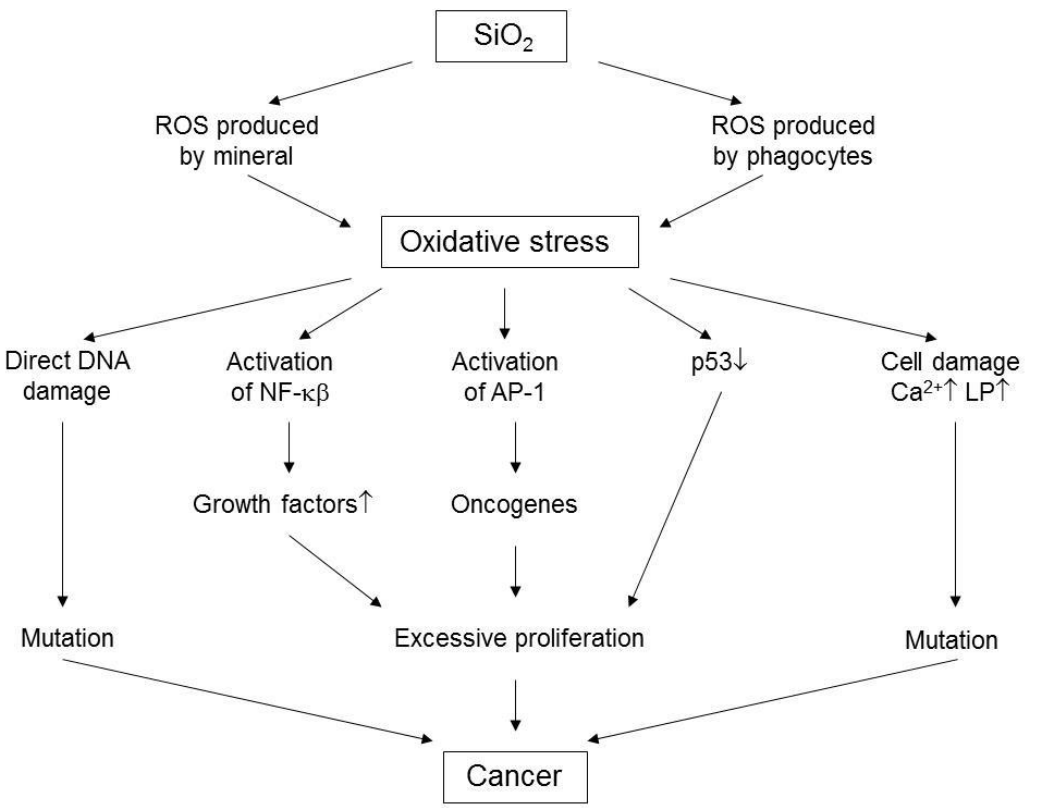

Figure 1. Representation of silica-produced ROS and mechanisms through which they contribute to the development of lung cancer (adapted from Shi et al. 1998).

The involvement of oxidative stress as a result of increased free radical generation, and the production of ROS with early and low grade simple pneumoconiosis was demonstrated by Altin et al. (2004) in measurements of the activities of blood plasma antioxidant enzymes, superoxide dismutase and glutathione peroxidase, and the concentration of the lipid peroxidation end product malondialdehyde (MDA). Further support for the involvement of ROS in the initiation step in pneumoconiosis was obtained by Nadif et al. (1998), who reported elevated levels of superoxide dismutase and catalase in coal workers, and suggested that these enzymes might have potential value as markers of early stages of pneumoconiosis. Furthermore, Engelen et al. (1990), observed a correlation between superoxide dismutase, catalase and glutathione peroxidase with diseased but not control miners.

Subsequently, Knaapen et al. (2004) suggested that the generation of both ROS and reactive nitrogen species (RNS) can stimulate the development of lung cancer by inhaled dust particles. They pointed out that two independent mechanisms can operate: a) the generation of oxidizing agents by clay particles primarily as a result of physicochemical characteristics of the surfaces, and b) the stimulation of cellular oxidant generation by the presence of clay mineral particles. Furthermore, there are various mechanisms for the generation of cellular ROS/RNS, including the production of an inflammatory response and the activation of NAD(P)H-oxidase enzymes in the mitochondria. Thus, a further subdivision can be made between primary (induced by the mineral particle) and secondary (as a result of inflammation) formation of oxidants. In addition, clay particles may carry surface-adsorbed carcinogenic components into the lung. Each of these pathways can impact on genotoxicity and cell proliferation, as well as on feedback mechanisms involving DNA repair or apoptosis. Also, although there is strong evidence that ROS/RNS mediate genotoxicity and mutagenesis, there is little information on the subsequent steps that lead to neoplastic changes, and since most proposed molecular mechanisms for mineral-induced carcinogenesis have been derived from *in vitro* studies, there is still a need for *in vivo* assessment of the relative contributions of primary and secondary pathways.

In experiments on the effects on rat lung parenchyma of exposure to coal dust, Pinho et al. (2004) used various assays to demonstrate the involvement of ROS. These included (a) measurements of the amounts of thiobarbituric acid-reactive substances (TBARS), (b) determination of carbonyl groups to assess the oxidative damage to proteins, (c) measurement of the total radical-trapping antioxidant parameter (TRAP) by luminol chemoluminescence emission, (d) assessing catalase activity by the rate of decrease of H_2O_2, and (e) determining superoxide dismutase activity by inhibition of adrenaline autooxidation. Overall the results suggested a biphasic inflammatory response, and the involvement of oxidative damage in coal dust-induced lung damage. At the present time, it is not clear as to the nature of the inflammatory response associated with clay mineral inhalation, especially since some minerals have considerably higher toxicity than coal dust.

ELECTRON PARAMAGNETIC RESONANCE (EPR) SPECTROSCOPY AND ITS USE IN THE STUDY OF FREE RADICAL REACTIONS

Electron paramagnetic resonance (EPR) spectroscopy is one of the most important techniques for investigating free radical processes, since it detects specifically chemical

species containing unpaired electrons. "Stable" paramagnetic species can be characterized directly, but there are also procedures for determining the presence of very unstable free radicals. In this respect, spin trapping methodology, in which an unstable free radical reacts with a diamagnetic "spin trap" to produce a (more) stable radical (as illustrated in Figure 2a for the spin trap phenyl-N-t-butylnitrone (PBN)), has proven to be of great importance for the identification of the hydroxyl radical and the superoxide radical anion in chemical and biological systems (e.g., Janzen 1980). Hyperfine splittings ($a(^{14}N)$ and $a(^{1}H)$) resulting from the ^{14}N and ^{1}H atom on the α-carbon is observed in the EPR spectra, and their magnitudes vary according to the chemical nature of the trapped radical $R^{\cdot}$.

Although there are differences in the accessibility of individual spin traps to different types of tissue, and in their selectivities for different types of radical, by appropriate choice it is possible to distinguish both the source and identity of biologically generated radicals. However, very reactive radicals, such as $^{\cdot}OH$, may react indiscriminately with organic molecules in their vicinity to produce the more stable C-centred radicals, which could be the main species observed after reaction with the spin trap.

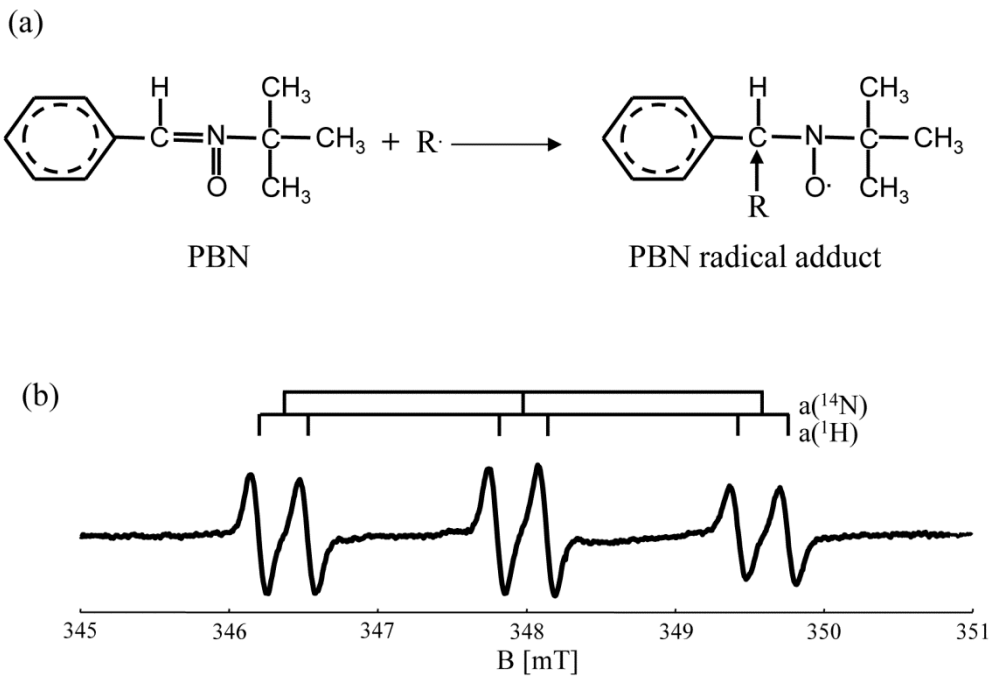

Figure 2 (a) Mechanism for the formation of an adduct of a free radical $R^{\cdot}$ with the spin trap PBN, and (b) its resulting EPR spectrum.

EXPERIMENTAL EVIDENCE FOR THE ASSOCIATION OF FREE RADICAL REACTIONS WITH MINERAL SURFACES

The ability of clay mineral surfaces to catalyze chemical reactions is well-known (e.g., Solomon and Swift 1967; Solomon 1968), and they are able to act as electron donors and/or

acceptors depending on their composition. In addition, various types of surface functional group can exist in a single mineral sample; for example in kaolinites much of the cation exchange capacity is associated with edge sites (Ma and Eggleton 1999). Thus the chemical properties of clay minerals are influencd by their particle sizes as well as their compositions. Furthermore, many surface sites can be changed by adjusting the pH as a result of protonation/deprotonation reactions.

It should also be recognized that that clay minerals can either catalyze or inhibit free radical reactions. For example, in the early work of Solomon and Swift (1967) on the influence of alumino- and magnesio-silicates on the free-radical polymerization of methyl methacrylate, it was concluded that octahedrally-coordinated Al was primarily responsible for inhibition of the reaction through radical termination reactions. However, as described in the chapter by Worasith et al. (2014), there are many examples of free radical centres located in clay minerals, and of the production of free radicals on mineral surfaces. Indeed, as described in this chapter, several studies have suggested that pulmonary toxicity to asbestos and silica may be mediated through oxidant-induced cell injury, and surface radicals associated with freshly fractured silica may be a factor in the initiation of pulmonary disease.

The formation of free radicals by O_2 reduction on asbestos in a cell-free system was demonstrated by Zalma et al. (1987) using EPR spectroscopy and a spin trapping agent, and for quartz by Shi et al. (1988), who also reported that grinding increased the generation of radicals. However, the potential of freshly ground quartz dust to generate hydroxyl radicals decreased rapidly with time in air and dropped by 50% after one day, a result which demonstrates rapid O_2-induced surface modification of ground quartz. It was also demonstrated that $^{\cdot}OH$ generation involves mainly the silica surface and H_2O rather than the Fenton reaction, which requires the presence of transition metals. Nevertheless, there is also ample evidence that transition metals can play an important role in the production of hydroxyl radicals by clay minerals (Garrido-Ramírez et al. 2010).

Reactions of $^{\cdot}OH$ could be important in lipid peroxidation and the fibrogenicity of quartz dust, especially in acute silicosis, and a mechanism for their production by the reduction of O_2 at mineral surfaces was reported by Pezerat et al. (1989). Surface activity due to the presence of electron donor sites, is generally linked to structural Fe^{2+} ions. The reducing properties of the surfaces of some mineral fibres, such as chrysotile, nemalite, and freshly ground amphiboles in aqueous buffer medium, are highly effective in producing radicals from dissolved O_2, as measured by the intensities of EPR spectra of DMPO adducts of $^{\cdot}OH$ and $R^{\cdot}$. It was also shown that the reducing activity of certain fibres can be increased by prior treatment with Fe^{2+} or adding glutathione to the reaction medium, thus suggesting that the carcinogenic activity may be the result of the reducing properties of their surfaces. Such reducing properties may either be present at the time of inhalation or acquired in the biological medium. Since antioxidant molecules are reducing agents, it is possible that they could exacerbate health problems associated with the inhalation of mineral dust particles.

Formation of superoxide and hydroxyl radicals as a result of O_2 reduction also occurs on the surfaces of smectite clays, and Gournis et al., (2002) showed that the yield of $^{\cdot}OH$ was mainly a function of clay particle size and depended to a lesser extent on Fe content of the clay mineral. Of three samples investigated, synthetic laponite clay with small platelet size (~20 nm) but no structural iron had the highest level of $^{\cdot}OH$ production followed by montmorillonite (~200 nm), whereas fluorohectorite (~2000 nm) did not generate hydroxyl radicals by O_2 reduction. However, one might expect that it is only the Fe^{2+} form of iron that

would be effective in radical generation, so the total iron content of a mineral might not be an important parameter. The relative importance of the forms of Fe in hydrogen atom abstraction and ·OH formation mechanisms at the interfaces between mineral particles and biological fluids was investigated by Fenoglio et al. (2001) using crocidolite asbestos fibres that had been modified by thermal treatments. Both radical mechanisms were active with the original fibres, but hydrogen atom abstraction was dependent on the amount and location of Fe^{2+}, and was suppressed by surface oxidation, whereas $HO^{\cdot}$ release appeared to be independent of the oxidation state of iron. In similar measurements with quartz specimens containing different concentrations of Fe, a commercial sample with trace levels of iron was active in both tests. However, its reactivity was not fully suppressed by treatment with desferrioxamine, which should remove/inactivate iron, and the radical yield was close to that of a pure quartz dust, suggesting the presence of active sites other than iron. Both crocidolite and quartz react with ascorbic acid, and this reaction would be expected to deplete the antioxidant defences after deposition of such particles in the lung. However, the radical yield was increased with quartz, but decreased with asbestos after treatment with ascorbic acid, a result which may be explained by selective removal of Fe and Si from the mineral surfaces.

BIOLOGICAL RADICAL GENERATION IN RESPONSE TO MINERAL DUST INHALATION

Despite the evidence presented in the previous paragraph, Vallyathan (1994) questioned the relevance of assaying for ·OH radical generation in predicting the cytotoxicity and pathogenicity of minerals. Based on comparisons of the ability of several minerals to generate hydroxyl radicals and their lipid peroxidation potentials with their cytotoxicity, it was suggested that the ability induce lipid peroxidation is a more relevant assay. Support for this idea was generated from a study of a group on minerals in which it was shown that crystalline silica, which was the most potent cytotoxic and pathogenic, had the lowest ·OH radical generating ability, but induced the highest levels of lipid peroxidation, whereas coal mine dust had the highest ·OH radical generation ability, but was the least cytotoxic in bioassays of toxicity and induced the lowest levels of lipid peroxidation. Further support for this conclusion was obtained from the investigations of Dalal et al. (1990) into the role of free radicals in the mechanisms of hemolysis and lipid peroxidation by silica, in which comparative EPR and cytotoxicity studies were used to examine specifically the role of the fracture-induced Si-based radicals (Si· and SiO·) and silica-generated hydroxyl (·OH) radicals in cell membrane damage. Concentrations of Si· and SiO· radicals were controlled through decay processes, thermal annealing, and boiling, whilst that of ·OH radicals was varied by using catalase, superoxide dismutase, $KMnO_4$, Na_2SeO_3, ascorbic acid, and metal ions. From a comparison of hemolysis and EPR results it was deduced that the radicals play little or no role in the silica-induced hemolysis, although lipid peroxidation data indicated that the radicals might be involved in the initiation of an oxidative chain reaction leading to the macrophage membrane damage through lipid peroxidation.

In a comparison of the effects of freshly fractured silica, aged silica, amosite, crocidolite, chrysotile, and a nontoxic dust, barite, on the *in vitro* generation of O_2-derived free radicals from human neutrophils and rat alveolar macrophages, Vallyathan et al. (1992) showed a

direct relationship between the relative toxicity index and EPR peak heights for radical adducts of the spin trap PBN (Figure 3). Radical generation was prevented by the addition of catalase, dimethyl sulfoxide, 1,3 dimethyl-2-thiourea, sodium benzoate, or mannitol, whereas addition of carmustine, a glutathione reductase-glutathione peroxidase inhibitor, resulted in a 5-fold increase in radical generation. Thus, whereas any damage resulting from the generation of free radicals at low concentrations by nontoxic dusts can be repaired by the normal cellular defense system, the higher levels of free radical generation with toxic dusts, such as silica, amosite, chrysotile, and crocidolite, increase the probability of the cellular defence system being overwhelmed and resulting in permanent cell injury. Vallyathan et al. (1992) also showed that the membrane-based oxidase system was the probable primary source of radicals, and that the generation of O_2-derived free radicals is an important primary event in cell injury induced by both silica and asbestos minerals.

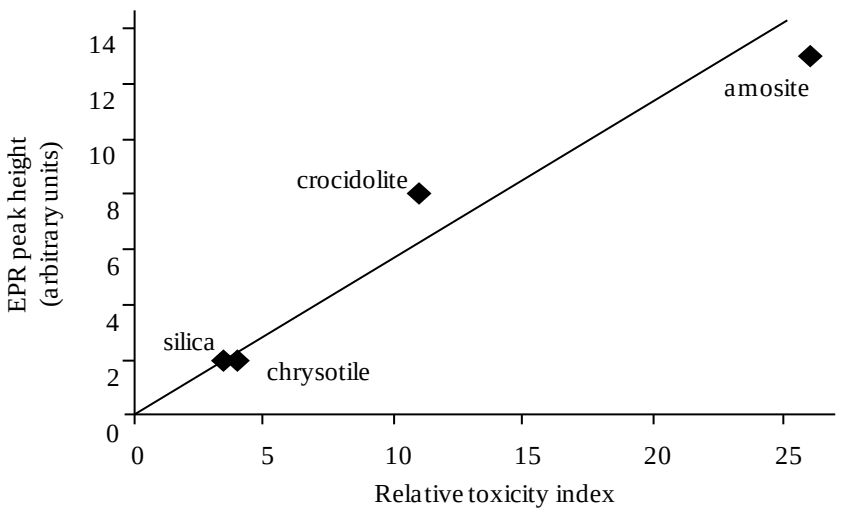

Figure 3. Relationship between the relative mineral toxicity index and EPR peak heights of the PBN radical adduct normalized for surface area (adapted from Vallyathan et al. (1992)).

Support for the involvement of a free radical mechanism for *in vitro* DNA damage and in the *in vivo* toxicity of asbestos was presented by Fubini et al. (1995), in an investigation of the formation of hydroxyl and carboxylate radicals in aqueous suspensions of three different types of iron-containing minerals (two asbestos fibers (chrysotile and crocidolite), an iron-exchanged zeolite), and two iron oxides (magnetite and haematite) by observing the EPR spectra of their DMPO adducts. Two target molecules were considered: the formate ion to provide evidence for the potential for hydrogen abstraction from any organic molecule, and H_2O_2, which is always present during phagocytosis. Iron was implicated in free radical generation, but the amount of iron at the mineral surface was unrelated to the amount of radicals formed, and only a few surface ions in a particular redox and coordination state were found to be active. Evidence was produced for three different types of active site (i) for H atom abstraction, (ii) a heterogeneous catalyst for $^{\cdot}OH$ production, and (iii) a catalyst for H_2O_2 disproportionation. For both free radical generation mechanisms, the Fe-exchanged zeolite behaved similarly to the asbestos samples, whereas the two oxides were mostly inert.

However, magnetite was an excellent catalyst for H_2O_2 disproportionation, whereas haematite was also inactive in this reaction.

In rats injected intratracheally with crocidolite, Ghio et al. (1998) showed the development of a neutrophilic inflammatory response within 24 hours by histologic examination. EPR spectroscopy and the spin trap 4-POBN demonstrated the production of C-centred free radicals and provided strong evidence for *in vivo* free radical production and lipid peroxidation resulting from asbestos exposure.

CURRENT STATUS OF THE ROLES OF MINERALS IN LUNG DISEASE AND PRIORITY PROBLEMS

As can be seen from the discussion in the previous paragraphs there is still uncertainty concerning the extent to which free radicals generated by mineral particles have a causative role in lung disease compared to free radical responses in lung tissue initiated by the presence of specific types of mineral particle. However, it seems likely to us that free radicals generated by mineral surface reactions may be a factor in the initiation of tissue response to the presence of mineral particles, but it is also not the only factor.

In a critical evaluation of the pathogenesis of silicosis, Vallyathan et al. (1995) considered possible early events that occur in lungs of rats after inhalation of freshly fractured or aged quartz. In both cases, the number of bronchoalveolar lavage cells and biochemical markers of lung injury increased lipid peroxidation, and the ability of pulmonary phagocytes to produce more O_2-derived radicals were elevated after a 2-week exposure. However, all were higher in freshly ground compared to aged quartz, whereas antioxidant enzymes showed lower concentrations in the group that was exposed to freshly fractured quartz. Furthermore, free radical concentrations associated with the freshly milled quartz were significantly higher than those for aged quartz.

Rates of clearance from lungs of stable free radicals were monitored *in vivo* by Vallyathan et al. (1997) using the intensity of the EPR signal at L-band frequencies from the stable nitroxide radical TEMPO instilled into the lungs of rats. The contents of the antioxidant enzymes superoxide dismutase (SOD) and glutathione peroxidase (GPx), and the amount of lipid peroxidation were also measured in whole lungs of rats exposed to crystalline silica (quartz) and sham exposed controls. Clearance of TEMPO followed first order kinetics and the rate was consistent with oxidative stress in the rats exposed to quartz. This conclusion was supported by measurements of SOD and GPx, which were up regulated in quartz exposed animals. Increased lipid peroxidation also supported a role for enhanced generation of ROS in the pathogenesis of silica-induced lung injury. These *in vivo* experiments demonstrated directly that silicotic lungs are in a state of oxidative stress, and that increased generation of ROS is associated with enhanced levels of oxidative enzymes and lipid peroxidation.

Clay mineral particles may also be instrumental in the environmental transformation of other pollutants into either more or less toxic species. For example, Lomnicki et al. (2008) have suggested that persistent free radicals associated with combustion-generated particles may be responsible for oxidative stress resulting in cardiopulmonary disease and probably cancer that have been attributed to exposure to airborne fine particles. Substituted phenoxyl and semiquinone radicals were detected by EPR spectroscopy and it was postulated that they

were formed via a mechanism that involves initial physisorption on particulate matter, followed by chemisorption via elimination of water or hydrogen chloride, and electron transfer which results in the simultaneous reduction of metal ions. Such radicals may be part of a catalytic biochemical cycle that results in the formation of hydroxyl radicals and other ROS. However, clay minerals have also been shown to participate in the transformation of environmental pollutants to less toxic species (e.g., Worasith et al. 2014), probably through mechanisms that involve generation od the hydroxyl radical.

POTENTIAL APPROACHES FOR AMELIORATING HEALTH PROBLEMS ASSOCIATED WITH MINERAL INHALATION

Lung diseases caused by mineral dust inhalation such as asbestosis and silicosis are generally regarded as incurable, so prevention is the only practical method for decreasing the numbers of these debilitating diseases. Measures to limit asbestosis have now been in place in many countries for a number of decades, and have shown success because of control in the use of asbestos minerals combined with the development of safer alternative materials to replace them. Pneumoconioses in general are, however, a growing problem and likely to remain so for the near future, at least partly because aging populations are increasingly likely to have been exposed to toxic dusts at some time during their lives.

Prevention is always a better option than cure, but with profit motives driving modern societies, there is often little incentive for industries to adopt preventative measures unless there are appreciable financial penalties for failing to do so. However, in industrial settings the use of efficient extraction systems and protective masks and headwear can go a long way towards minimizing the risks to workers of dust inhalation, but the risks of ambient mineral dusts to populations as a whole are more difficult to address, especially in dry climates, where the use of water to minimize air-borne dust is limited. Furthermore, the composition of ambient dusts is not a constant factor, and is influenced by particulates from industrial and automobile emissions, and the increasing use of concrete in developing countries means that there is likely to be an increasing amount of related dusts in urban areas. Nevertheless, soil-derived clay minerals will continue to represent an appreciable fraction of inhaled inorganic dusts, and will at the same time also function as carriers of potentially toxic chemicals.

CONCLUSION

Inhalation of silica or aluminosilicate mineral dusts can lead to the development of pneumoconioses, which are initiated by reactions between mineral surfaces and lung tissue. Oxidative stress as a result of free radical generation and seen by lipid peroxidation appears to be a trigger for the onset of these diseases. The size (and shape) of clay mineral particles is the major factor governing their toxicity, but their chemical compositions are also important, and there appears to be a wide range of toxicities associated with a single type of particle, such as silica. Furthermore, although there are chemical assays to identify and determine free radicals produced by mineral surface reactions, and to measure the potential of various systems to oxidize lipids, there is still not a reliable method to evaluate the potential toxicity

of ambient dust particles of complex composition. Nor are there effective treatments for the pneumoconioses associated with the inhalation of inorganic mineral dusts.

The increased use of concrete in developing countries is also a cause for concern, though not necessarily despair, since free radical generation associated with silica dust drops off rapidly with its aging after fracture. Nevertheless, at the present time there are insufficient experimental data available to assess the extent of risks to the general population in many (near) urban environments, where the compositions of dusts represent a combination of particles from soil, industrial, and automobile inputs. Furthermore, such risks could be highly variable over relatively short distances and timescales, and thus represent greater hazards to the very young and elderly.

REFERENCES

Altin, R., Armutcu, F., Kart, L., Gurel, A., Savranlar, A. & Özdemir, H. (2004). Antioxidant response at early stages and low grades of simple coal worker's pneumoconiosis diagnosed by high resolution computed tomography. *International Journal of Hygiene and Environmental Health, 207,* 455-462.

Becklake, M.R. (1992). The mineral dust diseases. *Tubercle and Lung Disease*, *73*, 13-20.

Bluvshtein, N., Mahrer, Y., Sandler, A. & Rytwo, G. (2011). Evaluating the impact of a limestone quarry on suspended and accumulated dust. *Atmospheric Environment*, *45*, 1732-1739.

Branquinho, C., Gaio-Oliveira, G., Augusto, S., Pinho, P., Máguas, C. & Correia, O. (2008). Biomonitoring spatial and temporal impact of atmospheric dust from a cement industry. *Environmental Pollution*, 151, 292-299.

Churg A. & Wright J.L. (1983). Small-airway lesions in patients exposed to nonasbestos mineral dusts. *Human Pathology*, 14, 688-693.

Clouter, A., Brown, D., Höhr, D., Borm, P. & Donaldson, K. (2001). Inflammatory effects of respirable quartz collected in workplaces versus standard DQ12 quartz: particle surface correlates. *Toxicological Sciences*, *63*, 90-98.

Collins, J.F., Salmon, A.G., Brown, J.P., Marty, M.A. & Alexeeff, G.V. (2005). Development of a chronic inhalation reference level for respirable crystalline silica. *Regulatory Toxicology and Pharmacology*, *43*, 292-300.

Daher, N., Saliba, N.A., Shihadeh, A.L., Jaafar, M., Baalbaki, R. & Sioutas, C. (2013). Chemical composition of size-resolved particulate matter at near-freeway and urban background sites in the greater Beirut area. *Atmospheric Environment*, *80*, 96-106.

Daher, N., Saliba, N.A., Shihadeh, A.L., Jaafar, M., Baalbaki, R., Shafer, M.M., Schauer, J.J. & Sioutas, C. (2014). Oxidative potential and chemical speciation of size-resolved particulate matter (PM) at near-freeway and urban background sites in the greater Beirut area. *Science of the Total Environment*, *470–471*, 417-426.

Dalal, N.S., Shi, X. & Vallyathan, V. (1990). Role of free radicals in the mechanisms of hemolysis and lipid peroxidation by silica: Comparative ESR and cytotoxicity studies. *Journal of Toxicology and Environmental Health*, *29*, 307-316.

Ding, M., Chen, F., Shi, X., Yucesoy, B., Mossman, B. & Vallyathan, V. (2002). Diseases caused by silica: mechanisms of injury and disease development. *International Immunopharmacology*, *2*, *173-182*.

Donaldson, K. & Borm, P.J.A. (1998). The quartz hazard: a variable entity. *Annals of Occupational Hygiene*, *42*, 287-294.

Engelen, J.J., Borm, P.J., van Sprundel, M. & Leenaerts, L. (1990). Blood antioxidant parameters at different stages of pneumoconiosis in coal workers. *Environmental Health Perspectives, 84*, 165-172.

Fenoglio, I., Prandi, L., Tomatis, M. & Fubini, B. (2001). Free radical generation in the toxicity of inhaled mineral particles: the role of iron speciation at the surface of asbestos and silica. *Redox Report*, *6*, 235-241.

Fishwick, D. & Barber, C. (2012). Pneumoconiosis. *Medicine*, *40*, 310-313.

Fubini, B. (1998). Surface chemistry and quartz hazard. *Annals of Occupational Hygiene, 42*. 521-530.

Fubini, B., Mollo, L. & Giamello, E. (1995). Free radical generation at the solid/liquid interface in iron containing minerals. *Free Radical Research, **23***, 593-614.

Fujiwara, F., Rebagliati, R.J., Dawidowski, L., Gómez, D., Polla, G., Pereyra, V., Smichowski, P. (2011). Spatial and chemical patterns of size fractionated road dust collected in a megacity. *Atmospheric Environment, 45*, 1497-1505.

Garrido-Ramírez, E.G., Theng, B.K.G. & Mora, M.L. (2010). Clays and oxide minerals as catalysts and nanocatalysts in Fenton-like reactions - A review. *Applied Clay Science, 47*, 182-192.

Geh, S., Shi, T., Shokouhi, B., Schins, R.P.F., Armbruster, L., Rettenmeier, A.W. & Dopp, E. (2006). Genotoxic potential of respirable bentonite particles with different quartz contents and chemical modifications in human lung fibroblasts. *Inhalation Toxicology*, *18*, 405-412.

Ghio, A.J., Kadiiska, M.B., Xiang, Q.-H. & Mason, R.P. (1998). *In vivo* evidence of free radical formation after asbestos instillation: an ESR spin trapping investigation. *Free Radical Biology and Medicine*, *24*, 11-17.

Gibbs, A.E., Pooley, F.D., Griffiths, D.M., Mitha, R., Craighead, J.E., Ruttner, J.R. (1992). Talc pneumoconiosis: a pathologic and mineralogic study. *Human Pathology*, *23*, 1344-1354.

Gournis, D., Karakassides, M.A. & Petridis, D. (2002). Formation of hydroxyl radicals catalyzed by clay surfaces. *Physics and Chemistry of Minerals*, *29*, 155-158.

Huang, Y., Zhang, M., Zou, H., Li, X., Xing, M., Fang, X. & He, J. (2013). Genetic damage and lipid peroxidation in workers occupationally exposed to organic bentonite particles. *Mutation Research*, *751*, 40-44.

IARC Working Group on the Evaluation of Carcinogenic Risks to Humans, International Agency for Research on Cancer, & World Health Organization. (1997). *Silica, some silicates, coal dust and para-aramid fibrils* (Vol. 68). World Health Organization.

Janzen, E.G. (1980). A critical review of spin trapping in biological systems. In: Free Radicals in Biology, Vol. IV, (Ed. Pryor, W.A.), New York, Academic Press, pp. 115-154.

Kanarek, M.S. (2011). Mesothelioma from chrysotile asbestos: update. *Annals of Epidemiology*, *21*, 688-697.

Kang, J.-H., Keller, J.J., Chen, C.-S. & Lin, H.-C. (2012). Asian dust storm events are associated with an acute increase in pneumonia hospitalization. *Annals of Epidemiology, 22*, 257-263.

Knaapen, A.M., Borm, P.J.A., Albrecht, C. & Schins, R.P.F. (2004). Inhaled particles and lung cancer. Part A: Mechanisms. *International Journal of Cancer, 109*, 799-809.

Leung, C.C., Yu, I.T.S. & Chen, W. (2012). Silicosis. *The Lancet, 379*, 2008-2018.

Lomnicki, S., Truong, H., Vejerano, E. & Dellinger, B. (2008). Copper oxide-based model of persistent free radical formation on combustion-derived particulate matter. *Environtal Sciience & Technology, 42*, 4982-4988.

Ma, C. & Eggleton, R.A. (1999) Cation exchange capacity of kaolinite. *Clays and Clay Minerals, 47*, 174-180.

Martínez, C., Prieto, A., García, L., Quero, A., González, S. & Casan, P. (2010). Silicosis: a disease with an active present. *Archivos de Bronconeumología, 46*, 97-100.

Nadif, R., Bourgkard, E., Dusch, M., Bernadac, P., Bertrand, J.-P., Mur, J.-M., Pham, Q.-T. (1998). Relations between occupational exposure to coal mine dusts, erythrocyte catalase and Cu^{++}/Zn^{++} superoxide dismutase activities, and the severity of coal workers' pneumoconiosis. *Occupational and Environmental Medicine, 55*, 533-540.

Newhouse, M.L. & Thompson, H. (1965). Mesothelioma of pleura and peritoneum following exposure to asbestos in the London area. *British Journal of Industrial Medicine, 22*, 261-268.

Niklinski, J., Niklinska, W., Chyczewska, E., Laudanski, J., Naumnik, W., Chyczewski, L. & Pluygers, E. (2004).The epidemiology of asbestos-related diseases. *Lung Cancer, 45*, S7-S15.

Pezerat, H., Zalma, R., Guignard, J. & Jaurand, M.C. (1989). Production of oxygen radicals by the reduction of oxygen arising from the surface activity of mineral fibres. *IARC Sci Publ.* 1989 (90), 100-111.

Pinho, R.A., Bonatto, F., Andrades, M., Frota, M.L.C. Jr., Ritter, C., Klamt, F., Dal-Pizzol, F., Uldrich-Kulczynski, J.M. & Moreira, J.C.F. (2004). Lung oxidative response after acute coal dust exposure. *Environmental Research, 96*, 290-297.

Schenker, M.B. (2010). Inorganic agricultural dust exposure causes pneumoconiosis among farmworkers. *Proceedings of the American Thoracic Society, 7*, 107-110.

Schenker, M.B., Pinkerton, K.E., Mitchell, D., Vallyathan, V., Elvine-Kreis, B. & F.H.Y. Green (2009). Pneumoconiosis from agricultural dust exposure among young California farmworkers. *Environmental Health Perspectives, 117*, 988-994.

Shi, X., Dalai, N.S. & Vallyathan, V. (1988). ESR evidence for the hydroxyl radical formation in aqueous suspension of quartz particles and its possible significance to lipid peroxidation in silicosis. *Journal of Toxicology and Environmental Health, 25*, 237-245.

Shi, X., Castronova, V., Halliwell, B. & Vallyathan, V. (1998). Reactive oxygen species and silica-induced carcinogenesis. *Journal of Toxicology and Environmental Health, Part B, 1*, 181-197.

Solomon, D.H. (1968). Clay minerals as electron acceptors and/or electron donors in organic reactions. *Clays and Clay Minerals, 16*, 31-39.

Solomon, D.H. & Swift, J.D. (1967). Reactions catalyzed by minerals. Part II. Chain termination in free-radical polymerizations. *Journal of Applied Polymer Science, 11*, 2567-2575.

Vallyathan, V. (1994). Generation of oxygen radicals by minerals and its correlation to cytotoxicity. *Environ Health Perspectives, 102*(Suppl 10), 111-115.

Vallyathan, V., Castranova, V., Pack, D., Leonard, S., Shumaker, J., Hubbs, A.F., Shoemaker, D.A., Ramsey, D.M., Pretty, J.R. & McLaurin, J.L. (1995). Freshly fractured quartz inhalation leads to enhanced lung injury and inflammation. Potential role of free radicals. *American Journal of Respiratory and Critical Care Medicine, 152*, 1003-1009.

Vallyathan, V., Leonard, S., Kuppusamy, P., Pack, D., Chzhan, M., Sanders, S.P, & Zweir, J.L. (1997). Oxidative stress in silicosis: Evidence for the enhanced clearance of free radicals from whole lungs. *Molecular and Cellular Biochemistry, 168*, 125-132.

Vallyathan, V., Mega, J.F., Shi, X. & Dalal, N.S. (1992). Enhanced generation of free radicals from phagocytes induced by mineral dusts. *American Journal of Respiratory Cell and Molecular Biology, 6*, 404-413.

Wagner, G.R. (1997). Asbestosis and silicosis. *The Lancet, 349*, 1311-1315.

Wagner, J.C., Sieggs, C.A. & Marchand, P. (1960). Diffuse pleural mesothelioma and asbestos exposure in the North Western Cape Province. *British Journal of Industrial Medicine, 17*, 260-271.

Worasith, N., Ninlaphurk, S., Mungpayaban, H., Deng, W. & Goodman, B.A. (2014). Characterization of Paramagnetic Centres in Clay Minerals and Free Radical Surface Reactions by EPR Spectroscopy. *Clays and Clay Minerals: Geological Origin, Mechanical Properties and Industrial Application, 13*, 335-360.

Zalma, R., Bonneau, L., Guignard, J., Pezerat, H. & Jauand, M.-C. (1987). Formation of oxy radicals by oxygen reduction arising from the surface activity of asbestos. *Canadian Journal of Chemistry, 65***,** 2338-2341.

Zhang, M., Li, X., Lu, X., Fang, X., Chen, Q., Xing, M. & He, J. (2011). Studying the genotoxic effects induced by two kinds of bentonite particles on human B lymphoblast cells *in vitro*. *Mutation Research, 720*, 62-66.

In: Clays and Clay Minerals
Editor: Liam R. Wesley
ISBN: 978-1-63117-779-8

Chapter 15

INDUSTRIAL APPLICATION OF CLAYS AND CLAY MINERALS

Ivana Savic[1,*], Stanisa Stojiljkovic[1], Ivan Savic[1] and Dragoljub Gajic[2,3]

[1]Department of Chemical Engineering, Faculty of Technology, University of Nis, Serbia
[2]Department of Signals and Systems,
School of Electrical Engineering, University of Belgrade, Serbia
[3]Department of Information Engineering,
Computer Science and Mathematics, University of L'Aquila, Italy

ABSTRACT

Clays are among the most widespread sedimentary rocks, which are mainly composed of clay minerals like kaolinite, illite, montmorillonite and other aluminum silicates as well as other various ingredients, e.g., quartz grains, apatite, granite, iron hydroxide, etc. According to their mineralogical composition, there are three main groups of clays: kaolinite, montmorillonite and illite as well as around 30 different types of pure clays within these categories. However most of natural clays are mixtures of these different types. Due to their specific properties, e.g., high capillarity, unique rheological properties, hardening, plasticity, thixotropy, high degree of swelling, clays are widely used in various industries. For example, because of their excellent colloidal properties clays are often used as drilling fluids for oil and gas wells as well as other boreholes to lubricate and cool the cutting tools, to remove cuttings, and help prevent blowouts. The possibility of swelling allowes clays to occupy an important role in mining and geology while the high swelling degree of clays is exploited in the construction industry. In contact with freshly poured concrete, clays swell and create a waterproof barrier that is used during construction of underground facilities, sewerage systems, water tanks, nuclear and other waste storages, etc. Clays have been widely used as a foundary-sand bond in the steelmaking industry as well as a binding agents in the manufacturing of iron

* Address for Correspondence: Dr Ivana M. Savic, Department of Pharmacy, Faculty of Technology, Bulevar oslobodjenja 124, 16000 Leskovac, Serbia. Tel.: +381 16 242859, Fax: +381 16 242859. E-mail: vana.savic@yahoo.com.

ore pellets. One of the important properties of clays is adsorption and ability to interact with the metal ions from the surrounding environment. Therefore clays take a prominent place in the list of natural sorbents and can be used to remove heavy metals ions and organic compounds from industrial water, that represents one of the major challenges of the modern civilization. Besides being used in environmental protection, the use of clays as adsorbents is found in the food industry as well, e.g., for clarification of wine. In addition, clays are also very important in medicine and cosmetics where mixed with water create a colloidal solution, which when consumed acts as a natural laxative absorbing both organic and inorganic contaminants, heavy metals and free radicals. Clays and clay minerals are ingredients in a large number of skin care products as creams but also independently applied to eczema and different types of rashes. Recently a lot of studies have been performed in order to investigate the use of clays as a thermal energy storage medium since they are able to perform reversible direct hydration/dehydration process. The first results clearly showed that a few types of clays can be even considered as an efficient energy storage materials compared to the others used in this purpose.

Keywords: Clays, clay minerals, industrial applications

1. INTRODUCTION

1.1. Definition, Grouping and Properties of Clay and Clays Minerals

The definition of "clay" was formalized in 1546 by Agricola [1]. However it has been revised many times since then although the fundamentals involving plasticity, particle size, and fire hardening were retained by most [2]. Clay is an earth material that is plastic when moist but hard when fired, and composed mainly of fine particles of hydrous aluminum silicates and other minerals [3]. Based on composition it is crystallized aluminum silicate which contains other impurities. Secondary components of clay can be quartz grains of and, more rarely, zircon, apatite, granite and others [4]. Clays often contain admixtures as iron hydroxides. Also clays can contain an organic substance. Small amounts of manganese rock greenish color. According to their mineralogical composition, there are four main groups of clays: kaolinite ($Al_4(OH)_8Si_4O_{10}$), montmorillonite (complex hydrated silicates of Al, Mg and Na), illite (complex hydrated silicates of Al, Mg, Fe i Na) and haloizit ($Al_4(OH)_8Si_4O_{10}\times 4H_2O$) as well as around 30 different types of pure clays within these categories [5]. One subgroup of the montmorillonite is bentonite clay.Due to their quite useful properties [6-8] such as high capillarity, unique rheological properties, hardening, plasticity, thixotropy, high degree of swelling as well as high degree of efficiency for M^+ cation exchange, today clays have an important role in modern industry. The high capillary and porosity of clay enables the absorption of large amounts of water. The thixotropy is property of some clays when kneaded they become more viscous. Kneading also increases the shaping ability that is a consequence of a change in the electrical nature of clay surface layers. Swelling is a very important feature of clay minerals that enables their wide application in various industries in the field of geotechnical engineering, environmental engineering and other industrial applications. High degree of efficiency for M^+ cation exchange is the result of

charge imbalances in clay structure caused by exchange of Al^{3+} for Si^{4+} in the tetrahedral sheets, and of Mg^{2+} for Al^{3+} cations in the octahedral sheets.

In addition to the above-mentioned physical and chemical properties, clays have another good advantages, such as:

- They are locally available.
- Their mining, processing, transportation and maintenance is not that much energy-intensive.
- They are not harmful to human health, i.e. do not cause any harmful emissions, do not irritate skin, they are odorless, do not have chemical additives, are not electrostatic, absorb harmful radiation.
- Clay additives are even more environmentally friendly (e.g., straw, wood waste, sand, etc.).
- Clays contribute to a comfortable room climate by absorbtion of moisture that is under different conditions rereleased into the room, regulate the room temperature by cooling in the summer and heating in the winter climate, absorb smells.
- Stability and durability of clay construction elements is almost unlimited.
- Clay products do not require additional thermal insulation.
- Clays are recyclable.

1.2. Bentonite Clays Characteristics and Properties

1.2.1. Characteristics

The name bentonite was applied as erly as 1848 by Knight to a highly plastic clay material appearing near Fort Benton, Wyoming [9]. Bentonite is a colloidal aluminum-silicate clay [10] formed by alteration of volcanic material [11, 12]. It consists of several minerals out of which the dominant one is montmorillonite that makes at least 70% of its composition [13]. Bentonite, in addition to montmorillonite, contains a small portion of other mineral matter, usually quartz, feldspar, volcanic glass, organic matter, gypsum, or pyrite whose total share in bentonite is about 30% [14]. There are different types of bentonite named based on the dominant chemical element such as potassium, sodium, calcium, and aluminium. From industrial applications point of view the most common are the sodium and calcium bentonites [15]. These are three-layer alumino-silicate clays with an ability to swell and increase volume when in contact with water. Sodium bentonite shows higher swelling capacity compared to the calcium bentonite because the sodium cations may be hydrolyzed to a greater extent than the calcium cations [15, 16]. This feature provides bentonite an excellent cohesiveness and makes it an excellent bonding and sealing material.

1.2.2. Physical-chemical Properties

Bentonite clays ususally have pale-green color. However due to the presence of different cations they could also be yellow, red or brown [17]. These are some of the most important properties of bentionite clays:

- In contact with water, they show a property of thixotropy, and passes into a gel.
- May absorb 12-15 times larger amount of water relative to the dry form [18] due to process diffusion process and capillary suction. This water retention and swelling capacity depends on temperature and pressure [19].
- Great cation exchange capacity. Bentonite clays are characterized by an octahedral sheet of aluminum atoms being infixed between two tetrahedral layers of silicon atoms [20]. It has net negative electric charge due to the isomorphic substitution of Al^{3+} with Fe^{2+} and Mg^{2+} in the octahedral sites and Si^{4+} with Al^{3+} in the tetrahedral sites and is balanced by the cations such as Na^{+} and Ca^{2+} located between the layers and surrounding the edges [21]. These cations are interchangeable because of the weak links and therefore provide bentonite with high cation exchange capacity. Clay cations are able to bind not only with the inorganic compounds, but also organic compounds such as herbicides, bioorganic particles, viruses and pathogenic proteins.

1.3. Application of Clays and Clay Minerals

An early use of clays dates in the time of Jericho, 7800 years BC, when used to build a tower, while the ancient Greeks and Romans used clays to build their houses because it was a cheap material. In recent years, clays have experienced a revival. The great cation exchange capacity, bonding capacity, plasticity, strong tendency to react with organic compounds and thixotropy are the main key features for their use in the modern world. Some other features are presence of manganese, iron and potassium, color, purity, and efficiency under the acidic and/or basic conditions. For example clay minerals also has many other applications in various fields which include the production of bonding, filling and solidification agents, oil drilling, cosmetics, pharmaceuticals, sealants, farming and hydraulic containment [22]. Also, today an application of clay minerals in environmental protection is especially very interesting and important since it is used to remove heavy metallic ions from waste water [23, 24].

Table 1. Primary and secondary properties of clay

Primary properties	Secondary properties
Chemical composition	Granulometric composition
Density	Adsorptive capacity
Hardness	Specific density
Surface properties	Abrasiveness
Colour	Precipitation behavior
Wettability	Rheological performance

1.3.1. The requirements for the quality of the clay

Industrial application defines the requirements for clay quality which can include: mineral composition, content of Al_2O_3 and SiO_2, impurity content, pH value, chemical stability, swelling, fire resistance, coarseness of particles, whiteness [25, 26].

Depending on the application and customer requirements, clays must have certain properties:

- For the paper production, a high degree of whiteness as well as a low abrasiveness is necessary.
- The paint industry needs a high degree of whiteness, a large proportion of the fine particles and good dispersion properties.
- In the plastics industry, requirements are mainly related to the particle size.
- Ceramics industry primarily requires good shaping ability.
- Production of refractory materials, e.g., fine and coarse bricks, requires a high content of aluminum oxide.

In adition there are also some limitations based on the chemical content and application, e.g.,

- For the ceramics industry allowed contents are: Fe_2O_3 lower than 1.5%, loss on ignition lower than 12%, Al_2O_3 minimum 31%, SiO_2 maximum 55%, CaO than 1%.
- Kaolin clay used in the ceramics industry should meet the following requirements: Fe_2O_3 maximum content around 0.6-1.5%, TiO_2 maximum content around 0.6-1.2%, CaO up to 0.8%, Al_2O_3 content higher than 30%.

1.4. The Use of Bentonite Clay in the Construction Industry and Natural Environment

The use of bentonite in the construction industry has grown significantly over the last few years especially due to the ability of bentonite to retain water in long term, due to the chemical resistance, compatibility with the environment and easy of administration. Building applications provide appropriate market for bentonite where it is traditionally used as a thixotropic agent, support to or lubrication in walls and foundations, in construction of tunnels and drilling. Also, bentonite is used for sealing purposes in dike construction, hydraulic engineering and landfill construction, especially for encapsulation of old wastes deposits [27].

A liner system in an engineered landfill acts as a barrier for substances and prevents contamination of to the surrounding environment. Thus the liner system becomes one of the critical design considerations. Bagchi [28] and Jayasekera [29] studied the hydraulic conductivity of different landfill liners and according to the results a landfill liner is intended to be a low permeabillity barrier which generally involves an application of clay. Puma et al. aimed to evaluate the reuse of incinerator slag, mixed with sodium bentonite, for landfill capping system components [30]. A characterization was performed on pure bottom ash (BA) samples from an incinerator in the north of Italy. After investigation, the results were pointed to the BA-bentonite mixture qualified as a suitable material for landfill cover in Italy. Moreover, owing to the low release of toxic compounds, the proposed cover system would have no effect on the leachate quality in the landfill. Roberts and Shimaoka [31] investigated the possibility of the application of bentonite coated gravel as a liner material for waste landfills. Bentonite coated gravel has proven to be a very effective capping material and method for the remediation of contaminated sediments in aquatic environments.

Soil-bentonite vertical slurry cut-off wall is a useful treatment for urban industrial contaminated sites. Due to the clay-heavy metal interaction, significant changes may occur in the engineering behavior of soil-bentonite cut-off walls. Fan et al. [32] were conducted a series of oedometer tests to investigate the effects of lead on the compressibility and the permeability of kaolin-bentonite mixtures, a simplified model of in-situ soil-bentonite cut-off wall backfills. It was found that the fabric of kaolin-bentonite mixture, depending on the particle-particle interaction subjected to different ranges of pH and lead concentration, governs the sedimentation behavior and permeability.

The cut-off wall is embedded aggregate which serves as a semi impervious area during the placement of the slurry wall [33]. The cut-off wall is made from a mixture of bentonite, cement and ground slag. Thanks to the adequate properties cement-bentonite cut-off walls can be an excellent and cost efficient material in the development of dry docks. Cracks in the foundation rock allow water to enter the dry dock. Applying the cement-bentonite cut-off wall can be performed by foundation grouting and in this way its permeability decreased.

The adsorption mechanism, migration patterns and permeation behavior of soil-bentonite barrier materials for metal ions with different valences are investigated by Lv and Zhao [34]. The obtained results showed that the adsorption process for metal ions with different valences by soil-bentonite barrier materials is fast, and the higher the valence, the greater the adsorption capacity is. Pseudo-second-order adsorption kinetics and Langmuir-Freundlich adsorption equation explain that chemical adsorption is the dominating state and the surface has certain heterogeneity.

Bentonite, as drilling fluid additive, is important for the oil, gas and geothermal drilling industry. Its main functions are improvement of the mud viscosity in order to reduce the fluid loss to the formation. During the research, Abdou et al. were studied both natural and nano-bentonite as drilling mud [35]. Nano-bentonite has been prepared by nano-grinding. The rheological properties, filtration and gel strength before and after treatment with viscosities and filter loss agent, were used for comparison with the American Petroleum Institute API bentonite. After testing it was found that with decreasing the grain size of bentonite to the nano-scale, the results were not in accordance with the API standard.

During the construction of a tunnel in cohesive soil area, the main force need to resist adhesive force generated around the machine, but also to reduce the frictional force coming from rocks [36]. In this case, the most commonly used lubrication is bentonite mud, which is injected through ports in the jacking head and filled outside of the pipes.

In addition some modifications of bentonite clay improve its properties and allow better useage in construction. Scalia et al. [37] modified bentonite to prevent alterations in hydraulic conductivity when permeated with aggressive inorganic solutions. The tests indicated that a bentonite-polymer composite, polymerized with acrylic acid, swells more and retains low hydraulic conductivity compared with natural sodium bentonite when contacted with aggressive inorganic solutions. Also, it is known that sodium bentonite has been shown to exhibit semipermeable membrane behavior. For this reason, it can be used as barrier for hydraulic containment applications. However, degradation of such membrane behavior due to the diffusion of cations into the bentonite is occurring. This degradation increases with increasing salt concentration and increasing valence of the salt cation. In order to improve membrane behavior of traditional bentonite, Bohnhoff et al. [38] have carried out the polymerization of bentonite referred to as a bentonite-polymer nanocomposite. However, complete degradation of the membrane behavior was ultimately observed for specimens of

the bentonite-polymer nanocomposite exposed to 10 mmol/dm^3 $CaCl_2$ for a test conducted in a rigid-wall cell and 20 mmol/dm^3 $CaCl_2$ for a test conducted in a flexible-wall cell.

1.4.1. Mineral Flotation Using Bentonite

Clay minerals are often associated with copper, gold and other valuable minerals and place a widespread problem in mineral flotation. During the research, Cruz et al. [39] tried to explain how the rheological behavior of kaolinite and bentonite suspensions at natural pH and how the pH modifier, collector and frother normally used in copper-gold flotation affect the rheological properties. It was found that bentonite has a stronger effect on the viscosity of suspensions than kaolinite. The pH modifier, collector and frother have a potential to alter the rheological behavior of kaolinite and bentonite suspensions and the effect of the pH modifier is more pronounced. However, the presence of clays in mineral beneficiation circuits can cause a wide range of different problems, including that of slime coatings on valuable minerals and elevated viscosities of flotation pulps. Forbes et al. [40] have attempted to decouple and estimate the relative magnitudes of the slime coatings and pulp rheology effects on the natural floatability of chalcopyrite mineral in a model system. They found that that these two phenomena can be partially isolated and that they both have a detrimental effect on flotation performance.

1.4.2. The Materials for the Heat Storage

Due to a constant growth in population and thus in energy consumption too, the world has begun to be much more aware of limited energy resources as well as capacity of the atmosphere to receive the combustion byproducts. In order to overcome this problem, the industrialized countries have become very interested in developing technologies based on intensive use of renewables. Recently, there is also a growing interest in the construction of buildings which use solar energy that is quite reasonable since buildings represent huge proportion in overall residential energy consumption, i.e. around 40-50%, while cooling and heating loads contribute the most to this share. In addition, reduction of heat losses in buildings has a significant impact on total emissions of the greenhouse gases. Traditional insulation materials have been used in thin or multiple layers in order to achieve a higher thermal resistance but caused more complex construction details. For this reason, in recent years an attention has been focused on phase-change materials (e.g., hydrated salts, paraffin, fatty acids) [41] and materials with good absorption properties as thingy and bentonite [42], which have an ability to store the thermal energy in a latent form. In this way, the capacity of heat storage per unit volume can be increased compared to that of conventional building materials. Li et al. investigated the thermal performances of paraffin/bentonite composite phase-change material [43]. During the research they found that the heat transfer rate of prepared paraffin/bentonite composite was enhanced by bentonite.

1.5. The Use of Bentonite in Electrical Engineering

Clay minerals can be used as insulation in electrical engineering. The bentonite gels are used as “thickening agents” for electrolytes, which are used in electrical capacitors. Bentonite has also been used as an excipient for the polymer batteries [44]. In the literature it is possible

to find information about some tests on the effectiveness of bentonite for improvement of electrical grounding materials [45]. There is also a research conducted on the effectiveness of mixture of bentonite with some chemicals such as Na_2SO_4, Na_2CO_3, $MgSO_4$ and $MgCO_3$ as grounding material improvement [46]. Lim et al. [47] conducted a study in order to find out why certain properties of bentonite make it highly applicable as grounding material improvement, and also some critical issues of using bentonite for that. Rozynek et al. studied the electric-field-induced structuring of kaolinite and halloysite particles in respect to their electrorheological response in silicone oil and in paraffin dispersions [48]. It was found that kaolinite particle dispersions have an improved electrorheological response relative to dispersions of halloysite particles.

1.6. Application of Bentonite in the Agriculture and Farming

1.6.1. Application of Bentonite in Soil Fertilization

Soil preparation in agriculture depends on the amount of clay included in it. The presence of colloidal clay increases the viscosity and elasticity of earth as well as impermeability to water and a tendency to fast dry. Impermeability to water provides slower swelling of soluble fertilizer and thus rational use of fertilizers. The main advantage of bentonite in the soil is moisture retention and a slow release of fertilising elements [49, 50]. This ensures continuity of dosing, regulates the respiration of soil, enhances the effect of heat exchange and keep longer soil temperature overnight. In other words, the bentonite in the surface layer of the earth does not allow rapidly salting and leaving nutrient components into the deeper layers. The use of bentonite is more intense in the desert areas and sandstone. The use of bentonite would result in a greater flexibility and improved strength of the field as well as better water impermeability. The presence of bentonite in the soil increases its drying and thus there is an increase in the pH of soil which is of great importance for the plants growing in such a soil. The use of bentonite was suggested for superphosphates [51] and mixed fertilizers with a super-phosphate, nitrogen and potassium hydroxide. In these fertilizer proportion of bentonite is from 0.25 to 0.5% with a pH of 7 to 9, which is mixed with 7.5 to 10% of fertilizers.

1.6.2. Bentonite as a Basis for the Preparation of Insecticides and Fungicides

Insecticide or fungicide should be toxic to insects, fungi or mold of plants, but should not poses a danger to all plants. In particular, should not be a danger to the leaves (branches). Application of clays and clay minerals in pesticide formulations is currently attracting considerable interest. To increase pesticide efficiency that reversible binding of the pesticide on clay minerals has been suggested. For proper use of insecticides and fungicides in the form of emulsions is necessary to add larger amounts of substrate. One of the substances that can effectively meet this task is bentonite. It is inert, and has no detrimental effect on the branches and can build nutritive elements to the insects. Having in mind that the bentonite with the oil builds a solid emulsion and solutions with water, it may be prepared for various fungicides as well.

Recently, research attention is increasingly focused in the development of controlled release formulations, because of the leaching of herbicides through soil can be minimized in this way. Perez et al. [52] incorporated the insecticide-nematicide carbofuran in alginate-

based granules to obtain controlled-release properties. The basic formulation was modified by addition of natural and acid-treated bentonite (0.5 and 1.0 mol/dm^3 H_2SO_4). Alginate-bentonite controlled release formulations might be efficient systems for reducing carbofuran leaching in clay soils, which would reduce the risk of groundwater pollution. Bentonite and anthracite have been used as modifying agents in alginate-based controlled release formulations prepared with chloridazon and metribuzin [53]. These controlled release formulations have been evaluated in a calcareous soil. The obtained results have shown that the use of controlled release formulations reduces the presence of herbicides in the leachate compared to technical products, mainly for chloridazon. Also, it found that one could design a right profile in the release rate of active ingredients from controlled release formulations in each agro-environmental situation. In this way can prevent the environmental pollution that derived from the use of chloridazon and metribuzin.

The use of particle film technologies is one of the approaches to suppress arthropod pests of crops [54]. In the literature there are data on the application of kaolin particle films in a number of different crops (mainly fruit) against a range of different pests [55, 56]. The material is chemically inert over a wide pH range, and therefore has no direct toxicity to animals or plants. In this case, kaolin is used as an aqueous suspension which is sprayed onto the crop, forming a white particle film between the pest and its host plant. This hampers insect movement in plants, prevents the feeding and other physical activities of insect. Abd El-Aziz [57] in his work tried to explore the efficacy of particle films of kaolin and bentonite clay in laboratory and field experiments against onion thrips, *Thrips tabaci* on onion plants. He concluded that kaolin had the strongest effect and significantly suppressed feeding and had the least leaf damage compared with bentonite particle films, in laboratory evaluation. Kazemi et al. [58] tested the calcium bentonite as toxin binder for decreasing the probably deleterious effects of phosalone on rumen degradability of dry matter. During this experiment they examined the effects of the different levels (0, 0.7, 2.8 and 5.6 mg) of phosalone as an insecticide with different levels of calcium bentonite (0 and 100 mg) on the in vitro dry matter disappearance.

1.7. Bentonite in the Food Industry

Fruit and vegetable storage technologies available today consume a lot of electricity and generate more pollutants. However, recently more and more attention is paid to the design of equipment that should be a low cost technology, eco-friendly, affordable and easy to handle. Al-Arfaj et al. were focused on bentonite clay pyramid for storing household fruits and vegetables [59]. They used two storage systems like refrigerator and room temperature as control. The efficiency of the bentonite clay pyramid is estimated by determining the physiological loss of weight, heterotrophic microbial count and organoleptic quality for the stored products such as bitter guard, chilly and orange. From the result obtained it may be concluded that the clay pyramid storage system is a more effective method than storage room and refrigerated storage. Therefore, this pyramid could be used as a best eco-friendly, electricity free, zero cost mechanisms.

Thanks to its adsorption properties, bentonite has been applied in clarification of alcoholic and non-alcoholic beverages, oil bleaching and esterification reactions. In addition to gelatin, casein and albumin, bentonite is used as clarification agent for red and white wines

[60-63]. In this case, clarification shall be made by binding protein from wines on the bentonite. However, through electrostatical interaction it may bind anthocyanins [60]. In order to improve the clarification effect of clay, Li et al. used a combination of bentonite and chitosan for clarification of apple juices [64]. In addition, a bentonite clay as the adsorbent may be used for soybean oil bleaching [65] and cotton oil to produce edible oil products [66]. Interest is the use of bentonite as a catalyst in esterification reactions. Jeenpadiphat and Tungasmita [67] have exerted the esterification of oleic acid in palm oil using the acid-activated bentonite. During this process, the acid-activated bentonite exhibited the best catalytic activity. In addition, despite the use for food products in literature can be found some information about the implementation of nanocomposites based on clay minerals in the food packaging industry [68].

1.8. The Use of Bentonite in the Textile Industry

The textile industry has been required to develop new methods and technologies through introduction of some new materials in various processes. Gashti et al. [69] developed a method that provides a simple and practical solution for improving the dyeability of cotton with direct and basic dyes. During the experiment, the fibers were dyed with basic and direct dyes after the nanoclay pre-treatment. In this case, the nanoclay was used as received. Based on obtained results, it was concluded that the basic dyes showed a higher dyeability on the clay pre-treated samples compared to raw materials.

Various methods have been developed for modifying the surface of textile fibers in order to improve their dyeability with natural dyes [70, 71]. However, sometimes these methods may cause some physical, chemical, and mechanical damage to the textile fibers. The use of nanoclays was mainly directed towards the dye removal from textile effluent because of their favorable ion exchange ability, followed by π-electron interactions and hydrogen bonding with dyes [72]. A coating of nanoclay on cotton could reduce its flammability, thermal degradation, and wrinklability in comparison with untreated cotton [73]. Gashti et al. [74] have shown that the nanoclay may be useful for the natural dyeing of wool both from the economic and from the environmental point of view. During the dyeing of textiles using a bentonite gel, acids and electrolytes get in thickened mixes which are used as an acid dyestuff [75]. The water content, in this case, is much higher than when the mineral composition is used. This feature is very important for the rapid diffusion of color over the fabric and getting quality paint. The mixtures were inert, with no odor and do not damage the material. After use and a long drying, bentonite restores its colloidal properties, which means it is easy to remove by washing.

In paints, as a base are generally used oil emulsions. Bentonite, due to its large specific surface area and adsorption capacity increases emulsion stability, and thus extends the shelf life of product. For example, the stability of the flax oil paint is increased by addition of bentonite, and disabled by the separation of pigment (barium sulphate) from the oil. These bentonite emulsions, due to the ability to absorb water by bentonite, reduce the water permeability which results in a greater protection of objects from corrosion. Also, in the paint industry, the bentonite is used as a tanning agent for the dye.

The cotton fabric can be coated with flame retardant intumescent formulations containing bentonite nanoclay. In this way the thermal stability of cotton fabric is increased after 300 °C [76].

1.9. Application Bentonite in the Production of Detergents

In the literature one can find a number of publications in which the washing mechanisms have been studied, as well as those parameters which are of interest for washing process [77]. From a scientific point of view, the detergent should possess good emulsifying ability, the ability to suspend contaminants and to exert a protective colloid effect.The ability of dispersion and deflocculation are important parameters during the washing process, but also a significant surface and interfacial adsorption layer. The presence of alkaline earth metal ions or polyvalent cations Ca^{2+} and Mg^{2+} has a negative effect on the ability of washing surfactants. Adsorption of polyvalent cations reduces the electrical potential which makes it difficult to remove impurities and facilitates its re-entry to the substrate fabrics. Clay binds alkaline earth metals, and it is itself negatively charged so that the negative potential increases and thereby increases the effect of washing. Clay can replace polyphosphates in laundry detergents. Clay does not allow agglomeration of the impurity particles by reducing the Van der Walls's force of attraction that exists between them. Also, clay does not allow return of the impurities from the washing solution on the material. Bentonite was mixed with the surfactants used in ecological detergents. So, detergents with bentonite are characterized by valuable benefits such as:

- Large contact area.
- The formation of abundant and light foam.
- The ability to facilitate the dissolution of detergent, to penetrate well into the fibers, and to absorb the impurity.
- The ability to soften hard water through ion exchange [78].
- Clay allows the integration of fatty substances, creating a stable suspension in the solution.
- Underwear after washing, softer and longer retains the freshness [79, 80].

Fite and Javier [81] attempted to apply ecological surfactants to attain improvement of the softness of cotton fabric during the washing process. To achieve this goal microparticules sodium bentonite was added to the detergent formulations.

1.10. The Use of Bentonite in Environment Protection

Bentonite adsorption mechanism is mainly based on their surface or ionic charge. As a rule, the edges of bentonite are the positively charged and surface at these locations can enable negatively charged ions adsorption (SO_4^{-2}, Cl^-, HCO_3^-). It is carried out on the adsorption of positively charged ions (Ca^{2+}, Mg^{2+}, Fe^{2+}, Mn^{2+}). In acidic environments bentonite behaves as a hydrophilic colloid with a negative charge.

Contamination of the environment, especially water resources is often the result of uncontrolled and irrational discharges of toxic substances from various industrial facilities in the immediate area. Among them the heavy metal cations can be found as well. The main sources of these metals are mining, metallurgical, chemical manufacturing, tannery, battery manufacturing industries, fossil fuels, etc. The modern chemical industry is based largely on catalysts, out of which many are metals or metal compounds. Also production of plastics, such as polyvinyl chloride, involves the use of metal compounds, particularly as heat stabilizers [82]. These heavy metal bearing wastewaters are of considerable concern because they are non-biodegradable, highly toxic and probably carcinogen [83]. However, despite the law, the recommendations and guidelines on drinking water quality, often the cations of heavy metals found in concentrations are above permissible levels.

Some of the conventional techniques for removal of these metals from industrial wastewater include chemical precipitation, adsorption, solvent extraction, membrane separation, ion exchange, electrolytic techniques, coagulation/flotation, sedimentation, filtration, membrane process, biological process and chemical reaction. During the adsorption process the most commonly used adsorbents are: granulated activated Carbon, fly ash, peat, recycled alum sludge, peanut hulls, resins, kaolinite, manganese oxides, zeolite, and biomaterials. However, as one of the important properties of clay is adsorption and ability to interact with metal ions, that can be used as another way of removing heavy metal ions and treatment of industrial and drinking water. The metal cations interact with the clay and adsorption is carried out on account of ion exchange and precipitation of the hydroxide on the surface of the clay. Also, the clay contains organic matter that can form complexes with metals from the surrounding medium. The pH value of the environment is one of the critical factors in determining the interaction of the natural clay, and heavy metal ions.

Cantavong et al. [84] during their study investigated the adsorption characteristics of clay in Thailand, for the removal of ions Cd (II), Cr (III), Cu (II), Ni (II), Pb (II) and Zn (II) in the form of nitrates. Based on the obtained results the adsorption of metal ions from solution by the individual success of the removal took place in the following order: Pb> Cr> Cd> Zn> Cu> Ni. Orumvens [85] studied the removal of lead ions from water by adsorption on kaolinite (clay from Nigeria). During this experiment the effect of time (0-120 min), concentrations (5, 10, and 75 mg/dm^3), pH (3 to 9.5) and temperature (30, 40, and 50 °C) on the adsorption capacity of the clay was examined. The results showed that the adsorption capacity of the clay to remove lead increases with increasing solution temperature. The maximum adsorption capacity of lead of 6.457 mg/g was achieved at 50 °C. Adsorption of lead is reduced from 93% to 82% with the increase of the pH value of the solution. Also, it was found that the presence of negative charge on the silicon surface of the adsorbent is responsible for the adsorption of lead. Naseem and Tahir [86] investigated the removal of lead from aqueous and acidic solutions by using bentonite as an adsorbent. The maximum adsorption of Pb (II) (more than 96%) was obtained in aqueous solution under optimum conditions for 10 min, whereas 86% of the adsorbed Pb (II) is obtained by using bentonite in an acidic medium (1×10^{-5} mol/dm^3 HCl required 0.5 g of bentonite). Adsorption decreases when the concentration of the electrolyte increases. Savic et al. [87] optimized the adsorption of Fe(III) from water using response surface methodology and artificial neural network. In this process, bentonite clay served as an adsorbent. After determination of adsorbed Fe (III) from water, it was found that bentonite clay is an efficient adsorbent for the removal of Fe (III) ions.

In the textile industry many colors and their degradation products are cancerogenic, mutagenic or toxic for organism [88]. Methylene blue is dark blue dye that can be found in wastewater. Having in mind the mentioned side effects, methylene blue has become the subject of strict legal regulations. The most efficient and cost effective procedure for maximal removal of methylene blue from aqueous medium is adsorption. The different adsorbents such as activated carbons [89, 90] and natural zeolite [91] were used for adsorption of methylene blue from aqueous solutions. Husein et al, [92] defined the level of porosity and adsorption properties of bentonite clay during adsorption process of methylene blue.

Serious environmental problems arise from the use of pesticides. To reduce pesticide leaching into the environment like air and water, one of the feasible solutions is reversible binding of the pesticide on clay minerals. Many studies have been focused on adsorption of pesticides by clay minerals for their removal from water [93, 94].

1.11. Biomedical Application of Bentonite

1.11.1. Application Bentonite in Pharmacy and Cosmetics

Clays play an important role in medicine [95]. Clay therapy is based on the ability of clays and clay minerals to adsorb and retain harmful and toxic substances. Because of their properties as a high specific area and sorptive capacity, rheological properties, chemical inertness and low or null toxicity for the patient, clay and clay minerals are extensively used in the formulation of various pharmaceutical and cosmetic products [96]. The therapeutic properties of clay come from its complex chemical composition and those are antitoxicity, antiseptic properties, bacteriocidity, anti-inflammatory properties, absorption, and demineralization [97].

In pharmaceutical formulations, they are used as active substance orally administered (osmotic oral laxative, antidiarrehoeaics, gastrointestinal protectors) or administered topically (dermatological protectors, cosmetics) and as excipients (lubricants, delivery systems, inert bases, emulsifiers) [98]. In recent times, bentonite clay has once again been gaining popularity. When taken correctly, it can help for providing minerals for the body, calming to skin itching from eczema, psoriasis, chicken pox, etc and to speed healing, digestive disturbances like acid reflux, constipation, bloating and gas, internal and external detoxification. Also, bentonite clay can be used as a compress to help soothe wounds, cuts, muscle damage, bruises and pain associated with carpel tunnel. Bentonite and other healing clays have being used internally to help reduce radiation exposure, in alternative cancer treatments, and in infections.

Clay minerals are often used in a variety of commercial beauty products, because of the emulsion stabilizing [99] and binding properties. In cosmetic products clay has an ability to stabilize oil-in-water emulsions at low concentrations, increasing internal phase viscosity to inhibit coalescence. Also in cosmetics, bentonite has many advantages as suspending agents. The colloidal structure of bentonite clay provides excellent suspension of fine particles in aqueous systems. Its high yield value enables the successful suspension of even high-density particulates. Clay minerals are used in the form of creams, powders and emulsions. Also, they can be applied as antiperspirants to give the skin opacity, remove shine and cover blemishes. Having in mind that during the perspiration sodium, cloro, potassium and urea can activate the metabolic change and the excretion of catabolites, their use is eliminated by using

bentonite. Application of these formulations for treatment of blemishes, cellulite, eczema and wrinkles is very important [98]. In some beauty products clay minerals are used as a treatment for dark circles under the eyes. Because of its ability to draw toxins from the epidermis and dirt from the pores, clay minerals are active principles in face mask. The face masks are recommended for inflammatory processes such as boils, acne, ulcers. Also bentonite massage creams have an ability to open the skin pores and facilitate the penetration of active ingredients. As abrasive, bentonite may be incorporated in the toothpaste compositions [100]. Its concentration in the toothpaste is in the range of from 5 to 40% in weight. Recently, a new formulation of powders, depilatories, blush, among other components must contain bentonite. Skin is constantly assaulted by sun exposure and terrestrial solar ultraviolet radiation is a major factor deleterious to our health. The most reliable approach to sun protection is to cover up the skin by using a thin film of a topical sunscreen formulation. Adequate optical properties of bentonite clay enabled the development of new sunscreen formulations. Bhatt et al. have observed a diffusive and an oscillatory light transport in the aqueous bentonite colloids [101]. It is observed that the oscillatory behaviour is not visible above 55% volume concentration of bentonite. *Movahedi et al.* introduced a novel sun lotion with considerable UV absorption properties compared to commercially available sunscreens [102]. This formulation, containing bentonite and zeolite minerals, was capable of absorbing the highest level of UV light compared to that of the commercially available sun lotion.

The interaction of clay with biomolecules, polymers and the cells oriented in the direction of the biomaterial design and regenerative medicine. Hydrogels are of great interest in the biomedical engineering field because of their similarity to soft tissues. However, the low mechanical strength of hydrogels often limits their practical applications. In order to improve the mechanical strength of hydrogels with implications for tissue engineering and regenerative strategies clay nanoparticles were used as either fillers or cross-linkers to strengthen the polymer network [103].

1.11.2. Application Bentonite in Spas and Aesthetic Medicine

Due to appropriate properties such as absorption/adsorption capacity, high cation exchange capacity, plastic properties, rheological properties, grain size and cooling index, clay minerals have become useful in spas, geotherapy, pelotherapy and paramuds [98]. The mixture of clays and water in geotherapy is directly applied upon the skin to treat dermatological diseases and to alleviate the pain caused by chronic rheumatic inflammations and sport traumatism. A mixture of minero-medicinal water with clay minerals (peloids) in the pelotherapy have a stimulatory, antiphlogistic, analgesic action and are indicated for chronic rheumatic processes, degenerative osteoarthrosis in any part of the body, dysendocrine arthropathies, spondilo-arthritis ankylopoietic, spondylosis, myalgias, nueralgias, etc. In aesthetic medicine, peloids are used for the same purposes as geotherapy. Paramuds are a mixture of paraffin and clay minerals. They are used to moisturise the skin and act as anti-inflammatory [104]. They are also used in aesthetic medicine to treat compact lipodystrophies in their initial state.

1.12. New Field of Mineral Clay: Organ Clay and Nanocomposite Clay

In recent years, the interest in clays has increased dramatically due to its composition and structure which can be easily modified to serve different purposes. Largely due to structural flexibility and its small particle size, clay nanostructure can be modified to tune rheological and mechanical properties.

Modified clays can be divided into pillared layered clays, organoclays, nanocomposites, acid- and salt-induced [105], as well as thermally and mechanically induced modified clays [106]. When treated with acid, bentonite has great ionic adsorption capacity. Thus, it can be used as adsorbent in catalyst, bleaching earth for adsorbing impurities from edible and industrial oils, and also in the preparations of organoclay, and nanocomposites. Today, organic treatment of clay caused an explosive interest in a class of materials called polymer-clay nanocomposites.

A relatively easy method of modifying the clay surface, making it more compatible with an organic matrix, is ion exchange [107]. The cations are not strongly bound to the clay surface, so small molecule cations can replace the cations present in the clay. Isomorphic substitution leads to the decrease of positive charge in layers, compensated by interlayer exchangeable cations such as Na^+, Ca^{2+}, K^+, Mg^{2+}. In the ion exchange reaction interlayer cations can be replaced with various organic cations [108]. Often in that purpose is used the ammonium surfactants. The surfactants usually contain short aliphatic chains, benzyl or hydroxyl groups, as well as the long aliphatic chain (C 12-C 18), which causes the expansion of distance between the layers [109]. Other clay modifiers include alkyl amines [110], alkyl carbazol, poly(dimethylsiloxane) and quinolinium or pyridinium [111]. Other ammonium surfactants are more complex molecules [112, 113], oligomers [114, 115] and reactive groups [116]. The substitution of exchangeable metal organic ammonium cations drastically change the surface properties of clay. The results of this are organoclays which unlike the natural are a highly effective sorbent.

The studies of intercalation of organic molecules into the interlayer space of clay minerals started in the 1920s [117]. This leads to the development of new materials with a predefined structure and performance. Nanocomposite polymer–clay represents a combination of structural, physical and chemical properties of both clay and polymer, where one component has nanometric dimensions.

Organoclay today has found wide application in chemical, cosmetics, petrochemical industry, medicine and environmental protection. It is very effective sorbent of organic contaminants from the environment [118]. Especially important is the application organoclay in wastewater treatment in textile industry [119]. The textile dyes and their degradation products are extremely toxic to the environment. Zapata et al. developed silica/clay organo-heterostructures to promote polyethylene-clay nanocomposites by *in situ* polymerization [120]. Sodium montmorillonite clay was modified with three different unnatural amino acids in order to design intercalated clay structures that may be used for bone biomaterials applications [121]. Nikolic et al. [117] was prepared a new class of functional composites based on the polymerically modificated montmorillonite and methacrylic acid. Poly(ethylenimine) with a molecular weight of 60000 was used for montmorillonite clay particle modifications. The purpose of this modification of the clay was to improve its thermal properties. Stojiljkovic et al. organically modified bentonite clay using the monomer ethenyl acetate. The exchange of inorganic intralayer cations of the clay was achieved using a

cationic surfactant (Genamine CTAC). Organoclay modified in this way was incorporated in Luviskol, Carbopole and purine. The adsorptive properties of the obtained composites of organoclays were investigated along with their capability for removing toxic Pb^{2+} from water in charged systems [122]. Thanks to its high specific surface, charge, the existance of a high number of macro, micro and submicro pores in the structure of the composite, as well as a high number of active centers on its surface, the material shows good adsorptive characteristics towards Pb^{2+} ions, which was confirmed by the decrease of the value of the electrical conductivity. The efficiency of clays modifies many different properties of the polymer, such as sorbancy, ion exchange capabilities and thermal and solvent resistance. They give improved mechanical properties and accelerated diffusion of oxygen, which is important for the packaging industry. To reduce costs and improve the comprehensive water absorbing properties of superabsorbent materials based on acrylic monomers, grafting acrylic monomers onto clay and fabricating a composite consisting of a polymer and clay is a priority. Organically modified clays are proposed as a good option for removal of oil from produced water [123-125]. The adsorption for some organic pollutants using bentonite organoclay has been studied [125]. Recently, Abdelwahab [126] was reported the modified bentonite is an excellent alternative in the adsorption of hydrocarbon from oil-water emulsion removal with the highest adsorption capacity (48 mg/g at 2 g/dm^3). Additionally, interest in the synthesis of polymer-clay nanocomposites in tissue engineering is growing as it is cheap, easily available, and environmentally friendly [127]. The structure of clay allows the interclaysion of different biomolecules between the clay layers. These biomolecules can be released in a controlled manner which can be utilised in drug delivery and cosmetic applications.

CONCLUSION

The use of clays in various fields is well known due to their vast abundance, low cost, low impact from both the environmental protection and resource savings point of view, effective recycling and other particular properties mentioned above. Because of its excellent swelling capacity and sedimentation volume, bentonite in purified form could be used as suspending and disintegrating agent. The high cation exchange capacity, high surface area and pore size distribution suggest their use as a good adsorbent. The promising potential of nanoclays offers novel perspectives for a wide use in building materials, ceramics, paper coatings, pharmaceuticals, ion exchangers, separators, paints, plastics, pesticides and cosmetics. Increasing attention has been recently given to novel nanocomposites of clay mineral with biomaterials, including vitamins, drugs, and DNA strands for possible future developments in cosmetics, pharmaceutics, and medicine as well as information storage.

ACKNOWLEDGMENTS

The support from the Marie Curie FP7-ITN "ENERGY-SMARTOPS", Contract No: PITN-GA-2010-264940, the Erasmus Mundus Action II EUROWEB Project and the Ministry

of Education, Science and Technological Development of the Republic of Serbia under the project TR-34012 is gratefully acknowledged.

REFERENCES

[1] Guggenheim, S. & Martin, R. T. (1995). Definition of clay and clay mineral: joint report of the aipea nomenclature and cms nomenclature committees. *Clay. Clay Miner*., *43(2)*, 255-256.

[2] Ni, J., Lin, J., Wei, R., Yang, H. & Yang, Y. (2013). Does the Distribution of Polycyclic Aromatic Hydrocarbons in Soil Particle-Size Separates Affect Their Dissipation During Phytoremediation of Contaminated Soils?. In *Functions of Natural Organic Matter in Changing Environment*, Springer, Netherlands, pp. 669-672.

[3] Rao, K. S. (2013). Strategic use of soil in war operations: the role of dispersion flocculation thixtrophy and plasticity of clay. *Defence Sci. J.*, *1(2)*, 192-204.

[4] Saba, S., Delage, P., Lenoir, N., Cui, Y. J., Tang, A. M. & Barnichon, J. D. (2014). Further insight into the microstructure of compacted bentonite–sand mixture. *Eng. Geol.*, *168*, 141-148.

[5] Uddin, F. (2008). Clays, Nanoclays, and Montmorillonite Minerals, Metall. *Mater. Trans. A*, *39A*, 2804-2814.

[6] Parvinzadeh, M., Moradin, S., Rashidi A. & Yazdanshenas, M. E. (2010). Ultrasonic assisted finishing of cotton with nonionic softener. *Polym. Plast. Technol. Eng.*, *49*, 874-884.

[7] Hajiraissi, R. & Parvinzadeh, M. (2011). Preparation of polybutylene terephthalate/silica nanocomposites by melt compounding: Evaluation of surface properties. *Appl. Surf. Sci.*, *257*, 8443-8450.

[8] Parvinzadeh Gashti, M. & Eslami, S. (2012). Structural, optical and electromagnetic properties of aluminum–clay nanocomposites. *Superlattices Microstruct.*, *51*, 135-148.

[9] Hosterman, J. W. & Patterson, S. H. (1992). Bentonite and Fuller's earth resources of the United States. U.S. Geological Survey Professional Paper 1522. United States Government Printing Office, Washington D.C., USA.

[10] Grim, R. & Guven, N. (1978). Bentonite: Geology, Mineralogy, Properties *and* Uses. *Elsevier Science Publishing Co., Inc., New York.*

[11] Bergaya, F. & Lagaly, G. (2000). General introduction: clays, clay minerals and clay science. Bergaya, F., Theng, B. K. G. & Lagaly, G. (Eds.), Handbook of Clay Science. Elsevier, Amsterdam, pp. 1–18.

[12] Carrado, K. A., Decarreau, A., Petit, S., Bergaya, F. & Lagaly, G. (2006). Synthetic clay minerals and purification of natural clays. Bergaya, F., Theng, B. K. G. & Lagaly, G. (Eds.), Handbook of Clay Science, Elsevier, Amsterdam, pp. 115–139.

[13] Abdou M. I. & Ahmed H. E.-S. (2011). The Compatibility of Egyptian Bentonite during Drilling Shale Formations. *Petrol. Sci. Technol*., *29(1)*, 59-68.

[14] Gates, W. P., Anderson, J. S., Raven, M. D. & Churchman, G. J. (2002). Mineralogy of a bentonite from Miles, Queensland, Australia and characterisation of its acid activation products. *App. Clay Sci*., *20(4–5)*, 189–197.

[15] *Gleason, M. H., Daniel, D. E. & Eykholt G. R.* (1997). Calcium and sodium bentonite for hydraulic containment applications. *J. Geotech. Geoenviron., 123*, 438-445.
[16] Mitchell, J. K. (1993). Fundamentals of soil behavior, 2nd Ed., John Wiley & Sons, New York.
[17] Brindley, G. W. & Brown, G. (1980). Crystal structures of clay minerals and their X-ray identification. London, Mineralogical Society.
[18] Shen, Y. H. (2001). Preparations of organobentonite using nonionic surfactants. *Chemosphere, 44(5)*, 989-995.
[19] Villar, M. V. & Lloret, A. (2004). Influence of temperature on the hydro-mechanical behaviour of a compacted bentonite. *Appl. Clay Sci., 26*, 337-350.
[20] Safa Ozcan, A. & Ozcan, A. (2004). Adsorption of acid dyes from aqueous solutions onto acid-activated bentonite. *J. Colloid Interf. Sci., 276*, 39-46.
[21] Onal, M. & Sarıkaya, Y. (2007). Preparation and characterization of acid-activated bentonite powders. *Powder Technol., 172*, 14-18.
[22] Croker, J., Poss, R., Hartmann, C. & Bhuthorndharaj, S. (2004). Effects of recycled bentonite addition on soil properties, plant growth and nutrient uptake in a tropical sandy soil. *Plant Soil, 267*, 155-163.
[23] Wang, S. W., Dong, Y. H., He, M. L., Chen, L. & Yu, X. J. (2009). Characterization of GMZ bentonite and its application in *the* adsorption of Pb(II) from aqueous solutions. *Appl. Clay Sci, 43*, 164-171.
[24] Al-Qunaibit, M. H., Mekhemer, W. K. & Zaghloul, A. A. (2005). The adsorption of Cu(II) ions on bentonite- *a* kinetic study. *J. Colloid Interf. Sci., 283*, 316-321.
[25] Velde, B. (1995). Composition and mineralogy of clay minerals, in Velde, B., ed., Origin and mineralogy of clays. New York, Springer-Verlag, p. 8-42.
[26] Garzon, E., Sanchez-Soto, P. J. & Romero, E. (2010). Physical and geotechnical properties of clay phyllites. *Appl. Clay Sci., 48(3)*, 307–318.
[27] Koch, D. (2002). Bentonites as a basic material for technical base liners and site encapsulation cut-off walls. *Appl. Clay Sci., 21(1–2)*, 1–11.
[28] Bagchi, A. (2004). Design of landfills and integrated solid waste management. 3rd edition, John Wiley and Sons Inc., pp 400.
[29] Jayasekera, S. (2007). Long term effects of landfill leachate on volume change and hydraulic conductivity properties of expansive clays. Proceedings of the Sri Lankan geotechnical society's first international conference on soil & rock engineering, 5-11 August 2007, Colombo, Sri Lanka.
[30] Puma, S., Marchese, F., Dominijanni, A. & Manassero, M. (2013). Reuse of MSWI bottom ash mixed with natural sodium bentonite as landfill cover material. *Waste Manag. Res., 31(6)*, 577-584.
[31] Roberts, A. A. & Shimaoka, T. (2008). Analytical study on the suitability of using bentonite coated gravel as a landfill liner material. *Waste Manag., 28(12)*, 2635–2644.
[32] Fan, R., Du, Y., Liu, S. & Chen, Z. (2013). Engineering behavior and sedimentation behavior of lead contaminated soil-bentonite vertical cutoff wall backfills. *J. Cent. South Univ., 20(8)*, 2255-2262.
[33] Soucy, E. (2013). Cement-Bentonite Cut Off Walls: A Comparison of the Hebron and Hibernia Bund Wall. *Proto-Type*, 1.

[34] Lv, S. Q. & Zhao, Y. S. (2013). The effect of metal ions with different valences on the retardation of soil–bentonite barrier materials and its mechanism. *Chinese Chem. Lett., 24(12)*, 1075–1079.

[35] Abdou, M. I., Al-sabagh, A. M. & Dardir, M. M. (2013). Evaluation of Egyptian bentonite and nano-bentonite as drilling mud. *Egyptian J. Petrol., 22(1)*, 53–59.

[36] Mengpeng, C., Zhang, W., Sun, P. & Huang. L. (2013). The Use of bentonite mud in the MTBM of the rock areas. In *ICPTT 2012@ sBetter Pipeline Infrastructure for a Better Life*, pp. 1665-1672.

[37] Scalia, J., Benson, I., Bohnhoff, C., Edil, G. & Shackelford, T. (2013). Long-term hydraulic conductivity of a bentonite-polymer composite permeated with aggressive inorganic solutions. *J. Geotech. Geoenviron. Eng., in press*.

[38] Bohnhoff, G. L., Shackelford, C. D., & Sample-Lord, K. M. (2013). calcium-resistant membrane behavior of polymerized bentonite. *J. Geotech. Geoenviron. Eng.*, DOI: org/10.1061/(ASCE)GT.1943-5606.0001042.

[39] Cruz, N., Peng, Y., Farrokhpay, S. & Bradshaw, D. (2013). Interactions of clay minerals in copper–gold flotation: Part 1 – Rheological properties of clay mineral suspensions in the presence of flotation reagents. *Miner. Eng., 50–51*, 30–37.

[40] Forbes, E., Davey, K. J. & Smith, L. (2014). Decoupling rehology and slime coatings effect on the natural flotability of chalcopyrite in a clay-rich flotation pulp. *Miner. Eng., 56*, 136–144.

[41] Farid, M. M., Khudhair, A. M., Ali, S., Razack, K. & Al-Hallaj, S. (2004). A review on phase change energy storage: materials and applications. *Energ. Convers. Manage., 45*, 1597–1615.

[42] Lim, S. C., Gomes, C. & Kadir, M. Z. A. A. (2013). preliminary grounding performance of bentonite mixed concrete encased steel cage under high soil resistivity condition. *Int. J. Elec. Power, 47*, 117-128.

[43] Li, M., Wu, Z., Kao, H., & Tan, J. (2011). Experimental investigation of preparation and thermal performances of paraffin/bentonite composite phase change material. *Energ. Convers. Manage., 52(11)*, 3275-3281.

[44] Aradilla, D., Estrany, F., Casellas, F., Iribarren, J. I. & Aleman, C. (2014). All-polythiophene rechargeable batteries. *Org. Electron., 15(1)*, 40–46.

[45] Tu, Y. P., He, J. L. & Zeng, R. (2006). Lightning impulse performances of grounding devices covered with low-resistivity materials. *IEEE Transactions on Power Delivery, 21*, 1706-1713.

[46] Al-Ammar, E., Khan, Y., Malik, N. & Wani, N. (2010). Development of low resistivity material for grounding resistance reduction. *IEEE Int.Energy Conf. and Exhibition* 700-703.

[47] Lim, S. C., Gomes, C. & Kadir, M. Z. A. A. (2013). Characterizing of bentonite with chemical, physical and electrical perspectives for improvement of electrical grounding systems. *Int. J. Electrochem. Sci., 8*, 11429 – 11447.

[48] Rozynek, Z., Zacher, T., Janek, M., Caplovicova, M., Fossum, J. O. (2013). Electric-field-induced structuring and rheological properties of kaolinite and halloysite. *Appl. Clay Sci., 77–78*, 1–9.

[49] Tian, L., Liu, J., Guo, X., Li, L. & Liu, X. (2013). Effects of water saving materials on soil physical characters and maize yield in loess plateau. *Adv. J. Food Sci. Technol., 5(2)*, 186-191.

[50] Pateiro-Moure, M., Novoa-Munoz, J. C., Arias-Estévez, M., Lopez-Periago, E., Martinez-Carballo, E. & Simal-Gandara, J. (2009). Quaternary herbicides retention by the amendment of acid soils with a bentonite-based waste from wineries. *J. Hazar. Mater*., *164(2–3)*, 769–775.

[51] Xiaoyu, N., Yuejin, W., Zhengyan, W., Lin, W., Guannan, Q. & Lixiang, Y. (2013). A novel slow-release urea fertiliser: Physical and chemical analysis of its structure and study of its release mechanism. *Biosyst. Eng*., *115(3)*, 274–282.

[52] Fernandez-Perez, M., Villafranca-Sanchez, M., Gonzalez-Pradas, E., Martinez-Lopez, F. & Flores-Cespedes, F. (2000). Controlled release of carbofuran from an alginate−bentonite formulation: water release kinetics and soil mobility. *J. Agric. Food Chem*., *48(3)*, 938–943.

[53] Flores Cespedes, F., Perez Garcia, S., Villafranca Sanchez, M. & Fernandez Perez, M. (2013). Bentonite and anthracite in alginate-based controlled release formulations to reduce leaching of chloridazon and metribuzin in a calcareous soil. *Chemosphere*, *92(8)*, 918–924.

[54] Glenn, D. M., Puterka, G. J., Vanderzwet, T., Byers, R. E. & Feldhake, C. (1999). Hydrophobic particle films: A new paradigm for suppression of arthropod pests and plant diseases. *J. Econ. Entomol*., *92*, 759-771.

[55] Abd El-Aziz, Sh, E. (2003a). Kaolin & Bentonite clays particle films as a new trend for suppression of chewing and sucking insects of cotton plants. *Arab. Univ. J. Agric. Sci*., *11(1)*, 373-385.

[56] Abd El-Aziz, Sh, E. (2003b). Evaluation of particle films as a physical control method for controlling melon ladybird, Epilachna chrysomelina (F.) (Coleoptera: Coccinellidae) on cantaloupe plants. *Bull. Ent. Soc. Egypt*, *29*, 21-34.

[57] Abd El-Aziz, Sh. E. (2013). Laboratory and field Evaluation of Kaolin and Bentonite particle films against onion thrips, Thrips tabaci (Lind.) (Thysanoptera : Thripidae) on onion plants. *J. Appl. Sci. Res*., *9(4)*, 3141-3145.

[58] Kazemi, M., Tahmasbi, A. M., Valizadeh, R., Naserian, A. A., Vakili, A. R. & Sonei, A. (2012). Poisonous effects of phosalone as an insecticide on rumen degradability of dry matter according to *in situ* technique. *Int. J. Agr. Inn. Res*., *1(3)*, 71-74.

[59] Al-Arfaj, A. A., Murugan, A. M., Chinnathambi, A. & Al-Hazmi, M. I. (2013). Cost-effective bentonite clayed pyramid technologies for household fruits and vegetables storage. *J. Food Agr. Environ*., *11(2)*, 175-180.

[60] Diblan, S. & Ozkan, M. (2013). Effects of various clarification agents on the anthocyanins of red wines. *GIDA - J. Food*, *38(1)*, 47-54.

[61] Kaur, M., Sharma, H. K., Patil, S. & Shitandi, A. (2013). Optimization of ethanol concentration, glycerol concentration and temperature conditions of grape-mahua wine to maximize the quality and overall acceptability. *J. Microbiol. Biotechnol. Food Sci*.,*2(6)*, 2426-2430.

[62] Lira, E., Salazar, F. N., Rodriguez-Bencomo, J. J., Vincenzi, S., Curioni, A. & Lopez, F. (2013). Effect of using bentonite during fermentation on protein stabilisation and sensory properties of white wine. *Inter. J. Food Sci. & Technol.*, DOI: 10.1111/ijfs.12402

[63] Lambri, M., Dordoni, R., Giribaldi, M., Violetta, M. R. & Giuffrida, M. G. (2012). Heat-unstable protein removal by different bentonite labels in white wines. *LWT-Food Sci. Technol.*, *46(2)*, 460-467.

[64] Li, Z. X., Wang, G. M. & Liang, Q. (2013). Preparation and properties of the novel adsorbent agent for juices clarification. *Adv. Mater. Res.*, *791*, 248-251.

[65] Foletto, E. L., Paz, D. S. & Gundel, A. (2013). Acid-activation assisted by microwave of a Brazilian bentonite and its activity in the bleaching of soybean oil. *Appl. Clay Sci.*, *83–84*, 63–67.

[66] Lacin, O., Sayan, E. & Kirali, E. G. (2013). Optimization of acid-activated bentonites on bleaching of cotton oil. *J. Chem. Soc. Pak*, *35(4)*, 1053-1059.

[67] Jeenpadiphat, S. & Tungasmita, D. N. (2014). Esterification of oleic acid and high acid content palm oil over an acid-activated bentonite catalyst. *Appl. Clay Sci.*, *87*, 272-277.

[68] Rodriguez, F. J., Torres, A., Penaloza, A., Sepulveda, H., Galotto, M. J., Guarda, A. & Bruna, J. (2013). Development of an antimicrobial material based on a nanocomposite cellulose acetate film for active food packaging. *Food Addit. Contam. Part A, in press.*

[69] Gashti, M. P., Rashidian, R., Almasian, A. & Zohouri, A. B. (2013). A novel method for colouration of cotton using clay nano-adsorbent treatment. *Pigm. Resin Technol.*, *42(3)*, 175-185.

[70] Parvinzadeh, M. & Ebrahimi, I. (2011). Influence of atmospheric-air plasma on coating of nonionic lubricating agent on polyester fiber. *Radiat. Effects Defects Solids*, *166*, 408-416.

[71] Parvinzadeh, M. & Ebrahimi, I. (2011). Atmospheric air-plasma treatment of polyethylene terephthalate fiber to improve the performance of nanoemulsion silicone. *Appl. Surf. Sci.*, *257*, 4062-4068.

[72] Bujdak, J. (2006). Effect of the layer charge of clay minerals on optical properties of organic dyes. A review. *Appl. Clay Sci.*, 34, 58-73.

[73] Yuen, C. W. M., Kan, C. W. & Lee, H. L. (2006). Improving wrinkle resistance of cotton fabric by montmorillonite, *Fibers Polym.*, *7*, 139-145.

[74] Parvinzadeh Gashti, M., Katozian, B., Shaver, M. & Kiumarsi, A. (2014). Clay nanoadsorbent as an environmentally friendly substitute for mordants in the natural dyeing of carpet piles. *Color. Technol.*, *130(1)*, 54-61.

[75] Stojiljkovic, S. (2003). The power of clay. Faculty of Technology, University of Nis, Serbia.

[76] Nehra, S., Dahiya, J. B. & Kumar, S. (2013). Effect of nanoclays on thermal and flame retardant properties of intumescent coated cotton fabric. *Asian J. Res. Chem.*, *6(7)*, 676-682.

[77] Ersoy, O. G., Kaya, M., Birci, E., Ersoy Akova, A. & Ulger, Z. (2013). European Patent No. EP 1999308. Munich, Germany.

[78] Jha, A. K., Jha, A. K., Mishra, A. K., Kumari, V. & Mishra, B. (2011). Softening of hard water by bentonite mineral. *Asian J. Water, Environ. Pol.*, *8(4)*, 93-96.

[79] Feng-LG, H. (2011). Aqueous detergent composition containing ethoxylated fatty acid di-ester. European Patent No. EP 1753853.

[80] Reyes, A. (2011). European Patent No. EP 2360233. Munich, Germany.

[81] Fite, C. & Javier, F. (2009). The effect of bentonite microparticles in the washing of cotton fabric. "9th World Textile Conference AUTEX 2009". Cesme-Izmir, 1180-1186.

[82] Atieh, M. A. (2011). Removal of zinc from water using modified and non-modified carbon nanofibers, *2nd International Conference on Environmental Science and Technology IPCBEE*, Singapore, Vol. 6, pp. V1-220 - V1-223,

[83] Dermentzis, K., Christoforidis, A. & Valsamidou, E. (2011). Removal of nickel, copper, zinc and chromium from synthetic and industrial wastewater by electrocoagulation. *Int. J. Environ. Sci., 1*, 697-710.

[84] Chantawong, V., Harvey, N. W. & Bashkin, V. N. (2003). Comparison of heavy metal adsorptions by Thai kaolin and ballclay. *Water, Air, and Soil Poll., 148(1-4)*, 111-125.

[85] Orumwense, F. F. (1996). Removal of lead from water by adsorption on a kaolinitic clay. *J. Chem. Technol. Biot., 65(4)*, 363-369.

[86] Naseem, R. & Tahir, S. S. (2001). Removal of Pb (II) from aqueous/acidic solutions by using bentonite as an adsorbent. *Water Res., 35(16)*, 3982-3986.

[87] Savic, I. M., Stojiljkovic, S. T., Stojanovic, S. B. & Moder, K. (2012). Modeling and optimization of Fe (III) adsorption from water using bentonite clay: Comparison of central composite design and artificial neural network. *Chem. Eng. Technol., 35(11)*, 2007-2014.

[88] Mathur, N., Bhatnagar, P. & Bakre, P. (2006). Assessing mutagenicity of textile dyes from Pali(Rajasthan) using Ames bioassay. *Appl. Ecol. Environ. Res., 4(1)*, 111-118.

[89] Hassan, A. F., Abdel-Mohsen, A. M. & Fouda, M. M. (2014). Comparative study of calcium alginate, activated carbon, and their composite beads on methylene blue adsorption. *Carbohyd. Polym., 102*, 192-198.

[90] Pezoti Junior, O., Cazetta, A. L., Gomes, R. C., Barizao, E. O., Souza, I. P., Martins, A. C., Asefa, T. & Almeida, V. C. (2014). Synthesis of $ZnCl_2$-activated carbon from macadamia nut endocarp (*Macadamia integrifolia*) by microwave-assisted pyrolysis: Optimization using RSM and methylene blue adsorption, *J. Anal. Appl. Pyrol., 105*, 166-170.

[91] Han, R., Wang, Y., Zou, W., Wang, Y. & Shi, J. (2007). Comparison of linear and nonlinear analysis in estimating the Thomas model parameters for methylene blue adsorption onto natural zeolite in fixed-bed column. *J. Hazard. Mater., 145*, 331-335.

[92] Hussein, H., Khudhaier, H., Al-Khafaji, N., Hadi, H. & Ali, H. (2007). Study of the adsorption of methylene blue from aqueous solution: a comparison between iraqi & english bentonite activity as adsorbents. *J. Kerbala Univ., 5*, 1-16.

[93] Donia, A. M., Atia, A. A., Hussien, R. A. & Rashad, R. T. (2012). Comparative study on the adsorption of malathion pesticide by different adsorbents from aqueous solution. *Desalin. Water Treat., 47(1-3)*, 300-309.

[94] Chevillard, A., Angellier-Coussy, H., Peyron, S., Gontard, N. & Gastaldi, E. (2012). Investigating ethofumesate–clay interactions for pesticide controlled release. *Soil Sci. Soc. Am. J., 76(2)*, 420-431.

[95] Mukherjee, S. (2013). Clays for Medicines and Fillers. In *The Science of Clays*, Springer, Netherlands, pp. 151-158.

[96] Lopez-Galindo, A., Viseras, C. & Cerezo, P. (2007). Compositional, technical and safety specifications of clays to be used as pharmaceutical and cosmetic products. *Appl. Clay Sci., 36*, 51–63.

[97] Fratzl, P. & Weinkamer, R. (2007). Nature's hierarchical materials. *Prog. Mater. Sci., 52*, 1263-1334.

[98] Isabel Carretero, M. (2002). Clay minerals and their beneficial effects upon human health. A review. *Appl. Clay Sci., 21*, 155 – 163.

[99] Ray, S. S. & Okamoto, M. (2003). Polymer/layered silicate nanocomposites: a review from preparation to processing. *Prog. Polym. Sci., 28*, 1539–1641.

[100] Shira, P., Masters, J. & Sullivan, R. (2012). Anti-erosion toothpaste composition. U.S. Patent No. 20,120,251,466.

[101] Bhatt, H., Baladhia, J. & Patel, R. (2013). Diffusive light transmission in bentonite colloids. *J. Optics*, 1-5.

[102] Movahedi, M. M., Alipour, A., Mortazavi, S. A. R. & Tayebi, M. (2013). production of a novel mineral-based sun lotion for protecting the skin from biohazards of electromagnetic radiation in the UV region. *J. Biomed. Physics Eng.*, *3(4)*, 1-4.

[103] Wu, C. J., Gaharwar, A. K., Schexnailder, P. J. & Schmidt, G. (2010). Development of biomedical polymer-silicate nanocomposites: a materials science perspective. *Materials*, *3(5)*, 2986-3005.

[104] Choy, J. H., Choi, S. J., Oh, J. M. & Park, T. (2007). Clay minerals and layered double hydroxides for novel biological applications. *Appl. Clay Sci.*, *36(1)*, 122-132.

[105] Vlasova, M., Dominguez-Patino, G., Kakozey, N., Dominguez-Patino, M., Juarez-Romero, D. & Enriquez-Mendez, Y. (2003). Structural-phase transformations in bentonite after acid treatment. *Sci. Sinter*., *35*, 155-166.

[106] Basak, B. B., Pal, S. & Datta, S. C. (2012). Use of modified clays for retention and supply of water and nutrients. *Curr. Sci. India*., *102(9)*, 1272-1278.

[107] Greesh, N., Hartmann, P. C., Cloete, V. & Sanderson**,** R. D. (2008). Adsorption of 2-acrylamido-2-methyl-1-propanesulfonic acid (AMPS) and related compounds onto montmorillonite clay. *J. Colloid Interf. Sci*., *319(1)*, 2-11.

[108] Grim, R. E. (1968). Clay Minerology, 2nd ed., McGraw-Hill, New York.

[109] Carastan, D. & Demarquette, N. (2006). Microstructure of nanocomposites of styrenic polymers. *Macromol. Symposia*, *233*, 152-160.

[110] Li, Y. & Ishida, H. (2005). A study of morphology and intercalation kinetics of polystyrene-organoclay nanocomposites. *Macromolecules*, *38*, 6513-6519.

[111] Chigwada, C., Wang, D. & Wilkie, C. (2006). Polystyrene nanocomposites based on quinolinium and pyridinium surfactants. *Polym. Degrad. Stabil*., *91*, 848-855.

[112] Yao, H., Zhu, J., Morgan, A. & Wilkie, C. (2002). Crown ether-modified clays and their polystyrene nanocomposites. *J. Appl. Polymer Sci*., *86*, 2492-2501.

[113] Yei, D., Kuo, S., Fu, H. & Chang, F. (2005). Enhanced thermal properties of PS nanocomposites formed from MMT treated with a surfactant/cyclodextrin inclusion complex. *Polymer*, *46*, 741-750.

[114] Chen, K. & Vyazovkin, S. (2006). Mechanistic differences in degradation of polystyrene and polystyrene-clay nanocomposite: thermal and thermo-oxidative degradation. *Macromol. Chem. Phys*., *207*, 587-595.

[115] Lagaly, G. & Ziesmer, S. (2005). Surface modification of bentonites. iii. sol-gel transitions of Na-montmorillonite in the presence of trimethylammonium-end capped poly(ethylene oxides). *Clay Miner*., *40*, 523-536.

[116] Bourbigot, S., Vanderhart, D., Gilman, J., Awad, W., Davis, R., Morgan, A. & Wilkie, C. (2003). Investigation of nanodispersion in polystyrene–montmorillonite nanocomposites by solid-state NMR. *J. Polym. Sci. Polym. Phys*., *41*, 3188–3213.

[117] Nikolic, Lj., Ristic, I., Stojiljkovic, S., Vukovic, Z., Stojiljkovic, D., Nikolic, V. & Budinski-Simendic, J. (2012). The influence of montmorillonite modification on the properties of composite material based on poly(methacrylic acid). *J. Compos. Mater*., *46(8)*, 921-928.

[118] Chaari, I., Medhioub, M. & Jamoussi, F. (2011). Use of clay to remove heavy metals from Jebel Chakir landfill leachate. *J. Appl. Sci. Environ. Sanitation*, *6(2)*, 143-148.

[119] Tahir, S. S. & Rauf, N. (2006). Removal of a cationic dye from aqueous solutions by adsorption onto betonite clay. *Chemosphere*, *63*, 697-702.

[120] Zapata, P. A., Belver, C., Quijada, R., Aranda, P. & Ruiz-Hitzky, E. (2013). Silica/clay organo-heterostructures to promote polyethylene–clay nanocomposites by *in situ* polymerization. *Appl. Catal. A: General*, *453*, 142–150.

[121] Katti, K., Ambre, A. H., Peterka, N. & Katti, D. R. (2010). Use of unnatural amino acids for design of novel organomodified clays as components of nanocomposite biomaterials. *Phil. Trans. R. Soc. A*, *368*, 1963–1980.

[122] Stojiljkovic, S., Stamenkovic, M., Kostic, D., Miljkovic, M., Arsic, B., Savic, I., Savic, I. & Miljkovic, V. (2013). The influence of organic modification on the structural and adsorptive properties of bentonite clay and its application for the removal of lead. *Sci. Sinter.*, *45*, 363-376.

[123] Oliveira, G. C., Mota, M. F., Silva, M. M., Rodrigues, M. G. F. & Laborde, H. M. (2012). Performance of natural sodium clay treated with ammonium salt in the separation of emulsion oil in water. *Braz. J. Petrol. Gas*, *6(4)*, 171–183.

[124] Mowla, D., Karimi, G. & Salehi, K. (2013). Modeling of adsorption breakthrough behaviors of oil from salty waters in a fixed bed of commercial organoclay/sand mixture. *Chem. Eng. J.*, 218, 116–125.

[125] Masooleh, M. S., Bazgir, S., Tamizifar, M. & Nemati, A. (2010). Adsorption of petroleum hydrocarbons on organoclay. *J. Appl. Chem. Res*., *4(14)*, 19–23.

[126] Abdelwahab, E. (2013). Modified activated carbon and bentonite used to adsorb petroleum hydrocarbons emulsified in aqueous solution. *Am. J. Environ. Protect*., *2(6)*, 161-169.

[127] Chrzanowski, W., Kim, S. Y. & Neel, E. A. A. (2013). Biomedical applications of clay. *Aust. J. Chem.*, *66(11)*, 1315-1322.

In: Clays and Clay Minerals
Editor: Liam R. Wesley
ISBN: 978-1-63117-779-8

Chapter 16

SOME APPLICATIONS OF CLAYS IN RADIOACTIVE WASTE MANAGEMENT

Hosam El-Din M. Saleh*
Radioisotope Department, Nuclear Research Center,
Atomic Energy Authority, Dokki, Giza, Egypt

ABSTRACT

Clay as inorganic material present naturally is considered as additional mater for immobilization and containment of radioactive wastes. The use of natural clays as an additive to facilitate the incorporation of organic radioactive wastes seems to be an acceptable route to counteract the retarding effect of these hazardous wastes and to obtain a well-standing structural stable monolith. The waste form composite has to optimally comply with the advised requirements of chemical, physical and mechanical characterizations for the safe long-term disposal even at very exaggerating conditions. Radioactive waste generated from the nuclear applications should be properly isolated by a suitable containment such as, multi-barrier systems. Multi-barrier technology is a promising method for keeping the radioactive waste safe against the flooding events and keeping the radiation dose in the permissible level during the transportation and long-term disposing processes.

The capacity of a multi-barrier system including economical material and other additives such as clays and clay minerals to isolate radioactive wastes is an important point for study.

INTRODUCTION

Clays and clay minerals are considered as an important topic in applied sciences. These materials occur in weathering crusts and soils, continental and marine sediments, volcanic deposits, geothermal fields, altered wallrock produced by the intrusion of plutonic rocks and hydrothermal fluids, and very low grade metamorphic rocks [1].

* E-mail address: hosamsaleh70@yahoo.com

Clays and clay minerals as in situ lithologic components and engineered barriers are characterized by favorable properties from the viewpoint of radioactive waste emplacement. Their high sorptivity, longevity, and low permeability make them promising candidates for retaining most natural and anthropogenic long-lived radionuclides within the contaminated and engineered disposal sites [2].

The utilization of clay minerals in controlling radionuclide concentrations in waste effluents or their use as engineered barriers in disposal sites of radioactive wastes is widely accepted due to their natural availability in large quantities, their relatively good sorption properties, their low permeability and their stability compared to organic exchangers. Sorption processes of various radionuclides onto natural soils and clay minerals have been studied by several authors [3].

Natural clays achieve equilibrium with the local groundwater to ensure that their permeability remains relatively constant. When used in the disturbed zone of a disposal facility, engineered and imported clays have not achieved this equilibrium and their permeability may be modified by the evolving chemistry of the disturbed zone. Examples of mechanisms that may change the permeability include dimensional changes in the clay lattice induced by ion replacement. Both local clays from the site and engineered clays (bentonite – crushed limestone) have been used to provide barriers to groundwater infiltration. The extensive use of grout suggests that the clay may be affected by an alkaline aqueous phase. The indigenous clay showed no degradation in performance. The permeability is variable for the clay samples used (6.4×10^{-8} – 4.1×10^{-10} m/s), but remains unchanged when treated with an alkaline solution. The engineered clay shows an increase in permeability from 1×10^{-11} m/s to 6×10^{-11} m/s, but its performance remains superior to the natural clay. It was concluded, therefore, that these clay barriers would remain intact despite the perturbed chemistry of the disturbed zone [4].

Clays could be used in nuclear waste packages, composite with solidified waste forms and backfills as well as additive barrier during long-term storage and disposal.

1. CLAYS IN MULTI-BARRIER SYSTEMS FOR ISOLATION OF NUCLEAR WASTES

1.1. Isolation of High-Level Radioactive Waste [5]

Deep disposing is required for high-level radioactive waste encapsulated in metal containers since it can give off radionuclides that can migrate through groundwater for long-term disposal. An important matter is if a repository has to be constructed in virgin rock or if deep mines can be adapted to become repositories.

Multi-barriers in contaminants are very important to prevent or at least retard migration of waste from the disposal site.

Barriers in the form of metal containers (canisters, casks) and clay are proposed for creating multi-barrier systems (Figure 1). High-level radioactive waste (HLW) that represents the most hazardous waste because of the double effect of gamma radiation and release of radionuclides have to isolate from the environment.

Crystalline, argillaceous, and salt rock are host rock candidates depending on the geological conditions in the respective countries. Argillaceous rock like clay shale is very tight but the physical stability of underground rooms at depth is commonly rather poor. Salt rock contains fluid water in local brine lenses and undergoes strong time-dependent strain that can make it difficult to localize and retrieve waste containers after a few hundred years if this is required [5].

1.2. Isolation of Nuclear Fuel As a Waste Product [6]

Spent nuclear fuel is removed from a reactor as a radioactive waste product and requires careful management. Although its radioactivity decreases with time, chemical toxicity persists and the used fuel will remain a potential health risk for many hundreds of thousands of years.

A series of engineered and natural barriers will used together to contain and isolate used nuclear fuel from the biosphere. Each of these barriers provides a unique and stand-alone level of protection; if any of the barriers deteriorate, the next one will come into play.

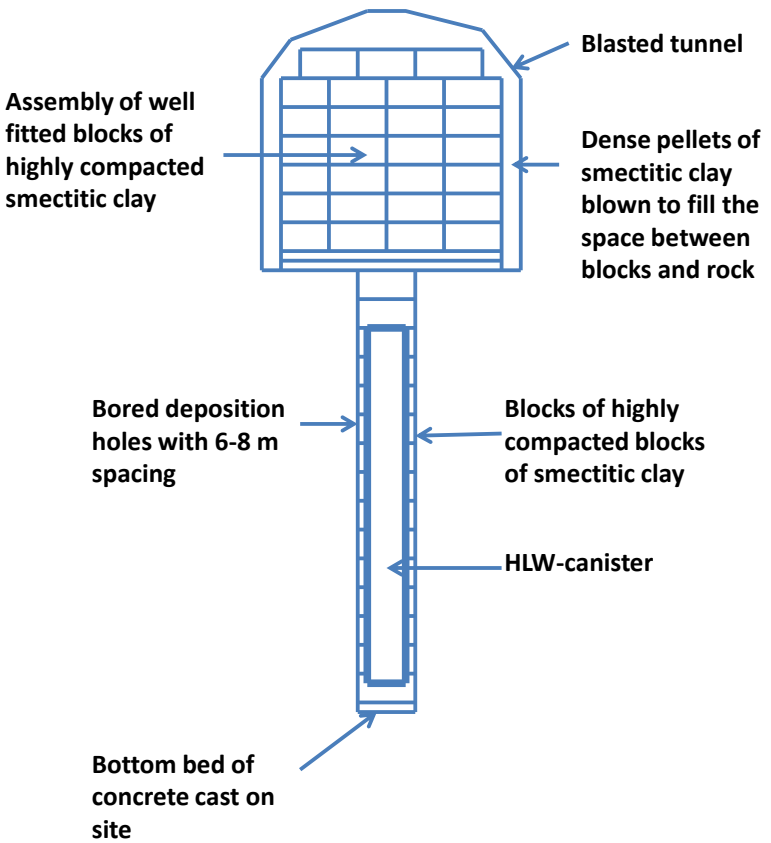

Figure 1. Isolation of HLW. The tunnels have height and width of about 5 m. The diameter of the 8 m deep deposition holes is 1.9 m. The canisters have a length of about 5 m and a diameter of about 1 m (Source: Pusch et al., 2012).

Natural barriers such as bentonite clay were used as backfill and sealants. After the used nuclear fuel containers are placed in the repository, all open spaces in each underground chamber will be filled with engineered materials designed to minimize any seeping of water through the repository.

During placement, each used nuclear fuel container will be surrounded by compacted bentonite clay (Figure 2), a natural material proven to be a powerful barrier to water flow. Bentonite swells when exposed to water, making an excellent sealing material. Bentonite is also very stable, typically formed millions to hundreds of millions of years ago.

As placement rooms are filled with containers, the open spaces will be filled with engineered materials – backfill and sealants made from mixtures of clay, sand and rock to minimize the flow of water. Once completely filled, placement rooms will be sealed with bulkheads of special, high performance concrete. Although very unlikely, if a used nuclear fuel container did fail, the chemical properties of the bentonite clay, backfill and sealants would make it difficult for radionuclides to travel, greatly slowing their release.

Before closing the repository, all tunnels and shafts will be filled with similar backfill and sealants, isolating the repository from the biosphere [6].

Bentonite clay is a very stable material formed naturally from volcanic ash released millions of years ago.

Bentonite is widely used as a sealant and an absorbent.

Figure 2. Bentonite clay as present in nature or processed as sealant or absorbent.

(Source: Nuclear Waste Management Organization, 2010).

1.3. Natural Clay in Liquid Radioactive Wastes Treatment [7]

Nuclear industry generates considerable amounts of liquid wastes that require advanced treatment. Evaporation, precipitation, ion exchange, or adsorption on clay surface may be used to concentrate wastes for further treatment or disposal.

Many natural mineral compounds, such as clays (e.g., bentonite, kaolinite and illite), vermiculite and zeolites (e.g., analcite, chabazite, sodalite and clinoptilolite), exhibit ion exchange properties. Natural zeolites were the first materials to be used in ion exchange processes. Clay materials are often employed as backfill or buffer materials for radioactive waste disposal sites because of their ion exchange properties, low permeability and easy workability. Clays can also be used in batch ion exchange processes but are not generally suited to column operation because their physical properties restrict the flow through the bed. Treatment of real salt-containing low-level radioactive waste. The efficiency of sorption

recovery of Cs and Sr radionuclides with finely dispersed mineral sorbents under static conditions was investigated in relation to the sorption time, pH, size of mineral granules, sorbent amount, salt content and chemical composition of solutions, and number of successive sorption steps. It was found that the studied natural sorbents can decrease the activity of treatment of the real salt-containing waste by 2–3 orders of magnitude owing to recovery of Cs and Sr. In another study, the utilization of Romanian modified clays for the treatment of radioactive liquid waste containing UO_2 ions was assessed. It was found that the adsorption of UO_2 ions from aqueous solution depended on the concentration of uranium in simulated wastewater, on contact time and on the ratio of sorbent/solution value and that the sorption process was spontaneous and endothermic. The previous study by Abdel Rahman et al. concluded that Romanian modified clays could be used for the treatment of radioactive liquid waste containing UO_2 [7].

2. CLAYS AS COMPOSITE MATERIAL WITH CEMENT FOR IMMOBILIZATION OF NUCLEAR WASTES

Composite of cement and clay is candidate to solidify/stabilize the organic spent liquid scintillator wastes. This composite should fulfill the mechanical, thermal, physical, structural, etc. requirements needed for the subsequent transportation and disposal processes specified by the Nuclear Regulatory Commission (NRC) [8]. The use of natural clay as an additive to facilitate the incorporation of real spent liquid scintillator seem to be an acceptable route to counter act upon the retarding effect of the organic waste and to obtain a well standing structural stable monolith. The temperature changes during the cement hydration and solidification of the nuclear waste revealed that the final waste form did not suffer any thermal stress and no cracklings were visually detected. Furthermore, visual inspection of the four-drop test showed a slight deformation in the rounded edge of the specimen other than the impacted edge. Consequently, the proposed cement-clay composite exhibited good structural durability even in case of immobilizing 15% liquid scintillator by the weight of the composite under unexpected transportation events [9].

Previous studies showed that presence of additives such as kaolin in the cemented waste form reduces leach rates during long-term disposal and conserves the mechanical strength with the safety requirements [10-11]. Clay minerals are beneficial to cement reactions, while organic matter may be deleterious when exposure occurs after cement hydration [12]. The organic deterioration effect could be minimized by using organophilic clays as pre-solidification adsorption additive [13]. Calcium hydroxide, lime, produced during the hydration of Portland cement can react with silicate and aluminate of the clay soil and results in more coating gel materials. Presence of organic matter can hinder the formation of that gel by immobilizing the Ca^{+2} [14].

The novelty is studying the immobilization of the hazardous organic wastes in very cheap material, cement, while the retarding effect of that waste was overcame by adding the natural clay.

Recently, an extensive array of leaching studies has been addressed to reduce the leachability of different radionuclides from immobilized waste matrices processed by mixing the cement with various materials having a significant sorption capacity such as clay [15].

These additives were utilized either to enhance the compressive strength of the grout mixture or to increase its resistivity to leaching of radiocontaminants [16].

For long-term storage and disposal processes, immobilization should be an irreversible process, which avoids a back release of radiocontaminants from the matrix during aggressive conditions of storage and disposal [17-18].

A key property of any waste form is its leaching resistance, which determines how well the radionuclides of concern are retained within the waste form in a wet environment. Estimating the rate of leaching from a matrix during disposal is a key consideration in assessing the immobilization method. Low matrix solubility means reduced likelihood of radionuclide release. The leaching behavior of cemented radioactive waste form is important to ultimately ensure the overall safety of a storage/disposal system. Dedicated experiments are carried out to identify leaching behavior of cemented waste form and to demonstrate their acceptance for storage and disposal [19-20].

Local natural clays present in Egypt have been investigated to determine their efficiency as cement admixture material and to evaluate the effect of their addition on the leaching behavior of the immobilized waste matrix. Leaching tests data for solidified waste form including 15% actual liquid scintillator waste with different concentrations of natural clay immersed in groundwater were recorded at different time intervals and represented in Figure 3.

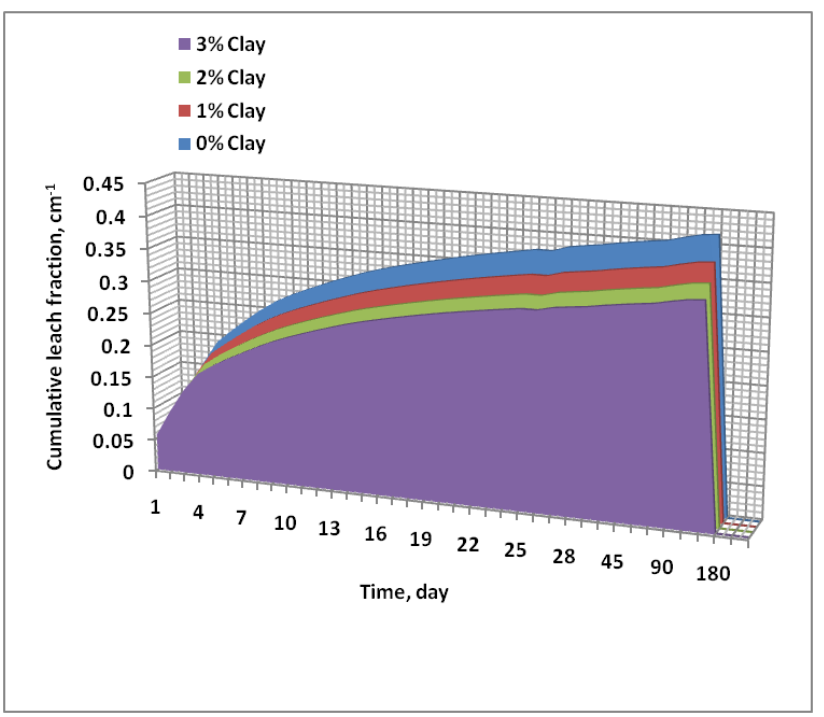

Figure 3. Radioactivity leached from the solidified waste form including 15% radioactive spent liquid scintillator waste containing different ratios of natural clay at water/cement ratio of 0.3 and leached in groundwater.

Moreover, diffusion coefficient (De) values were calculated and represented in Table 1. It is worth mentioning that the diffusion coefficient values were generally ranged from 10^{-5} cm^2/s for very mobile species to 10^{-15} cm^2/s for immobile species [21].

It could be notified from the data represented in Table 1 that De values were decreased with increasing the clay content mixed with the cemented waste form. Due to the mechanical characterization studied and reported in the literatures previously, the ratio of 3% natural clay was recommended for preparing the cement-clay composite [8]. In addition, all leaching indexes records represented in Table 1 showed values higher than the figure that is the limit specified by Nuclear Regulatory Commissions (NRC) [22].

Table 1. Diffusion coefficients and leaching indexes of the solidified waste form containing different ratios of natural clay and immobilizing 15% radioactive spent liquid scintillator waste at water/cement ratio of 0.3 and immersed in groundwater (dynamic mode)

Clay, %	Diffusion coefficient, cm^2/s	Leach index
0	2.023×10^{-11}	10.69
1	1.600×10^{-11}	10.80
2	1.270×10^{-11}	10.89
3	1.110×10^{-11}	10.95

Accordingly, the radioactive wastes were retained well within the candidate cement-clay composite as a solidified waste form [23].

The obtained results are revealing that natural clay improved the capability of Portland cement to immobilize the actual radioactive liquid scintillator waste due to its high sorptivity [24]. Cumulative fraction leached and diffusion coefficients were decreased with increasing the concentration of natural clay, up to 3%, in the solidified waste form. On the other hand, leaching index values were increased with the increase of the clay content. Based on the previously published studies, mixing of 3% clay with Portland cement has more processing value and therefore, it was the optimum ratio for the final waste form composition.

According to the data obtained from experimental results and the analyses performed under various leaching conditions, it could be recommended the usage of this composite as a solidifying agent for up to 15% organic radioactive spent liquid scintillator wastes originating from various applications of liquid scintillation. Cumulative fraction leached, diffusion coefficients and leaching indexes values as a key characteristic for leaching studies were computed during various conditions. The proposed waste form composite could optimally comply with the advised requirements for the disposal process even at very drastic conditions.

2.1. Durability of Cement-Clay Composite Containing Organic Waste Form Due to Frost Event

During the long-term disposal, very low temperature can exist; therefore, freeze/thaw (F/T) cycling test was performed to evaluate the stability and suitability of the cement–clay

composite as a matrix for incorporating liquid scintillator waste. The repeated F/T cycles have a cumulative effect rather than the single occurrence frost attacks that causes damage [25].

The final solid waste forms are required to permit sufficient strength and shape stability to meet the demands of the safe waste management regime [26].

The visual inspection of the waste form incorporating liquid scintillator does not show any cracking for all F/T cycles. There was no noticeable difference in the physical appearance of the waste form and the control specimens. This indicates that the proposed cement–clay matrix is an adequate monolith composite for solidification/stabilization of organic liquid scintillator spent wastes. Mass durability index (K_m) of the tested specimen subjected to increasing F/T cycles (up to 75 cycles) are represented in Table 2.

Table 2. Durability index (K_m) based on mass-loss % for plain cement and final waste forms subjected to 75 freezing/thawing cycles

F/T, cycles	Plain cement, %	Waste form, %	Differences
0	99.1	96.1	3
7.5	98.9	95.5	3.4
15	98.5	95.2	3.3
30	98.2	94.8	3.4
45	97.8	94.2	3.6
60	97.5	94	3.5
75	97	93.5	3.5

The results show that only a 2.6% decrease in K_m at the end of the F/T cycles (150 days). This behavior is also highly comparable to plain cement with water/cement ratio is 0.30 and subjected to the same F/T cycles intervals, where 2.1% decrease in K_m was recorded. In addition, the differences between K_m for plain cement and waste form not exceeding 3.6% even in the presence of deteriorating organic liquid scintillator in the waste form. Decrease in mass durability indices may be attributed to the deterioration that may start in the cement matrix due to the repeated freezing and thawing effect [27] and can be explained based on the following: when cured cement specimens subjected to freezing, moisture present inside pores, at −50 ^{o}C, was frozen and expands inside the hardened cement, then when the sample transport to thaw, at +60 ^{o}C leads to evaporation of that frozen water leading to empty pores and shrinkage may be occurred. The following F/T cycle repeats these actions. Furthermore, cycles of expansion and shrinkage for hardened cement pastes cause deterioration effect on cement and accordingly detectable mass-loss was distinguished.

The damage evolution of the waste form subjected to increasing F/T exposure periods has been, traditionally, assessed, by means of mechanical integrity degradation as well as the micro structural changes [28].

At the end of each F/T period, apparent porosity, volume of open pores, volume of impervious portion, water absorption, specific gravity, bulk density and compressive strength were also determined to evaluate the adequacy of cement–clay composite for solidification and stabilization of radioactive spent organic liquid scintillator wastes under frost attack. The same trend was recorded for plain cement blocks treated in similar way, under the identical temperatures and numbers of freezing/thawing cycles.

The results collectively reveal that minor decrease in compressive strength, bulk density, specific gravity, volume of impervious portion values and slight increases in apparent porosity, volume of open pores and water absorption values with the number of freezing–thawing cycles were reported. It should be notified that these changes are related to the figures obtained for waste form did not exposed to frost event.

The loss in compressive strength of the waste form did not exceed 1.6MPa after 75 cycles. It should be noted also that the control specimen lose about 5MPa due to the same freezing/thawing duration.

Cement and clay, as many porous materials, absorbs and retains moisture that makes it particularly vulnerable when exposed to repeated F/T cycles. Because of expansion, the structure suffers from internal micro cracking that leads to the low diminishing in the mechanical criteria distinguishing the waste form [29]. However, it should be mentioned that even after 75 cycles of F/T cycles at −50 ^{o}C and +60 ^{o}C, the compressive strength of the composite is still higher than that recommended by the Nuclear Regulatory Commission (NRC) for transport and disposal requirements [26].

The undetectable diminishing in all studied characters of the waste form during freeze/thaw cycles from 0 to 75 cycles indicates that the candidate cement–clay composite for immobilizing the spent liquid scintillator is agreeably to Skripkiunas et al. [30]. The very small decrease in the bulk density due to F/T cycles (from 1.566 to 1.535 g/cm^3) is accompanied with a proportional decrease in compressive strength values from 9.8 to 8.2 MPa.

It is clear from Figure 4 that a smooth increase in the apparent porosity of waste form is accompanied by a gradual decrease in compressive strength values. This approves that the slight damage evolution during freezing/thawing cycles of the composite incorporating the liquid scintillator waste involved detriments that accumulating gradually cycle by cycle.

The refinement in the pore structure of the waste form by adding clay leads to reduce permeability of the hydrated cement paste and can dispose retardation in moisture migration through cement matrix. This can induce build-up of internal hydraulic pressure that causes cracking in the composite. The pore refinement due to clay addition may also appear in the minor reduction in the mechanical integrity and the slight increase in the porosity of the cement–clay composite waste form [31]. Additional changes in cement structure can occur due to crystallization processes within pore system by adding clay as admixture [32]. The main roles of clay addition could be classified as filling materials, high pozolanity and as a surface-active agent.

According to classical frost action theories, the capillary porosity is the driving factor in frost deterioration processes [33]. In addition, Fagerlund [34] suggested that there is a critical moisture content at which each cement material will stand to deteriorate under freeze/thaw cycles. The data obtained for water absorption indicated that only an increase of about 2% in water absorption was calculated for the cement–clay composite by increasing the F/T cycles up to 75 cycles. Based on Fagerlund theory, the slight deteriorations in micro structural parameters and consequently in the mechanical integrity of the waste form subjected to F/T treatment could be discussed. Calming, similar trends were recorded for plain cement blocks (water/cement = 0.30) treated in identical way, under the same temperature and equal numbers of F/T cycles.

2.2. Stability of Cement-Clay Composite Containing Organic Waste Form Due to Flooding Effect

The data obtained from the solidified specimens immersed in water were compared to that non-immersed which prepared by the same way and cured under the same conditions and revealed that an increase in compressive strength, bulk density, specific gravity and volume of impervious portion values were recorded. On the other hand, decrease in mass loss, volume of open pores, water absorption and apparent porosity values with the increase of immersion time up to 18 months were detected.

The Nuclear Regulatory Commission (NRC), USA, recommended a minimum compressive strength of 6 MPa for the waste form to insure it remains stable under the compression load inherent in a disposal environment [26]. It is evident from the data obtained that the strength of the waste form was greater than the regulations requirement for all samples at immersion and non–immersion conditions. It is evident that the samples from the interior volume of the blocks are characterized by higher density and lower porosity, resulting in the enhanced strength.

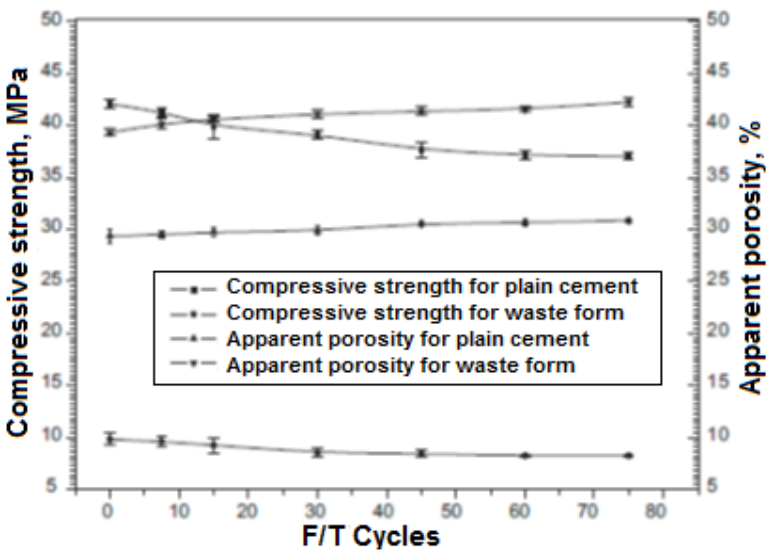

Figure 4. Apparent porosity and compressive strength for plain cement and waste form samples subjected to freezing/thawing cycles.

It could be noticed from characterization of the cement that the durability of hardened cement depends on the degree of hydration. As the hydration progressed with the increase in the curing time, the amount of hydration products was increased, which fill the pores present in the specimens leading to enhancement in the microstructural properties, especially, the porosity.

Durability of the hardened cement matrix immersed in the three types of water was higher than that of the reference sample (non–immersed) especially in case of seawater and had the sequence:

Seawater > groundwater > freshwater > non–immersed.

Elevation in the mechanical durability for the immersed samples in seawater may be due to the formation of $CaCO_3$ (calcite) as a result of the reaction of lime liberating during hydration of cement paste with CO_2 present in seawater. Calcite can act as filler for pore cement matrix and accelerate the hydration of tri-calcium aluminate (C_3A) to form calcium carboaluminate hydrates, i.e. fill up the empty pores inside the waste form, therefore, the durability of the waste form was enhanced [35]. Filling up the empty pores inside the waste form increases the strength and water resistance of the hardened cement block [36]. In addition, the formation of secondary minerals, primarily calcite, can suppress the migration of radionuclides [37], which decreases their leaching. Consumption of $Ca(OH)_2$ (lime) by the reaction with pozzolans materials, such as clay, and/or carbonation can result in greatly enhanced durability strength [38], where Portland–pozzolana cements gain strength slowly and may require curing over a comparatively long period and the long-term strength is high [25].

Migration of moisture through pore structure of the cement matrix can induce build-up of internal hydraulic pressure that causes cracking in the composite and consequently can affect negatively on the physicomechanical properties. The refinement of pore structure in the waste form by adding clay leads to reduce the permeability of the hardened cement composite and can dispose retardation in moisture migration through cement matrix so that physicomechanical properties will be enhanced [8]. Additional changes in the cement structure can occur due to crystallization processes within pore system by adding clay as admixture leading to enhancement of the physicomechanical properties [32].

REFERENCES

[1] E. Gala´n and R.E. Ferrell, Chapter 3 – Genesis of Clay Minerals, *Developments in Clay Science*, 5, 83–126 (2013).

[2] S. Y. Lee and R.W. Tank, Role of clays in the disposal of nuclear waste: A review, *Applied Clay Science* 1(1-2), 145-162. (1985).

[3] A. Zaki, M. I. Ahmad and R. O. Abdel Rahman, Evaluation of the Use of Natural Clay as a Barrier for the Retardation of Some Radionuclides, *International Journal of Environmental Engineering* Science, 2(2), 239-254 (2011).

[4] International Atomic Energy Agency, Performance of engineered barrier materials in near surface disposal facilities for radioactive waste, *IAEA-TECDOC*-1255, (2001).

[5] R. Pusch, S. Knutsson and M. H. Mohammed, Isolation of hazardous waste in crystalline, *Journal of Earth Sciences and Geotechnical Engineering*, 2(3), 57-75 (2012).

[6] Nuclear Waste Management Organization, Multiple-Barrier System, *Backgrounder* 2010, www.nwmo.ca

[7] R. O. Abdel Rahman, H. A. Ibrahium and Yung-Tse Hung, Liquid Radioactive Wastes Treatment: A Review, *Water*, 3, 551-565, (2011).

[8] S. B. Eskander, S. M. Abdel Aziz, H. El–Didamony and M. I. Sayed, Immobilization of low and Intermediate Level of Organic Radioactive Wastes in Cement Matrices. *Journal of Hazardous Materials* 190, 969–979 (2011).

[9] T. A. Bayoumi, H. M. Saleh and S. B. Eskander, Solidification of hot real radioactive liquid scintillator waste using cement-clay composite, Monatshefte fur Chemie - *Chemical Monthly*, 144(12), 1751-1758, (2013).

[10] A. M. El–Kamash, M. R. El–Naggar and M. I. El–Dessouky, Immobilization of cesium and strontium radionuclides in zeolite–cement blends. *Journal of Hazardous Materials* 136(2), 310–316 (2006).

[11] A. E. Osmanlioglu, Immobilization of radioactive waste by cementation with purified kaolin clay. *Waste Management* 22(5), 481–483 (2002).

[12] D. G. Wareham and J. R. Mackechnie, Solidification of New Zealand harbor sediments using cementitious materials. *Journal of Materials in Civil Engineering* 18(2), 311–315 (2006).

[13] D. M. Montgomery, C. J. Sollars, R. Perry, S. E. Tarling, P. Barnes and E. Henderson, Treatment of organic-contaminated industrial wastes using cement-based stabilization/ solidification-I. Microstructural analysis of cement-organic interactions. *Waste Management & Research* 9(2), 103–111 (1991).

[14] F. Hsai–Yang, Foundation Engineering Handbook, Second Edition. Sixth Printing by Kluwer Academic Publisher, USA. (2002).

[15] T. A. Bayoumi, S. M. Reda and H. M. Saleh, Assessment study for multi-barrier system used in radioactive borate waste isolation based on Monte Carlo simulations, *Applied Radiation and Isotopes* 70, 99–102. (2012).

[16] Plecas, Leaching study on the process of solidification of radionuclide 60Co in concrete. *Polish Journal of Environmental Studies* 14(5), 699–701. (2005).

[17] H. M. Saleh and S. B. Eskander, Long-term effect on the solidified degraded cellulose-based waste slurry in cement matrix. *Acta Montanistica Slovaca* 14(4), 291-297 (2009).

[18] H. M. Saleh, T. A. Bayoumi and H. A. Shatta, Mechanical and Chemical Characterizations of Polyester Modified Cement Immobilizing Nuclear Wastes. *Advances in Chemical Science* 1(1), 12-17 (2012).

[19] H. M. Saleh, M. E. Tawfik and T. A. Bayoumi, Chemical stability of seven years aged cement–PET composite waste form containing radioactive borate waste simulates. *Journal of Nuclear Materials* 411(1-3), 185-192 (2011).

[20] H. M Saleh, Treatment and Solidification of Hazardous Organic Wastes: Radioactive Cellulose-Based Wastes, Book ISBN 978-3-659-18564-9, LAP Lambert Academic Publishing, Germany. (2012).

[21] D. H. Moon and D. Dermatas, An evaluation of lead leachability from stabilized/solidified soils under modified semi-dynamic leaching conditions. *Engineering Geology* 85(1-2), 67–74 (2006).

[22] J. M. Lee, J. Whang, C. L. Kim and J. W. Park, Leachability of radionuclides from cement-solidified waste form produced at Korean nuclear power plant. Journal of Environmental Science and Health, Part A: *Toxic/Hazardous Substances and Environmental Engineering* 37(2), 201–212 (2002).

[23] Pariatamby, C. Subramaniam, S. Mizutani and H. Takatsuki, Solidification and stabilization of fly ash from mixed hazardous waste incinerator using ordinary Portland cement. *Environmental Science* 13(5), 289–296 (2006).

[24] R. O. Abdel Rahman, A. A. Zaki and A. M. El–Kamash, Modeling the long–term leaching behavior of 137Cs, 60Co, and 152,154Eu radionuclides from cement–clay matrices. *Hazardous Materials* 145(3), 372–380 (2007).

[25] A. M. Neville and J. J. Brooks, Concrete Technology, Longman Singapore Publisher (Pte), Ltd.: Singapore, 286 (1994).

[26] R. Voke, G.H. Jonsson and S. Guriven, Final waste forms for LLW/ILW/TRU mixed wastes: a comparison between BNFL and US tested requirements, in: *Proceeding of the International Topical Meeting on Nuclear and Hazardous Wastes Management*, vol. II, Spectrum, 96, August, 18–23, Seattle, WA, USA, pp. 290–296 (1996).

[27] S. B. Eskander, T. A. Bayoumi and M. E. Tawfik, Immobilization of borate waste simulate in cement–water extended polyester composite based on poly (ethylene terephthalate) waste, *Polymer-Plastics Technology and Engineering* 45, 939–945 (2006).

[28] Vegas, J. Urreta, M. Frais and R. Garcia, Freeze–thaw resistance of blended cements containing calcined paper sludge, *Construction and Building Materials* 23, 286–2868 (2009).

[29] A. S. Klemm and M. Wieloch, Multicriterim optimization approach in a design of cementitious composites with improved resistance to freezing/thawing, in: *High Performance Structures and Materials*, vol. II, WIT Press, Ancona, Italy, (2004).

[30] G. Skripkiunas, V. Sasnauskas, M. Dauksys and D. Palubinskaite, *Mater. Sci. Poland* 25 (3) 625–635 (2007).

[31] B. B. Sabir, Mechanical properties and frost resistance of silica fume concrete, *Cement and Concrete Composites* 19, 285–299 (1997).

[32] G. A. Varlakova, Z. I. Golubeva, A. S. Barinov, I. A. Sobolev and M.I. Ojovan, Properties and composition of cemented radioactive wastes extracted from the moundtype repository, *Materials Research Society Symposium Proceedings* Q05–07, 1124 (2009).

[33] Lea's, in: Hewlett (Ed.), Chemistry of Cement and Concrete, fourth ed., Butterworth–Heinemann, Oxford, UK, (2001).

[34] G. Fagerlund, Critical moisture contents at freezing of porous materials, in: Second CIB/RILEM Symposium on Moisture Problems in Buildings, Rotterdam, pp. 1–17 (1974).

[35] S. A. El–Alfi, H. Darweesh and H. El–Didamony, Addition of limestone in the low heat portland cement, *Ceramics–Silikaty*, 44, 107–111 (2000).

[36] L. G. Shpynova (ed.), Formation and Genesis of Microstructure of Concrete. *Electronic Stereomicroscopy of Concrete*, Vishcha Shkola, L'vov (1975).

[37] M. Toyohara, M. Kaneko, F. Matsumara, et al., Study on effects of hydraulic transport of ground water in cement, in: Sci. Basis for Nuclear Waste Management XXIV. *Materials Research Society Symposium Proceedings* 608, 263–283 (2000).

[38] K. P. Moravelaki, A. Bakolas, I. Koratosios and V. Kilikoglou, Hydraulic lime mortars for the restoration of historic masonry in concrete, *Cement and Concrete Research* 35, 1577–1586 (2005).

In: Clays and Clay Minerals
Editor: Liam R. Wesley
ISBN: 978-1-63117-779-8

Chapter 17

GENESIS, PROPERTIES AND INDUSTRIAL APPLICATIONS OF BAUXITIC LITHOMARGIC CLAY

A. Andrews,[1,*] S. K. Y. Gawu,[2] Zs. Momade[3] and F. W. Y. Momade[1]

[1]Department of Materials Engineering,
Kwame Nkrumah University of Science and Technology, Kumasi, Ghana
[2]Department of Geological Engineering,
Kwame Nkrumah University of Science and Technology, Kumasi, Ghana
[3]Department of Chemical Engineering,
Kwame Nkrumah University of Science and Technology, Kumasi, Ghana

ABSTRACT

Primary clays underlying Awaso lateritic bauxite deposits in southwestern Ghana, known as lithomargic clays are thought to have resulted from an indirect or incomplete bauxitization process. The physical, genetic, geochemical and mineralogical relations characterizing these clay types have been examined enabling their potential use for the production of alumino-silicate refractories and aluminium sulphate (alum). Kaolinite and gibbsite are the dominant minerals whilst accessory minerals found included goethite, rutile, biotite and muscovite with quartz conspicuously absent. The gibbsitic fraction has successfully been separated from the kaolinitic fraction using a 90 μm sieve making it possible to produce refractories of varying alumina content. Being residual, lithomargic clays of low iron content (< 1.5%) are not plastic and therefore difficult to produce refractory bodies. An improvement in the plasticity of the clay has been achieved by addition of a clay binder. This report reviews the advances made towards the industrial utilization of lithomargic clays. The effect of processing route on the structure, physical and mechanical properties as well as performance of products from lithomargic clay is discussed.

* Corresponding author email: anthonydrews@gmail.com.

1. GENESIS OF LITHOMARGIC CLAYS

Lithomargic clays constitute an important group of residual clays underlying lateritic bauxite deposits in Ghana. Lateritic bauxites are those developed over rocks other than limestone or dolomite and constitute between 84% and 75% of the world's reserves and resources [1, 2]. Two major processes have been reported to be responsible for the formation of most lateritic bauxite deposits in the tropical and subtropical regions of the world [3]. The first process involves a direct transformation of alumino-silicate source rocks through interplay of physical, chemical and biological weathering processes resulting in a residual deposit rich in aluminium. The second is an indirect process characterized by the weathering of source rocks through a clay-mineral stage, followed by, a transformation to bauxite by a further removal of alkali, alkaline earths and silica. Kesse [4] believes that all bauxite deposits in Ghana resulted from indirect bauxitization processes because lithomargic clay is always found separating the deposits from the underlying bedrock.

The existence of a clay-mineral transition zone is not sufficient to elucidate the order of events leading to the formation of these lateritic bauxite deposits. It is not certain whether clay minerals formed first and later underwent intense weathering in parts to form bauxite thereby leaving lithomarge clay below the bauxite layer or the bauxite formed directly from the alumino-silicate source rocks and later, alumina and silica recombined to form the lithomarge. Studies of weathering profile of Awaso lateritic bauxite deposit in southwestern Ghana by Gawu [5] indicate that the bauxite evolved in three stages similar to the bauxite-bearing laterite of Boknur-Navge plateau in Karnataka [6]. In stage one, phyllite was converted to lithomargic clay through the intermediate stage of altered phyllite; the conversion of lithomargic clay to ferruginous laterite accounted for the second stage and the concentration of Fe-rich, Al-rich and Al-Si-rich units occurred in stage three. Stage two is essentially characterised by the gradual changes in the contents of gibbsite and goethite until kaolinite almost completely disappears in the final part of the stage. This requires a solution with a pH above 4 and an Eh of below 0.3 mV [7]. The final stage involved the segregation into lateritic and bauxitic units as a result of the changes in the pH-Eh. It is characterised by concentration changes of gibbsite as well as of the iron minerals, since kaolinite is now almost completely leached out. The complete absence of quartz from the profiles, although present in the underlying phyllite, indicated that gibbsite was formed through the dissolution of kaolinite when the pH of the infiltrating water was above 4.2 [8]. Iron minerals were dissolved by solutions having a pH of approximately 4.2 and Eh below 0.3 mV.

Evidence for the indirect bauxitization process includes:

i) the preservation of the relict texture of the source rock in the laminated bauxite litho-unit which occurs immediately above the lithomarge;
ii) the observation under the microscope of gibbsite surrounding a central clay nucleus in some concretions. If it were a direct alteration to gibbsite, the silica to form this clay nucleus would have to pass through the gibbsite at the margin to reach the core and change the gibbsite to kaolinite. However, the gibbsite at the margin was not also resilicated to kaolinite hence partial resilication could not have been restricted to the core;

iii) the relatively high silica content of the laminated bauxite litho-unit also appears to be an incomplete leaching process and finally no evidence has been found to support the fact that the lithomarge is a resilicated product.

The weathering process can be simplified by reaction (1) as follows:

$$K_2O \cdot Al_2O_3 \cdot 6SiO_2 + H_2O + CO_2 = 2Al(OH)_3 + 6SiO_2 + K_2CO_3 \quad (1)$$

When the weathering process is via clay-mineral formation, there is an accumulation of lithomargic clay below the bauxite layer, separating it from the underlying source rock according to reaction (2).

$$K_2O \cdot Al_2O_3 \cdot 6SiO_2 + 2H_2O + CO_2 = Al_2(Si_2O_5)(OH)_4 + 4SiO_2 + K_2CO_3 \quad (2)$$

From the evidence adduced, it can be concluded that the lateritic bauxite of the Awaso deposit evolved through an indirect bauxitization process under intense tropical weathering conditions which culminated into the leaching of K, Na, Ca, Mg, and silica.

2. Physical, Chemical and Mineralogical Properties of Lithomargic Clays

The lithomargic clay, a transition zone material, which occurs at a minimum depth of about 15 meters is made up of variegated soft clays in shades of brown, white and orange yellow. The usual relict textures are commonly found in this zone. The thickness of this zone may well be over 8 meters. Eight samples taken randomly from various horizons of the clay layer showed varied colours from yellowish white to reddish brown depending on the iron oxide content of the sample [9]. Chemical analysis of the samples indicated an Al_2O_3 content of between 31-46% whilst the SiO_2 and Fe_2O_3 contents varied between 27-39 and 0.3-19%, respectively. Other measurable components include TiO_2 (1-3%), Na_2O (0.1-0.2%), and K_2O (0.4-2%). The MgO and CaO were in trace quantities, all lower than 0.05%. There seems to be a strong correlation between iron oxide content and plasticity index (PI) of lithomargic clays. Table 1 summarises the chemical composition and plasticity indices of selected lithomargic clays underlying the Awaso bauxite deposits. It could be observed that as the Fe_2O_3 content increased, the PI also increased. Generally, clays of iron oxide content less than 1.5% seem to have low PI whilst clays of iron content greater than 1.5% have relatively high PI.

Mineralogical analysis of samples using differential thermoanalyser (DTA) and x-ray diffraction (XRD) [10] showed the main minerals components as kaolinite/nacrite and gibbsite. Iron was present as goethite and titanium as rutile. Muscovite was also seen on the x-ray diffraction patterns. Figure 1 presents the x-ray diffraction patterns of low-iron grade and high-iron grade samples.

Table 1. Chemical composition and plasticity indices of selected lithomargic clays underlying the Awaso bauxite deposits

Sample ID	Sample Description	Composition, %						PI
		SiO_2	Al_2O_3	Fe_2O_3	TiO_2	K_2O	Na_2O	
A1	Whitish greasy	37.60	44.02	0.37	1.24	0.13	0.05	8.00
A2	Yellowish white	27.00	45.90	1.22	2.20	0.41	0.12	13.00
A3	Pale pinkish white	36.40	38.50	0.70	1.40	0.40	0.01	13.85
A4	Light brown	33.10	35.20	4.70	1.30	0.40	0.02	16.54
A5	Reddish brown	33.90	43.70	9.92	1.96	1.78	0.19	23.51

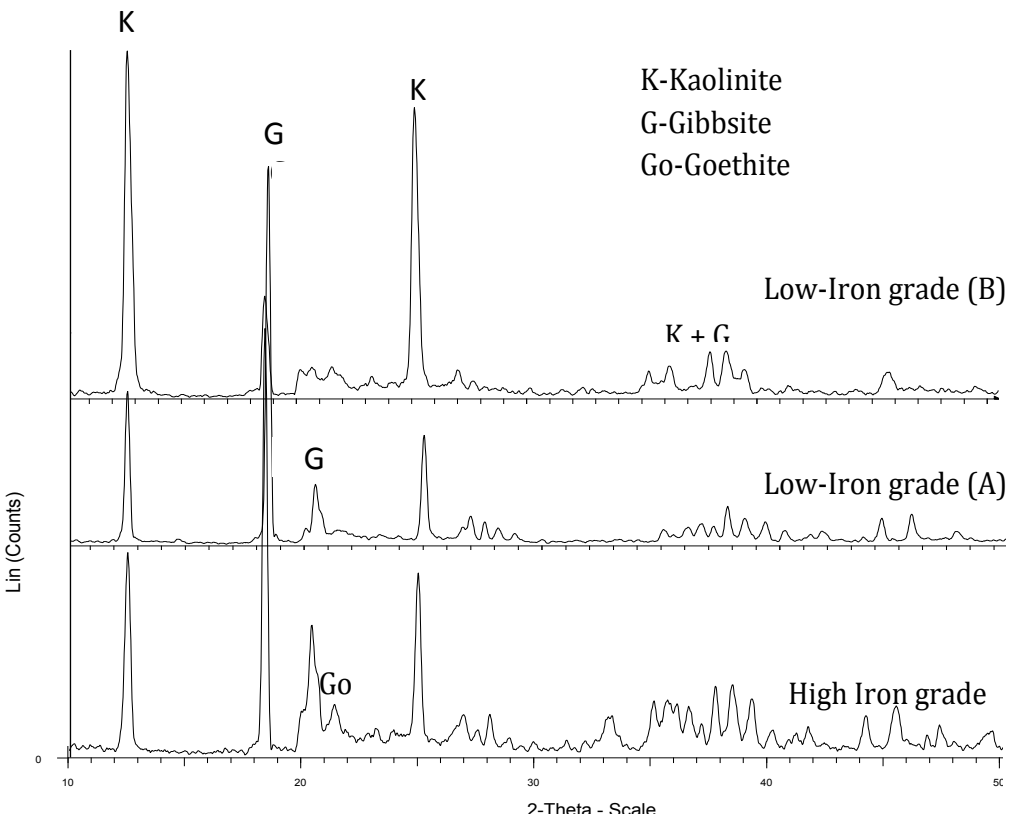

Figure 1. X-ray diffraction patterns of low-iron grade and high-iron grade lithomargic samples.

Visual observation of the bigger particles obtained during screening and washing tests indicated that, macroscopically the gibbsite particles appeared to be laminated or foliated with kaolinite existing between these foliates. The implication is that if wet screening were used as a beneficiation tool then the coarse gibbsite product could still be diluted by significant amounts of kaolinite.

3. POTENTIAL INDUSTRIAL APPLICATIONS

Based on the chemical composition, lithomargic clay can be classified into two grades, namely, the low-iron (containing less than 1.5% as Fe_2O_3) and the high-iron (containing more than 1.5% as Fe_2O_3) grades [11]. The low-iron grade has diverse range of applications in, for example, the production of aluminium sulphate (alum), aluminosilicate refractories, and anorthite bodies. It also has the potential to be used as an adsorbent in the removal of fluoride in water. With the high-iron grade, lithomargic clay can be calcined and used as pigments in paint manufacture. In this review, three areas of potential applications are considered in more detail: that is, production of aluminosilicate refractories, aluminium sulphate, and anorthite bodies.

3.1. Aluminosilicate Refractories

Refractories are fundamental materials for any high temperature operation. They are physically and chemically stable at high temperatures. Generally, the oxides of aluminium (alumina), silicon (silica) and magnesium (magnesia) are the most important materials used in the production of refractories. Aluminosilicate refractories are normally produced using refractory clays mainly composed of kaolinite clay mineral. This group of refractories can be classified as semi-alumina, fireclay and high alumina refractories depending on their alumina and silica contents [12, 13]. The fireclay subgroup is that having alumina content of between 25-45% [14, 15]. Even though new types of refractory materials have been developed, fireclay refractories are still widely used due to their ease of fabrication, resistance to chemical attack and low cost. According to the Al_2O_3–SiO_2 phase diagram [16], the fireclay subgroup occurs with eutectic point (T_e) at 5.5% Al_2O_3 and eutectic temperature of about 1595^{o}C whereas the eutectic point of high alumina refractory subgroup exists at 78% Al_2O_3 and eutectic temperature of about 1840^{o}C. Thus, the refractory quality of high-alumina is usually higher than that of fireclay bearing refractories.

Lithomargic clay has been used to produced fireclay refractories as well as high alumina refractories. The possibility to produce high alumina refractories from lithomargic clay stem from the fact that lithomargic clay can be separated into kaolinitic and gibbsitic fractions using a 90 µm sieve. This provides the option to blend the two fractions in various ratios to produce refractories of varying composition and hence varying properties for different application areas. Good combinations of properties of refractories produced from lithomargic clay have been reported [17-20]. Refractories produced from lithomargic clay could be used as low to high heat duty applications such as insulation behind hot-face materials, furnace linings, and specialty applications such as laboratory crucibles.

3.2. Aluminium Sulphate (Alum)

Aluminium sulphate is a chemical compound with the formula $Al_2 (SO_4)_3$. It is mainly used in the purification of drinking water, waste water treatment plants and also in paper production, pharmaceutical industry and textile dyeing industry. Aluminium sulphate is

sometimes referred to as alum. Alum is normally available in hydrated form as $Al_2(SO_4)_3 \cdot 18H_2O$. There are two grades of alum commercially available on the market – the technical grade and the iron-free grade. The iron-free grade contains only 0.01% Fe_2O_3 as compared to about 0.04% Fe_2O_3 in technical grade alum. The iron-free grade is used in the production of special high quality papers, dyes and pharmaceuticals.

Alum can be produced by adding aluminium hydroxide (Al $(OH)_3$), aluminium silicates (clay) or bauxite to sulphuric acid (H_2SO_4). Based on the chemical and mineralogical compositions, lithomargic clay is therefore a potential candidate for the production of technical grade of alum. Additionally, the iron content could further be reduced by the presence of gibbsite in lithomargic clay. Previous work by Gawu and Momade [9] and Momade and Sraku-Lartey [21] indicated that alum can best be produced by first calcining the lithomargic clay at 700^{o}C to break the kaolinite structure, followed by leaching with H_2SO_4. Alum crystals produced via this process compares very well in performance with commercially available alum [11].

3.3. Anorthite

Anorthite ($CaAl_2Si_2O_8$) is one of the most important members of the plagioclase feldspar family. It is a rare constituent in magmatic and metamorphic rocks. Anorthite is composed of 20.2% CaO, 36.6% Al_2O_3 and 43.2% SiO_2. Lithomargic clay can potentially be used as raw material for the production of anorthite bodies by addition of lime. Lightweight anorthite bodies can be produced by addition of combustible materials such as saw dust. The synthesis of dense anorthite ceramics are promising materials for substrate applications in electronics industry due to their good physical properties such as thermal expansion coefficient of $4.8x10^{-6}$ /K and low dielectric constant of 6.2 at 1 MHz [22]. Other application areas include supports of catalysts for the conversion of combustion gases from engines in industrial heat exchangers and from gas turbines due to their low thermal expansion coefficient, high thermal shock resistance and low dielectric constant [23]. The fluorapatite–anorthite binary system can be used as material for joint prostheses or dental roots [24, 25].

4. ADVANCES IN ALUMINOSILICATE REFRACTORIES PRODUCED FROM LITHOMARGIC CLAY

Refractories are the primary materials used by the metallurgical industry in the construction of internal linings of furnaces for melting, smelting in vessels, for holding and transporting molten metal and slag in furnaces. This is because refractories can withstand very high temperatures without physical and chemical deterioration. Aluminosilicate refractories are manufactured using refractory clays. They mainly are composed of kaolinite clay mineral ($Al_2O_3 \cdot 2SiO_2 \cdot 2H_2O$). Refractory clays are usually contaminated with limited amounts of impurity oxides, including TiO_2, Fe_2O_3, CaO, MgO and alkali oxides which act as fluxing agents at high temperatures [26]. According to the Al_2O_3–SiO_2 phase diagram [16], there exist two eutectic points at 5.5% Al_2O_3 and eutectic temperature of about 1595°C and at 78% Al_2O_3 and eutectic temperature of about 1840°C. Even though fluxing agents decrease

the eutectic temperature of aluminosilicate refractories, the amount of fluxes is normally kept at minimal to minimise their effect on the development of liquid phase at higher temperatures [15].

The chemical and mineralogical characteristics indicate that lithomargic clays consist mainly of kaolinite and gibbsite. The SiO_2 (mainly from the kaolinite) and Al_2O_3 contents vary between 27-39% and 31-46%, respectively. The impurities include Fe_2O_3, TiO_2, K_2O, CaO, MgO and Na_2O [11, 27]. The high alumina content of lithomargic clay makes this clay suitable for use as fireclay aluminosilicate refractory. Studies have also shown that lithomargic clay type A1 (see Table 1) is light in weight; has a soft texture, resistant to chemical and oxidation attack [11]. However, production of refractory ceramic bodies from this sample without a suitable binder is not possible due to its low plasticity as shown in Table 1. There are a number of possible local clays which have good plasticity and therefore could be used as a binder to improve the plasticity of lithomargic clay. Local clays that have been considered thus far to have good plasticity include Mfensi, Afari and Fosu clays. Table 2 shows the results of the Atterberg limits determined for Mfensi, Afari, and Ofosu clays. The Atterberg limit of lithomargic clay sample A1 has been added for comparison. The plasticity indices (PI), except for lithomargic clay, falls within the range 10–60% recommended for ceramic clays [28]. It must be noted that severe shrinkage during drying and firing of refractory bricks are not desirable and must be reduced to the barest minimum. For low shrinkage property, the PI must be within 10-20%. Additionally, binders used should be able to minimize the adverse effect on the refractoriness of the refractory bricks produced. The chemical compositions of the three binders, determined using X-ray florescence spectrometer (XRF–Spectro X-LAB 2000), are shown in Table 3. The major constituents are alumina and silica, forming over 70% of the total chemical compositions. Impurities in the raw materials include oxides of iron, sodium, magnesium, titanium, calcium and potassium. Afari clay has the highest Al_2O_3 and Fe_2O_3 contents of 26.6 and 6.7%, respectively. Fosu clay had the highest SiO_2 content compared to the other clay binders.

Table 2. Atterberg limits of Mfensi, Afari, Fosu and Lithomargic clays

Clay type	Liquid Limit (LL)	Plastic Limit (PL)	Plasticity Index (PI)
Mfensi	43.62	21.72	21.90
Afari	60.17	27.55	32.62
Fosu	51.76	27.79	23.98
Lithomargic (A1)	32.60	24.60	8.00

Table 3. Chemical composition of raw materials

Clay type	Composition, %									
	Al_2O_3	SiO_2	Fe_2O_3	Na_2O	MgO	TiO_2	CaO	K_2O	MnO	LOI
Lithomargic (A1)	44.0	37.6	0.4	0.1	0.0	1.3	0.3	0.2	0.5	14.0
Afari	26.6	48.9	6.7	1.7	1.6	0.8	0.2	0.1	0.0	12.0
Fosu	17.8	72.5	0.6	0.1	0.3	1.0	0.2	2.3	0.0	5.2
Mfensi	23.4	58.6	3.63	2.1	1.4	0.9	0.1	1.3	0.0	8.0

Based on the Atterberg limits and chemical composition analyses, Mfensi clay could be the most suitable binder which can be used to improve the plasticity and properties of lithomargic clay based refractories. Nevertheless, Afari and Fosu clays have also been used as binders and properties reported [20]. This section focuses on advances made on the production of aluminosilicate refractories bricks from lithomargic clay type A1 using different clay binders.

4.1. Materials Preparation

Lithomargic (sample A1), Mfensi, Afari and Fosu clays were used as starting materials. Clay samples were allowed to dry in an oven at 105ºC for 24 hours before processing. The dried clay samples were crushed to smaller particle sizes in a mortar to liberate the mineral constituents. Principal alkalis and dead organic matters were removed by washing i.e. soaking the crushed clay in water for 48 hours and the water filtered off. This treatment was necessary since the presence of alkalis (Na and K) and organics are known to lower refractoriness and strength. They also increase porosity and shrinkage as they burn-off during firing. Particle size analyses were carried out on the starting clay samples using Malvern analyzer (Mastersizer 2000) and the results are shown in Figure 2. The average grain sizes (d_{50}) of lithomargic, Afari, Fosu and Mfensi clays were 18.51, 44.95, 39.81 and 34.67 µm, respectively. The lithomargic clay has the least average grain size whilst Afari clay has the highest. The particle size and distribution of lithomargic clay was the smallest and narrow whilst binders contained coarse and wide particle size distribution with Mfensi clay having the least coarse particle size distribution.

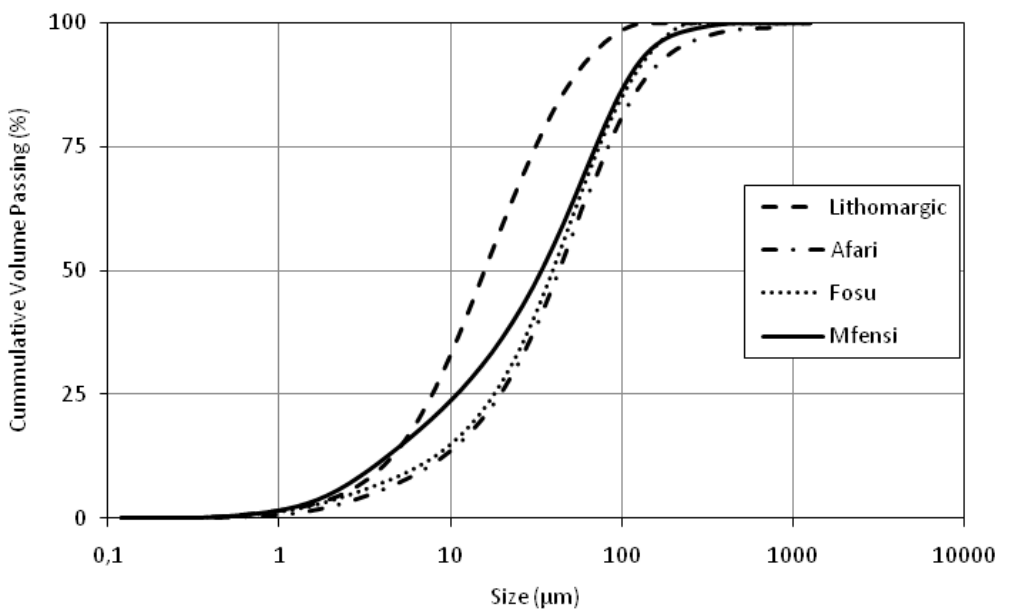

Figure 2. Particle size distribution of investigated clay materials.

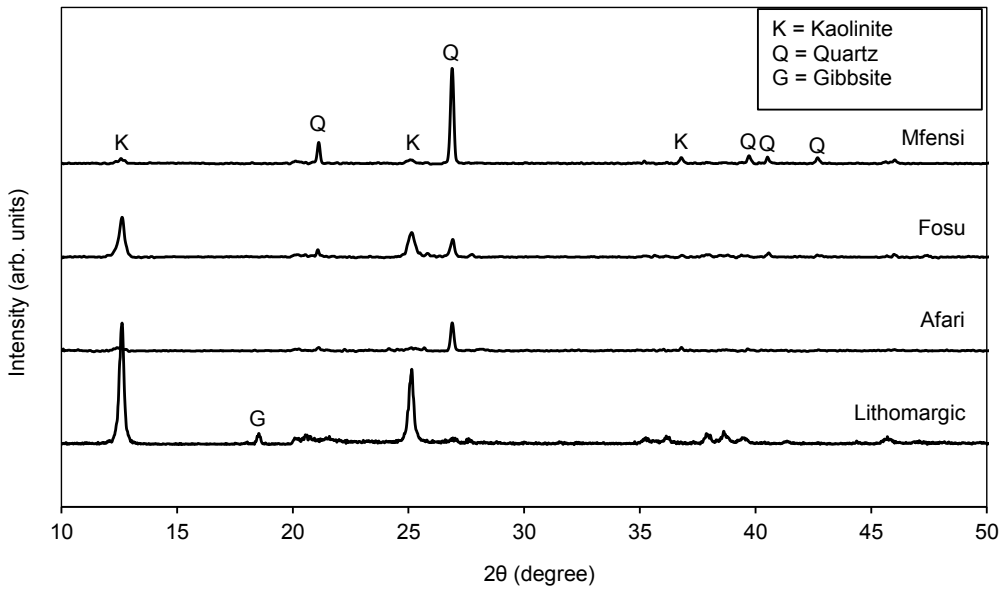

Figure 3. XRD patterns of investigated clay samples.

Table 4. Formulation matrices of lithomargic-binder clay samples. Included in the table are the firing conditions

Sample ID	Composition, %				Firing Temp., °C	Soaking time, min
	Lithomargic (L)	Mfensi (M)	Afari (A)	Fosu (F)		
L90M10	90	10	0	0	1200-1400	60
L85M15	85	15	0	0	1200-1400	60
L80M20	80	20	0	0	1200-1400	30-120
L80A20	80	0	20	0	1350	120
L80F20	80	0	0	20	1350	120

The mineralogical compositions of clay binders were analysed using X-ray diffractometer (Siemens D5000) operating at 40 kV and 40 mA and using Cu Kα radiation. Samples were scanned from 10–50^{o} (2θ) at a step size of 0.02^{o}. Figure 3 shows the XRD patterns of the materials. Mfensi clay consists mainly of quartz with minor fraction of kaolinite. Afari and Fosu clays have relatively low concentrations of quartz and kaolinite. The mineralogical composition of lithomargic clay used (i.e. sample A1), consist of two major crystalline phases; kaolinite and gibbsite, with the kaolinitic peaks having higher relative peak intensity than that of the gibbsite.

4.2. Formulation, Moulding and Drying

Clay samples were oven dried for 24 hours at 105^{o}C. The dried clay samples were ground into powder using a pestle and mortar. Various lithomargic-binder clay formulations were prepared by mechanical agitation at varying proportions by weight as shown in Table 4.

Clay samples for each formulation mix were moulded by adding appropriate amount of water to the mix, tempered and thoroughly worked until plastic state was achieved. Bricks of dimensions 5.2 cm × 5.2 cm × 5.2 cm were moulded. For thermal cycling tests, moulded bricks were of dimensions 15 cm × 2 cm × 2 cm. Drying was done in open air for 24 hours followed by oven drying at a temperature of 105^{o}C for 48 hours. Gauge marks were made on samples of the moulded bricks to determine the drying and firing shrinkages.

4.3. Firing of Moulded Bricks

The dried moulded bricks were fired in a muffle furnace (HF2). Firing temperatures ranged from 1200 to 1400^{o}C for samples L90M10, L85M15 and L80M20. For samples L80M20, soaking time was varied from 30 to 120 minutes in an attempt to optimize the firing conditions. Before reaching the sintering temperature, bricks were fired to 600^{o}C and soaked for 60 minutes due to the displacive transformation between high and low quartz at about 573^{o}C that is usually accompanied by 2% volume change which can lead to fracture of bricks containing large amounts of quartz, which is the case in the current work.

4.4. Characterisation of Fired Bricks

The fired bricks were characterised based on surface appearance, mineralogical composition, linear firing shrinkage, apparent porosity, water of absorption, bulk density, cold crushing strength, modulus of rupture and thermal shock resistance. Densification parameters were determined from linear firing shrinkage (ASTMC326-09), apparent porosity (ASTM C20-00) and bulk density using the water displacement (Archimedes) method according to ASTM C134-95. The thermal stability of the samples was measured using the water-quench test according to ASTM (C1171-05).

4.5. Results and Discussion

The various findings of the work have been published. Table 5 summarizes the major conclusions from these works.

4.5.1. Effect of Firing Temperature on Densification

Linear firing shrinkage, bulk density and apparent porosity are used as direct measures of extent of densification. Andrews *et al.* [17] has reported the effect of temperature on densification of fireclay bricks produced from lithomargic clay using Mfensi clay as a binder (i.e. samples L90M10, L85M15 and L80M20). Bricks were fired from 1200 to 1400^{o}C for 1 hour. The linear firing shrinkage increased as the firing temperature increased in all formulation mix. Linear firing shrinkage increased strongly within the temperatures of 1250 to 1300^{o}C due to volume expansion accompanying quartz to cristobalite phase transformation. This phase transformation can result in pore closure within the fired bricks enhancing densification [29, 30]. With an increase in linear firing shrinkage, the bulk

density of the fired bricks can also increase. It was also reported that as the binder content increased, the bulk density increased, with sample L80M20 recording a maximum bulk density at 1400°C. An improved densification at high temperatures can result in low apparent porosity due to pore closure. From the work, it was concluded that dense fireclay refractories can be produced from lithomargic clay using 20% Mfensi clay and firing at 1400°C for 1 hour.

5.4.2. Effect of Soaking Time on Densification

In another report [18], lithomargic-Mfensi clay formulated bricks (L80M20) were fired at 1350 and 1400°C at varying soaking time (30 to 120 minutes at an interval of 30 minutes) in an attempt to optimize the firing conditions of the refractory bricks.

Table 5. Measured properties of lithomargic clay-based refractories

Research team	Aim	Firing temp., °C	Highlights	Publication year
Gawu and Momade [9]	Potential utilization of lithomargic clay as refractory material.	1250	Separation of gibbsite from kaolinite was successful using 90µm sieve size. Phases: Mullite and Cristobalite. Corundum formed with > 90µm fraction	1998
Momade and Momade [31]	Effect of impurities on mullitilization of lithomargic clay.	1300	Addition of boiler waste (slag) did not enhanced mullite formation. Laterite addition influenced mullite formation. Phases: Mullite, Cristoballite, Quartz	2012
Andrews et al. [17]	Develop densed fireclay refractory bricks from lithomargic clay using Mfensi clay as binder	1200 - 1400	Optimum properties obtained with 20wt% binder at 1400°C with apparent porosity less than 4%. Phases: Mullite, Cristoballite, Quartz	2012
Andrews et al. [18]	Optimize synthesis condition of lithomargic clay refractories using 20 wt% Mfensi clay as binder	1350 - 1400	Full densification achieved either at 1350°C for 120 minutes or 1400°C for 30 minutes. Phases: Mullite, Cristoballite, Quartz	2013
Andrews et al. [20]	Effect of binder type on properties of lithomargic clay refractories	1350	Mfensi clay showed good combination of properties with low water absorption, high cold crushing strength and thermal shock resistance. Phases: Mullite, Cristoballite, Quartz	2014
Andrews et al. [19]	Produce high alumina refractories from lithomargic clay using gibbsite as alumina source	1350	Gibbsite addition improved mullite formation, increased bulk density, cold crushing strength and decreased apparent porosity. Phases: Mullite, Alumina, Cristoballite, Quartz	2014

The linear firing shrinkage at 1350°C increased from 30 to 90 minutes and remained constant up to 120 minutes. At 1400°C, the linear firing shrinkage increased from 30 to 60

minutes and thereafter remained constant. The shrinkage at the two firing temperatures reached equilibrium after 120 minutes soaking time. Marginal differences in bulk densities and apparent porosities of bricks fired at both temperatures were observed. Nevertheless, density and apparent porosity measured at 1350^{o}C were slightly lower than at 1400^{o}C for the various soaking times except at 120 minutes. Thus bricks fired at 1400^{o}C for 30 minutes have similar physical properties compared to bricks fired at 1350^{o}C for 120 minutes. It was therefore recommended that for energy efficient production of this type of refractories, bricks can be produced at relatively low temperature (1350°C) for 120 minutes.

4.5.3. Effect of Binder Type on Densification

The effect of binder type on densification of lithomargic clay-based refractories has been studied [20]. Three different binders have been considered namely, Mfensi, Afari and Fosu clays. Samples L80M20, L80A20 and L80F20 bricks were fired at 1350^{o}C for 2 hours. Sample L80M20 recorded the highest linear firing shrinkage, followed by L80A20 and L80F20, respectively. The shrinkage values correspond linearly with the plasticity indices and impurity levels of the clay binders. Sample L80M20 recorded the highest bulk density (1.64 g/cm^{3}) followed by L80A20 (1.63 g/cm^{3}) and L80F20 (1.61 g/cm^{3}), respectively. Thus, strong correlation exists between linear firing shrinkage and bulk density.

4.5.4. Effect of Firing Conditions on Cold Crushing Strength

It has been reported that cold crushing strength of samples L90M10, L85M15 and L80M20 increases with increasing firing temperatures [17]. The cold crushing strengths of refractory bricks are usually influenced by their phase composition. The mineralogical composition of the fired bricks consisted of cristobalite, mullite and quartz. On the one hand, the high cold crushing strength values was attributed to the presence of highly refractory mullite and cristobalite phases as firing temperature increased. On the other hand, porosity decreased as firing temperature increased which could have also resulted in the high strength values.

In another investigation [18], the effect of soaking time on cold crushing strength (CCS) of sample L80M20 was reported. The cold crushing strength of bricks fired at 1350^{o}C showed an increase from 11.02 MPa to 11.81 MPa after soaking for 30 and 60 minutes, respectively. Thereafter, there was a gradual increase in strength at 90 minutes (11.90 MPa) and 120 minutes (11.96 MPa). It was further explained that the cold crushing strength values at such high temperatures for longer soaking time are influence more by enhanced densification rather than phase composition.

The effect of binder type on the cold crushing strength of lithomargic clay based refractories has also been reported by [20]. The cold crushing strength was significantly high for sample L80M20 (16.14 MPa), followed by L80A20 (12.11 MPa) and L80F20 (8.14 MPa), respectively suggesting that Mfensi clay provides the best combination of properties among all the clay binder investigated.

4.5.5. Effect of Binder Type on the Thermal Shock Resistance

Andrews *et al.* [20] investigated the effect of binder type on the thermal shock resistance of lithomargic clay based refractories using water quench method. The modulus of rupture (MOR) before and after thermal cycling was measured. Before the water quench test, sample L80F20 had the highest average MOR (4.4 MPa) followed by L80A20 (4.21 MPa) and

L80M20 (3.55 MPa), respectively. After the first water quench test, sample L80F20 and L80A20 lost more than 50% of their MOR values whilst sample L80M20 only lost about 15%. Thus, even though sample L80F20 recorded the highest MOR, it had the lowest retained strength after thermal cycling whilst sample L80M20 which recorded the least average MOR has the highest retained strength after thermal cycling. It has been reported that refractories with low MOR values tend to have high thermal shock resistance due to poor resistance to crack propagation [32].

4.5.6. Effect of Gibbsite on Properties

Andrews *et al.* [19] investigated the production of high alumina refractories from lithomargic clay by using gibbsite as alumina source. Gibbsite fraction was separated from lithomargic clay using 90 μm sieve size. Gibbsite fraction in lithomargic clay was varied from 0-40%, moulded and fired at 1350^{o}C for 2 hours. Linear firing shrinkage increases with increasing gibbsite content up to 40% due to evaporation of structural water in gibbsite upon heating, as gibbsite has chemically bonded water content higher than that of kaolinite. The bulk densities of the fired bricks increases linearly with a corresponding decrease in apparent porosity as gibbsite content increased. The cold crushing strength increased with increasing gibbsite content reaching a maximum of 19.1 MPa.

Momade and Momade [31] investigated mullite and corundum formation at different kaolinitic and gibbsite ratios by varying the kaolinitic to gibbsitic fractions at 20:80, 30:70; 50:50, 80:20 and 90:10%. These admixtures were fired at 1300^{o}C for 2 hours and x-ray diffraction patterns analysed. The diffraction patterns between 2Θ values of 20 and 40 are presented in Figure 4 and a plot of the intensities of the peaks at 2Θ = 25.3 for corundum and 25.9 and 26.3 for mullite are shown in Figure 5.

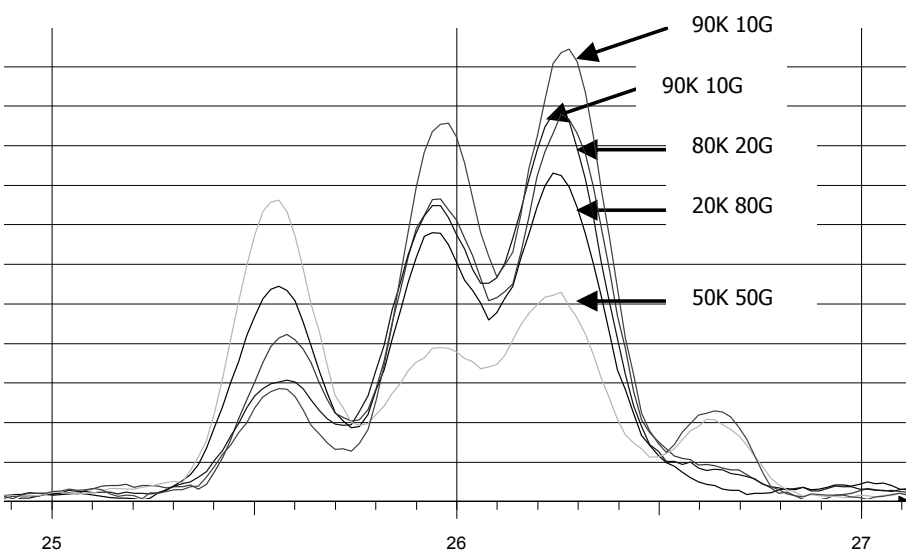

Figure 4. Diffraction patterns of different admixture between 2θ values of 25 and 27 showing corundum, mullite and silica peaks.

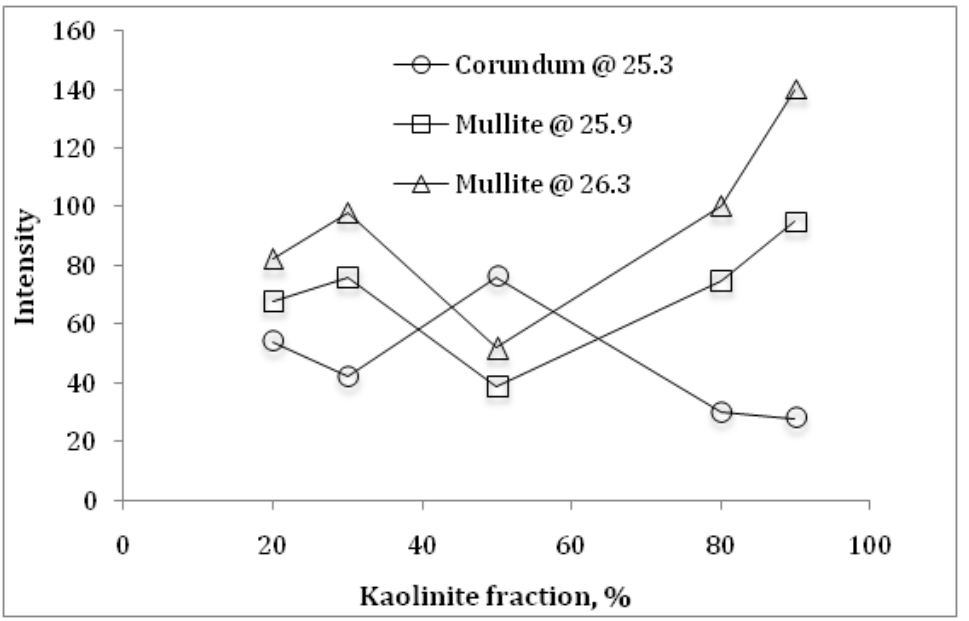

Figure 5. Peak intensities between 2Θ values of 25 and 27 as a function of amount of kaolinitic fractions in the admixtures.

Table 6. Chemical composition of oil mill boiler waste (slag)

Sample	Composition, %									
	Al_2O_3	SiO_2	Fe_2O_3	Na_2O	MgO	TiO_2	CaO	K_2O	MnO	LOI
Boiler slag	10.6	67.4	2.3	1.4	4.8	0.21	2.9	4.2	0.06	3.3

Corundum formation was expected to decrease as the gibbsitic ratio in the mixture was decreased. Instead a sharp increase in peak intensity was observed at 50:50 ratio followed thereafter by a decrease. At the same time the peak intensity of the mullite phase decreased sharply. The increase in peak intensity, which is proportional to the amount of free alumina, may be due to two reasons. Firstly, some of the alumina contributions from gibbsite at the higher ratios may have been used in the formation of mullite with silica rejected during kaolinite transformation which may have not occurred to a large extent with the 50:50 admixing (silica peaks at 2Θ values of 26.5 are present for only the 50:50 and 90:10 ratios). Secondly but not probably, there could be a rejection of alumina from mullite at lattice.

4.5.7. Effect of Impurity on Mullitilization

The effect of some impurities on mullitilization has been investigated by Momade and Momade [31]. Impurities that have been considered included oil mill boiler waste (slag) and laterite containing mainly goethite, hematite and kaolinite. The chemical composition of the oil mill boiler slag is presented in Table 6.

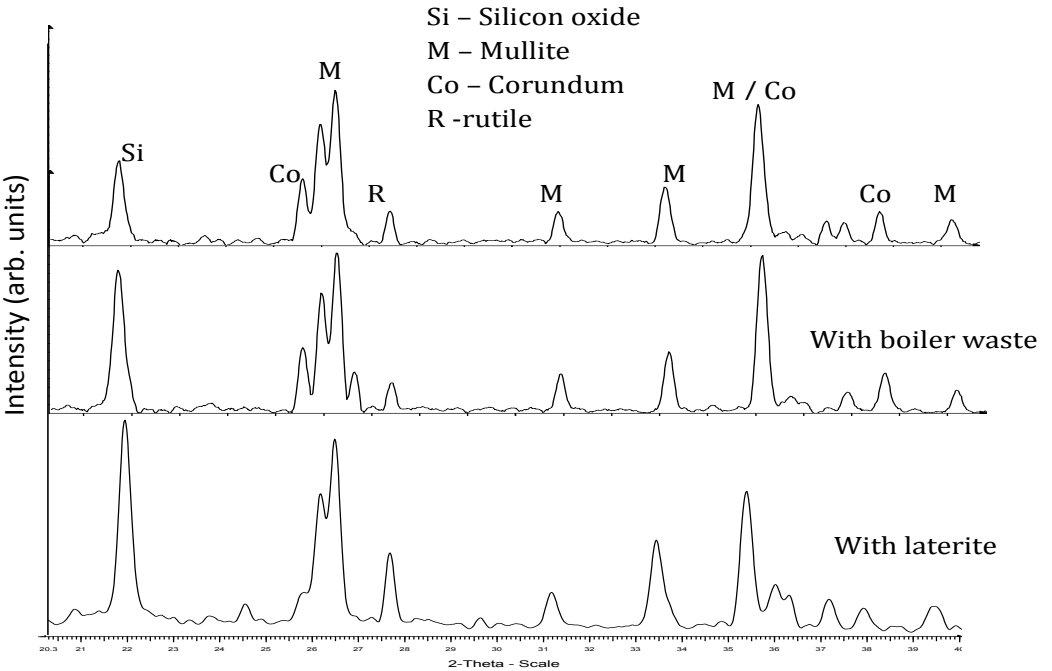

Figure 6. X-ray diffractogram of kaolinitic to gibbsitic ratio of 70:30 admixed with 2% boiler waste and laterite and fired at 1300^{o}C for 2 hours.

Samples containing 70:30 kaolinitic to gibbsitic ratio were mixed with 2% boiler waste and laterite and fired at 1300^{o}C for 2 hours. The x-ray diffractograms of these are presented in Figure 6. On the one hand, the addition of oil mill boiler ash did not seem to have any significant effect on mullite formation. On the other hand, addition of laterite resulted in shifts in mullite peaks suggesting changes in lattice constants.

CONCLUSION

The characteristics of bauxitic lithomargic clays from the Awaso bauxite deposit were investigated through physical, chemical and mineralogical analyses. The clay consists of varying iron oxide contents hence could be exploited as raw material for different applications. Extensive research conducted on the low-iron grade of the clay suggests that the clay could be used to produce aluminosilicate refractories of varying alumina and mullite contents, aluminium sulphate for water purification and anorthite bodies for use in electronic industry. Refractories produced from lithomargic clay could be used as low to high heat duty applications such as insulation behind hot-face materials, furnace linings, and specialty applications such as laboratory crucibles.

REFERENCES

[1] Anon., Principles and Methods of Bauxite Prospecting: Group training in Production of Alumina, in, ALUTERV-FKI, Budapest, UNIDO, 1979, pp. 1-145.

[2] S. H. Patterson, Bauxite and Nonbauxitic Aluminium Resources and Production, in: J.J. Leonard (Ed.) An Update in Bauxite Proceedings of the 1984 Bauxite Symposium, Los Angeles, California, 1984, pp. 3-30.

[3] C. S. Hurburt, W. E. Sharp, Dana's Minerals and How to Study Them, John Wiley & Sons, NY, 1998, pp.189-190.

[4] G. O. Kesse, The Mineral and Rock Resources of Ghana, A. A. Balkema, Rotterdam, Netherlands, 1985, p.169.

[5] S. K. Y. Gawu, Ore Petrology and Geochemistry of the Ichiniso Bauxite Deposit, Awaso, Ghana, Kwame Nkrumah University of Science and Technology, Kumasi, MPhil Thesis, 1993.

[6] R. B. Krishna, P. N. Satish, M. S. Sethumadhav, Syngenetic and epigenetic features and genesis of bauxite-bearing laterite of Boknur-Navge plateau, Belgaum district, Karnataka, *J. Geol. Soc.*, India, 34 (1989) 46-60.

[7] S. A. Norton, Laterite and Bauxite Formation, *Economic Geology*, 68 (1973) 353-361.

[8] L. R. Gardner, A Chemical Model for the Origin of Gibbsite from Kaolinite, *The American Mineralogist*, 55 (1970) 1380-1389.

[9] S. K. Y. Gawu, F. W. Y. Momade, Progress Report on Characterization of the Awaso Lithomargic Clay for the Ghana Chamber of Mines, Report 2, 1998.

[10] F. W. Y. Momade, S. K. Y. Gawu, Progress Report on the Characterisation of the Lithomargic Clay for the Chamber of Mines, Report 3, (1999).

[11] F. W. Y. Momade, S. K. Y. Gawu, Geochemical and mineralogical characteristics of lithomargic clay types from Awaso bauxite deposit, Ghana: implications for possible industrial utilization, *Journal of Science and Technology*, 29 (2009) 386–392.

[12] V. A. Krivandin, B. L. Markov, Metallurgical Furnaces, Mir Publishers, Moscow, 1980, pp.239-242.

[13] F. Shackelford, R. H. Doremus, Ceramic and Glass Materials: Structure, Properties and Processing, (2008) p.1.

[14] K. Shaw, Refractory and their uses, Applied Science Publishers, London, 1972, p. 19.

[15] J. H. Chesters, Refractories: Production and Properties, Iron and Steel Institute London, 1973, pp.10-11.

[16] S. Aramaki, R. Roy, Revised phase diagram for Al_2O_3–SiO_2, *Journal of American Ceramic Society*, 45 (1962) 229.

[17] A. Andrews, J. Adam, S. K. Y. Gawu, Development of fireclay aluminosilicate refractory from lithomargic clay deposits, *Ceramic International*, 39 (2012) 779–783.

[18] A. Andrews, J. Adam, S. K. Y. Gawu, P. A. Olubambi, Synthesis Optimization of Fireclay Refractories from Lithomargic Clay, *Ceramic Forum International*, 90 (2013) E1-E3.

[19] A. Andrews, E. Nsiah-Baafi, S. K. Y. Gawu, P. A. Olubambi, Synthesis of high alumina refractories from lithomargic clay, *Ceramics International*, 40 (2014) 6071-6075.

[20] A. Andrews, S. K. Y. Gawu, M. Appiah, A. Indome, A. Fudzi, J. Abaka, Strength of lithomargic clay based refractories after thermal cycling, *Refractories and Industrial Ceramics*, In press (2014).
[21] F. W. Y. Momade, K. Sraku-Lartey, Studies into the preparation of alum from slime waste from the Awaso bauxite washing plant, *Hydrometallurgy*, 101 (2010) 93-98.
[22] R. A. Gdula, Anorthite ceramic dielectrics, *American Ceramic Society Bulletin*, 50 (1971) 555-557.
[23] M. R. Boudchicha, S. Achour, A. Harabi, Crystallization and sintering of cordierite and anorthite based binary ceramics, *Journal of Materials Science Letters*, 20 (2001) 215-217.
[24] X. Cheng, S. Ke, Q. Wang, H. Wang, A. Shui, P. Liu, Fabrication and characterization of anorthite-based ceramic using mineral raw materials, *Ceramics International*, 38 (2012) 3227-3235.
[25] S. Agathopoulos, D. U. Tulyaganov, P. A. A. P. Marques, M. C. Ferro, M. H. V. Fernandes, R. N. Correia, The fluorapatite–anorthite system in biomedicine, *Biomaterials*, 24 (2003) 1317-1331.
[26] A. C. Schacht, Refractories Handbook, Marcel Dekker, Inc, NY, 2004, pp. 81-85.
[27] F. W. Y. Momade, S. K. Y. Gawu, M. Affam, Characterization of lithomargic clay from the Awaso bauxite deposit, in: 90th Anniversary International Conference and Exhibition of the Geological Survey Department of Ghana, International Conference Centre, Accra, Ghana, 2004.
[28] E. E. Nnuka, C. Enejor, Characterization of Nahuta Clay for Industrial and Commercial Applications, *Nigerian Journal of Engineering and Materials*, 2 (2001) 9-12.
[29] R. M. German, Sintering theory and practice, John Wiley & Sons, Inc, New York, 1996, pp. 480-485.
[30] S. C. Carniglia, G. L. Barner, Handbook of Industrial Refractories Technology: Principles, Types, Properties and Applications, Noyes Publications, Park Ridge, NJ, 1992, pp. 528-529.
[31] F. W. Y. Momade, Zs. Momade, Effect of impurities on the mullite formation of lithomargic clay., in: Report on lithomargic clays underlying Awaso bauxite deposits, Kwame Nkrumah University of Science and Technology, Kumasi, 2012.
[32] N. Ntakaburimvo, C. Allaire, J. Sebbani, Influence of the firing temperature and mineralogy on the thermo-mechanical behavior of aluminosilicate refractory castables, in: 44th Metallurgist of CIM; Metal/Ceramic Interactions, Canadian Institute of Mining, Metallurgy and Petroleum, Canada, 2002, pp.261-280.

In: Clays and Clay Minerals
Editor: Liam R. Wesley
ISBN: 978-1-63117-779-8

Chapter 18

CONFUSION IN THE LITERATURE OF VERMICULITE

Ernest M. M. Marwa •
Sokoine University of Agriculture, Morogoro, Tanzania

ABSTRACT

In many studies, vermiculite, hydrobiotite and a mixture of vermiculite, mica and hydrobiotite are grouped together as 'vermiculite'. This is due to the fact that the name 'vermiculite' is used as a mineral at the same time as a traded commodity. Any mineral that shows the property of exfoliation when flash-heated is named as 'vermiculite', regardless whether is vermiculite, hydrobiotite or a mixture of vermiculite, hydrobiotite and/or mica. This generalisation is making confusion and difficult to compare available data in literature. True vermiculite does not expand when heated or treated with chemicals and it is rarely used as a commercial commodity in civil engineering works because of high bulk density and poor thermal exfoliation. It differs significantly from other minerals that are regarded as commercial vermiculites in chemical compositions as well as in physic-chemical properties. Thus, it is recommended in this chapter that this generalisation should stop because it is misleading the public.

INTRODUCTION

Vermiculite is a secondary 2:1 phyllosilicate mineral with a net negative layer charge falling between -0.6 and -0.9 per formula unit (Bailey, 1980; Guggenheim et al., 2006). This layer charge is less than that of micas but higher than that of smectites and is both directly and indirectly responsible for many of the useful properties of vermiculite. The mineral has a general chemical formula $(Mg, Ca)_{0.6\text{-}0.9}(Mg, Fe^{3+}, Al)_{6.0}[(Si, Al)_8O_{20}](OH)_4.nH_2O$ (Deer et al., 1992). In macroscopic scale, vermiculite looks like mica, but it exists in a wide range of colours, such as light yellow, brown and /or black (Van Gosen et al., 2005). Unheated 'true' vermiculite has a hardness of 1.5, specific gravity of 2.2-2.5, and a perfect (001) cleavage (Walker, 1951). It occurs both in dioctahedral and trioctahedral forms (Brindley and Brown,

• E-mail: emagesa@yahoo.com.

1984). However, most macroscopic trioctahedral vermiculite results from the alteration of micas, in particular, biotite, phogopite or muscovite. Some can to a less extent form from alteration of chlorite, olivine, serpentine, pyroxene or amphibole (Basset, 1963; Bush, 1976). The alteration of micas to vermiculites involves the release of K^+, oxidation of Fe^{2+} to Fe^{3+}, and re-orientation of hydroxyl ions (Douglas, 1989). The dioctahedral varieties, which are common in soils, originate from the alteration of dioctahedral illite (Brindley and Brown, 1984). Distinction between trioctahedral and dioctahedral vermiculites is based on the position of reflection (060) on their XRD patterns. Dioctahedral vermiculites show an interlayer space value *d*(060) between 0.149 nm and 0.150 nm, while trioctahedral vermiculites have *d*(060) between 0.151 nm and 0.153 nm (Bailey,1980).

Structurally, vermiculite consists of an octahedral sheet sandwiched between two opposing tetrahedral sheets. The dimensions of the tetrahedral sheets vary with the size and charge of the cations occupying the octahedral sites (Bailey, 1966). The adjacent tetrahedral sheets (silicate layers) are separated by a double layer of water molecules arranged in a distorted hexagonal pattern around Mg^{2+} ions. Its hydration state is defined by the number of layers saturated with water molecules between the silicate sheets (Suzuki et al., 1987). This interlayer water facilitates the exchange and migration of cations in the interlayer space (Douglas, 1989). Apart from the structural water, the mineral vermiculite occurs with a varying amount of non-structural water (Walker, 1951).

A regularly mixed layer structure of biotite and vermiculite is referred to as hydrobiotite in ‘mineralogical sense’ (Brindley et al., 1983) and not simply vermiculite as it appear in some literature. When vermiculite is regularly interstratified with phlogopite, it is sometimes called hydrophlogopite (Schoeman, 1989). Interestingly, commercially and in literature true vermiculite, hydobiotite, hydrophlogopite or a mixture of vermiculite and some hydromica all are grouped together as vermiculite (Frank and Edmond, 2001). Dugarlite, Mondalite, Strong-lite, and Zonolite are among the commercial names also used to refer to commercial vermiculite and related products (Hindman, 2006). This generalization is making confusion and difficult to compare research findings on vermiculite.

VERMICULITE IDENTIFICATION

Vermiculite is difficult to identify and quantify because of its broad structural diversity (Środoń, 2006). A number of methods are currently in use, but X-ray diffraction (XRD) remains the principal tool commonly employed for identifying clay minerals including vermiculite (Hillier, 2003). With XRD, it is also possible to identify and quantify other mineral phases that are present in vermiculite. The use of both random powders and oriented clay fractions is recommended as they are complementary. The random powders provide absolute abundances of different mineral phases while oriented clay fractions enhance the signals from the basal plane (001) which facilitates recognition of individual clay mineral phases (Kahle et al., 2002).

Cation saturation with ethylene glycol and heating are commonly used in combination with XRD to distinguish vermiculite from smectite (Thorez, 1976). The smectite swells when solvated with ethylene glycol show a significant increase in the d-spacing in the XRD patterns while vermiculite and other similar layer silicates are not significantly affected by this

treatment (Moore and Reynolds, 1997). Vermiculite and smectite is distinguished from chlorite by heating. When heated to 400 ^{o}C, smectite and vermiculite usually collapse to 9.6-10 Å while chlorite remains unaffected (Hardy and Tucker, 1988). Further heating to 550 ^{o}C causes dehydroxylation of the hydroxide sheet and the 7 Å component in chlorite is rendered amorphous and the intensity of the 001 reflection is increased (Moore and Reynolds, 1997). Vermiculite at 550^{o}C shows only a slight collapse or no further collapse (Hardy and Tucker, 1988). Thus, without this prior treatment, it is difficult to distinguish vermiculite and chlorite because they have similar XRD reflection patterns (Walker, 1949).

True vermiculite is identified by its first order basal spacings on the XRD patterns of between about 14 and 15 Å. True vermiculite shows a series of higher order basal peaks that are rational on the primary basal spacing (Brindley and Brown, 1984; de la Calle and Suquet, 1988). Hydrobiotite is distinguished from true vermiculite on the XRD patterns by most obviously strong but broad peaks at around 12 and 24 A˚. The broad peak at around 24 A˚ arises from an ordered interstratification of 10 A˚ (mica) and 14 A˚ (vermiculite) layers (Hillier et al., 2013). On solvation with ethylene glycol, the basal spacing (00l) of true vermiculites may decrease or increase depending on whether individual vermiculite is of low or high charge. For instance, true vermiculite (KL2) studied by Marwa (2009) showed a slight decrease in the basal spacing on solvation from around 14.4 to 14.2Å (Figure 1). This response to glycolation in the Mg-saturated state is a characteristic of high charge vermiculites (MacEwan and Wilson, 1984). The response is due to vermiculite imbibing one layer of ethylene glycol (Marwa et al., 2009a). The XRD patterns of this true vermiculite (KL2 in Figure 1) displayed a completely rational series of basal spacings with no sign of layer spacing heterogeneity.

The Air-dried and ethylene glycol solvated XRD patterns of commercial vermiculite from Palabora mines in South Africa (PB) were completely different from that of true vermiculite (Figure 1). The basal spacings of the discrete vermiculite and hydrobiotite in PB decreased slightly from its air-dried values. Mica in PB was not affected by glycolation and its basal spacing remained unchanged at 10.1Å. From the intensity of the peak it is obvious that PB had both vermiculite and hydrobiotite but the proportion of hydrobiotite was higher than that of vermiculite and mica. The XRD patterns of PB showed sign of layer spacing heterogeneity and display irrational series of basal spacings, which are completely different from that of true vermiculite. This proves that vermiculite is different from hydrobiotite and should not be grouped together.

EXFOLIATION CHARACTERISTICS

True vermiculite in ‘mineralogical sense’ does not and should not exhibit the property of exfoliation when heated or treated with chemicals (Hillier et al., 2013). Minerals that exhibit the property of exfoliation when heated or treated with chemicals are either hydrobiotite or those with interstratifications of vermiculite, hydrobiotite and /or mica phases, which are called commercial vermiculites. In their study, Hillier et al. (2013), used six samples comprising of true vermiculite, phlogopite, and hydrobiotite with/without vermiculite to prove that true vermiculite does not exfoliate when heated or treated with chemicals. Phlogopite was incorporated in that study as a control. True vermiculite and phlogopite did

not show significant exfoliation when heated at 400 and 900^{o}C, while hydrobiotite and / or mixture of vermiculite, hydrobiotite and /or chlorite exfoliated significantly.

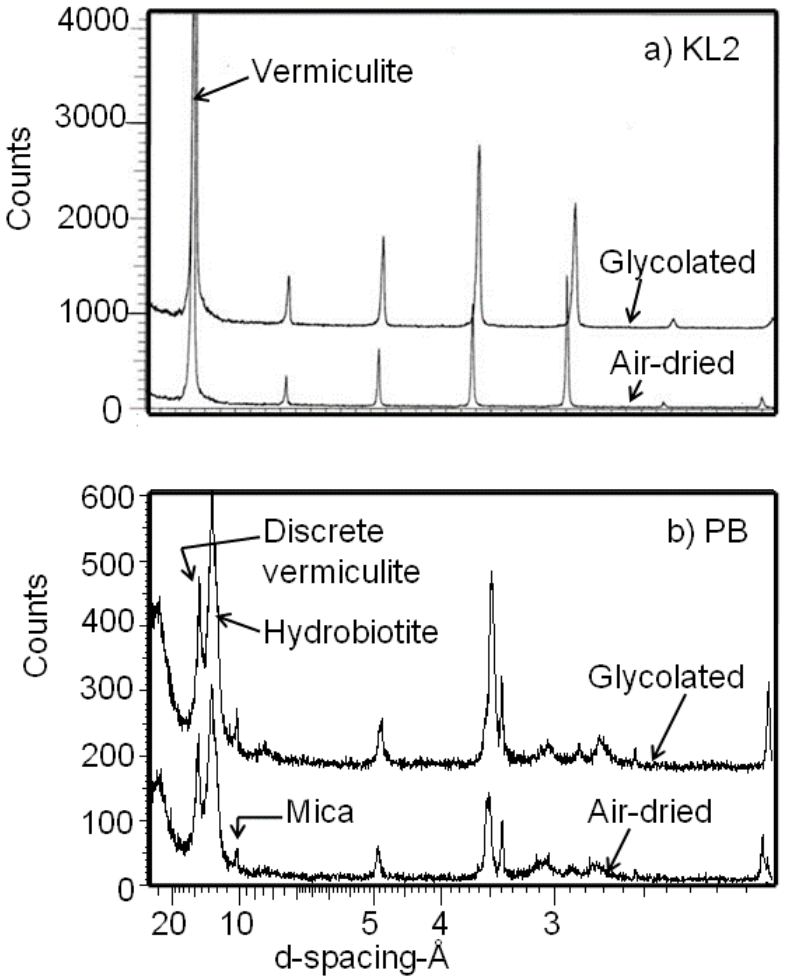

Marwa (2009).

Figure 1. XRD patterns in the air-dried and ethylene glycol solvated conditions for a) KL2 (true vermiculite and b) PB (hydrobiotite with small amounts of vermiculite and mica). Intensity counts are offset for clarity.

In the actual sense, true vermiculite does not contain substantial amounts of potassium but minerals in literature that are reported to exhibit exfoliation property have a substantial amount of potassium in their chemical compositions. True vermiculite used by Hillier et al. (2013) had <0.05 wt% K_2O. Contrary to the eight commercial vermiculites reported by Hindman (2006) from Australia, China, Brazil, USA, Egypt, South Africa, Russia, and Canada, which had 0.50-4.24 wt% K_2O. Similarly, studies by El Mouzdahir et al. (2009) used what they called "vermiculite" from Palabora Mining Company in South Africa and concluded that "dehydration from 300-600^{o} C caused exfoliation and formation of low bulk density material of potential economic important". What they used was not true vermiculite; it

had 2.5 wt% K_2O and XRD patterns of raw sample show peaks of hydrobiotite. Also Gordeeva et al. (2002) used two samples KVK-2 and KR-1, which were regarded as vermiculites, to assess their response to heating. Close examination had shown that the samples were not true vermiculites because they had 0.70-0.87 and 3.0-6.0 Wt% K_2O, respectively. In that study, those with higher potassium exfoliated more than those with small amount of potassium. This is another example, which proves that what is regarded in literature as commercial vermiculites are not necessarily true vermiculites.

BULK DENSITY AND MASS LOSS

The difference between true vermiculites and commercial vermiculites on the basis of bulk density and mass loss is clear when heated at a temperature above 200 ^oC. According Hillier et al. (2013) and Marwa et al. (2009b), true vermiculites when heated lose more weight than hydrobiotite or a mixture of vermiculite and hydrobiotite and / or mica (Table 1). High loss in weight for vermiculite is attributed to the loss of both interlayer water and high-temperature hydroxyl water. Vermiculites lose more water on heating and consequently more weight because their crystal structures are more hydrated with a double layer of water (Tripathi et al., 1978). Previous studies have indicated that interlayer water is lost when heating is done at a temperature lower than 550 ^oC, while dehydroxylation starts at 500 ^oC and continues to higher temperature (Barshad, 1950; Walker, 1951).

Furthermore, vermiculites and hydrobiotites differ in the extent of losing hydroxyl water when heated at 900^oC. More hydroxyl water is lost in vermiculites than in hydrobiotites (Marwa et al., 2009b; Hillier et al., 2013). Using particle size 0.5-1mm, Marwa and other researchers, in unpublished data found the same trend whereby vermiculites KL2 and VER-18 in Table1 lost 7.7-9.5% hydroxyl water while hydrobiotite with varying amount of vermiculite and/or mica (MK1, VER-2 and PB) lost 4.7-5.6% (Table 1). The presence of a larger amount of potassium ions in hydrobiotites has been found to hinder the release of hydroxyl water on heating (Marcos et al., 2009). Phlogopite (PHL-3) lost only 0.3% (Table 1). This could be due to the fact that phlogopite has high amounts of K and does not have interlayer water and OH ions are strongly held in the structure and thus, not easily lost on heating.

Although true vermiculites lost a lot of water on heating, their bulk densities did not decrease as that of hydrobiotite or a mixture of vermiculite and hydrobiotite (Table 1). This is due to the fact that true vermiculites do not exfoliate when heated. The decrease in bulk density in vermiculites is attributed to the loss of interlayer and hydroxyl waters. This finding is in agreement with previous studies which show more exfoliation and hence, decrease in bulk density in hydrobiotites than true vermiculites (Hillier et al., 2013; Justo et al., 1989; Midgley and Midgley, 1960).

Table 1. Variation in bulk density and mass loss on heating at 20, 400 and 900° C. Each value represents a mean of three replicates with a standard error

Sample	Bulk density, kg/m^3			Mass loss, %	
	20 °C	400 °C	900 °C	400 °C	900 °C
PHL-3	280±8	283±10	251±4	1.0±0.0	1.3±0.4
KL2	624±11	565±22	479±3	12.7±1.4	20.4±0.1
VER-18	800±8	753±14	287±3	10.1±0.4	19.6±0.0
VER-2	779±21	594±32	175±0.0	9.0±1.2	14.6±0.4
MK1	909±0	740±62	192±2	8.4±2.9	14.0±0.5
PB-	525±24	467±13	159±0.5	3.9±1.9	8.6±0.0

Source: Unpublished data using same samples as in Hillier et al. (2013), but with 0.5-1.0mm sized particles.

PHL-3=Phlogopite; KL2=Vermiculite; VER-18=Vermiculite with small amount of chlorite;

VER -2 and MK1=Vermiculite + Hydrobiotite and PB=Hydrobiotite with traces of vermiculite and mica.

CATION EXCHANGE CAPACITY

Cation exchange capacity (CEC) is a measure of the available quantity of exchangeable cations in a medium that can neutralise the negative charge in the soil at a given pH. In clay minerals including vermiculites, the CEC is equivalent to the layer charge which is represented by the sum of the exchangeable charge-compensating cations in a mineral (Bergaya et al., 2006). It is widely determined by the displacement of interlayer cations with index cations. It can also be deduced from the chemical analysis, provided vermiculite is not contaminated with other minerals and its chemical composition is accurately known (Bergaya et al., 2006).

Studies indicate that true vermiculites have a high CEC broadly ranging between 50 and 150 $cmol_{(+)}$/kg (Hindman, 2006; Van Straaten, 2002). Higher values of 180 up to 210 $cmol_{(+)}$/kg are also in literature. The CEC of vermiculite is attributed to the surface and interlayer ion exchange associated with the isomorphic replacement of Al^{3+} for Si^{4+} in its tetrahedral sheets and Al^{3+} and / or Fe^{3+} for Mg^{2+} in the octahedral layers. This substitution creates a deficiency of positive charges on the surface of vermiculite which is compensated by exchangeable cations (Ramirez-Valle et al., 2006). The isomorphic substitution accounts for 80 % of the CEC of vermiculite and the remaining 20 % is contributed by the broken bonds around the edges of the silica-alumina unit which give rise to unsatisfied charges (Grim, 1953).

Studies indicate that the CECs of true vermiculites are about 6 fold more than that of hydrobiotites or a mixture of vermiculites, hydrobiotites and / or micas (Marwa et al., 2009a and 2009b). In hydrobiotites or in a mixture of vermiculite and hydrobiotite the CEC

increases with the increase in the proportion of vermiculite (Table 2). The higher CEC in vermiculites is attributed to the high interlayer water that facilitates the exchange and migration of cations in the interlayer space (Douglas, 1989). The interlayer water in hydrobiotite is small and is only contributed by vermiculite component. This makes hydrobiotites to have low CEC.

Heating affected the CEC of true vermiculite differently from that of hydrobiotite or other hydromica. The CECs of true vermiculites were decreased by more than 89% of their original values when heated to a temperature of more than 600^{o}C (Table 2). This was caused by loss of interlayer and hydroxyl waters. Loss of interlayer water caused the interlayer space to decrease while loss of hydroxyl ions lowered the negative charges and consequently, the ability of vermiculite to adsorb cations.

Table 2. Variation in cation exchange capacity with heating temperature. Each value represent mean of three replicates with standard error

Samples	Heating temperature, ^{o}C				
	15	200	400	600	800
KL1	127.60±3.99	80.93±3.75	61.52±4.61	15.20±2.72	13.26±3.15
KL2	120.34±4.51	108.17±6.55	113.07±4.66	83.64±7.28	7.83±3.57
MS	148.26±4.31	124.30±5.80	133.97±4.41	103.47±3.46	3.89±1.05
MK2	104.22±4.55	60.42±3.50	52.16±4.52	69.67±5.23	27.96±3.46
MK1	23.19±3.86	25.29±3.70	16.65±3.33	19.89±1.21	22.90±1.72
PB	14.33±1.14	9.44±6.42	45.89±11.88	92.17±22.87	28.36±9.91

(Marwa, 2009).

KL1, KL2 and MS were true vermiculite while MK2 comprised of 60% vermiculite,16% hydrobiotite and 15% pyroxene and amphibole, MK1 contained 15% vermiculite,74% hydrobiotite and 7% quartz and PB had 1% vermiculite, 87% hydrobiotite and 11% mica.

According to Hindman (2006), if vermiculite is exfoliated, the CEC can decrease by 5-10 % from the unheated product. This is true if Hindman (2006) is referring to commercial vermiculites (hydrobiotites) but not true vermiculites.

The CECs of hydrobiotites are less affected on heating because of the increase in the availability of exchangeable K^{+} from mica (Figure 2). In addition, the presence of exchangeable K^{+} retards the release of hydroxyl water from hydrobiotites (Marcos et al., 2009). It implies the lost of the negative charges is less from hydrobiotites during dehydroxylation than from vermiculites. Heating of hydrobiotites makes potassium ions easily extractable. Significant increase in exchangeable K^{+} occurred when heated to a temperature of more than 400 ^{o}C. It implies that the conversion of interlayer K^{+} into exchangeable form in hydrobiotites occurs during the dehydroxylation stage. This is possible because potassium ions are not fixed in hexagonal sites due to their large ionic radii as compared to the other interlayer cations (Kawano and Tomita, 1991).

In contrast to potassium, heating decreases the availability of exchangeable Mg^{2+}, Ca^{2+}, and Na^{+} in both vermiculites and hydrobiotites (Marwa et al., 2009b). This could be probably due to fixation of the cations in the silicate sheet.

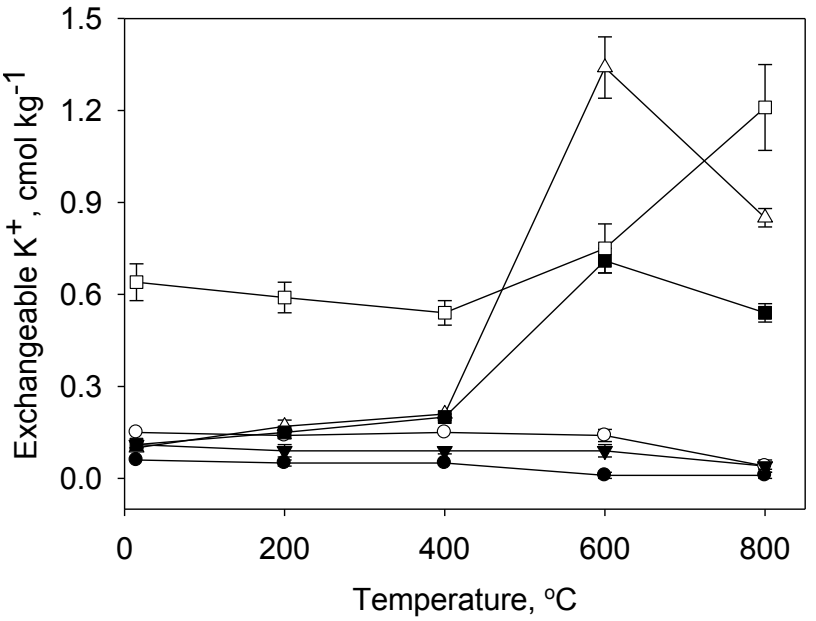

(Marwa (2009)).

Figure 2. Effect of heating vermiculites and hydrobiotites on the availability of exchangeable potassium. Shaded circles refer to vermiculite sample KL1; open circles vermiculite sample KL2; shaded triangles vermiculite sample MS; open triangles hydrobiotite and vermiculite sample MK1; shaded squares vermiculite and hydrobiotite sample MK2; and open squares hydrobiotite with small amount of vermiculite and mica (sample PB). Each plotted value represents a mean of three replicates with the standard error shown by a vertical bar.

The release of the interlayer water destabilizes the interlayer cations. Walker (1956) has shown that the interlayer cations on heating could migrate into the hexagonal sites of the silicate sheet and get fixed.

The decrease in the availability of exchangeable cations is a sign of fixation. The only place where these cations can be fixed permanently is in the hexagonal vacant sites.

CONCLUSION

True vermiculite is different from hydrobiotite or a mixture of hydrobiotite and vermiculite, which are regarded in literature as commercial vermiculites**.** It does not exfoliate when heated as compared to commercial vermiculites. It differs significantly from commercial vermiculites in chemical and mineralogical compositions as well as in physic-chemical properties. Thus, damping true vermiculite under commercial vermiculites is misreading the public and should stop to enable precisely comparison of research findings.

REFERENCES

Bailey, S. W. (1966). The status of clay mineral structures. *Clays and Clay Minerals*, **14:** 1–23.

Bailey, S. W. (1980). Comment: Summary of recommendations of AIPEA Nomenclature Committee. *Clays and Clay Minerals*, 28**:**73-78.

Barshad, I. (1950). The effect of interlayer cations on the expansion of the mica type of crystal lattice. *American Mineralogist*, 35:225-238.

Basset, W. A. (1963). The geology of vermiculite occurrences. *Clays and Clay Minerals*, 10:61-69.

Bergaya, F., Lagaly, G. and Vayer, M. (2006). Cation and anion exchange. In: Bergaya, F., Theng, B. K. G and Lagaly, G. (Eds.). Developments in Clay Science, Volume 1: Handbook of Clay Science. Elsevier, Amsterdam. pp. 979-1001.

Brindley, G. W. and Brown, G. (Eds.) (1984). Crystal Structures of Clay Minerals and their X-ray Diffraction. Mineralogical Society, Monograph No.5. London. 495pp.

Brindley, G. W., Zalba, P. E. and Bethke, C. M. (1983). Hydrobiotite, a regular 1:1 interstratification of biotite and vermiculite layers. *American Mineralogist*, 68**:**420-425.

Bush, A. L. (1976). Vermiculite in the United States, In: 11th Industrial Minerals Forum. Montana Bureau of Mines and Geology Special Publication. 74:145-155.

Deer, W. A., Howie, R. A. and Zussman, J. (1992). An Introduction to the Rock-Forming Minerals. 2nd edition, Longman, England, 696pp.

De la Calle, C. and Suquet, H. (1988). Vermiculite. In: Bailey, S.W. (Ed.). Hydrous Phyllosilicates (Exclusive of Micas): Reviews in Mineralogy. Mineralogical Society of America. Washington, D.C. pp.455-496.

Douglass, L. A. (1989). Vermiculites. In: Dixon, J. B. and Weed, S. B. (Eds.). Minerals in Soil Environments. 2nd edition. Soil Science Society of America, Book series no.1. pp.635-674.

El Mouzdahir, Y., Elmchaouri, A., Mahboub, R., Gil, A. and Korili, S. A. (2009). Synthesis of nano-layered vermiculite of low density by thermal treatment. *Powder Technology*, 189 (1): 2–5.

Frank, D. and Edmond, L. (2001). Feasibility for identifying mineralogical and geochemical traces for vermiculite ore deposits. United States Environmental Protection Agency. Region 10, EPA 910-R-01-002.

Gordeeva, L. G., Moroz, E. N., Rudina, N. A. and Aristov, Y. I. (2002). Formation of porous vermiculite in the course of swelling. Inorganic Synthesis and Industrial Inorganic Chemistry. *Russian Journal of Applied Chemistry*.75 (3):357-361.

Grim. R. E. (1953). Clay Mineralogy. McGraw-Hill Publishing Company Ltd, London, UK. 384pp.

Guggenheim, S., Adam, J. M., Bain, D. C., Bergaya, F., Brigatti, M. F., Drits, V. A., Formoso, M. L. L., Galán, E., Kogure, T. and Stanjek, H. (2006). Summary of recommendations of nomenclature committees relevant to clay mineralogy: report of the Association Internationale Pour l'Etule de Argiles (AIPEA) Nomenclature Committee for 2006. *Clay Minerals*, 41**:**863-877.

Hardy, R. and Tucker, M. (1988). X-ray powder diffraction of sediments. In: Tucker, M. (ed.). Techniques in Sedimentology, Blackwell Science Ltd., Avon. pp.191-228.

Hillier, S. (2003). Quantitative analysis of clay and other minerals in sandstones by X-ray powder diffraction (XRPD). International Association of Sedimentology. Special Publication. 34:213-251.

Hillier, S., Marwa, E. M. M. and Rice, C. M. (2013): On the mechanism of exfoliation of 'Vermiculite'. *Clay Minerals*, 48:563-582.

Hindman, J. R. (2006). Vermiculite. In: Kogel, J. E.,Trivedi, N. C, Barker, M. J., and Krukowski, S. (Eds.). Industrial Minerals and Rocks, Commodities, Markets and Uses. 7th edition. Society of Mining, Metallurgy and Exploration. pp. 1015-1026.

Justo, A., Maqueda, C., Perez-Rodriguez, J. L. and Morillo, E. (1989). Expansibility of some vermiculite. *Applied Clay Science*, 4 (5-6):509-519.

Kahle, M., Kleber, M. and Jahn, R. (2002). Review of XRD-based quantitative analyses of clay minerals in soils: the suitability of mineral intensity factors. *Geoderma*, 109:191-205.

Kawano, M. and Tomita K. (1991). Dehydration and rehydration of saponite and vermiculite. *Clays and Clay Minerals*, 39 (2):174-183.

MacEwan, D. M. C. and Wilson, M. J. (1984). Interlayer and intercalation complexes of clay minerals. In: Brindley, G. W and Brown, G. (Eds.). Crystal Structures of Clay Minerals and their X-ray Identification. Mineralogical Society Monograph No.5, reprint. London. pp. 197-248.

Marcos, C., Arango, Y. C. and Rodriguez, I. (2009). X-ray diffraction studies of the thermal behaviour of commercial vermiculites. *Applied Clay Science*, 42: 368-378.

Marwa, E. M. M. (2009). Characterization of vermiculites from the Mozambique Belt of Tanzania for agricultural applications. Unpublished PhD thesis. University of Abeerden. 192pp.

Marwa, E. M. M., Hillier, S., Rice, C. M. and Meharg, A. A. (2009a). Mineralogical and chemical characterization of some vermiculites from the Mozambique Belt of Tanzania for agricultural use. C*lay Minerals,* 44:1-17.

Marwa, E. M. M., Meharg, A. A. and Rice, C. M. (2009b). The effect of heating temperature on the properties of vermiculites from Tanzania with respect to potential agronomic application. *Applied Clay Science*, 43:376-382.

Midgley, H. G. and Midgley, C. M. (1960). The mineralogy of some commercial vermiculites. *Clay Minerals*, 4(23):142-150.

Moore, D. M. and Reynolds, R. C. Jr. (1997). X-ray Diffraction and the Identification and Analysis of Clay Minerals. Oxford University Press, Inc. Madison Avenue, New York, 378pp.

Ramírez-Valle, V., Jiménez de Haro, M. C., Avillés, L. A. Pérez-Maqueda, L. A., Durán, A., Pascual, J. and Pérez-Rodriquez, J. L. (2006). Effect of interlayer cations on high-temperature phases of vermiculite. *Journal of Thermal Analysis and Calorimetry*, 84 (1): 147-155.

Schoeman, J. J. (1989). Mica and vermiculite in South Africa. *Journal of South African Institute of Mining and Metallurgy*, 89(1):1-12.

Środoń, J. (2006). Identification and quantitative analysis of clay minerals. In: Bergaya, F., Theng, B. K. G and Lagaly, G. (Eds.). Developments in Clay Science, Volume 1: Handbook of Clay Science. Elsevier, Amsterdam. pp. 765-787.

Suzuki, M., Wada, N., Hines, D. R., and Whittingham, M. S. (1987). Hydration states and phase transitions in vermiculite intercalation compounds. *Physical Review B*, 36 (5):2844-2851.

Thorez, J. (1976). Practical Identification of Clay Minerals: A Handbook for Teachers and Students in Clay Mineralogy. G. Lelotte Dison, Belgique, 90pp.

Tripathi, R. P., Chandra, U., Chandra, R. and Lokanathan, S. (1978). A Mössbauser study of the effects of heating biotite, phlogopite and vermiculite. *Journal of Inorganic and Nuclear Chemistry*, 40:1293-1298.

Van Gosen, B. S.; Lowers, H. A; Bush, A. L; Meeker, G. P; Plumlee, G. S; Brownfield, T. K. and Sutley, S. J. (2005). Reconnaissance study of the geology of U.S. vermiculite deposits – Are asbestos minerals common constituents? Version 2.0, USGS, Bulletin 2192, 8pp.

Van Straaten, P. (2002). Rocks for Crops: Agro-minerals of Sub-Saharan Africa. International Centre for Research in Agroforestry Project. Nairobi, Kenya. 388pp.

Walker, G. F. (1949). Water layers in vermiculite. *Nature*, 163:726.

Walker, G. F. (1951). Vermiculites and some related mixed-layer minerals. In: Brindley, G. W. (ed.). X-ray Identification and Crystal Structures of Clay Minerals. Mineralogical Society, London. pp.199-223.

Walker, G. F. (1956). The mechanism of dehydration of Mg-vermiculite. *Clays and Clay Minerals*, 4:101-115.

INDEX

A

B

C

D

E

F

G

H

I

J

K

L

M

N

O

P

Q

R

S

T

U

V

W

X

Y

Z